

TOPICS IN CURRENT CHEMISTRY

281

Volume Editors V. Balzani · S. Campagna

Photochemistry and Photophysics of Coordination Compounds II

 Springer

281

Topics in Current Chemistry

Editorial Board:

**V. Balzani · A. de Meijere · K. N. Houk · H. Kessler · J.-M. Lehn
S. V. Ley · S. L. Schreiber · J. Thiem · B. M. Trost · F. Vögtle
H. Yamamoto**

Topics in Current Chemistry

Recently Published and Forthcoming Volumes

Photochemistry and Photophysics of Coordination Compounds II

Volume Editors: Balzani, V., Campagna, S.
Vol. 281, 2007

Photochemistry and Photophysics of Coordination Compounds I

Volume Editors: Balzani, V., Campagna, S.
Vol. 280, 2007

Metal Catalyzed Reductive C–C Bond Formation

A Departure from Preformed Organometallic Reagents
Volume Editor: Krische, M. J.
Vol. 279, 2007

Combinatorial Chemistry on Solid Supports

Volume Editor: Bräse, S.
Vol. 278, 2007

Creative Chemical Sensor Systems

Volume Editor: Schrader, T.
Vol. 277, 2007

In situ NMR Methods in Catalysis

Volume Editors: Bargon, J., Kuhn, L. T.
Vol. 276, 2007

Sulfur-Mediated Rearrangements II

Volume Editor: Schaumann, E.
Vol. 275, 2007

Sulfur-Mediated Rearrangements I

Volume Editor: Schaumann, E.
Vol. 274, 2007

Bioactive Conformation II

Volume Editor: Peters, T.
Vol. 273, 2007

Bioactive Conformation I

Volume Editor: Peters, T.
Vol. 272, 2007

Biominerization II

Mineralization Using Synthetic Polymers and Templates
Volume Editor: Naka, K.
Vol. 271, 2007

Biominerization I

Crystallization and Self-Organization Process
Volume Editor: Naka, K.
Vol. 270, 2007

Novel Optical Resolution Technologies

Volume Editors:
Sakai, K., Hirayama, N., Tamura, R.
Vol. 269, 2007

Atomistic Approaches in Modern Biology

From Quantum Chemistry to Molecular Simulations
Volume Editor: Reiher, M.
Vol. 268, 2006

Glycopeptides and Glycoproteins

Synthesis, Structure, and Application
Volume Editor: Wittmann, V.
Vol. 267, 2006

Microwave Methods in Organic Synthesis

Volume Editors: Larhed, M., Olofsson, K.
Vol. 266, 2006

Supramolecular Chirality

Volume Editors: Crego-Calama, M., Reinhoudt, D. N.
Vol. 265, 2006

Photochemistry and Photophysics of Coordination Compounds II

Volume Editors: Vincenzo Balzani · Sebastiano Campagna

With contributions by

A. Barbieri · F. Barigelletti · E. C.-C. Cheng · L. Flamigni
T. Gunnlaugsson · R. A. Kirgan · D. Kumaresan · J. P. Leonard
C. B. Nolan · D. P. Rillema · C. Sabatini · R. H. Schmehl
K. Shankar · F. Stomeo · B. P. Sullivan · S. Vaidya · B. Ventura
J. A. G. Williams · V. W.-W. Yam

The series *Topics in Current Chemistry* presents critical reviews of the present and future trends in modern chemical research. The scope of coverage includes all areas of chemical science including the interfaces with related disciplines such as biology, medicine and materials science. The goal of each thematic volume is to give the nonspecialist reader, whether at the university or in industry, a comprehensive overview of an area where new insights are emerging that are of interest to a larger scientific audience.

As a rule, contributions are specially commissioned. The editors and publishers will, however, always be pleased to receive suggestions and supplementary information. Papers are accepted for *Topics in Current Chemistry* in English.

In references *Topics in Current Chemistry* is abbreviated Top Curr Chem and is cited as a journal.

Visit the TCC content at springerlink.com

ISSN 0340-1022

ISBN 978-3-540-73348-5 Springer Berlin Heidelberg New York

DOI 10.1007/978-3-540-73349-2

This work is subject to copyright. All rights are reserved, whether the whole or part of the material is concerned, specifically the rights of translation, reprinting, reuse of illustrations, recitation, broadcasting, reproduction on microfilm or in any other way, and storage in data banks. Duplication of this publication or parts thereof is permitted only under the provisions of the German Copyright Law of September 9, 1965, in its current version, and permission for use must always be obtained from Springer. Violations are liable for prosecution under the German Copyright Law.

Springer is a part of Springer Science+Business Media

springer.com

© Springer-Verlag Berlin Heidelberg 2007

The use of registered names, trademarks, etc. in this publication does not imply, even in the absence of a specific statement, that such names are exempt from the relevant protective laws and regulations and therefore free for general use.

Cover design: WMXDesign GmbH, Heidelberg

Typesetting and Production: LE-TeX Jelonek, Schmidt & Vöckler GbR, Leipzig

Printed on acid-free paper 02/3180 YL - 5 4 3 2 1 0

Volume Editors

Prof. Vincenzo Balzani

Dipartimento di Chimica "G. Ciamician"
Università di Bologna
Via Selmi 2
40126 Bologna
Italy
vincenzo.balzani@unibo.it

Prof. Sebastiano Campagna

Dipartimento di Chimica Inorganica
Chimica Analitica e Chimica Fisica
University of Messina
Via Sperone 31
98166 Vill. S. Agata, Messina
Italy
campagna@unime.it

Editorial Board

Prof. Vincenzo Balzani

Dipartimento di Chimica „G. Ciamician“
University of Bologna
via Selmi 2
40126 Bologna, Italy
vincenzo.balzani@unibo.it

Prof. Jean-Marie Lehn

ISIS
8, allée Gaspard Monge
BP 70028
67083 Strasbourg Cedex, France
lehn@isis.u-strasbg.fr

Prof. Dr. Armin de Meijere

Institut für Organische Chemie
der Georg-August-Universität
Tammanstr. 2
37077 Göttingen, Germany
ameijer1@uni-goettingen.de

Prof. Steven V. Ley

University Chemical Laboratory
Lensfield Road
Cambridge CB2 1EW
Great Britain
Svl1000@cus.cam.ac.uk

Prof. Dr. Kendall N. Houk

University of California
Department of Chemistry and
Biochemistry
405 Hilgard Avenue
Los Angeles, CA 90024-1589
USA
houk@chem.ucla.edu

Prof. Stuart L. Schreiber

Chemical Laboratories
Harvard University
12 Oxford Street
Cambridge, MA 02138-2902
USA
sls@slsiris.harvard.edu

Prof. Dr. Horst Kessler

Institut für Organische Chemie
TU München
Lichtenbergstraße 4
86747 Garching, Germany
kessler@ch.tum.de

Prof. Dr. Joachim Thiem

Institut für Organische Chemie
Universität Hamburg
Martin-Luther-King-Platz 6
20146 Hamburg, Germany
thiem@chemie.uni-hamburg.de

Prof. Barry M. Trost

Department of Chemistry
Stanford University
Stanford, CA 94305-5080
USA
bmtrost@leland.stanford.edu

Prof. Dr. Hisashi Yamamoto

Department of Chemistry
The University of Chicago
5735 South Ellis Avenue
Chicago, IL 60637
USA
yamamoto@uchicago.edu

Prof. Dr. F. Vögtle

Kekulé-Institut für Organische Chemie
und Biochemie
der Universität Bonn
Gerhard-Domagk-Str. 1
53121 Bonn, Germany
voegtle@uni-bonn.de

Topics in Current Chemistry Also Available Electronically

For all customers who have a standing order to Topics in Current Chemistry, we offer the electronic version via SpringerLink free of charge. Please contact your librarian who can receive a password or free access to the full articles by registering at:

springerlink.com

If you do not have a subscription, you can still view the tables of contents of the volumes and the abstract of each article by going to the SpringerLink Homepage, clicking on “Browse by Online Libraries”, then “Chemical Sciences”, and finally choose Topics in Current Chemistry.

You will find information about the

- Editorial Board
- Aims and Scope
- Instructions for Authors
- Sample Contribution

at springer.com using the search function.

Preface

Photochemistry (a term that broadly speaking includes photophysics) is a branch of modern science that deals with the interaction of light with matter and lies at the crossroads of chemistry, physics, and biology. However, before being a branch of modern science, photochemistry was (and still is today), an extremely important natural phenomenon. When God said: "Let there be light", photochemistry began to operate, helping God to create the world as we now know it. It is likely that photochemistry was the spark for the origin of life on Earth and played a fundamental role in the evolution of life. Through the photosynthetic process that takes place in green plants, photochemistry is responsible for the maintenance of all living organisms. In the geological past photochemistry caused the accumulation of the deposits of coal, oil, and natural gas that we now use as fuels. Photochemistry is involved in the control of ozone in the stratosphere and in a great number of environmental processes that occur in the atmosphere, in the sea, and on the soil. Photochemistry is the essence of the process of vision and causes a variety of behavioral responses in living organisms.

Photochemistry as a science is quite young; we only need to go back less than one century to find its early pioneer [1]. The concept of coordination compound is also relatively young; it was established in 1892, when Alfred Werner conceived his theory of metal complexes [2]. Since then, the terms coordination compound and metal complex have been used as synonyms, even if in the last 30 years, coordination chemistry has extended its scope to the binding of all kinds of substrates [3, 4].

The photosensitivity of metal complexes has been recognized for a long time, but the photochemistry and photophysics of coordination compounds as a science only emerged in the second half of the last century. The first attempt to systematize the photochemical reactions of coordination compounds was carried out in an exhaustive monograph published in 1970 [5], followed by an authoritative multi-authored volume in 1975 [6]. These two books gained the attention of the scientific community and certainly helped several inorganic and physical chemists to enter the field and to enrich and diversify their research activities. Interestingly, 1974 marked the beginning of the series of International Symposia on the Photochemistry and Photophysics of Coordi-

nation Compounds. The venue of the 17th symposium of this series is Dublin and will be held in June 2007.

Up until about 1975, most activity was focused on intramolecular photochemical reactions. Subsequently, due partly also to the more diffuse availability of flash techniques, the interest of several groups moved to investigations of luminescence and bimolecular energy and electron transfer processes. In the last decade of the past century, with the development of supramolecular chemistry, it was clear that photochemistry would play a very important role in the achievement of valuable functions, such as charge separation, energy migration and conformational changes [7], related to applications spanning from solar energy conversion to signal processing and molecular machines [8, 9]. In the last few years, an increasing number of scientists have become involved in these fields. Because of their unique ground and excited state properties, metal complexes have become invaluable components of molecular devices and machines exploiting light (often sunlight) to perform useful functions [8, 9, 10]. The photochemistry of coordination compounds can also contribute to solving the energy crisis by converting sunlight into electricity or fuel [11]. In the meantime, the basic knowledge of the excited state properties of coordination compounds of several metal ions has increased considerably. However, this has resulted in an unavoidable loss of general knowledge and an increase in specialization. Currently, all scientists working in the field of the photochemistry and photophysics of coordination compounds have their own preferred metal. There is, therefore, an urgent need to spread the most recent developments in the field among the photochemical community. To write an exhaustive monograph like [5], however, would now be an impossible enterprise. For this reason, we decided to ask experts to write separate chapters, each one dealing with a specific metal whose complexes are currently at the frontier of research. It has been a delight as well as a privilege to work with an outstanding group of contributing authors and we thank them for all their efforts. We would also like to thank all the members of our research groups for their support.

Bologna and Messina, March 2007

Vincenzo Balzani
Sebastiano Campagna

References

1. Ciamician G (1912) *Science* 36:385
2. Werner A (1893) *Zeit Anorg Chem* 3:267
3. Lehn J-M (1992) From coordination chemistry to supramolecular chemistry. In: Williams AF, Floriani C, Merbach AE (eds) *Perspectives in coordination chemistry*. VCH, Weinheim, p. 447
4. Balzani V, Credi A, Venturi M (1998) *Coord Chem Rev* 171:3
5. Balzani V, Carassiti V (1970) *Photochemistry of Coordination Compound*. Academic Press, London

6. Adamson AW, Fleischauer PD (eds) (1975) Concepts in inorganic photochemistry. Wiley-Interscience, New York
7. Balzani V, Scandola F (1991) Supramolecular photochemistry. Horwood, Chichester
8. Balzani V, Credi A, Venturi M (2003) Molecular devices and machines. Wiley-VCH, Weinheim
9. Kelly TR (ed) (2005) Molecular machines, Top Curr Chem 262
10. Kay EU, Leigh DA, Zerbetto F (2007) Angew Chem Int Ed 46:72
11. Armaroli N, Balzani V (2007) Angew Chem Int Ed 46:52

Contents

Photochemistry and Photophysics of Coordination Compounds:

Lanthanides

J. P. Leonard · C. B. Nolan · F. Stomeo · T. Gunnlaugsson 1

Photochemistry and Photophysics of Coordination Compounds:

Rhenium

R. A. Kirgan · B. P. Sullivan · D. P. Rillema 45

Photochemistry and Photophysics of Coordination Compounds:

Osmium

D. Kumaresan · K. Shankar · S. Vaidya · R. H. Schmehl 101

Photochemistry and Photophysics of Coordination Compounds:

Iridium

L. Flamigni · A. Barbieri · C. Sabatini · B. Ventura · F. Barigelletti 143

Photochemistry and Photophysics of Coordination Compounds:

Platinum

J. A. G. Williams 205

Photochemistry and Photophysics of Coordination Compounds:

Gold

V. W.-W. Yam · E. C.-C. Cheng 269

Author Index Volumes 251–281 311

Subject Index 325

Contents of Volume 280

Photochemistry and Photophysics of Coordination Compounds I

Volume Editors: Balzani, V., Campagna, S.

ISBN: 978-3-540-73346-1

Photochemistry and Photophysics of Coordination Compounds: Overview and General Concepts

V. Balzani · G. Bergamini · S. Campagna · F. Puntoriero

Photochemistry and Photophysics of Coordination Compounds: Chromium

N. A. P. Kane-Maguire

Photochemistry and Photophysics of Coordination Compounds: Copper

N. Armaroli · G. Accorsi · F. Cardinali · A. Listorti

Photochemistry and Photophysics of Coordination Compounds: Ruthenium

S. Campagna · F. Puntoriero · F. Nastasi · G. Bergamini · V. Balzani

Photochemistry and Photophysics of Coordination Compounds: Rhodium

M. T. Indelli · C. Chiorboli · F. Scandola

Photochemistry and Photophysics of Coordination Compounds: Lanthanides

Joseph P. Leonard · Claire B. Nolan · Floriana Stomeo ·
Thorfinnur Gunnlaugsson (✉)

School of Chemistry, Centre for Synthesis and Chemical Biology,
Trinity College Dublin, Dublin 2, Ireland
gunnlaut@tcd.ie

1	Introduction	2
2	Luminescent Lanthanide Complexes	2
2.1	Physical Properties of Lanthanides	2
2.2	The Sensitisation Process	5
2.2.1	Chromophore Excitation	5
2.2.2	Triplet-Mediated Energy Transfer	6
2.3	Designing Luminescent Lanthanide Complexes	7
2.3.1	Choice of Lanthanide	8
2.3.2	Choice of Antenna	8
2.3.3	Degree of Coordination and Solvent Effects	9
2.4	Ligands Employed for Lanthanide Complexes	10
2.4.1	Podands	11
2.4.2	Cryptates	12
2.4.3	Calixarenes	13
2.4.4	Macrocyclic and Bicyclic Ligands	14
2.5	Modulating the Luminescence of a Lanthanide Complex	15
3	Lanthanide Luminescent Sensors and Switches	17
3.1	Sensors Based on Method A	18
3.2	Sensors Based on Method B	20
3.3	Sensors Based on Methods C and D	27
4	Simple Self-Assemblies Using <i>f-d</i> Mixed Metal Ions	34
5	Conclusion	38
	References	38

Abstract This article is concerned with the recent advantages in the design of lanthanide complexes as luminescent devices such as sensors and switches. Herein the fundamental concepts of how to produce lanthanide complexes that can have their luminescence properties manipulated by external sources is first discussed, followed by a review of selected examples from the recent literature.

Keywords Lanthanide luminescence · Luminescent devices · Sensors · Switches · Tb(III) and Eu(III) complexes

1

Introduction

The development of luminescent signalling systems is an active area of research in supramolecular chemistry because of their many possible applications [1–19]. The use of metal-based complexes for *in vivo* applications is well documented and the majority of applications have focused on using such complexes as therapeutic drugs, biological probes and assays [20–32], as they can overcome the problematic issue of autofluorescence [33–35]. This chapter will focus on some examples of the use of lanthanide complexes as luminescent signalling systems. This is a fast growing area, as the lanthanides have become popular for use in biological applications because of their unique photophysical properties such as their relatively long-lived luminescence [36–38]. The majority of research in this area has concentrated on lanthanide ions that emit in the visible and near infrared spectrum, which is advantageous for *in vivo* applications, and the main part of the discussion herein focuses on these ions [39]. We will then focus our attention towards the development of higher order lanthanide complexes, made by the use of $f-f$ and mixed $f-d$ ions. However, this review starts with a short summary of the physical properties of the lanthanide ions and in particular their photophysical properties.

2

Luminescent Lanthanide Complexes

2.1

Physical Properties of Lanthanides

The unique magnetic and photophysical properties of the metals in the lanthanide series have attracted great interest over the past few years, due to their potential in medical diagnostics [40, 41], optical imaging [42, 43] and high technological applications [44, 45]. The importance of lanthanides for magnetic and optical materials has long drawn attention to their physical properties and solid-state chemistry, which have both been extensively studied [46]. More recently the development of contrast agents for medical magnetic resonance imaging (MRI) and luminescent chemosensors for optical imaging of cells has shifted the focus towards their coordination chemistry in solution [47, 48]. Moreover, anions can also bind directly to lanthanide ions, or more importantly, as part of their coordination environment, such as when coordinative unsaturated ligands are used. Hence, the sensing of anion by such coordination is possible (exchange of coordination ligands).

Despite their name, “rare earth elements”, lanthanides are in fact not especially rare: each is more common in the earth’s crust than silver, gold or platinum. They possess characteristic $4f$ open-shell configurations and exhibit

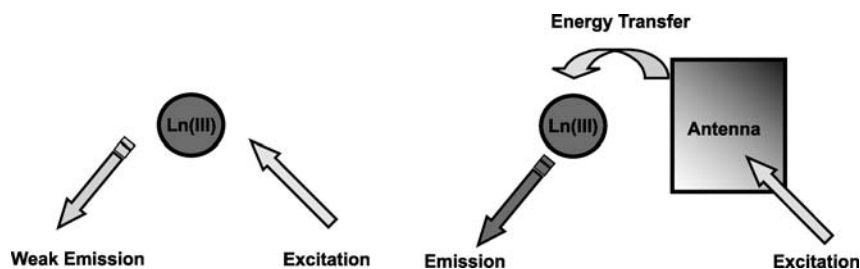
a close chemical resemblance across the periodic series due to the small and regular decrease in their ionic radii. This decrease in radii is known as the lanthanide contraction [47, 48]. Their most stable oxidation state is + 3, particularly in water, with a $[\text{Xe}]4f^n$ configuration. The lanthanide ions possess relatively high charge densities and have a strong electrostatic nature in their bonding, as the ions are polarising and hard Lewis acids. They can coordinate to a variety of ligands with different coordination numbers, most typically eight to ten. The hard Lewis acidity of the lanthanide ions results into a specific preference towards ligands incorporating atoms that can act as hard Lewis bases or can be easily polarised. Therefore, combinations of amines and carboxylic groups are commonly used in lanthanide complexation [42, 43]. Indeed, one of the most popular ligands in the complexation of lanthanides is 1,4,7,10-tetrakis(carboxymethyl)-1,4,7,10-tetraazacyclododecane (commonly known as DOTA). Its popularity is largely due to its use as a magnetic resonance contrast agent with gadolinium [39, 49–51], where the ion coordinates to the four nitrogens of the cyclen ring and the four carboxylates of the pendant arms, giving rise to an octa-coordination environment.

The role played by the lanthanide ions in many supramolecular systems is mostly based on their optical features and coordination requirements. Lanthanides present special spectroscopic properties due to the shielding of the $4f$ orbitals, with forbidden intra-configuration $f-f$ electronic transitions resulting in very low extinction coefficients (ϵ typically $0.1 \text{ mol}^{-1} \text{ dm}^3 \text{ cm}^{-1}$) [52] and characteristic narrow line-like emission bands, mostly in the visible and near infrared ranges. Most of the lanthanide ions are luminescent, some more than others. Their emission depends on how efficiently their excited state(s) can be populated and their non-radiative deactivation pathways minimised. The main advantage is that the $f-f$ electronic transitions are easily recognisable for they are almost independent of the chemical environment of the ion. They can be either fluorescent (e.g. Pr(III), Nd(III), Ho(III), Er(III) and Yb(III)) or phosphorescent (e.g. orange Sm(III), red Eu(III), Gd(III) which emits in the UV, green Tb(III), yellow Dy(III) and blue Tm(III)), following the IUPAC rules regarding molecular luminescence spectroscopy [53]. According to these rules, the term “fluorescence” refers to processes that occur without change in spin, typically $S_1 \rightarrow S_0$ or $\text{Yb}(^2F_{5/2} \rightarrow ^2F_{7/2})$ transitions. The term “phosphorescence” refers to transitions involving a change in spin, typically $T_1 \rightarrow S_0$ or $\text{Eu}(^5D_4 \rightarrow ^7F_7)$ transitions [47, 48]. Two ions, La(III) and Lu(III), have no $f-f$ transitions and are therefore not luminescent.

The photophysical properties of Eu(III) and Tb(III) have generated the most interest to date of all the lanthanides because their emissions occur in the visible region. For example, Eu(III) emits in the red (550–750 nm) while Tb(III) emits in the green (450–650 nm). In terms of energy gap, Eu(III) ($\Delta E = 12\,300 \text{ cm}^{-1}$, $^5D_0 \rightarrow ^7F_6$), Gd(III) ($\Delta E = 32\,200 \text{ cm}^{-1}$, $^6P_{7/2} \rightarrow ^8S_{7/2}$) and Tb(III) ($\Delta E = 14\,800 \text{ cm}^{-1}$, $^5D_4 \rightarrow ^7F_0$) are the best ions for an efficient population of their excited states. However, and as stated above, while Eu(III)

and Tb(III) emit in the visible region of the spectrum, Gd(III) emits in the UV. This makes the latter unsuitable as a luminescent probe for bio-analysis due to the absorption and emission interference (light scattering, etc.) from the organic part of the complexing molecule. The sizable energy gap displayed by Eu(III) and Tb(III) explains why luminescent probes containing these ions have been so popular during the last decade. Besides Sm(III) ($\Delta E = 7400 \text{ cm}^{-1}$, $^4G_{5/2} \rightarrow ^6F_{11/2}$) and Dy(III) ($\Delta E = 7850 \text{ cm}^{-1}$, $^4F_{9/2} \rightarrow ^6F_{3/2}$), which have been employed in dual luminescent time-resolved immunoassays [54–56], the other lanthanide ions have not found similar applications, due to their very low quantum yield in aqueous solution. $^5\text{Pr(III)}$ emits both in the visible and near-infrared (NIR) ranges [57] and is often a component of solid state optical materials. This is due to its blue up-conversion, that is the blue emission from 3P_0 upon two- or three-photon pumping into the 1G_4 or 1D_2 states [58]. Thulium is a blue emitter from its 3P_0 , 1D_2 and 1G_4 levels and as such has found use in electroluminescent devices [44, 45]; it is known to be one of the first ions having shown up-conversion [58]. The ions Nd(III), Dy(III), Ho(III) and Er(III) also display up-conversion processes [47, 48]. Moreover, Nd(III), Ho(III), Er(III) and Yb(III) have stirred particular interest in the design of lasers (especially Nd(III)) and telecommunication devices owing to their ability to emit in the NIR part of the electromagnetic spectrum [59]. In addition, Nd(III), Er(III) and Yb(III) have been recently employed in the development of luminescent probes for time-resolved imaging of biological tissues, as they are able to efficiently transmit light in the NIR spectral range [60–62].

As explained above, the lanthanide $f-f$ transitions (electric dipole transitions) are “Laporte-forbidden”, therefore, the generation of fluorescence from the lanthanide ion can be difficult. Direct excitation of the lanthanide ion can be achieved, but this only becomes practical with the use of lasers or at high ion concentrations. However, such inherent disadvantages can be overcome by using sensitisation techniques [63–66] (Scheme 1). This involves using indirect excitation of the lanthanide ion with a sensitising chromophore (often termed as an antenna) [67, 68] usually through an intramolecular energy transfer process [64–66, 69, 70]. The antenna needs to be in close prox-



Scheme 1

imity to the lanthanide ion, which is achieved through coordination of the lanthanide to a ligand containing an antenna. This process will now be discussed.

2.2

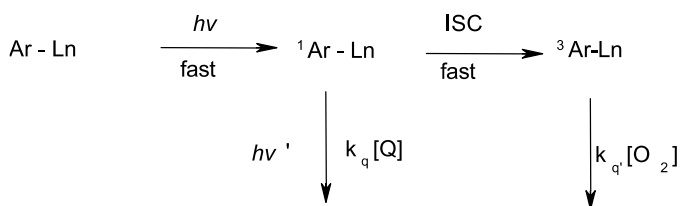
The Sensitisation Process

The sensitisation process associated with producing lanthanide luminescence consists of a number of steps, including excitation of the antenna and energy transfer to the lanthanide. The details of this process and the considerations required in designing complexes working on this principle are discussed in the following sections.

2.2.1

Chromophore Excitation

Aromatic systems are commonly used as antennae in the sensitisation process although recently, the use of transition metal complexes have also been shown to be useful as visible and near infra-red emitting lanthanide devices [71, 72]. Using organic compounds as antenna, lanthanide luminescence begins with the excitation of the antenna chromophore (sensitiser, denoted Ar in Scheme 2) from the ground state, S_0 , (Ar-Ln), to the singlet-excited state, S_1 , (1 Ar-Ln). Following the formation of this excited state a number of processes are possible, such as classical non-radiative decay of the 1 Ar-Ln (e.g. internal conversion, not shown in Scheme 2). But more importantly, deactivation to the ground state (Ar-Ln), with an associated ligand fluorescence emission ($h\nu'$), can occur. It is also possible for this excited state to be quenched ($k_q[Q]$) by other means such as electron transfer (e.g. photoinduced electron transfer). A triplet-excited state, T_1 , (3 Ar-Ln) can also be formed via intersystem crossing (ISC). Singlet and triplet excited states share a common geometry where their potential curves intersect. However, intersystem crossing from an S_1 to a T_1 is a spin-forbidden process. Nevertheless, singlet-triplet transitions may occur in the presence of spin-orbit coupling, which is largely promoted by the presence of heavy atoms (e.g. lanthanides) which makes this process more efficient [73]. This triplet 3 Ar-Ln state can be



Scheme 2 Initial steps of sensitisation process – the antenna excitation

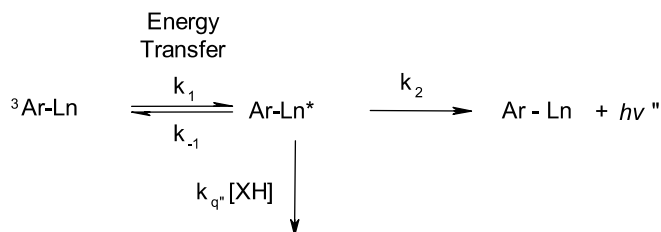
lost by quenching from oxygen, ($k_q'[\text{O}_2]$). It is also possible to transfer the excited state of the antenna ($^3\text{Ar-Ln}$) to the lanthanide excited state ($^5\text{D}_4$ and $^5\text{D}_0$ for Tb(III) and Eu(III), respectively) by way of an energy transfer process, resulting in Ar-Ln^* [74].

The lanthanide(III) ions have the advantage of possessing long-lived excited state lifetimes, provided that deactivations by non-radiative pathways as discussed above are minimised (see also Sect. 2.3.1). The lifetime of emission from the excited state of the lanthanide ions falls in the range of microseconds (e.g. Yb, Nd) to sub-milliseconds (e.g. Eu and Tb) [75]. Such long-lived emissions have led to numerous applications of lanthanide-based systems as luminescent probes and sensors [42, 43, 46, 75]. This is due to the possibility of time-resolved detection, which allows a relatively easy discrimination between the desired luminescent signal and the auto-fluorescence of the background. Such methods are based on a delay set between the excitation of the probe and the measurement of the lanthanide luminescence, so that the shorter-lived (nanosecond time frame) fluorescence and light scattering of the biological background (auto-fluorescence) decay to negligible levels [52]. This provides good signal-to-noise ratio, which enables more accurate determination of the analyte in real time.

2.2.2

Triplet-Mediated Energy Transfer

The process by which triplet-mediated energy transfer occurs [$^3\text{Ar-Ln} \leftrightarrow \text{Ar-Ln}^*$] has two proposed mechanisms. Firstly, Dexter energy transfer involves an exchange interaction requiring a mutual electronic exchange between the antenna and the metal-centre acceptor [76]. Energy transfer occurs through the overlapping orbital of the antenna and the metal ion and hence, requires physical contact between the two components. Secondly, Förster energy transfer [77, 78] involves a columbic interaction that arises when the dipole of the excited antenna induces a dipole in the acceptor (lanthanide metal centre). This is a “through space” process that does not require physical contact between the sensitiser and the acceptor, the Ln(III) ion. The rate of energy transfer (k_1) via the Förster mechanism is distance-dependent with dependence proportional to r^{-6} , where r is the intramolecular distance between the sensitising chromophore and the metal centres. The formation of the lanthanide excited state (Ar-Ln^*) is a reversible process (Scheme 3) that can result in the reformation of the antenna triplet excited state ($^3\text{Ar-Ln}$). It is also possible to quench this lanthanide excited state via vibrational quenching from energy-matched oscillators, ($k_q'[\text{XH}]$) such as O – H, N – H and C – H (see later). In situations where the energy transfer is efficient in forming Ar-Ln^* and the quenching conditions are minimised, a lanthanide emission can occur. The resulting lanthanide emission involves transitions from this state. These transitions are $^5\text{D}_4 \rightarrow ^7\text{F}_j$. The most common of these transitions ob-



Scheme 3 Final steps of sensitisation process – lanthanide luminescence

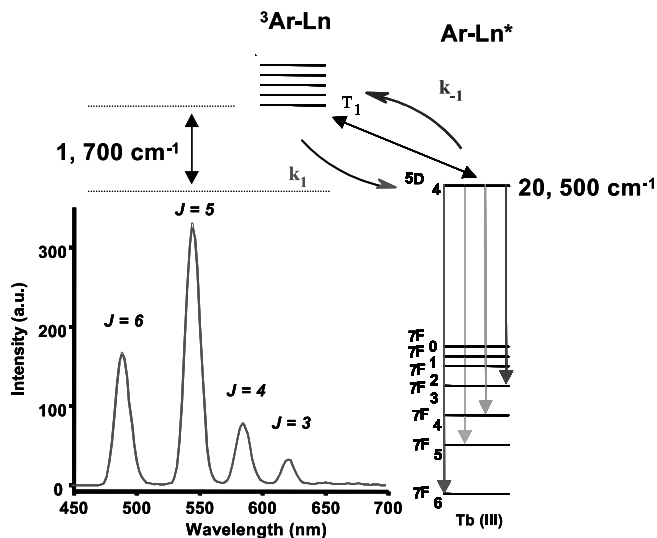


Fig. 1 Illustration of energy transfer to the lanthanide ion in sensitisation process for Tb(III), from triplet state of the antenna and the corresponding emission spectra for Tb(III)

served are those of $J = 6, 5, 4$ and 3 , whereas for Eu(III) (${}^5D_0 - {}^7F_J$) these transitions are observed at $J = 0, 1, 2, 3$ and 4 . Some of these emission bands are sensitive to the local coordination environment, which means that changes in their band structure, intensity and lifetime can be employed for analysis of their coordination environment.

2.3

Designing Luminescent Lanthanide Complexes

A number of factors must be considered during the designing of luminescent lanthanide complexes, some of the most important factors will now be discussed. These factors include the nature of the lanthanide ion, choice of antenna, degree of coordination, solvent, etc.

2.3.1

Choice of Lanthanide

The choice of the lanthanide ion is important and needs to be considered in terms of their emission properties. For some of the lanthanide ions the energy gap is quite large and the emission wavelength appears in the ultra violet region, e.g. at ca. 300 nm as in the case of Gd(III). However, for others, the emission occurs at long wavelengths due to smaller energies gaps, e.g. Nd(III) and Yb(III), both of which emit in the NIR. The lanthanides also usually possess relatively long-lived excited states, which unfortunately can be quenched with appropriate molecules such as those rich in O–H and N–H functional groups [79–83]. This occurs through a non-radiative quenching process, which is one of the most important in determining the luminescence quantum yield. This non-radiative deactivation usually occurs through energy transfer to vibrational modes that match the energy of the excited state of the lanthanide ion. The high frequency vibrations of O–H, N–H, and even C–H oscillators, strongly dissipate the energy of the lanthanide excited state resulting in quenching of the lanthanide luminescence [85].

The lower the excited state energy of the lanthanide earth ion, the more efficient the energy dissipation process. Also, the direct coordination of water and other solvent molecules to the lanthanide centre has a large effect on the deactivation of the excited state through non-radiative paths, and on the efficiency and lifetime of the emission process. In order to minimise vibration-induced deactivation processes, a rigid metal-ion environment is needed that is free of high energy vibrations and that can protect the Ln(III) ion from solvent coordination. Macrocyclic ligands often satisfy the criteria of high coordination and rigidity, and as such are commonly employed in lanthanide coordination chemistry. Because of this, most of the examples discussed herein will focus on examples where ligands such as macrocycles are used. We refer to some recent excellent reviews for those interested in the use of linear polydentate ligands [85].

2.3.2

Choice of Antenna

The triplet energy of the sensitising chromophore is quite an important consideration when choosing an antenna [69, 70]. The lowest excited states of Eu(III) and Tb(III) are $17\,200\text{ cm}^{-1}$ and $20\,500\text{ cm}^{-1}$, respectively, which restrict the choice of antenna. The energy of the triplet excited state needs to be at least 1700 cm^{-1} above the excited state of the lanthanide ion for efficient population to the lanthanide excited state, Ar-Ln*, to prevent a thermally initiated back energy-transfer process, from Ar-Ln* to $^3\text{Ar-Ln}$ (Scheme 3). Hence, if this energy gap is less than 1500 cm^{-1} , such thermally activated back-energy transfer competes to repopulate the triplet state of the antenna. Hence, a balance needs

to be reached between these opposing factors. For this reason the choice of chromophore that can be used for sensitising Eu(III) and Tb(III) is limited. This is further complicated because sometimes suitable ligands can still lead to non-luminescent complexes due to additional deactivation processes such as ligand-to-metal charge transfer (LMCT), examples of which will be discussed. A final consideration when choosing an antenna is the excitation wavelength. To be of practical use, the excitation wavelength should be above ca. 330 nm, negating the need for expensive quartz optics that would significantly increase the costs for medical diagnostic applications. As required by both the Förster and the Dexter mechanisms (but especially by the latter), the lanthanide centre must be in close proximity to the antenna for efficient population of the excited state. A variety of ligands bearing aromatic sensitising chromophores has been devised for such sensitisation, including bipyridines [86], terpyridines [87], substituted phenyls [88], and naphthyl groups [89], where these are proximally positioned to the lanthanide ions through coordination.

2.3.3

Degree of Coordination and Solvent Effects

As discussed above, the presence of coordinated and solvent O – H, N – H and C – H oscillators associated with unsaturated complexes has significant implications because non-radiative quenching of the lanthanide excited states can occur through vibrational harmonics of these oscillators. Only the effects of Eu(III) and Tb(III) will be discussed here. In water (or alcoholic solvents), the rate constant for luminescence ($k_{\text{H}_2\text{O}}$) or lifetimes ($\tau_{\text{H}_2\text{O}}$) of the lanthanide excited states are often significantly shorter than the rate constant for luminescence ($k_{\text{D}_2\text{O}}$) or lifetimes ($\tau_{\text{D}_2\text{O}}$) in the deuterated solvent analogues, where such quenching is absent. Formation of lanthanide complexes where the high coordination requirement of the lanthanide ion is fulfilled, negates this deactivation pathway; for example, designing lanthanide complexes that are free from metal-bound water molecules can greatly improve the lifetime and emission intensity of a complex. Measuring the rate of decays of the lanthanide emission in H_2O and D_2O allows the hydration state to be measured and can be used to assess the suitability of a ligand to fully coordinate a lanthanide metal centre. The hydration state (q), the number of metal-bound water molecules of lanthanide complexes, can then be calculated using the equations derived by Horrocks et al. [60, 90, 91] and by Parker et al. [61, 92] to account for quenching from N – H oscillators):

$$[q \pm 0.5] : q^{\text{Eu(III)}} = A[(1/\tau_{\text{H}_2\text{O}} - 1/\tau_{\text{D}_2\text{O}}) - 0.25 - 0.075x] \quad (1)$$

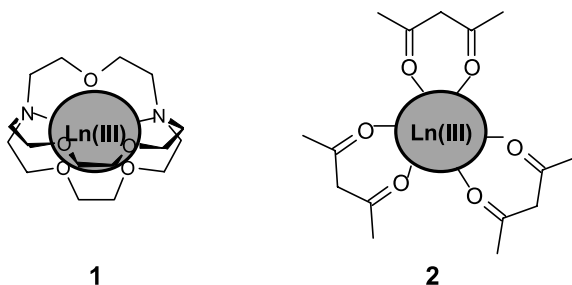
$$[q \pm 0.5] : q^{\text{Tb(III)}} = A[(1/\tau_{\text{H}_2\text{O}} - 1/\tau_{\text{D}_2\text{O}}) - 0.06] , \quad (2)$$

where A is a proportionality constant specific to a given lanthanide ion that mirrors the sensitivity of the ion to quenching from metal-bound waters, and

x is the number of N – H oscillators in the complex. While Eq. 1 takes account for N – H oscillators of amides, Horrocks has recently modified this equation to account for closely located O – H oscillators, or N – H oscillators of amines. This equation is particularly good when dealing with systems with large q -values [90]. In the case of Tb(III) and Eu(III), A is 5.0 ms and 1.2 ms, respectively. For an efficient luminescent device, the number of metal-bound excitation deactivating molecules should be kept small to prevent this type of quenching.

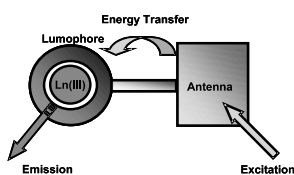
2.4 Ligands Employed for Lanthanide Complexes

The formation of luminescent lanthanide complexes relies on a number of factors. The choice of coordinating ligand and the method by which the antenna chromophore is attached to it, as well as the physical properties of the antenna, are important. In order to fully coordinate a lanthanide ion, either a high-level polydentate ligand such as a cryptate **1** or a number of smaller ligands (such as 1,3-diketones, **2**) working in cooperation are required. Both **1** and **2** are two of the simplest coordination complexes possible for lanthanide ions. In both cases there are no antennae present. However, the number of bound solvent molecules is decreased considerably from nine (for lanthanide ions in solution) to one to two for the cryptate and three for the 1,3-diketone complexes.



In both these examples the coordinating groups are either oxygen or nitrogen atoms. Ln(III) ions can be classified as “hard acids” and coordination occurs via ionic bonding interactions, which leads to a strong preference for negatively charged or neutral donor groups possessing large ground state dipole moments. In aqueous solution, donor groups containing neutral oxygen or nitrogen atoms generally bind when present in multidentate ligands (such as podands, crown ethers and cryptates) because water molecules and hydroxide ions are good ligands for lanthanide ions [93–95]. Over the past 20 years a significant amount of research has been carried out into the development of encapsulating ligands for the formation of stable lanthanide complexes and the reader can be directed to excellent reviews [96, 97].

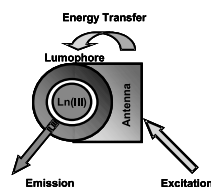
In this review a brief highlight of how an antenna can be incorporated into coordinating ligands to allow for the formation of luminescent complexes is discussed. Scheme 4 shows the most common ligand types, where (method A) the antenna is covalently incorporated to the coordinating ligand but not involved in coordination and (method B) the antenna is incorporated into the coordinating ligand and is involved in the coordinating process directly.



Producing Luminescent lanthanide complexes using antenna

Antenna covalently attached to coordinating ligand

A.



Producing Luminescent lanthanide complexes using antenna

Antenna integrated into coordinating ligand

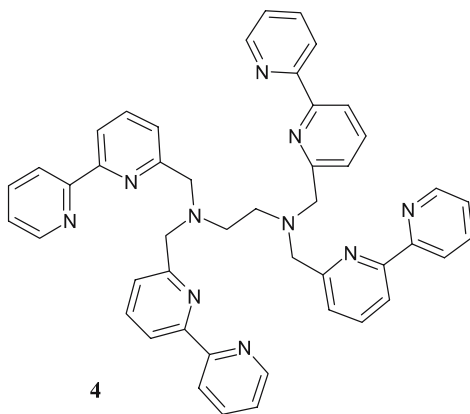
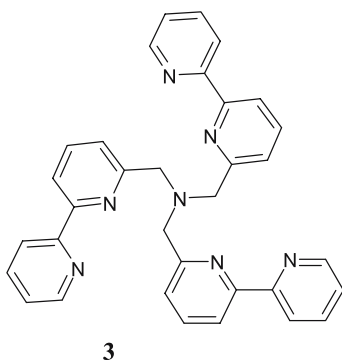
B.

Scheme 4 Two common methods (A and B) of incorporating antenna into coordinating ligands

2.4.1

Podands

There are many examples of “podand-type” ligands [98–100] and the bipyridyl (bpy)-based podand ligands **3** and **4** have been used to form lanthanide complexes. These can be considered as ligands with integrated antenna as shown in Scheme 4. In both examples, the bipyridine moiety is directly incorporated into the coordinating ligand and serves a dual role of coordinating to the metal centre as well as acting as the antenna. The



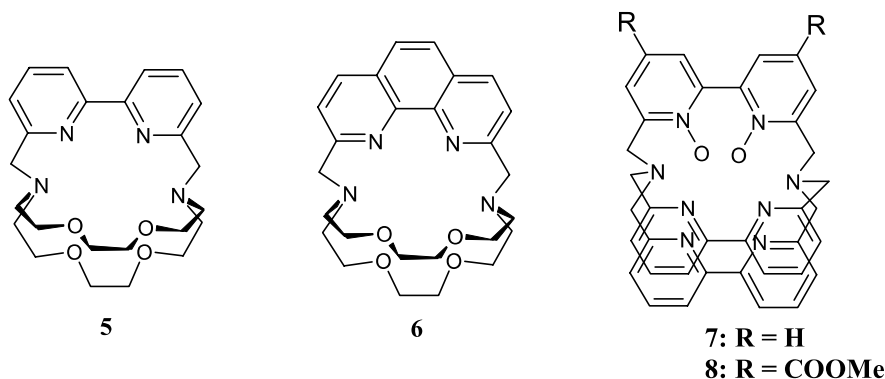
lowest triplet energy of the bpy unit (${}^3\pi\pi^*$) at ca. $23\,000\text{ cm}^{-1}$ is ideal for use as a sensitizer. The Eu(III) emission is produced when the bpy moiety is excited at 300 nm and is assigned to an energy transfer from the coordinated ligand to the metal centre. However, the Eu(III) complexes formed by coordination of the ligands were shown to be unstable in aqueous solution and lifetime studies (q) revealed that two water molecules were bound to Eu-3 with a quantum yield of $\phi = 0.1$. This q value of 2 indicates that all of the nitrogens of the ligand were involved in coordination. The complex, Eu-4 showed a quantum yield (ϕ) of 0.003 in water and 0.07 in methanol. It was observed from the lifetime studies that OH quenching was very efficient and more severe in Eu-4. This suggests that although acyclic systems cannot produce stable complexes they do demonstrate the effectiveness of incorporating antenna into coordinating ligands to produce luminescent complexes. It should be noted that a number of podand-type ligands have been shown to be effective in the formation of Gd(III) complexes [101].

2.4.2

Cryptates

By redesigning the above acyclic podand-type ligand **3** into a cyclic cryptate, the issue of stability can be resolved resulting in kinetically stable complexes (Scheme 4) [102]. The Tb(III) and Eu(III) complexes of cryptate **5** show an increase in lanthanide emission lifetimes of 0.72 ms and 0.41 ms, respectively, upon excitation at 310 nm. Similar results are found with the phenanthroline analogue **6** with Eu(III). A large number of modifications of these cryptates have been reported, all showing enhancements in the lanthanide ion emission [103–106].

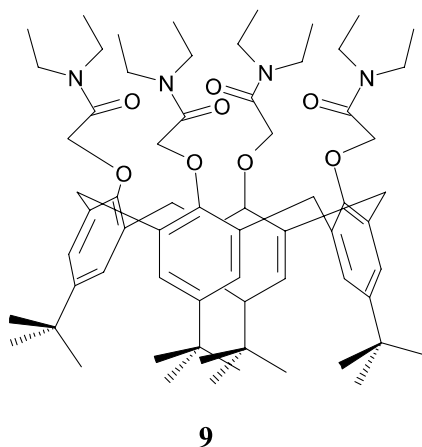
N-Oxide derivatives of similar cryptates [107–111] have also been developed with **7** and **8** shown as examples. An improvement in coordination efficiency was observed from the q values reported. In these examples, the *N*-oxide cryptates were shown to have a higher quantum yield than the

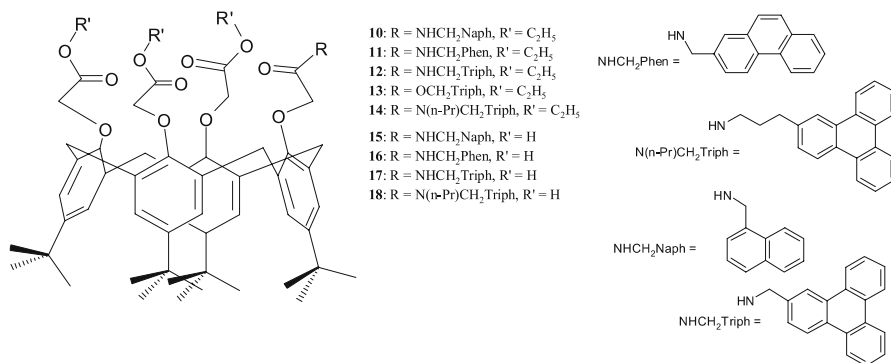


nitrogen analogues. This improvement was attributed to the N – O moiety increasing the efficiency in which the $^3\pi\pi^*$ energy level was populated [112]. These good shielding characteristics and high quantum yields show *N*-oxide cryptates as promising ligands for the formation of excited state in these lanthanide complexes.

2.4.3 Calixarenes

Calixarenes modified on the lower rim with ether, acetate, ketone and amide functional groups have been shown to readily form complexes with ions and neutral molecules [113]. Sabbatini et al. [114] have shown that Tb(III) and Eu(III) complexes of **9**, a calix[4]arene functionalised with *t*-butyl groups on the upper rim and amido groups functionalised on the phenols of the lower rim, are readily formed. In these examples the aromatic residues of the calix[4]arene function as the sensitiser, while the phenoxy and amido oxygens are involved in the coordination of the metal centre. These systems can be considered as integrated systems, as depicted in Scheme 4. The complexes were studied in water and methanol. Both Eu·**9** and Tb·**9** yielded q values of ca. 1. Of the two complexes, the Tb·**9** complex was found to be highly luminescent with a quantum yield of $\phi = 0.2$, compared to $\phi = 0.002$ for Eu·**9**. The high quantum yield of Tb·**9** was due to efficient ligand-to-metal energy transfer and good shielding from solvent deactivation. Like the cryptand examples above, the formation of stable complexes with moderate quantum yields is possible. With further modification of the calixarene ligands on the lower rim many examples of Eu(III) and Tb(III) complexes with varying luminescence properties are possible. Another advantage of using calixarenes is that the phenoxy moieties can be functionalised to have complexes with specific properties for desired applications. For example, the inclusion of sul-





fate groups in the *para* position of a calix[4]arene led to a water-soluble complex [115].

The tris esters, 10–14 and tris acid 15–16 functionalised calix[4]arene ligands were developed [116] where the fourth phenol position was functionalised with a naphthalene, (naph) phenanthrene, (phen) or triphenylene (triph) moiety by way of an amide link, or in the case of 13, by an ester link. Once again the phenoxy oxygens of the calixarene and the ester or acid are involved in the coordination of the metal centre. However, the calixarene aromatic moieties were not utilised as antenna and this function was undertaken by the naph, phen, or triph appendages. These can all be considered as covalently attached antenna coordinating ligands because the antenna is tethered to the coordinating ligand but not involved in the coordination itself (method A in Scheme 4). From studies of the Eu(III) and Tb(III) complexes in methanol, it was found that these complexes were stable and luminescent. The degree of luminescence was found to be similar for all complexes whether neutral or charged. However, these complexes are sensitive to the type of spacer used as the complexes were found to be more luminescent when an ester linkage was used instead of the amide. Calix[4]arene ligands have also been used in the formation of luminescent complexes where they serve merely as a structural scaffold to accommodate the coordinating antenna. The reader is directed to the work of groups such as Ulrich and Ziessel [117] for such examples.

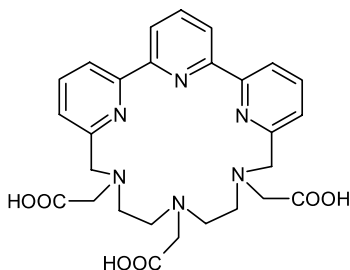
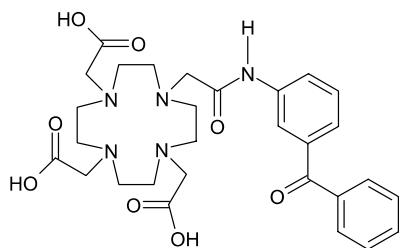
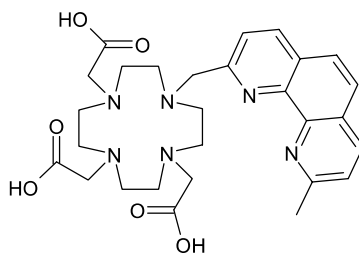
2.4.4

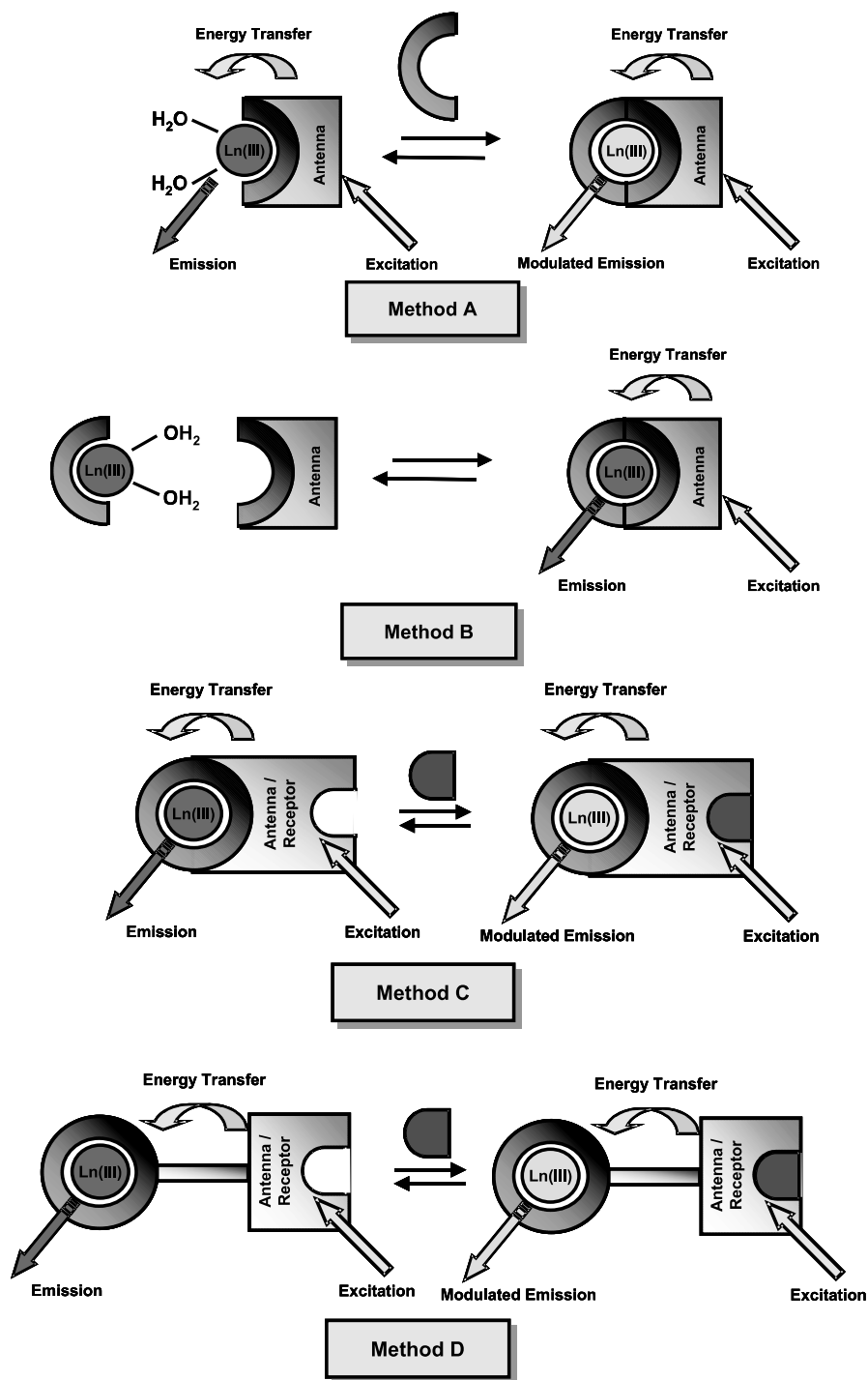
Macrocyclic and Bicyclic Ligands

Many aza-crown macrocyclic ligands [118] have been used to produce stable, well-shielded lanthanide complexes that have good photophysical properties. The aza-crown macrocyclic ligand 19 has a terpyridine moiety incorporated into it to act as a sensitizer. Quantum yields of $\phi = 0.18$ and $\phi = 0.21$ were determined in water for the Eu(III) and Tb(III) complexes respectively. 19 is an

example of an “attached antenna”-type ligand. However, many examples exist of the alternative variety where the sensitiser is covalently attached to the ligand but not coordinating to the metal centre, (Scheme 4). The structure **20** is an example of a cyclen-based ligand functionalised with three carboxylic pendant arms and a benzophenone chromophore attached to the fourth cyclen nitrogen through an amide bridging group based on such a design. This results in the formation of an overall charge-neutral lanthanide complex [119] with quantum yields of $\phi = 0.095$ for Eu·**20** and $\phi = 0.27$ for Tb·**20** when measured in water. By changing the sensitising chromophore to phen as in **21** [120], it was shown that binding occurs through both of the nitrogens of the phen substituent resulting in a nonodentate ligand with optimal shielding of the lanthanide centre. This good shielding ability is explained by the rigidity of the phenanthroline chromophore and its spatial arrangement within the complex. Stability in water and high luminescence efficiencies were seen, as well as an increase in the quantum yields of $\phi = 0.21$ for Eu·**21** as compared to Eu·**20** above.

This brief overview has shown that there are many possibilities when choosing ligands for the design of luminescent lanthanide complexes. From the examples shown it is apparent that the most luminescent of the lanthanide complexes are formed when macrocyclic ligands are used that fully or almost fully coordinate the metal centre. It should also be apparent that there are many examples and options available when it comes to choosing possible antenna within the criteria set out above (Sect. 2.3.2).

**19****20****21**



2.5

Modulating the Luminescence of a Lanthanide Complex

Previously we mentioned how incorporating sensitising chromophores into the lanthanide-coordinating ligand allows the indirect excitation of the lanthanide ion, via intramolecular energy transfer (Schemes 1–4). The efficiency of the sensitisation process depends on many factors such as the structure and the excited state energy of the antenna (E_{S_1} and E_{T_1}), the redox potentials (HOMO/LUMO energies), as well as the rate of ISC from $S_1 \rightarrow T_1$ and various quenching pathways e.g., by electron transfer or MLCT and solvent quenching (Schemes 3–4). Many of these parameters can be manipulated, allowing the lanthanide luminescence emission to be modulated. Scheme 5 shows a number of common methods by which modulation of the emission of a lanthanide complex can be achieved.

Method A involves luminescent complexes that can be modulated by changes in their coordination environment. The complex is composed of an unsaturated coordinating ligand resulting in a complex that contains labile solvent ligands. Displacement of these labile ligands by other coordinating ligands can have an effect on lifetimes and quantum yields as the coordinating ligands may not be able to quench the lanthanide excited state in the same way as solvents such as water.

Method B is similar to the concept described above in method A, except modulation is due to the displacement of solvent molecules by a coordinating group containing an antenna capable of sensitisation.

Method C and **Method D** are again similar to that described above. In each case the antenna is structurally modified to accommodate a receptor allowing for the inclusion of a guest. This guest inclusion results in changes in the antenna properties, such as alterations in the effectiveness of the sensitisation process, the intensity/quantum yield, as well as to the lifetime of the metal-centred luminescence.

3

Lanthanide Luminescent Sensors and Switches

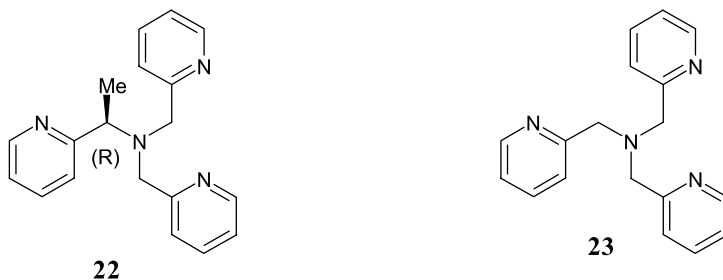
In this section, a number of systems that have been shown to act as sensors and/or switches will be discussed. These systems have been subdivided based on their mode of operation as described in Scheme 5. In the following section these modes of operation, in conjunction with the concept of modulation, will be shown to produce lanthanide luminescent sensors and switches.

◀ **Scheme 5** Illustration of most common methods for modulating lanthanide luminescence

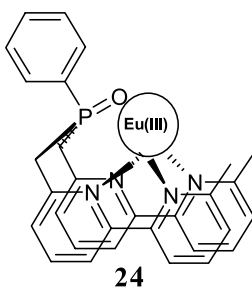
3.1 Sensors Based on Method A

Method A has been successfully applied in anion sensing. As mentioned previously, lanthanide ions can coordinate to anions such as acetate, fluoride, etc., which modulates the lanthanide luminescence. Examples of such systems will now be discussed.

The Eu(III)-based complexes formed using the podand-type ligands **22** and **23**, containing three pyridine moieties, can be modulated by changes in the coordinating ligand environment [121, 122]. In both cases the lanthanide complexes were studied in acetonitrile. The lanthanide luminescence emissions of these complexes were found to be modulated to different degrees when titrated with various anions. Complex Eu·**22** was found to be somewhat selective to NO_3^- over all other anions tested, showing a 4.9-fold increase in emission intensity. The circular dichroism signal of Eu·**22** was observed at 260 nm and was intensified on addition of NO_3^- , indicating that modification to the 3-D arrangement of the pyridines had occurred. When the metal centre was Tb(III), the anion selectivity of Tb·**22** was found to change to Cl^- . This indicated that the nature of the lanthanide ion dramatically effects anion sensing selectivity despite their similar ionic radii. Similar results for anion responsive selectivity have been reported for the achiral complexes Eu·**23** and Tb·**23**, however, the change in emission intensities were significantly lower.



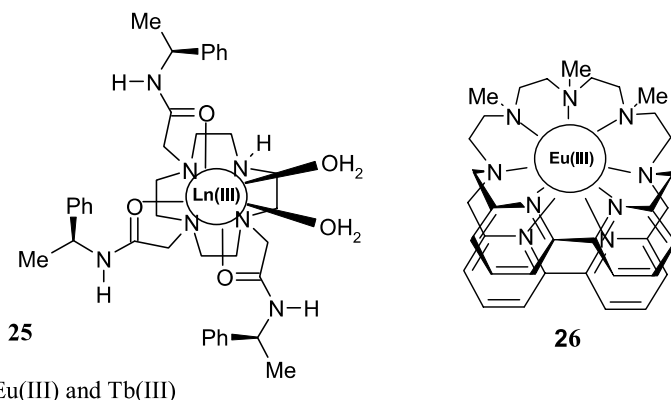
These elegantly simple complexes show there is much scope using this mode of sensing to develop anion-specific sensing devices by careful control of the lanthanide ion employed (i.e. different ionic radii, Lewis acid strength and anion affinity) and the nature of the ligand used. In a similar example, the bis-bpy-phenyl phosphine oxide ligand **24** was designed as an anion sensor when complexed with Eu(III) [123, 124]. As with the previous example, this pentadentate ligand is unable to fully satisfy the high coordination requirement of the lanthanide, thus leaving an open face (occupied by solvent molecules) that acts as the receptor site for anion coordination. The luminescent emission was produced by energy transfer following excitation of



the bpy moiety. The complexes were made in situ in acetonitrile with either Eu(III) triflate or nitrate salts. For complexes containing the triflate counter anions, infrared analysis indicated that the triflate anions were coordinated in the first coordination sphere. In studies with a number of anions, an 11-fold enhancement in emission intensity was observed upon addition of two equivalents of NO_3^- compared to increases of 5, 1.8 and 1.5 for Cl^- , AcO^- and F^- , respectively. These sensing events also showed an increase in both the lifetime and quantum yields of Eu-24. From the changes in the symmetry-sensitive transitions, $J = 2$ and $J = 4$ (mentioned in Sect. 2.2.2) it was clear that the emission enhancements were directly related to the coordination of these anions to the lanthanide metal centre caused by displacement of the coordinated solvent molecules.

In all of the above examples, the complexes were formed with podand-type ligands but have limited stability in aqueous solution. Parker et al. have made some subtle modifications to these systems to develop anion-sensing devices that can operate in aqueous conditions for potential in vivo applications [125, 126]. This was achieved by alkylating three of the four amine positions in the cyclen moiety with [*R*]-*N*-(2-chloroethanoyl)-2-phenyl-ethylamine, to form Tb-25 and Eu-25 complexes, which were found to have two water molecules bound directly to the metal centre. In solution, it was observed that both water molecules could be displaced in the presence of hydrogen carbonate resulting in the formation of a reversible 1 : 1 adduct, leading to a large change in the lifetimes as well as the lanthanide emission intensities. Studies were carried out in solutions containing MES buffer with pH ranging between 6.4 and 7.3, and in the presence of high ionic strength. This study demonstrated that stable lanthanide complexes can be produced that can detect the presence of anions under simulated physiological conditions. Further evidence for the formation of 1 : 1 adducts with lanthanide complexes of this ligand was later reported [127] with a crystal structure of Yb-25, which formed a 1 : 1 adduct with (*S*)-lactate. The Eu(III) complex of 25 has also recently been used by Parker et al. [128] as a sensor for phosphorylated amino acids.

In a final example, a Eu(III) cryptate complex has been reported as an example of a pH sensing device [129]. This is an example of a bis bipyridyl-



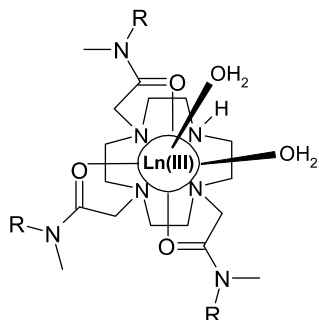
based cryptate with a poly N-methylated flexible arm, **26**. This type of cryptate resulted in the formation of a stable complex. The nine amines were incorporated within the ligand allowing for a well-coordinated complex, thus reducing luminescence quenching from OH oscillators. Modulation of the emission was produced by changes in the coordination environment upon protonation of the cryptate N-methylated backbone. In aqueous solution **Eu·26** gave characteristic Eu(III) emissions arising from energy transfer from the bipyridyl moiety of the cryptate excited triplet state to the metal centre. This emission was dramatically affected by pH. The complex showed a maximum intensity around pH 7, decreasing in intensity above and below pH 7 by almost 50%, but showing a second maximum of lower intensity around pH 3.5. The reduction in emission intensity in acidic environments was attributed to protonation of the aliphatic amines preventing them from being involved in coordination to the metal centre. Therefore, upon protonation the coordination environment was altered because the coordinated methyl amines were replaced by water molecules, leading to the deactivation in the excited state of the Eu(III) metal centre. This was confirmed by q value analysis. At pH 2, a q value of 2 was determined while at pH 6.8 a q value of 1 was determined, showing that when deprotonated the complex shields the metal centre more efficiently. When conditions are made more basic, the amines are deprotonated and can contribute to the complexation of the metal centre, leading to longer lifetimes and higher emission intensities. At very high pH, loss of emission is attributed to the formation of a hydroxylated Eu(II) species.

3.2

Sensors Based on Method B

The following examples are partially coordinated complexes where the ligand does not contain an antenna (method B, Scheme 5) [130–132]. In the first ex-

amples (**27** and **28**) the presence of the two metal-bound water molecules for the Tb(III) and Eu(III) complexes was confirmed by lifetime measurements of the 5D_4 and 5D_0 excited states, respectively, as well as by X-ray crystallography. Studies on all of these complexes were performed with *p*-dimethyl amino benzoic acid (DMABA), which acts as an antenna, coordinating to the ion through the carboxylate, and as such has the potential to sensitise both Eu(III) and Tb(III). However, these studies showed that the formation of luminescent lanthanide complexes was only possible with the Tb(III) complexes with enhancements of up to 680-fold.



Eu. 27 : R' = CH₃, Ln(III) = Eu(III)

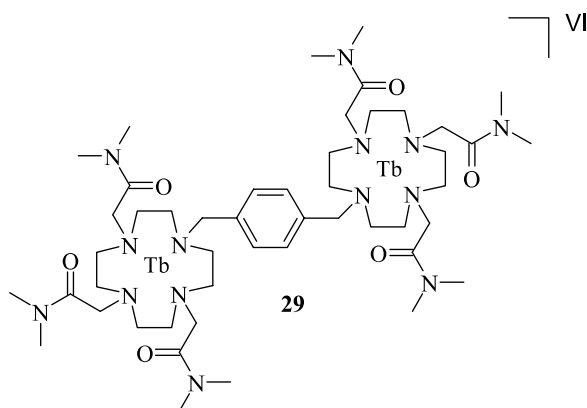
Tb. 27 : R' = CH₃, Ln(III) = Tb(III)

Eu. 28 : R' = H, Ln(III) = Eu(III)

Tb. 28 : R' = H, Ln(III) = Tb(III)

The formation of these ternary luminescent lanthanide complexes was the result of displacement of the two labile metal-bound water molecules, which was necessary because the energy transfer process between the antenna and the Ln(III) metal centre is distance-dependent. This ternary complex formation was confirmed by analysis of the emission lifetimes in the presence of DMABA and showed the water molecules were displaced by a change in the hydration state q from 2 to 0, with binding constants of $\log K_a = 5.0$. The Eu(III) complexes were not modulated in either water or buffered solutions at pH 7.4. Lifetime analysis of these complexes showed that the metal-bound water molecules had not been displaced and that the ternary complex was not formed. Of greater significance, both Tb·27 and Tb·28 could selectively detect salicylic acid while aspirin was not detected in buffered solutions at pH 7.4, using the principle as discussed for DMABA where excitation of the binding antenna resulted in a luminescent emission upon coordination of salicylic acid to the complex.

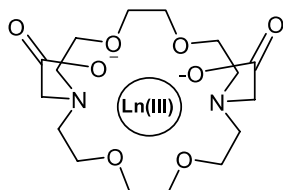
We have recently extended this design principle towards the formation of bis-lanthanide complexes, where the two lanthanide centres were covalently attached by a short spacer. Here the two parts of the ligand **27** were employed, and connected by a simple xylene spacer, giving **29**. This complex gave rise to large enhancement in the Tb(III) emission upon binding to several bis-carboxylates, where the binding was found to be in a 1 : 1 ratio. Using DMABA, each of the metal centres were found to bind one anion, giving rise to 1 : 2 ternary complex formation. Interestingly, with either L- or D-tartaric acid, the



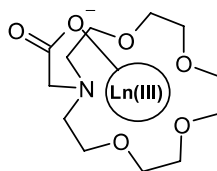
Tb(III) emission was quenched, possibly due to more efficient O – H quenching by the bound anion [133].

The detection of aromatic carboxylates via the formation of ternary complexes using lanthanide ion complexes of functionalised diaza-crown ethers **30** and **31** has been demonstrated [134]. Like the previous examples, these complexes contained vacant coordination sites but the use of carboxylic acid arms resulted in overall cationic 2^+ or 1^+ complexes. Furthermore, the formation of luminescent ternary complexes was possible with both Tb(III) and Eu(III). A number of antennae were tested including picolinate, phthalate benzoate and dibenzoylmethide. The formations of these ternary complexes were studied by both luminescence and mass spectroscopy. In the case of Eu·**30** and Tb·**30**, the 1 : 1 ternary complexes were identified. When the Tb(III) and Eu(III) complexes of **30** were titrated with picolinic acid, luminescent enhancements of 250- and 170-fold, respectively, were recorded. The higher values obtained for Tb(III) was explained because there was a better match between the triplet energy of the antenna and a charge transfer deactivation pathway compared to the Eu(III) complex.

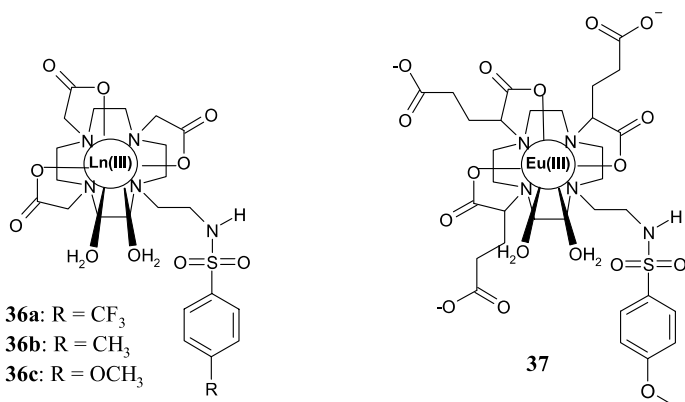
The Eu(III) complex Eu·**31** was studied with the same coordinating antenna. A 1 : 2 ternary complex was expected because there were more avail-



Ln(III) = Eu(III) and Tb(III)



Ln(III) = Eu(III) and Tb(III)



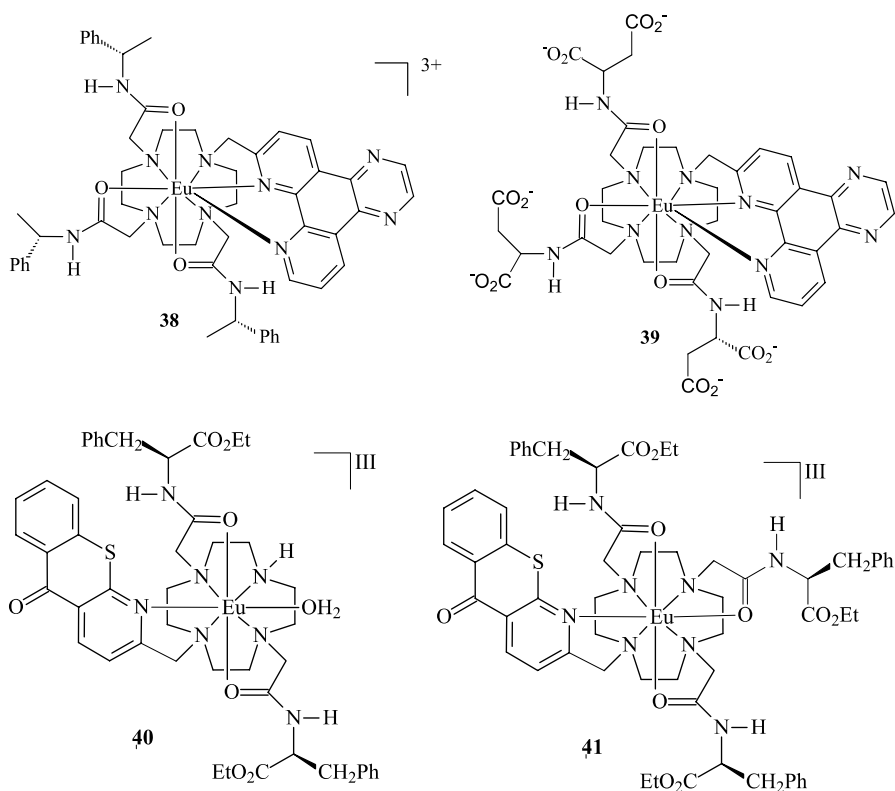
Ln(III) = Eu(III) or Tb(III)

the ring was reduced, which resulted in a change in pK_a by one log unit. A disadvantage to this type of system was its limited use under physiological conditions because of competition with other anions such as carbonates, lactates, citrates and phosphates.

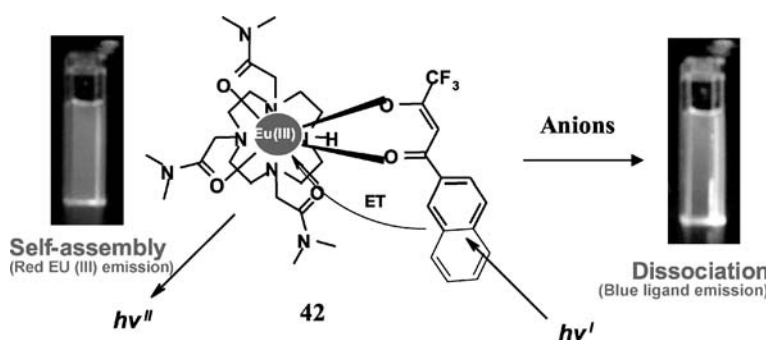
These disadvantages were overcome by modifying the coordinating arms of the complex to produce **37**, where three carboxyethyl substituents were attached α to the cyclen ring nitrogens. This reduced the affinity of the complex to competitive anions allowing coordination of the aryl sulfonamide to take preference. In repeat pH titrations in a simulated physiological environment, the response was shown to be identical to that in water indicating the success of the modified arms in preventing competitive anion binding [140]. This example shows these highly stable complexes are promising for future applications, especially for in vivo applications where careful design of the complex can lead to controlled selectivity in a competitive media.

Parker et al. have recently elegantly extended their use of coordinatively unsaturated lanthanide complexes for anion sensing, for interacting with DNA as well as for imaging of stained or living cells [141]. Compound **38** was developed for the intercalation into DNA [142], while the structurally related molecule **39** (also formed as the Tb(III) complex) has been developed for the detection of anions such as uric acid [143]. The two structures are related, however, **39** is overall anionic, while **38** is cationic. Compounds **40** and **41** have also been developed by Parker et al. The former was developed as a chemoselective sensor for the citrate anion using ratiometric analysis [144]. The latter, which is structurally related, was used for selective nucleoli staining of NIH 3T3, HeLa and HDF cells, in life and for fixed cell imaging [141, 145].

The above examples have demonstrated the use of coordinatively unsaturated complexes that either lack the antenna or become luminescent upon coordination of antennae such as carboxylates etc. Recently, a new addition of



lanthanide complexes based on this design was developed by us, where we used the Eu(III) complex of **29a**. In aqueous solution at pH 7.4, the europium complex formed the self-assembly ternary complex **42**, with β -diketonate, which gave rise to intense luminescence from the Eu(III) centre upon excitation of the antenna [146]. However, in a similar manner to that observed for **36**, the formation of this self-assembly was pH-dependent, and the Eu(III) emission



was only observed within the physiological pH range. Moreover, the self-assembly could also be dissociated (see below) by displacing the antenna with suitable anions such as bicarbonate, fluoride and dicarboxylates such as lactates. We are currently working on other analogues of **42**, with the aim of achieving more selective anion sensing.

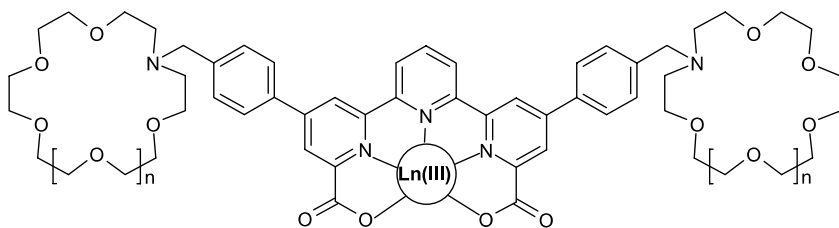
3.3

Sensors Based on Methods C and D

This final section will look at complexes where the antenna is integrated into the lanthanide complex and are purposely designed with a receptor incorporated, leading to modulation of the sensitisation process upon guest recognition.

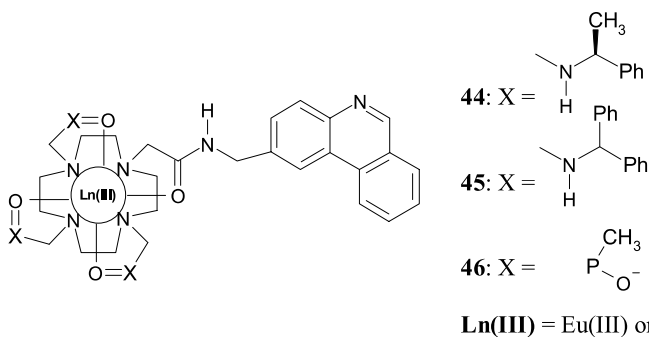
We begin with a review of the two crown ether-based systems **43a** and **b**, respectively, which are among the first examples of where the lanthanide emission could be modulated by external inputs such as cations. These examples were developed by de Silva et al., who previously had developed analogue examples where the input was a proton. For both of these complexes, **43a** and **43b**, an order of magnitude enhancement in the Eu(III) luminescent emission of **42** and **43** was observed when titrated with Na^+ and K^+ , respectively. The switching on of the Eu(III) luminescent emission was attributed to alkali cation-induced suppression of PET from the aza-crown. Similar results were obtained for Tb-**42** and Tb-**43** but the quantum yields (ϕ) were found to be less than 0.0016 in both cases compared to 0.47 for the Eu(III) analogues. This was explained by the presence of a low-lying triplet state, which allows for efficient back energy transfer process (as described in Scheme 3) [147].

One of the most important design changes in the evolution of this type of sensor was to produce complexes stable in aqueous media. The cyclen-based ligands and their stable Eu(III) and Tb(III) complexes, **44–46**, represent examples of sensors developed by Parker et al. for pH, pO_2 , halide and hydroxide ion sensing, [148–150]. The ligand used was based on cyclen substituted in one of the four positions with phenanthridine as the antenna and receptor. The other three positions were substituted with various pendant

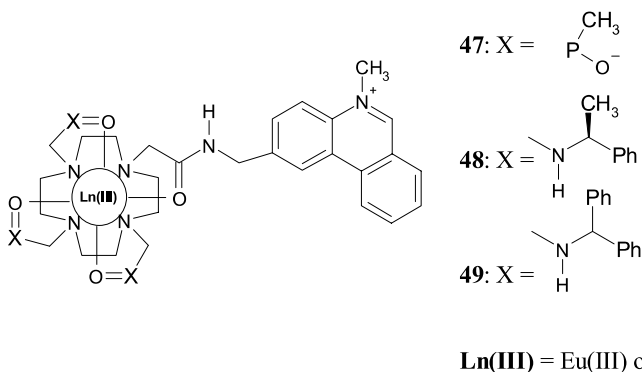


43a: $n = 0$

43b: $n = 1$ Ln(III) = Eu(III) or Tb(III)



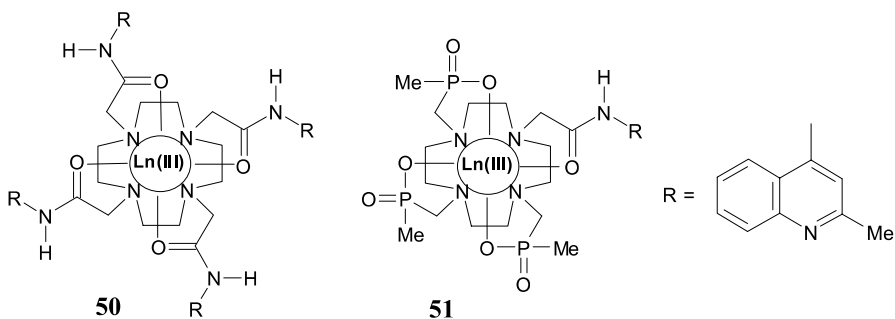
arms, such as chiral amides in the case of **44** and **45** and phosphinate esters in **46**. Upon excitation of the phenanthridine antenna, the complexes showed lanthanide luminescent emissions depending on pH in aqueous solution. A luminescence enhancement factor of over 500 was recorded for Eu-**46** when the phenanthridine was excited at 370 nm. In the case of Tb-**46**, no emission was observed upon excitation of phenanthridine when protonated, due to a phenanthridine low-lying triplet state. Parker also developed other luminescent sensors of these molecules by simply methylating the nitrogen position of the phenanthridine ligand, which prevented its use as a pH sensor. However, the results, Eu-**47**, Eu-**48** and Eu-**49**, were found to be sensitive to chloride anions in the physiological pH range with a quenching of luminescence upon chloride recognition. Quenching of the luminescent emission occurred by way of charge transfer from the halide to the singlet excited state, S_1 , of the electron-poor cationic chromophore, which prevented population of the triplet excited state, T_1 [151].



The lanthanide luminescence of the Tb(III) complexes of **47** and **48** was pH-independent over the range 1–10. However, sensitivity to pO_2 , in the pH range 2–9, was reported and was attributed to the quenching of the aromatic

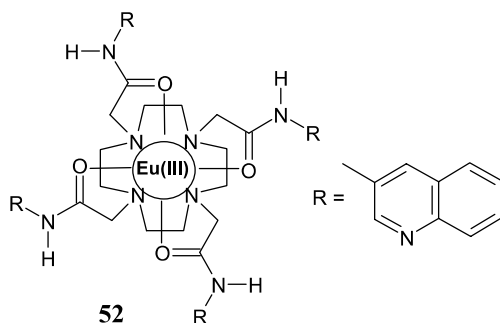
triplet state. The lanthanide luminescence of the Eu(III) complexes **47** and **48** was sensitive to hydroxide anions. The Eu(III) emission was independent of pH up to pH 9; however, above this there was a significant decrease in the emission, which was zero by pH 13.5. The Eu(III) emission was found to decrease with increasing amounts of KOH. This occurred because the *N*-methyl phenanthradine moiety was attacked by OH⁻ at the C-6 position in a reversible manner, leading to a decrease in the longest wavelength absorption band of phenanthradine. In a similar study on the Tb(III) complexes of **47** and **48**, the Tb(III) emission was found to be switched on with the addition of KOH at ca. pH 9, reaching a maximum at pH 11.2 and then decreasing by a factor of two beyond pH 13. The switching on of the Tb(III) emission was due to an increase in the triplet energy of the *N*-methylated phenanthradine moiety upon formation of the hydroxylated species. No explanation was given for the decrease in Tb(III) emission beyond pH 11.2. However, this was found to be a reversible process over a number of acid/base cycles [151].

Other complexes based on quinolyl derivatives can act as pH sensors. Here cyclen-based ligands are used that contain four quinolyl-based proton receptors/sensitising moieties for pH sensing, attached via amide-bridged pendant arms, **50** [152–154]. A modified version, which contained only one quinolyl-based receptor **51**, was also reported as a pH sensor in both solution and in soft material such as hydrogel [152–154]. The pH profiles of the Eu-**51** and Eu-**50** complexes showed sigmoidal characteristics upon excitation of the quinolyl moiety at 330 nm. The p*K*_a was determined to be ca. 4.6 and ca. 5.8 for Eu-**51** and Eu-**50**, respectively. In both cases, luminescence was switched on in acidic conditions. Interestingly, the Tb(III) complex of **51** only produced lanthanide luminescence when the complex was in acidic conditions *and* in the absence of molecular oxygen. This development was the first example of a lanthanide luminescent molecular logic gate where the luminescent output could be described as mimicking the *inhibit* logic gate function [155, 156].

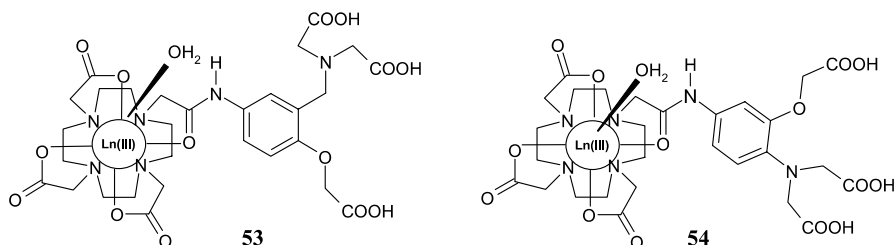


Ln(III) = Eu(III) or Tb(III)

Another related example is **52** [157], which is a tetra-substituted cyclen ligand with four quinoline receptor moieties capable of sensing protons in a similar manner to **50**. The lanthanide emission was found to be switched on in highly acidic conditions, with a luminescent enhancement of over 300-fold. Luminescent enhancement was attributed to an enhancement in the population of the S_1 and subsequent T_1 excited states of the quinoline chromophore when in acidic media. A bell-shaped pH profile was found to exist at pH 1.8–3.5, whereas at more acidic pH the emission was switched off.



So far in this section the examples discussed have comprised of hetero aromatic antenna receptors, which mainly function as pH sensors. The detection of metal cations in biological, medical and ecological applications is of major interest. However, this requires more elaborate receptors that can selectively bind a specific metal cation. Naturally, the more elaborate the receptor required, the more challenging its synthesis becomes. The synthesis of lanthanide-based sensors of **53** and **54** has been reported with each ligand incorporating an antenna/receptor selective for zinc(II) [158, 159]. In both cases the receptors are structurally similar, with **53** synthesised from benzylamine and **54** from aniline.

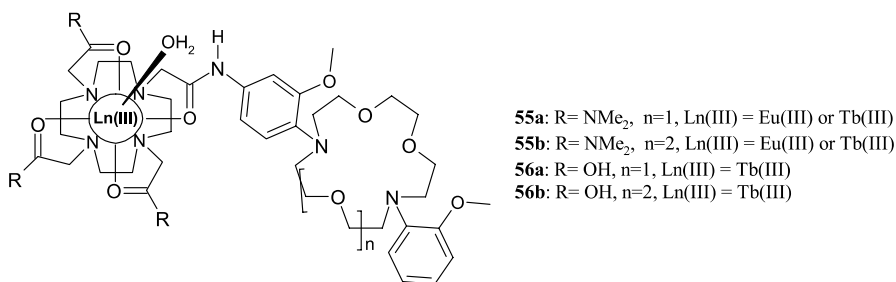


Ln(III) = Eu(III) and Tb(III)

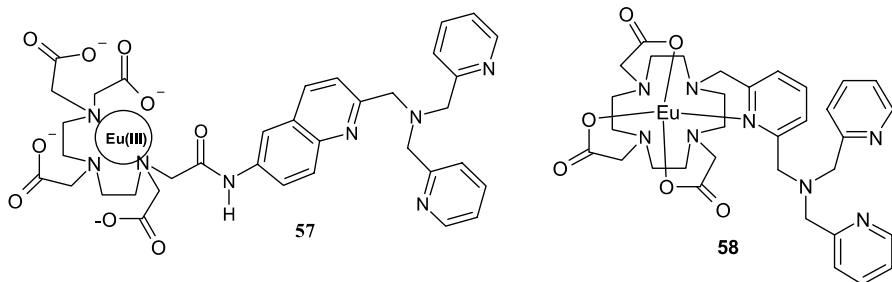
On addition of zinc (as $ZnCl_2$) to a solution of Ln-**53**, under simulated physiological conditions, the luminescent emission of the lanthanide was en-

hanced with the Tb-53 complex showing an enhancement of 26%, while Eu-53 showed an enhancement of 42%. The luminescence emission enhancements were much lower than those observed in the examples discussed above. For Ln-54 it was suggested that the binding of Zn(II) resulted in the deconjugation of the aniline nitrogen lone pair, resulting in suppression of PET from or to the intermediate aryl singlet excited state of the aniline moiety, which leads to luminescent enhancement. Regardless of this, these complexes showed great selectivity for Zn(II) over other cations such as Mg(II) and Ca(II) and can be said to be the first examples of lanthanide-based sensors for metal sensing.

The Tb(III) and Eu(III) complexes of 55–56 were prepared, where modulation of the lanthanide emission was expected upon addition of group I cations due to the incorporation of group I specific antenna/receptor fragments [160, 161]. These examples are the first reported devices that are kinetically stable and show selectivity for group I cations in buffered solutions. This was achieved by conjugating an aromatic crown ether moiety onto one of the pendant arms of the cyclen structure forming a bis-macrocyclic structure. Compounds 55a and 55b are examples of this design, yielding overall cationic complexes, whereas 56a and 56b are the corresponding charge-neutral complexes. Of the Eu(III) and Tb(III) complexes formed, only the Tb(III) complexes gave a lanthanide emission that was modulated upon detection of either Na⁺ or K⁺. This was most likely due to the inefficient sensitisation of the Eu(III) excited state, or because of a competitive electron transfer or MLCT quenching of the Eu(III) state yielding Eu(II), which is not emissive.



The Tb(III) complexes of 55 and 56 showed luminescence emission which was switched on with a corresponding order of magnitude enhancements at pH ~ 3.2 with pK_a of ca. 2.4 (depending on pH). The pK_as were particularly low and suggested that there was a significant inductive effect enforced by the Tb(III) ion and the subsequent delocalisation of the aromatic amino moiety of the aniline centre adjacent to the Tb(III)–cyclen complex. For 55 and 56, the emission was also significantly affected in alkaline pH (above pH 10), giving rise to an overall “on–off–on” pH profile. This inverted-bell shaped curve



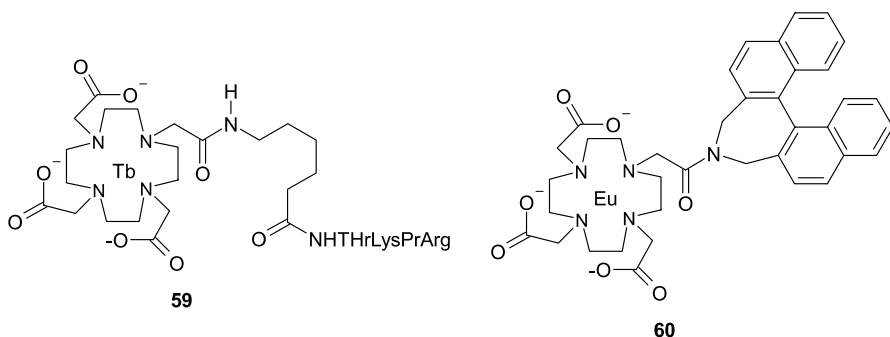
was absent in the charge-neutral complexes **57** and **58**, which was unexpected because of the similarity of the complexes. This phenomenon is still under investigation. Another unexpected observation with these complexes was that the Tb(III) emission was switched on at pH 7.4, upon addition of either Na⁺ or K⁺, but only at high concentration of the ions (> 0.1 mM). For both **56** and **58** selective K⁺ recognition was observed with large order, ca. 30- to 40-fold, enhancements in the Tb(III) emission. In contrast, for **55** and **57** selective Na⁺ recognition was observed but with more moderate, ca. seven- to ninefold, enhancements. In all cases, protonation or metal cation binding was found to cause substantial increases in the lifetime of the lanthanide luminescence with increases from 0.18 ms to 1.29 ms recorded. These observations indicate that sensitisation of the Tb(III) centre is made more efficient upon binding of the guest cation within the diaza-crown receptor. We have recently extended this design principle to other crown ethers [162].

Nagano et al. have also prepared Eu(III) and Tb(III) complexes for Zn(II) sensing [163, 164]. Acyclic ligands with a pyridine-based receptor/antenna were used to complex the lanthanide cation. **59** was prepared from a diethylenetriaminepentaacetic acid (DTPA) moiety covalently attached to a quinoline-containing tetrakis(2-pyridylmethyl)ethylenediamine (TPEN)-based antenna/receptor, which is known to be selective for Zn(II). Investigations into the effect of pH on the modulation of the lanthanide emission found that Eu-**57** was pH-independent between pH 3.6 and 8.8. Studies performed with a selection of group I, II and transition metal ions showed Eu-**57** was selective for Zn(II), with significant modulation of the Eu(III)-based emission. Unlike the previous Zn(II) sensor examples where the modulation was modest, the modulated emission of Eu-**57** upon the addition of Zn(II) led to an increase in luminescence by a factor of about five. Compound Eu-**57** was also found to be ideal for testing in living cells because of the relatively long excitation wavelength of 340 nm.

Pope and Laye developed the related Eu(III) complex **58**, using the picolyl unit as a Zn(II) receptor. This elegant example involves one of the pyridyl nitrogen moieties in the coordination of the lanthanide ion prior to the Zn(II) sensing. The antenna can thus both populate the reporter effectively, being coordinated to the metal ion, as well as fulfilling the high coordination re-

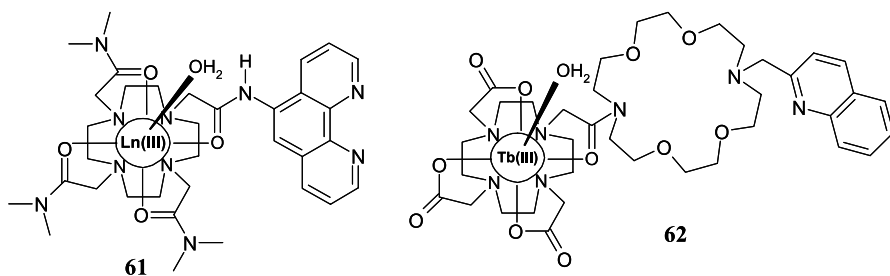
quirement of the ion, as q was reported to be 0. However, upon addition of Zn(II), the Eu(III) emission is quenched as now all the pyridyl moieties coordinate to the Zn(II). This means that the Eu(III) is no longer 8-coordinated and becomes di-aqua coordinated. This quenches the Eu(III) excited state and hence the Eu(III) emission is significantly reduced as a function of Zn(II) concentration [165].

As discussed previously, compounds such as **40** and **41** have been developed to target biological macromolecules, where the emission from the lanthanide centre is modulated upon the interaction of these complexes with the biomolecules. In a similar manner, both compounds **59** and **60** have been developed to target such species. The former was developed by Faulkner et al. for the targeting and is based on the use of Tb(III)-DOTA derivative [166], functionalised with a peptide conjugate. The latter, having a binaphthyl antenna, was developed by Lowe et al. for targeting human serum albumin (HAS) [167]. Both of these examples demonstrate the versatility of the use of cyclen-based lanthanide complexes for the targeting of such species.



The Eu(III) complex of **61** has been reported as a sensor that is selective for H^+ or Cu(II) [168]. The ligand is a cyclen-based system with a 1,10-phenanthridine (*phen*) moiety incorporated as an antenna/receptor. A pH titration of Eu-**61** showed a bell-shaped pH profile where the emission can be described as being switched off-on-off as a function of pH. This bell-shaped pH-dependence was fully reversible and gave pK_{a} s of 3.8 and 8.1. The pK_{a} s were assigned to the protonation of the phen nitrogen moiety and the subsequent deprotonation of the aryl amide. The changes in the lanthanide luminescence emission in the alkaline region were due to the reduction of Eu(III) to Eu(II). In the physiological pH range, the emission was “almost” pH-independent and switched on. Studies in buffered solution at pH 7.4, showed Eu-**61** to be an effective sensor for Cu(II) and selective over Co(II), Fe(II) and Fe(III). Upon addition of Cu(II) to a solution of Eu-**61** the Eu(III) emission was switched off. The only disadvantage to this system was the use of the short excitation wavelength of 278 nm, which suggests that the system is not suitable for in vivo detection.

The Tb(III) complex, **62**, is a dual-component recognition device for H^+ and K^+ in four independent pH windows, in aqueous buffered solutions [169]. This example clearly shows how slight modifications to the existing design can lead to new and unprecedented signalling responses. At first glance, Eu-**62** appears to be similar to the examples discussed above, but utilises a cyclen macrocycles that has been alkylated at three of its positions with acetate pendant arms, giving an overall neutral Tb(III) complex. As with the other examples, a receptor antenna moiety is tethered to the complex but is covalently attached through the receptor, and not the antenna, resulting in unexpected response characteristics.



Studies on the dual-component sensing behaviour of Tb-**62** were performed with the addition of K^+ over a wide pH range of 0.8–12.0. Results showed that the Tb(III) emission was silent and immune to the addition of K^+ in alkali solution (pH 9.2–12.0). However, quenching of the Tb(III) emission, in the pH range 1.0–3.4, was seen upon addition of K^+ , whereas emission was enhanced gradually in the pH range 4.1–9.0. Selectivity for K^+ over other group I and II cations was demonstrated at both pH 6.3 and 2.2. However, the concentration of the metal cation required to modulate the Tb(III) emission is considerably higher, making Tb-**62** impractical, at the moment, for in vivo applications.

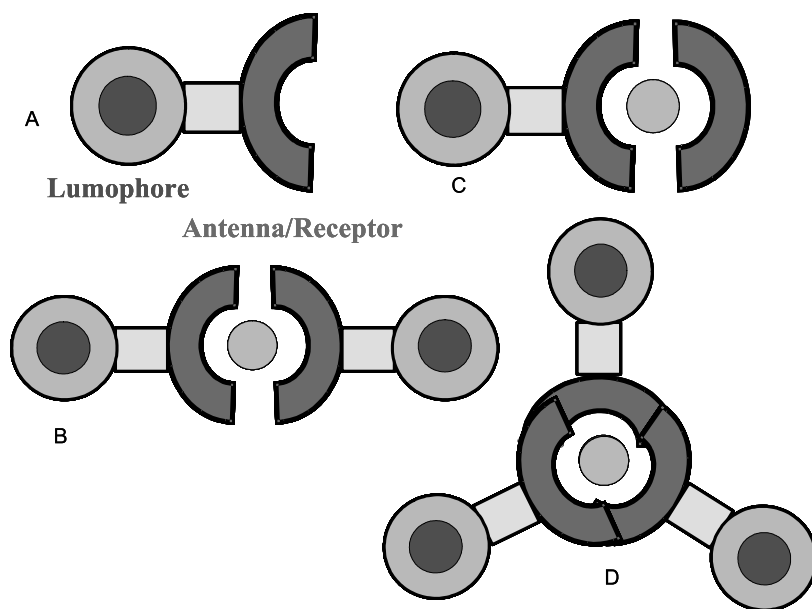
4

Simple Self-Assemblies Using $f-d$ Mixed Metal Ions

This last section deals with a few examples of the formation of self-assembly structures from lanthanide complexes, which are formed by using transition metal ions. This area of research is very novel and relatively few examples have been developed to date. While the lanthanide ions have been used to mediate the formation of supramolecular structures, such as helicates, many of which can have both $f-f$ and $f-d$ metal ions, etc. the focus here will be on the use of lanthanide complexes and ligand structures similar to those described above [170–173].

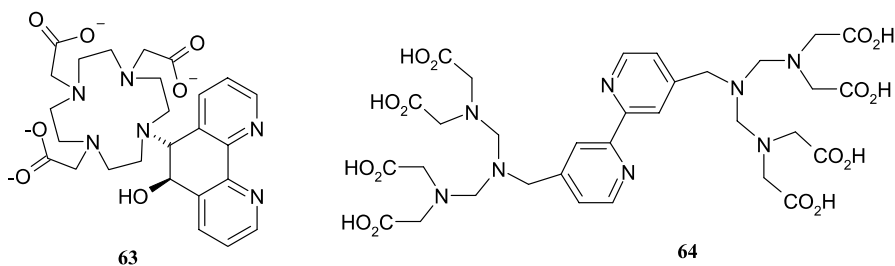
In recent years a few examples of mixed $f-d$ self-assemblies have been developed. One of the driving forces for such work has been that the excited states of NIR-emitting ions such as Yb(III), Eb(III), and Nd(III) in particular, can be formed by excitation in the visible region [174–176]. As many transition metal complexes often have strong MLCT absorption bands in the visible region, then these are ideal as antennae for the population of these ions. This has been elegantly shown by many researchers [177–179]. This is of particular interest as it opens up new potentials for sensing of biological systems in the NIR. Moreover, the photophysics of transition metal complexes is well established and explored, and many varieties of ligands are available that can be used to construct mixed $f-d$ metal ion self-assemblies. With this in mind we set out to self-assembly structures based on the phen derivative **61** [180].

Compound **61** can be depicted in a cartoon manner as **A** in Scheme 6. Our idea was to form the linear $f-d-f$ assembly (**B**) by simply using a Cu(II), Fe(II) or Zn(II) ion as the bridging unit; where these would coordinate to the phen ligand and as such bring two of the lanthanide complexes together. While the formation of a self-assembly was successful, the desired structure (**B** in Scheme 6) was not exclusively formed. Using Cu(II) we showed that upon addition of **61**, at pH 7.4, the Eu(III) emission was switched off. Moreover, the absorption spectra were shifted to the red and the singlet



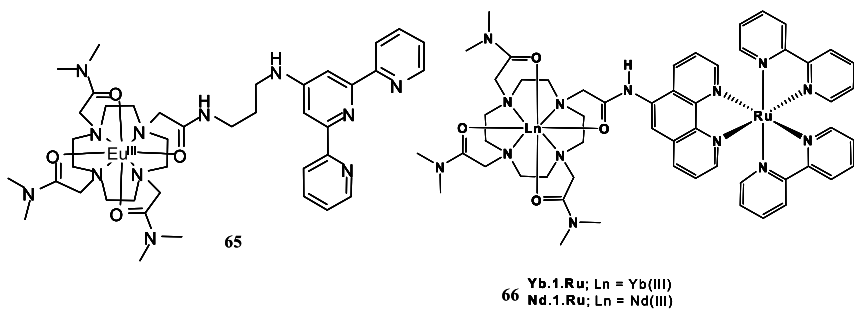
Scheme 6 The various self-assembly structures possible for simple $f-d$ mixed coordination based compounds

excited state was quenched. Analysis of these changes showed that in fact both structure **B** and **D** were formed. In a related work, Desreux et al. have developed self-assembly complexes using the 6-hydroxy-1,6-dihydro-1,10-phenanthroline appended cyclen derivative **63** [181]. While these were formed as MRI contrast agents using Gd(III), they showed that using either Fe(II) or Ni(II) the self-assembly complexes formed were structurally identical to **D** in Scheme 6. Similarly, Livramento et al. have used an octa-acidic acid derivative of the 2,2'-bipyridine moiety **64** as an MRI contrast agent, which was formed by self-assembly around a Fe(II) ion, giving a 6 : 1 ratio between the *f* and the *d* metal ions in the self-assembly [182].



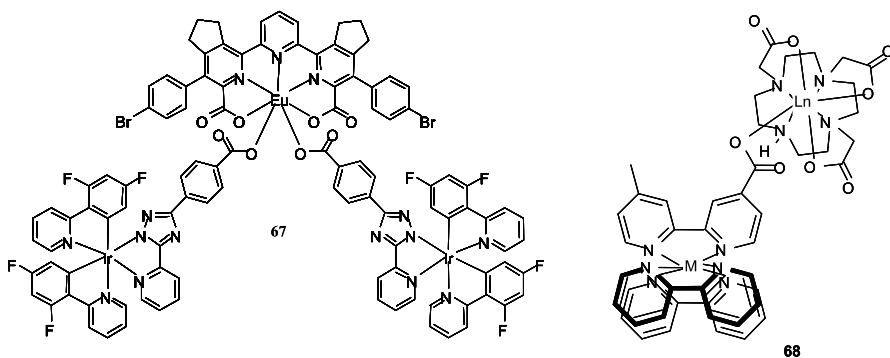
With the aim of achieving the linear assembly **B**, we made the Eu(III) complex **65**. Unlike that seen for **61** and **63**, the terpyridine antenna was now conjugated into the cyclen ring via a spacer [183]. However, this antenna indeed ensured that the desired assembly was formed. Upon addition of ions such as Fe(II) and Co(II), the MLCT band was clearly formed, and only 0.5 equivalents of the metal ion were needed to achieve saturation. Fitting the changes to using non-linear least squares regression analysis indeed showed the formation of the desired complex. Moreover, the singlet excited state of the phen ligand was quenched. However, the most important changes were observed in the Eu(III) emission, where the emission was reduced in intensity, most likely due to energy transfer from the $^5D_0 \rightarrow ^3MLCT$ upon binding to Fe(II). From these changes, the stoichiometry was determined to be 2 : 1 (complex : Fe(II)). More importantly, the Eu(III) ion is an *impartial luminescent reporter* as it does not participate directly in the binding of the transition metal ions. Hence, the changes in the Eu(III) centre in **65** can be considered a direct measure of the coordination changes occurring at the antenna and therefore of the formation of the self-assembly complex **B** (Scheme 6). Moreover, as the Eu(III) complex does not take part directly in the formation of the self-assembly, the Eu(III) complexes can be considered as impartial observers in the determination of the structural nature of the resulting assembly in solution.

The final example of self-assembly structures shown schematically in Scheme 6 is **D**. This was developed with the aim of achieving NIR emission



from Nd(III) and Yb(III), respectively, by exciting into the MLCT band of the complex. Here a Ru(II) complex was used and the Yb(III) or the Nd(III) complex of **61** [184]. By simply using Ru(bipy)₂²⁺ as a capping or ancillary ligand, the desired structure **D** (Scheme 6), **66**, was formed. Indeed the excitation of the MLCT band gave rise to efficient energy transfer/sensitisation to the lanthanide excited state and the NIR emission was observed. However, for the two complexes, the Nd(III) analogue was found to be more emissive and is currently being investigated further in our laboratory.

In an analogous manner, other examples of such mixed *f-d* self-assemblies have been developed. Compounds **67** and **68** are examples of two such complexes. In the former, developed by DeCola et al., the system consists of a heterotrimetallic complex, in which the excitation of the Eu(III) occurs via energy transfer from a Ir(III)-based metal-based antenna [185]. Interestingly, the emission of almost-white light can be observed if there is only partial energy transfer from the excited Ir(III)-based chromophore. If this occurs, the Eu(III) red emission combined with the residual blue emission from the iridium complex gives rise to a global white light emission. In the latter, developed by Faulkner et al. [186], the system is based on the use of coordinatively unsaturated Eu(III) and Tb(III) ligands, similar to those discussed



for 41, and M = Ru(II) or the Os(II) complexes. These transition metal complexes have carboxylate functionality that can be used to coordinate to the metal centre. Upon excitation of the MLCT band of these complexes a sensitised lanthanide emission (Ln = Yb(III), Nd(III) or Er(III)) was observed. Other examples of such designs have appeared in the last few years and demonstrate the significant interest that such self-assemblies based on lanthanide ions are gathering [187].

5 Conclusion

From the systems discussed in this chapter, it can be seen that in the last few years the development of lanthanide ion luminescent complexes, sensors, switches and self-assemblies has come a long way with many wonderful examples being developed. In each section, this evolution of lanthanide-based photochemistry has been highlighted and selective examples discussed as well as their development to overcome issues such as complex stability and, in some cases, their ability to overcome competition from physiological medium to produce highly selective and sensitive sensors. It is clear that much work has been achieved but that there is still much to be done to push this field of research to the next stage and to the incorporation of these complexes onto solid supports or gels for use in diagnostic equipment, as has happened for fluorescent sensing devices, or even further to the point where in vivo applications can be envisaged. The field of NIR-emissive complexes and the use of lanthanide ions in the formation of coordination networks are fast growing fields of research and very exciting! It will thus be interesting to follow all these exciting developments in the near future.

Acknowledgements The authors would like to thank the many students and postdoctoral fellows that have worked in our laboratory in Dublin on the many examples discussed above. We also like to thank University of Dublin, Trinity College, Kinerton Ltd. (now Ipsen Ltd.), Enterprise Ireland Science Foundation Ireland, IRCSET, CSCB and the Wellcome Trust for financial assistance through the years.

References

1. Callan JF, de Silva AP, Magri DC (2005) *Tetrahedron* 36:8551
2. Gunnlaugsson T, Ali HDP, Glynn M, Kruger PE, Hussey GM, Pfeffer FM, dos Santos CMG, Tierney J (2005) *J Fluoresc* 15:287
3. de Silva AP, McCaughan B, McKinney BOF, Querol M (2003) *Dalton Trans*, p 1902
4. Balzani V (2003) *Photochem Photobiol Sci* 2:459
5. Balzani V, Credi A, Venturi M (2003) *Pure Appl Chem* 75:541
6. Martínez-Máñez R, Sancenón F (2003) *Chem Rev* 103:4419
7. Raymo FM (2002) *Adv Mater* 14:401

8. de Silva AP, Gunaratne HQN, Gunnlaugsson T, Huxley AJM, McCoy CP, Rademacher JT, Rice TE (1997) *Chem Rev* 97:1515
9. Venturi M, Credi A, Balzani V (2003) *Molecular devices and machines – a journey into the nanoworld*. Wiley, Weinheim
10. Feringa BL (ed) (2001) *Molecular switches*. Wiley, Weinheim
11. Gunnlaugsson T, Glynn M, Tocci (née Hussey) GM, Kruger PE, Pfeffer FM (2006) *Coord Chem Rev* 250:3094
12. Parkesh R, Lee TC, Gunnlaugsson T (2007) *Org Biomol Chem* 5:310
13. Gunnlaugsson T, Kruger PE, Jensen P, Tierney J, Ali HDP, Hussey GM (2005) *J Org Chem* 70:10875
14. Pfeffer FM, Gunnlaugsson T, Jensen P, Kruger PE (2005) *Org Lett* 7:5375
15. Gunnlaugsson T, Leonard JP, Murray NS (2004) *Org Lett* 6:1557
16. Gunnlaugsson T, Lee TC, Parkesh R (2003) *Org Biomol Chem* 1:3265
17. Gunnlaugsson T, Bichell B, Nolan C (2002) *Tetrahedron Lett* 43:4989
18. Gunnlaugsson T, Lee TC, Parkesh R (2003) *Org Lett* 5:4065
19. Gunnlaugsson T, Nieuwenhuyzen M, Richard L, Thoss V (2001) *Tetrahedron Lett* 42:4725
20. Stochel G, Wanat A, Kuliš E, Stasicka Z (1998) *Coord Chem Rev* 171:203
21. Wing-Wah V, Yam K, Kam-Ying Lo (1998) *Coord Chem Rev* 184:157
22. Thunus L, Lejeune R (1999) *Coord Chem Rev* 184:125
23. Perry LM, Winefordner JD (1990) *Talanta* 37:965
24. Gudgin Dickson EF, Pollak A, Diamandis EP (1995) *J Photochem Photobiol B: Biol* 27:3
25. Coates J, Sammes PG, West RM (1996) *J Chem Soc Perkin Trans 2*, p 1275
26. Coates J, Sammes PG, West RM (1996) *J Chem Soc Perkin Trans 2*, p 1283
27. De Horroks WWE, Sudnick DR (1981) *Acc Chem Res* 14:384
28. Sammes PG, Yahioğlu G (1996) *Nat Prod Rep*, p 1
29. Parker D, Dickins RS, Puschmann H, Cossland C, Howard JAK (2002) *Chem Rev* 102:1977
30. Bünzli J-CG, Piguet C (2002) *Chem Rev* 102:1977
31. Selvin PR (2001) *J Am Chem Soc* 123:7067
32. Piguet C, Bünzli J-CG (1999) *Chem Soc Rev* 28:347
33. Lis S, Elbanowski M, Makowska B, Hnatejko Z (2002) *J Photochem Photobiol A: Chem* 150:233
34. Bazin H, Preaudat M, Trinquest E, Mathis G (2001) *Spectrochim Acta A* 57:2197
35. Choppin GR, Peterman DR (1998) *Coord Chem Rev* 174:283
36. Gunnlaugsson T, Stomeo F (2007) *Org Biomol Chem* 5:1999
37. Gunnlaugsson T, Leonard JP (2005) *Chem Commun*, p 3114
38. Alpha B, Lehn J-M, Ballardini R, Balzani V, Perathoner S, Sabbatini N (1990) *Photochem Photobiol* 52:299
39. Merbach AE, Toth É (eds) (2001) In: *The chemistry of contrast agents in medical magnetic resonance imaging*. Wiley, West Sussex, England
40. Toth E, Burai L, Merbach AE (2001) *Coord Chem Rev* 216:363
41. Aime S, Botta M, Fasano M, Terreno E (1998) *Chem Soc Rev* 27:19
42. Faulkner S, Matthews JL (2003) In: Ward MD (ed) *Applications of coordination chemistry*. *Comprehensive coordination chemistry II*, vol 9, 2nd edn. Elsevier, Amsterdam, p 913
43. Petoud S, Cohen SM, Bünzli J-CG, Raymond KN (2003) *J Am Chem Soc* 125:13324
44. Bünzli J-CG (2006) *Acc Chem Res* 39:53
45. Bünzli J-CG, Piguet C (2005) *Chem Soc Rev* 34:1048

46. Bünzli J-CG (2006) *J Alloys Compounds* 408:934
47. Bünzli J-CG (2004) In: Sigel A, Sigel H (eds) *Metal ions in biological systems*, vol 42. Marcel Dekker, The Netherlands, p 39
48. Sigel A, Sigel H (eds) (2003) *The lanthanides and their interrelations with biosystems. Metal ions in biological systems*, vol 40. Marcel Dekker, New York
49. Caravan P, Ellison JJ, McMurray TJ, Lauffer RB (1999) *Chem Rev* 99:2293
50. Aime S, Botta M, Fasano M, Terreno E (1999) *Acc Chem Res* 32:941
51. Lauffer RB (1987) *Chem Rev* 87:901
52. Bünzli J-CG (1989) In: Bünzli J-CG, Choppin GR (eds) *Lanthanide probes in life, chemical and earth sciences; theory and practice*. Elsevier, New York, p 219
53. Parker D, Williams JAG (2003) In: Sigel A, Sigel H (eds) *Metal ions in biological systems*, vol 40. Marcel Dekker, New York, p 233
54. Melhuish WH (1984) *Pure Appl Chem* 56:231
55. Hemmilä I, Ståhlberg TPM (1995) *Bioanalytica applications of labelling technologies*. Wallac Oy, Turkey
56. Hemmilä I, Mukkala VM (2001) *Crit Rev Clin Lab Sci* 38:441
57. Voloshin AI, Shavaleev NM, Kazakov VPJ (2001) *Lumin* 93:199
58. Auzel F (2004) *Chem Rev* 104:139
59. Stouwdam JW, Hebbink GA, Huskens J, vanVeggel FCJM (2003) *Chem Mater* 15:4604
60. Shavaleev NM, Pope SJA, Bell ZR, Faulkner S, Ward MD (2003) *Dalton Trans*, p 808
61. Werts MHV, Woudenberg RH, Emmerink PG, Gassel RV, Hofstraat JW, Verhoeven JW (2000) *Angew Chem Int Ed* 39:4542
62. Imbert D, Cantuel M, Bünzli JCG, Bernardinelli G, Piguet C (2003) *J Am Chem Soc* 125:15698
63. Parker D, Williams JAG (1996) *J Chem Soc Perkin Trans 2*, p 1581
64. Parker D (2000) *Coord Chem Rev* 205:109
65. Sabbatini N, Guardigli M, Lehn J-M (1993) *Coord Chem Rev* 123:201
66. Wolbers MPO, Veggel FCJM, Snellink-Ruel BHM, Hofstraat JW, Geurts FAJ, Reinhoudt DN (1998) *J Chem Soc Perkin Trans 2*, p 2141
67. Petoud S, Muller G, Moore EG, Xu J, Sokolnicki J, Riehl PJ, Le UN, Cohen SM, Raymond KN (2007) *J Am Chem Soc* 129:77
68. Beeby A, Parker D, Williams JAG (1996) *J Chem Soc Perkin Trans 2*, p 1565
69. Tremblay MS, Zhu Q, Martí AA, Dyer J, Halim M, Jockusch S, Turro NJ, Sames D (2006) *Org Lett* 8:2723
70. Woods M, Sherry AD (2003) *Inorg Chem* 42:4401
71. Coppo P, Duati M, Kozhevnikov VN, Hofstraat JW, De Cola L (2005) *Angew Chem* 177:1840
72. Imbert D, Cantuel M, Bünzli J-CG, Bernardinelli G, Piguet C (2003) *J Am Chem Soc* 125:15698
73. de Silva AP, Gunaratne HQN, Rice TE (1996) *Angew Chem Int Ed* 35:2116
74. Beeby A, Faulkner S, Parker D, Williams JAG (2001) *J Chem Soc Perkin Trans 2*, p 1268
75. Zucchi G, Ferrand AC, Scopelliti R, Bünzli JCG (2002) *Inorg Chem* 41:2459
76. Dexter DL (1953) *J Chem Phys* 21:836
77. Forster T (1984) *Ann Phys* 2:55
78. Forster TH (1959) *Discuss Faraday Soc* 27:7
79. Aime S, Botta M, Parker D, Williams JAG (1996) *J Chem Soc Dalton Trans*, p 17
80. Dickens RS, Parker D, de Sousa AS, Williams JAG (1996) *Chem Commun*, p 697
81. Hass Y, Stein G (1971) *J Phys Chem* 75:1093
82. Stein G, Wurzburg E (1975) *J Chem Phys* 62:208

83. Beeby A, Clarkson IM, Dickens RS, Faulkner S, Parker D, Royle L, de Sousa AS, Williams JAG, Woods M (1999) *J Chem Soc Perkin Trans 2*, p 493
84. Shinoda S, Miyake H, Tsukube H (2005) *Handbook of the physics and chemistry of rare earths*, vol 35. Elsevier, The Netherlands
85. Lowe MP, Parker D, Reany O, Aime S, Botta M, Castellano G, Gianolio E, Pagliarin R (2001) *J Am Chem Soc* 123:7601
86. Lehn J-M (1990) *Angew Chem Int Ed* 29:1304
87. de Silva AP, Gunaratne HQN, Rice TE (1996) *Angew Chem Int Ed* 35:2116
88. Dickins RS, Howard JAK, Maupin CL, Moloney JM, Parker D, Riehl JP, Siligardi G, Williams JAG (1999) *Chem Eur J* 5:1095
89. Beeby A, Parker D, Williams JAG (1996) *J Chem Soc Perkin Trans 2*, p 1565
90. Supkowski RM, Horrocks WD (2002) *Inorg Chem Acta* 340:44
91. Horrocks WD, Sundick DR (1981) *Acc Chem Res* 14:384
92. Beeby A, Clarkson IM, Dickens RS, Faulkner S, Parker D, Royle L, de Sousa AS, Williams JAG, Woods M (1999) *J Chem Soc Perkin Trans 2*, p 493
93. Suarez S, Mamula O, Scopelliti R, Donnio B, Guillion d Terazzi E, Piguët C, Bünzli J-CG (2005) *New J Chem* 29:1323
94. Horrocks WD, Sudnick DR (1979) *Science* 206:1194
95. Bünzli J-CG, Wessner D (1981) *Helvet Chim Acta* 64:582
96. Tsukube H, Shinoda S (2002) *Chem Rev* 102:2389
97. Tsukube H, Shinoda S, Tamiaki H (2002) *Coord Chem Rev* 226:227
98. Balzani V, Berghmans E, Lehn JM, Sabbatini N, Terode R, Ziessel R (1990) *Helv Chim Acta* 73:2083
99. Ziessel R, Lehn J-M (1990) *Helv Chim Acta* 73:1149
100. Lehn J-M, Ziessel R (1987) *Chem Commun*, p 1292
101. Thompson MK, Botta M, Nicolle G, Helm L, Aime S, Merbach AE, Raymond KN (2003) *J Am Chem Soc* 125:14274
102. Rodriguez-Ubis J-C, Alpha B, Plancheral D, Lehn J-M (1984) *Helv Chim Acta* 67:2264
103. Alpha B, Lehn J-M, Mathis G (1987) *Angew Chem Int Ed Engl* 26:266
104. Lehn J-M, Roth CO (1991) *Helv Chim Acta* 74:572
105. Blasse G, Dirksen GJ, van der Voort D, Sabbatini N, Perathoner S, Lehn J-M, Alpha B (1988) *Chem Phys Lett* 146:347
106. Alpha B, Balzani V, Lehn J-M, Perathoner S, Sabbatini N (1987) *Angew Chem Int Ed Engl* 26:1266
107. Xue G, Bradshaw JS, Kent N, Dalley P, Savage B, Izatt RM, Prodi L, Monalti M, Zaccheroni N (2002) *Tetrahedron* 58:4809
108. Paul-Roth CO, Lehn J-M, Guilhem J, Pascard C (1995) *Helv Chim Acta* 78:1895
109. Pietraszkiewicz M, Karpiuk J, Kumar RA (1993) *Pure Appl Chem* 65:563
110. Alpha B, Anklam E, Deschenaux R, Lehn J-M, Pietraszkiewicz M (1988) *Helv Chim Acta* 71:1042
111. Lehn J-M, Pietraszkiewicz M, Karpiuk J (1990) *Helv Chim Acta* 73:106
112. Prodi L, Maestri M, Balzani V (1991) *Chem Phys Lett* 180:45
113. Atwood JL, Davies JED, Macnicol DD, Vogtle F, Lehn J-M (eds) (1996) *Comprehensive supramolecular chemistry*, vol 1. Pergamon, Oxford
114. Sabbatini N, Guardigli M, Mecati A, Balzani V, Ungaro R, Ghidini E, Casnati A, Pochini A (1990) *Chem Commun*, p 878
115. Sato N, Yoshida I, Shinkai S (1993) *Chem Lett*, p 621
116. Steemers FJ, Verboom W, Reinhoudt DN, van der Tol EB, Verhoeven JW (1995) *J Am Chem Soc* 117:9408
117. Ulrich G, Ziessel R (1994) *Tetrahedron Lett* 35:6299

118. Galup C, Couchet JM, Picard C, Tisnes P (2001) *Tetrahedron Lett* 42:6275
119. Beeby A, Bushby LM, Maffeo D, Williams JAG (2000) *J Chem Soc Perkin Trans 2*, p 1281
120. Quici S, Marzanni G, Cavazzini M, Anelli PL, Botta M, Gianolio E, Accorsi G, Araroli N, Barigelletti F (2002) *Inorg Chem* 41:2777
121. Yamada T, Shinoda S, Sugimoto H, Uenishi J-I, Tskube H (2003) *Inorg Chem* 42:7932
122. Yamada T, Shinoda S, Tskube H (2002) *Chem Commun*, p 1218
123. Charbonniere LJ, Ziessel R, Monalti M, Prodi L, Zacheroni N, Boehme C, Wipff G (2002) *J Am Chem Soc* 124:7779
124. Montalti M, Prodi L, Zacheroni N, Charonniere L, Douce L, Ziessel R (2001) *J Am Chem Soc* 123:12694
125. Bruce JI, Dickens RS, Govenlock LJ, Gunnlaugsson T, Lopinski S, Lowe MP, Parker D, Peacock RD, Perry JJB, Aime S, Botta M (2000) *J Am Chem Soc* 122:9674
126. Dickins RS, Gunnlaugsson T, Parker D, Peacock RD (1998) *Chem Commun*, p 1643
127. Dickins RS, Love CS, Puschmann H (2001) *Chem Commun*, p 2308
128. Atkinson P, Murray BS, Parker D (2006) *Org Biomol Chem* 4:3166
129. Bazzicalupi TC, Bencini A, Bianchi A, Giogi C, Fusi V, Masotti A, Valtancoli B, Roque A, Pina F (2000) *Chem Commun*, p 56
130. Gunnlaugsson T, Leonard JP, Mulready S, Nieuwenhuyzen M (2004) *Tetrahedron* 60:105
131. Gunnlaugsson T, Harte AJ, Leonard JP, Nieuwenhuyzen M (2002) *Chem Commun*, p 2134
132. Gunnlaugsson T, Harte AJ, Leonard JP, Nieuwenhuyzen M (2003) *Supramol Chem* 15:505
133. Harte AJ, Jensen P, Plush SE, Kruger PE, Gunnlaugsson T (2006) *Inorg Chem* 45:9465
134. Magennis SW, Craig J, Gardner A, Fucassi F, Gragg PJ, Robertson N, Parson S, Pikramenou Z (2003) *Polyhedron* 22:745
135. Li C, Wong W-T (2002) *Chem Commun*, p 2034
136. Li C, Wong W-T (2004) *Tetrahedron Lett* 45:6055
137. Pope SJA, Burton-Pye BP, Berridge R, Khan T, Skabara PJ, Faulkner S (2006) *Dalton Trans*, p 2907
138. Faulkner S, Burton-Pye BP, Khan T, Martin LR, Wray SD, Skabara PJ (2002) *Chem Commun*, p 1668
139. Lowe MP, Parker D (2000) *Chem Commun*, p 707
140. Lowe MP, Parker D (2001) *Inorg Chim Acta* 317:163
141. Yu J, Parker D, Pal R, Poole RA, Cann MJ (2006) *J Am Chem Soc* 128:2294
142. Bretonnière Y, Cann MJ, Parker D, Slater R (2004) *Org Biomol Chem* 2:1624
143. Poole RA, Kielar F, Richardson SL, Stenson PS, Parker D (2006) *Chem Commun*, p 4084
144. Parker D, Yu JH (2005) *Chem Commun*, p 3141
145. Pandya S, Yu J, Paker D (2006) *Dalton Trans*, p 2757
146. Leonard JP, dos Santos CMG, Plush SE, McCabe T, Gunnlaugsson T (2007) *Chem Commun*, p 129
147. de Silva AP, Gunaratne HQN, Rice TE, Stewart S (1997) *Chem Commun*, p 1891
148. Parker D, Senanayake K, Williams JAG (1997) *Chem Commun*, p 1777
149. Parker D, Senanayake K, Williams JAG (1998) *J Chem Soc, Perkin Trans 2*, p 2129
150. Parker D, Williams JAG (1998) *Chem Commun*, p 245
151. Govenlock LJ, Mathieu CE, Maupin CL, Parker D, Riehl JP, Sligardi C, Williams JAG (1999) *Chem Commun*, p 1699
152. Gunnlaugsson T, Parker D (1998) *Chem Commun*, p 511

153. Gunnlaugsson T, McCoy CP, Stomeo F (2004) *Tetrahedron Lett* 45:8403
154. McCoy CP, Stomeo F, Plush SE, Gunnlaugsson T (2006) *Chem Mater* 18:4336
155. Gunnlaugsson T, Mac Donnell DA, Parker D (2001) *J Am Chem Soc* 123:12866
156. Gunnlaugsson T, Mac Donnell DA, Parker D (2000) *Chem Commun*, p 93
157. Gunnlaugsson T (2001) *Tetrahedron* 42:8901
158. Reany O, Gunnlaugsson T, Parker D (2000) *Chem Commun*, p 473
159. Reany O, Gunnlaugsson T, Parker D (2000) *J Chem Soc Perkin Trans 2*, p 1819
160. Gunnlaugsson T, Leonard JP (2005) *Dalton Trans*, p 3204
161. Gunnlaugsson T, Leonard JP (2003) *Chem Commun*, p 2424
162. Gunnlaugsson T, Plush SE (2007) *Org Lett* 7:1919
163. Hanaoka K, Kikuchi K, Kojima H, Urano Y, Nagano T (2003) *Angew Chem Int Ed* 42:2996
164. Hanaoka K, Kikuchi K, Kojima H, Urano Y, Nagano T (2004) *J Am Chem Soc* 126:12470
165. Pope SJA, Laye RH (2006) *Dalton Trans*, p 3108
166. Aarons RJ, Notta JK, Meloni MM, Feng JH, Vidyasagar R, Narvainen J, Allan S, Spencer N, Kauppinen RA, Snaith JS, Faulkner S (2006) *Chem Commun*, p 909
167. Hamblin J, Abboyi N, Lowe MP (2005) *Chem Commun*, p 657
168. Gunnlaugsson T, Leonard JP, Sénéchal K, Harte AJ (2003) *J Am Chem Soc* 125:12062
169. Li C, Law G-L, Wong W-T (2004) *Org Lett* 6:4841
170. Senegas J-M, Koeller S, Bernardinelli G, Piguët C (2005) *Chem Commun*, p 2235
171. Floquet S, Borkovec M, Bernardinelli G, Pinto A, Leuthold L-A, Hopfgartner G, Imbert D, Bünzli J-CG, Piguët C (2004) *Chem Eur J* 10:1091
172. Elhabiri M, Hamacek J, Bünzli J-CG (2004) *Eur J Inorg Chem*, p 51
173. Cantuel M, Bernardinelli C, Muller G, Riehl JP, Piguët C (2004) *Inorg Chem* 43:1840
174. Imbert D, Cantuel M, Bünzli J-CG, Bernardinelli C, Piguët C (2003) *J Am Chem Soc* 125:15698
175. Herrera JM, Ward MD, Adams H, Pope SJA, Faulkner S (2006) *Chem Commun*, p 1851
176. Bassett AP, Magennis SW, Glover PB, Lewis DJ, Spencer N, Parson S, Williams RM, De Cola L, Pikramenou Z (2004) *J Am Chem Soc* 126:9413
177. Klink SI, Keizer HF, van Veggel CJM (2000) *Angew Chem Int Ed* 39:4319
178. Sambrook MR, Curiel D, Hayes EJ, Beer PD (2006) *New J Chem* 30:1130
179. Beer PD, Szemes F, Passaniti P, Maestri M (2004) *Inorg Chem* 43:3965
180. Gunnlaugsson T, Leonard JP, Sénéchal K, Harte AJ (2004) *Chem Commun*, p 782
181. Paris J, Gameraio C, Humblet V, Mohapatra PK, Jacques V, Desreux JF (2006) *Inorg Chem* 45:5092
182. Livramento JB, Tóth É, Sour A, Borel A, Merbach AE, Ruloff R (2005) *Angew Chem Int Ed* 44:1480
183. Sénéchal-David K, Leonard JP, Plush SE, Gunnlaugsson T (2006) *Org Lett* 8:2727
184. Sénéchal-David K, Pope SJA, Quinn S, Faulkner S, Gunnlaugsson T (2006) *Inorg Chem* 45:10040
185. Faulkner S, Burton-Pye BP (2005) *Chem Commun*, p 259
186. Coppo P, Duati M, Kozhevnikov VN, Hofstraat JW, De Cola L (2005) *Angew Chem Int Ed* 44:1806
187. Ward MD (2007) *Coord Chem Rev* 251:1663

Photochemistry and Photophysics of Coordination Compounds: Rhenium

Robert A. Kirgan² · B. Patrick Sullivan¹ (✉) · D. Paul Rillema²

¹Department of Chemistry, University of Wyoming, Laramie, WY 82071-3838, USA
bpat@uwyo.edu

²Department of Chemistry, Wichita State University, Wichita, KS 67260, USA

1	Introduction	46
2	Complexes with Metal-element Multiple Bonds	46
2.1	High-valent Oxorhenium Complexes	46
2.2	Complexes with the ReO ₂ ⁺ Core	48
2.3	Nitridorhenium Complexes	52
3	Complexes of Re(II)	53
4	Rhenium Hydride Complexes	54
5	Complexes with Rhenium – Rhenium Bonds	54
6	Complexes of Re(I) with Pyridine and Diimine Ligands	55
6.1	Photophysical Properties	56
6.2	Photophysical Mechanisms	69
6.3	Transient Detection	75
6.4	Photochemistry	76
6.5	Polymer Systems	80
6.6	Molecular Polygons	82
6.7	Host-Guest Molecules	85
6.8	Carbon Dioxide Reduction	86
6.9	Bioinorganic Applications	87
6.10	Light Emitting Devices	91
6.11	Sensors	93
7	Other Re(I) Carbonyl Complexes	95
	References	97

Abstract This review describes recent advances in the photochemistry of complexes of the element rhenium. It covers not only fundamental chemistry but the recent applications of these complexes to supramolecular chemistry, carbon dioxide reduction, bioinorganic chemistry, sensors, and light-emitting devices.

Keywords Photochemistry · Photophysics · Rhenium · Luminescence · Excited-state

Abbreviations

DFT density functional theory

TDDFT time dependent density functional theory

MLCT	metal to ligand charge transfer
LMCT	ligand to metal charge transfer
HOMO	highest occupied molecular orbital
AOM	angular overlap model
RHF	restricted Hartree-Fock

1

Introduction

The photochemistry of rhenium complexes occupies a prominent position in the photochemistry of transition metal complexes. Along with early preparative studies on photosubstitution of carbonyl species like $\text{Re}(\text{CO})_5\text{X}$, the preparation of the remarkably stable yellow complex *fac*- $\text{Re}(\text{CO})_3(\text{phen})\text{Cl}$ foreshadowed the discovery of the a large class of related luminescent materials by Wrighton and co-workers in the 1970s [1]. As pointed out by Vogler and Kunkley, the current photochemistry of rhenium complexes is rich, spanning eight oxidation states from formal $\text{Re}(0)$ (for example, $\text{Re}_2(\text{CO})_{10}$) to formal $\text{Re}(\text{VII})$ (for example MeReO_3) [2].

This review covers recent developments in the photochemistry of rhenium complexes and covers approximately the last five years. Older literature is referred to when it clarifies or substantiates the newer studies. Like all reviews, the perspective of the authors is offered here. In general, we have not reviewed preparative photochemistry when it is not a primary focus of the study, or where it does not offer chemical insight. We refer the reader instead to the earlier monographs on transition metal photochemistry, which are the best source for these important preparative procedures [1, 3–5]. We have reported the studies that best characterize the state of the field as far as the significant fundamental photochemical advances, and the applications of the photochemistry of rhenium complexes. The organization of this review follows the complex type in terms of the structure and formal oxidation state. Not surprisingly given the history of rhenium photochemistry, the bulk of the work has been published in the area of polypyridine and other dimine ligands involving $\text{Re}(\text{I})$ with carbon monoxide as a coligand. Many of these studies emphasize applications of excited states properties of this class of complex, for example, sensors and photocatalysis among others.

2

Complexes with Metal-element Multiple Bonds

2.1

High-valent Oxorhenium Complexes

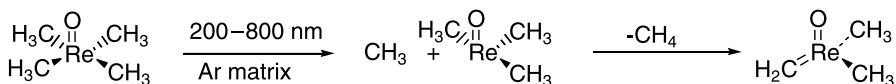
Low temperature Ar matrix studies of the mixed methyl-oxo complexes MeReO_3 , Me_3ReO_2 and Me_4ReO have been fruitful in characterizing their

photochemistry both directly through IR and Raman spectroscopic measurements (with isotopic labeling) and indirectly by reference to supporting DFT calculations. Interest in these complexes stems from the utility of MeReO_3 in olefin metathesis reactions. Broadband irradiation of Me_3ReO_2 (200–800 nm) in an Ar matrix leads to methane elimination and the formation of the methyldene complex $\text{H}_2\text{C} = \text{ReMeO}_2$ (Eq. 1), which is assigned a distorted tetrahedral structure [6]. A secondary photolysis also occurs to possibly yield a derivative tentatively assigned as $(\text{H}_2\text{C})\text{Re}(\text{O})\text{OH}$.



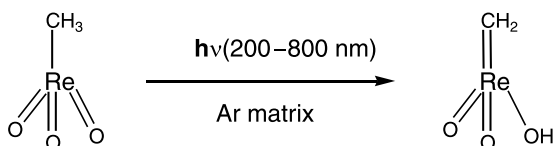
Equation 1

Likewise, irradiation of Me_4ReO also leads to methane elimination and the formation of $\text{H}_2\text{C} = \text{Re}(\text{O})\text{Me}_2$, as shown in Eq. 2, via methyl radical involvement [7, 8].



Equation 2

A similar chemical motif (methyl radical elimination) had been observed earlier with MeReO_3 (here with 254 nm irradiation in an Ar matrix) where both deuterium and C-13 labeling studies and IR spectroscopy had been utilized to characterize the methyldene photo product, $\text{H}_2\text{C} = \text{ReO}_2(\text{OH})$ (Eq. 3) [9]. Previous studies had identified the $\text{Re} - \text{Me}$ bond cleavage reaction as the primary process in higher temperature nonaqueous solutions [2]. It is proposed that in the caged low temperature environment of the Ar matrix the primary step is also $\text{Re} - \text{Me}$ bond cleavage, but that the methyl radical recombines to form the methyldene complex. Interestingly, broad band irradiation eventually leads to an apparent CO complex, tentatively assigned as $\text{H}_2\text{Re}(\text{CO})\text{O}(\text{OH})$. For both MeReO_3 and MeReO_4 complexes DFT calculations suggest that the excited states responsible for the transformations in



Equation 3

Equations 1–3 have substantial Re – Me to metal-oxo character, thus providing a weakening of the Re – Me bond in the excited state. In addition, in the MeReO_4 case, there is possibility of the population of orbitals that are antibonding with respect to the Re – Me bond.

A recent re-investigation of the electronic structure of MeReO_3 by both DFT/TDDFT and more highly correlated methods leads to the conclusion that the second transition (ca. 240 nm) has both methyl carbon and oxo character (by DFT/TDDFT). Use of CASSCF/MS-CASPT2 calculations shows more oxo and less C contribution, demonstrating that the level of theory is important in interpreting the photochemistry [10].

Several reaction products of MeReO_3 have been examined for their photochemical behavior. An example is the reductive photochemistry of the yellow adduct, $(\text{PPh}_3)\text{MeReO}_3$ [11], which possess an absorption at 380 nm that is assigned as a LMCT transition from phosphorus to Re. Irradiation of the complex in methylene chloride initially leads to the formation of triphenylphosphine oxide and a Re(V) complex formulated as MeReO_2 . Further evolution of the reaction gives the putative mixed-valence complex $\text{MeRe}^{\text{V}}(\text{PPh}_3)_2\text{O}_2\text{Re}(\text{O})_3\text{Me}$. A second study is of the photodecomposition of the peroxide complex, $\text{MeRe}(\text{O})(\text{O}_2)_2$, which gives rise to MeReO_3 and O_2 upon irradiation at 260 nm into the intraligand (peroxo) absorption [12]. The primary photochemical step is proposed to involve a radical pair or $[\text{MeRe}(\text{O}_2)(\text{O})]^+$ and superoxide ion.

2.2

Complexes with the ReO_2^+ Core

Ever since the discovery [13] of the luminescence of complexes of the type *trans*- ReO_2L_4^n (where L is for example py, or 4-pic, $n = 1+$ or cyanide, $n = 3-$), there have been a number of fundamental studies highlighting the proton acceptor and electron transfer behavior of the emitting state [4]. For these complexes excitation of the type $^1\text{A}_{1g}$ to $^1\text{E}_{1g}$ (in D_{4h} symmetry) is rapidly followed by intersystem crossing to yield emission from $^3\text{E}_{1g}$ back to the $^1\text{A}_{1g}$ ground state. The excited triplet has electron density redistributed onto the oxo ligands and the empty $d\pi$ orbitals at the metal. Other older work, primarily of Reber and coworkers has concentrated on fundamental photophysical studies relating emission energies and vibrational structure in the emission band to electronic structure [14] of the complexes. Extended Hückel calculations show an expected variation of emission energies with antibonding π type interactions of the in plane ligands with the d_{xy} orbital, which is a component of the HOMO. Therefore, the weaker π -donor ligand would destabilize the HOMO increasing the absorption and emission energies. The actual ordering of $\text{en} < \text{MeIm} < \text{py}$ (en is ethylenediamine and MeIm is 1-methylimidazole) is essentially opposite of the predicted order. Consideration of electron-electron repulsions in a crystal field model allows

the rationalization of the order, predicting an increase in the energy of the $^3E_{1g}$ relative to the $^1A_{1g}$ ground state. This work illustrates the limitations and strengths of simple calculation models to rationalize excited state properties.

The *trans*-dioxo complexes are extremely valuable to transition metal photochemistry because they exhibit well-defined vibrational progressions, which enables the identification of the modes involved in the lowest-energy transition and therefore a quantitative characterization of excited state geometry. In the cases of other emitting states, for example, in many metal-to-ligand charge transfer excited states, this information is largely absent due to severe line broadening, even at low temperatures, which means that indirect fitting procedures must be employed to extract excited state geometries.

Analysis of the emission manifold for ReO_2^+ complexes in general shows two vibrational progressions in their luminescence spectra, one corresponding to a totally symmetric OReO mode and the other a totally symmetric Re–L mode of the in-plane ligands. This was first reported by Winkler and Gray [13], but has been examined in great detail by Savoie and Reber [14] and Grey, Butler and Reber [15, 16]. It was initially noted that the vibronic structure was not consistent with a purely harmonic model. To account for this, coupling of the ground state surface to a single excited state surface, that of an $^1A_{1g}$, was proposed initially from the results of fitting the dual vibrational progressions to a harmonic model. Studies of the pressure dependence

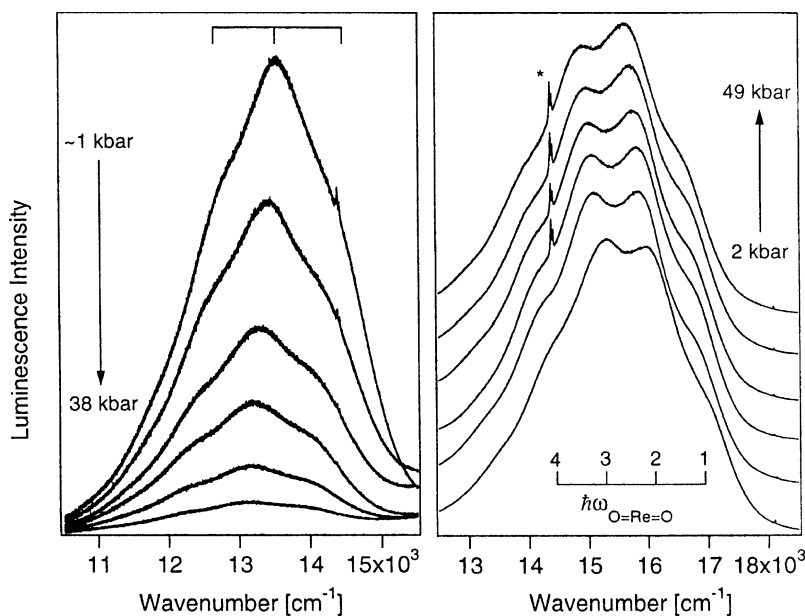


Fig. 1 Examples of pressure dependent emission spectra of $[\text{ReO}_2(\text{en})_2]\text{Cl}$ (left) from 1 to 38 kbar and $[\text{ReO}_2(\text{tmen})_2]\text{Cl}$ from 2 to 49 kbar

of the emission behavior showed, in fact, that this was too simple for complexes with low energy excited states. Although pressure effects on emission spectra can be manifested in both an intra- and intermolecular sense, absence of phase transitions in these molecules point to an intramolecular origin. As pressure is increased, the potential minima of the ground and excited states shift to lower values of the normal coordinate, Q . The excited state surface appears to be more affected leading to a decrease of ΔQ , the difference in these quantities. The net result is pressure-induced changes of not only ΔQ but in the electronic origins, the band maxima and the vibrational frequencies in the excited state. For the Re dioxo complexes, only a model where coupling to two excited state surfaces (both the excited triplet and singlet A_{1g} states) comes into play is sufficient to describe the pressure dependent spectral data (See Fig. 1). This model is shown in Fig. 2. A recent short review summarizes how coupled coordinates arise from the interactions between electronic states with different equilibrium geometries [17].

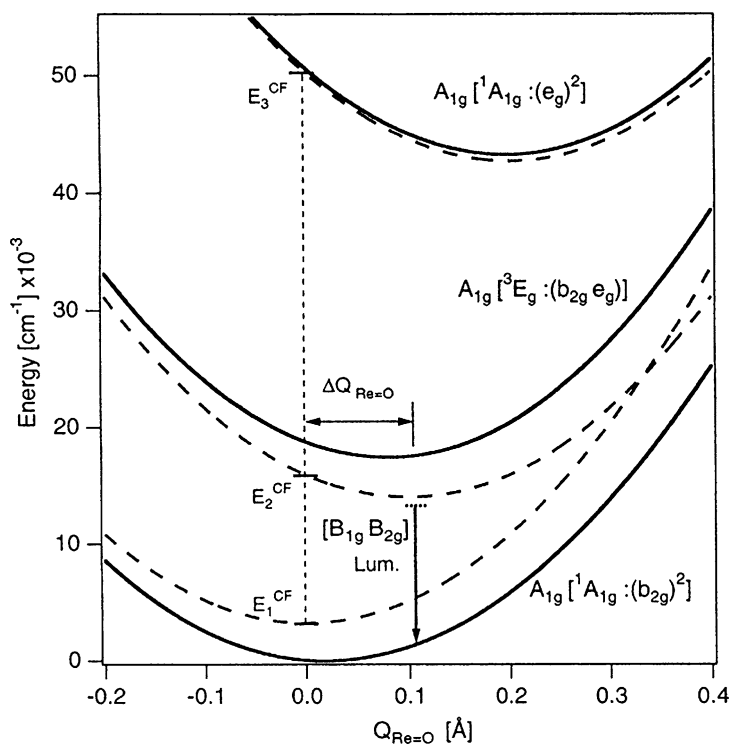


Fig. 2 The model of coupled potential energy surfaces used to explain the vibronic spectral features in Re dioxo complexes. *Solid and dashed lines* represent adiabatic and diabatic surfaces, respectively. The lowest adiabatic surface corresponds to the electronic ground state used to calculate the luminescence spectra. The crystal field energies for all three A_{1g} states are given along the *vertical dashed line*

Several comparative photophysical studies of isoelectronic dioxo complexes of other metals have been published. One compares the emission spectral properties of *trans*-dioxo Os(VI) with that of Re(V) [18]. For complexes of the type *trans*-OsO₂²⁺ and *trans*-ReO₂⁺ containing ethylenediamine, imidazole and oxalate ligands, the emission energies were found to be in the range of 620–900 nm. Even though the Os complexes exhibited unresolved spectra, their band shapes deviated from that expected for a harmonic ground state potential surface. The three surface interaction model was used to describe the discrepancy.

A recent report concerns the emission from the technetium dioxo core, and directly compares the appropriate Re analogs [19]. Emission from complexes of the formulation *trans*-TcO₂(L)₄ⁿ (L is py or pic, *n* is 1+; L is CN, *n* is 3-) occurs ca. 0.2 eV below that of the Re analogs. The relative lower energy for the *trans*-TcO₂⁺ core is predicted by TDDFT calculations, as is an electronic structure that closely mirrors that of the Re analogs. Low temperature spectra show the similar vibrational progressions for the Tc complexes as for Re, consisting of a dominant O=Tc=O symmetric mode and a Tc-L symmetric, in plane mode that is displaced ca. 50 cm⁻¹ to lower energy due to the differences in the metals. Comparison of the vibrational structure for the *trans*-[MO₂(pic)₄]BPh₄ complexes is shown in Fig. 3. Although more comparisons of isoelectronic metal complexes are needed it appears that the emission maxima for presumed isostructural complexes *trans*-MO₂L₄ⁿ vary in the order Re > Os > Tc.

Preparative studies and luminescence studies have been conducted on the diphosphine derivative *trans*-O₂Re(dmppe)₂⁺, including an X-ray crystal structure of this complex (dmppe is 1,2-*bis*(di-4-methylphenylphosphino)ethane) [20]. The complex excited state emits both in the solid state and in CH₃CN solution with a 1.1 μs lifetime in the solid. The emission energy is

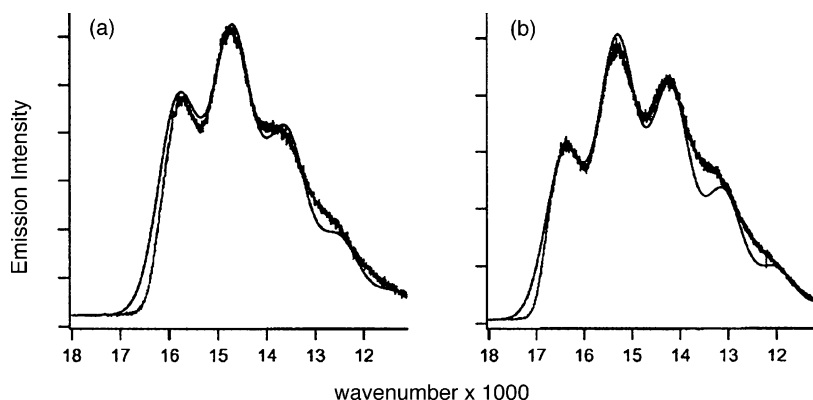


Fig. 3 Experimental (*thick noisy line*) and calculated (*fitted solid line*) emission spectra for ReNCl₂(PCy₃)₂ (a) and ReNBr₂(PCy₃)₂. The *fitted line* is consistent with a lengthening of the ReN bond in the excited state of ca. 0.08–0.09 Å

similar to that of other derivatives (broad 596–612 nm) and is likely a composite emission from ${}^3B_{2g}$ and ${}^3B_{3g}$ excited states due to the lowered (D_{2h}) symmetry. Low temperature (77 K) spectra also show vibrational structure – presumably due to the symmetric OReO mode.

2.3

Nitridorhenium Complexes

Complexes of the type *trans*-NRe(diphos)Cl⁺ and *trans*-NRe(dmppe)Lⁿ (where diphos is a 1,2-*bis*(diphenylphosphino)ethane substituted in the four positions with methyl and fluoro substituents and L is either Cl or CH₃CN) are luminescent in both the solid state and in CH₃CN solution [20]. It is likely that the emission is derived from the (d_{xy})¹(d_{xz})¹ [3B_2] and (d_{xy})¹(d_{yz})¹ [3B_1] excited states, whose weak absorptions occur in the 390–500 nm region. The vibrational structure in the transition corresponds to the ReN modes, which supports this assignment. Higher energy, intense absorptions have been tentatively assigned to overlapping LMCT (involving N and/or Cl ligands) and π - π^* transition localized on the phosphine. Remarkably, the *trans*-NRe(dmppe)(CH₃CN)²⁺ exhibits a lifetime of 8.1 μ s in deaerated CH₃CN whereas the other complexes are all less than 0.1 μ s. The first reported reductive electron transfer quenching studies of Re-nitrido complexes show that they are moderately potent excited states oxidants. For example, *trans*-NRe(dmppe)(CH₃CN)²⁺ exhibits a value of + 1.39 V (NHE) from a Marcus analysis of the bimolecular rate constants for a series of arylamine quenchers.

Like the Re-dioxo complexes, Re-nitrido complexes exhibit vibrational structure at low temperature making the determination of excited state distortions possible. The study of a series of *five-coordinate* pseudo-square pyramidal complexes of the type ReNX₂(PR₃)₂, where the nitrido ligand is apical, demonstrates this quite nicely (X = Cl or Br, R is phenyl or cyclohexyl) [21]. The excited state arises from a d_{xy} to d_{yz} transition where the latter orbital is mixed in an antibonding fashion with N_p functions. The nitridorhenium frequencies for the complexes occur in the range 1095–1101 cm⁻¹ as seen in Fig. 4. Fitting the vibronic components in the complexes gives a Re–N bond length that is 0.08–0.09 Å longer in the excited state, consistent with the antibonding contribution of the nitrido ligand and also consistent with a reduction in bond order from 3 to 2.5.

The trends in the emission energies (origins) are rationalized by AOM calculations that show that the phosphine tunes the transition very little because the change in energy for the d_{xy} to d_{yz} transition contains only terms for halide and nitride ligands. Accordingly, the E_{00} decreases by 425–600 cm⁻¹ upon substitution of Br with Cl, because chloride as the better π -donor, destabilizes the filled d_{xy} orbital.

Photolysis of *trans*-NRe(CN)₄(H₂O)²⁻ in water with added ethylenediamine is reported to yield a dimeric product, where two distorted octahedral

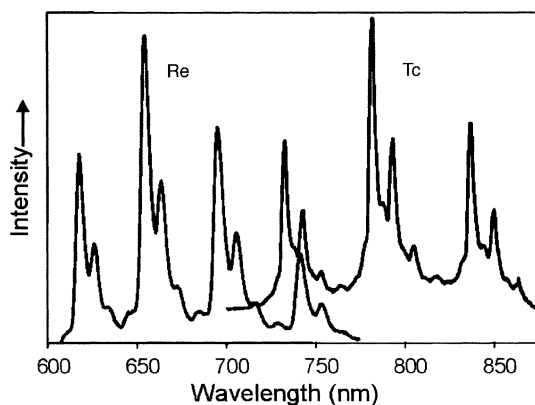


Fig. 4 Structure on the low-temperature emission spectra of $[\text{MO}_2(\text{pic})_2]\text{BPh}_4$. *Left* spectrum is for $\text{M}=\text{Re}$, *right* for $\text{M}=\text{Tc}$

Re centers are bridged by an en ligand [22]. Apparently this reaction, which involves displacement of water is not thermally rapid under the synthesis conditions. The study appears to be the first example of photosubstitution of a rhenium-nitrido complex.

3

Complexes of Re(II)

There are several classes of Re(II) complexes that exhibit luminescence in both solution and in the solid state, the cyclopentadienyl systems Cp_2Re and Cp^*_2Re [23] and the singular case of the homoleptic diphosphine, $\text{Re}(\text{dmpe})_3^{2+}$ (Cp^* is pentamethylcyclopentadienyl) [24]. Emission has been shown to be LMCT in nature (Re – P sigma bond to $d\pi$ Re(II)). These complexes are also rare examples in transition metal photochemistry of doublet-double emission, i.e., a fluorescence.

A new study of the excited state properties of $\text{Re}(\text{dmpe})_3^{2+}$ and its Tc analog, demonstrates that both complexes have among the highest excited state oxidation potentials of any simple coordination complex, a property that was not previously recognized [25]. This was ascertained by reductive quenching (in CH_3CN) with a series of aromatic hydrocarbons and the use of a Rehm–Weller analysis. The latter analysis is reminiscent of excited state potential determinations for organic singlet states. The complexes were found to have potentials of +2.61 and +2.52 (Re and Tc, respectively) compared to the saturated calomel electrode. The nature of the quenching as electron transfer from the hydrocarbon was supported by a novel steady state photolysis experiment where the radical cation of 10-methyl phenothiazine was photocatalytically produced using the autoxidation of $\text{Re}(\text{dmpe})_3^+$ to regenerate

$\text{Re}(\text{dmpe})_3^{2+}$. Of interest is that both complexes make available extremely oxidizing excited states using a visible photon, since their absorption and emission energies are 528 nm (600 nm) for Re, and 590 nm (681 nm) for Tc, respectively. Unrestricted open shell TDDFT calculations confirm the nature of the transitions as LMCT and predict the proper relative energies of Re versus Tc.

4

Rhenium Hydride Complexes

Rhenium is an element known for its abundance of metal hydride complexes spanning a variety of oxidation states, for example, from Re(I), $\text{Re}(\text{CO})_5\text{H}$ to Re(VII), ReH_9^{2-} . However, despite the recent interest in light-driven H_2 formation from different substrates (such as water) there are few recent photochemical studies of Re hydride complexes.

The complex $\text{CpRe}(\text{PPh}_3)_2\text{H}_2$ has been of primary concern because of its thermal and photochemically-induced C – H activation chemistry [26, 27]. Upon UV photolysis the complex undergoes PPh_3 substitution with a variety of entering groups (L), for example, phosphine, CO or ethylene to yield both $\text{CpRe}(\text{L})(\text{PPh}_3)\text{H}_2$ and CpReL_2H_2 . The ratio of the products depends upon reaction conditions and entering group. Under similar conditions, the complex $\text{CpRe}(\text{PPh}_3)\text{H}_4$ undergoes photolysis to lose dihydrogen and capture a ligand, regenerating a $\text{CpRe}(\text{L})(\text{PPh}_3)\text{H}_2$ type structure.

Theoretical studies have been published concerning complexes of the formulation $\text{M}(\text{chelate})(\text{CO})_3\text{H}$ (M is Mn and Re and chelate is a diazabutadiene ligand, for example, the parent, *cis*- $\text{HN}=\text{C}(\text{H})(\text{H})\text{C}=\text{NH}$). These point to a rich photoreactivity similar to the alkyl derivatives (see later) that arises from potential surfaces accessible from the initially formed MLCT excited manifold [28, 29]. The initially formed states are predicted to be photodissociative by virtue of mixing of the sigma-bond to ligand (π^*) charge transfer (SBLCT) excited state configurations into the MLCT excited state configurations, which are multiplicity dependent. Experimental results for Mn complexes have previously been published, and the calculations suggest that the photoreactivity of the Re analogs will be enhanced relative to those because of greater mixing of configurations. This metal hydride chemistry should be fertile area for future research.

5

Complexes with Rhenium – Rhenium Bonds

Measurement of action spectra for the photolysis of $\text{M}_2(\text{CO})_{10}$ (M is Mn or Re) provides new evidence for the excited state origin of the well-studied

primary photoprocesses [30] in these systems, i.e., metal-metal bond homolysis yielding $\text{Re}(\text{CO})_5$, and CO loss yielding $\text{Re}_2(\text{CO})_9\text{L}$ [31]. For Mn, using the appropriate traps in investigating the wavelength dependence, it was found that both photoprocesses could occur from the low-lying excited states, but that higher energy excitation clearly favors the CO loss pathway. However, the data do not clearly establish that all the metal-metal bond cleavage comes from surface crossing to the $^3(\sigma-\sigma^*)$ photodissociative state. For Re, the mechanism appears more complex, with population of the upper states also leading to the cleavage of the metal-metal bond. It is noted here that the role of solvent (as opposed to the complexes in the gas phase) in determining the shapes of the potential surface may profoundly affect the photochemistry.

Recent work has focused on the substituted dimer, $[\text{fac-Re}(\text{bpy})(\text{CO})_3]_2$ partially because of its potential involvement in photocatalytic processes, for example, CO_2 reduction (see later). A fundamental question that has been explored is why a metal-metal bond cleavage is different for this complex than for $\text{Re}_2(\text{CO})_{10}$. Fujita and Muckerman have attempted to answer this by employing DFT, RHF and MP2 calculations [32]. They find that the most stable ground state geometry is a skewed, *cis* conformation, which is in agreement with experimental data. For this geometry the $\sigma^*(\text{MM})$ excited state is not immediately accessible, i.e., excitation followed by rearrangement would be necessary to achieve bond cleavage. Of note is that upon photolysis in THF, the radical, $\text{Re}(\text{bpy})(\text{CO})_3$ is produced, though inefficiently compared to $\text{Re}_2(\text{CO})_{10}$. Apparently, solvation rapidly results in the formation of $[\text{Re}(\text{bpy})(\text{CO})_3(\text{THF})]$, which has an apparent dimerization rate that is much slower than $\text{Re}(\text{CO})_5$. It is suggested that this is due to blocking of the coordination site by the THF ligand.

Earlier work had examined the apparent dimerization rate of $[\text{Re}(\text{dmbpy})(\text{CO})_3(\text{THF})]$ (dmbpy is 4,4'-dimethyl-2,2'-bipyridine) in competition with CO_2 . In this case the slow rate is an advantage for the reduction reaction to compete [33]. Apparently, the complex yields CO through an intermediate CO_2 bridged dimer formulated as $[(\text{dmbpy})\text{Re}(\text{CO})_3]_2(\text{CO}_2)$.

6

Complexes of Re(I) with Pyridine and Diimine Ligands

Complexes of Re(I) containing polypyridine or diimine donors, usually with three carbon monoxide co-ligands, continue to be an intense area of interest. These studies will be described under the following headings: photophysical properties, photophysical mechanisms, transient detection, photochemical properties, polymer systems, molecular polygons, guest-host molecules, carbon dioxide reduction, bioinorganic applications and usages as sensors and light emitting-diodes.

6.1 Photophysical Properties

Photophysical properties of the rhenium(I) bi- and tricarbonyl complexes with pyridine and polypyridine ligands of note are summarized in Tables 1–4. In addition to the carbonyl ligands, the complexes contain the diimine ligand located in the left hand column; the monodentate ligands labeled L_x are shown in Figs. 5–12 at the end of the tables. Information about the photophysical properties of the rhenium complexes are listed in the remaining columns sequentially according the solvent used in the study, the temperature of the measurement, the excitation wavelength, the emission wavelength, the emission quantum yield and the emission lifetime (in the tables the emission and excitation wavelength is in nm). The references in the right hand column can be consulted for additional details.

In Table 1, the diimine ligands were either 2,2'-bipyridine or 1,10-phenanthroline, or one of their derivatives, although 2,2'-bipyrazine and derivatives of 2,2'-bipyrimidine are also listed. Some monodentate chelating ligands contained one or more pyridine functionality and could bind an

Table 1 Rhenium tricarbonyl complexes with multidentate ligands

Complex	Solvent	Temp (K)	Ex.	Em.	QY	Life (ns)	Refs.
Re(CO) ₃ (bpy)(L1) ⁺	CH ₂ Cl ₂	273	350	568	0.007	550	[34]
Re(CO) ₃ (bpy)(L2) ⁺	CH ₂ Cl ₂	273	350	563	0.044	610	[34]
Re(CO) ₃ (dmb)(L1) ⁺	CH ₂ Cl ₂	273	350	558	0.008	570	[34]
Re(CO) ₃ (dmb)(L2) ⁺	CH ₂ Cl ₂	273	350	552	0.049	740	[34]
Re(CO) ₃ (phen)(L1) ⁺	CH ₂ Cl ₂	273	350	552	0.012	2040	[34]
Re(CO) ₃ (phen)(L2) ⁺	CH ₂ Cl ₂	273	350	549	0.061	3080	[34]
Re(CO) ₃ (3,4,7,8-Mephen)(L1) ⁺	CH ₂ Cl ₂	273	350	525	0.002	520	[34]
Re(CO) ₃ (3,4,7,8-Mephen)(L2) ⁺	CH ₂ Cl ₂	273	350	515	0.075	12 500	[34]
Re(CO) ₃ (L3)Cl	CH ₂ Cl ₂	298	436	576	–	< 100	[35]
	Glass	77	436	526	–	–	
	LB Film	298	430	–	–	–	
Re(CO) ₃ (L4)Cl	CH ₂ Cl ₂	298	488	615	–	< 100	[35]
	Glass	77	488	536	–	–	
Re(CO) ₃ (L5)Cl	CH ₂ Cl ₂	298	430	–	–	–	[35]
Re(CO) ₃ (L6)Cl	CH ₂ Cl ₂	298	430	–	–	–	[35]
Re(CO) ₃ (bpy)(L7) ⁺	CH ₂ Cl ₂	298	396	554	–	< 100	[35]
	Glass	77	396	492	–	–	
	LB Film	298	388	–	–	–	
Re(CO) ₃ (bpy)(L8) ⁺	CH ₂ Cl ₂	298	370	540	–	< 100	[35]
	Glass	77	370	492	–	–	
	LB Film	298	366	530	–	–	

Table 1 (continued)

Complex	Solvent	Temp (K)	Ex.	Em.	QY	Life (ns)	Refs.
Re(CO) ₃ (bpy)(L9) ⁺	CH ₂ Cl ₂	298	370	536	–	< 100	[35]
	Glass	77	370	494	–	–	
	LB Film	298	366	–	–	–	
Re(CO) ₃ (L10)Cl	CH ₂ Cl ₂	298	400	–	–	–	[35]
	Glass	77	400	622, 675	–	–	
Re(CO) ₃ (bpy)(L11) ⁺	CH ₂ Cl ₂	298	344	550	–	500	[36]
Re(CO) ₃ (phen)(L11) ⁺	CH ₂ Cl ₂	298	450	563	–	200, 1500	[36]
Re(CO) ₃ (bpy)(L12) ⁺	CH ₂ Cl ₂	298	340	530	–	630	[36]
	CH ₃ CN	298	334	540	–	460	
Re(CO) ₃ (phen)(L12) ⁺	CH ₂ Cl ₂	298	400	548	–	2300	[36]
Re(CO) ₃ (bpy)(L13) ⁺	CH ₃ CN	298	346	540	–	–	[36]
Re(CO) ₃ (phen)(L13) ⁺	CH ₂ Cl ₂	298	348	550	–	–	[36]
	CH ₃ CN	298	346	550	–	–	
Re(CO) ₃ (bpy)(L14) ⁺	CH ₃ CN	298	348	540	–	230	[36]
	Solid	298	–	510	–	1500	
	Solid	77	–	500	–	–	
Re(CO) ₃ (phen)(L14) ⁺	CH ₂ Cl ₂	298	368	550	–	2000	[36]
	CH ₃ CN	298	363	571	–	1400	
	Solid	298	–	515	–	1900	
	Solid	77	–	500	–	–	
Re(CO) ₃ (L15)(NCCH ₃) ⁺	CH ₃ CN	298	310	370	–	–	[37]
Re(CO) ₃ (L16)(NCCH ₃) ⁺	CH ₃ CN	298	310	417	–	–	[37]
Re(CO) ₃ (L17)(NCCH ₃) ⁺	CH ₃ CN	298	–	–	–	–	[37]
Re(CO) ₂ (L18)(L19) ⁺	CH ₃ CN	298	~ 380	~ 610	0.003	8450	[38]
	CH ₂ Cl ₂	298	~ 380	~ 610	0.014	8864	
Re(CO) ₂ (L20)(L19) ⁻	CH ₃ CN	298	~ 380	~ 610	0.003	7836	[38]
	CH ₂ Cl ₂	298	~ 380	~ 610	0.011	10 550	
Re(CO) ₃ (phen)(L21) ⁺	CH ₂ Cl ₂	298	–	536	0.25	2690	[39]
	CH ₃ CN	298	–	552	0.079	1370	
	Buffer	298	–	552	0.027	790	
Re(CO) ₃ (phen)(L22) ⁺	CH ₂ Cl ₂	298	–	536	0.30	2920	[39]
	CH ₃ CN	298	–	550	0.13	1750	
	Buffer	298	–	550	0.12	1070	
Re(CO) ₃ (phen)(L23) ⁺	CH ₂ Cl ₂	298	–	540	0.49	2850	[39]
	CH ₃ CN	298	–	554	0.16	1460	
	Buffer	298	–	554	0.096	840	
Re(CO) ₃ (3,4,7,8-Mephen)(L21) ⁺	CH ₂ Cl ₂	298	–	510	0.16	7810	[39]
	CH ₃ CN	298	–	518	0.072	7320	
	Buffer	298	–	522	0.026	11 110	

Table 1 (continued)

Complex	Solvent	Temp (K)	Ex.	Em.	QY	Life (ns)	Refs.
Re(CO) ₃ (3,4,7,8-Mephen)(L22) ⁺	CH ₂ Cl ₂	298	-	516	0.19	13 540	[39]
	CH ₃ CN	298	-	522	0.051	9900	
	Buffer	298	-	518	0.041	14 060	
Re(CO) ₃ (3,4,7,8-Mephen)(L23) ⁺	CH ₂ Cl ₂	298	-	518	0.27	13 280	[39]
	CH ₃ CN	298	-	522	0.12	8540	
	Buffer	298	-	522	0.078	11 620	
Re(CO) ₃ (2,9-diMe-4,7-diPh-phen)(L21) ⁺	CH ₂ Cl ₂	298	-	540	0.22	7220	[39]
	CH ₃ CN	298	-	550	0.079	6780	
	Buffer	298	-	556	0.011	6010	
Re(CO) ₃ (2,9-diMe-4,7-diPh-phen)(L22) ⁺	CH ₂ Cl ₂	298	-	542	0.19	15 480	[39]
	CH ₃ CN	298	-	550	0.13	9410	
	Buffer	298	-	554	0.012	7850	
Re(CO) ₃ (2,9-diMe-4,7-diPh-phen)(L23) ⁺	CH ₂ Cl ₂	298	-	542	0.18	11 650	[39]
	CH ₃ CN	298	-	552	0.053	6960	
	Buffer	298	-	558	0.028	5080	
Re(CO) ₃ (dpz)(L21) ⁺	CH ₂ Cl ₂	298	-	548	0.28	1120	[39]
	CH ₃ CN	298	-	568	0.086	400	
	Buffer	298	-	572	0.034	110	
Re(CO) ₃ (dpz)(L22) ⁺	CH ₂ Cl ₂	298	-	544	0.15	1240	[39]
	CH ₃ CN	298	-	562	0.065	520	
	Buffer	298	-	566	0.033	210	
Re(CO) ₃ (dpz)(L23) ⁺	CH ₂ Cl ₂	298	-	548	0.24	1100	[39]
	CH ₃ CN	298	-	568	0.054	400	
	Buffer	298	-	572	0.032	130	
Re(CO) ₃ (bpy)(L24) ⁺	CH ₂ Cl ₂	298	370	539	0.007	660	[40]
	Glass	77	370	499	-	-	
	LB Film	298	368	527	-	-	
Re(CO) ₃ (bpy)(L25) ⁺	CH ₂ Cl ₂	298	370	540	0.006	700	[40]
	Glass	77	370	492	-	-	
	LB Film	298	366	530	-	-	
Re(CO) ₃ (bpy)(L26) ⁺	CH ₂ Cl ₂	298	364	548	0.078	930	[40]
	Glass	77	364	491, 528, 555	-	-	
	LB Film	298	354	546	-	-	
Re(CO) ₃ (L27)Cl	CH ₂ Cl ₂	298	380	497	0.001	-	[41]
Re(CO) ₃ (L27)(L28) ⁺	CH ₂ Cl ₂	298	380	474	0.003	-	[41]
Re(CO) ₃ (bpy)(L29)	CH ₂ Cl ₂	298	361	571	0.003	-	[42]
	CH ₃ CN	298	345	573	0.004	-	
	Solid	77	361	525	-	-	

Table 1 (continued)

Complex	Solvent	Temp (K)	Ex.	Em.	QY	Life (ns)	Refs.
Re(CO) ₃ (phen)(L29)	CH ₂ Cl ₂	298	353	568	0.022	–	[42]
	CH ₃ CN	298	341	571	0.041	–	
	Solid	77	353	544	–	–	
Re(CO) ₃ (bpy)Cl	1 : 4 H ₂ O : Dioxane pH = 2.5	298	368	605	0.004	29	[43]
		77	368	536	–	2900	
Re(CO) ₃ (L30)Cl	1 : 4 H ₂ O : Dioxane pH = 2.5	298	394	678	0.0001	1.5	[43]
		77	394	580	–	700	
Re(CO) ₃ (L31)Cl	1 : 4 H ₂ O : Dioxane pH = 2.5	298	390	648	0.0002	0.5	[43]
		77	390	541	–	900	
Re(CO) ₃ (L32)Cl	1 : 4 H ₂ O : Dioxane pH = 8	298	375	625	0.002	7	[43]
		77	375	–	–	–	
Re(CO) ₃ (L31)(L33) ⁺	1 : 4 H ₂ O : Dioxane pH = 2.5	298	366 _(sh)	592	0.015	77	[43]
		77	366 _(sh)	523	–	3100	
Re(CO) ₃ (L32)(L33)	1 : 4 H ₂ O : Dioxane pH = 8	298	350 _(sh)	583	0.045	75	[43]
		77	350 _(sh)	–	–	–	
Re(CO) ₃ (L30)(L34) ⁺	1 : 4 H ₂ O : Dioxane pH = 2.5	298	370	612	0.004	12	[43]
		77	370	533	–	1500	
Re(CO) ₃ (L30)(L35)	1 : 4 H ₂ O : Dioxane pH = 8	298	370	610	0.005	10	[43]
		77	370	–	–	–	
Re(CO) ₃ (L30)(L33)	1 : 4 H ₂ O : Dioxane pH = 2.5	298	360	614	0.005	48	[43]
		77	360	521	–	2800	
Re(CO) ₃ (L31)(L34)	1 : 4 H ₂ O : Dioxane pH = 2.5	298	370 _(sh)	605	0.005	12	[43]
		77	370 _(sh)	528	–	1500	
Re(CO) ₃ (L32)(L35) ⁻	1 : 4 H ₂ O : Dioxane pH = 8	298	355 _(sh)	587	0.04	50	[43]
		77	355 _(sh)	–	–	–	
[(Re(CO) ₃ (4,4'-bpy)Br)(L36)] ₂ ^a	CH ₂ Cl ₂	298	352	611	–	86	[44]
[(Re(CO) ₃ (4,4'-bpy)Br)(L37)] ₂ ^a	CH ₂ Cl ₂	298	357	616	–	72	[44]
[(Re(CO) ₃ (4,4'-bpy)Br)(L38)] ₂ ^a	CH ₂ Cl ₂	298	351	616	–	495	[44]
Re(CO) ₃ (bpy)(L39) ⁺	CH ₂ Cl ₂	298	355	426 533			[45]
Re(CO) ₃ (dmb)(L39) ⁺	CH ₂ Cl ₂	298	355	426 533			[45]
Re(CO) ₃ (4,4'-di ^t Bu-bpy)(L29) ⁺	CH ₂ Cl ₂	298	355	426 533			[45]
Re(CO) ₃ (4,4'-di ^t Bu-bpy)(L40) ⁺	CH ₂ Cl ₂	293	360	524	0.39	11 000	[46]

Table 1 (continued)

Complex	Solvent	Temp (K)	Ex.	Em.	QY	Life (ns)	Refs.
Re(CO) ₃ (4,4'-di ^t Bu-bpy)(L41) ⁺	CH ₂ Cl ₂	293	360	552	0.042	2100	[46]
Re(CO) ₃ (L42)Cl	CH ₂ Cl ₂	298	420	722		< 100	[47]
	Glass	77	420	642		1900	
Re(CO) ₃ (L43)Cl	CH ₂ Cl ₂	298	420	695		< 100	[47]
	Glass	77	420	600		3500	
Re(CO) ₃ (L44)Cl	CH ₂ Cl ₂	298	420	633		< 100	[47]
	Glass	77	420	–		–	
Re(CO) ₃ (L45)Cl	CH ₂ Cl ₂	298	420	633		< 100	[47]
	Glass	77	420	–		–	
Re(CO) ₃ (L46)Cl	Benzene	298	480	595		260	[48]
	Solid	298	480	558		< 100	
	Solid	77	480	562		1900	
	Glass	77	480	535		7200	
Re(CO) ₃ (L47)Cl	Benzene	298	580	626		< 100	[48]
Re(CO) ₃ (bpy)(L48) ⁺	CH ₃ CN	293	370	562	0.0018	132	[49]
Re(CO) ₃ (L49)Cl	CH ₂ Cl ₂	298	400	598	0.018	960	[50]
	Glass	77	400	527		456 000	
				570 620			
Re(CO) ₃ (L50)Cl	CH ₂ Cl ₂	298	400	598	0.008	163	[50]
	Glass	77	400	504		30 000	
				543		410 000	
				585			
Re(CO) ₃ (phen)Cl	CH ₂ Cl ₂	298	400	606	0.013	227	[50]
	Glass	77	400	535		7600	
Re(CO) ₃ (phen)(L51) ⁺	C ₂ H ₅ OH	298	364	508	0.77	18 640	[51]
				459, 490		17 080	
	Glass	77		524, 565			
				505, 483	0.70	17 350	[51]
Re(CO) ₃ (4-Mephen)(L51) ⁺	C ₂ H ₅ OH	298	364	505, 483	0.70	17 350	[51]
	Glass	77		461, 495		15 840	
				529, 568			
				505, 481	0.61	15 400	[51]
Re(CO) ₃ (4,7-diMephen)(L51) ⁺	C ₂ H ₅ OH	298	360	505, 481	0.61	15 400	[51]
	Glass	77		465, 498			
				535, 571			

Table 1 (continued)

Complex	Solvent	Temp (K)	Ex.	Em.	QY	Life (ns)	Refs.
Re(CO) ₃ (3,4,7,8-Mephen)(L51) ⁺	C ₂ H ₅ OH	298	364	505, 476	0.52	16 300	[51]
	Glass	77		465, 500, 535, 575			
Re(CO) ₃ (2,9-diMephen)(L51) ⁺	C ₂ H ₅ OH	298	364	498	0.22	–	[51]
	Glass	77		452, 483, 513, 552			
Re(CO) ₃ (2,9-diMe-4,7-diPh-phen)(L51) ⁺	C ₂ H ₅ OH	298	376	529	0.39	–	[51]
	Glass	77		495, 523, 562			
Re(CO) ₃ (5-Clphen)(L51) ⁺	C ₂ H ₅ OH	298	364	524	0.78	1500 171 000	[52]
	Glass	77		474, 505, 546, 583			
Re(CO) ₃ (5-nitro-phen)(L51) ⁺	C ₂ H ₅ OH	298	370	–	–	–	[52]
	Glass	77		490, 526, 562			
Re(CO) ₃ (5-Mephen)(L51) ⁺	C ₂ H ₅ OH	298	372	510	0.83	20 200 231 000	[52]
	Glass	77		463, 495, 532, 571			
Re(CO) ₃ (5,6-diMephen)(L51) ⁺	C ₂ H ₅ OH	298	377	493, 518	0.56	30 900 229 000	[52]
	Glass	77		483, 518, 556, 602			
Re(CO) ₃ (php)(L51) ⁺	C ₂ H ₅ OH	298	410	541	0.11	6200 268 000	[52]
	Glass	77		500, 538, 578, 625			
Re(CO) ₃ (bpy)(L51) ⁺	C ₂ H ₅ OH	298	370	518	0.27	1220 8800	[53]
	Glass	77		450, 478, 510, 556			
Re(CO) ₃ (L52)Cl	CHCl ₃	298	464	635			[54]

Table 1 (continued)

Complex	Solvent	Temp (K)	Ex.	Em.	QY	Life (ns)	Refs.
Re(CO) ₃ (L53)Cl	CHCl ₃	298	460	561			[54]
Re(CO) ₃ (L54)Cl	CHCl ₃	298	431	529			[54]
Re(CO) ₃ (L52)(NCCH ₃) ⁺	CH ₃ CN	298	388	520			[54]
Re(CO) ₃ (L53)(NCCH ₃) ⁺	CH ₃ CN	298	379	509			[54]
Re(CO) ₃ (L54)(NCCH ₃) ⁺	CH ₃ CN	298	380	504			[54]
Re(CO) ₃ (L52)(L55) ⁺	CH ₃ CN	298	396	528			[54]
Re(CO) ₃ (L53)(L55) ⁺	CH ₃ CN	298	386	523			[54]
Re(CO) ₃ (L54)(L56) ⁺	CH ₃ CN	298	383	519			[54]
Re(CO) ₃ (L53)(L56) ⁺	CH ₃ CN	298	388	550			[54]
Re(CO) ₃ (L57)Cl	EtOH : MeOH	298	420	705	0.0001		[55]
	Glass	77		656		98	
Re(CO) ₃ (L58)Cl	EtOH : MeOH	298	404	718	0.0007	–	[55]
	Glass	77		641		2537	
Re(CO) ₃ (L57)(L59) ⁺	EtOH : MeOH	298	388	684	0.0017	25	[55]
	Glass	77		632		1522	
Re(CO) ₃ (L58)(L59) ⁺	EtOH : MeOH	198	374	669	0.0089	95	[55]
	Glass	77		617		5507	
Tridentate Ligands							
Re(CO) ₃ (L60) ⁺		298	325				[56]
	(CH ₂ OH) ₂						
	N ₂			559	0.0162		
	<i>air</i>			565	0.0056		
	CH ₃ CN						
	N ₂			554	0.0125		
	<i>air</i>			552	0.0004		
Re(CO) ₃ (L61) ⁺		298	325				[56]
	(CH ₂ OH) ₂						
	N ₂			428,557	0.0234		
	<i>air</i>			429,558	0.0085		
	CH ₃ CN						
	N ₂				0.0163		
	<i>air</i>			424,559			
Re(CO) ₃ (L62) ⁺		298	325				[56]
	(CH ₂ OH) ₂			427,555			
	N ₂			428,554	0.0162		
	<i>air</i>				0.0060		
	CH ₃ CN						
	N ₂				0.0146		
	<i>air</i>			418,554			
				421			

Table 1 (continued)

Complex	Solvent	Temp (K)	Ex.	Em.	QY	Life (ns)	Refs.
Re(CO) ₃ (L63) ⁺	(CH ₂ OH) ₂	298	280				[57]
	N ₂			575	0.0077		
	air				0.0021		
Re(CO) ₃ (L64) ⁺	(CH ₂ OH) ₂	298	320	555			[57]
	N ₂				0.022		
	air				0.0080		
Re(CO) ₃ (L65) ⁺	(CH ₂ OH) ₂	298	290	327			[57]
	N ₂				0.048		
	air				0.045		
Re(CO) ₃ (L66) ⁺	(CH ₂ OH) ₂	298	320	440			[57]
	N ₂				0.021	14 380	
	air				0.023	16 010	

^a = rectangle

Table 2 Rhenium dimer and trimer complexes

Complex	Solvent	Temp (K)	Ex.	Em.	QY	Life (ns)	Refs.
(bpy)(CO) ₃ Re(L67)Re(CO) ₃ (bpy) ²⁺	CH ₂ Cl ₂	298	366	535	–	1040	[36]
(bpy)(CO) ₃ Re(L68)Re(CO) ₃ (bpy) ²⁺	CH ₃ CN	298	360	415	–	< 100	[36]
				556		240	
(phen)(CO) ₃ Re(L68)Re(CO) ₃ (phen) ²⁺	CH ₃ CN	298	406	423	–	< 100	[36]
(bpy)(CO) ₃ Re(L69)Re(CO) ₃ (bpy) ²⁺	CH ₃ CN	298	347	586	–	200	[36]
	Solid	298	–	508	–	1200	
	Solid	77	–	508	–	–	
(phen)(CO) ₃ Re(L69)Re(CO) ₃ (phen) ²⁺	CH ₂ Cl ₂	298	383	550	–	2500	[36]
	CH ₃ CN	298	368	570	–	1500	
	Solid	298	–	557	–	1100	
	Solid	77	–	540	–	–	
Cl(CO) ₃ Re(L70) ₂ Re(CO) ₃ Cl	Water	298	480	665	–	–	[58]
(4,4'-di ^t Bu-bpy)(CO) ₃ Re(L71)	CH ₂ Cl ₂	298	350	542	0.026	1060	[59]
Re(CO) ₃ (4,4'-di ^t Bu-bpy) ²⁺							
(4,4'-di ^t Bu-bpy)(CO) ₃ Re(L72)	CH ₂ Cl ₂	298	350	540	0.026	1010	[59]
Re(CO) ₃ (4,4'-di ^t Bu-bpy) ²⁺							
(4,4'-di ^t Bu-bpy)(CO) ₃ Re(L73)	CH ₂ Cl ₂	293	360	536	0.2	4800	[47]
Re(CO) ₃ (4,4'-di ^t Bu-bpy) ²⁺							

Table 2 (continued)

Complex	Solvent	Temp (K)	Ex.	Em.	QY	Life (ns)	Refs.
(6 MeBpy)(CO) ₃ Re(L72)Re(CO) ₃ (6-MeBpy) ²⁺	CH ₂ Cl ₂	293	360	544	0.083	3800	[47]
(4,4'-di ^t Bu-Bpy)(CO) ₃ Re(L74)Re(CO) ₃ (4,4'-di ^t Bu-Bpy) ²⁺	CH ₂ Cl ₂	293	360	538	0.16	6200	[47]
(4,4'-di ^t Bu-bpy)(CO) ₃ Re(L75)Re(CO) ₃ (4,4'-di ^t Bu-bpy) ²⁺	CH ₂ Cl ₂	293	360	538	0.22	5400	[47]
(4,4'-di ^t Bu-bpy)(CO) ₃ Re(L76)Re(CO) ₃ (4,4'-di ^t Bu-bpy) ²⁺	CH ₂ Cl ₂	293	360	532	0.27	5900	[47]
[Re(CO) ₃ (bpy)] ₃ (L77) ³⁺	CH ₃ CN	293	380	574	0.0014	15	[60]
[Re(CO) ₃ (bpy)] ₃ (L78) ³⁺	CH ₃ CN	293	380	576	0.030	250	[60]
[Re(CO) ₃ (dmb)] ₃ (L77) ³⁺	CH ₃ CN	293	380	562	0.001	10	[60]
[Re(CO) ₃ (dmb)] ₃ (L78) ³⁺	CH ₃ CN	293	380	566	0.061	510	[60]
[Re(CO) ₃ (4,4'-diPhbpy)] ₃ (L77) ³⁺	CH ₃ CN	293	380	582	0.0043	15.5	[60]
[Re(CO) ₃ (4,4'-diPhbpy)] ₃ (L78) ³⁺	CH ₃ CN	293	380	582	0.040	220	[60]
[Re(CO) ₃ (4,4'-di ^t Bu-bpy)] ₃ (L77) ³⁺	CH ₃ CN	293	380	560	0.003	8.2	[60]
[Re(CO) ₃ (4,4'-di ^t Bu-bpy)] ₃ (L78) ³⁺	CH ₃ CN	293	380	562	0.026	610	[60]
[Re(CO) ₃ (5,5'-diMebpy)] ₃ (L77) ³⁺	CH ₃ CN	293	380	568	0.008	12.1	[60]
[Re(CO) ₃ (5,5'-diMebpy)] ₃ (L78) ³⁺	CH ₃ CN	293	380	566	0.070	830	[60]
[Re(CO) ₃ (6,6'-diMebpy)] ₃ (L77) ³⁺	CH ₃ CN	293	380	556	0.008	9.9	[60]
[Re(CO) ₃ (6,6'-diMebpy)] ₃ (L78) ³⁺	CH ₃ CN	293	380	554	0.045	540	[60]
[Re(CO) ₃ (6-Mebpy)] ₃ (L77) ³⁺	CH ₃ CN	293	380	568	0.0015	16.2	[60]
[Re(CO) ₃ (6-Mebpy)] ₃ (L78) ³⁺	CH ₃ CN	293	380	568	0.030	440	[60]
[Re(CO) ₃ (phen)] ₃ (L77) ³⁺	CH ₃ CN	293	380	560	0.0015	17.6	[60]
[Re(CO) ₃ (phen)] ₃ (L78) ³⁺	CH ₃ CN	293	380	562	0.052	1850	[60]
[Re(CO) ₃ (4-Mephen)] ₃ (L77) ³⁺	CH ₃ CN	293	380	554	0.0004	5.4	[60]
[Re(CO) ₃ (4-Mephen)] ₃ (L78) ³⁺	CH ₃ CN	293	380	552	0.035	2180	[60]
[Re(CO) ₃ (4,7-diPhphen)] ₃ (L77) ³⁺	CH ₃ CN	293	380	578	0.0017	20.5	[60]
[Re(CO) ₃ (4,7-diPhphen)] ₃ (L78) ³⁺	CH ₃ CN	293	380	578	0.023	1070	[60]
[Re(CO) ₃ (2,9-diMe-4,7-diPhphen)] ₃ (L77) ³⁺	CH ₃ CN	293	380	564	0.0002	4.9	[60]
[Re(CO) ₃ (2,9-diMe-4,7-diPhphen)] ₃ (L78) ³⁺	CH ₃ CN	293	380	562	0.027	1420	[60]
[Re(CO) ₃ (en)] ₃ (L77) ³⁺	CH ₃ CN	293	380	538	0.000	–	[60]
[Re(CO) ₃ (en)] ₃ (L78) ³⁺	CH ₃ CN	293	380	536	0.091	920	[60]

equivalent number of rhenium centers giving rise to mono- or multi-metal complexes. The most emissive complexes and with the longest emission lifetimes contained 2,6-dimethylphenylisocyanide; others with more elaborate organic functionalities were less emissive and had shorter emission lifetimes.

Table 3 Rhenium complexes with less than three carbonyl groups

Complex	Solvent	Temp (K)	Ex.	Em.	QY	Life (ns)	Refs.
Re(CO) ₂ (dmb)(L79) ₂ ⁺	CH ₃ CN	298	415	618	0.07	1224	[61]
Re(CO) ₂ (dmb)(L80)(L80) ⁺	CH ₃ CN	298	411	608	0.09	1101	[61]
Re(CO) ₂ (dmb)(L80) ₂ ⁺	CH ₃ CN	298	402	600	0.08	1074	[61]
Re(CO) ₂ (dmb)(L80)(L81) ⁺	CH ₃ CN	298	400	598	0.07	1003	[61]
Re(CO) ₂ (dmb)(L81) ₂ ⁺	CH ₃ CN	298	396	595	0.10	1046	[61]
Re(CO) ₂ (dmb)(L82) ₂ ⁺	CH ₃ CN	298	395	592	0.13	1220	[61]
Re(CO) ₂ (dmb)(L79)(L83) ⁺	CH ₃ CN	298	388	612	0.03	601	[61]
Re(CO) ₂ (dmb)(L80)(L84) ⁺	CH ₃ CN	298	382	606	0.05	511	[61]
Re(CO) ₂ (dmb)(L81)(L85) ⁺	CH ₃ CN	298	379	602	0.06	665	[61]
Re(CO) ₂ (dmb)(L83) ₂ ⁺	CH ₃ CN	298	366	605	0.03	381	[61]
Re(CO) ₂ (dmb)(L84) ₂ ⁺	CH ₃ CN	298	365	603	0.03	355	[61]
Re(CO) ₂ (dmb)(L84)(L85) ⁺	CH ₃ CN	298	363	602	0.05	361	[61]
Re(CO)(bpy)(L51) ₃ ⁺	C ₂ H ₅ OH Glass	298 77	382	– 485	–	– 6300	[53]

Table 4 Results from solvent or binding studies

Complex	Solvent	Temp (K)	Ex.	Em.	QY	Life (ns)	Refs.		
L86	CH ₃ CN	298	409				[62]		
	H ₂ O								
	100			0	666	0.0004	11		
	90			10	634	0.0005	13		
	80			20	612	0.0016	120		
	70			30	611	0.0017	124		
	60			40	613	0.0021	135		
	50			50	613	0.0024	137		
	40			60	612	0.0026	140		
	30			70	611	0.0031	167		
	20			80	604	0.0047	176		
10	90	602	0.0065	212					
Re(CO) ₃ (bpy)(L87) ⁺	CH ₃ CN	298	355	600	0.0035	< 1	[63]		
	+Li ⁺							0.0055	12
	+Na ⁺							0.0042	10
	+K ⁺							0.0012	< 1
	+Mg ²⁺							0.0470	140
	+Ca ²⁺							0.0130	56
	+Ba ²⁺							0.0087	47
	+H ⁺							0.0280	140

Replacement of Cl⁻ by pyridine, or one of its derivatives, lead to an enhancement of emission properties of rhenium(I) complexes as noted by entries in Table 1.

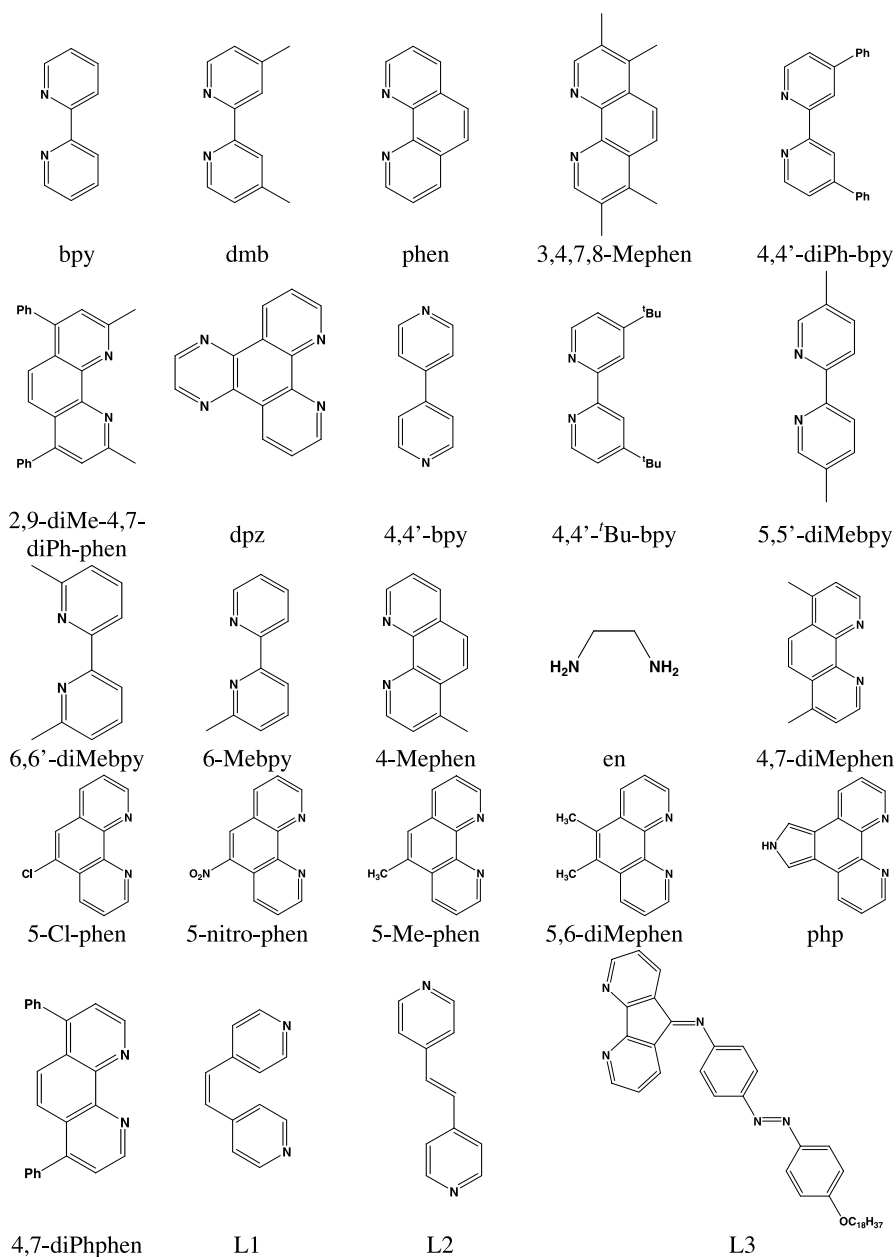


Fig. 5 Structures of ligands with acronyms and L1-L3

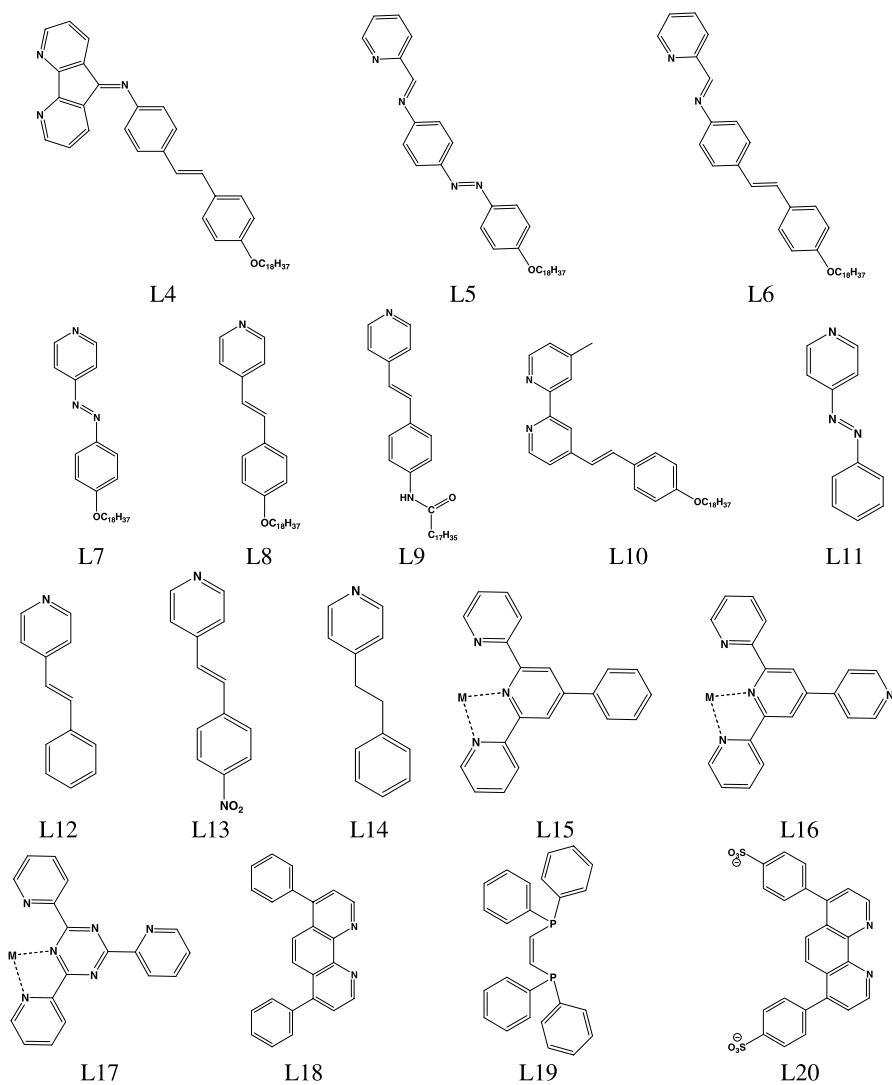


Fig. 6 Structures of ligands L4–L20

Complexes containing the multidentate dentate ligands listed in Table 2 and those with less than three carbonyl ligands listed in Table 3 have also been prepared. Some of the multidentate ligands contained a nucleotide; others an ester or acid side chain. Finally, some results from solvent or binding studies are listed in Table 4.

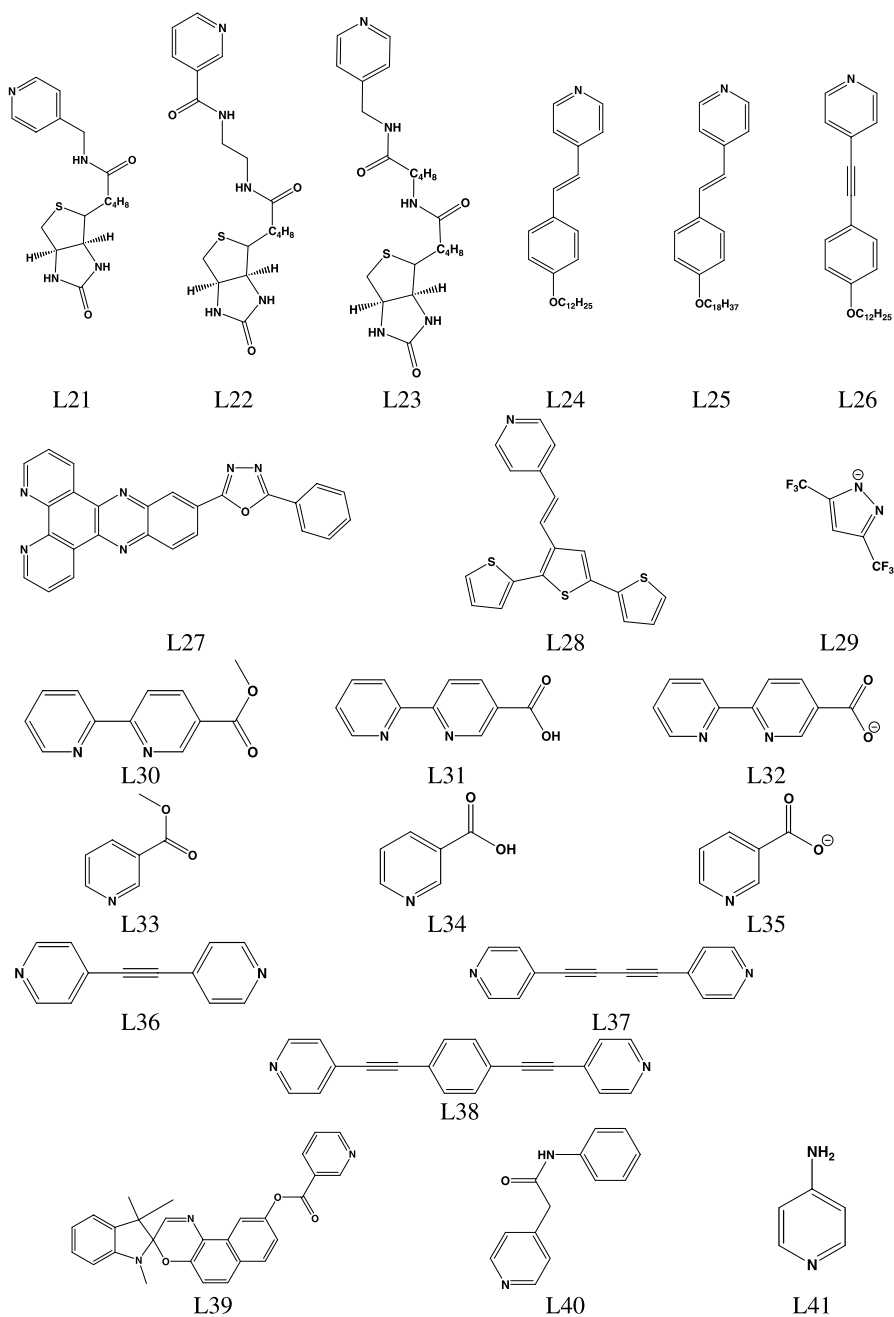


Fig. 7 Structures of ligands L21–L41

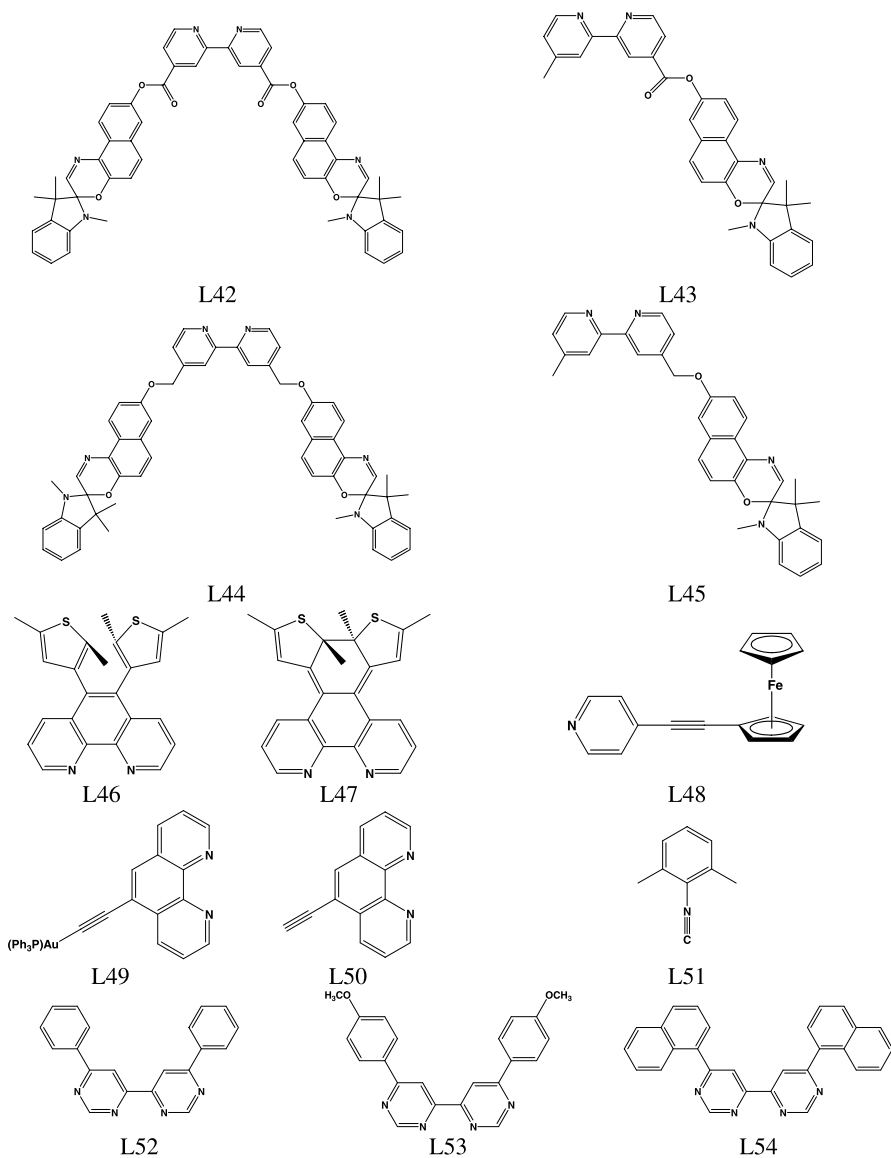


Fig. 8 Structures of ligands L42–L54

6.2 Photophysical Mechanisms

Figure 13 illustrates two models used to explain the photochemical properties of rhenium carbonyl complexes. The MLCT absorption band often

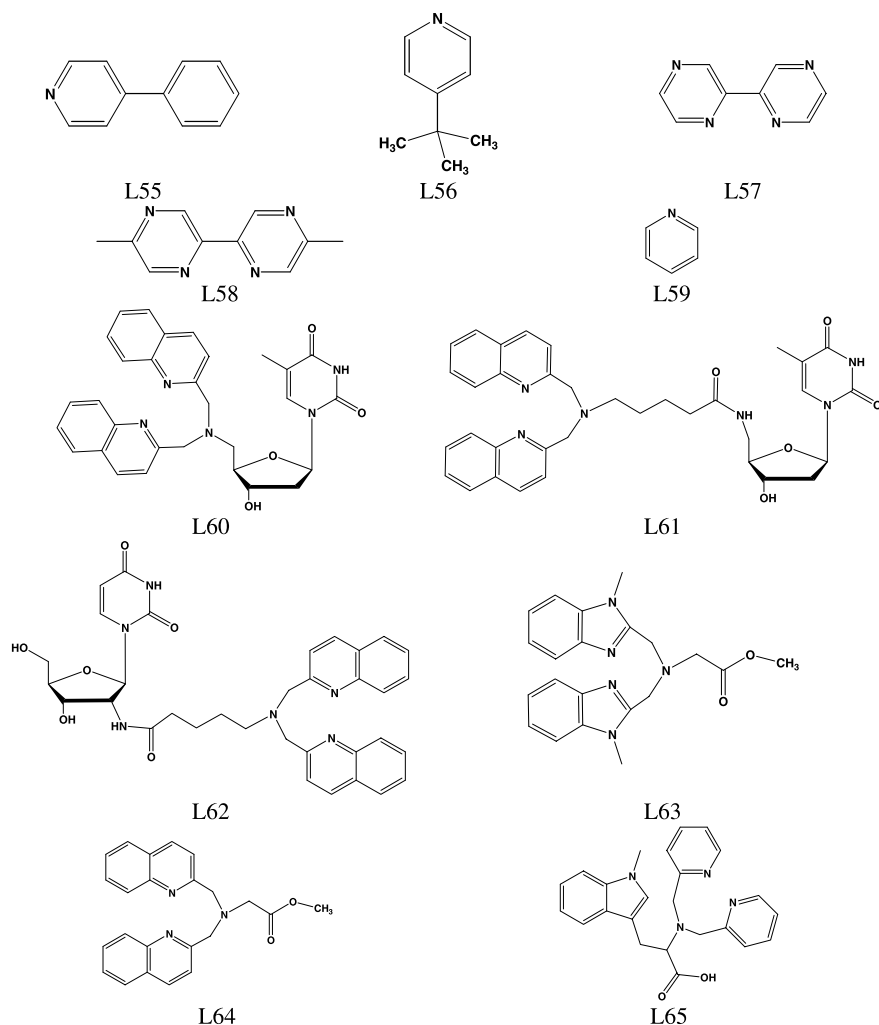


Fig. 9 Structures of ligands L55–L65

lies at lower energy on the shoulder of the $\pi \rightarrow \pi^*$ diimine ligand centered transition (LC); hence, both the $^1\text{MLCT}$ and $^1\text{LC}^*$ levels are often populated simultaneously. Further, the $^3\text{MLCT}$ and $^3\text{LC}^*$ vary in energy relative to one another. Consequently, emission spectra are often found to occur in the 500 nm region with strong vibronic character consistent with a large $^3\text{LC}^*$ contribution; in other cases the spectra occur near 600 nm and are structureless and assignable to a $^3\text{MLCT}$ state. Because the emission envelope of the coordinated diimine ligand is red-shifted from that of the free ligand, a combination ^3LC , $^3\text{MLCT}$ state is often employed to account for the emission behavior.

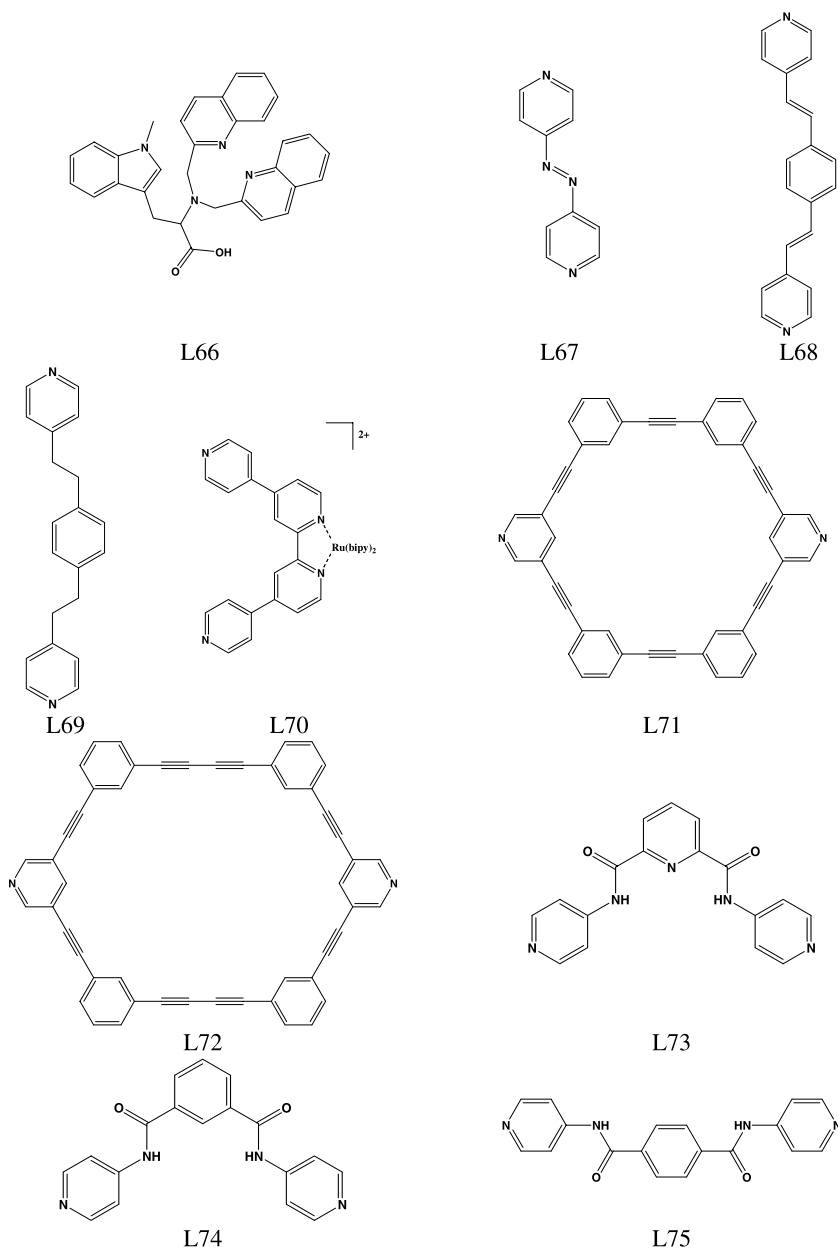


Fig. 10 Structures of ligands L66–L75

Emission spectra are also temperature dependent. At 77 K in a frozen matrix, the ³MLCT state in some cases is found to rise above the ³LC state resulting in ligand centered emission in some systems [50].

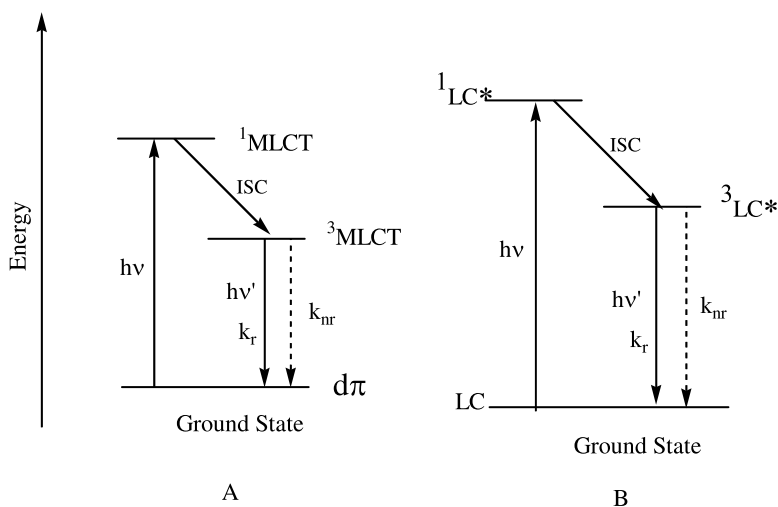


Fig. 13 Jablonski Diagrams for $[\text{Re}(\text{diimine})(\text{CO})_3\text{L}]$ Complexes: **A** MLCT Model; **B** Ligand-Centered Model

More recently, density functional theory and time dependent density functional theory have provided new insights into the appropriateness of these models [51–53]. For the “parent complexes”, $[\text{Re}(\text{bpy})(\text{CO})_3\text{Cl}]$ and $[\text{Re}(\text{bpy})(\text{CO})_3(\text{py})]^+$, the highest occupied molecular orbital contained 50% or greater Re_d character along with $\sim 20\%$ contributions each from CO and Cl for $[\text{Re}(\text{bpy})(\text{CO})_3\text{Cl}]$ and $\sim 20\%$ contributions from CO for $[\text{Re}(\text{bpy})(\text{CO})_3(\text{py})]^+$. The lowest unoccupied molecular orbitals consisted of 80% or greater diimine ligand π^* character in both cases. Thus the lowest energy optical transition was assigned as a metal-ligand-to-ligand charge transfer transition (MLLCT) [53].

TDDFT calculations results were consistent with the band shapes of the optical spectra of the “parent complexes” and are shown in Fig. 14. The calculated optical transitions are shown as bars under the experimental spectra and consist of MLLCT, ligand-to-ligand charge transfer transitions (LLCT), intraligand $\pi \rightarrow \pi^*$ transitions (IL), and metal-complex delocalized-charge transfer transitions (MCDCT). Triplet state energies were also calculated based on a $^3\text{MLLCT}$ state and correlated with experimental emission spectral results [53].

Similar calculations were applied to $[\text{Re}(\text{diimine})(\text{CO})_3(\text{RNC})]^+$ complexes, where RNC is 2,6-dimethylphenylisocyanide and diimine = phen derivatized with electron donor groups [51] or electron withdrawing groups [52]. In general the HOMOs contained 45% or greater Re_d character and 27% or greater RNC character and the LUMO contained $> 81\%$ diimine π^* character. The lowest optical transition was assigned as MLLCT and emis-

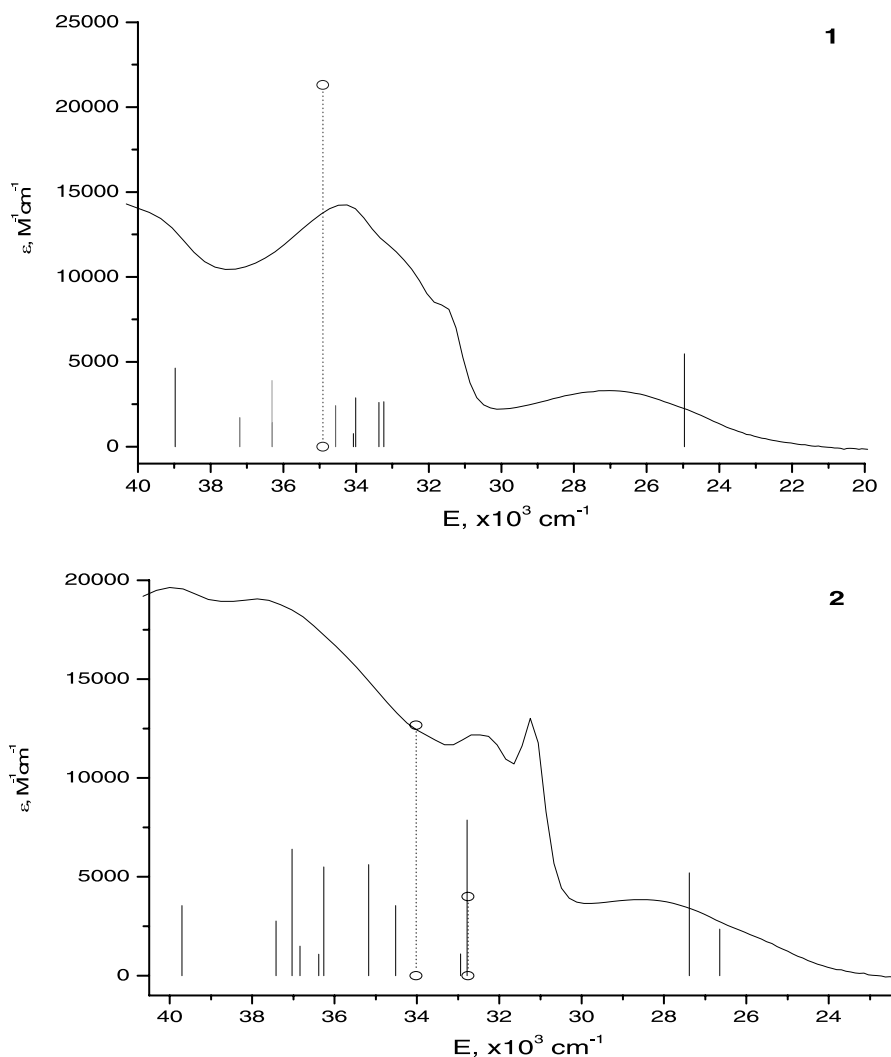


Fig. 14 Experimental absorption spectra of 1, $[\text{Re}(\text{bpy})(\text{CO})_3\text{Cl}]$, and 2, $[\text{Re}(\text{bpy})(\text{CO})_3(\text{py})]^+$, and calculated singlet excited-states. The excited states are shown as *vertical bars* with height equal to the extinction coefficient. *Black* = MLLCT, *green* = LLCT, *blue* = $\pi \rightarrow \pi^*$, *red* = MCDCT, *orange* = Re_d , *CNx* \rightarrow Re_s mixed excited-state (with permission from ACS)

sion was assigned as $^3\text{MLLCT}$. The HOMOs of complexes of the type $[\text{Re}(\text{bpy})(\text{CO})_3(\text{ER})_2]$, where $\text{ER} = \text{NHPh}$, $\text{N}(4-\text{CH}_3\text{Ph})_2$, PPh_2 , were located on the amido and phosphido ligands and the LUMOs were located on the bpy π^* levels. Thus, for the latter complexes the lowest energy transition was assigned as LLCT and emission as $^3\text{LLCT}$ [64].

6.3

Transient Detection

Time resolved absorption (TRA), infrared (TRIR), and Resonance Raman (TRRR) methods were used to detect transients of photoexcited rhenium(I) carbonyl complexes. The $^3\text{MLCT}$ nature of the excited state was confirmed by detecting the existence of the diimine radical (diimine $^-$) using time resolved absorption measurements [44, 50, 61, 65, 66]. For $[\text{Re}^1(\text{dmb-tol})(\text{CO})_3\text{Cl}]^*$, where dmb-tol was 4-methyl-4'-(*N*-methyl-*p*-tolylaminomethyl)-2,2'-bipyridine, the transient absorption spectrum was consistent with the formation of the redox separated state $[\text{Re}^1(\text{dmb}^-\text{tol}^+)(\text{CO})_3\text{Cl}]$ [67]. For the compound $[\text{Re}^1(\text{bpy-YH})(\text{CO})_3\text{CN}]$ shown in Fig. 15, the transient absorption spectrum of $[\text{Re}^1(\text{bpy-Y}^-)(\text{CO})_3\text{CN}]^*$ was attributed to the redox intermediate $[\text{Re}^1(\text{bpy}^-\text{Y})(\text{CO})_3\text{CN}]^*$ [68]. TRA was also used to probe the excited state behavior of $[\text{RCO}_2\text{-Re}(\text{CO})_3(\text{bpy})]$, where RCO_2^- = naphthalene-2-carboxylate, anthracene-9-carboxylate, pyrene-1-carboxylate and acetate anions. Two excited states were observed: the $^3\text{LLCT}$ state of the arene and the $^3\text{MLCT}$ state of Re-bpy component [69].

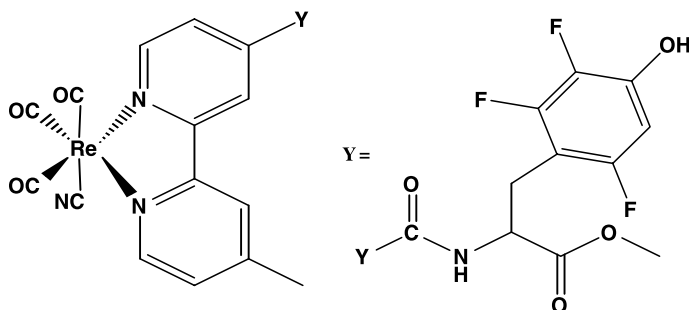


Fig. 15 Structure of $[\text{Re}(\text{bpy}-\text{Y})(\text{CO})_3\text{CN}]$

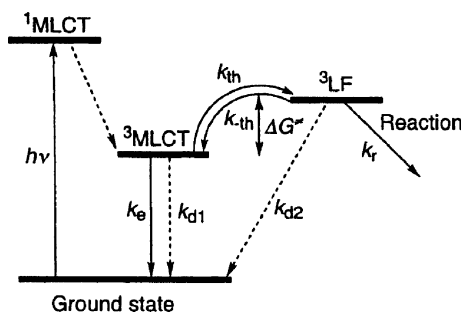
The detection of intermediates related to changes in CO stretching frequencies has provided additional insight into the photophysics of rhenium carbonyl complexes. Vlcek's group has extensively examined two rhenium tricarbonyl systems by TRIR, $[\text{Re}(\text{ER})_2(\text{CO})_3(\text{bpy})]$, where ER = NHPh, N(4-CH $_3$ Ph) $_2$, and PPh $_2$, and $[\text{Re}(\text{R})(\text{CO})_3(\text{dmb})]$, where R = CH $_3$ and C $_2$ H $_5$. TRIR measurements in the picosecond and nanosecond time domains revealed complex excited state dynamics for $[\text{Re}(\text{ER})_2(\text{CO})_3(\text{bpy})]$ initiated by LLCT and ending in a low lying excited state consisting of an aminyl/phosphinyl radical-cationic ligand [64]. The dynamics of excited state decay for $[\text{Re}(\text{R})(\text{CO})_3(\text{dmb})]$ was also complex. After initial population of the $^3\text{MLCT}$ state, TRIR revealed formation of $[\text{Re}(\text{R})(\text{CO})_3(\text{dmb})]^-$ by reaction with solvent, then $[\text{Re}(\text{R})(\text{CO})_3(\text{dmb})]$, and finally $[\text{Re}(\text{R})(\text{CO})_3(\text{dmb})]$ [70].

TRRR measurements for $[\text{Re}(\text{dppz-X})(\text{CO})_3\text{Cl}]$, where dppz is dipyrido[3,2-a:2',3'-c]phenazine and $X = \text{Br}$ and COOC_2H_5 were examined for dppz-X vibrations. The results were in agreement with a $^3\text{MLCT}$ excited state assignment [71].

6.4 Photochemistry

Although many of the complexes of the type $\text{Re}(\text{bpy})(\text{CO})_3\text{L}^n$, where L is a weak field ligand like pyridine or halide are photostable to irradiation into the MLCT manifold, efficient photochemical ligand substitution is found for *fac*- $\text{Re}(\text{X}_2\text{bpy})(\text{CO})_3(\text{PR}_3)^+$ to yield substitution trans to the axial PR_3 group by CO loss (X_2bpy is 4,4'- X_2 -2,2'-bpy where X is H, CF_3 , OEt or Ph and PR_3 is a tertiary phosphine or phosphite) [72]. The *cis-trans*- $\text{Re}(\text{X}_2\text{bpy})(\text{CO})_2(\text{PR}_3)\text{L}^n$ form with chloride, py or CH_3CN as the entering group. Isolated yields ranged from ca. 50–95%. A follow-up study probed the mechanism of this reaction. For a series of complexes where X is either CF_3 or H and photolysis takes place in CH_3CN to yield the appropriate solvent complex, the temperature dependence of the emission yield and lifetime was interpreted as indicating an activated process proceeding from a $^3\text{MLCT}$ state to a ^3LF state as shown in Scheme 1 [73]. Activation energies for photosubstitution were found to be between 3200 and 4800 cm^{-1} , and photosubstitution yields were generally in the range of 0.1 to 0.55. Labeling (^{13}C) studies demonstrated that the axial CO was indeed labilized, consistent with a dissociative mechanism, and an associated excited state kinetic trans effect. Interestingly, the photostability of *fac*- $\text{Re}(\text{bpy})(\text{CO})_3\text{py}^+$ and $\text{Re}(\text{bpy})(\text{CO})_3\text{Cl}$ and related bpy-substituted complexes is proposed to be due to the weaker trans-labilizing ability of the py or chloride ligand compared to a phosphorus donor and not a larger activation energy to reach the ^3LF state.

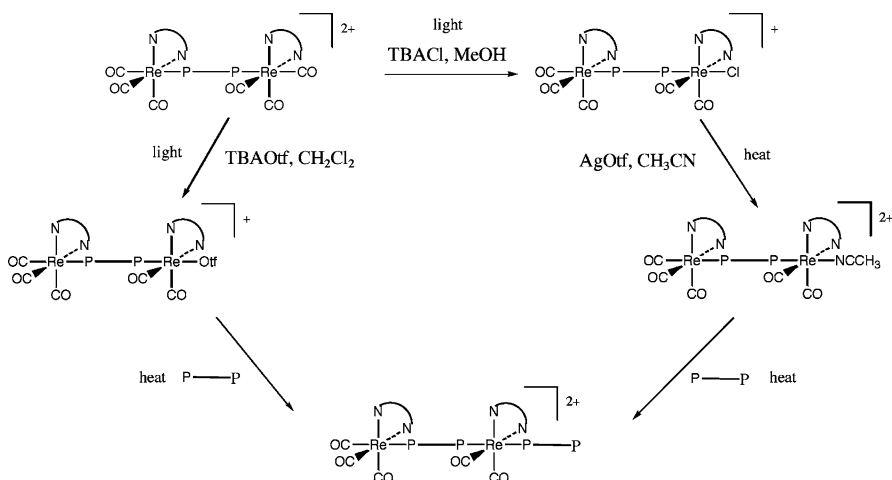
For the complex *fac*- $\text{Re}(\text{bpy})(\text{CO})_3(\text{TEP})^+$ (TEP is triethynylphosphine) both possible trans-axial labilization products are observed in CH_3CN so-



Scheme 1 Jablonski diagram for the dissociative, activated loss of the ligand trans to PR_3 in *fac*- $[\text{Re}(\text{bpy})(\text{CO})_3(\text{PR}_3)]^+$ complexes

lution, i.e., *cis-trans*-Re(bpy)(CO)₂(TEP)(CH₃CN)⁺ and *fac*-Re(bpy)(CO)₃(CH₃CN)⁺ in ca. a 2 : 1 ratio. This may indicate that the kinetic trans effect of TEP and CO is comparable. *fac*-Re(bpy)(CO)₃(TEP)⁺ also exhibits a structured high energy luminescence suggestive of ligand-localized origin [74]. In fact, DFT/TDDFT calculations predict a mixed ligand-localized (bpy) and MLCT state to be lowest in energy; however, they do little to shed light on the unique photosubstitution behavior.

Photosubstitution of diphosphine-bridged bimetallic complexes has been used to produce precursors for oligometallic materials where only one end of the complex has been ligated [75]. This chemistry as shown in Scheme 2 utilizes 1,2-*trans*-bis-diphenylphosphinoethylene as the bridging ligand and can proceed with quantum yields as high as 0.35. The chemistry is unique in that it proceeds to substitute at only one trans position. This is proposed to be due to “self-quenching”, i.e., intramolecular energy transfer transfer from the high-energy chromophore that proceeds efficiently to the low energy, photo-stable ligand substituted chromophore. In fact, TRIR studies demonstrate this rapid energy transfer by monitoring the change in the ground and excited state Re – CO modes. Another related study has used dppe as a bridging ligand and under similar conditions and has produced up to tetrametallic complexes using only Re(I) dicarbonyl units as building blocks [76].



Scheme 2 Photochemical and thermal transformations of the ligand bridged complex $[(\text{bpy})(\text{CO})_3\text{ReP}-\text{PRe}(\text{CO})_3(\text{bpy})]^{2+}$ (P-P is *trans*-1,2-bis-diphenylphosphinoethylene)

Recent preparative studies of a series of mixed-ligand bpy and phen complexes of the formulation *cis*-[Re(CO)₂(chelate)(diphos)]⁺ and *cis-trans*-[Re(bpy)(CO)₂(PR₃)₂]⁺ (diphos is for example dpmm or dppe) are emissive in solution with lifetimes in the range of 25 to 1147 ns and emission quantum

yields of between 0.002 and 0.11 [77]. The complexes represent a new class of photosensitizers with tunable ground and excited state properties.

A study reported the homolysis of the metal alkyl bond for $[\text{Re}(\text{R})(\text{CO})_3(\text{dmb})]$ ($\text{R} = \text{CH}_3$ and C_2H_5) [71]. The photoactive excited state was identified as $^3\text{MLCT}$ (metal-to-ligand charge transfer) with an admixture of $^3\text{SBLCT}$ (sigma bond-to-ligand charge transfer) character. Excited state decay of $[\text{Re}(\text{C}_2\text{H}_5)(\text{CO})_3(\text{dmb})]$ led only to homolytic cleavage of the $\text{Re}-\text{C}_2\text{H}_5$ bond, whereas for $[\text{Re}(\text{CH}_3)(\text{CO})_3(\text{dmb})]$ both homolytic cleavage of the $\text{Re}-\text{CH}_3$ bond and decay from the excited state to the ground state occurred in a 1 : 1 ratio.

Trans to *cis* isomerization of azo and ethylene linkages associated complexes of the type $[\text{Re}(\text{diimine})(\text{CO})_3\text{L}]^+$, where L are ligands shown in Fig. 16, was examined by several groups [34–36, 63, 77]. The process is outlined in Scheme 3. Optical excitation in the visible caused *trans* to *cis* isomerization along with a marked enhancement of emission.

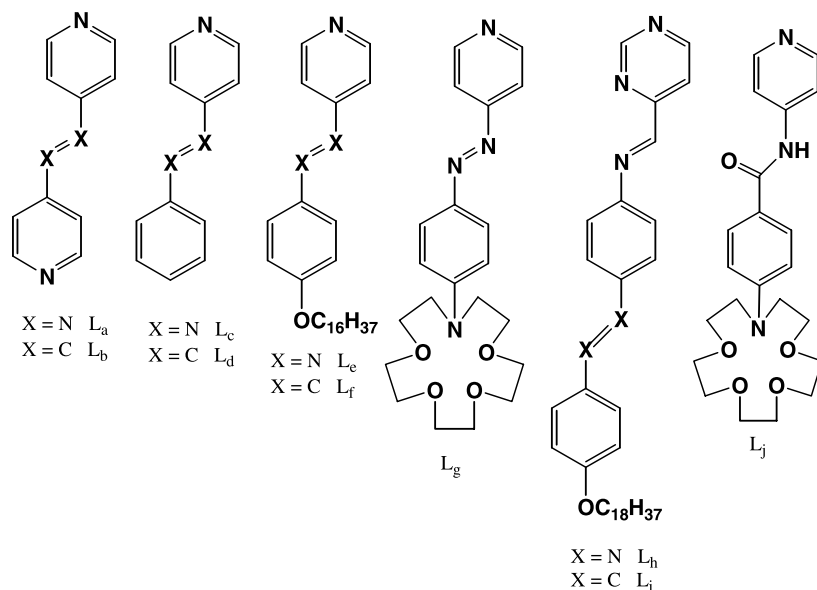
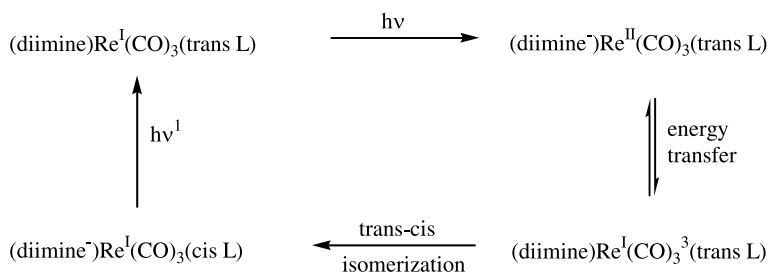
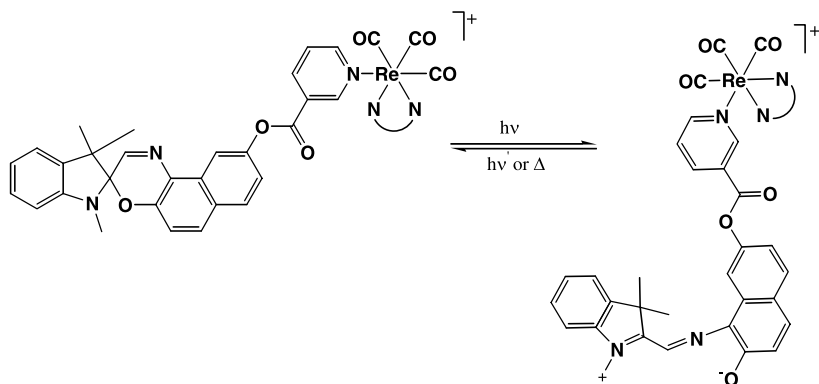


Fig. 16 Azo, ethylenic and crown ligands

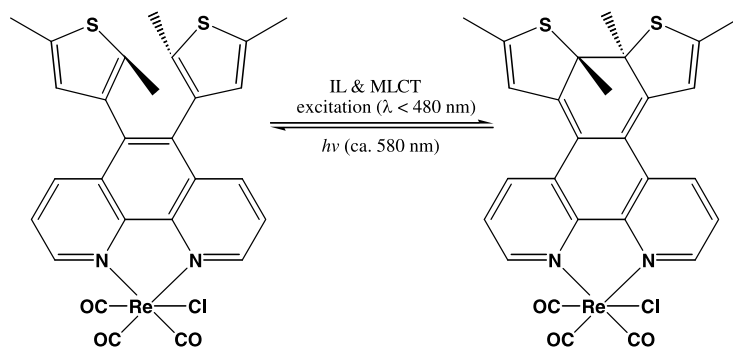
The isomerization was caused by energy transfer from a $^3\text{MLCT}$ to a ^3IL (intraligand) state when the ligand was in the *trans* form. The ^3IL state is higher in energy than the $^3\text{MLCT}$ state in the *cis* form, accounting for the increase in emission intensity observed for the complex after isomerization. The presence of protons was required to isomerize $[\text{Re}(\text{diimine})(\text{CO})_3\text{L}_g]^+$ [78]. The reverse process of *cis* to *trans* isomerization was studied in two cases and required exciting the complexes at higher



Scheme 3 Photoinduced *cis-trans* isomerization of complexes with C = N linkages



A. Ring-opening, spirooxazines



B. Ring Closure, Dioxyethenes

Scheme 4 Photo-induced (A) ring-opening and (B) ring-closing reactions

energy than the energy needed to cause *trans* to *cis* isomerization [34, 35]. $[\text{Re}(\text{diimine})(\text{L}_h)(\text{CO})_3]\text{Cl}$ underwent reversible isomerization in the forward direction upon irradiation at 450 nm and in the reverse direction at 365 nm $[\text{Re}(\text{diimine})(\text{CO})_3\text{L}_a]^+$ required irradiation at 250 nm to cause *cis* to *trans* isomerization [35]. The high energy required resulting in some decompos-

ition [34]. The reversible *trans* to *cis* and *cis* to *trans* behavior resulting from excitations at differing frequencies was equated to a *photoswitch*.

Light controlled ion switching was observed for the nanosecond release and microsecond recapture of alkali and alkaline earth metal ions for $[(\text{bpy})\text{Re}(\text{CO})_3\text{L}_j]^+$, where L_j contains an azacrown ether [63]. Photosensitization studies of ring-opening [45, 47] and ring-closing [48] have been studied by Yam's group for rhenium complexes containing spirooxazine and diarylethenes moieties attached to either the pyridine or diimine ligands. The reactions are shown in Scheme 4.

6.5

Polymer Systems

Five different polymeric species containing rhenium(I) tricarbonyl complexes are shown in Fig. 17. Polymer A contained $\{\text{Re}(\text{CO})_3\text{Cl}\}$ units attached to a dipyridyphenazine ligand [79]. The polymer components were varied from $x = 0.1$ and $y = 0.9$ to $x = 1$ and $y = 0$ with the latter variation providing the most evidence for the presence of the rhenium complex. A shoulder located at ca. 550-600 nm was attributed to the characteristic MLCT optical transition for the rhenium complex. The photoluminescence spectrum gave a continuous decrease of emission ($\pi^*-\pi$) from the poly(*p*-phenylenevinylene) backbone at ~ 550 nm with an increase in emission intensity ($\pi^*-\text{d}$) at ~ 690 nm as the rhenium loading increased.

Polymer B was synthesized using $\text{M}_2(\text{O}_2\text{CR}_4)$, where $\text{M} = \text{Mo}$, $\text{R} = \text{CF}_3$; $\text{M} = \text{Rh}$, $\text{R} = \text{CH}_3$, and $[\text{Re}(\text{L})_2(\text{CO})_3\text{Br}]$, where $\text{L} = 4,4'$ -bipyridine [80]. Only the oligomers obtained were too insoluble to characterize.

A more conventional polymer is shown for C which contains 2,2'-bipyridine (bpy) groups built into a polymer backbone [81, 82]. The π conjugated co-polymers $\{\text{P}[\text{Re}]_x\}$ ($x = 0.1, 0.2, 0.5$) contained $\{\text{Re}(\text{CO})_3\text{Cl}\}$ units coordinated to the bpy sites. The $\{\text{P}[\text{Re}]_x\}$ polymers showed a $\pi-\pi^*$ absorption at ~ 375 nm and a $\text{d}\pi(\text{Re})-\pi^*(\text{bpy})$ absorption at ~ 420 nm. Excitation of the $\{\text{P}[\text{Re}]_x\}$ polymers at 380 nm gave photoluminescence spectra consisting of $\pi^*-\pi$ emission at about 485 nm from the polymer backbone and $^3\text{MLCT}$ emission from the rhenium centers peaking at $\sim 590-600$ nm. Electroluminescence measurements indicated the efficiency was < 0.1 cd/A for the co-polymers which is much lower when compared to $\{(\text{bpy})\text{Re}(\text{CO})_3\}$ stand alone systems. A possible reason postulated for the difference was charge carrier recombination due to the separation of localized electron-hole pairs.

Two approaches were taken to prepare polymer D [83]. The synthesis of the polymer involved combining methacrylate and styrene monomers with either a free pyridine ligand or a pyridine with $\{\text{Re}(\text{phen})(\text{CO})_3\}$ attached. For the polymer with the free pyridine, $\{\text{Re}(\text{phen})(\text{CO})_3\}$ was attached in a second step. Both routes led to polymers with similar properties.

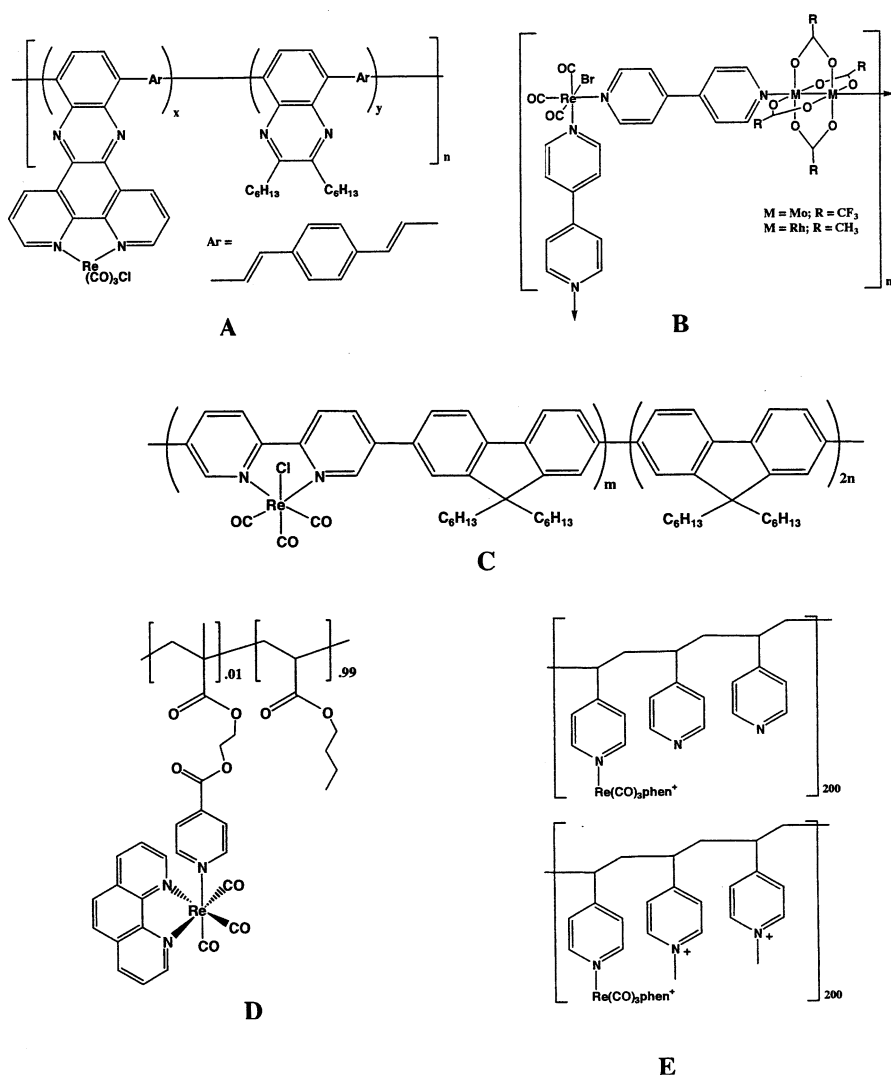


Fig. 17 Polymers incorporating rhenium into their structures

Absorption and emission properties were similar to those of unattached $[Re(phen)(CO)_3(py)]^+$ with high quantum efficiencies and long emission lifetimes. Quenching of the emission occurred in the presence of O_2 suggesting their use for dioxygen sensors.

A study compared the photophysical properties of the polymers (E) $\{(vpy - CH_3)_2^+ - vpyRe(CO)_3(phen)^+\}_{200}$, where vpy = vinylpyridine, $phen$ = 1,10-phenanthroline, to those of $\{(vpy - vpyRe(CO)_3(phen)^+)\}_{200}$. Electron transfer was observed in the former; energy transfer in the latter [84].

6.6 Molecular Polygons

Rhenium molecular squares and triangles are shown in Fig. 18 [44, 62, 85–90]. In general, Re complexes form the corners of the squares and rectangles or corners of the triangles [44, 62, 85–89] except for one rectangle which contains two rhenium and two palladium complexes in opposite corners [90]. Most often the spacers holding the metal centers in place were based on ligands containing pyridine functionalities on opposite ends of an organic linker [44, 62, 85–90], although alkoxide [62, 85] and diimine bridges [86, 88, 89] were also reported. In two cases, the bridging ligand itself contained a metal complex [88, 89] resulting in adding additional metal centers to the rectangles. One bridging ligand contained Zn salen [88]; the

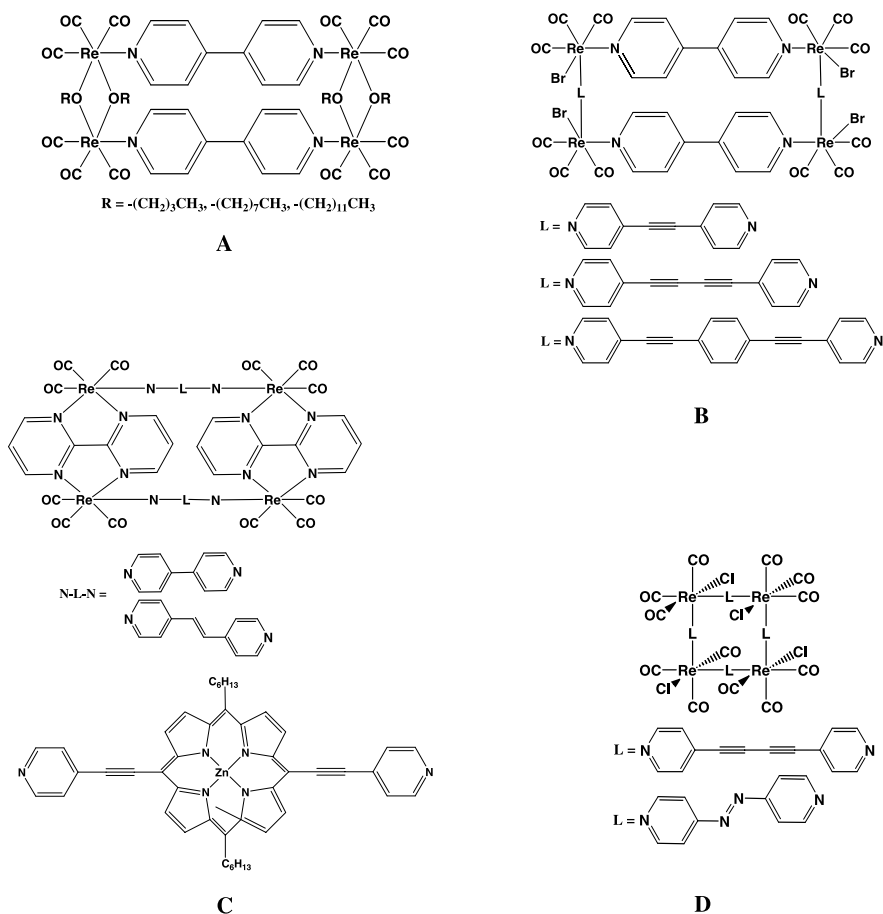


Fig. 18 Squares, Rectangles, Triangles

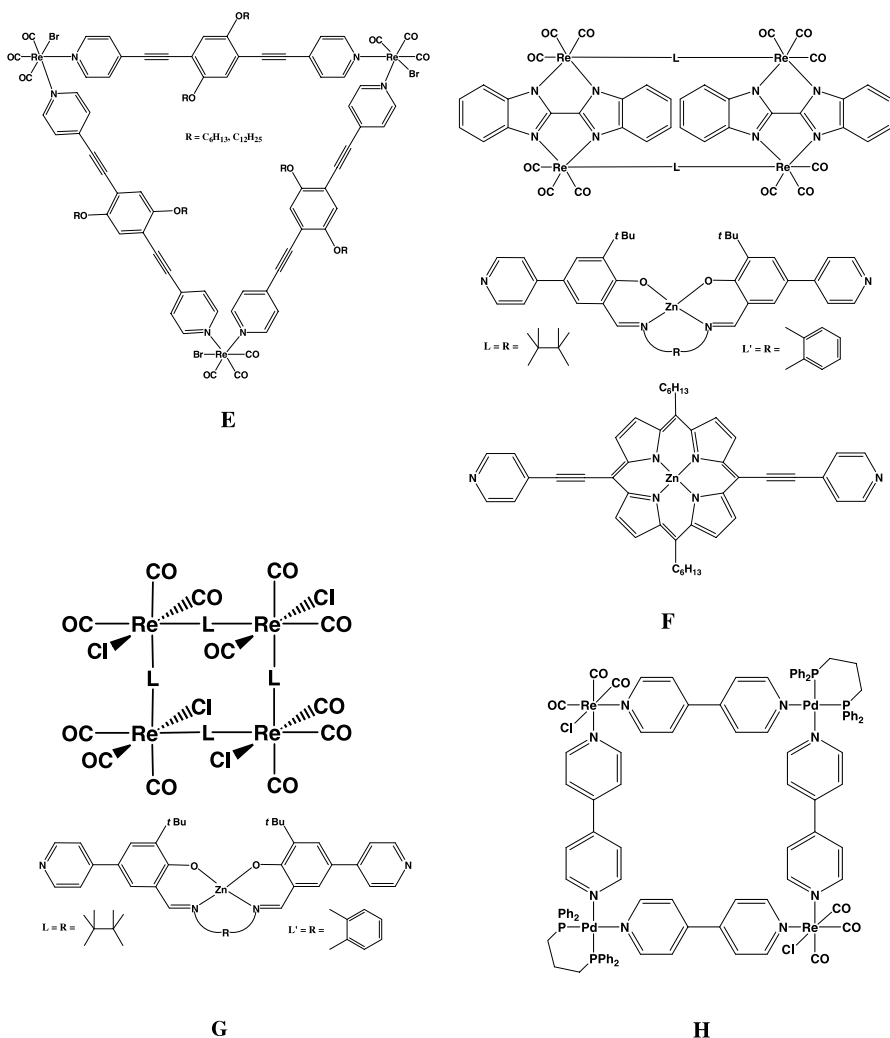


Fig. 18 (continued)

other contained zinc porphyrin [89]. Two synthetic procedures were followed. First, the molecular bridged rhenium dimers were prepared and then another bridging ligand was added to form the rectangle. Thus, in these cases, the same bridging ligands were located on opposite sides of the rectangle as shown in Fig. 18. Second, squares were formed by a one pot synthesis of $[Re(CO)_5Cl]$ with the bridging ligand.

The room temperature emission characteristics of the molecular polygons varied. The emission maximum of rectangle A ($R = -(CH_2)_{11}CH_3$) was located near 600 nm and its intensity was dependent on the solvent.

Its quantum efficiency and lifetime increased respectively from 0.39×10^{-3} and 0.39 ns in CH_3CN to 6.54×10^{-3} and 212 ns in a 1 : 9 $\text{CH}_3\text{CN}:\text{H}_2\text{O}$ mixture [62]. Aggregation was the reason given for the emission enhancement in the presence of water. Other **A** molecules ($\text{R} = \text{OH}, \text{OCH}_3, \text{OC}_2\text{H}_2\text{C}_2\text{H}_2\text{OH}$), were not emissive in solution at room temperature [85]. Emission maxima for **B** in CH_2Cl_2 were located near 600 nm and emission lifetimes varied from 86 ns ($L = 1$) to 495 ns ($L = 3$) [11]. Molecular rectangle **C** was not emissive at room temperature [86] in agreement with results reported for the monomer, $[\text{Re}(\text{bpm})(\text{CO})_3\text{Cl}]$, where bpm is 2,2'-bipyrimidine, which is also nonluminescent [91]. Rectangle **D** ($L = 1$) gave the characteristic $^3\text{MLCT}$ emission of $\text{Re}(\text{diimine})(\text{CO})_3\text{Cl}$ complexes located at 635 nm with a short emission lifetime of 39 ns and low emission quantum yield of 8.5×10^{-4} [87]. Emission from **E** was observed in the 470–500 nm spectral region with an emission lifetime of ~ 360 ps and low quantum yields of 0.012 ($\text{R} = \text{C}_{12}\text{H}_{25}$) and 0.032 ($\text{R} = \text{C}_6\text{H}_{13}$) [87]. The blue shift in emission was attributed to a mixed $\pi-\pi^*$, $^3\text{MLCT}$ state. Emission from **F** was similar to that observed for **E**; emission lifetimes were near 1 ns and emission quantum yields near 0.1 [88]. Only singlet emission was observed from the molecular rectangles containing zinc porphyrins (**G**) with emission lifetimes were near 1 ns [89]. The Re/Pd square (**H**) showed emission from the $^3\text{MLCT}$ state with a maximum at ~ 625 nm and an emission lifetime of 17 ns [90].

In general, emission intensity in the molecular polygons examined here was significantly diminished from that of the monomolecular rhenium complexes. This can be attributed to a decrease in the emission lifetime due to quenching by the additional vibronic components.

One of the reasons for synthesizing molecular polygons was to examine their use for guest-host interactions and possible catalysis. Quinones were found to quench the emission of **A** by both dynamic and static quenching and the binding constant with methyl-*p*-benzoquinone was determined to be $4.1 \times 10^2 \text{ M}^{-1}$ [62]. Electron transfer quenching of **B** with various amines followed Stern–Volmer behavior at low amine concentrations but deviated at higher concentrations with *N,N,N',N'*-tetramethylphenylenediamine producing an upward curvature of the Stern–Volmer plot and a blue shift in the emission maximum of the rectangle which was interpreted as the result of substrate binding [44]. The 2,9-naphthalenedisulfonate dianion was found by NMR techniques to bind to **C** ($L = 2$) with an association constant of $2.3 \times 10^3 \text{ M}^{-1}$ [86]. Nitro-substituted aromatic amines were found to quench the emission of **D** ($L = 3$) in THF [87] with quenching rate constants that ranged from 4.94×10^8 to $9.12 \times 10^9 \text{ s}^{-1}$. When **D** was cast as a film, 60% quenching occurred upon exposure to dinitrotoluene vapors. Similar quenching experiments with nitro-substituted aromatic amines with **E** were attempted without success. The size of the hole as calculated was too small to hold the guests [87]. Binding of guests such as DABCO (1,4-diazobicyclo[2.2.2]octane) in **F** based on the metalloporphyrin bridging ligand were unsuccessful. The cavity was too narrow for guest

incorporation [89]. The guest in **G** was a special Zn-salen spacer, G-1, which bonded to both Zn atoms in the bridge. Energy transfer was noted by decreases in the emission spectra of both the guest and host as a function of the concentration of added guest [88]. Encapsulation of ClO_4^- increased the emission intensity for **H**. The increase was attributed to a decrease of the quenching rate constant [90].

The N-L-N spacers in **C** were replaced by redox active diimine ligands such as 4,4'-bipyridine and the singly reduced rectangles were generated, placing the added electron on one of the N-L-N ligands. Intervalence electron transfer was observed at 5100 cm^{-1} for N-L-N = 4,4'-bipyridine and attributed to a transition from $\text{N-L-N}^{\cdot-}$ to the other N-L-N ligand. Due to the closeness of the two N-L-N ligands, the process was attributed to direct orbital overlap rather than superexchange through the metal centers [92].

6.7

Host-Guest Molecules

The novel host-guest molecules **A** shown in Fig. 19 were designed to observe charge separation between the rhenium bpy core of the guest and the viologen located on the end of the host. The host and guest were synthesized separately and then allowed to self assemble. Transient absorption data were in agreement with photoinduced electron transfer from the excited state of the rhenium complex to the viologen-host molecule [65]. Molecules **B**

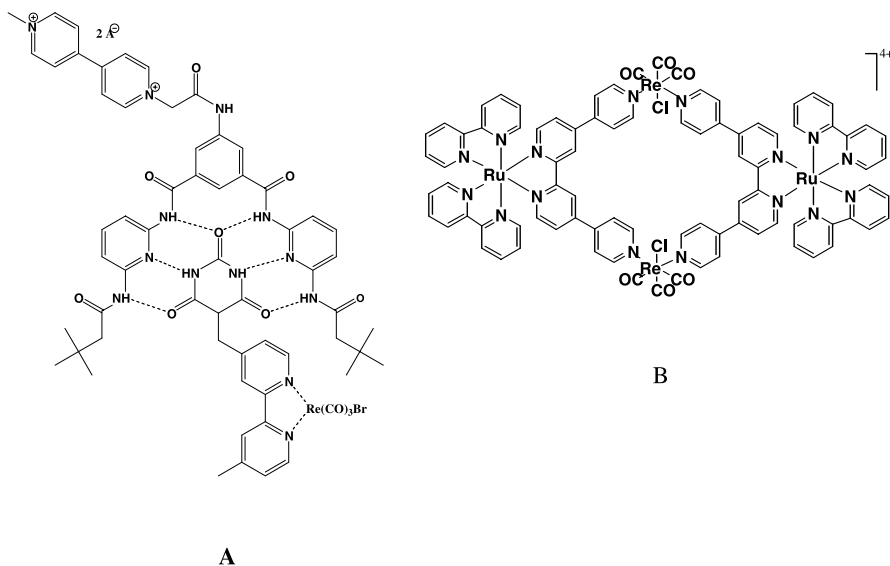


Fig. 19 Host-guest molecules

shown in Fig. 19 house mono- and bicyclic organic molecules such as 1,4-diaminobenzene and 1-naphthol as guests. Instead of changes in emission spectra, it was possible to follow concentration changes of the guests by monitoring changes in the optical spectrum [58]. Other host-guest interactions are discussed in the section on sensors.

6.8

Carbon Dioxide Reduction

Advances in CO₂ reduction using visible irradiation were made in a number of areas. First, photo-oxidant properties of complexes of the type Re(dmb)(CO)₂(P(p-XPh)₃)₂⁺, where X = CH₃O, F, and Cl, were enhanced by increasing the excited state oxidant power due to π-π, CH-π, and CH-π-π interactions resulting from close proximity of the CH(aryl)-π (pyridine)-π (aryl) components. However, the presence of CO₂ did not quench the excited state [61]. CO₂ reduction to CO was affected photocatalytically by Re(4,4'-bpy)(CO)₃PR₃⁺, X = H, CH₃; R = P(OC₂H₅)₃, P(O-i-C₃H₇)₃, in quantum efficiencies of 16–20%. The one electron reduced species generated by excited state quenching by triethanolamine reacted with CO₂ to produce CO [93]. Efficiencies of 9 to 12% for CO production were obtained for the Ru-Re dimer (A) and Ru-Re₃ tetramer (B) shown in Fig. 20. The excited states were quenched by 1-benzyl-1,4-dihydronicotinamide yielding a species with the electron on the Re-bound bpy end of the bridging ligand which migrated to the Re-bound bpy end of the bridging ligand prior to reaction with CO₂ [94].

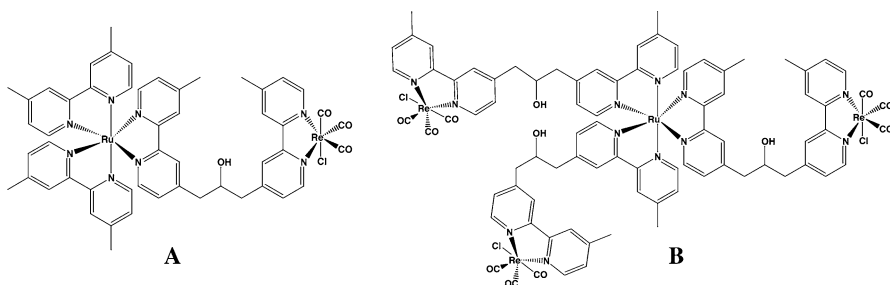
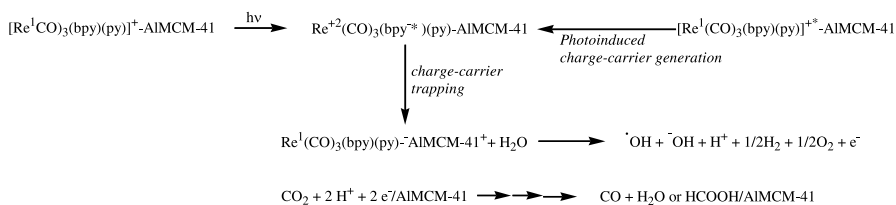


Fig. 20 Multimetallic carbon dioxide reduction photocatalysts

In another study, [Re(bpy)(CO)₃(py)]⁺ was encapsulated into microporous NaY and mesoporous AlMCM-41 molecular sieves. Irradiation of the molecular sieve encapsulated rhenium complex in the presence of CO₂ and H₂O (either gaseous or adsorbed onto the matrix) led to formation of CO and carbonate species. The proposed photoinduced process is outlined in Scheme 5 [95, 96].



Scheme 5 Photocatalytic activation mechanism of CO_2 under visible light irradiation using $[\text{Re}(\text{CO})_3(\text{bpy})(\text{py})]^+$

The use of high pressure photocatalysis resulted in greater turnover number for photocatalytic reduction of CO_2 to CO with $\text{Re}(\text{bpy})(\text{CO})_3\text{Cl}$ and $[\text{Re}(\text{bpy})(\text{CO})_3(\text{POiPr})_3]^+$, in addition to greater catalyst stability [97, 98]. For example, for sacrificial quenching in DMF solution the former exhibited 5.1 times the turnover number at normal pressure (0.1 Pa) using a pressure of 2.45 Pa of CO_2 . The latter showed a 3.8 times increase at 3.8 Pa.

A study involving the photocatalytic properties of two series of complexes of the type $\text{Re}(\text{diimine})(\text{CO})_3\text{X}$ was conducted, where the diimine was substituted a bpy or phen or other related ligands, and X was Cl, CN and other common pseudohalides. It demonstrated that all the complexes that exhibited luminescence were capable of CO_2 reduction under nonaqueous conditions using sacrificial quenching [99]. No clear correlation of activity with structure was discerned; however it was clearly demonstrated that this extended class of materials has a great potential for photocatalytic CO_2 reduction. Of note is that $\text{Tc}(\text{bpy})(\text{CO})_3\text{Cl}$ also is emissive, and is a photocatalyst.

Although not directly a photochemical study, Gibson and co-workers [100] have prepared or isolated a number of species that could be intermediates in the photocatalytic CO_2 reduction to CO or formate, including $\text{Re}(\text{dmbpy})(\text{CO})_3\text{X}$ (dmbpy is 4,4'-dimethyl bipyridine and X is COOH, CHO, OH) and dimeric complexes such as the bicarbonato-bridged complex $[\text{Re}(\text{dmbpy})(\text{CO})_3](\text{OCO}_2)[\text{Re}(\text{dmbpy})(\text{CO})_3]$, the hydrido bridged species $[\text{Re}(\text{dmbpy})(\text{CO})_3]_2(\text{H})[\text{Otf}]$, the CO_2 bridged complex $[\text{Re}(\text{dmbpy})(\text{CO})_3](\text{CO}_2)[\text{Re}(\text{dmbpy})(\text{CO})_3]$. It is suggested that the reactions of $\text{Re}(\text{dmbpy})(\text{CO})_3(\text{COOH})$ could yield CO and formate by parallel paths, one forming $\text{Re}(\text{dmpby})(\text{CO})_4^+$ that subsequently releases CO , and one giving $\text{Re}(\text{dmbpy})(\text{CO})_3\text{CHO}$ that is the source of formate.

6.9

Bioinorganic Applications

Rhenium carbonyl complexes were used as probes in biological systems. Photoexcitation of $[\text{Re}(\text{phen})(\text{CO})_3(\text{H83})]^+\text{AzM}^{2+}$ and $[\text{Re}(\text{phen})(\text{CO})_3(\text{H107})]^+\text{AzM}^{2+}$ ($\text{Az} = \textit{Pseudomonas aeruginosa azurin}$; $\text{M} = \text{Cu or Zn}$) in the presence of the oxidative quencher, $\text{Co}(\text{NH}_3)_5\text{Cl}$, resulted in the formation

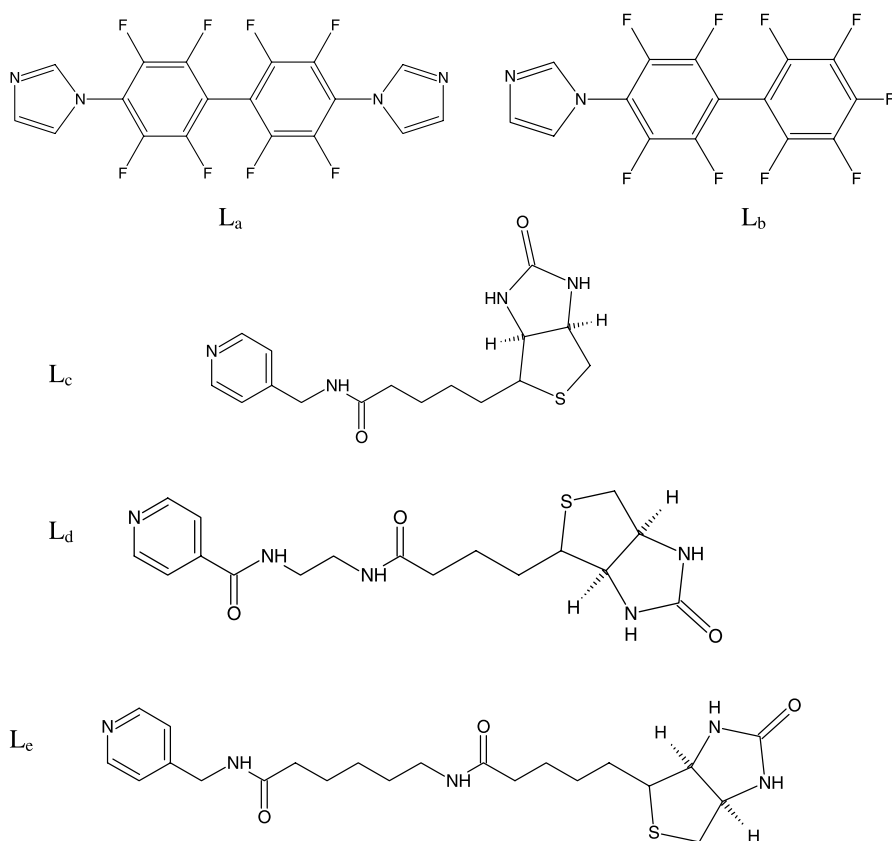


Fig. 21 Imidazole tetrafluorobenzene ligands

of tryptophan and tyrosyl radicals in the protein and their presence was verified by EPR spectroscopy [101]. $[\text{Re}(4,7 - (\text{CH}_3)_2\text{phen})(\text{CO})_3L_a]^+$ and $[\text{Re}(4,7 - (\text{CH}_3)_2\text{phen})(\text{CO})_3L_b]^+$, where L_a and L_b are shown in Fig. 21, bind in the active site of nitric oxidase synthase truncated at residue 114 [102].

Such molecules that invade the active site of the enzyme may provide a means of inhibiting electron transfer from the reductase to the oxygenase domain. $[\text{Re}(\text{diimine})(\text{CO})_3L_{c,d,e}]^+$ complexes, where $L_{c,d,e}$ are shown in Fig. 21; diimine = phen, 3,4,7,8- $(\text{CH}_3)_4\text{phen}$, 2,9- $(\text{CH}_3)_2$ -4,7- Ph_2phen and dipyrido[3,2-*f*:2',3'-*h*]quinoxaline, contain the ligand L with the coordinating pyridine linked to biotin. Biotin binds to the protein avidin and upon binding enhanced the emission of the rhenium chromophore; hence, the complex served as a recorder for the presence of avidin [39].

An interesting use of $\text{Re}(\text{bpy})(\text{CO})_3\text{CN}$ as an excited state oxidant of fluoro-tyrosines (substituted at a number of positions) was published emphasizing the driving force dependence of the reaction using a Marcus analysis (see

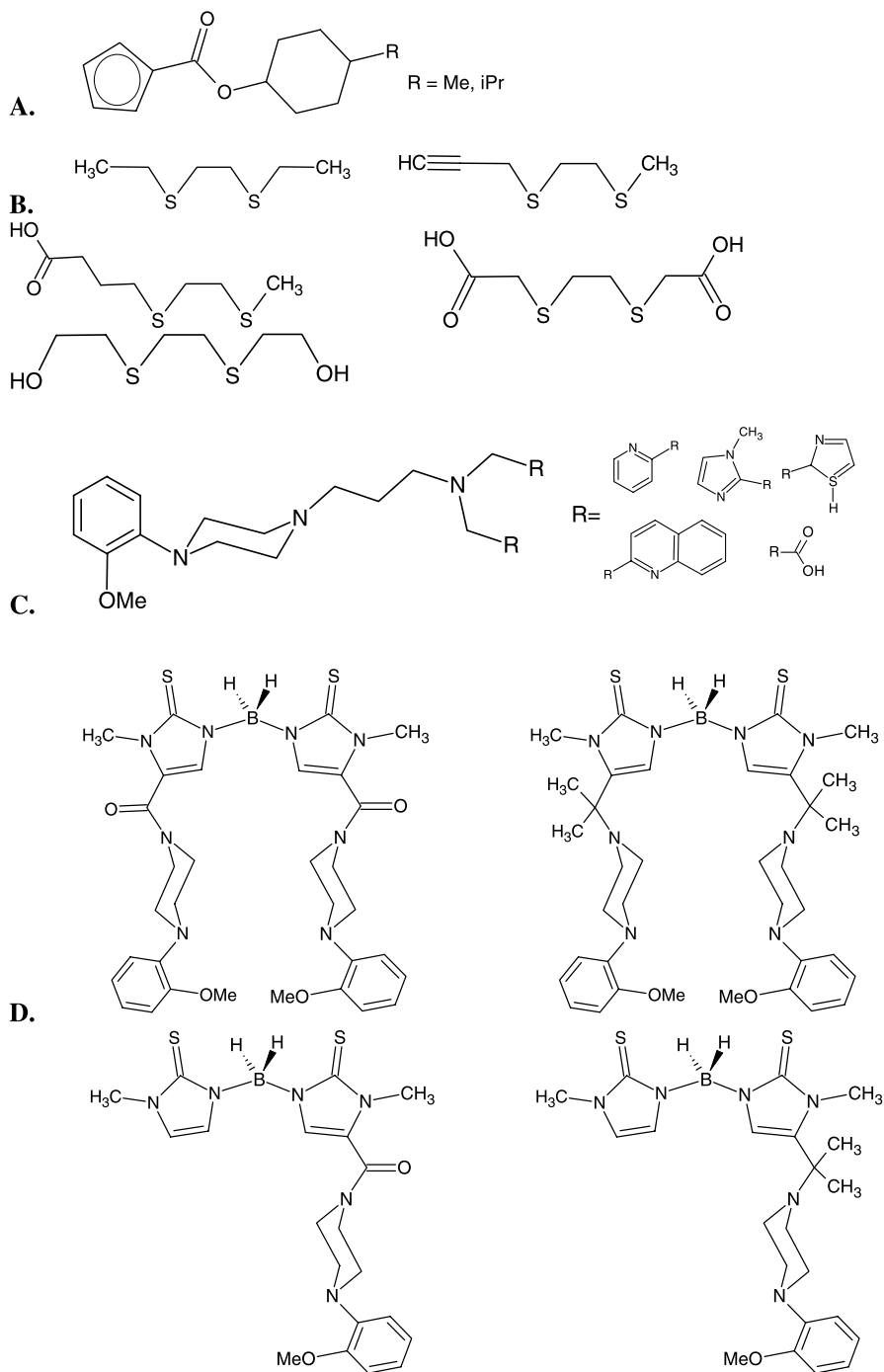


Fig. 22 Ligands bonded to the $\{\text{Re}(\text{CO})_3\}^+$ unit

transient detection section). The fluorotyrosines are presented as powerful probes of charge transport properties in enzymes [68].

Although not necessarily involving photoactive complexes, a variety of approaches have been used to design radiopharmaceuticals for imaging central nervous system receptors. Ultimately, such studies are an important extension of photochemical applications of Re complexes since the design of radiopharmaceuticals that luminescence (for detection) and are therapeutic (by radiation) is a topic of current interest [19]. Re complexes are usually studied prior to the preparation of Tc derivatives since their chemistries are so similar, although the use of Re isotopes for therapy is also possible.

Rhenium tricarbonyl complexes containing, substituted cyclopentadienyl ligands, dithioether ligands and tridentate ligands derived from arylpiperazines were synthesized as models for similar $\{^{99m}\text{Tc}(\text{CO})_3\}^+$ complexes. (Fig. 22) Complexes **A** showed high uptake in the brains of Wistar rats and underwent fast blood clearance. Autoradiographic studies indicated binding to 5-HT_{1A} and adrenergic receptors [103]. $\{\text{Re}(\text{CO})_3\}^+$ complexes bonded to dithioether ligands, **B** in Fig. 22, served as good representatives of $\{^{99m}\text{Tc}(\text{CO})_3\}^+$ which were subjected to biodistribution studies in rats. The low molecular weight, neutral complexes showed brain uptake; a more hydrophilic and an anionic complex exhibited only low brain uptake [104]. Thirteen tridentate arylpiperazine ligands of the form shown in Fig. 22 were

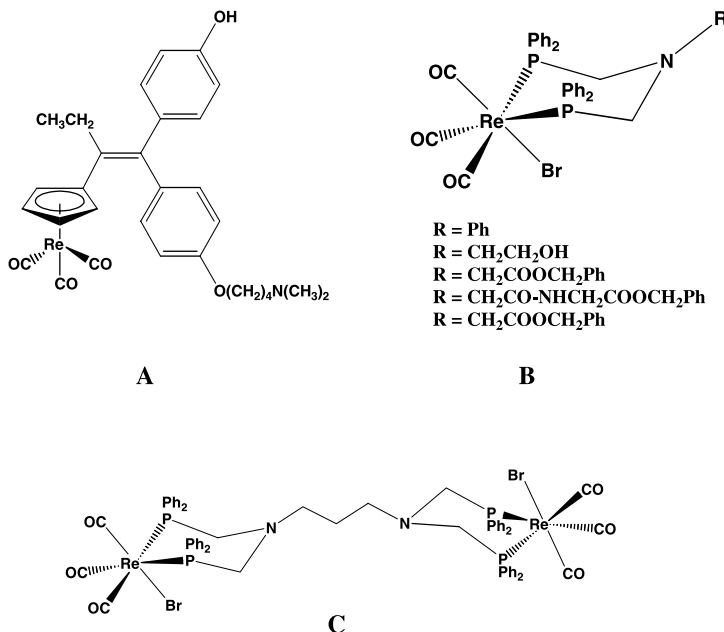


Fig. 23 Rhenium Complexes used in Cancer Studies

synthesized and coordinated to $\{\text{Re}(\text{CO})_3\}^+$ yielding **C** as scaffolds for potential use as pharmacologically specific radiopharmaceuticals. These tridentate chelating ligands form libraries that can be radiolabeled with radioisotopes of Tc and Re [105]. In addition, an umbrella ligand with boron as the central atom (**D**) connected to $\{\text{Re}(\text{CO})_3\}^+$ were reported [106]. Metal complexes based on ligands containing derivatives of 1-(2 methoxy)arylpiperazine were the focus since these components have been most often used as targets for the 5-HT_{1A} subclass of serotonergic receptors.

Rhenium tricarbonyl complexes containing substituted cyclopentadienyl and *bis* diphenylphosphine ligands also were investigated as anti-cancer agents. The antiproliferative effects on breast cancer of complex **A** shown in Fig. 23 were examined relative to the known active metabolite, 4-hydroxytamoxifen, and found to have a similar effect [107]. The cytotoxicity of five rhenium tricarbonyl bis-diphenylphosphine complexes **B** shown in Fig. 23 was examined for 18 different human cancer cell lines. The tests showed that all the complexes were active against specific tumor cell lines, especially a line of breast and uterine cancer [108].

Metallo dendrimers designed as infrared probes for immunological reagents were prepared by tethering $\{(\text{cyclopentadienyl})\text{Re}(\text{CO})_3\}$ complexes to poly(amidoamine) dendrimers. Polyethylene glycol groups were added to improve the solubility [109]. Amplification of the IR signal was anticipated in the CO stretching region.

6.10 Light Emitting Devices

Rhenium 2,2'-bipyridine surfactant complexes, $[\text{Re}(\text{bpy})(\text{CO})_3(\text{L})]\text{PF}_6$ ($\text{L} = \textit{trans}$ -4-dodecyloxy-4'-stilbazole (**L**₂₄), *trans*-4-octadecyloxy-4'-stilbazole (**L**₂₅) and 4-(4'-dodecyloxyphenylethynyl)pyridine) (**L**₂₆) formed stable Langmuir-Blodgett films which served as the emitting layer in organic light emitting diodes (OLEDs). An OLED consisting of 25 layers with ITO glass on the bottom and Al on top took 7 V to turn-on and 18 V to reach 9 cd/cm² [40]. Rhenium 2,2'-bipyridine moieties were used to cap both ends of a polyfluorene yielding $\{\text{Re}(\text{bpy})(\text{CO})_3(\text{py})\text{-X-(py)}(\text{CO})_3(\text{bpy})\text{Re}\}^{2+}$ polymers, where X = polyfluorene of unknown length. The polymer with and without the Re caps were spin-coated from their solutions in CH₂Cl₂ onto an ITO surface previously modified with a layer of poly(styrene sulfonic acid) doped poly(ethylenedioxythiophene). The LED was then topped with a layer of Ca/Al. The photoluminescence (PL) and electroluminescence (EL) showed luminescence consistent with the presence of $[\text{Re}(\text{bpy})(\text{CO})_3(\text{py})]^+$. Further details about the stability and luminescence power were not given [110].

The trifunctional molecule **A** shown in Fig. 24 was synthesized integrating three functions needed for efficient operation of OLEDs. The molecule contains and emissive chromophores (a Re^I polypyridyl complex containing

dipyrido[3,2-a2',3'-c]phenazine), an electron-transporting 1,3,4-oxadiazole group, and a hole-transporting terthiophene unit. The HOMO-LUMO gap of the complex was between that of the poly(N-vinylcarbazole) (PVK) host polymer, a property suggesting its potential use as an OLED [41]. Further investigation in this area should prove fruitful.

Polymers based on 1,10-phenanthroline and chlorotricarbonylrhenium(I) were fabricated into single-layer light emitting devices. The turn-on voltage was ~ 7 V with a 125 cd/m^2 output. The electroluminescence maximum was broad and occurred at 700 nm [111].

One of the brightest Re containing OLEDs reported was based on either $[\text{Re}(\text{bpy})(\text{CO})_3(\text{L})]^+$, complex B shown in Fig. 24, or $[\text{Re}(\text{phen})(\text{CO})_3(\text{L})]^+$, where $\text{L} = 3,5\text{-bis}(\text{trifluoromethyl})\text{pyrazolate}(\text{btpz})$ [42]. The complexes were dopants in host materials 4,4'-dicarbazolyl-1-1'-biphenyl (CBP) and 2,2',2''-(1,3,5-benzenetriyl)tris[1-phenyl-1H-benzimidazole] (TBPI) and sublimable in the 150–165 degree range for vacuum deposition. For $[\text{Re}(\text{bpy})(\text{CO})_3(\text{btpz})]^+$, electrophosphorescence emission occurred at 530 nm at a turn-on voltage of 6 V with luminescence power of 0.72 lm/W and luminescence of 2300 cd/m^2 at a current density of 100 mA/cm^2 [42]. Another rhenium complex, $\text{Re}(\text{CO})_3\text{ClL}$ ($\text{L} = 2\text{-(1-ethylbenzimidazol-2-yl)pyridine}$), was vacuum

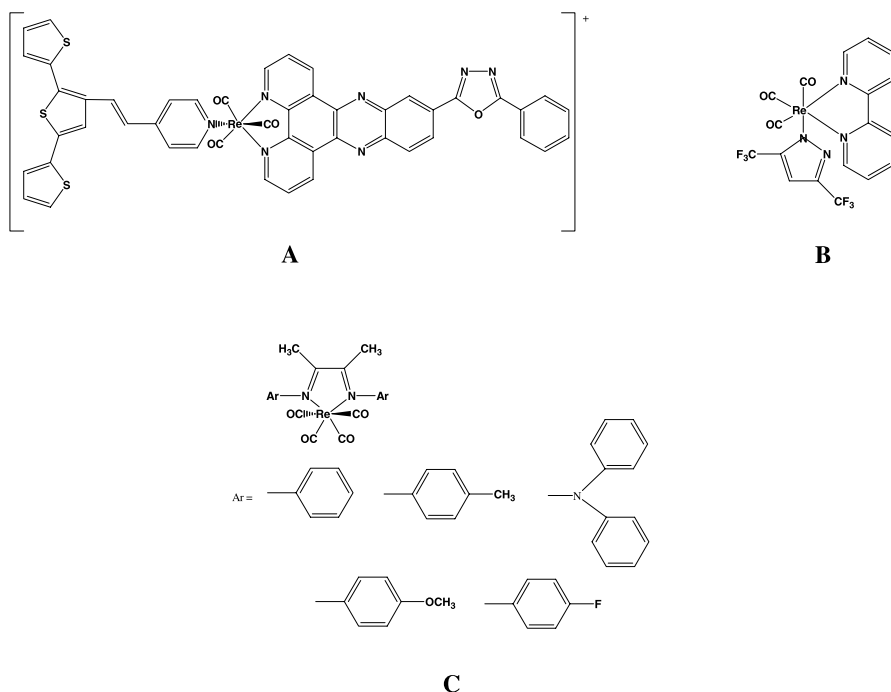


Fig. 24 OLED molecules

deposited onto ITO to form an OLED, and its electroluminescence properties were examined. The maximum output was 113 cd/m^2 at a 11 V bias voltage [112]. Complex system C, also shown in Fig. 24, was examined for its potential use as an electrochemical device. But the lack of the diimine π structure like bpy or phen and the low energy gap gave a poor performance [113].

6.11 Sensors

$[\text{Re}(\text{CO})_3(5\text{-COOH-bpy})\text{Cl}]$ was found to have potential for use as a pH sensor. It was weakly emissive in its protonated form, while it underwent a 10 fold luminescence increase in its deprotonated form. Its $\text{p}K_{\text{a}}$ value was 5.39 [45, 114]. A sol-gel based luminescence pH sensor capable of responding over a wide range from pH 2.3–12 based on the hydrolysis product of $[\text{Re}(\text{py-pzH})(\text{CO})_3\text{L}]^+$, where $\text{py-pzH} = 3\text{-(pyridine-2-yl)pyrazole}$; $\text{L} = 3\text{-N-(pyridine-4-methylene) (aminopropyltriethoxysilane)}$ Fig. 25, spin-coated onto glass slides was reported. The pH dependence was related to the protonation/deprotonation of the 3-(pyridine-2-yl)pyrazole ligand. The excited state $\text{p}K_{\text{a}}^*$ for $[\text{Re}(\text{py-pzH})(\text{CO})_3(\text{py})]^+$ was 7.05 [115]. The acid-base behavior of $[\text{Re}(\text{bpy})(\text{CO})_3(\text{PCA})]^+$ and $[\text{Re}(\text{bpy})(\text{CO})_3(\text{PCA})\text{Re}(\text{bpy})(\text{CO})_3]^{2+}$, $\text{PCA} = 4\text{-pyridinecarboxaldehydeazine}$, [Fig. 25] was opposite to the examples above. Emission increased in the presence of H^+ and was attributed to protonation of one of the N atoms of the $\text{C}=\text{N}-\text{N}=\text{C}-\text{PCA}$ ligand. The excited state $\text{p}K_{\text{a}}^*$ was 2.7 [116].

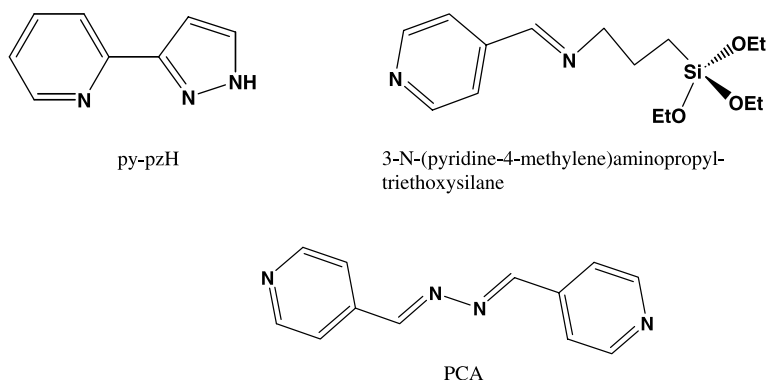
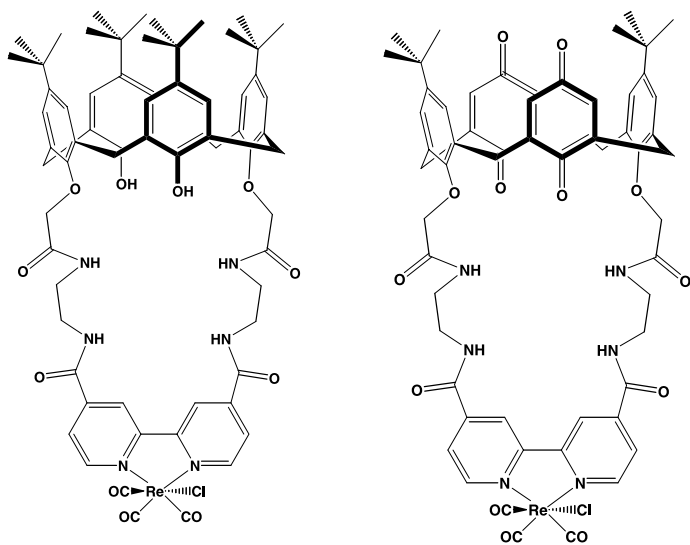
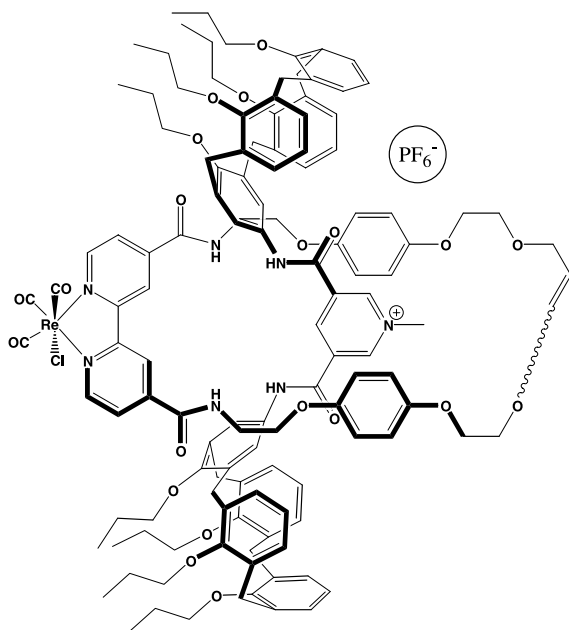


Fig. 25 Proton sensor ligands

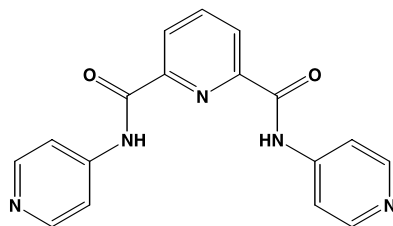
Luminescence sensing was used for anion recognition [49, 117, 118]. Beer et al. [117] reported the use of a modified 2,2'-bipyridine ligand bonded to $\{\text{Re}(\text{CO})_3\text{Cl}\}$ [see Fig. 26 A]. The modified bipyridine ligand contained a macrocyclic $(\text{NH})_4$ cavity capped with a calix [4]arene strapped on its back. The cavity was of sufficient size to accommodate anions. An increase in emis-



A



B

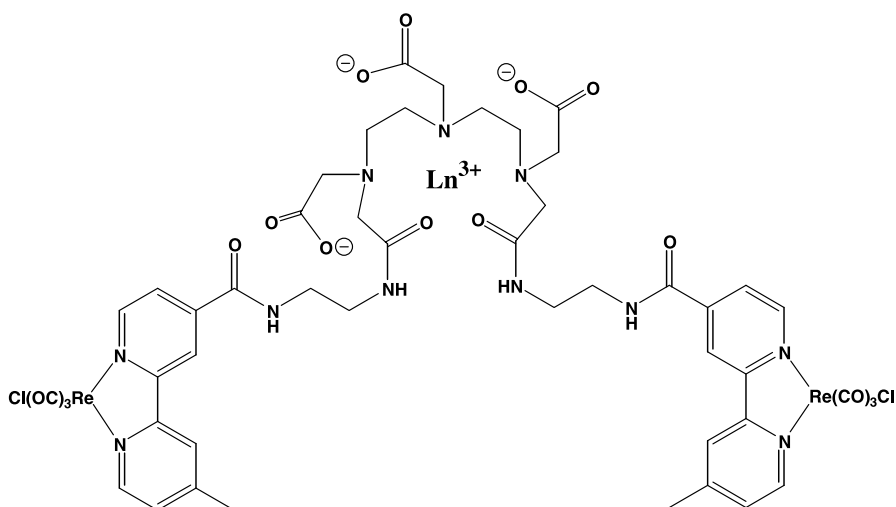


C

◀ **Fig. 26** Anion sensor molecules

sion was found upon addition of Cl^- , $\text{C}_2\text{H}_3\text{O}_2^-$, H_2PO_4^- with a preference for $\text{C}_2\text{H}_3\text{O}_2^-$. Another more complex molecular cavity, also shown in Fig. 26 B, but attached to the same $\{\text{Re}(\text{CO})_3\text{Cl}\}$ core, was more sensitive to HSO_4^- than other anions. Emission in this case also increased [118]. A simpler approach was used by Lee's group. Re-bpy complexes of the type shown in Fig. 26 C containing amide-type receptors served as anion binding sites. In this case emission intensity was quenched in the presence of an anion series: CN^- , F^- , Cl^- , Br^- , I^- , $\text{C}_2\text{H}_3\text{O}_2^-$, H_2PO_4^- , NO_3^- , and ClO_4^- . The sensitivity for CN^- and F^- was so high that quenching of 10% was observed in 10^{-8} M CN^- and F^- [46].

Cation recognition by luminescence sensing has also been reported. As referred to above, release and recapture of alkali and alkaline earth metal ions for $[(\text{bpy})\text{Re}(\text{CO})_3\text{L}_j]^+$, where L_j contains an azacrown ether [63] was controlled by light. A sensor for lanthanide ions is shown in Fig. 27. The photoactive center was Re^{I} ("bpy") and its emission was quenched by the lanthanide ion [119].

**Fig. 27** Lanthanide sensor

7

Other Re(I) Carbonyl Complexes

The primary photolytic step upon UV photolysis of $\text{Cp}^*\text{Re}(\text{CO})_3$, CO loss, has been utilized to study the oxidative-addition of the putative $\text{Cp}^*\text{Re}(\text{CO})_2$ fragment in substituted benzenes. Although preparative chemistry in a gen-

eral sense is not covered in this review, the importance of this reaction to activation of CH, CF and CCl bonds is notable. Thus, $\text{Cp}'\text{Re}(\text{CO})_3$ (Cp' is Cp or Cp^*) afforded oxidative addition products of the type $\text{Cp}'\text{Re}(\text{CO})_2(\text{Ar})\text{H}$ (Ar is C_6F_5 or 2,3,5,6- C_6H_4) as the principal photochemical products, demonstrating CH and activation [120]. Several minor products are produced that are consistent with C-F activation.

Studies with chloroarenes and $\text{Cp}'\text{Re}(\text{CO})_3$ under UV irradiation show oxidative addition products derived from C–Cl bond activation. For example, pentachlorobenzene at 350 nm yields *trans*- $\text{Cp}'\text{Re}(\text{CO})_2(\text{Ar})\text{Cl}$ (Ar is 2,3,4,5- $\text{C}_6\text{Cl}_4\text{H}$) as the primary type of product [121]. Studies of di- and tri-chlorobenzenes [122] and of disubstituted dichloroarenes [123] also show C–Cl bond activation. In the latter case, unusual directing effects were observed, for example, a C–Cl bond across the ring from either CF_3 and CH_3 is selectively activated depending upon the system [123].

The use of photochemical dinitrogen loss has been selectively employed in similar reactions with some notably enlightening results [124, 125]. An early study shows that $\text{Cp}^*\text{Re}(\text{CO})(\text{L})(\text{N}_2)$ (L is $\text{P}(\text{OEt})_3$, $\text{P}(\text{OMe})_3$, PMe_2Ph) photochemically produces *trans*- $\text{Cp}^*\text{Re}(\text{CO})(\text{L})(\text{Ph})\text{Cl}$ under UV irradiation in chlorobenzene, similar to the reports above [124]. However, the analogous reaction of $\text{Cp}^*\text{Re}(\text{CO})_2(\text{N}_2)$ with 1,4-difluorobenzene, produces both the C–H oxidative addition product $\text{Cp}'\text{Re}(\text{CO})_2(\text{Ar})\text{H}$ (Ar is 2,5- $\text{C}_6\text{F}_2\text{H}_3$) and the coordinated benzene product, $\text{Cp}'\text{Re}(\text{CO})_2(\eta^2\text{-1,4-}\text{C}_6\text{F}_2\text{H}_4)$ [125]. The two isomers interconvert around 213 K.

An interesting low-temperature study that directly bears on the reactivity of the $\text{Cp}'\text{Re}(\text{CO})_2$ photofragment identifies three different isomeric pentane adducts in the region of 163–193 K [126]. Proton NMR experiments demonstrate that preferential binding of methylene over methyl group occurs and that the η^2 -binding mode (C–H) is preferred. Deuterium labeling studies support these interpretations and show that H-atom binding is slightly preferred compared to D-atom binding.

The photochemistry of the nitrosyl complex $\text{Cp}^*\text{Re}(\text{CO})_2(\text{NO})^+$ appears superficially similar to the complexes above in that photolysis at wavelengths greater than 310 nm in the presence of PPh_3 gives photosubstitution of CO. The kinetics of product formation for $\text{Cp}^*\text{Re}(\text{CO})(\text{PPh}_3)(\text{NO})^+$ exhibit isosbestic behavior during the early phases of the reaction [127]. Despite this behavior, the low energy transitions in the 320–380 nm range are assigned as metal to nitrosyl charge transfer. Interestingly a weak emission is observed in the solid (570 nm), but not in solution. This is probably the only M to NO charge transfer emission reported.

In a complimentary study, Bitterwolf [128], examined the photochemistry in a triethyloctylammonium hexafluorophosphate matrix at ca. 90 K by IR spectroscopy. Irradiation > 450 nm did not yield products; however, an irradiation wavelength of 400 nm led to a mixture of linkage isomers of Re-NO, i.e., in addition to the N-bound form, the O-bound and side-bound (η^2) prod-

ucts were observed. This is clearly a fascinating system from a fundamental point-of-view apparently exhibiting emission and possibly, two or more types of photoreactions.

Acknowledgements BPS would like to thank the National Science Foundation for financial support.

References

1. Geoffroy GL, Wrighton MS (1979) *Organometallic Photochemistry*. Academic Press, New York
2. Kunkley H, Vogler A (2000) *Coord Chem Rev* 200–202:991
3. Balzani V, Carassiti V (1970) *Photochemistry of Coordination Compounds*. Academic Press, New York
4. Roundhill DM (1994) *Photochemistry and Photophysics of Metal Complexes*. Plenum Press, New York
5. Ferraudi GJ (1988) *Elements of Inorganic Photochemistry*. Wiley, New York
6. Downs A, Dierker G, Green JC, Greene TM, McGrady G, Morris LJ, Scherer W, Sirsch P (2002) *Dalton Trans* 3349
7. Morris LJ, Downs A, Dierker G, Green JC, Greene TM, Teat SJ, Parsons SP (2002) *Dalton Trans* 3142
8. Morris LJ, Downs A, Greene TM, McGrady G, Hermann WA, Sirsch P, Scherer W, Gropen O (2001) *Organometallics* 20:2344
9. Morris LJ, Downs A, Greene TM, McGrady G, Hermann, WA, Sirsch P, Gropen O, Scherer W (2000) *Chem Commun*, p 67
10. Costa PJ, Calhorda MJ, Bossert J, Daniel C, Romao CC (2006) *Organometallics* 25:5235
11. Kunkely H, Vogler A (2000) *J Organomet Chem* 606:207
12. Kunkely H, Vogler A (2005) *Inorg Chem Comm* 8:467
13. Winkler J, Gray HB (1985) *Inorg Chem* 24:346
14. Savoie C, Reber C (1998) 171:387
15. Grey JK, Butler IS, Reber C (2002) 124:11699
16. Grey JK, Butler IS, Reber C (2004) *Can J Chem* 82:1083
17. Landry-Hum J, Tessier V, Ernzerhof M, Reber C (2002) *Coord Chem Rev* 233:63
18. Savoie C, Reber C (2000) *J Am Chem Soc* 122:844
19. Del Negro AS, Wang Z, Seliskar CJ, Heineman WR, Sullivan BP, Hightower SE, Hubler TL, Bryan SA (2005) *J Am Chem Soc* 127:14978
20. Yam W-W, Pui L-Y, Man-Chung Wong K, Cheung K-K (2000) *Inorg Chim Acta* 300:721
21. Bailey SE, Eikey RA, Abu-Omar MM, Zink JI (2002) 41:1755
22. Van der Westhuizen HJ, Purcell W, Basson SS (2002) *Trans Metal Chem* 27:506
23. Bell SEJ, Hill JN, McCamley A, Perutz RN (1990) *J Phys Chem* 94:3876
24. Lee YF, Kirchoff JR (1994) *J Am Chem Soc* 116:3599
25. Del Negro AS, Seliskar CJ, Heineman WR, Sullivan BP, Hightower SE, Bryan SA (2006) *J Am Chem Soc* 128:16494
26. Jones WD, Maguire JA, Rosini GP (1998) *Inorg Chim Acta* 270:77
27. Jones WD, Maguire JA, Rosini GP (1999) *Organometallics* 18:1754
28. Guillaumont D, Finger K, Hachey MR, Daniel C (1998) *Coord Chem Rev* 171:439

29. Guillaumont D, Daniel C (1998) *Coord Chem Rev* 177:181
30. Meyer TJ, Caspar JV (1985) *Chem Rev* 85:187
31. Sarakha M, Ferraudi G (1999) *Inorg Chem* 38:4605
32. Fujita E, Mukerman JT (2004) *Inorg Chem* 43:7636
33. Yukiko H, Shouichi K, Brunshawig BS, Fujita E (2003) *J Am Chem Soc* 125:11976
34. Wenger OS, Henling LM, Day MW, Winkler JR, Gray HB (2004) *Inorg Chem* 43:2043
35. Yam VW-W, Yang Y, Zhang J, Chu BW-K, Zhu N (2001) *Organometallics* 20:4911
36. Yam VW-W, Lau VC-Y, Wu L-X (1998) *J Chem Soc Dalton Trans* 1461
37. Metcalfe C, Spey S, Adams H, Thomas J (2002) *J Chem Soc Dalton Trans* 4732
38. Shen Y, Maliwal B, Lakowicz J (2001) *J Fluorescence* 11:315
39. Lo KK-W, Hui W-K, Chung C-K, Tsang KH-K, Lee TK-M, Li C-K, Lau JS-Y, Ng DC-M (2006) *Coord Chem Rev* 250:1724
40. Yam VW-W, Li B, Yang Y, Chu BW-K, Wong KM-C, Cheung K-K (2003) *Eur J Inorg Chem* 4035
41. Lundin N, Blackman A, Gordon K, Officer D (2006) *Angew Chem Int Ed* 45:2582
42. Ranjan S, Lin S-Y, Hwang K-C, Chi Y, Ching W-L, Liu C-S (2003) *Inorg Chem* 42:1248
43. Costa I, Montalti M, Pallavicini P, Perotti A, Prodi L, Zaccheroni N (2000) *J Organomet Chem* 593-594:267
44. Thanasekaren P, Liao R-T, Manimaran B, Liu Y-H, Chou P-T, Rajagopal S, Lu K-L (2006) *J Phys Chem A* 110:10683
45. Yam VW-W, Ko C-C, Wu L-X, Wong KM-C, Cheung K-K (2000) *Organometallics* 19:1820
46. Sun S-S, Lees A, Zavalij PY (2003) *Inorg Chem* 42:3445
47. Ko C-C, Wu L-X, Wong KM-C, Zhu N, Yam VW-W (2004) *Chem Eur J* 10:766
48. Ko C-C, Kwok W-M, Yam VW-W, Phillips DL (2006) *Chem Eur J* 12:5840
49. Sun S-S, Tran D, Odongo O, Lees A (2002) *Inorg Chem* 41:132
50. Pomestchenko IE, Poluansky DE, Castellano FN (2005) *Inorg Chem* 44:3412
51. Villegas JM, Stoyanov SR, Huang W, Rillema DP (2005) *Dalton Trans* 1042
52. Villegas JM, Stoyanov SR, Huang W, Rillema DP (2005) *Inorg Chem* 44:2297
53. Stoyanov SR, Villegas JM, Cruz AJ, Lockyear LL, Reibenspies JH, Rillema DP (2005) *J Chem Theory Comput* 1:95
54. Ioachim E, Medlycott E, Hanan G (2006) *Inorg Chim Acta* 359:2599
55. Kirgan R, Rillema DP, unpublished observations
56. Wei L, Babich J, Eckelman W, Zubieta J (2005) *Inorg Chem* 44:2198
57. Wei L, Babich J, Ouellette W, Zubieta J (2006) *Inorg Chem* 45:3057
58. de Wolf P, Heath S, Thomas J (2002) *Chem Commun*, p 2540
59. Sun S-S, Lees A (2001) *Organometallics* 20:2353
60. Sun S-S, Lees A (2002) *Organometallics* 21:39
61. Tsubaki H, Sekine A, Ohashi Y, Koike K, Takeda H, Ishitani O (2005) *J Am Chem Soc* 127:15544
62. Manimaran B, Thanasekaren P, Rajendran T, Lin R-J, Chang I-J, Lee G-H, Peng S-M, Rajagopal S, Lu K-L (2002) *Inorg Chem* 41:5323
63. Lewis JD, Perutz RN, Moore JN (2004) *J Phys Chem A* 108:9037
64. Gabrielsson A, Busby M, Matousek P, Towrie M, Hevia E, Cuesta L, Perez J, Zácic S, Vlcek A Jr (2006) *Inorg Chem* 45:9789
65. Dirksen A, Kleverlaan CJ, Reek JNH, De Cola L (2005) *J Phys Chem A* 109:5248
66. Ishitani O, George MW, Ibusuki T, Johnson FPA, Koike K, Nozaki K, Pac C, Turner JJ, Westwell JR (1994) *Inorg Chem* 33:4712
67. Partigianoni CM, Chodorowski-Kimmes S, Treadway J, Strilin D, Trammell SA, Meyer TJ (1999) *Inorg Chem* 38:1193

68. Reece SY, Seyedsayamdost MR, Stubbe J, Nocera DG (2006) *J Am Chem Soc* 128:13320
69. Wolcan E, Torchia G, Tocho J, Piro OE, Juliarena P, Ruiz G, Féiz MR (2002) *J Chem Soc Dalton Trans* 2194
70. Gabrielsson A, Blanco-Rodriguez AM, Matousek P, Towrie M, Vlcek A Jr (2006) *Organometallics* 25:2148
71. Walsh PJ, Gordon KC, Lundin NJ, Blackman AG (2005) *J Phys Chem A* 109:5933
72. Koike K, Tanabe J, Toyama S, Tsubaki H, Sakamoto K, Westwell JR, Johnson FPA, Hori H, Saitoh H, Ishitani O (2000) *Inorg Chem* 39:2777
73. Koike K, Okoshi N, Hori H, Takeuchi K, Ishitani O, Clark IP, George MW, Johnson FPA, Turner JJ (2002) *J Am Chem Soc* 124:11448
74. Hightower SE, Corcoran RC, Sullivan BP (2005) *Inorg Chem* 44:9601
75. Del Negro AS, Woessner SM, Sullivan BP, Dattelbaum DM, Schoonover JR (2001) *Inorg Chem* 40:5056
76. Ishitani O, Kanai K, Yamada Y, Sakamoto K (2001) *Chem Commun*, p 1514
77. Smithback JL, Helms JB, Schutte E, Woessner SM, Sullivan BP (2006) *Inorg Chem* 45:2163
78. Lewis JD, Perutz RN, Moore JN (2000) *Chem Commun*, p 1865
79. Chan WK, Ng PK, Gong X, Hou S (1999) *J Mater Chem* 9:2103
80. Xue W-M, Kün FE, Herdtweck E (2001) *Polyhedron* 20:791
81. Zhang M, Lu P, Wang X, He L, Xia H, Zhang W, Yang B, Liu L, Yang L, Yang M, Ma Y, Feng J, Wang D, Tamai N (2004) *J Phys Chem B* 108:13185
82. Zhang M, Lu P, Wang XM, Xia H, Zhang W, Yang B, Liu LL, Yang L, Yang M, Ma YG, Feng JK, Wang DJ (2005) *Thin Solid Films* 447:193
83. Bignozzi CA, Ferri V, Scoponi M (2003) *Macromol Chem Phys* 204:1851
84. Feliz MR, Ferraudi G (2004) *Inorg Chem* 43:1551
85. Woessner SM, Helms JB, Shen Y, Sullivan BP (1998) *Inorg Chem* 37:5406
86. Benkstein KD, Hupp JT, Stern CL (1998) *J Am Chem Soc* 120:12982
87. Sun S-S, Lees AJ (2000) *J Am Chem Soc* 122:8956
88. Splan KE, Massari AM, Morris GA, Sun S-S, Reina E, Nguyen ST, Hupp JT (2003) *Eur J Inorg Chem* 2348
89. Benkstein KD, Stern CL, Splan KE, Johnson RC, Walters KA, Vanhelmont FWM, Hupp JT (2002) *Eur J Inorg Chem* 2818
90. Slone RV, Yoon DI, Calhoun RM, Hupp JT (1995) *J Am Chem Soc* 117:11813
91. Vogler A, Kisslinger J (1986) *Inorg Chim Acta* 115:193
92. Dinolfo PH, Williams ME, Stern CL, Hupp JT (2004) *J Am Chem Soc* 126:12989
93. Koike K, Hori H, Ishizuka M, Westwell JR, Takeuchi K, Ibuski T, Enjouji K, Konno H, Sakamoto K, Ishitani O (1997) *Organometallics* 16:5724
94. Gholamkhash B, Mametsuka H, Koike K, Tanabe T, Furue M, Ishitani O (2005) *Inorg Chem* 44:2326
95. Hwang J-S, Chang J-S, Park S-E, Ikeue K, Anpo M (2005) *Topics Catal* 35:311
96. Hwang J-S, Kim DS, Lee CW, Park S-E (2001) *Korean J Chem Eng* 18:919
97. Hori H, Takano Y, Koike K, Sasaki Y (2003) *Inorg Chem Comm* 6:300
98. Hori H, Koike K, Kazuhide S, Ishizuka M, Tanaka J, Takeuchi K, Sasaki Y (2002) *J Mol Cat A* 179:1381
99. Kurz P, Probst B, Springler B, Alberto R (2006) *Eur J Inorg Chem* 2966
100. Gibson DH, Yin X, He H, Mashuta MS (2003) *Organometallics* 22:337
101. Di Bilio AJ, Crane BR, Wehbi WA, Kiser CN, Abu-Omar MM, Carlos RM, Richards JH, Winkler JR, Gray HB (2001) *J Am Chem Soc* 123:3181

102. Dunn AR, Belliston-Bittner W, Winkler JR, Getzoff ED, Stuehr DJ, Gray HB (2005) *J Am Chem Soc* 127:5169
103. Saidi M, Seifert S, Kretzschmar M, Bergmann R, Pietzsch H-J (2004) *J Organomet Chem* 689:4739
104. Pietzsch H-J, Gupta A, Reisgys M, Drews A, Seifert S, Syhre R, Spies H, Alberto R, Abram U, Schubiger PA, Johannsen B (2000) *Bioconjugate Chem* 11:414
105. Wei L, Banerjee SR, Levadala MK, Babich J, Zubieta J (2004) *Inorg Chim Acta* 357:1499
106. Garcia R, Xing Y-H, Paulo A, Domingos Â Santos I (2002) *J Chem Soc Dalton Trans* 4236
107. Jaouen G, Top S, Vessières A, Pigeon P, Leclercq G, Laios I (2001) *Chem Commun*, p 383
108. Zhang J, Vittal JJ, Henderson W, Wheaton JR, Hall IH, Hor TSA, Yan YK (2002) *J Organomet Chem* 650:123
109. Heldt J-M, Fischer-Durand N, Salmain M, Vessières A, Jaouen G (2004) *J Organomet Chem* 689:4775
110. Lee P-I, Hsu SL-C, Chung C-T (2006) *Synthetic Metals* 156:907
111. Ng PK, Gong X, Chan SH, Lam LSM, Chan WK (2001) *Chem Eur J* 7:4358
112. Wang K, Huang L, Gao L, Jin L, Huang C (2002) *Inorg Chem* 41:3353
113. Lam LSM, Chan WK (2001) *Chem Phys Chem* 4:252
114. Amendola V, Bacchilega D, Costa I, Gianelli L, Montalti M, Pallavicini P, Perotti A, Prodi L, Zaccheroni N (2003) *J Photochem Photobiol A: Chem* 159:249
115. Lam MHW, Lee DYK, Man KW, Lau CSW (2000) *J Mater Chem* 10:1825
116. Cattaneo M, Fagalde F, Katz NE (2006) *Inorg Chem* 45:6884
117. Beer PD, Timoshenko V, Maestri M, Passaniti P, Balzani V (1999) *Chem Commun*, p 1755
118. Curiel D, Beer PD (2005) *Chem Commun*, p 1909
119. Pope SJA, Coe BJ, Faulkner S (2004) *Chem Commun*, p 1550
120. Godoy F, Higgitt CL, Klahn AH, Oelckers B, Parsons S, Perutz R (1999) *Dalton Trans* 2039
121. Klahn AH, Toro A, Oelckers B, Buono-Core GE, Manriquez V, Wittke O (2000) *Organometallics* 19:2580
122. Klahn AH, Carreno M, Godoy F, Oelckers B, Pizarro A, Toro A, Reyes A (2001) *J Coord Chem* 54:379
123. Abally A, Clot E, Eisenstein O, Garlan MT, Godoy F, Klahn AH, Munoz JC, Oelckers B (2005) *New J Chem* 29:226
124. Leiva C, Sutton D (1998) *Organometallics* 17:4568
125. Carbo JJ, Eisenstein O, Higgitt CL, Klahn AH, Maseras F, Oelckers B, Perutz RN (2001) *Dalton Trans* 1472
126. Lawes DJ, Geftakis S, Ball GE (2005) *J Am Chem Soc* 127:4134
127. Kunkley H, Powlowski V, Vogler A (2002) *Inorg Chim Acta* 335:147
128. Bitterwolf TE (2004) *J Photochem Photobiol A* 163:209

Photochemistry and Photophysics of Coordination Compounds: Osmium

Duraisamy Kumaresan · Kalpana Shankar · Srivathsa Vaidya ·
Russell H. Schmehl (✉)

Department of Chemistry, Tulane University, New Orleans, LA 70118, USA
russ@tulane.edu

1	Introduction and Scope	102
2	Classical Transition Metal Complexes of Os	102
2.1	Complexes with Imine Ligands	102
2.2	Other Classical Transition Metal Complexes	111
3	Energy and Electron Transfer Reactions	112
3.1	Intramolecular Electron Transfer	112
3.2	Os Complexes as Quenchers in Energy and Electron Transfer Systems	115
3.3	Energy Transfer Involving Aromatic Hydrocarbon Donors/Acceptors	124
4	Photochemistry and Photophysics of Organometallic Os Complexes	128
4.1	Os Carbonyl Cluster M–M Cleavage	128
4.2	Complexes Exhibiting CO Loss	131
4.3	Other Organometallic Photoreactions	131
5	Photonic Applications of Os Complexes	133
5.1	Sensors and Biological Applications	133
5.2	Photovoltaic Cells	135
5.3	Electroluminescent Devices	138
	References	139

Abstract This review provides an overview of research since the year 2000 relating to photochemical and photophysical processes involving complexes of osmium. The review is broken into four focus subjects. The photophysical investigations of Os(II) imine complexes and other classical transition metal complexes is presented, including a brief discussion of theoretical approaches to understanding electronic structure. An overview of light induced energy and electron transfer reactions involving Os complexes is also covered. Photoreactions of organometallic Os complexes are discussed, focusing on mechanistic aspects of metal–metal cleavage in diosmium and triosmium carbonyl complexes. Finally, reports of applications of Os complexes to sensors, dye sensitized solar cells, electroluminescent devices, and biological systems are presented.

Keywords Bipyridyl · Energy transfer · Osmium complexes · Osmium photochemistry · Osmium photophysics · Photosubstitution · Terpyridyl

1

Introduction and Scope

This article is intended to review the published work on the photochemistry and photophysics of osmium complexes that has appeared in the literature over the past several years. We have attempted to cover, albeit somewhat selectively, literature dating back to the year 2000. A variety of reviews pertaining to particular aspects of osmium photophysics and photochemistry were published prior to 2000. A few reviews discuss the photophysical behavior of primarily monometallic Os complexes in solution [1, 2]. Several earlier reviews discuss light induced energy and electron transfer reactions involving osmium complexes; in much of this work the Os complex is not the chromophore [3–6]. Finally, one review exists discussing the photochemistry of Os carbonyl complexes [7].

In examining the published work in this area over the past 5 years, searches were done using Chemical Abstracts SciFinder and SCOPUS. The searches cover work published through October 2006. From the results, manuscripts were grouped into the divisions that appear in this article. There was a significant body of work discussing the photophysical and photochemical behavior of osmium imine complexes, expanding and refining work published in the 1980s and 1990s. By far the most active area since 2000 has been studies of photoinduced intramolecular energy and electron transfer reactions involving Os complexes. The photochemistry of a variety of organometallic species was also reported. Finally, osmium complexes have been used in a variety of applications ranging from DNA sensing to sensitization of dye sensitized solar cells. This review is not, nor is it intended to be, comprehensive. Our hope is that we have managed to present examples of the majority of systems involving interaction of light with osmium complexes, and that this review may serve as a starting point for persons interested in particular areas of osmium photochemistry. Ligands other than those typically described in textbooks of inorganic chemistry are gathered in Scheme 1 and are organized alphabetically by the acronyms presented in the text.

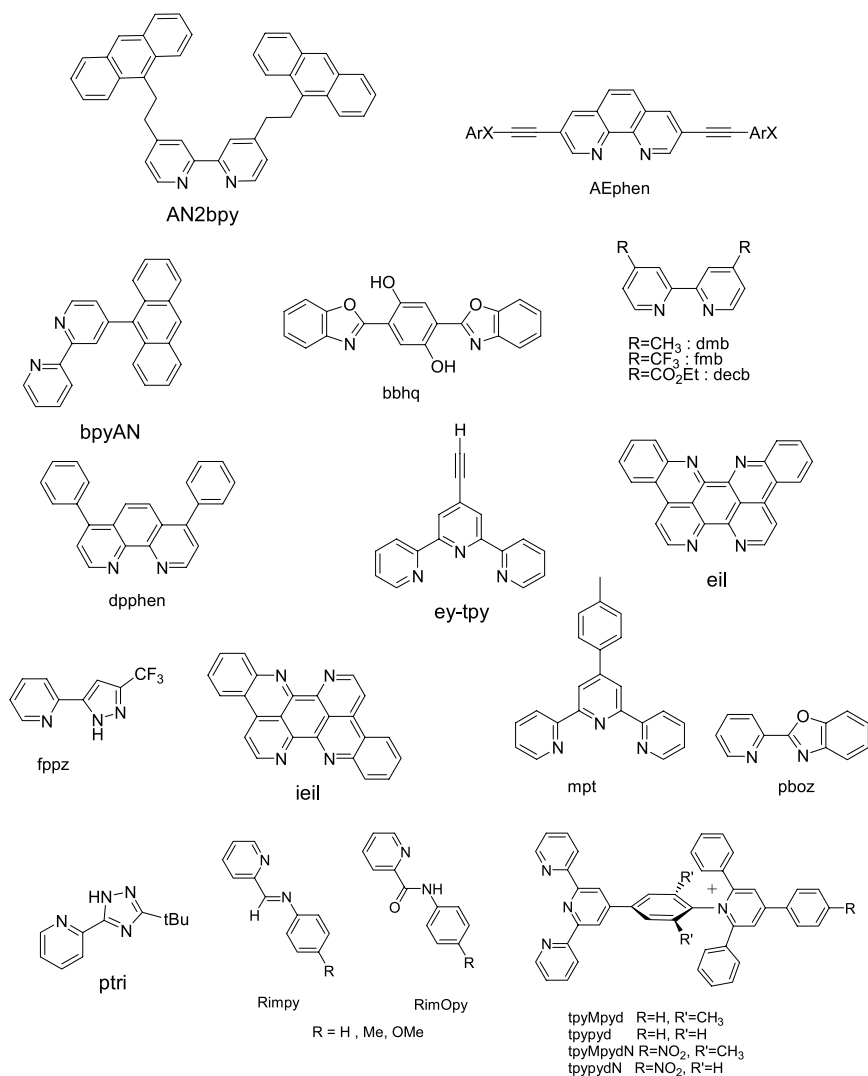
2

Classical Transition Metal Complexes of Os

2.1

Complexes with Imine Ligands

The photophysical behavior of the parent complex of this series, $[\text{Os}(\text{bpy})_3]^{2+}$ (bpy = 2,2'-bipyridine) has been thoroughly investigated by Meyer, Sutin, Yersin, and others, predominantly in the 1980s [8–11]. They established the relationship between the photophysics of Ru(II) diimine and Os(II) diimine



Scheme 1 Structures of simple ligands used

complexes, illustrating that the emissive excited state is Os to diimine metal-to-ligand charge transfer (MLCT) in character. Luminescence from Os(II) complexes is generally at lower energy than that from the related Ru(II) complexes, in part due to the significantly more negative one-electron oxidation potential of the Os(II) complexes. Earlier work also demonstrated that the excited state lifetimes of Os(II) diimines are generally shorter than those of the corresponding Ru(II) complexes and explained this through spin-orbit coupling and energy gap considerations.

Terpyridyl complexes of Ru(II) generally have MLCT states with very short excited state lifetimes [12]. Relaxation is via thermally activated population of a ligand field (LF) excited state that decays rapidly to the ground state. In recent work of Benniston and Harriman, thermally activated nonradiative relaxation was examined for $[\text{Os}(\text{tpy})_2]^{2+}$ ($\text{tpy} = 2,2',6',2''$ -terpyridine) and an ethynylated terpyridyl derivative, $[\text{Os}(\text{ey} - \text{tpy})_2]^{2+}$. For the tpy complex they observed two states accessible by thermal activation: one, believed to be a higher lying MLCT state 640 cm^{-1} above the ground state and the other, a LF state 3500 cm^{-1} higher in energy than the ground state. Surprisingly, they found that the ey-tpy derivative had a much smaller barrier for population of the LF state [13].

Other recent work on the temperature dependence of the luminescence behavior of Os(II) diimine complexes was reported by Ogawa and coworkers in the investigation of $[\text{Os}(\text{bpy})_2(4,4'\text{-dcbpy})]$ and $[\text{Os}(\text{bpy})_2(3,5\text{-dcbpy})]$, where $4,4'\text{-dcbpy} = 4,4'$ -dicarboxy-2,2'-bipyridine and $3,5\text{-dcbpy} = 3,5$ -dicarboxy-2,2'-bipyridine. The $4,4'\text{-dcbpy}$ complex exhibited a decrease in the luminescence lifetime with increasing temperature and had an activation barrier of approximately 350 cm^{-1} . The luminescence lifetime of the $3,5\text{-dcbpy}$ complex, however, increased with increasing temperature. This surprising observation remains unexplained [14].

Interligand electron transfer dynamics in the $^3\text{MLCT}$ excited state of $[\text{Os}(\text{bpy})_3]^{2+}$ and other mixed ligand Os(II) complexes has been examined by Papanikolas et al. using femtosecond spectroscopy [15–17]. They used polarization anisotropy measurements following excitation at various wavelengths (different levels of the potential energy manifold). Figure 1 illustrates that excitation is into both the singlet and triplet MLCT manifolds and that vertical excitation could result in population of different surfaces, corresponding to different degrees of ligand localization of the MLCT state in both the singlet and triplet manifolds. Upon excitation into the lower energy portion of the direct absorption into the $^3\text{MLCT}$ state, the excitation energy appears to be partially localized and the timescale for hopping from one ligand to another is on the order of 9 ps. Excitation higher into the $^3\text{MLCT}$ manifold results in energy dissipation in part into solvent vibrational modes, and the complex remains vibrationally cold. Excitation into the red edge of the $^1\text{MLCT}$ transition results in subpicosecond intersystem crossing, vibrational cooling of the vibrationally excited $^3\text{MLCT}$ state on the order of 16 ps, and interligand energy migration on the 4–5 ps timescale. The results of this work contrast with those of an earlier report of interligand energy migration in $[\text{Os}(\text{bpy})_3]^{2+}$ [18].

The lower energy luminescence of Os(II) complexes relative to the corresponding Ru(II) complexes has led to a number of studies seeking complexes that absorb throughout the visible (black chromophores) and have emissive excited states in the near-infrared. Kol and Barigelletti reported the photophysical properties of Os(II) complexes of eilatin (eil, Scheme 1) and isoeilatin (ieil) bis-phenanthroline derivatives. The eil com-

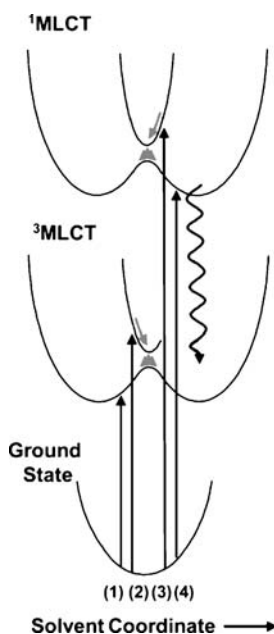


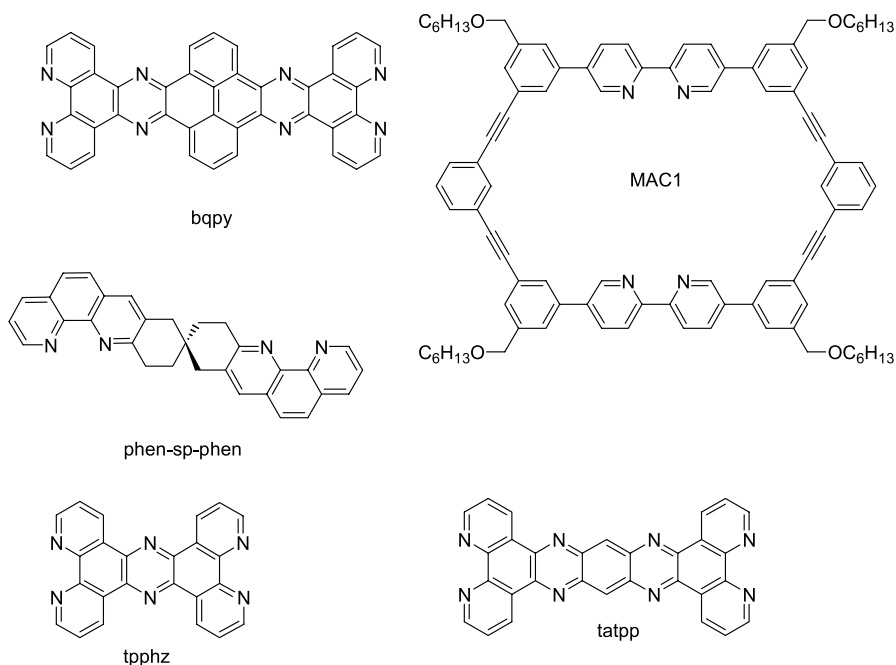
Fig. 1 Potential energy surfaces of the ¹MLCT and ³MLCT states of [Os(bpy)₃]²⁺ for a model in which the excitation can be localized on a single bipyridine [16]

plex [Os(eil)₃]²⁺ exhibits near-infrared emission at 1060 nm with a very low luminescence quantum yield. The ieil complexes studied, [Os(bpy)₂(ieil)]²⁺ and [{Os(bpy)₂]₂{μ-ieil}]⁴⁺, absorb throughout the visible, and thus appear as nearly black chromophores. Only the monometallic complex is luminescent with a maximum of 1240 nm. The emission was too weak for luminescence lifetimes to be obtained for these complexes [19–21].

The synthesis and near-infrared photoluminescence of [Os(bpy)₂(3,8-diarylethynyl-1,10-phenanthroline)]²⁺ complexes (AEphen; A = methoxyphenyl, biphenyl, nitrophenyl) have recently been reported. These phenanthroline complexes exhibit emission in the 790–830 nm region. The nitrophenylethynyl derivative exhibits no room temperature luminescence, presumably because of intramolecular electron transfer quenching [22].

A bimetallic Os(II) complex of the macrocyclic ligand MAC1 (Scheme 2) was prepared and characterized by Venturi et al. Each Os(II) center of the complex has a [(bpy)₂Os(II)] fragment attached to one of the bipyridyl units of MAC1. The complex has absorption and luminescence behavior reasonably similar to that of [Os(bpy)₃]²⁺ with an absorption maximum of 488 nm and emission with a maximum of 740 nm ($\tau_{RT} = 59$ ns, $\phi_{RT} = 0.003$). The complex may be used in the development of supramolecular assemblies [23].

Chirboli, Scandola, Campagna, and McDonnell have examined bimetallic Os complexes having the bridging ligand 9,11,20,22-tetraazatetrapyrido[3,2-



Scheme 2 Structures of bridging ligands

a:2',3'-c:3'',2''-l:2''',3'''-n]pentacene (tatpp, Scheme 2). The complex prepared, $[(\text{phen})_2\text{Os}(\text{tatpp})\text{Os}(\text{phen})_2]^{4+}$ (phen = 1,10-phenanthroline), has absorption and redox characteristics similar to the tris-phenanthroline complex, except the one-electron reduction of the tatpp ligand is very low (near 0 V vs SCE). The complex is nonluminescent in solution at room temperature and the photophysical behavior was examined using transient absorption spectroscopy. The excited bimetallic complex has a lifetime of approximately 60 ps at room temperature. The authors were able to conclude that, while the bimetallic Ru(II) complex has a ligand centered excited state, the Os(II) dimer has an Os to bridging ligand MLCT excited state [24].

A number of bimetallic Os(II) imine complexes have been prepared with a variety of bridging ligands (BL). Often these complexes are reported along with mixed metal Ru(II)(BL)Os(II) systems in which energy transfer from the Ru(II) imine complex to the Os(II) complex is examined. The mixed metal complexes are reviewed in Sect. 3, and structures of bridging ligands are shown in Scheme 2. A typical example is from the work of Juris et al., in which a set of complexes of this type was prepared using spirohexane linked bis-phenanthroline ligands as bridging ligand [25].

An active area of research in transition metal complex photophysics has been the preparation of complexes exhibiting blue or green phosphorescence with high quantum yields for emission, for potential application in electro-

luminescent devices. Recent work on Os(II) imine complexes has yielded some interesting results, particularly with mixed imine carbonyl complexes. Collected luminescence maxima and quantum yields are presented in Table 1. One example comes from the work of Wu et al. on the preparation and photophysical investigation of complexes of the pyridylpyrazolate ligand fppz (Scheme 1). The structure of the neutral complex $[\text{Os}(\text{fppz})_2(\text{CO})_2]$ shown in Fig. 2 demonstrates the two pyrazoyl substituents are *cis* to one another. The complex exhibits structured emission in solution at room temperature from a ligand localized $\pi-\pi^*$ state with maxima at 430, 457, and 480 nm, an emission quantum yield of 0.14, and an excited state lifetime of over 18 μs [26]. The blue phosphorescence, high quantum yield, and absence of charge on the complex make this complex potentially attractive for organic light-emitting diode (OLED) applications.

More recently, this group has published a very elegant examination of related Os(II) complexes that exhibit significant luminescence solvatochromism. Starting with $[\text{Os}(\text{fppz})_2(\text{CO})_2]$, it was demonstrated that one of the CO ligands could be substituted with a variety of substituted pyridines. For complexes having pyridazine (pdz), 4,4'-bipyridine (4,4'-bpy), or 4-cyanopyridine (CNpy) as the substituting ligands, luminescence was observed in the green to red, depending on solvent, with emission quantum yields of a few percent and lifetimes typically in the tens of nanoseconds. Density functional studies of the complexes indicated the excited state had significant fppz to L (CNpy, 4,4'-bpy, pdz) character and that it was this large charge displacement that gave rise to the solvatochromism. A few of these complexes are included in Table 1 [27].

Table 1 Room temperature (RT) photophysical properties of mixed imine/carbonyl complexes of Os(II)

Complex	Abs λ_{max} , nm ^b	λ_{max} , RT em, nm	τ_{em} , RT, μs	ϕ_{em} , RT	Refs.
$[\text{Os}(\text{fppz})_2(\text{CO})_2]$		430, 457, 480	18	0.14	[26]
$[\text{Os}(\text{fppz})_2(\text{CO})(\text{pdz})]^{\text{a}}$	396, 420	654	0.086	0.01	[27]
$[\text{Os}(\text{fppz})_2(\text{CO})(\text{CNpy})]^{\text{a}}$	389, 429	710	0.004	0.001	[27]
$[\text{Os}(\text{bpy})(\text{CO})_2(\text{I})_2]$	350, 404	606	0.239	0.15	[28]
$[\text{Os}(\text{dbbpy})(\text{CO})_2(\text{I})_2]$	350, 390	583	0.025	0.02	[28]
$[\text{Os}(\text{dpphen})(\text{CO})_2(\text{I})_2]$	327, 395	604	0.556	0.39	[28]
$[\text{Os}(\text{pboz})(\text{CO})_2(\text{I})_2]$	325, 421	650	0.295	0.02	[28]
$[\text{Os}(\text{dbpboz})(\text{CO})_2(\text{I})_2]$	338, 354	640	0.083	0.02	[28]

^a In CH_3CN

^b Absorption spectra also have lower energy bands with lower absorptivity

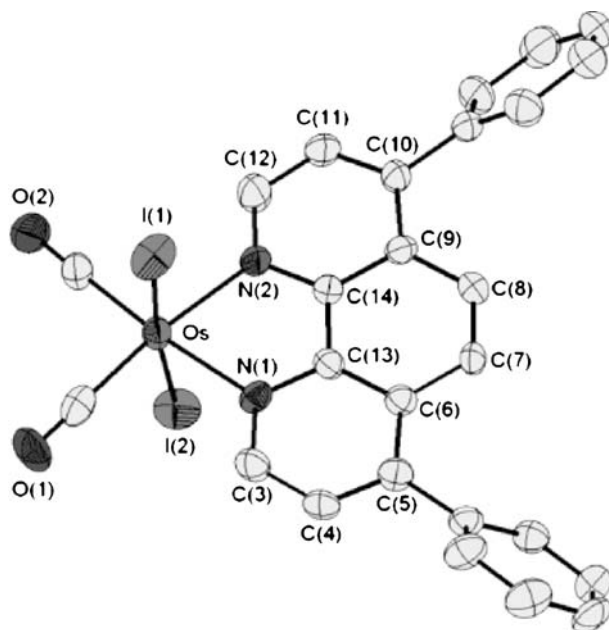


Fig. 3 X-ray structure of $[\text{Os}(\text{CO})_2(\text{I})_2(\text{dpphen})]$ [28]

plex is luminescent, photoisomerization is observed to occur ($\phi_{\text{isom}} = 0.04$) on the subnanosecond timescale. Figure 4 shows absorption spectra of the starting S,S complex and the photoproduct S,O complex, as well as the emission spectrum of the S,S complex. Isomerism beyond the S,O complex does not occur and thermal relaxation to the more stable S,S complex occurs over several hours at elevated temperatures. Interestingly, the closely related complex $[\text{Os}(\text{bpy})_2\text{Cl}(\text{DMSO})]^+$ does not exhibit photoisomerism.

Upon investigation of the carbonyl complex *trans*-(Cl)- $[\text{Os}(\text{bpy})(\text{CO})_2\text{Cl}_2]$, Hartl and coworkers observed that photoirradiation in acetonitrile with $\lambda \geq 320$ nm light gives rise to substitution of a CO ligand, with the formation of *trans*-(Cl)- $[\text{Os}(\text{bpy})(\text{CO})(\text{CH}_3\text{CN})\text{Cl}_2]$ [31]. Carbonyl loss is also observed upon one-electron oxidation of the *trans*-(Cl) dicarbonyl complex in acetonitrile. Electrochemical oxidation in noncoordinating solvents does not lead to CO loss. The mono-solvento photoproduct is stable to further ligand loss.

The photostability of Os(II) bipyridyl complexes with covalently attached hydroquinone was investigated by Keyes and coworkers. In the complex $[\text{Os}(\text{bpy})_2(\text{bbhq})]^+$ (Scheme 1) the Os(II) center is coordinated to one ligand nitrogen and one of the oxygens of the central hydroquinone. The complex has an Os to bpy MLCT absorption with a maximum of 493 nm, but is non-luminescent. Photolysis in acetonitrile in the presence of excess Cl^- did not yield any measurable photodegradation [32].

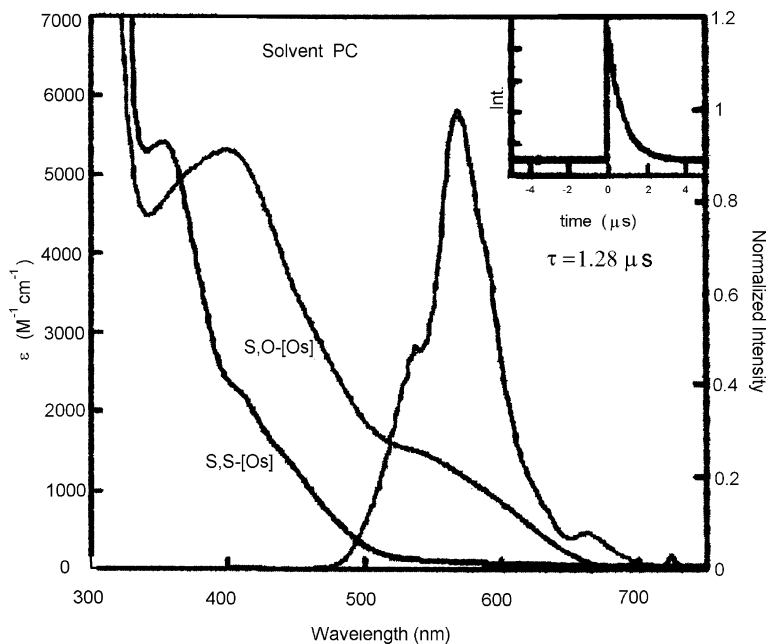


Fig. 4 Absorption and luminescence spectra of $[\text{Os}(\text{bpy})_2(\text{DMSO})_2]^{2+}$. Spectra shown are for the starting S,S bound bis-DMSO and the photoproduct S,O bound bis-DMSO. The inset shows the luminescence decay of the S,S complex [30]

Photosensitized generation of singlet oxygen from ruthenium(II) and osmium(II) bipyridyl complexes has been reported by Abdel-Shafi and co-workers. The work reports oxygen quenching rate constants for a variety of complexes and discusses the relationship between the excited state and redox characteristics of the chromophores and the overall efficiencies for producing singlet oxygen. Os(II) chromophores examined include $[\text{Os}(\text{bpy})_3]^{2+}$, $[\text{Os}(\text{bpy})_2(\text{CO})\text{Cl}]^+$, and $[\text{Os}(\text{bpy})_2(\text{CH}_3\text{CN})\text{Cl}]^+$. One key observation is that rate constants for singlet oxygen formation for Os(II) complexes are faster than rate constants for the corresponding Ru(II) complexes, possibly due to differences in spin-orbit coupling between the two metal centers [33].

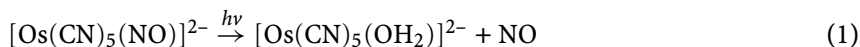
Photoinduced and chemical oxidation of coordinated imines to amides in isomeric osmium(II) complexes of *N*-arylpyridine-2-carboxaldimines has been studied by Ghosh and coworkers [34]. The complexes $[\text{Os}(\text{Br})_2(\text{Rimpy})_2]$ (Scheme 1) were prepared and characterized structurally, indicating the pyridines of the two Rimpy ligands are *trans* to one another and the bromides are *cis*. Broadband photolysis of the complex in aerated acetonitrile resulted in oxidation of one Rimpy ligand to yield the RimOpy ligand and oxidation of the osmium to Os(III). The overall yield of the photochemical process is reported to be greater than 95%. The authors propose a mech-

anism involving electron transfer from the excited state of the complex to oxygen and subsequent attack of the superoxide on the ligand imine carbon to make an Os(III) peroxo intermediate that eliminates a hydroxyl radical to yield [Os(III)(Br)₂(Rimpy)(RimOpy)].

2.2

Other Classical Transition Metal Complexes

The photorelease of nitrogen monoxide (NO) from pentacyanonitrosyl coordination compounds of trivalent Fe, Ru, and Os (Eq. 1) was reported by Videla, Braslavsky, and Olabe.



The work reports wavelength dependent quantum yields for the photoreaction and photosubstitution yields for the Os(III) complex are much lower than those of the iron or ruthenium analogs. The authors also report that the complexes exhibit weak luminescence in the green; the Os(III) complex has a reported emission yield of 0.008 [35].

Taube and coworkers prepared η^6 -arene Os(II) complexes with the ligands tmtacn, tacn, and triamine completing the coordination sphere (tmtacn = 1,4,7-trimethyl-1,4,7-triazacyclononane; tacn = 1,4,7-triazacyclononane). Photolysis of the [$(\eta^6$ -arene)Os(II)(tacn)] complexes in acetonitrile results in clean conversion to the [(CH₃CN)₃Os(II)(tacn)] complex. The photolyses were carried out in the presence of biphenyl, a strong absorber of 254-nm light, to screen the photoproduct from photolysis. Interestingly, the tmtacn complexes proved to be photostable when the arene is *p*-cymene and the photosubstitution takes place *much* more slowly for the benzene complex, [(benzene)Os(II)(tmacn)], relative to the unmethylated tacn complex. While quantum yields were not reported for the process, the qualitative effect was large. The observed difference in reactivity was attributed to steric effects and this contention was supported by the fact that the [$(\eta^6$ -arene)Os(II)(NH₃)₃] complexes readily substituted upon photolysis in acetonitrile [36].

As a last example of work on non-imine coordination complex photochemistry, Coppens and coworkers observed crystallographic evidence for side-on coordination of N₂ to a single Os center in a photoinduced metastable state. Irradiating crystals of the complex [(NH₃)₅Os(N₂)], they noted a decrease in the infrared stretch associated with coordinated N₂, which could reasonably be explained as linkage isomerism of the N₂ to a side-on coordination. At low temperatures, thermal conversion back to the end-on coordination isomer is slowed, allowing photochemical conversion of the end-on complex to the metastable side-on complex. Through very elegant X-ray crystallographic analysis the authors were able to obtain a difference electron density map, and thus a structure of the side-on dinitrogen. Figure 5 shows the

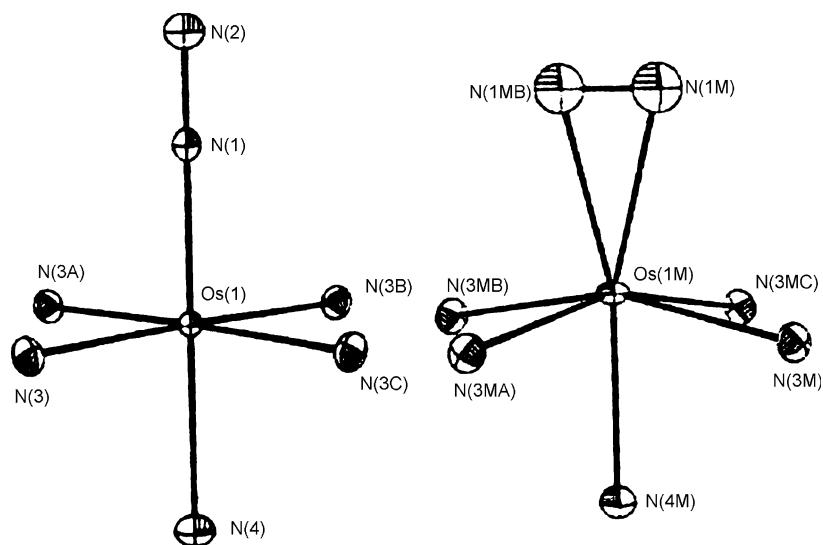


Fig. 5 X-ray structures of end-on and side-bound N_2 in $[Os(NH_3)_5(N_2)]^{2+}$ [37]

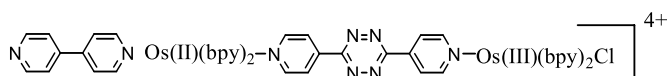
structures obtained for the starting complex and the metastable photolysis product [37].

3 Energy and Electron Transfer Reactions

Over the past 5 years there has been a tremendous amount of work examining intramolecular energy and electron transfer reactions involving Os(II) and Os(III) diimine complexes. Several themes run through the work and in much of the work the Os center serves as the energy or electron acceptor, particularly in systems involving mixed Ru(II)/Os(II) or Ru(II)/Os(III) complexes. The discussion below is broken into three sections: photoinduced reactions involving intramolecular electron transfer, systems involving Os(II) centers as energy acceptors, and systems in which Os(II) complexes are linked to aromatic hydrocarbons.

3.1 Intramolecular Electron Transfer

Forster and Keyes prepared the tetrazine containing $[Os(II)(BL)Os(III)]$ dimer (see below) and examined light induced intramolecular electron transfer in the system. They also measured heterogeneous electron transfer rate constants for oxidation of the complex at a Pt electrode [38]. The work is

**Structure 1**

a unique combination of thermal and photophysical measurements and the results indicate that the photoinduced electron transfer rate constant is on the order of 10^7 s^{-1} , significantly slower than the rate constant measured for oxidation of a monolayer of the monometallic $[(\text{BL})\text{Os}(\text{II})(\text{bpy})_2\text{Cl}]^+$ on a Pt electrode.

Additional work by the Forster group, making use of transient emission spectroscopy, probed the rate of photoinduced electron transfer between metal centers within a novel trimeric complex $\{[\text{Os}(\text{II})(\text{bpy})_2(\text{bpe})_2][\text{Os}(\text{II})(\text{bpy})_2\text{Cl}]_2\}^{4+}$, where bpy is 2,2'-bipyridyl and bpe is *trans*-1,2-bis-(4-pyridyl)ethylene. Transient emission experiments on the trimer, and on $[\text{Os}(\text{bpy})_2(\text{bpe})_2]^{2+}$ in which the $[\text{Os}(\text{bpy})_2\text{Cl}]^+$ quenching moieties are absent, reveal that the rate of photoinduced electron transfer (PET) across the bpe bridge is $1.3 \pm 0.1 \times 10^8 \text{ s}^{-1}$. The electron transfer is believed to be from the peripheral Os(II)Cl metal centers to the $[\text{Os}(\text{bpy})_2(\text{bpe})_2]^{2+}$ chromophore. Comparison to rate constants for reduction of monolayers at a Pt electrode reveals that the photoinduced process is significantly faster [39].

Lainé and coworkers have published several papers on triarylpyridinium functionalized terpyridyl ligands as electron acceptors in Os(II) complex systems exhibiting photoinduced electron transfer [40–43]. The work focuses on the issue of intramolecular reduction of the pendant triarylpyridinium moiety when ligands of the type tpyXpydY (Scheme 1) are coordinated to Os(II). In a study of $[(\text{mpt})\text{Os}(\text{tpypyd})]^{2+}$ [41] the authors concluded that photoreduction of the coordinated pyridinium is observed based on a combination of spectroelectrochemical and nanosecond resolved transient absorption work, but the free energy for the intramolecular electron transfer is thought to be slightly endergonic. When the pyridinium moiety is functionalized with a nitro substituent, photoreduction becomes clearly evident [42]; however, the decay of the charge separated state has a component on the picosecond timescale and a much longer component. The long component comes from formation of a ligand localized triplet state on the nitro substituted pyridinium ligand; the triplet state energy has been found by low temperature luminescence spectroscopy to be very close in energy to the Os to tpy MLCT energy. Figure 6 shows a state diagram for the complexes $[(\text{mpt})\text{Os}(\text{tpypydN})]^{2+}$ and $[(\text{mpt})\text{Os}(\text{tpyMpydN})]^{2+}$, indicating that reversible energy transfer to populate the ligand centered state competes with electron transfer to the lower energy charge separated state. It is found that electron transfer dominates in $[(\text{mpt})\text{Os}(\text{tpyMpydN})]^{2+}$, while energy transfer is dominant in the complex lacking the methyl substituents to force an increased torsion angle between the terpyridyl and pyridinium portions of the ligand. The relative

both energy transfer and electron transfer from the porphyrin to the Os(II) complex are possible. The authors speculate that electron transfer dominates the quenching of the Os(II) center luminescence in this preliminary report.

Also, Hossain and coworkers have reported photoinduced electron transfer in mixed metal Ru/Os dyads and triads having functionalized diimide ligands [46].

3.2

Os Complexes as Quenchers in Energy and Electron Transfer Systems

A significant amount of work has been done on complexes in which a Ru(II) diimine complex serves as an energy donor and an Os(II) diimine complex is the acceptor. In these systems the Ru complex emission is from a $^3\text{MLCT}$ state and, in general, energy transfer sensitized an Os complex $^3\text{MLCT}$ state. Much discussion has revolved around the question of the mechanism of the process. Since the spin forbidden ground state to $^3\text{MLCT}$ state absorption in Os imine complexes has significant oscillator strength (because of the large spin-orbit coupling matrix element of Os), it is possible that energy transfer is by a Förster or resonant energy transfer mechanism. However, it is also possible that the process occurs via an electron exchange mechanism and the significant body of work published prior to the year 2000 has focused on this question. Much of this earlier work is cited in the more recent work reported in this review.

In continuing studies addressing the resonance versus exchange energy transfer mechanistic question, Keene and Ghiggino examined energy transfer within dyads involving polypyridyl-ruthenium(II) and -osmium(II) centers separated by rigid alicyclic bridges (Fig. 8). Their results for energy transfer from the Ru(II) $^3\text{MLCT}$ state to the $^3\text{MLCT}$ state of the Os(II) complex ($k_{\text{en}} \sim 10^7 \text{ s}^{-1}$) could be fit assuming a Förster model for energy transfer [47].

Furue and his group studied competitive energy and electron transfer quenching across a peptide bridge in polypyridine ruthenium(II)/osmium(II) binuclear systems [48]. The bridging ligands, including mb-leu-bp and mb-pro-bp (Scheme 3), have Ru(II) with either two bpy or two fmb (Scheme 1) ligands completing the coordination environment and the accepting Os(II) center has bipyridyl ligands.

Energy transfer rate constants for the $[\text{Ru(II)(bpy)}_2]$ donor are a factor of 7–10 times faster than the complexes having $[\text{Ru(II)(fmb)}_2]$ as donor. The results were fit using a Förster model and explained by the fact that the dipole of the Ru complex MLCT state is localized toward the bridge in the $[\text{Ru(bpy)}_2]$ complex, but toward the spectator fmb ligands in the Ru(fmb)_2 complex, giving rise to a longer energy transfer distance.

Constable and Barigelletti reported recently trimetallic OsRu_2 and pentametallic OsRu_4 complexes prepared using the ligand tpOt2 (Scheme 4). For the complexes $\{(\text{tpy})\text{Os}(\text{tpOt2})[\text{Ru}(\text{tpy})_2]\}^{6+}$ and $\{\text{Os}(\text{tpOt2})$

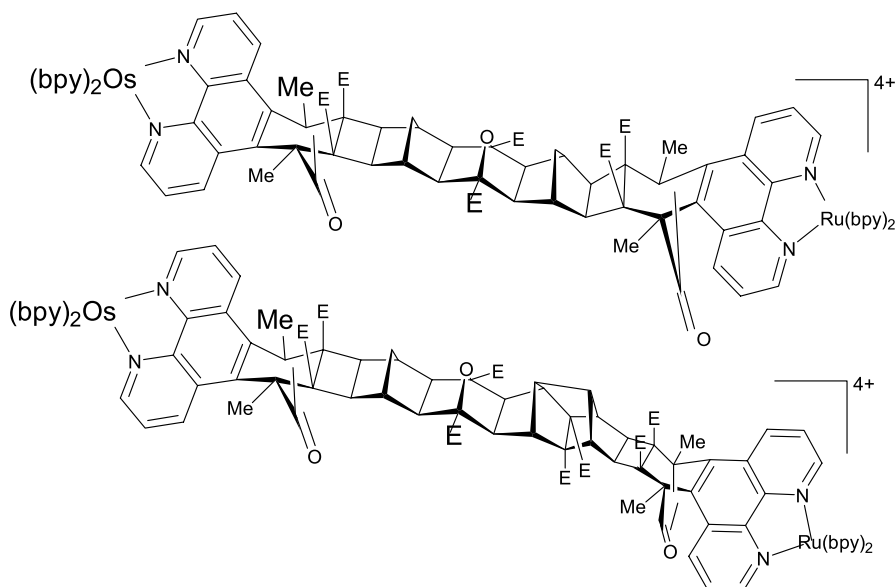
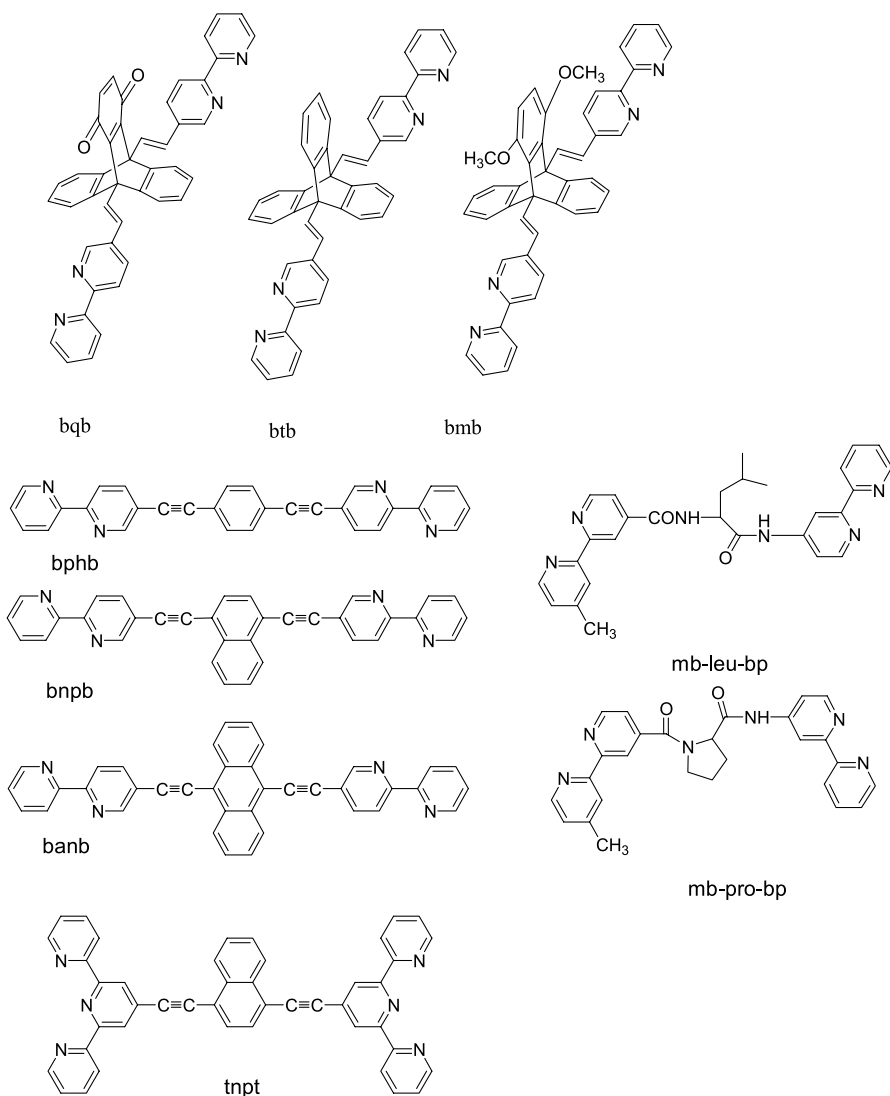


Fig. 8 Rigidly bridged Ru diimine donor/Os diimine acceptor [47]

$(\text{Ru}(\text{tpy}))_2\}_2^{10+}$, room temperature luminescence measurements indicated that nonradiative relaxation of the Ru to tpy $^3\text{MLCT}$ state ($k_{\text{nr}} > 10^8 \text{ s}^{-1}$) is significantly faster than energy transfer to populate the Os to tpy $^3\text{MLCT}$ state [49, 50].

Beyeler and Belser investigated intramolecular energy migration from Ru(II) imine chromophores to Os(II) diimines through the derivatized bicyclooctyl containing bridging ligands bqb, btb, and bmb (Scheme 3). The ligand bqb allows for control of energy or electron transfer via a redox switch prior to excitation [51]. Figure 9 illustrates the operation of the redox switch. When the bqb ligand is in the quinone state, electron transfer quenching occurs following excitation of the Ru(II) center and no Os diimine luminescence is observed. If the quinone is reduced to the hydroquinone the energy transfer path to populate the emissive Os to bipyridine MLCT state is allowed and the luminescence is observed.

Intramolecular energy transfer from Ru(II) tris-bipyridyl units to Os(II) bipyridyl units attached to a polystyrene backbone was studied by Meyer and coworkers [52, 53]. They observed complex kinetics and were able to account for nearest neighbor energy transfer quenching and energy hopping between adjacent Ru(II) donor chromophores. Energy transfer from a Ru(II) bipyridyl chromophore to a neighboring Os(II) center was observed to occur on the 400-ps timescale. This, and related work by the North Carolina group, has been reviewed recently and includes systems in which the Os(II) center acts as an energy acceptor from Ru(II) bipyridyl complex donors and as an electron

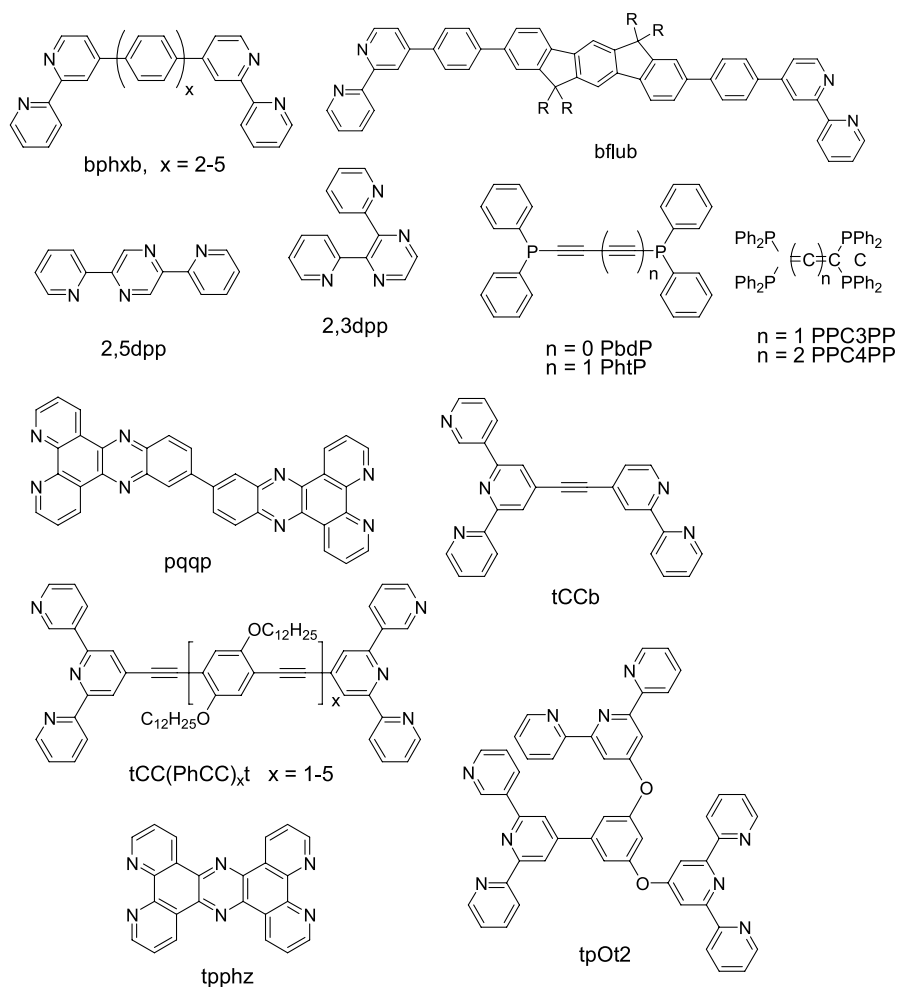


Scheme 3 Structures of bridging ligands

donor to Ru(III) centers formed by irreversible oxidative electron transfer to an aryldiazonium ion in solution [54].

Campagna and coworkers recently reviewed energy donor/acceptor systems, including Ru complex donor/Os complex acceptor chromophores. The review provides an overview of a number of light harvesting systems [55].

Over the past several years, energy donor/acceptor systems have been prepared in which the electronic coupling of the bridging ligand is increased



Scheme 4 Structures of bridging ligands

significantly relative to systems having saturated bridging ligands. There are a number of bridging ligands with polyphenylene or polyphenylene ethynylene moieties as the bridge. Very often, energy transfer processes are in the picosecond time domain. In an elegant collaboration of the Ziessel and Hariman groups, mixed Ru/Os complexes having the bridging ligands bphb (phenyl), bnpb (naphthalene), and banb (anthracene) (Scheme 3) were prepared. The relative energy levels of the Ru(II) complex 3MLCT state, the $^3(\pi-\pi^*)$ state of the aromatic component of the bridging ligand, and the 3MLCT state of the Os(II) imine chromophore are shown in Fig. 10. The authors were able to map out energy transfer rate constants from the Ru(II) 3MLCT state directly to the Os(II) 3MLCT state for the bphb bridge ($8 \times 10^8 \text{ s}^{-1}$).

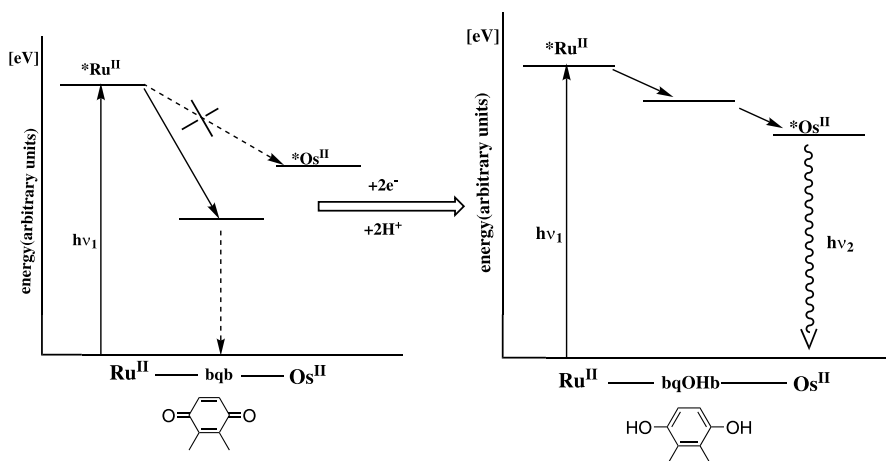


Fig. 9 Energy level diagram indicating redox control of Os(II) complex luminescence [51]

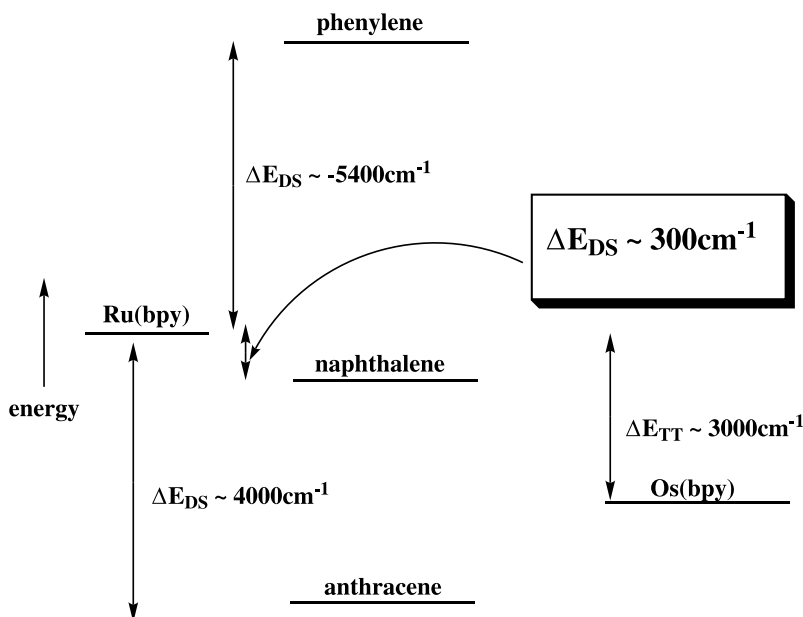


Fig. 10 State diagram for a Ru-aromatic hydrocarbon-Os complex bridge (E_{DS} = the energy gap between the donor and the spacer in the bridging ligand) [56]

The other complexes were more complicated and involved stepwise energy transfer from the 3MLCT state of the Ru(II) chromophore to the Os(II) chromophore. For the case of the banb bridging ligand, the bridge anthracene $^3(\pi-\pi^*)$ state is the lowest energy excited state and both the Ru chromophore

and the Os center sensitize this state with rate constants in excess of 10^{10} s^{-1} . This work is expanded by closely related work with butadiynyl components in the bridging ligands [56, 57].

In the case of the strongly coupled bridging ligands 2,3dpp and 2,5dpp, Hammarstrom and coworkers found that Ru to Os energy migration was complete within 400 fs for complexes of the type $[(\text{bpy})_2\text{Ru}(\text{BL})\text{OsL}_2]^{4+}$ (BL = bpy, biq; biq = 2,2'-biquinoline), a timescale that is fast relative to vibrational relaxation of the Franck–Condon excited state [58]. However, this timescale is comparable to that found by McCusker and coworkers for intersystem crossing in $[\text{Ru}(\text{bpy})_3]^{2+}$ and suggests the energy transfer process could actually follow formation of the $^3\text{MLCT}$ state of the Ru(II) complex donor. More recent work on the closely related tetrametallic complex $\{[(\text{bpy})_2\text{Ru}(2,3\text{dpp})]_3\text{Os}\}^{8+}$ by Andersson et al. further indicates that energy migration from the Ru(II) MLCT states to the Os(II) MLCT manifold takes place on the 60-fs timescale, significantly faster than the intersystem crossing timescale [59, 60]. This elegant work was preceded by a report of the synthesis and luminescence behavior of related mixed metal fragment 2,3dpp complexes [61].

Harriman and Ziesel recently reported the acetylide bridged bimetallic complex $[(\text{mpt})\text{Os}(\text{tCCb})\text{Ru}(\text{bpy})_2]^{4+}$ (tCCb shown in Scheme 4) [62]. Excitation of the Ru(II) center resulted in nearly 100% efficient energy transfer to the Os to mpt MLCT state with a rate constant of $7 \pm 2 \times 10^{10} \text{ s}^{-1}$. Analysis of the Förster overlap factor led to the prediction of a much lower rate constant for resonant energy transfer and the authors concluded that the process was dominated by an electron exchange transfer mechanism.

Bimetallic donor/acceptor systems having a Ru(II) tris-bipyridyl donor, a polyphenylene bridge, and an Os(II) tris-bipyridine acceptor have been studied by DeCola and coworkers [63–65]. The bridging ligands are shown in Scheme 4 as bphxb ($x = 2-5$). Rate constants for Ru to Os energy transfer ranged from $2.5 \times 10^{11} \text{ s}^{-1}$ for $x = 2$ to $4.8 \times 10^8 \text{ s}^{-1}$ for $x = 5$. The energy transfer process is reported to follow an exchange energy transfer mechanism and the rate constant is expected to fall off exponentially with distance as shown in Eq. 2,

$$k_{\text{en}} = k_0 \exp(-\beta(r - r_0)) \quad (2)$$

where r_0 is the contact distance of the donor and acceptor and β reflects the magnitude of the distance dependence. The β value obtained in this work, 0.5 \AA^{-1} , compares favorably with that obtained by Barigelletti for a related polyphenylene bridged Ru/Os donor/acceptor system [66].

Another distance dependence investigation was carried out by Harriman, Ziesel, and coworkers on $[(\text{tpy})\text{Ru}(\text{BL})\text{Os}(\text{tpy})]^{4+}$ donor/acceptor complexes having a bridging ligand (BL) with the structure tCC(PhCC)xt (Scheme 4, $x = 1-5$). While the absolute energy transfer rate constants ranged from $1.1 \times 10^8 \text{ s}^{-1}$ for $x = 1$ to $2 \times 10^6 \text{ s}^{-1}$ for $x = 5$, the resulting distance dependence yielded a very small β value of 0.2 \AA^{-1} . The authors comment on the

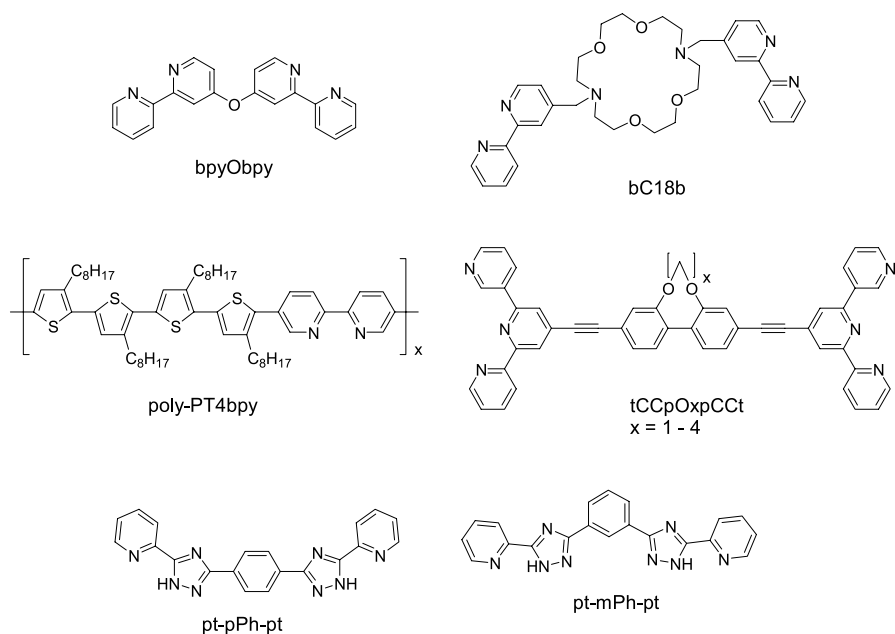
fact that excited states localized on the bridging ligand do not seem to be involved in the energy transfer process, and they suggest that systems with very long energy transfer distances could be made using the repeating phenylene ethynylene bridge [67].

Hong's group examined energy transfer in $[(\text{bpy})_2\text{ClRu(II)(P-BL-P)Os(II)Cl}(\text{bpy})_2]^{2+}$ (P – BL – P = PbDP, PhtP, Scheme 4) [68]. The energy transfer rate constants were believed to follow an exchange energy transfer mechanism; for these complexes rate constants were on the order of $2\text{--}3 \times 10^9 \text{ s}^{-1}$ at the approximate distance dependence of 0.02 \AA^{-1} . This is a remarkably small distance dependence and systems of this sort should be investigated in greater detail.

Natarajan developed and characterized mono-, di-, and tetranuclear homo/heterometallic complexes of Ru(II) and Os(II) based on the bridging ligand bis-dipyrido[3,2-*a*:2',3'-*c*]phenazine (pqpp, Scheme 4) [69]. In the mixed metal system, the energy transfer rate constant was found to be $5 \times 10^7 \text{ s}^{-1}$; this rate constant is nearly a factor of 100 slower than that of a closely related system reported earlier that has tpphz as bridging ligand [70]. In this system, energy migration from the Ru to tpphz $^3\text{MLCT}$ state to the Os to tpphz $^3\text{MLCT}$ state exhibits complex kinetics that have been interpreted as energy transfer from the promptly formed $^3\text{MLCT}$ state with a lifetime of 18 ps and energy transfer from the relaxed $^3\text{MLCT}$ state of the Ru chromophore with a lifetime of 13 ps. In the pqpp complex the bridging ligand is nonplanar (can twist about a single C – C bond) and the distance between metal centers is greater, and this is thought to contribute to the significantly slower energy transfer rate constant.

Intramolecular energy transfer was also reported for the complexes $[(\text{bpy})_2\text{Ru}(\text{pt-mPh-pt})\text{Os}(\text{bpy})_2]^{2+}$ and $[(\text{bpy})_2\text{Ru}(\text{pt-pPh-pt})\text{Os}(\text{bpy})_2]^{2+}$ (Scheme 5) [71]. In room temperature solution luminescence from both the Ru(II) and Os(II) MLCT states was observed with energy transfer rate constants of $1.5 \times 10^8 \text{ s}^{-1}$ for both complexes, and, as with other complexes, calculated rate constants for Förster energy transfer were slow relative to the experimental values, implying some degree of exchange coupling contributing to the room temperature process.

Recent work of Benniston, Harriman, and others explores the torsion angle dependence of intramolecular energy transfer rate constants in Ru/Os systems having the bridging ligand tCCpOxpCCt (Scheme 5 and a related series not shown here). For the ligand tCCpO1pCCt, the authors examined the temperature dependence of energy transfer in the complex $\{[(\text{tpy})\text{Ru}(\text{tCCpO1pCCt})]_2\text{Os}\}^{6+}$ and found that both exchange and resonance energy transfer processes were operative, with the resonance energy transfer dominating in frozen matrices when the thermally activated exchange process was essentially shut down. The authors found two thermally activated processes that they attributed to superexchange and electron hopping mechanisms [72]. They were also able to systematically tune the torsion angle between the two central phenyl residues between 37 and 94° . The



Scheme 5 Structures of bridging ligands

exchange energy transfer rate constant is temperature dependent and also depends on the electronic coupling through the bridging tCCpO_xCCt ligand. Electronic coupling matrix elements, extracted from temperature dependent rate constant data, indicate that quadratic dependence on the torsion angle is obtained with the minimum coupling being when the two central phenyl rings are perpendicular to one another [73].

In somewhat related work of Venturi et al., the dinuclear complex [(bpy)₂Ru(MAC1)Os(bpy)₂]⁴⁺ was examined (Scheme 2). Luminescence spectral data show that the emission band of the Ru(II) unit is almost completely quenched with concomitant sensitization of the emission of the Os(II) unit. Electronic energy transfer from the Ru(II) to the Os(II) ³MLCT state takes place by two distinct processes ($k_{\text{en}} = 2.0 \times 10^8$ and $2.2 \times 10^7 \text{ s}^{-1}$ at 298 K) [74].

Another example of the conformational influence of energy transfer was provided by Barigelletti and coworkers. Using the complex [(bpy)₂Ru(bC18b)Os(bpy)₂]⁴⁺ (Scheme 5), they illustrated modulation of photoinduced energy transfer between Ru(II) and Os(II) termini by a conformational change induced by Ba²⁺ binding at a central macrocyclic site [75]. Upon addition of Ba²⁺ the Ru(II) to Os(II) energy transfer rate constant decreased from 1.1×10^8 to $4.7 \times 10^7 \text{ s}^{-1}$; the authors attribute this to a resonance energy transfer process in which the Förster coupling decreases because of an increase in the donor/acceptor separation following coordination of Ba²⁺.

Jukes, DeCola, and others reported a fascinating study of competition between energy transfer and photocyclization for a dinuclear Ru/Os complex containing a photoresponsive dithienylethene (dte) derivative as bridging ligand and [76, 77]. By using the photochromic dte moiety incorporated into a bridging ligand, the authors were able to induce ring closure via direct irradiation of the dithienylethene absorption, as shown in Fig. 11. In the Ru/Ru bimetallic complex, irradiation into the Ru to bpy MLCT absorption resulted in photocyclization of the dte with an efficiency paralleling that for excitation into the dte localized absorption. However, in both the Ru/Os mixed metal complex and the Os/Os complex, photolysis in the lower energy MLCT region resulted in much lower quantum yields for dte cyclization because the $^3\text{MLCT}$ state of

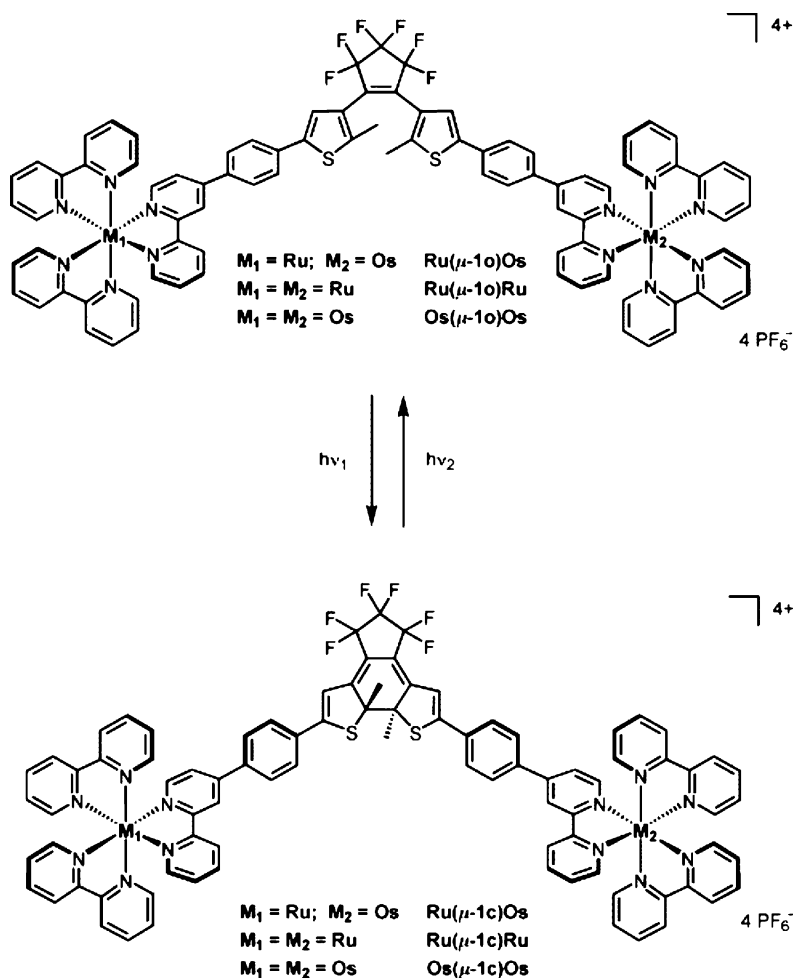


Fig. 11 Photocyclization of dithienylethene bridged bimetallic complexes [76, 77]

the Os center served as an energy drain, deactivating the triplet state localized on the dte ligand.

Finally, in systems involving Ru(II) to Os(II) energy transfer, there have been several recent examples of energy transfer between $[\text{Ru}(\text{bpy})_3]^{2+}$ and $[\text{Os}(\text{bpy})_3]^{2+}$ in single crystals of the Ru(II) complex doped with the Os(II) complex. Ohno and collaborators measured energy transfer and electron transfer in crystals of $[\text{Os}_x\text{Ru}_{1-x}(\text{bpy})_3]\text{X}_2$ ($x = 0-0.23$) [78]. An energy transfer rate constant of $2 \times 10^{11} \text{ s}^{-1}$ was determined for heavily doped crystals in which energy transfer from a Ru(II) center to an adjacent Os(II) center is presumed; the rate constant for energy transfer to the next nearest neighbor was estimated to be $< 10^9 \text{ s}^{-1}$. In an elegant extension, Yersin and Kratzer examined energy transfer in crystals of $\Lambda\text{-Ru}(\text{bpy})_3]^{2+}/\Delta[\text{Os}(\text{bpy})_3]^{2+}$; the structure is built up of homochiral layers of the Ru complex followed by homochiral layers of the Os complex. Very efficient exchange energy transfer is observed and, at low temperatures, the emission of the Os(II) acceptor site appears to be highly vibrationally resolved. Magnetic field effects were also examined in some detail [79]. Chirality effects on energy transfer from diphenylphenanthroline Ru(II) to Os(II) complexes were examined for mixtures of the complexes in Langmuir–Blodgett films [80].

Far fewer studies have been done of energy transfer from the Re(I) complex $^3\text{MLCT}$ state to Os(II) complexes. Intramolecular energy transfer processes in the complex $[(\text{CO})_3(\text{phen})\text{Re}(\text{L})\text{Os}(\text{tpy})(\text{bpy})]^{3+}$ (L = 4,4'-bipyridine, bis-4-pyridylethane, bis-4-pyridylethylene) were reported by Argazzi and coworkers. Along with energy transfer, the Re(I) chromophore can be quenched by reductive electron transfer from the Os(II) complex. They were able to determine that energy transfer was dominant and had to occur with a rate constant greater than $5 \times 10^7 \text{ s}^{-1}$ [81].

Hong et al. examined energy migration from a Re(I) complex excited state to an Os(II) MLCT state through the bridging cumulene ligands PPC3PP and PPC4PP (Scheme 4). The complexes, $[(\text{CO})_3\text{ClRe}(\text{PPCxPP})\text{Os}(\text{bpy})_2]^{2+}$, both exhibit 100% efficient energy transfer from the postulated Re(I) to phosphine MLCT state to the Os(II) centered MLCT state [82].

3.3

Energy Transfer Involving Aromatic Hydrocarbon Donors/Acceptors

In some systems examined the Os(II) center is involved in energy transfer with an excited state localized on a ligand. Very often the energy transfer process would differ from that of the corresponding Ru(II) complex in that the lower energy state in the Os(II) complexes is the $^3\text{MLCT}$ state. An interesting example was presented by Schanze and coworkers who investigated polythiophene polymers (poly-PT4bpy, Scheme 5) having pendant Os(II) diimine chromophores. In the Os(II) polymer the MLCT state is lower in energy than the polythiophene-based $^3\pi-\pi^*$ state and $^3\text{MLCT}$ emission is observed.

The transient absorption spectrum of the Os(II) containing polymer reflects features of the thiophene polymer triplet [83].

Prodi examined the photophysical properties of supramolecular assemblies containing polypyridine complexes and pyrene chromophores. Using the complex $[(bpy)_2Os(bpyObpy)]^{2+}$ (Scheme 5) and pyrene-1-carboxylic acid, the authors demonstrated that, upon addition of Zn^{2+} , complex formation occurs in which the Zn^{2+} links together the free bpy of the Os complex and the carboxyl of the pyrene. Excitation of the Os(II) MLCT absorption results in exclusive emission from the 3MLCT state of the Os complex [84].

The ligand AN2bpy (Scheme 1) and the corresponding complex $[Os(AN2bpy)_3]^{2+}$ were recently investigated by Campagna's group, along with other mixed pyrene/anthracene substituted bipyridines and the Ru(II) and Os(II) complexes. In this complex the anthracene localized triplet is approxi-

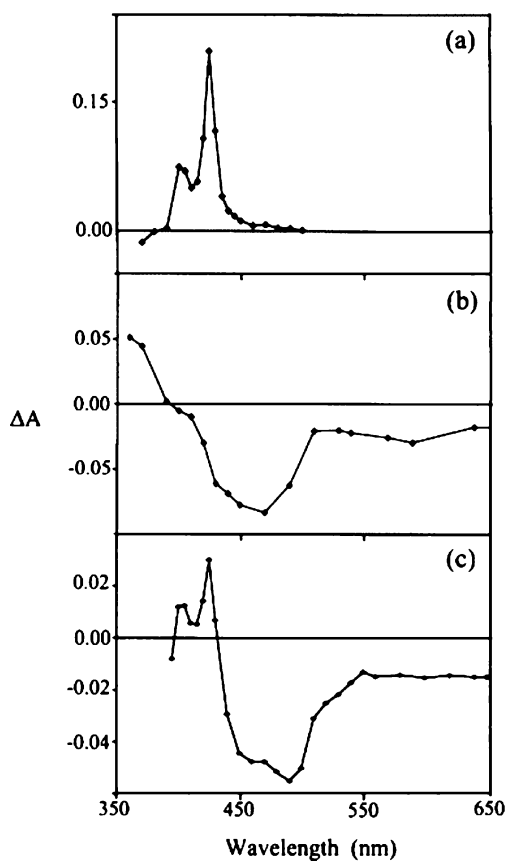


Fig. 12 Nanosecond transient absorption spectra of the AN2bpy ligand (a), $[Os(bpy)_3]^{2+}$ (b), and $[Os(AN2bpy)_3]^{2+}$ (c) [85]

- ◀ **Fig. 13** Redox state dependence of energy transfer efficiencies in a coumarin/Ru/Os triad complex. The lower portion of the figure does not show the direct coumarin to Os complex energy transfer for simplicity [87]

Two Os(II) complexes of the ligand bpyAN, $[(bpy)_2Os(bpyAN)]^{2+}$ and $[(bpyAN)_2Os(CO)Cl]^{2+}$, were prepared by Balazs and Schmehl [86]. The 3MLCT state of the CO chloride complex $[(bpy)_2Os(CO)Cl]^{2+}$ is approximately 900 cm^{-1} higher in energy than that of the $[Os(bpy)_2(bpyAN)]^{2+}$. Transient absorption spectra of the two anthracene containing complexes show that $[Os(bpy)_2(bpyAN)]^{2+}$ has a spectrum reflecting only the 3MLCT state, while the transient absorption spectrum of $[(bpyAN)_2Os(CO)Cl]^{2+}$ consists *only* of features of the anthracene.

Os(II) chromophore centers were found to serve as energy donors in the complexes Osptytp and OsptyZntpp (Fig. 7), in which each Os(II) center has a $[(bpy)_2Os(CO)(py)]^{2+}$ environment. The 3MLCT state of the Os(II) donor chromophore has an emission maximum of 590 nm in CH_2Cl_2 at room tem-

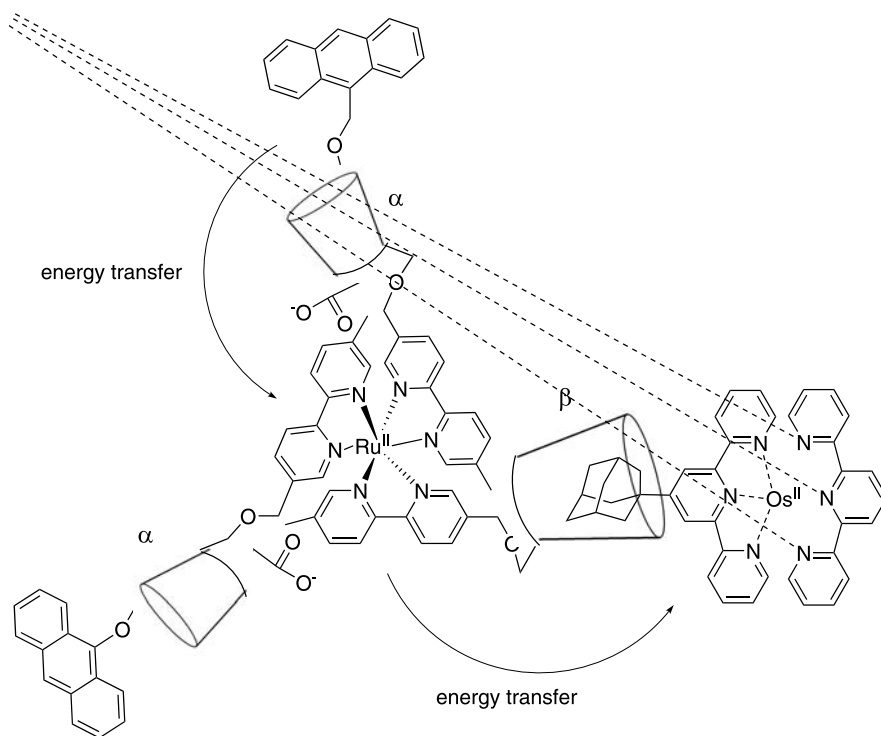


Fig. 14 Energy transfer cascade in self-assembling anthracene-Ru complex-Os complex light harvesting array linked by cyclodextrins [88]

perature, higher in energy than both the porphyrin singlet and triplet excited states. Luminescence investigation of Os₂pytpp clearly indicates only weak emission from the porphyrin singlet. The Zn porphyrin complex Os₂pyZntpp exhibits only very weak emission from the porphyrin. No transient absorption studies were done and so direct investigation of triplet sensitization or photoinduced electron transfer products was not reported [45].

A few studies of singlet energy transfer from substituents on ligands to the MLCT state of Os(II) complexes have also been reported. In the work of Akasaka et al., bimetallic and trimetallic complexes were prepared and studied involving coumarin as a chromophore and energy donor and Os(II) and Ru(II) terpyridyl complexes as acceptors. As shown in Fig. 13, energy transfer directly from the coumarin to the remote Os(II) ³MLCT state occurs when the bridging azo functionality between the Ru(II) and Os(II) centers is reduced and luminescence is observed from the Os(II) complex [87].

In an elegant self-assembling system based on the use of cyclodextrin hosts, DeCola and coworkers noncovalently linked an alkylcarboxyanthracene to an α -cyclodextrin bearing Ru(II) complex that also had an Os(II) bipyridyl derivative attached to the Ru complex (Fig. 14). The system yields an energy transfer cascade from the photoexcited anthracene to the Ru to bpy ³MLCT state, which in turn transfers energy to the Os(II) complex ³MLCT state. All rate constants are $> 10^8 \text{ s}^{-1}$ [88].

4

Photochemistry and Photophysics of Organometallic Os Complexes

Over the past few years there has been a growing body of literature on the photophysics and photochemistry of organometallic Os complexes. A significant portion of the literature has focused on the photochemistry and transient photophysical characterization of triosmium clusters involving Os – Os bond homolysis. There is also a significant body of literature on CO loss from diosmium and triosmium complexes.

4.1

Os Carbonyl Cluster M–M Cleavage

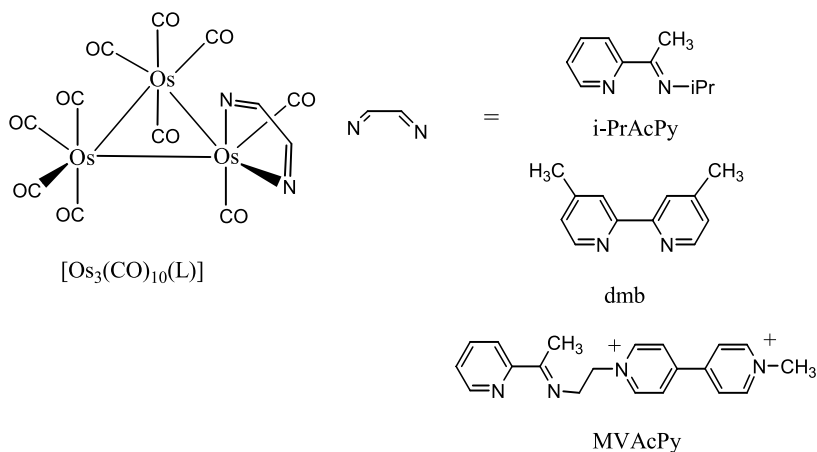
Leadbetter examined the photoreactivity of $[\text{Os}_3(\text{CO})_{12}]$ in the presence of various monodentate coordinating ligands including PPh₃, CH₃CN, and C₂H₄. With PPh₃ photosubstitution of CO occurs to yield the mono, bis, and tris PPh₃ complexes (stereochemistry not specified). In CH₃CN the mono and bis CH₃CN complexes are formed, and in ether solutions saturated in C₂H₄ the η_2 ethene complex is formed [89]. This photochemistry differs from that of the corresponding Ru analog which yields products that result from Ru – Ru bond

cleavage. Time dependent DFT calculations have been done recently which support the notion that the Os complex has a much smaller degree of metal centered orbital character in the lowest unoccupied orbitals [90].

Bakker and others conducted a mechanistic study of the photofragmentation of the clusters $[\text{Os}_3(\text{CO})_{10}(\text{diene})]$ (diene = *cis*-1,3-butadiene, 1,3-cyclohexadiene). The photolysis yields $[\text{Os}(\text{CO})_3(\text{diene})]$ and $[\text{Os}_2(\text{CO})_7]$ which can be trapped with CO to yield $[\text{Os}_2(\text{CO})_9]$. The authors report direct observation of the open-triangle primary photoproduct having two bridging CO ligands. The intermediate was characterized with nanosecond time-resolved infrared and UV/visible spectroscopy; the nanosecond IR spectrum showed two new CO absorption bands at 1857 and 1801 cm^{-1} [91]. The low-lying excited states and primary photoproducts of the clusters were further studied by picosecond time-resolved IR spectroscopy and by density functional theory. The results show a transient at 1815 cm^{-1} forms in less than 5 ps; this gives way over a period of 20 ps to new bands at 1857 and 1801 cm^{-1} , representing formation of a CO bridged intermediate [92].

Stufkens and Hartl observed light induced formation of zwitterions and biradicals from the diimine clusters $[\text{Os}_3(\text{CO})_{10}(\text{iPr-AcPy})]$ and $[\text{Os}_3(\text{CO})_{10}(\text{dmb})]$ using picosecond UV/vis and nanosecond IR spectroscopies. Picosecond transient spectra indicated generation of the ligand anion radical and evolution over approximately 50 ps to a much longer lived transient that was attributed to an opened cluster with an associated ligand on the diimine metal. Figure 15 shows the proposed evolution of species in the photoreaction [93, 94].

The photophysical and photochemical reactivity of the mixed metal cluster, $[\text{Os}_2\text{Ru}(\text{CO})_{10}(\text{iPrAcPy})]$, was also examined by this group. Their observation is that zwitterionic products are formed preferentially for the complex



Structure 2

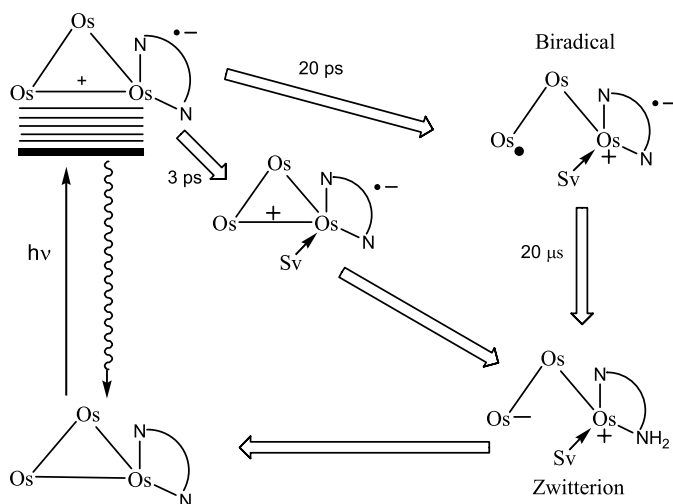


Fig. 15 Formation of zwitterions and biradicals from the diimine clusters $[\text{Os}_3(\text{CO})_{10}(\text{LL})]$ (LL = diimine ligand) [93, 94]

having the diimine ligand on the Ru center. In addition, the lower Lewis basicity of the Ru decreases the tendency to coordinate solvent and, as a consequence, recombination times are much shorter [95]. A comparison of products formed on electrochemical reduction with the photochemical reactivity was also recently reported [96].

The photochemistry of $[\text{Cp}(\text{CO})_2\text{Os}]_2$ has been examined recently by two separate groups. Bitterwolf and coworkers illustrated that photolysis of the complex in nujol at low temperature resulted in loss of CO and formation of a triply CO bridged species (Fig. 16). In benzene solution at room tempera-

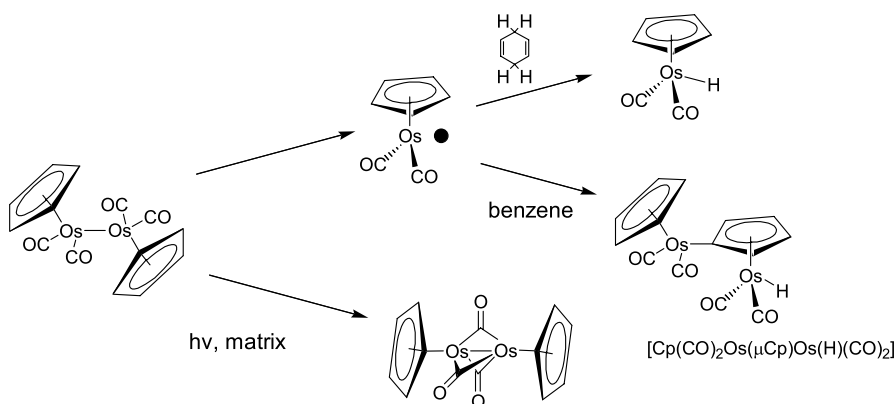


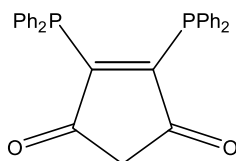
Fig. 16 Photoreactivity of $[\text{Cp}_2\text{Os}_2(\text{CO})_4]$ in frozen matrices and solution [97, 98]

ture, photolysis leads to homolysis of the Os – Os bond and formation of the Os-centered radical, $[\text{Cp}(\text{CO})_2\text{Os}^\cdot]$. This radical species abstracts a hydrogen atom from the Cp of another molecule and ultimately leads to formation of a bimetallic complex having a bridging Cp (from the radical) $[\text{Cp}(\text{CO})_2\text{Os}(\mu\text{-Cp})\text{Os}(\text{H})(\text{CO})_2]$ [97, 98]. Zhang, Bullock, and coworkers also observed photolytic C – H homolytic bond cleavage by the Os radical species. The authors report the direct spectroscopic observation of $[\text{Cp}(\text{CO})_2\text{Os}^\cdot]$ by isolation of the hydrido Os complex time-resolved infrared and the isolation of the hydrido Os complex kinetic analysis of H atom to isolation of the hydrido Os complex transfer from C to Os. Exhaustive photolysis in the presence of 1,4-cyclohexadiene led to isolation of the hydrido Os complex [98].

4.2

Complexes Exhibiting CO Loss

The reaction of the Os–Sb cluster $\text{Os}_3(\mu\text{-H})(\mu\text{-SbPh}_2)(\mu_3, \eta^2\text{-C}_6\text{H}_4)(\text{CO})_9$ with nitrile solvent results in loss of CO and solvent substitution to yield $\text{Os}_3(\mu\text{-H})(\text{SbPh}_2)(\mu_2, \eta^2\text{-C}_6\text{H}_4)(\text{CO})_9(\text{CN}^t\text{Bu})$. Photolysis of this complex results in CO loss on the Os center having four CO ligands. The product has an η^4 benzene in which all three Os centers are involved. Structural data are provided for the complexes [99].



bpcd

Structure 3

Ultraviolet photolysis of the diphosphine complex $[\text{Os}_3(\text{CO})_{10}(\text{bpcd})]$ (bpcd, Struct. 3) yields an orthometalated hydrido triosmium complex as the exclusive product (Fig. 17). The mechanism presumably involves initial CO loss with subsequent coordination of one phenyl of the diphenylphosphino unit followed by the insertion process [100].

4.3

Other Organometallic Photoreactions

In an extension of the work done on $[\text{Os}_3(\text{CO})_{10}(\text{iPr-AcPy})]$ (Struct. 2), a derivative was prepared having the ligand MV-AcPy $^{2+}$, where MV is a methyl viologen derivative. The picosecond time-resolved UV/vis spectra

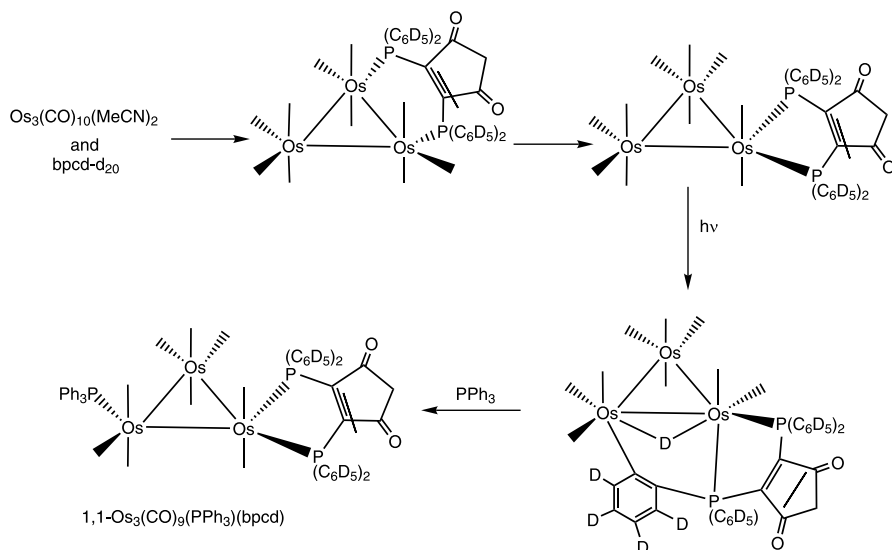


Fig. 17 Products from ultraviolet photolysis of the diphosphine complex $[\text{Os}_3(\text{CO})_{10}(\text{bpcd})]$ [100]

of the complex $[\text{Os}_3(\text{CO})_{10}(\text{MV-AcPy})]^{2+}$ clearly illustrate electron transfer from the cluster to the MV^{2+} moiety (the characteristic spectrum of reduced methyl viologen is observed). Also, transient spectroscopy of the one-electron reduced complex indicates that transient behavior similar to that of the parent complex $[\text{Os}_3(\text{CO})_{10}(\text{iPr-AcPy})]$ is observed (Fig. 14) in which M – M bond cleavage occurs [101].

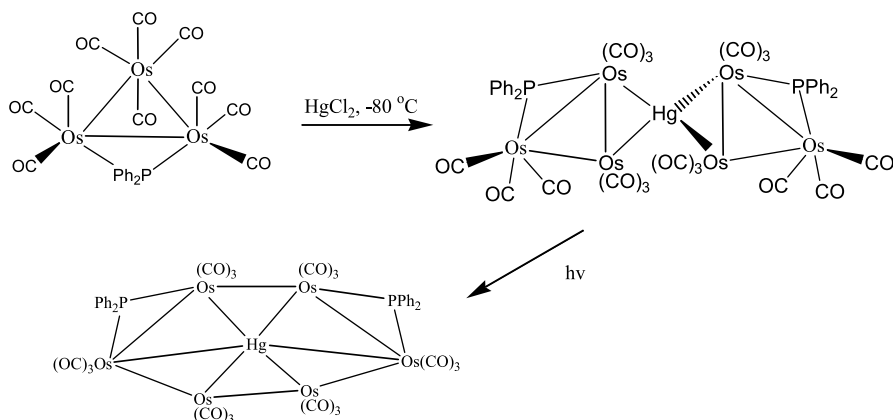


Fig. 18 Photoreaction of the photoproduct of $[\text{Os}_3(\text{CO})_{10}(\mu\text{-PPh}_2)]$ with Hg^{2+} to yield a cyclic heptametallal complex [102]

Egld and coworkers found that the product obtained by reaction of $[\text{Os}_3(\text{CO})_{10}(\mu\text{-PPh}_2)]$ with Hg^{2+} , shown in Fig. 18, produced a complex that was light sensitive. Upon exposure to daylight, a rearrangement took place to give the novel wheel-shaped cluster complexes $[\text{Os}_6(\mu_6\text{-Hg})(\mu\text{-PPh}_2)_2(\text{CO})_{20}]$. This unusual CO loss photochemistry could provide the avenue for the development of novel materials [102].

The mesityl complex $[(\text{mes})\text{Os}(\text{C}_2\text{H}_4)(\text{CH}_3\text{CN})]$ results in addition of benzene when irradiated with ultraviolet light in benzene solution (Fig. 19) [103]. Photolysis of the complex in perdeuterotoluene in frozen matrices results in D atom abstraction. Photolysis of Os(VI) dioxo complexes such as $[\text{Os}(\text{O})_2(\text{Bu-salch})]$ (Scheme 1) with olefins yields epoxides, in one instance with some degree of chiral selectivity [104].

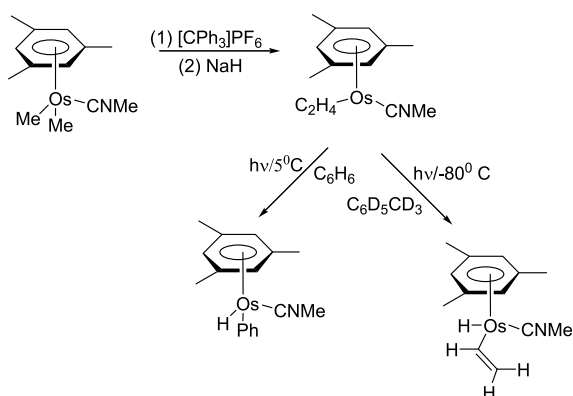


Fig. 19 C–H insertion into $[(\text{mes})\text{Os}(\text{C}_2\text{H}_4)(\text{CH}_3\text{CN})]$ following photolysis in benzene solution [103]

5 Photonic Applications of Os Complexes

5.1 Sensors and Biological Applications

The majority of Os(II) complexes exhibit weak luminescence and might not appear to be attractive candidates for use in various sensing schemes based on luminescence. Systems serving as oxygen sensors, including Os(II) complexes, have recently been reviewed [105]. Nonetheless, there are a few recent examples of applications of this sort and one recent application of a Ru(II)/Os(II) energy transfer based sensing system.

Webber et al. have used $[\text{Os}(\text{bpy})_3]^{2+}$ complex luminescence in a photoluminescence following electron transfer scheme for HPLC detection of amines

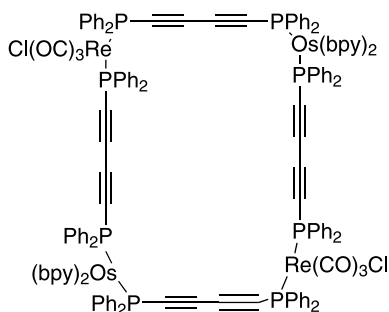
of biological importance (i.e., dopamine) and catechols. The use of the Os(III) complex as an oxidant of organics in the analyte followed by luminescence detection of the Os(II) complex is sensitive at the nanomolar level. Despite the fact that the $[\text{Os}(\text{bpy})_3]^{2+}$ luminescence has a significantly lower quantum yield than the Ru(II) complex, the background signal is much lower because Os(III) is a weaker oxidant and greater selectivity is achieved [106, 107].

A very interesting approach for specific immunoassays was recently reported by Wang, Yang, and Tan [108]. They employed silica nanoparticles of varying sizes with different mixtures of $[\text{Os}(\text{bpy})_3]^{2+}$ and $[\text{Ru}(\text{bpy})_3]^{2+}$ incorporated in the particles, imparting different relative emission intensities for the Ru and Os chromophores. The nanoparticles were then modified with either mouse or human IgG antibodies and exposed to microspheres modified with, for instance, anti-mouse IgG. Luminescence results revealed that the mouse IgG nanoparticles associated specifically with the anti-mouse IgG microspheres. Further, mixtures of the microspheres modified with anti-mouse and anti-human IgG could be distinguished because of selective doping ratios of the nanoparticles with the Os and Ru complexes.

The complex $[\text{Os}(\text{tpy})(\text{tact-tpy})]^{2+}$ was examined in detail for potential application as a luminescence sensor. The complex emission was demonstrated to be sensitive to Cu^{2+} and Ni^{2+} in mixed aqueous acetonitrile solutions. The Ni^{2+} complex serves as a sensor for the anions ATP, AMP, and Cl^- . Finally, the authors demonstrated that sol-gel silica films containing the complex exhibited luminescence sensitive to oxygen [109].

Hong and coworkers reported an interesting macrocyclic complex consisting of mixed Re(I) carbonyl chloro complexes linked through the diphosphine bridge (below) to $\text{Os}(\text{bpy})_2$ chromophores. Excitation of either the Re(I) or Os(II) visible light absorbing centers resulted in luminescence from the Os(II) diimine complex in the red. The emission was quenched to varying degrees by association of anisole, 1,4-dimethoxybenzene, and 1,3,5-trimethoxybenzene [110].

Use of a Ru imine complex to Os imine complex energy transfer scheme for detection of oligonucleotide sequences was recently reported [111]. The system



Structure 4

involves a split probe oligo detection system, in which the 3' end of one half of the oligo is tagged with the Os(II) complex acceptor and the 5' end of the second half of the oligo is tagged with the Ru(II) complex donor. The two halves will only associate with their complementary segments on a polynucleotide containing the full sequence. They demonstrated that reasonably effective energy transfer occurs for the oligonucleotide having a perfect match and minimal energy transfer is observed if there are two mismatches in the sequence.

Brewer et al. have examined light induced DNA cleavage by a series of complexes known to have metal-to-metal charge transfer (MMCT) excited states. The Os containing complex $\{[(bpy)_2Os(2,3dpp)]_2RhCl_2\}^{5+}$ (2,3dpp in Scheme 4) was shown to lead to the cleavage of pUC18 DNA, converting the supercoiled form to the nicked form cleanly, even in the absence of oxygen. The authors propose that, for complexes of this general structural type, the presence of a MMCT lower in energy than other, most particularly MLCT, states is required [112].

5.2

Photovoltaic Cells

Over the past 15 years there has been a wealth of research on development and application of transition metal complex sensitizers to the development of dye sensitized photoelectrochemical (solar) cells (DSSCs) [113]. Charge injection from the excited state of many sensitizers has been found to be on the sub-picosecond timescale, and a key objective has been to identify chromophores that absorb throughout the visible spectrum. For this reason, Os(II) complexes appear attractive and a variety of attempts were made to make use of these complexes in DSSCs in the 1990s [114–116]. Work has continued in this area in recent years and representative examples are given below.

Molecular rectification by a bimetallic Ru–Os compound anchored to nanocrystalline TiO_2 was reported by Kleverlaan et al. The complex $[(dcb)_2Ru(Cl)(bpa)Os(Cl)(bpy)_2]^{2+}$ adsorbs to TiO_2 via the carboxylate moieties of the dcb ligand and charge injection results following excitation of either the Ru(II) or the Os(II) center. The hole created in charge injection ends up as Os(III) (see Fig. 20), since back electron transfer from the injected electron is slow relative to intramolecular hole migration, allowing intramolecular electron transfer from Os(II) to Ru(III) centers created upon charge injection to dominate. DSSCs made from this bimetallic chromophore have no significant photocurrent because recombination of the injected electron is fast relative to reduction of the Os(III) center by the iodide reductant in the cell [117].

Vos and Bignozzi reported another Ru(II)/Os(II) donor/acceptor complex, $[(dcb)_2Ru(dpt)Os(bpy)_2]^{4+}$, as a sensitizer for TiO_2 photoelectrodes. Their work indicates that charge injection occurs from both Ru(II) and Os(II) centered excited states, but that the resulting transient species is the thermodynamic Ru(II)/Os(III) species [118].

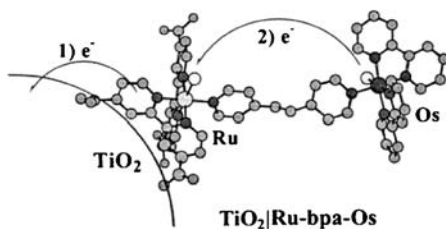


Fig. 20 Photoinduced charge injection into TiO_2 and subsequent hole migration to the Os(II) center in $[(\text{dcb})_2\text{Ru}(\text{Cl})(\text{bpa})\text{Os}(\text{Cl})(\text{bpy})_2]^{2+}$ [116]

The Lewis group has been active in this area for some time, and in 2001 they reported high quantum yields for sensitization of nanocrystalline TiO_2 with *cis*- $[\text{Os}(\text{CN})_2(\text{dcb})_2]$ and related derivatives [119]. The complex provided better response at long wavelengths than the leading Ru(II) complex dye, and open circuit photovoltages and photocurrents were comparable. Figure 21 illustrates the relative external quantum efficiencies as a function of wavelength for various sensitizers, including the Os(II) dicyano complex.

Charge injection and charge recombination dynamics have also been examined for $[(\text{dcb})_2\text{Os}(\text{CN})_2]$ and $[(\text{dcb})\text{Os}(\text{SCN})_2]$. Injection occurs with rate constants $> 10^8 \text{ s}^{-1}$ (probably much greater), but recombination rate constants are on the microsecond timescale. Detailed analysis of the combined

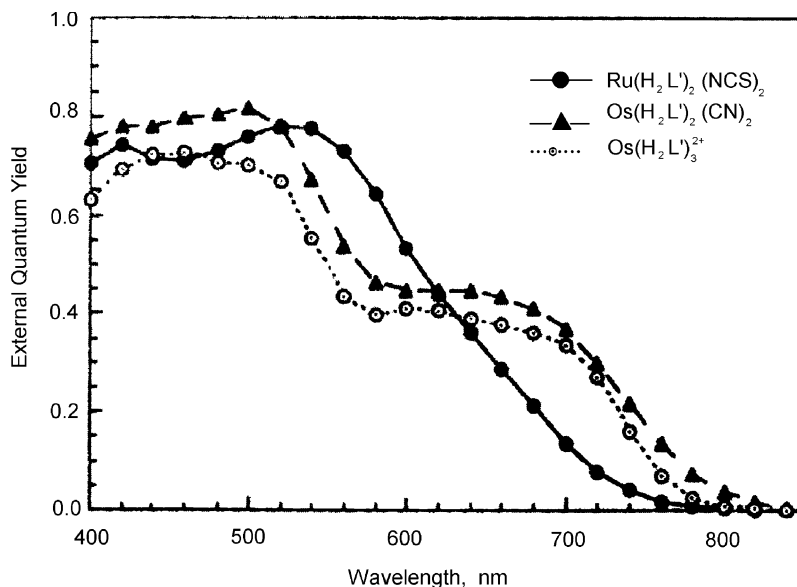
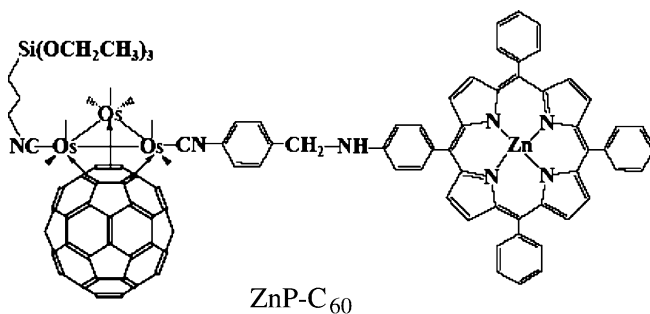


Fig. 21 Wavelength dependence of the external quantum yield for various sensitizers in dye sensitized solar cells ($\text{H}_2\text{L}' = 4,4'$ -dicarboxy-2,2'-bipyridine) [118]

kinetic data suggests the back electron transfer is in the Marcus inverted region. They also found that iodide reduction of the Os(III) generated competed effectively with back electron transfer for the CN complex only [120].

The photostability and photoelectrochemical behavior of a red sensitive Os(II) complex, $[(\text{tct})\text{Os}(\text{CN})_3]^-$ ($\text{tct} = 4,4',4''\text{-tricarboxy-2,2':6',2''-terpyridine}$), was investigated by Argazzi et al. The complex is stable to photosolvation in acetonitrile and methanol and, when used in DSSCs, exhibits efficient photocurrent generation at wavelengths in excess of 900 nm, comparable to the well studied $[(\text{tct})\text{Ru}(\text{SCN})_3]^-$ complex [121].

Os(II) complexes having phosphonic acid derivatized bipyridyl ligands (Scheme 1) have also been studied. The phosphonic acid complexes exhibit stronger adsorption to the semiconductor surface, which offers some advantages in devices. The complexes $[\text{Os}(\text{dpb})_3]^{2+}$, $[(\text{dpb})_2\text{Os}(\text{Cl})_2]$, and $[(\text{dpb})_2\text{Os}(\text{CN})_2]$ have been investigated by Zabri et al. [122]. The photo-physical properties of the complexes are reported and a comparison of the performance of DSSCs is made relative to $[(\text{dcb})_2\text{Ru}(\text{SCN})_2]$. Remarkably, absorption into the spin forbidden Os to dpb MLCT absorption resulted in high efficiencies in the 600–700-nm spectral region.



Structure 5

McCusker and coworkers investigated the dynamics of charge injection into ITO/TiO₂ electrodes from $[\text{Os}(\text{dcb})_2(\text{CN})_2]$ and $[\text{Os}(\text{dcb})_2(\text{SCN})_2]$. The key observation from the results is that the Os(II) complexes exhibit a smaller fraction of charge injection on the femtosecond timescale and a greater fraction on the picosecond timescale. The authors suggest that this is due to a greater portion of the charge injection coming from the thermalized ³MLCT state rather than the ¹MLCT or vibrationally excited ³MLCT states [123].

A unique approach to covalent modification of ITO electrode surfaces was presented by Cho and coworkers. Using the complex shown, covalent attachment to ITO is achieved with a siloxane linkage and the remainder of the sensitizer consists of C₆₀ linked to a triosmium carbonyl cluster that also links to a tetraphenylporphyrin derivative. The work describes a photocurrent generation quantum yield of over 19% [124].

Meyer and coworkers investigated the photophysical behavior of vinyl containing Ru(II) and Os(II) complexes electropolymerized into the channels of silica sol-gel modified ITO electrodes. The monomeric complexes, $[\text{Ru}(\text{vbpy})_3]^{2+}$ and $[\text{Os}(\text{vbpy})_3]^{2+}$ (vbpy = 4-methyl-4'-vinyl-2,2'-bipyridine), have excited state lifetimes of approximately 900 and 60 ns, respectively. Incorporation into the sol-gel pores and polymerization (reductive polymerization initiated at the ITO electrode) results in chromophores that exhibit a remarkably small amount of self-quenching and have domains that reflect relatively isolated chromophores with excited state lifetimes longer than the solution values [125].

5.3

Electroluminescent Devices

A complementary application to the use of Os complexes in photovoltaic cells is the use of luminescent Os complexes in electroluminescent devices. There has been a significant amount of work in this area, particularly as it applies to the development of Os complexes with high quantum yields for phosphorescence. A review of transition metal complexes used in OLED development was published in 2006 by Evans et al. [126]. Another very recent review discusses various Os(II) carbonyl complexes with diketonate, hydroxyquinolate, bipyridine, and phenanthroline ligands as emitters in OLED devices [127]. A few select examples of Os complexes in OLEDs are presented here.

Lu and coworkers have used neutral *trans*-bis-phosphine Os(II) complexes as red emitters in electroluminescent cells and found their performance to have high efficiency. The complexes *trans*- $[\text{Os}(\text{Ph}_2\text{MeP})_2(\text{fppz})]$, *trans*- $[\text{Os}(\text{PhMe}_2\text{P})_2(\text{fppz})]$, and *trans*- $[\text{Os}(\text{Ph}_2\text{MeP})_2(\text{ptri})]$ (ligands: Scheme 1) all exhibit strong emission in the red and show high electroluminescence intensities in EL devices having a fluorobiphenyl derivative as hole blocker and PVK (polyvinylcarbazole) incorporated into the Os containing layer [128]. Refinement of this work using *trans*- $[\text{Os}(\text{PhMe}_2)_2(\text{fppz})]$ as chromophore has yielded OLEDs with external quantum efficiencies greater than 12% [129].

Dalton et al. reported strong electroluminescence from mixed ligand Os(II) complexes having aryl substituted bipyridine or phenanthroline ligands (Arbpy or Arphen) and bidentate phosphine ligands such as diphenylphosphinoethane (dppe). The complexes, serving as dopants in a PVK layer of the OLED, exhibited relatively pure red luminescence and external quantum efficiencies of 0.6% [130, 131].

Doping of ionic electroluminescent films of $[\text{Ru}(\text{bpy})_3]^{2+}$ with $[\text{Os}(\text{phen})_3]^{2+}$ produced single layer OLEDs with luminescence emerging predominantly from the Os MLCT excited state, but the emission energy can be tuned to some extent by varying the concentration of the dopant. The devices prove to have better stability than devices prepared from either of the pure complexes [132].

Acknowledgements The authors would like to thank the US Department of Energy, Office of Chemical Sciences (DE-FG02-96ER14617), for support leading to the production of this review.

References

1. Serpone N (1985) NATO ASI Ser C, Math Phys Sci 146:351
2. Kalyanasundaram K (1993) J Ind Chem Soc 70:433
3. De Cola L, Belser P (1998) Coord Chem Rev 177:301
4. Baxter SM, Jones WE Jr, Danielson E, Worl L, Strouse G, Younathan J, Meyer TJ (1991) Coord Chem Rev 111:47
5. Denti G, Serroni S, Campagna S, Juris A, Balzani V (1993) Mol Cryst Liq Cryst A 234:79
6. Kochi JK (1990) Acta Chem Scand 44:409
7. Ford PC (1990) J Organomet Chem 383:339
8. Yersin H, Huber P, Braun D (1990) J Phys Chem 94:3560
9. Kober EM, Caspar JV, Lumpkin RS, Meyer TJ (1986) J Phys Chem 90:3722
10. Caspar JV, Westmorland TD, Allen GH, Bradley PG, Meyer TJ, Woodruff WH (1984) J Am Chem Soc 106:3492
11. Bergkamp MA, Gutlich P, Netzel TL, Sutin N (1983) J Phys Chem 87:3877
12. Hofmeier H, Schubert US (2004) Chem Soc Rev 33:373
13. Benniston AC, Harriman A, Li P, Sams CA (2005) J Phys Chem A 109:2302
14. Ranatunga A, Lasey RC, Ogawa MY (2001) Inorg Chem Commun 4:30
15. Shaw GB, Styers-Barnett DJ, Gannon EZ, Granger JC, Papanikolas JM (2004) J Phys Chem A 108:4998
16. Shaw GB, Brown CL, Papanikolas JM (2002) J Phys Chem A 106:1483
17. Shaw GB (2002) PhD dissertation, University of North Carolina
18. Cushing JPB, Kelley DF (1997) J Phys Chem A 101:7222
19. Bergman SD, Gut D, Kol M, Sabatini C, Barbieri A, Barigelletti F (2005) Inorg Chem 44:7943
20. Bergman SD, Goldberg I, Barbieri A, Kol M (2005) Inorg Chem 44:2513
21. Bergman SD, Goldberg I, Barbieri A, Barigelletti F, Kol M (2004) Inorg Chem 43:2355
22. Yang J, Dass A, Sotiriou-Leventis C, Tyson DS, Leventis N (2005) Inorg Chim Acta 358:389
23. Venturi M, Marchioni F, Balzani V, Opris DM, Henze O, Schlueter AD (2003) Eur J Org Chem 4227
24. Chiorboli C, Fracasso S, Ravaglia M, Scandola F, Campagna S, Wouters KL, Konduri R, MacDonnell FM (2005) Inorg Chem 44:8368
25. Juris A, Prodi L, Harriman A, Ziesel R, Hissler M, El-ghayoury A, Wu F, Riesgo EC, Thummel RP (2000) Inorg Chem 39:3590
26. Wu P-C, Yu J-K, Song Y-H, Chi Y, Chou P-T, Peng S-M, Lee G-H (2003) Organometallics 22:4938
27. Li S-W, Cheng Y-M, Yeh Y-S, Hsu C-C, Chou P-T, Peng S-M, Lee G-H, Tung Y-L, Wu P-C, Chi Y, Wu F-I, Shu C-F (2005) Chem Eur J 11:6347
28. Chen Y-L, Lee S-W, Chi Y, Hwang K-C, Kumar SB, Hu Y-H, Cheng Y-M, Chou P-T, Peng S-M, Lee G-H, Yeh S-J, Chen C-T (2005) Inorg Chem 44:4287
29. Baranovskii VI, Lyubimova OO (2003) Opt Spectrosc 94:502
30. Mockus NV, Petersen JL, Rack JJ (2006) Inorg Chem 45:8

31. Chardon-Noblat S, Da Costa P, Deronzier A, Mahabiersing T, Hartl F (2002) *Eur J Inorg Chem* 2850
32. Leane D, Keyes TE (2006) *Inorg Chim Acta* 359:1627
33. Abdel-Shafi AA, Worrall DR, Ershov AY (2004) *Dalton Trans* 30
34. Ghosh AK, Kamar KK, Paul P, Peng S-M, Lee G-H, Goswami S (2002) *Inorg Chem* 41:6343
35. Videla M, Braslavsky SE, Olabe JA (2005) *Photochem Photobiol Sci* 4:75
36. Wang R, Eberspacher TA, Hasegawa T, Day V, Ware DC, Taube H (2001) *Inorg Chem* 40:593
37. Fomitchev DV, Bagley KA, Coppens P (2000) *J Am Chem Soc* 122:532
38. Forster RJ, Keyes TE (2001) *J Phys Chem B* 105:8829
39. Brennan JL, Howlett M, Forster RJ (2002) *Faraday Discuss* 121:391
40. Lainé P, Amouyal E (1999) *Chem Commun* 935
41. Lainé P, Bedioui F, Amouyal E, Albin V, Berruyer-Penaud F (2002) *Chem Eur J* 8:3162
42. Lainé PP, Bedioui F, Loiseau F, Chiorboli C, Campagna S (2006) *J Am Chem Soc* 128:7510
43. Lainé PP, Loiseau F, Campagna S, Ciofini I, Adamo C (2006) *Inorg Chem* 45:5538
44. Ciofini I, Lainé PP, Bedioui F, Adamo C (2004) *J Am Chem Soc* 126:10763
45. Hyslop AG, Orphanide M, Javed U, Megehee EG (2003) *Inorg Chim Acta* 355:272
46. Hossain MD, Haga M-A, Gholamkhash B, Nozaki K, Tsushima M, Ikeda N, Ohno T (2001) *Collect Czech Chem Commun* 66:307
47. Kelso LS, Smith TA, Schultz AC, Junk PC, Warrenner RN, Ghiggino KP, Keene FR (2000) *J Chem Soc Dalton Trans* 2599
48. Furue M, Ishibashi M, Satoh A, Oguni T, Maruyama K, Sumi K, Kamachi M (2000) *Coord Chem Rev* 208:103
49. Constable EC, Handel RW, Housecroft CE, Morales AF, Ventura B, Flamigni L, Barigelletti F (2005) *Chem Eur J* 11:4024
50. Constable EC, Handel RW, Housecroft CE, Morales AF, Flamigni L, Barigelletti F (2003) *Dalton Trans* 1220
51. Beyeler A, Belser P (2002) *Coord Chem Rev* 230:28
52. Fleming CN, Dupray LM, Papanikolas JM, Meyer TJ (2002) *J Phys Chem A* 106:2328
53. Fleming CN, Maxwell KA, DeSimone JM, Meyer TJ, Papanikolas JM (2001) *J Am Chem Soc* 123:10336
54. Huynh MHV, Dattelbaum DM, Meyer TJ (2005) *Coord Chem Rev* 249:457
55. Serroni S, Campagna S, Puntoriero F, Loiseau F, Ricevuto V, Passalacqua R, Galletta M (2003) *C R Chim* 6:883
56. El-ghayoury A, Harriman A, Khatyr A, Ziessel R (2000) *J Phys Chem A* 104:1512
57. El-ghayoury A, Harriman A, Ziessel R (2000) *J Phys Chem A* 104:7906
58. Baudin HB, Davidsson J, Serroni S, Juris A, Balzani V, Campagna S, Hammarström L (2002) *J Phys Chem A* 106:4312
59. Andersson J, Puntoriero F, Serroni S, Yartsev A, Pascher T, Polivka T, Campagna S, Sundstrom V (2004) *Chem Phys Lett* 386:336
60. Andersson J, Puntoriero F, Serroni S, Yartsev A, Pascher T, Polivka T, Campagna S, Sundstroem V (2004) *Faraday Discuss* 127:295
61. Puntoriero F, Serroni S, Licciardello A, Venturi M, Juris A, Ricevuto V, Campagna S (2001) *J Chem Soc Dalton Trans* 1035
62. Harriman A, Hissler M, Khatyr A, Ziessel R (2003) *Eur J Inorg Chem* 955
63. Welter S, Salluce N, Benetti A, Rot N, Belser P, Sonar P, Grimdsdale AC, Muellen K, Lutz M, Spek AL, De Cola L (2005) *Inorg Chem* 44:4706
64. D'Aleo A, Welter S, Cecchetto E, De Cola L (2005) *Pure Appl Chem* 77:1035

65. Welter S, Salluce N, Belser P, Groeneveld M, De Cola L (2005) *Coord Chem Rev* 249:1360
66. Barigelletti F, Flamigni L, Guardigli M, Juris A, Beley M, Chodorowski-Kimmes S, Collin J-P, Sauvage J-P (1996) *Inorg Chem* 35:136
67. Harriman A, Khatyr A, Ziessel R, Benniston AC (2000) *Angew Chem Int Ed* 39:4287
68. Xu D, Zhang JZ, Hong B (2001) *J Phys Chem A* 105:7979
69. Bilakhiya AK, Tyagi B, Paul P, Natarajan P (2002) *Inorg Chem* 41:3830
70. Chiorboli C, Bignozzi CA, Scandola F, Ishow E, Gourdon A, Launay J-P (1999) *Inorg Chem* 38:2402
71. Weldon F, Hammarström L, Mukhtar E, Hage R, Gunneweg E, Haasnoot JG, Reedijk J, Browne WR, Guckian AL, Vos JG (2004) *Inorg Chem* 43:4471
72. Benniston AC, Harriman A, Li P, Sams CA (2005) *J Am Chem Soc* 127:2553
73. Benniston AC, Harriman A, Li P, Patel PV, Sams CA (2005) *Phys Chem Chem Phys* 7:3677
74. Venturi M, Marchioni F, Ribera BF, Balzani V, Opris DM, Schluter AD (2006) *Chem Phys Chem* 7:229
75. Paul RL, Morales AF, Accorsi G, Miller TA, Ward MD, Barigelletti F (2003) *Inorg Chem Commun* 6:439
76. Jukes RTE, Adamo V, Hartl F, Belser P, De Cola L (2005) *Coord Chem Rev* 249:1327
77. Jukes RTE, Adamo V, Hartl F, Belser P, De Cola L (2004) *Inorg Chem* 43:2779
78. Tsushima M, Ikeda N, Yoshimura A, Nozaki K, Ohno T (2000) *Coord Chem Rev* 208:299
79. Yersin H, Kratzer C (2002) *Coord Chem Rev* 229:75
80. Okamoto K, Takahashi M, Taniguchi M, Yamagishi A (2000) *Chem Lett* 740
81. Argazzi R, Bertolasi E, Chiorboli C, Bignozzi CA, Itokazu MK, Iha NYM (2001) *Inorg Chem* 40:6885
82. Ortega JV, Khin K, van der Veer WE, Ziller J, Hong B (2000) *Inorg Chem* 39:6038
83. Walters KA, Trouillet L, Guillerez S, Schanze KS (2000) *Inorg Chem* 39:5496
84. Juris A, Prodi L (2001) *New J Chem* 25:1132
85. Maubert B, McClenaghan ND, Indelli MT, Campagna S (2003) *J Phys Chem A* 107:447
86. Balazs GC, del Guerso A, Schmechl RH (2005) *Photochem Photobiol Sci* 4:89
87. Akasaka T, Mutai T, Otsuki J, Araki K (2003) *Dalton Trans* 1537
88. Faiz JA, Williams RM, Pereira Silva MJJ, De Cola L, Pikramenou Z (2006) *J Am Chem Soc* 128:4520
89. Leadbeater NE (1999) *J Organomet Chem* 573:211
90. Calhorda MJ, Costa PJ, Hartl F, Vergeer FW (2005) *C R Chim* 8:1477
91. Bakker MJ, Vergeer FW, Hartl F, Jina OS, Sun XZ, George MW (2000) *Inorg Chim Acta* 277:300–302
92. Vergeer FW, Matousek P, Towrie M, Costa PJ, Calhorda MJ, Hartl F (2004) *Chem Eur J* 10:3451
93. Vergeer FW, Bakker MJ, Kleverlaan CJ, Hartl F, Stufkens DJ (2002) *Coord Chem Rev* 229:107
94. Vergeer FW, Kleverlaan CJ, Stufkens DJ (2002) *Inorg Chim Acta* 327:126
95. Vergeer FW, Lutz M, Spek AL, Calhorda MJ, Stufkens DJ, Hartl F (2005) *Eur J Inorg Chem* 2206
96. Hartl F, Van Outersterp JW (2006) *Collect Czech Chem Commun* 71:237
97. Bitterwolf TE, Linehan JC, Shade JE (2001) *Organometallics* 20:775
98. Zhang J, Grills DC, Huang K-W, Fujita E, Bullock RM (2005) *J Am Chem Soc* 127:15684

99. Chen G, Deng M, Lee CKD, Leong WK, Tan J, Tay CT (2006) *J Organomet Chem* 691:387
100. Watson WH, Wu G, Richmond MG (2006) *Organometallics* 25:930
101. Vergeer FW, Kleverlaan CJ, Matousek P, Towrie M, Stufkens DJ, Hartl F (2005) *Inorg Chem* 44:1319
102. Egold H, Schraa M, Floerke U, Partyka J (2002) *Organometallics* 21:1925
103. Werner H, Wecker U (2000) *J Organomet Chem* 192:593-594
104. Zhang J, Liang J-L, Sun X-R, Zhou H-B, Zhu N-Y, Zhou Z-Y, Chan PWH, Che C-M (2005) *Inorg Chem* 44:3942
105. Amao Y (2003) *Microchim Acta* 143:1
106. Jung MC, Munro N, Shi G, Michael AC, Weber SG (2006) *Anal Chem* 78:1761
107. Jung MC, Weber SG (2005) *Anal Chem* 77:974
108. Wang L, Yang C, Tan W (2005) *Nano Lett* 5:37
109. Ros-Lis JV, Martinez-Manez R, Soto J, McDonagh C, Guckian A (2006) *Eur J Inorg Chem* 2647
110. Xu D, Khin KT, Van Der Veer WE, Ziller JW, Hong B (2001) *Chem Eur J* 7:2425
111. Bichenkova EV, Yu X, Bhadra P, Heissigerova H, Pope SJA, Coe BJ, Faulkner S, Douglas KT (2005) *Inorg Chem* 44:4112
112. Holder AA, Swavey S, Brewer KJ (2004) *Inorg Chem* 43:303
113. Hagfeldt A, Gratzel M (1995) *Chem Rev* 95:49
114. Heimer TA, Bignozzi CA, Meyer GJ (1993) *J Phys Chem* 97:11987
115. Alebbi M, Bignozzi CA, Heimer TA, Hasselmann GM, Meyer G (1998) *J Phys Chem* 102:7577
116. Farzad F, Thompson DW, Kelly CA, Meyer GJ (1999) *J Am Chem Soc* 121:5577
117. Kleverlaan C, Alebbi M, Argazzi R, Bignozzi CA, Hasselmann GM, Meyer GJ (2000) *Inorg Chem* 39:1342
118. Lees AC, Kleverlaan CJ, Bignozzi CA, Vos JG (2001) *Inorg Chem* 40:5343
119. Sauve G, Cass ME, Doig SJ, Lauermaun I, Pomykal K, Lewis NS (2000) *J Phys Chem B* 104:3488
120. Kuciauskas D, Freund MS, Gray HB, Winkler JR, Lewis NS (2001) *J Phys Chem B* 105:392
121. Argazzi R, Larramona G, Contado C, Bignozzi CA (2004) *J Photochem Photobiol A Chem* 164:15
122. Zabri H, Odobel F, Altobello S, Caramori S, Bignozzi CA (2004) *J Photochem Photobiol A Chem* 166:99
123. Kuciauskas D, Monat JE, Villahermosa R, Gray HB, Lewis NS, McCusker JK (2002) *J Phys Chem B* 106:9347
124. Cho Y-J, Ahn TK, Song H, Kim KS, Lee CY, Seo WS, Lee K, Kim SK, Kim D, Park JT (2005) *J Am Chem Soc* 127:2380
125. Yang J, Sykora M, Meyer TJ (2005) *Inorg Chem* 44:3396
126. Evans RC, Douglas P, Winscom CJ (2006) *Coord Chem Rev* 250:2093
127. Chou P-T, Chi YA (2006) *Eur J Inorg Chem* 3319
128. Lu J, Tao Y, Chi Y, Tung Y (2005) *Synth Met* 155:56
129. Niu Y-H, Tung Y-L, Chi Y, Shu C-F, Kim JH, Chen B, Luo J, Carty AJ, Jen AK-Y (2005) *Chem Mater* 17:3532
130. Carlson B, Phelan GD, Kaminsky W, Dalton L, Jiang X, Liu S, Jen AK-Y (2002) *J Am Chem Soc* 124:14162
131. Carlson B, Phelan GD, Jiang X, Kaminsky W, Jen AKY, Dalton LR (2003) *Proc Soc Photo Opt Instrum Eng* 4800:93
132. Hussein AR, Koh CY, Slinker JD, Flores-Torres S, Abruna HD, Malliaras GG (2005) *Chem Mater* 17:6114

Photochemistry and Photophysics of Coordination Compounds: Iridium

Lucia Flamigni · Andrea Barbieri · Cristiana Sabatini · Barbara Ventura ·
Francesco Barigelletti (✉)

Istituto per la Sintesi Organica e la Fotoreattività, Consiglio Nazionale delle Ricerche,
Via P. Gobetti 101, ISOF-CNR, I-40129 Bologna, Italy
franz@isof.cnr.it

1	Introduction	145
2	The Ir(III) Metal Center and the Octahedral Coordination	146
3	Mononuclear Complexes of Bidentate Ligands and Isomeric Species . . .	150
3.1	Interplay of Emissive Excited States	152
3.2	Phosphorescence Tuning in Ir(III)-Cyclometalated Complexes for OLED Applications	154
3.2.1	From Green to Yellow with Neutral Heteroleptic Complexes	154
3.2.2	From Green to Red with Neutral Homoleptic Complexes	157
3.2.3	Systematic Tuning Approaches Leading to Blue Emission	159
3.2.4	Cationic Ir(III)-Cyclometalated Complexes	163
3.3	Ir(III) Complexes for Oxygen Sensing	167
3.4	Photophysics of Ir(ppy) ₂ (LL) Complexes Covalently Linked to Substrates .	169
4	Mononuclear Complexes of Terdentate Ligands	172
4.1	Terdentate (N [^] N [^] N) Ligands	172
4.2	Terdentate Cyclometalating Ligands	176
5	Interplay of Excited States and the Role of MC Levels	178
6	Ir(III) Complexes in Multicomponent Systems	182
6.1	Binuclear Homometallic Complexes	182
6.2	Energy Transfer Processes	186
6.3	Electron Transfer Processes	193
6.4	Assemblies for Charge Separation	194
7	Conclusions	198
	References	199

Abstract Mononuclear Ir(III)-polyimine complexes show outstanding luminescence properties, i.e., high intensities, lifetimes in the μs time range, and emission wavelengths that can be tuned so as to cover a full range of visible colors, from blue to red. We discuss the approaches for the use of ligands that afford control on luminescence features. Emphasis is placed on subfamilies of cyclometalated complexes, whose recent enormous expansion is motivated by their potential for applications, including that as phosphorescent dopants in OLEDs fabrication. The interplay of the different excited states associated

with the luminescence, usually of MLCT and/or LC nature, is examined and the possible detrimental role of MC levels toward the luminescence properties is outlined. Ir(III)-polyimine moieties can be incorporated within multicomponent arrays where they can play as photoactive and/or electroactive units in photoinduced energy and electron transfer processes. The field is reviewed with attention to the processes of light collection and conversion into chemical energy.

Keywords Iridium complexes · Cyclometalating ligands · Phosphorescence · Electrochemistry · Multicomponent arrays · OLEDs · Photoinduced processes

Abbreviations

AN	acetonitrile
Av	avidine
Bu	butyl
CS	charge separation
CT	charge transfer
DFT	density functional theory
Et	ethyl
GS	ground state
HSA	human serum albumin
HOMO	highest occupied molecular orbital
IAA	iodoacetamide
ILCT	intra-ligand charge transfer
ITC	isothiocyanate
LC	ligand centered
LLCT	ligand-to-ligand charge transfer
LUMO	lowest unoccupied molecular orbital
LX	or LL ancillary ligands
MC	metal centered
MeO	methoxy
MLCT	metal-to-ligand charge transfer
MLLCT	metal-ligand-to-ligand charge transfer
OLED	organic light-emitting diode
Pr	propyl
SBLCT	sigma bond-to-ligand charge transfer
<i>t</i> -Bu	<i>tert</i> -butyl

Ligands – Further acronyms for ligands are indicated directly in the Figs.

acac	monoanion of acetyl acetone
biptpy	4'-(4-biphenyl)-2,2':6',2''-terpyridine
bpb	bianion of 1,4-bis(pyridine-2-yl)benzene
bpt	monoanion of 3,5-bis(pyridine-2-yl)-1,2,4-triazole
bpy	2,2'-bipyridine
dpb	2,3-bis(2-pyridyl)benzoquinoline
dpp	2,3-bis(2-pyridyl)pyrazine
HAT	1,4,5,8,9,12-hexaazaphenanthrene
nala	3-(2-naphthyl)alanine
ph	phenyl
phen	1,10-phenanthroline

pic	monoanion of picolinic acid
pppy	monoanion of phenyl-4,5-pinenopyridine
ppy	monoanion of phenyl-pyridine (2'-phenyl-pyridine)
ppyFF	monoanion of (4',6'-difluoro)phenyl-pyridine
py	pyridine
sal	monoanion of <i>N</i> -methyl salicylimine
TBA	tetrabutylammonium
terpy	2,2':6',2''-terpyridine
tpp	2,3,5,6-tetrakis(2-pyridyl)pyrazine
tpyada	4'-(1-adamantyl)9-2,2':6',2''-terpyridine

1

Introduction

A dozen years ago, the optical properties of a very few cases of Ir(III) complexes were known [1, 2]. In the same period, Ru(II)-, Os(II)- and Re(I)-polyimine complexes, for instance, were comparatively much more popular as a consequence of research efforts related to the theme of the interconversion between light and chemical energy [3–5]. In early times, the tricationic Ir(bpy)₃³⁺ species proved difficult to prepare, and was clearly identified only after closely related species were studied [1, 6, 7]; bpy is 2,2'-bipyridine, Fig. 1. At the same time, the neutral *fac*-Ir(ppy)₃ species initially appeared as a side-product of dichloro-bridged dimers of the type [Ir(ppy)₂Cl]₂ [8]; ppy is the cyclometalating anion from Hppy, Fig. 1. Today, we witness an impressive expansion of the literature on the luminescence of Ir(III) complexes, as illustrated by Fig. 2.

From this diagram, one may notice that ca. 90% of the known luminescent Ir(III) complexes, mostly from cyclometalating ligands, have been reported in the last 6 years. One relevant reason for this trend is related to the use of the cyclometalated complexes for OLED fabrication [9–12], with those of Ir(III) exhibiting relevant advantages with respect to complexes from other metals [13].

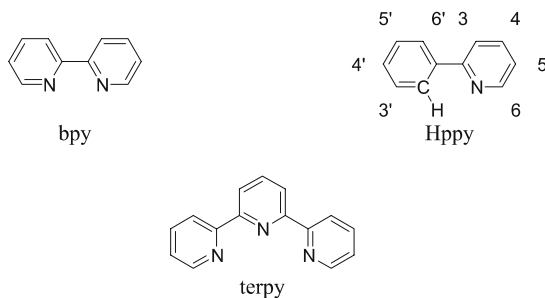


Fig. 1 Schematic structures

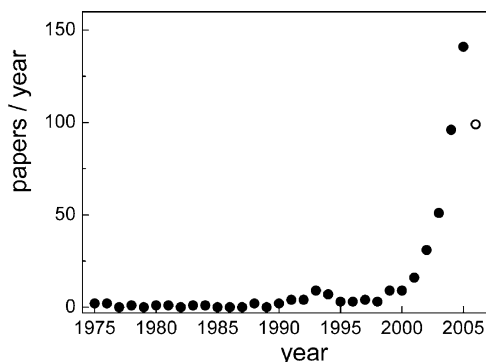


Fig. 2 Representative number of papers (*full points*) dealing with the luminescence of iridium(III) complexes in the indicated years; updating is set at August 2006 (*empty point*)

In this work, we will review the optical, and to some extent, the electrochemical properties, of selected subfamilies of Ir(III) complexes. This will be done having in mind mainly (i) the actual interest in the manipulation and tuning of the photophysical properties of complexes playing as phosphorescence emitters, (ii) the possible use of Ir(III) centers as templating units for multicomponent arrays, particularly in view of charge separation (CS) schemes for the interconversion of light and chemical energy.

2

The Ir(III) Metal Center and the Octahedral Coordination

The Ir(III) trication is a $5d^6$ center and the electronic properties of its polyimine complexes share several features with those of other well-known octahedral complexes of Fe(II) [14], Ru(II) [3], Os(II) [4], and Re(I) [5], whose metal centers are $3d^6$, $4d^6$, $5d^6$, and $5d^6$, respectively. Figure 3 depicts useful orbital and state energy diagrams for electronic transitions taking place in polyimine complexes of such d^6 metal centers.

As shown in Fig. 3a, the degenerate d orbitals of the Fe(II), Ru(II), Os(II), and Ir(III) cations are destabilized and split in an octahedral ligand field, by an amount Δ . Because of the different spatial extension for $3d$ (Fe), $4d$ (Ru), and $5d$ (Os and Ir) orbitals, this effect is smallest for the d orbitals with the lowest quantum number, $3d$. Of course, the amount of Δ depends also on the field strength exerted by the ligands, that can be ordered along a “spectrochemical series” [2]. It is likely that in this series, a cyclometalated ligand like ppy occupies a position among those causing the strongest effect. It should be noted that in all cases discussed here, light absorption is associated with electronic transitions from the ground state (GS) to, mostly, singlet levels of vari-

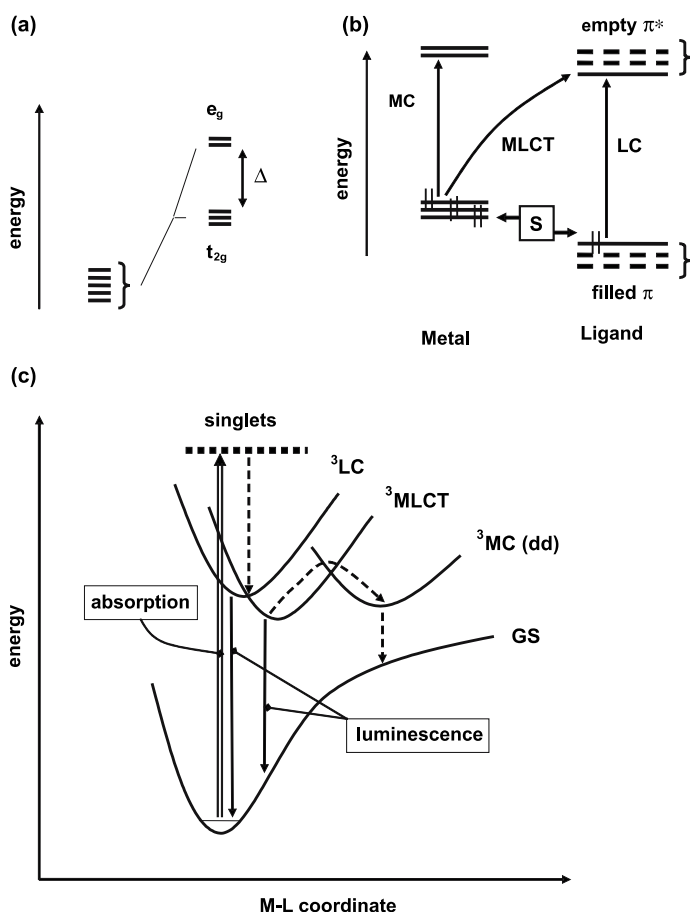


Fig. 3 **a** d orbitals in octahedral field; **b** orbital description of MC, MLCT, and LC transitions; S is a substituent group capable of exerting electron withdrawing or releasing effects (resulting in stabilization or destabilization, respectively, of the energy level of the filled d and π orbitals); **c** electronic transitions involving MC, MLCT, and LC excited states; the MC levels are not emissive

ous nature and electronic localization, ligand centered (1LC), metal-centered (1MC), and metal to ligand charge transfer (1MLCT). In addition, ligand-to-metal transitions (1LMCT) can in principle be involved. On the contrary, emission is always from triplet levels, 3MLCT or 3LC in nature, which actually include changeable amounts of the corresponding singlets [15]. This is a consequence of the high spin-orbit coupling constants of the metal centers taken into account, $\zeta = 431, 1042, 3381, 3909 \text{ cm}^{-1}$, for Fe, Ru, Os, and Ir, respectively [16].

A few basic issues regarding the known luminescent behavior of d^6 complexes from the families of Fe(II)-, Ru(II)-, and Os(II)-polyimines are shortly

reviewed below—this will help the survey of analogous properties exhibited by Ir(III) complexes.

- (i) For Fe(II) in an octahedral field, Δ (Fig. 3a) is small enough that the lowest-lying excited state for Fe(II)-polyimine complexes is most likely MC in nature, i.e., not emissive [14, 17], see Fig. 3c.
- (ii) On the contrary, for Os(II) and Ir(III), the ligand field splitting Δ is very large and the MC levels are pushed so high in energy that usually they do not affect the emission properties. These are traceable back to MLCT levels or LC levels, both of them being emissive. Os(II)-polyimine complexes display low-lying MLCT levels, around 1.6 eV [4, 18]. In this case, radiationless paths governed by the “energy-gap law” become effective [4, 18], which result in a low luminescence quantum efficiency, $\phi < 0.1$. By contrast, the energy content of the emitting levels for most Ir(III)-polyimine complexes is rather high (in the range 2.1 to 3 eV, see below), and their emission properties are practically void of complications from “energy-gap law” effects.
- (iii) For Ru(II)-polyimine complexes, one usually observes MLCT emission at around 2.1 eV [3]. However, MC levels are thermally accessible, see Fig. 3c, because Δ for the Ru(II) 4d orbitals has an intermediate value between the Fe(II) and Os(II) (and Ir(III)) cases. Thus, parasitic radiationless paths involving the MC levels contribute to deactivation of the MLCT emissive level for Ru(II)-polyimine complexes. A practical consequence is that also for this family of complexes, and apart from remarkable exceptions [19], ϕ rarely exceeds 0.1.

The spectroscopic and electrochemical properties of the archetypical cases of the tricationic Ir(bpy)₃³⁺ and Ir(terpy)₂³⁺ species, and of the neutral *fac*-Ir(ppy)₃ species, Table 1 [1, 6, 8, 20–25], reveal trends that will be recalled several times in the following (terpy is 2,2':6',2''-terpyridine, Fig. 1).

In particular, along the series Ir(bpy)₃³⁺, Ir(terpy)₂³⁺ and neutral *fac*-Ir(ppy)₃ (keeping in mind related properties exhibited by other *d*⁶ complexes), one can observe that:

- (i) The longest wavelength absorption peak ($\lambda_{\text{abs}}^{\text{max}}$) moves to lower and lower energy and the absorption intensity increases, Table 1. Notably, in all cases the absorption maximum does not exceed 400 nm, while for Ru(II)-polyimine complexes this is usually in the range 450–500 nm [3], as for the Os(II)-counterparts (in the latter case, forbidden transitions become apparent at even longer wavelengths) [4]; and for Fe(bpy)₃²⁺, $\lambda_{\text{abs}}^{\text{max}}$ is at ca. 520 nm [14].
- (ii) The emission peak (λ_{em}) follows the same trend, with the luminescence quantum yield (ϕ) increasing dramatically along the series; the luminescence lifetime (τ) stays around 1–2 μs . It's worth noticing that the energy content of the emitting level becomes lower and lower in the series. Nevertheless, it is as high as 2.5 eV for *fac*-Ir(ppy)₃, re-

Table 1 Spectroscopic and electrochemical properties of archetypical complexes of the Ir(III)-polypyridine family^a

	Absorption ^b		Emission ^c		τ μs	$E^{0,0,d}$ eV	Electrochemistry ^e	
	$\lambda_{\text{abs}}^{\text{max}}$ nm	ϵ $10^3 \text{ M}^{-1} \text{ cm}^{-1}$	λ_{em} nm	ϕ			Oxidation Ir ^{IV/III} V	Reduction Ir ^{III/II} ($\text{L}^{0/-1}$) V
Ir(bpy) ₃ (PF ₆) ₃	344	3.3	441	–	2.4	2.81	+2.1	–1.1
Ir(terpy) ₂ (PF ₆) ₃	352	5.8	458	0.03	1.2	2.71	>+2.4	–0.77
<i>fac</i> -Ir(ppy) ₃	375	7.2	494 ^f	0.38	1.9	2.50	+0.77	–2.19

^a Room temperature and acetonitrile solvent, unless otherwise noted; table compiled on the basis of data reported in [1, 6, 8, 20–25]

^b Lowest-energy absorption maximum with $\epsilon > 1500 \text{ M}^{-1} \text{ cm}^{-1}$

^c Oxygen-free solvent

^d Energy of the emitting excited state

^e Potentials vs. SCE (in some cases, adapted from the original works, according to $V_{\text{SCE}} = V_{\text{NHE}} - 0.24 \text{ V}$ and $V_{\text{SCE}} = V_{\text{Fc}^+/\text{Fc}} + 0.41 \text{ V}$)

^f At 77 K, in alcoholic solvent

- markably higher than for $\text{Ru}(\text{bpy})_3^{2+}$ and $\text{Os}(\text{bpy})_3^{2+}$ (2.1 and 1.6 eV, respectively).
- (iii) The electrochemical potentials (given vs. SCE in the Tables and concerned text for an easier comparison) are quite different for the complexes in Table 1 [1, 6, 8, 20–22, 24, 25].
- (iii-a) For $\text{Ir}(\text{bpy})_3^{3+}$, the first ligand reduction, occurring at -1.1 V, is easier than for the cases of both $\text{Ru}(\text{bpy})_3^{2+}$ and $\text{Os}(\text{bpy})_3^{2+}$, whose ligands can be reduced (first step) at around -1.3 V [16]. This is a consequence of the larger ionic charge in the Ir(III) center. For the same reason, the metal centered oxidation step is much more difficult in $\text{Ir}(\text{bpy})_3^{3+}$, $+2.1$ V, than in $\text{Ru}(\text{bpy})_3^{2+}$ and $\text{Os}(\text{bpy})_3^{2+}$, $+1.29$ and $+0.81$ V, respectively [16]. For the latter complex, the facile oxidation is ultimately understandable on the basis of the large spatial extension of the $5d$ orbitals [case of Os(II)] with respect to the $4d$ orbitals [case of Ru(II)], implying a larger destabilization of the occupied d levels of Os(II) upon ligand coordination, Fig. 3a.
- (iii-b) For *fac*- $\text{Ir}(\text{ppy})_3$, the negative charge on the ligand causes strong σ -donation through the Ir–C bonding. This results in facile metal-centered oxidation, $+0.77$ V, and in a difficult ligand-based reduction, -2.19 V, Table 1.

3

Mononuclear Complexes of Bidentate Ligands and Isomeric Species

In early times, it was noticed that spontaneous cyclometalation occurred upon C(3) coordination of one of the bpy ligands of the Ir-tris-bpy complex, that could therefore be denoted as $\text{Ir}(\text{bpy})_2(\text{bpy}-\text{C}^3, \text{N}')^{2+}$ [6]. This $\text{Ir}(\text{bpy})_3^{2+}$ species exhibits the interesting possibility of undergoing protonation at the external nitrogen, a property that could be useful in view of photocatalytic schemes [6]. The use of bpy and of the cyclometalating ppy ligand affords a full range of cyclometalated Ir(III) complexes, $\text{Ir}(\text{ppy})(\text{bpy})_2^{2+}$, $\text{Ir}(\text{ppy})_2(\text{bpy})^+$, and $\text{Ir}(\text{ppy})_3$, which appears to be a unique property of the Ir(III) ion.

For the case of $\text{Ir}(\text{ppy})_2(\text{bpy})^+$, three isomers A, B, and C, are in principle possible, Fig. 4a. Nevertheless, it is well-established that the cyclometalating carbons of the $(\text{C}^{\wedge}\text{N})_2\text{Ir}(\text{N}^{\wedge}\text{N})^+$ center occupy mutually *cis* positions, which are in turn *trans* to the nitrogen atoms of the $(\text{N}^{\wedge}\text{N})$ coordinating ligand, configuration A [1, 26].

The reasons for this outcome appear related to a so-called *trans* effect of the Ir–C bonds. These induce preferential labilization of the bonds located *trans* to them, which results in the stereochemical positioning of Ir–C and Ir–N bonds *trans* to one another. Such an effect is clearly observed for the stepwise reaction of $\text{Ir}(\text{acac})_3$ with ppy [24]. Here, after the first replacement

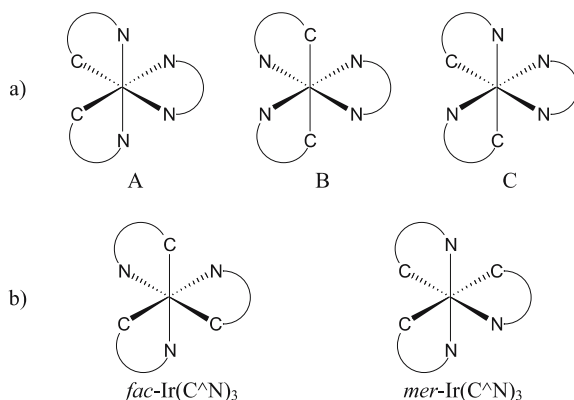


Fig. 4 Geometrical isomers: **a** A, B, C for $\text{Ir}(\text{ppy})_2(\text{bpy})^+$ and **b** *fac*- $\text{Ir}(\text{C}^{\wedge}\text{N})_3$ and *mer*- $\text{Ir}(\text{C}^{\wedge}\text{N})_3$

of a ppy ligand for an acac unit, the subsequent substitution steps are *trans*-directed and only *trans* C – Ir – N bonds form until the final *fac*- $\text{Ir}(\text{ppy})_3$ complex is obtained, Fig. 4b.

A widely followed path to prepare Ir(III)-cyclometalated complexes is based on the use of dichloro-bridged Ir(III) dimers, in turn obtained from IrCl_3 and a $(\text{C}^{\wedge}\text{N})$ ligand [26, 27]. Then, one way to the desired mononuclear complex is the treatment of the dimer with an excess of a suitable $(\text{C}^{\wedge}\text{N})$ or $(\text{N}^{\wedge}\text{N})$ ligand. This step can be performed at moderate temperature, for instance $T < 150^\circ\text{C}$, or at higher temperatures [28]. The *mer* isomer can be predominantly obtained in the former case, and can be subsequently converted, either thermally or photochemically, into the more stable *fac* isomer. Because of the differing *trans* influence of phenyl and pyridyl ligands, the *mer* and *fac* isomers exhibit slightly different structural properties: in a *fac* isomer the Ir – C and Ir – N bonds have nearly identical length; for the corresponding *mer* isomer, the bonds *trans* to the Ir – C bond are slightly longer than those *trans* to the Ir – N bonds [28, 29]. A practical consequence is that *fac* and *mer* isomers may show different electrochemical and spectroscopic properties [28, 30].

As early as 1991, the first extended series of *fac*-tris-cyclometalated complexes was reported by Watts and coworkers [24]. Table 2 collects photophysical and electrochemical results for these complexes [24, 31].

The ligands are 2-phenylpyridines with *S*-phenyl-substituted moieties. *S* ranges from electron releasing to electron withdrawing groups. These strongly affect the σ -donation at the C – Ir bond, leading to perturbation of the energy levels as schematized in Fig. 3b. The *S* substituents exert polar and mesomeric effects, whose intensity is related to the values of the Hammett substituent constants for *para* and *meta* substitution, σ_p and σ_m , respectively [31]. Positive and negative values of σ_p and σ_m for the employed

Table 2 Spectroscopic and electrochemical properties of *fac*-tris-cyclometalated Ir(III) complexes^a

	λ_{em}^b nm	τ^c μ s	$Ir^{IV/III,d}$ V	$E^{00,e}$ eV	σ_m^f	σ_p^f
$Ir(ppy)_3$	494	1.9	+ 0.77	2.51		
$Ir(5' - MeO - ppy)_3$	539	2.86	+ 0.55	2.30	+ 0.12	- 0.27
$Ir(4' - t - Bu - ppy)_3$	497	1.97	+ 0.66	2.50	- 0.10	- 0.20
$Ir(4' - Pr - ppy)_3$	496	1.93	+ 0.67	2.50	- 0.07	- 0.15
$Ir(4' - Me - ppy)_3$	493	1.94	+ 0.70	2.51	- 0.07	- 0.17
$Ir(4' - MeO - ppy)_3$	481	2.24	+ 0.75	2.58	+ 0.12	- 0.27
$Ir(4' - F - ppy)_3$	468	2.04	+ 0.97	2.65	+ 0.34	+ 0.06
$Ir(4' - F_3C - ppy)_3$	494	2.16	+ 1.08	2.51	+ 0.43	+ 0.54

^a From [24]; the substituent positions are indicated as in the original work

^b λ_{em} from measurements at 77 K in alcoholic glass

^c τ in Oxygen-free AN, room temperature

^d Potentials vs. SCE (internal reference $Fc^+/Fc = + 0.41$ V vs. SCE)

^e Energy of the emitting excited state

^f Hammett substitution constants for groups in *meta* and *para* positions [31] (with respect to the position of the C – Ir bond; of course, the effect by the pyridyl moiety should also be taken into account)

substituents, also listed in Table 2, indicate electron withdrawing and releasing effects, respectively. Thus, with respect to the potential for the unsubstituted *fac*- $Ir(ppy)_3$ complex ($Ir^{IV/III} = + 0.77$ V) and because of the influence on the σ -donation at the C – Ir bond, the electron-withdrawing groups (positive values or the σ constants) raise the metal centered oxidation of the concerned complex; the reverse happens for the electron-donating groups. For instance, for $S = F$ or CF_3 , the electron withdrawing effect transmitted via the σ -bonds, looks quite consistent, with a substantial increase of the oxidation potential, + 0.97 and + 1.08 V, respectively, vs. + 0.77 V for the bare *fac*- $Ir(ppy)_3$, Table 2. This is expected to affect the energy of the emitting level, E^{00} , consistent with its MLCT nature [32, 33].

3.1

Interplay of Emissive Excited States

For the reference case of *fac*- $Ir(ppy)_3$ (hereafter denoted simply $Ir(ppy)_3$), the lowest-energy absorption is of ¹MLCT nature and likewise the emission level is recognized to be of ³MLCT nature [1, 6, 8, 20–22, 24, 25], Fig. 3c. According to a simple description, this implies electron promotion of one *d* electron from the HOMO orbital located at the metal center to an empty π^* orbital, the ligand LUMO, mostly centered at the pyridine ring [34]. (Actually, the phenyl ring of *ppy* carries a negative charge and also the ligand localized HOMO

orbital is likely to contribute to the molecular HOMO). Higher-lying excited levels of ^3LC nature are also present, and evidence from several studies (vide infra) indicates that for several complexes derived from $\text{Ir}(\text{ppy})_3$, the energy separation of $^3\text{MLCT}$ and ^3LC levels might not be large—this is qualitatively depicted in Fig. 3c. In fact, we shall see that for some cyclometalated complexes discussed here, a reversal of the $^3\text{MLCT}$ - ^3LC energy ordering occurs. Owing to a small energy separation between these levels, the observed luminescence quantum yield of any complex of the $\text{Ir}(\text{III})$ -cyclometalated family, is best described as an admixture of luminescence efficiencies pertaining to $^3\text{MLCT}$ and ^3LC levels [35, 36],

$$\phi = a\phi(\text{CT}) + (1 - a)\phi(\text{LC}) \quad (1)$$

with a predominant $^3\text{MLCT}$ nature for $\text{Ir}(\text{ppy})_3$, $a \sim 1$. An assessment of the $^3\text{MLCT}$ or ^3LC nature of the phosphorescence is afforded by the photophysical properties, based on the following equation,

$$\phi = \frac{k_r}{k_r + k_{nr}} \quad (2)$$

where k_r and k_{nr} are the radiative and non-radiative rate constants, respectively, for deactivation of the emitting level, with $\tau = (k_r + k_{nr})^{-1}$. In the absence of non-radiative contributions, as happens at low temperature (77 K or lower [15]), one deals with the radiative lifetime, $\tau_r = 1/k_r$.

The interesting points for complexes of bidentate cyclometalating ligands are that:

- (i) for a typical $^3\text{MLCT}$ emission like that of $\text{Ir}(\text{ppy})_3$, $k_r \sim 2 \times 10^5 \text{ s}^{-1}$ ($\tau_r \sim 5 \mu\text{s}$), and,
- (ii) for a typical ^3LC emission, a much smaller k_r is found.

Regarding the latter issue, it has to be noticed that for the phosphorescence decay of isolated ligands, the values for τ_r may be in the ms to sec time range or longer [16]. For the complexes, the heavy atom effect may cause singlet-triplet mixing to an extent that a formal ^3LC level exhibits τ_r as short as tenths of μs [1]. Consistent with this, we shall see later that radiative lifetimes for ^3LC emitters of the $\text{Ir}(\text{III})$ -polyimine family are $\tau_r \sim 50 \mu\text{s}$ or larger ($k_r \sim 0.2 \times 10^5 \text{ s}^{-1}$ or smaller, Eq. 2).

In summary, for the complexes of *bidentate* cyclometalating ligands we deal with, one can guess the $^3\text{MLCT}$ or ^3LC nature of the emission based on $k_r \sim 2$ or $0.2 \times 10^5 \text{ s}^{-1}$, respectively. Regarding the *terdentate* ligands (see below), k_r is usually (but not always) found to be smaller by one order of magnitude and the difference between MLCT and LC emitters is less defined. Of course, other ways for judging the $^3\text{MLCT}$ vs. ^3LC nature of the emissions are available [35]. These include (i) the profile of the luminescence spectrum, which is structured for ^3LC emissions, and broad and unstructured for $^3\text{MLCT}$ ones, (ii) the rigidochromic effect, based on the fact that CT levels undergo blue-shifting on passing from fluid to frozen polar solvent, while

^3LC levels are either unaffected or slightly red-shifted under the same conditions, and (iii) the validity for $^3\text{MLCT}$ emissions, of a linear relationship between emission levels and “redox” energies, $\Delta E_{1/2} = e(E_{\text{ox}} - E_{\text{red}})$ eV (e is the elementary charge), see the equation below [3],

$$h\nu_{\text{em}} = B + b\Delta E_{1/2} \quad (3)$$

wherein B includes several interaction terms for the ^3CT species [37] and b is ideally close to 1 unit. All these aspects have been largely treated for cases of other metal complexes, in particular for the extensively studied Ru(II)-polyimine derivatives [3].

3.2

Phosphorescence Tuning in Ir(III)-Cyclometalated Complexes for OLED Applications

Ir(III) complexes of cyclometalated ligands can be employed, among other uses, for obtaining electrogenerated chemiluminescence [38–40], as sensitizers in solar cells [41], for photoinduced hydrogen production [42], and notably as emissive dopants in organic light emitting devices, OLEDs [10–12, 43]. This is due to the remarkable excited-state properties exhibited by these species; as seen above, for the prototypical Ir(ppy)₃ $\phi = 0.38$ and $E^{00} = 2.5$ eV (corresponding to green emission), Table 1. In addition, regarding the use of Ir(III)-cyclometalated complexes as phosphorescent dopants in OLEDs, it has to be noticed that even if under electrical excitation both singlets and triplet excitons are formed, with ~ 25 and 75% statistics [11], full conversion of singlets to triplets occurs, owing to the heavy metal effect (as noted above, the spin-orbit coupling constant of the Ir center is rather high, $\zeta_{\text{Ir}} = 3909 \text{ cm}^{-1}$ [16]). Other remarkable advantages are related to the fact that neutral species are more amenable to OLED fabrication processes than charged ones, and are obviously not subject to displacement effects under electrical fields. Finally, as it occurs also for the large families of Os(II) and Ru(II) d^6 complexes displaying $^3\text{MLCT}$ phosphorescence [3, 4], the possibility of changing the emission energy (and the electrochemical behavior) [24], affords the fine tuning of color variance within the electrophosphorescent devices [44]. In this respect and with reference to Fig. 3, systematic and effective approaches have been followed toward Ir(III) phosphors, so as to move from the green (reference case of Ir(ppy)₃) to the yellow and red on one hand [35, 44], and to the blue and near UV on the other hand [45].

3.2.1

From Green to Yellow with Neutral Heteroleptic Complexes

Table 3 lists properties of the neutral $(\text{C}^{\wedge}\text{N})_2\text{Ir}(\text{LX})$ complexes reported by Thompson, Forrest and coworkers [46, 47]. Figure 5a and b shows the ligands; LX are the ancillary bidentate monoanionic ligands from acetyl acetone

Table 3 Photophysical and electrochemical properties for neutral (C[^]N)₂Ir(LX) complexes^a

C [^] N	LX	Absorption ^b $\lambda_{\text{abs}}^{\text{max}}$ nm	ϵ $10^3 \text{ M}^{-1} \text{ cm}^{-1}$	Emission ^c λ_{em} nm	ϕ	τ μs	$\tau^{77\text{K}}$ μs	k_r^d 10^5 s^{-1}	Potential ^e Ir ^{IV/III} V
tpy	acac	460	2.5	512	0.31	3.1	4.5	1.0	+0.86
ppy	acac	460	1.6	516	0.34	1.6	3.2 ^f	2.1	+0.91
op	acac	456	3.2	520	0.14	2.3		0.6	
bo	acac	462	4.0	525	0.25	1.1		2.3	
bt	pic	475	5.0	541	0.37	2.3	3.6	1.6	
bzq	acac	500	1.6	548	0.27	4.5	23.3	0.6	+0.90
dpo	acac	443	7.9	550	0.10	3.0		0.3	
bt	acac	493	2.5	557	0.26	1.8	4.4	1.4	+1.04
bt	sal	450	5.0	562	0.22	1.4	3.1	1.6	
thpy	acac	453	3.2	562	0.12	5.3		0.2	
C6	acac	472	64.0	585	0.60	14.0		0.4	
bon	acac	491	10.0	586	0.11	1.3		0.8	
btth	acac	478	7.9	593	0.21	3.6		0.6	
β bsn	acac	496	3.2	594	0.16	2.2		0.7	
pq	acac	553	4.0	597	0.10	2.0		0.5	
bsn	acac	506	7.9	606	0.22	1.8	2.5	1.2	+0.97
α bsn	acac	506	7.9	606	0.22	1.8		1.2	
btp	acac	495	5.0	612	0.21	5.8		0.4	

^a Complexes of ligands depicted in Fig. 5, from [46, 47], in 2-MeTHF solvent unless otherwise indicated^b Lowest-energy absorption maximum with $\epsilon > 1500 \text{ M}^{-1} \text{ cm}^{-1}$ ^c Oxygen-free solvent^d Radiative rate constant, $k_r = \phi/\tau$ (from r.t. data)^e In CH₂Cl₂, potentials vs. SCE (adapted from [46], according to $V_{\text{SCE}} = V_{\text{Ag}/\text{AgCl}} + 0.04 \text{ V}$)

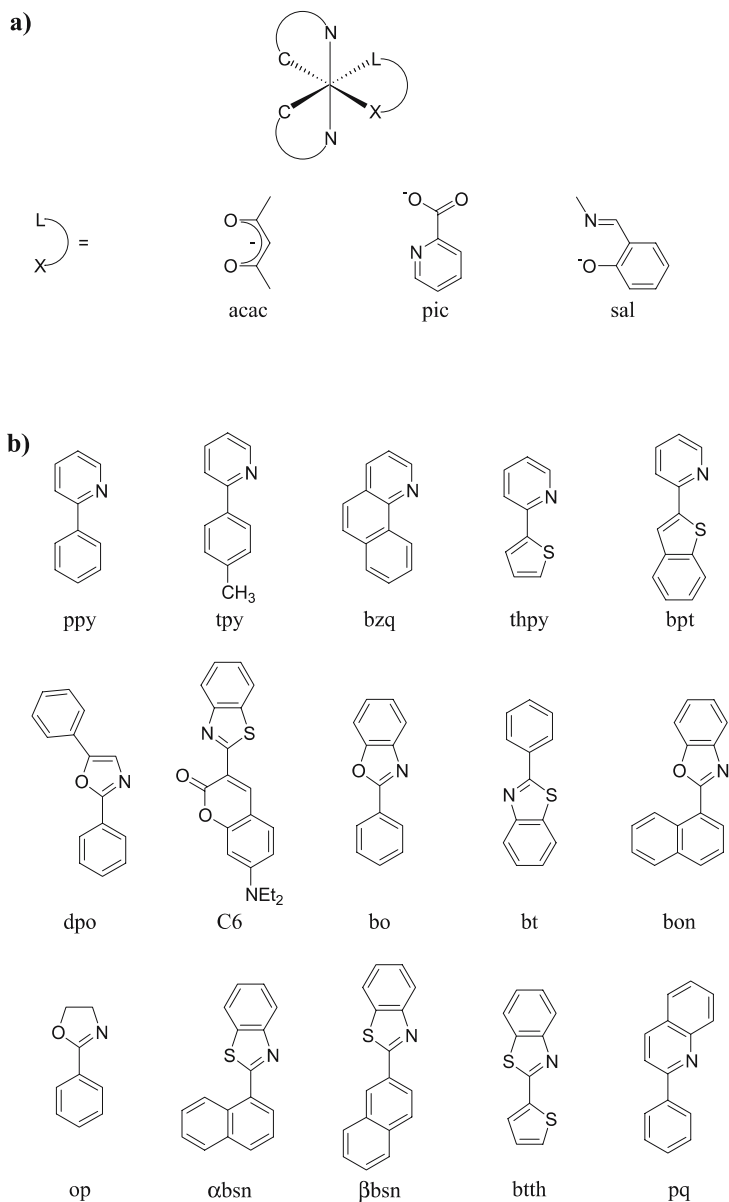


Fig. 5 **a** (XL) ligands of neutral $(C^N)_2Ir(LX)$ complexes of Table 3; **b** (C^N) ligands of the neutral $(C^N)_2Ir(LX)$ complexes of Table 3

(acacH), picolinic acid (picH), and *N*-methyl salicylimine (salH). For these complexes, the luminescence quantum yield ϕ is in the range 0.1–0.4. The emission peak changes in the range 512–612 nm, that allows color variation

from the green, for Ir(ppy)₃, to the yellow, for Ir(thpy)₃, and to the red (for complexes of Table 3 with an emission peak larger than 600 nm).

The color variation appears roughly related to the size of the ligand, i.e., a more extended electronic delocalization causes a lowering of the ligand-centered LUMO, in turn resulting in lower-lying levels both of ³MLCT and ³LC nature, Fig. 3c. For (ppy)₂Ir(acac), the emission is ascribable to ³MLCT character, with an evaluated radiative rate constant $k_r = 2.1 \times 10^5 \text{ s}^{-1}$. Along the series of Table 3, deviations in the k_r value might signal substantial ³LC contributions. For instance, for the case of (thpy)₂Ir(acac), $k_r = 0.2 \times 10^5 \text{ s}^{-1}$, the same value characterizing a genuine ³LC emitter like Pt(thpy)₂ [1, 48]. The only complex including a substituted aryl fragment is (tpy)₂Ir(acac), for which only a weak inductive and mesomeric effect is expected from the Me group, based on its small Hammett σ constants, Table 2; tpy is tolyl-pyridine.

3.2.2

From Green to Red with Neutral Homoleptic Complexes

Table 4 lists properties of the neutral homoleptic complexes with *facial* geometry, Ir(C[^]N)₃, whose ligands are illustrated in Fig. 6 [35].

The luminescence properties of this series of complexes reported by Tsuboyama and coworkers are similar to those of the (C[^]N)₂Ir(LX) complexes of Table 3, with the luminescence quantum yield ϕ being in the range 0.08–0.4. The emission peak changes are in the range 514–644 nm, which allows a wider color variation to the red side than for the complexes gathered in

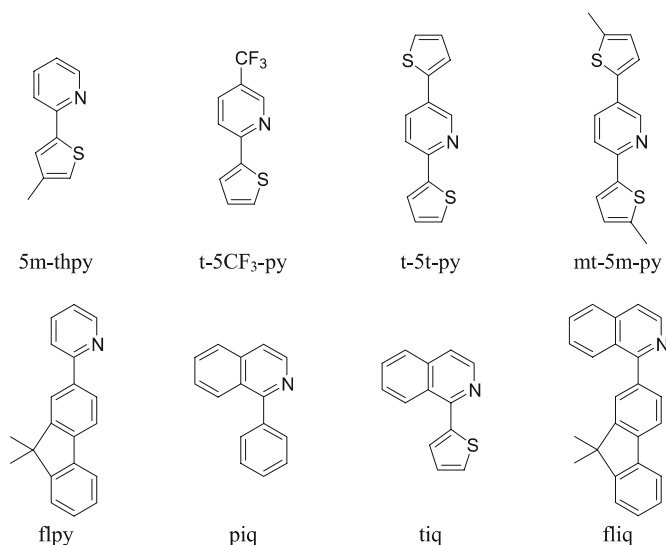


Fig. 6 (C[^]N) ligands of the neutral homoleptic Ir(C[^]N)₃ complexes of Table 4

Table 4 Photophysical properties for neutral homoleptic Ir(C[^]N)₃ complexes^a

C [^] N	Absorption ^b		Emission ^c		77 K			
	$\lambda_{\text{abs}}^{\text{max}}$ nm	ϵ 10 ³ M ⁻¹ cm ⁻¹	λ_{em} nm	ϕ	τ μs	k_r^d 10 ⁷ s ⁻¹	λ_{em} nm	τ μs
ppy			514	0.40	2.0	2.0	498	6.5
flpy	413	4.0	545	0.29	1.2	2.5	537	4.0
thpy			550	0.17	2.4	0.7	545	8.2
fliq	570	6.3	552	0.19	0.74	2.6	635	2.1
5m-thpy	460	10.0	558	0.08	0.99	0.8	533	10.2
t-5CF ₃ -py	472	10.0	563	0.19	1.1	1.7	557	6.5
btp	472	7.90	596	0.12	4.0	0.3	586	11.2
t-5t-py	472	12.6	613	0.12	4.6	0.3	605	19.2
piq	550	2.0	620	0.26	0.74	3.6	603	2.1
mt-5mt-py	482	12.6	627	0.08	4.7	0.2	620	10.8
tiq	472	6.3	644	0.17	0.74	2.3	638	3.5

^a Complexes of ligands depicted in Fig. 6, from [35] (thpy and btp are in Fig. 5).^b Toluene solvent at room temperature; toluene/ethanol/methanol mixture (5 : 4 : 1) at 77 K^c Lowest-energy absorption maximum with $\epsilon > 1500 \text{ M}^{-1} \text{ cm}^{-1}$ ^d Oxygen-free solvent^e Radiative rate constant, $k_r = \phi/\tau$ (from r.t. data)

Table 3. With reference to Eq. 1, comparison of results for the luminescence measurements at 77 K and room temperature (r.t.) allows some assessment of the predominant nature of the emission. Thus, the extent of the rigidochromic effect, i.e., the blue shifting of the emission peak on going from fluid to the frozen solvent, can be used to probe the CT nature of the emission [35]. For instance, the rigidochromic effect is relevant for Ir(ppy)₃, and a minor one for Ir(btp)₃. This is consistent with the evaluated k_r values, Table 4, that are 2×10^5 and $0.3 \times 10^5 \text{ s}^{-1}$, respectively, for the two complexes.

3.2.3

Systematic Tuning Approaches Leading to Blue Emission

As seen above, the approaches to Ir(III) complexes playing as luminescent dopants in the green-yellow-red range are mainly based on the manipulation/extension of the pyridine-like fragment of a cyclometalating ligand. Useful approaches to Ir(III)-based blue emission are less obvious and have been grouped as (a), (b), and (c) strategies by Thompson, Forrest and coworkers [45] and are conveniently commented here with reference to Fig. 3.

(a) Use of electron-withdrawing substituents (S [24], Fig. 3b) at the cyclometalating ring, for instance fluoride [28, 49, 50]. This has the effect of stabilizing the HOMO level (both from the metal and ligand orbitals) while only slightly affecting the ligand LUMO level. As a consequence, both the MLCT and LC transitions move to higher energy. Table 5 gathers examples of this approach for homoleptic complexes [28, 49, 50]. It may be noted that the blue shifting trend of the emission is accompanied by larger and larger Ir^{IV/III} potentials and that $k_r \sim 2 \times 10^5 \text{ s}^{-1}$, cases of Ir(3',4',5',6'-F₄-ppy)₃ and Ir(3',4',6'-F₃-ppy)₃ [50], consistent with a ³MLCT nature of the emission.

(b) Use of ancillary ligands (LL) to tune the HOMO energies of Ir(ppy)₂(LL) complexes, with the emission coming from the Ir(ppy) fragments [36, 50]; basically, an approach based on the electron perturbation of the HOMO-LUMO energy gap, as for case (a) above. Also in this case, the major effect manifests in the Ir^{IV/III} potentials. Table 6 lists representative cases; the ligands employed are shown in Fig. 7 [36, 50].

For some complexes, the drawn k_r value is very low. For instance, for LL = diphosphine chelate (dppe, Fig. 7), $k_r = 0.03 \times 10^5 \text{ s}^{-1}$, suggesting a ³LC emission. Consistent with this attribution, $\tau = 32.3 \mu\text{s}$ at 77 K, with only a small rigidochromic effect being observed [36]. For the cases of Table 6, a plot of the emission (peak) energy vs. the redox energy, $\Delta E_{1/2}$, Eq. 3, shows a satisfactory alignment, including cases of likely ³LC emitters, (tpy)₂Ir(PPh₂CH₂)₂BPh₂ and (tpy)₂Ir(dppe)(CF₃SO₃), Fig. 8 [36]. This might be taken as an indication that ³MLCT and ³LC levels are very close-lying.

(c) Replacement of the heterocyclic fragment of the (C[^]N) ligand with moieties bearing higher lying LUMO than for the pyridyl ring [28, 45, 51–56].

Table 5 Photophysical properties of Ir(III)-cyclometalated complexes for use as OLED phosphors^a. Neutral homoleptic Ir(C^N)₃ complexes

	Absorption ^b		Emission ^c		ϕ	τ μs	k_r^d 10^5 s^{-1}	Electrochemistry ^e		Refs.
	$\lambda_{\text{abs}}^{\text{max}}$ nm	ϵ $10^3 \text{ M}^{-1} \text{ cm}^{-1}$	λ_{em} nm	ϕ				Ir ^{IV/III} V	Ir ^{III/II} (L ^{0/-1}) V	
Ir(ppy) ₃			522					+ 0.83	- 2.20	[49]
Ir(5' - CF ₃ - ppy) ₃			517					+ 1.19	- 1.99	[49]
Ir(4' - F - ppy) ₃			514					+ 1.05	- 2.17	[49]
Ir(6' - F - ppy) ₃			506					+ 1.03	- 2.07	[49]
Ir(4', 6' - F ₂ - ppy) ₃	427	1.6	468			1.6		+ 1.29	- 2.0	[28]
Ir(3', 4', 5', 6' - F ₄ - ppy) ₃			468		0.53	2.3	2.3	+ 1.54	- 1.94	[50]
Ir(3', 4', 6' - F ₃ - ppy) ₃			459		0.30	1.6	1.9			[50]

^a Solvents indicated in the original works^b Lowest-energy absorption maximum with $\epsilon > 1500 \text{ M}^{-1} \text{ cm}^{-1}$ ^c Oxygen-free solvent^d Radiative rate constant, $k_r = \phi/\tau$ (from r.t. data)^e Potentials vs. SCE (when adapted from the original works, $V_{\text{SCE}} = V_{\text{Fc}^+/\text{Fc}} + 0.41 \text{ V}$ for AN solvent, $V_{\text{SCE}} = V_{\text{Fc}^+/\text{Fc}} + 0.51 \text{ V}$ for CH₂Cl₂ and DMF solvents)

Table 6 Photophysical properties of Ir(III)-cyclometalated complexes for use as OLED phosphors^a. (C[^]N)₂Ir(L-L) complexes; (LL) is an ancillary ligand

	Absorption ^b		Emission ^c		τ μs	k_r ^d 10^5 s^{-1}	Electrochemistry ^e		Refs.
	$\lambda_{\text{abs}}^{\text{max}}$ nm	ϵ $10^3 \text{ M}^{-1} \text{ cm}^{-1}$	λ_{em} nm	ϕ			Ir ^{IV/III} V	Ir ^{III/II} (L ^{0/-1}) V	
(tpy) ₂ Ir(acac)	451	2.8	512	0.38	1.4	2.7	+ 0.92	- 2.17	[36]
(tpy) ₂ Ir(pz) ₂ H	392	4.8	490	0.44	2.2	2.0	+ 1.06	- 2.14	[36]
(tpy) ₂ Ir(pz) ₂ BEt ₂	390	5.1	484	0.52	2.6	2.0	+ 1.14	- 2.15	[36]
(tpy) ₂ Ir(pz) ₂ Bpz ₂	383	5.1	480	0.52	3.5	1.5	+ 1.23	- 2.13	[36]
(3', 4', 5', 6' - F ₄ - ppy) ₂ Ir(acac)			479	0.31	1.8	1.7	+ 1.35	- 1.96	[50]
((tpy) ₂ Ir(pz) ₃ CH)(CF ₃ SO ₃)	377	4.9	476	0.33	3.0	1.1	+ 1.40	- 1.92	[36]
(tpy) ₂ Ir(PPh ₂ CH ₂) ₂ BPh ₂	370	4.5	468	0.038	4.7	0.08	+ 1.32	- 2.11	[36]
(3', 4', 6' - F ₃) ₂ Ir(acac)			465	0.15	0.68	2.2	+ 1.39	- 1.99	[50]
(tpy) ₂ Ir(dppe)(CF ₃ SO ₃)	358	5.7	458	0.005	2.1	0.03	+ 1.44	- 2.05	[36]

^a Solvents indicated in the original works^b Lowest-energy absorption maximum with $\epsilon > 1500 \text{ M}^{-1} \text{ cm}^{-1}$ ^c Oxygen-free solvent^d Radiative rate constant, $k_r = \phi/\tau$ (from r.t. data)^e Potentials vs. SCE (when adapted from the original works, $V_{\text{SCE}} = V_{\text{Fc}^+/\text{Fc}} + 0.41 \text{ V}$ for AN solvent, $V_{\text{SCE}} = V_{\text{Fc}^+/\text{Fc}} + 0.51 \text{ V}$ for CH₂Cl₂ and DMF solvents)

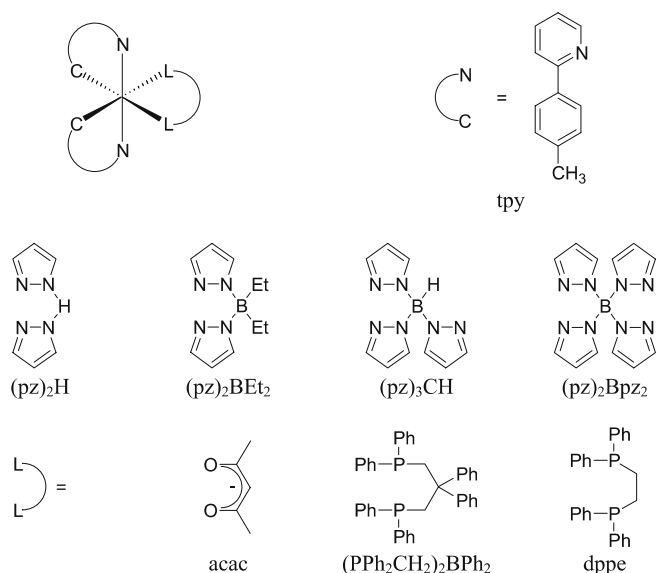


Fig. 7 Ligands of complexes of Table 6

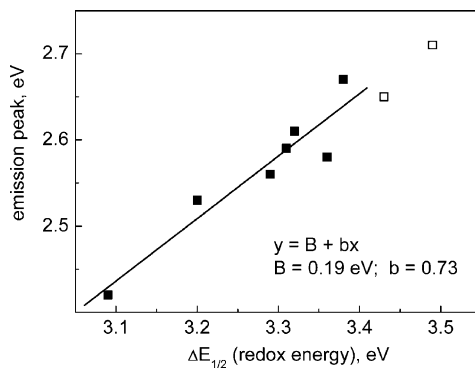


Fig. 8 Correlation between redox and emission energies, Eq. 3, for the series of Table 6. Empty points are for the ³LC emitters (tpy)₂Ir(PPh₂CH₂)₂BPh₂ and (tpy)₂Ir(dppe) (CF₃SO₃) [36]

These can be either *N*-pyrazolyl, triazolyl, or *N*-heterocyclic carbene-based moieties, Fig. 9, and the effect is to raise the energy of both MLCT and LC transitions.

Examples are listed in Table 7 [28, 45, 51, 52, 54, 56]. It is to be noted that in some cases reported in this Table, the luminescence quantum yield is smaller by ca. two orders of magnitude than for the reference Ir(ppy)₃ complex. For instance, for Ir(pmb)₃, $\phi = 0.04$, even if this complex is likely a ³MLCT emitter (the evaluated $k_r = 1.8 \times 10^5 \text{ s}^{-1}$). A possible explanation for this outcome is related to the fact that the emission level for Ir(pmb)₃ is rather high in energy,

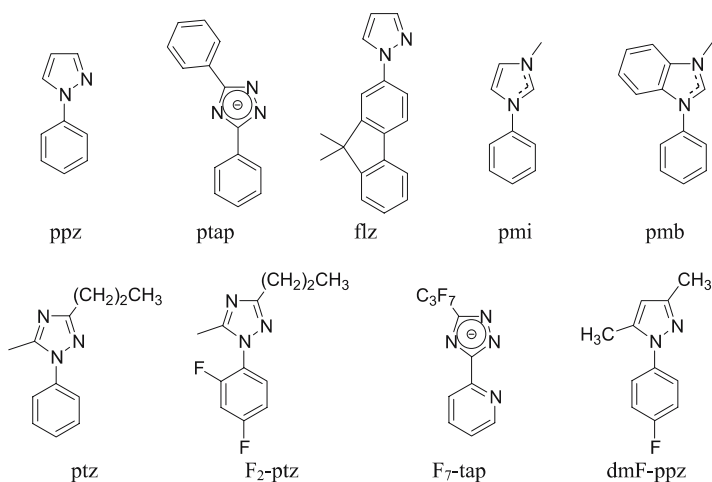


Fig. 9 Ligands of complexes of Table 7

$\lambda_{\text{em}} \sim 380$ nm (Table 7) [45]. With reference to Fig. 3c, it is possible that this results in a small ${}^3\text{MLCT} - {}^3\text{MC}$ energy gap, ΔE , despite the fact that the energy of the ${}^3\text{MC}$ level is predicted to be very high for the $5d^6$ Ir(III) complexes, as for the analogous $5d^6$ Os(II)-polyimine complexes [4]. We shall discuss the role of ${}^3\text{MC}$ levels in a subsequent section.

3.2.4

Cationic Ir(III)-Cyclometalated Complexes

Table 8 lists spectroscopic and electrochemical properties for two series of ionic Ir(III) complexes [57, 58]. In one case one deals with monoanionic species, $\text{TBA}[\text{Ir}(\text{ppy})_2\text{L}_2]$, with ancillary ligands $\text{L} = \text{CN}^-$, NCS^- , and NCO^- , Fig. 10 [57].

The ancillary ligands modulate the oxidation and reduction potentials as a consequence of their different ligand strength and electron-withdrawal capability toward the metal d orbitals, see Fig. 3. The overall effect goes along the sequence $\text{CN}^- > \text{NCS}^- > \text{NCO}^-$, i.e., the highest first oxidation and easiest first reduction, +1.42 and -1.19 V vs. SCE, respectively, are observed for $\text{Ir}(\text{ppy})_2(\text{CN})_2^-$. Accordingly, $\text{Ir}(\text{ppy})_2(\text{CN})_2^-$ results in a blue emitter, $\lambda_{\text{em}} = 470$ nm.

A more sophisticated tuning strategy leads to the sequence of the cationic complexes $\text{Ir}(\text{ppz} - \text{X})_2(\text{N}^{\wedge}\text{N})^+$, with $(\text{N}^{\wedge}\text{N})$ being a neutral diimine ligand, i.e., bpy, functionalized bpy, and 2,2'-biquinoline [58], Fig. 10. For this series, the energy levels of both diimine-based LUMO and HOMO are affected, resulting in wide variation of emission wavelength, from 625 nm to 493 nm, Table 8. Remarkably, according to DFT calculations, the HOMO level is de-

Table 7 Photophysical properties of Ir(III)-cyclometalated complexes for use as OLED phosphors^a. Neutral Ir(III) complexes with phenylpyrazolyl, phenyl-triazolyl, or *N*-carbene ligands

	Absorption ^b		Emission ^c		τ μs	k_r^d 10^5 s^{-1}	Electrochemistry ^e		Refs.
	$\lambda_{\text{abs}}^{\text{max}}$ nm	ε $10^3 \text{ M}^{-1} \text{ cm}^{-1}$	λ_{em} nm	ϕ			Ir ^{IV/III} V	Ir ^{III/II} (L ^{0/-1}) V	
Ir(4',6' - (CF ₃) ₂ - ppy) ₂ (ptap)			511	0.39	3.0	1.38	+ 1.51	- 2.03	[52]
Ir(ppy) ₂ (ppz)	403	5.2	504	0.72	1.45	5.0	+ 0.84	- 2.22	[51]
Ir(4',6' - F ₂ - ppy)(ppz) ₂	390	3.3	504	0.27	0.76	3.6	+ 1.02	- 2.15	[51]
Ir(ppy)(ppz) ₂	401	3.2	498	0.68	1.62	4.2	+ 0.87	- 2.23	[51]
Ir(ppy) ₂ (ptap)			489	0.45	1.9	2.4	+ 1.05	- 2.12	[52]
Ir(3',5' - F ₂ - ppy) ₂ (ptap)			484	0.38	2.4	1.6	+ 1.25	- 2.11	[52]
Ir(dmF - ppz) ₂ (F ₇ - tap)	353		469	0.008	0.005	14.7	+ 1.29	- 2.74(irr)	[54]
Ir(3',5' - (CF ₃) ₂ - ppy) ₂ (ptap)			466	0.30	3.7	0.8	+ 1.57	- 1.94	[52]
Ir(4',6' - F ₂ - ppy) ₂ (ppz)	380	6.6	465	0.50	1.13	4.4	+ 1.29	- 2.01	[51]
Ir(4',6' - F ₂ - ppy) ₂ (ptap)			461	0.27	1.4	1.9	+ 1.40	- 2.06	[52]
Ir(ptz) ₃			449	0.66	1.08	6.0	+ 0.85		[56]
Ir(4',6' - F ₂ - ptz) ₃			425	0.03	0.15	2.0	+ 1.29		[56]
Ir(ppz) ₃			414 ^f				+ 0.90		[45]
Ir(pmi) ₃			~ 380	0.02	0.40	0.5			[45]
Ir(pmb) ₃			~ 380	0.04	0.22	1.8			[45]
Ir(flz) ₃				0.38	37	0.1			[45]
Ir(4' - CF ₃ - ppz) ₃					0.05		+ 1.24		[28]
Ir(4',6' - F ₂ - ppz) ₃					0.05		+ 1.31		[28]

^a Solvents indicated in the original works^b Lowest-energy absorption maximum with $\varepsilon > 1500 \text{ M}^{-1} \text{ cm}^{-1}$ ^c Oxygen-free solvent^d Radiative rate constant, $k_r = \phi/\tau$ (from r.t. data)^e Potentials vs. SCE (when adapted from the original works, $V_{\text{SCE}} = V_{\text{Fc}^+/\text{Fc}} + 0.41 \text{ V}$ for AN solvent, $V_{\text{SCE}} = V_{\text{Fc}^+/\text{Fc}} + 0.51 \text{ V}$ for CH₂Cl₂ and DMF solvents)^f At 77 K

Table 8 Photophysical properties of charged Ir(III)-cyclometalated complexes^a

Absorption ^b		Emission ^c		Electrochemistry ^e		Refs.	
$\lambda_{\text{abs}}^{\text{max}}$ nm	ϵ $10^3 \text{ M}^{-1} \text{ cm}^{-1}$	λ_{em} nm	ϕ	τ μs	k_r^{d} 10^5 s^{-1}	Oxidation Ir ^{IV/III} V	Reduction Ir ^{III/II} ($\text{L}^{0/-1}$) V
Ir(ppy) ₂ L ₂ ⁻ complexes ^f							
Ir(ppy) ₂ (NCO) ₂ ⁻	2.36	538	0.99 ^g	0.85		+ 0.69	- 1.56
Ir(ppy) ₂ (NCS) ₂ ⁻	2.3	506	0.97 ^g	1.43		+ 0.96	- 1.44
Ir(ppy) ₂ (CN) ₂ ⁻		470	0.94 ^g	3.14		+ 1.42	- 1.19
Ir(ppz-X) ₂ (N [^] N) ⁺ complexes ^h							
Ir(ppz) ₂ (bpy-CO ₂ Et) ⁺	5.7	625	0.0012	0.10	0.1	+ 1.38	- 1.01
Ir(ppz-TB) ₂ (biq) ⁺	1.6	624	0.0068	0.56	0.1	+ 1.42	- 1.03
Ir(ppz-OMe) ₂ (bpy-TB) ⁺	8.5	615	0.0007	0.031	0.2	+ 1.03	- 1.49
Ir(ppz) ₂ (biq) ⁺	1.7	614	0.017	0.86	0.2	+ 1.45	- 0.95
Ir(ppz-Ph) ₂ (bpy-TB) ⁺	37.0	570	0.010	0.32	0.3	+ 1.25	- 1.47
Ir(ppz) ₂ (bpy) ⁺	9.7	565	0.17	0.48	3.5	+ 1.36	- 1.39
Ir(ppz) ₂ (bpy-TB) ⁺	8.9	550	0.076	0.72	1.1	+ 1.36	- 1.48
Ir(ppz) ₂ (bpy-OCH ₃) ⁺	9.2	550	0.032	0.53	0.6	+ 1.40	- 1.49
Ir(ppz-F ₂) ₂ (bpy-TB) ⁺	16.8	493	0.40	1.34	3.0	+ 1.66	- 1.42

^a Solvents indicated below^b Lowest-energy absorption maximum with $\epsilon > 1500 \text{ M}^{-1} \text{ cm}^{-1}$ ^c Oxygen-free solvent^d Radiative rate constant, $k_r = \phi/\tau$ (from r.t. data)^e Potentials vs. SCE (when adapted from the original works, $V_{\text{SCE}} = V_{\text{Fc}^+/\text{Fc}} + 0.41 \text{ V}$ for AN solvent, $V_{\text{SCE}} = V_{\text{Fc}^+/\text{Fc}} + 0.51 \text{ V}$ for CH_2Cl_2)^f In CH_2Cl_2 ^g Evaluated as explained in [57]^h Absorption spectra and electrochemical properties measured in AN, emission properties measured in 2-MeTHF [58]

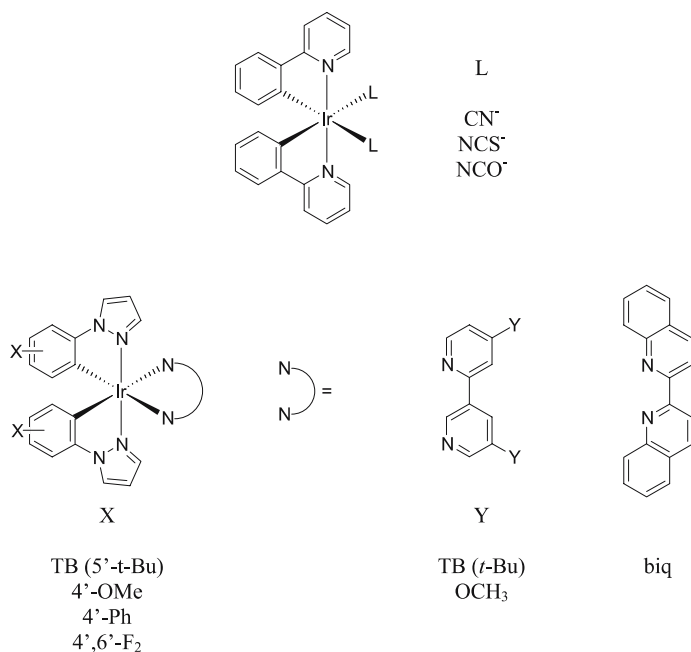


Fig. 10 Mono-anionic [57] and mono-cationic [58] complexes of Table 8

scribable as metal- and ppz-centered, which gives rise to ML→diimine CT transitions (MLLCT). Inspection of the redox properties reveals details of the approach followed for emission tuning. For instance, the reduction potential is -0.95 V and -1.39 V vs. SCE for $\text{Ir}(\text{ppz})_2(\text{biq})^+$ and $\text{Ir}(\text{ppz})_2(\text{bpy})^+$, respec-

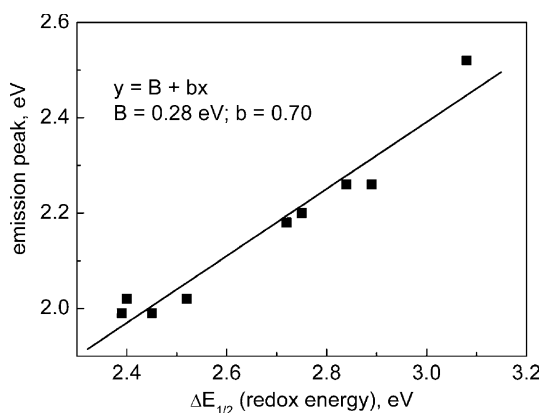


Fig. 11 Correlation between redox and emission energies, Eq. 3, for the series of cationic complexes of Table 8

tively, a consequence of the more extended conjugation of biq with respect to bpy. On the other hand, the oxidation potential is +1.36 V and +1.66 V vs. SCE for Ir(ppz)₂(bpy-TB)⁺ and Ir(ppz-F₂)₂(bpy-TB)⁺, respectively, owing to the already encountered influence of fluoride groups on the HOMO orbitals. A good relationship holds between the emission and the redox energies, Eq. 3, as illustrated by the plot of Fig. 11, pointing to a MLLCT nature of the emitting levels.

It can be noted that the k_r values for this series are in most cases one order of magnitude smaller than those typical of cyclometalated MLCT emitters, see Tables 5, 6 and 7 for instance. Some of these cationic Ir(ppz-X)₂(N[^]N)⁺ complexes were employed as phosphors in light-emitting electrochemical cells [58].

3.3

Ir(III) Complexes for Oxygen Sensing

Inspection of Tables 2 to 8 reveals that Ir(III) cyclometalated species are highly luminescent in oxygen-free solvent, with luminescence quantum yields as high as $\phi \sim 0.5$ and more [59–61], and lifetimes in the range of a few μ s. In air-equilibrated solvent, a remarkable quenching effect is registered, leading to a strong reduction in luminescence features with respect to degassed solutions—quenched ϕ_q and τ_q values can be as much as 60 times smaller than unquenched ϕ and τ ones [59]. This effect can therefore be conveniently exploited for oxygen-sensing devices [62, 63]. It is interesting to examine the type of mechanism involved in such luminescence quenching. This can be done in accord with the Stern–Volmer Eq. 4 [64] and with reference to the kinetic scheme of Eq. 5, wherein Q and ^{*}T denote dioxygen and the Ir(III)-based phosphorescence, respectively.

$$\frac{\tau}{\tau_q} = \frac{\phi}{\phi_q} = 1 + k_q \tau [\text{O}_2] \quad (4)$$



$$k_q = \frac{k_{diff} k_{de}}{k_{-diff} + k_{de}} \quad (6)$$

In the above equations, ^{*}T – Q is the collision associate, k_{diff} and k_{-diff} are the rate constants for formation and break up of the collision associate, and k_{de} is the rate constant for product formation from the associate [16]. Drawn values for k_q for some Ir(III) complexes are collected in Table 9 [21, 25, 59, 65–67].

Remarkably, for the Δ and λ isomers of *fac*-Ir(pppy)₃, $k_q = 2.6 \times 10^{10} \text{ M}^{-1} \text{ s}^{-1}$; pppy in Fig. 12 [59]. This is a value practically coincident with the diffusion constant for AN, $k_{diff} \approx 2.0 \times 10^{10} \text{ M}^{-1} \text{ s}^{-1}$ [16], which suggests that $k_{de} \gg k_{-diff}$, $k_q \sim k_{diff}$, Eq. 6. This appears to be among the highest values ever

Table 9 Rate constants for oxygen quenching of the luminescence.

	k_q^a $M^{-1} s^{-1}$	k_{diff}^b $M^{-1} s^{-1}$ (solvent)	ϕ_Δ^c	E_{ox} , V vs. SCE	Refs.
$Ir(\alpha - bsn)_2(acac)$	2.9×10^9	1.1×10^{10}	0.60	+ 0.97 ^d	[67]
$Ir(bt)_2(acac)$	5.9×10^9	(C ₆ H ₆)	0.86	+ 1.04 ^d	[67]
$Ir(pq)_2(acac)$	7.2×10^9		0.62		[67]
$\Delta/\lambda\text{-fac-Ir(pppy)}$	2.6×10^{10}	2.0×10^{10}		+ 0.54 ^e ± 0.3	[59]
$Ir(terpy)_2^{3+}$	$1\text{--}6 \times 10^8$	(AN)		>+ 2.4	[25, 65]
$Ir(bpy)_3^{3+}$	3.4×10^8	1.2×10^{10}	~ 1	+ 2.1 ^f	[21, 66]
$Ir(phen)_2^{3+}$	2.8×10^8	(CH ₃ OH)	~ 1		[66]

^a According to Eq. 4 of text

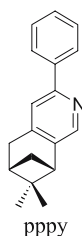
^b Diffusion controlled rate constant at 25 °C, from [16]

^c Quantum yield of sensitized singlet dioxygen (¹O₂) emission

^d In CH₂Cl₂, potentials vs. SCE (adapted from [46], according to $V_{SCE} = V_{Ag/AgCl} + 0.04 \text{ V}$)

^e In AN vs. SCE [59]

^f AN solvent

**Fig. 12** Schematic structure

reported for the luminescence quenching in transition complexes by dioxygen. For comparison purposes, k_q is ca. $2 \times 10^9 \text{ M}^{-1} \text{ s}^{-1}$ for both $Ru(bpy)_3^{2+}$ and $Os(bpy)_3^{2+}$, respectively [59], in the range $0.9\text{--}6 \times 10^8 \text{ M}^{-1} \text{ s}^{-1}$ for $Ir(terpy)_2^{3+}$ and derivatives [25, 65], and in the range $2\text{--}9 \times 10^9 \text{ M}^{-1} \text{ s}^{-1}$ for some Ir(III)-cyclometalated terdentate complexes [61] (all results in AN). This agrees well with most cases of oxygen quenching for several metal complexes [66, 68], where k_q was found to be significantly lower than k_{diff} , and where energy transfer was the predominant mechanism associated with k_{de} , Eq. 5. For the $Ir(C^{\wedge}N)_2(acac)$ cases listed in Table 9, the occurrence of energy transfer, taking place with efficiencies $\phi_\Delta > 0.6$ in C₆H₆ solvent, is demonstrated by the observed sensitization of the ¹O₂ luminescence (the two available excited states of the oxygen species are located at 1.6 and

1.0 eV [69]). Thus, when very high k_q values are observed, it seems possible that mechanisms based on charge transfer interactions might contribute to the overall quenching effect by dioxygen. To this occurrence, low values for the oxidation potential appear to be a determining factor in view of a favorable driving force toward formation of ion pairs (the reduction potential for oxygen is -0.78 vs. SCE [70]). By contrast, low k_q values and high efficiency of energy transfer are found when metal-centered oxidation is a difficult step, as in the cases of $\text{Ir}(\text{terpy})_2^{3+}$, $\text{Ir}(\text{bpy})_3^{3+}$, and $\text{Ir}(\text{phen})_2^{3+}$, Table 9.

3.4

Photophysics of $\text{Ir}(\text{ppy})_2(\text{LL})$ Complexes Covalently Linked to Substrates

The remarkable phosphorescence properties of Ir(III)-cyclometalated species (high luminescence quantum yield and long lifetimes, tunable emission peak), prove of use in several areas in addition to OLED application. We only mention here a few representative examples regarding the $\text{Ir}(\text{C}^{\wedge}\text{N})_2(\text{N}^{\wedge}\text{N})^+$ chromophores in (a)–(c) below. For these complexes as incorporated in suitable materials, the emission is expected of $\text{Ir} \rightarrow (\text{N}^{\wedge}\text{N})$ CT nature and the alteration of their luminescence features can be associated to other useful properties of the substrates.

(a) Along the series $\text{Ir}(\text{ppy})_2(\text{bpy})^+$, $\text{Ir}(\text{ppy})_2(\text{OAE1})^+$, and $\text{Ir}(\text{ppy})_2(\text{OAE2})^+$, Fig. 13 [71], one can see the effect of a large increase of the conjugation length of LL ($\text{N}^{\wedge}\text{N}$); the acronym OAE stands for conjugated oligo(arylene) ethynylene ligand. This example could be representative of what is expected upon grafting the $\text{Ir}(\text{ppy})_2^+$ unit to oligomeric fragments. Results are summarized in Table 10 [71] and the changes in k_r values suggest that on passing from LL = bpy to OAE1 and OAE2, there is a cross-over in the nature of the emission, from $^3\text{MLCT}$ to $^3\text{LC} (\pi\pi^*)$.

Interestingly, the luminescence quantum yield is reasonably constant along the series $\phi = 0.03 \pm 0.01$, an outcome ultimately ascribable to the high spin-orbit coupling of the metal center [71].

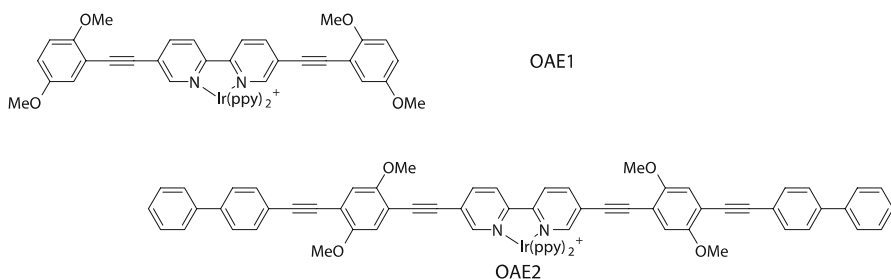


Fig. 13 Schematic structures

Table 10 Photophysical properties of selected Ir(pppy)₂(N[^]N)⁺ complexes^a

Absorption ^b		Emission ^c		Electrochemistry ^e		Refs.
$\lambda_{\text{abs}}^{\text{max}}$ nm	ϵ $10^3 \text{ M}^{-1} \text{ cm}^{-1}$	λ_{em} nm	ϕ	Ir ^{IV/III} V	Ir ^{III/II} ($\text{L}^{0/-1}$) V	
In THF Solvent ^a						
				k_{r}^{d} 10^5 s^{-1}	τ μs	
Complexes in AN solvent ^a ; derived bioconjugates in Oxygen-free 50 mM tris-Cl buffer at pH 7.4						
Ir(pppy) ₂ (bpy) ⁺	416	6.0	590	0.018	0.18	[71]
Ir(pppy) ₂ (OAE1) ⁺	406	31.6	620	0.036	0.44	[71]
Ir(pppy) ₂ (OAE2) ⁺	444	52.5	645	0.026	3.30	[71]
Ir(pppy) ₂ (bpy-NH ₂) ⁺	555	0.236	555	0.236	0.77	[79]
Ir(pppy) ₂ (bpy-ITC) ⁺	593	0.035	593	0.035	0.31	[79]
Ir(pppy) ₂ (bpy-ITC) ⁺ - HSA	558	0.150	558	0.150	2.7/0.53 ^f	[79]
Ir(pppy) ₂ (bpy-ITC) ⁺ - Av	560	0.043	560	0.043	0.8/0.15 ^f	[79]
Ir(pppy) ₂ (bpy-IAA) ⁺	582	0.022	582	0.022	0.30	[79]
Ir(pppy) ₂ (phen-NH ₂) ⁺	568	0.079	568	0.079	11.4	[79]
Ir(pppy) ₂ (phen-ITC) ⁺	608	0.079	608	0.079	0.41	[79]
Ir(pppy) ₂ (phen-ITC) ⁺ - HSA	563	0.071	563	0.071	1.0/0.18 ^f	[79]
Ir(pppy) ₂ (phen-ITC) ⁺ - Av	560	0.190	560	0.190	3.1/1.1 ^f	[79]
Ir(pppy) ₂ (phen-IAA) ⁺	590	0.228	590	0.228	0.59	[79]

^a Solvents as indicated within the Table^b Lowest-energy absorption maximum^c Oxygen-free solvent^d Radiative rate constant, $k_{\text{r}} = \phi/\tau$ ^e Potentials vs. SCE^f From dual exponential analysis [79]

* Denotes a quasi reversible or irreversible process

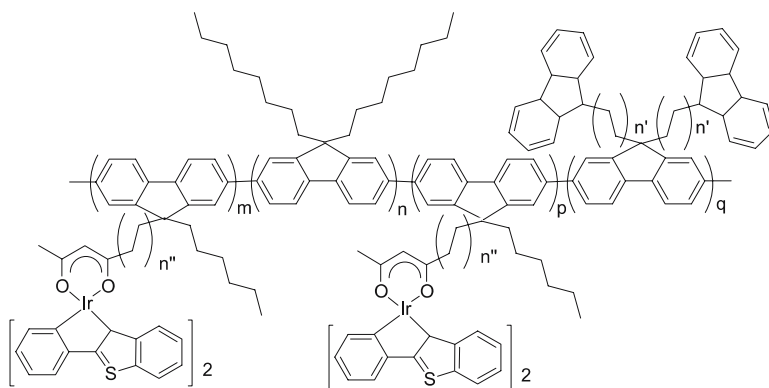


Fig. 14 Schematic structures

(b) Highly efficient electroluminescent (EL) polymers have been reported that incorporate Ir(III)-based phosphors [30, 72–75]. An example of an EL polymer is that resulting from the grafting of both Ir(III)-based phosphors and charge transport (carbazole) units onto polyfluorene main chains [76], Fig. 14.

The good EL performance of these devices results from the combination of the emission properties of the main chain (blue side) and the Ir(III) units (red side) and from modulation of the charge transport process by the incorporated carbazole units. These features are associated to a homogeneous single-layer material, which represents an advantage against using blends and multilayer structures that can be subject to phase separation.

(c) On the basis of consideration of possible alternatives to the use of radioactive isotopes [77, 78], Ir(C[^]N)(N[^]N)⁺ complexes [79], and related

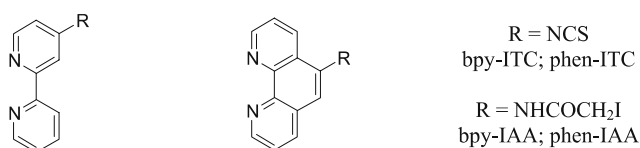
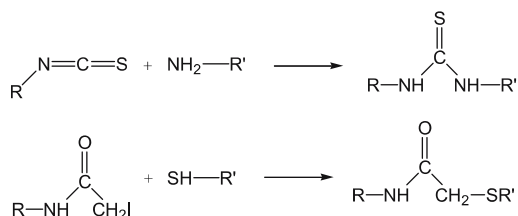


Fig. 15 Schematic structures



Scheme 1

species [80–83], have been proposed for biological labelling purposes (and likewise, Ru(II)- and Re(I)-polyimine derivatives [84, 85]). According to this approach, the (N[^]N) ligand can be functionalized with isothiocyanate (ITC) and iodoacetamide (IAA) groups, Fig. 15 (and Scheme 1), capable of undergoing reactions with primary amine and sulfhydryl groups, respectively.

On these bases, proteins like human serum albumin (HSA) and avidin (Av) have been labelled with such complexes. This yields bioconjugates that are strongly luminescent and can be used for recognition purposes [79]. In Table 10 are listed luminescence properties of some selected complexes and related bioconjugates [79].

4 Mononuclear Complexes of Terdentate Ligands

The luminescence properties of Ir(terpy)₂³⁺ have long been known [23], Table 1. With respect to the Ir(ppy)₃ complex (and most of its numerous derivatives), the luminescence quantum yield of Ir(terpy)₂³⁺ is lower, $\phi = 3 \times 10^{-2}$, even if the energy content and lifetime of the luminescent level are quite similar, $E^{00} \sim 2.7$ vs. 2.5 eV and $\tau = 1.2$ vs. 1.9 μ s, respectively. As a matter of fact, owing to the charge problem and to the lower emission intensity with respect to most of the tris-bidentate Ir(III)-cyclometalated complexes, the Ir(terpy)₂³⁺-type species have been devised for the building up of dyads and triads modeling photoenergy conversion schemes and not for use in EL devices [25, 65, 86, 87]. In this respect, Ir(terpy)₂³⁺-type units offer also the possibility to create linear arrays with geometrically opposite photoactive and electroactive units, e.g. electron donor (D) and acceptor (A) units. This allows us to circumvent the well-known problem of the geometrical isomers encountered for tris-bidentate arrangements [88]. This can be done by attaching suitable substituents at the 4'-position of the coordinated terpy's [89], similar to what happens for related Ru(II) and Os(II)-terpy type complexes [88]. In a subsequent section, we will deal with examples of such arrays and of the photoinduced processes taking place therein. Here, we restrict ourselves to an overview of the spectroscopic and electrochemical properties of Ir(III) complexes of (N[^]N[^]N), (N[^]C[^]N), and (C[^]N[^]C) ligands.

4.1 Terdentate (N[^]N[^]N) Ligands

Some properties of Ir(III) complexes of (N[^]N[^]N) ligands are listed in Table 11 [25, 65, 90, 91]; Fig. 16 displays schematic structures of the complexes. As noted above, for these non-cyclometalated complexes, the metal-centered oxidation step is difficult and is not observed in the usually explored potential range [25].

Table 11 Photophysical properties of selected Ir(III) complexes of terdentate (N[^]N[^]N) ligands^a

	Absorption ^b		Emission ^c		τ μs	k_r^d 10^5 s^{-1}	Electrochemistry ^e		Refs.
	$\lambda_{\text{abs}}^{\text{max}}$ nm	ϵ $10^3 \text{ M}^{-1} \text{ cm}^{-1}$	λ_{em} nm	$10^2 \times \phi$			Ir ^{IV/III} V	Ir ^{III/II} ($\text{L}^{0/-1}$) V	
Ir(terpy) ₂ ³⁺	352	5.8	458	3.0	1.2	2.5	f	-0.77	[25]
Ir(tterpy) ₂ ³⁺	373	29.0	506	11.5	9.5	1.2	f	-0.81 ^g	[25]
Ir(tBterpy) ₂ ³⁺	372	23.8	506	9.3	0.8	11.6	f	-0.74	[65]
Ir(BPAterpy) ₂ ³⁺	410	46.0	566	0.76	2.0	0.4	f	-0.76	[65]
Ir(BPterpy) ₂ ³⁺	381 ^h	44.3 ^h	562	0.58	17.0	0.03			[90]
Ir(terpy)(NMe ₂ terpy) ³⁺	~ 480	-	i	i	i				[90]
Ir(ABterpy) ₂ ³⁺	504	44.8	754	i	i				[91]

^a AN solvent unless otherwise noted^b Lowest-energy absorption maximum^c Oxygen-free solvent^d Radiative rate constant, $k_r = \phi/\tau$ ^e Potentials vs. SCE^f Estimated > 2.4 V [25]^g In CH₂Cl₂^h In waterⁱ Very weak luminescence [90, 91]

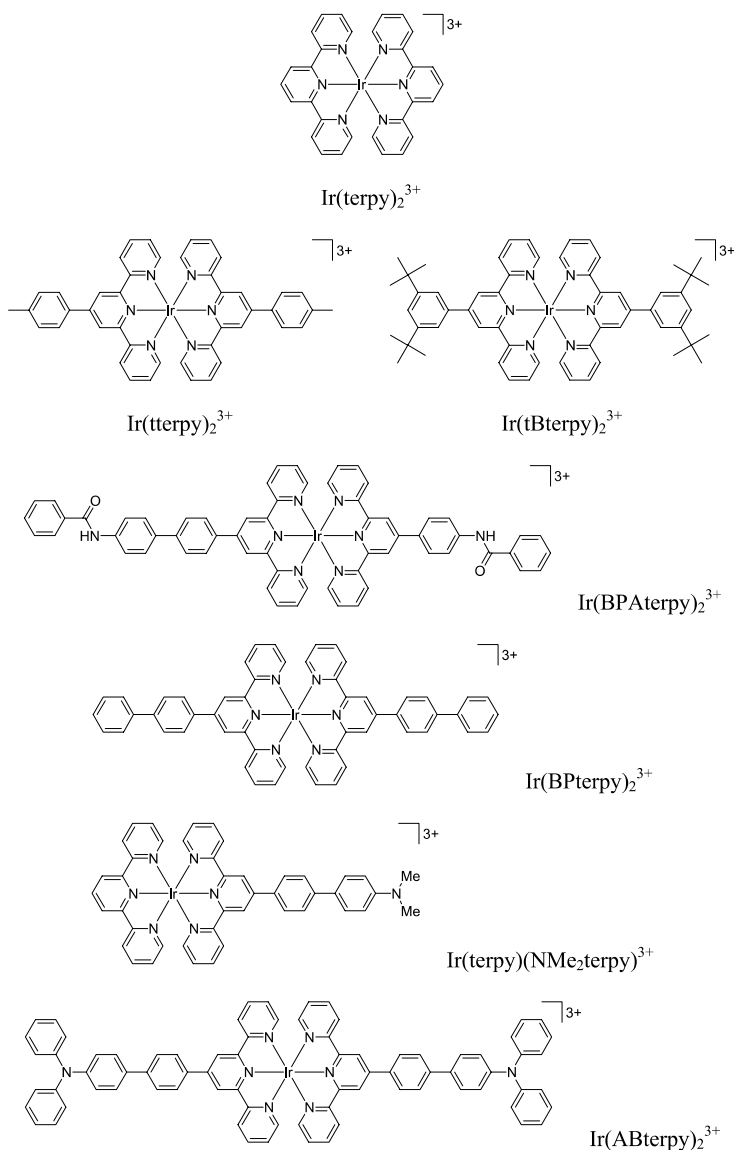


Fig. 16 Schematic structures of bis-terdentate complexes; the two terdentate planar systems are roughly perpendicular each other

Along the series of Table 11, the lowest-lying excited level, as monitored from the emission features, moves to lower and lower energy, a result mainly ascribable to a larger and larger ligand size. Interestingly, along this series the emission passes from a predominant ^3LC character ($\text{Ir}(\text{terpy})_2^{3+}$), to a mixed $^3\text{LC}/^3\text{MLCT}$ character ($\text{Ir}(\text{tterpy})_2^{3+}$ and $\text{Ir}(\text{tBterpy})_2^{3+}$); for $\text{Ir}(\text{BPterpy})_2^{3+}$

the emission is best ascribed to a ^3LC level, likely centered at the biphenyl moiety. These changes in the nature of the emission are signalled by the usual features: (i) emission profile; $^3\text{MLCT}$ emissions yield broad luminescence profiles, while spectra for ^3LC emissions are generally narrower and well resolved; some representative cases are illustrated by the luminescence profiles of Fig. 17, (ii) hypsochromic shift of the emission peak on passing from r.t. to 77 K in polar fluid solvent, that becomes frozen at the low temperature (see Fig. 17), and (iii) the k_r value, that for the series of Table 11 seems to be $\sim 10^5 \text{ s}^{-1}$ for $^3\text{MLCT}$ levels, and much smaller for ^3LC cases. For $\text{Ir}(\text{terpy})(\text{NMe}_2\text{terpy})^{3+}$, an intraligand charge transfer state (ILCT, of $\text{NMe}_2 \rightarrow \text{terpy}$ character) is thought to be the lowest-lying excited state, resulting in very weak emission intensity for the complex.

According to the interpretation advanced by the authors, this is in agreement with the ground state being more polar than the excited state, as evi-

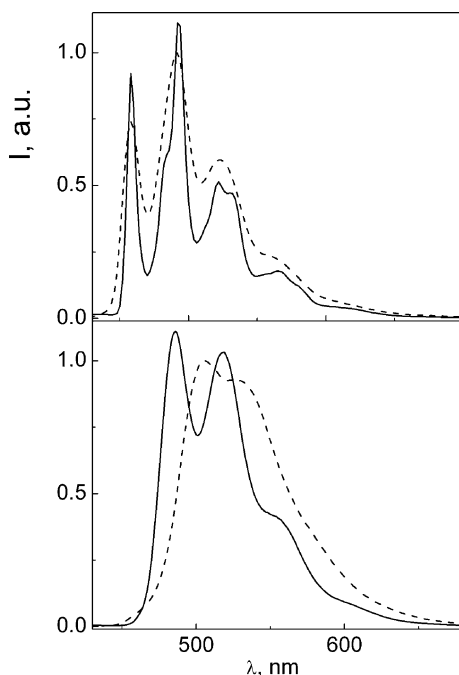


Fig. 17 Luminescence profiles at r.t. (*dashed line*) and at 77 K (*full line*) for a ^3LC emitter, $\text{Ir}(\text{terpy})_2^{3+}$ (*upper panel*), and a mixed $^3\text{LC}/^3\text{MLCT}$ emitter, $\text{Ir}(\text{tterpy})_2^{3+}$ (*bottom panel*); for the latter, distribution of configurations at the dihedral angle between proximate rings of tolyl and terpy fragments may contribute to broadening of the luminescence profile at r.t. [25]. Solvent was oxygen-free butyronitrile, $\lambda_{\text{exc}} = 350 \text{ nm}$. For $\text{Ir}(\text{terpy})_2^{3+}$, τ was 1.2 and 26 μs , at r.t. and 77 K, respectively. For $\text{Ir}(\text{tterpy})_2^{3+}$, τ was 9.5 and 39 μs , at r.t. and 77 K, respectively; for the latter complex, a hypsochromic shift of $\sim 600 \text{ cm}^{-1}$ is registered on passing from fluid (r.t.) to frozen (77 K) solvent

denced by pH titration of the absorption spectra [90]. A near-IR emission is also displayed by $\text{Ir}(\text{ABterpy})_2^{3+}$, Fig. 16, again resulting from an ILCT state wherein the aminobenzene fragment (AB) plays the donor and the bound terpy unit the acceptor.

4.2 Terdentate Cyclometalating Ligands

The first luminescent and redox-active Ir(III) complexes of terdentate cyclometalating ligands were reported by Campagna, Mamo and col-

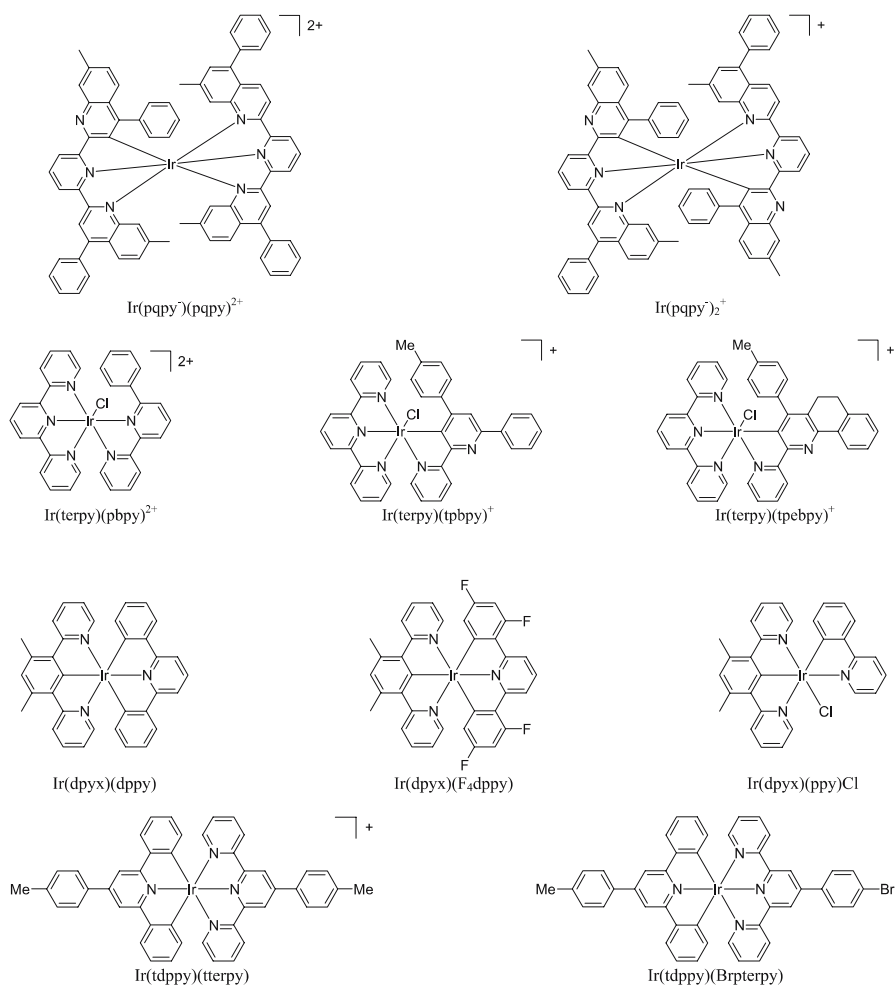


Fig. 18 Schematic structures of cyclometalated bis-terdentate complexes; the two terdentate planar systems are roughly perpendicular to each other

Table 12 Photophysical properties of selected Ir(III) complexes of terdentate cyclometalating ligands^a

	Absorption ^b		Emission ^c		τ μs	k_r^d 10^5 s^{-1}	Electrochemistry ^e		Refs.
	$\lambda_{\text{abs}}^{\text{max}}$ nm	ϵ $10^3 \text{ M}^{-1} \text{ cm}^{-1}$	λ_{em} nm	ϕ			Ir ^{IV/III} V	Ir ^{III/II} (L ^{0/-1}) V	
Ir(pqpy ⁻)(pqpy) ²⁺	390	44.3	620	0.005	0.33	1.5	-0.67	[92]	
Ir(pqpy ⁻) ₂ ⁺	418	6.5	630	0.066	2.3	3.0	-1.11	[92]	
Ir(terpy)(pbpy) ₂ ²⁺	322	25.8	539	0.007	1.5	0.5		[93]	
Ir(terpy)(tpbpy) ⁺	376	6.5	541	0.160	3.2	5.0		[93]	
Ir(terpy)(tpebpy) ⁺	381	5.6	562	0.160	2.4	7.0		[93]	
Ir(dpyx)(dppy)	510	7.3	585	0.210	3.9	5.4		[94]	
Ir(dpyx)(F ₄ - dppy)	487	5.2	547	0.410	3.7	11.0		[61]	
Ir(dpyx)(ppy)Cl	455	3.6	508	0.760	1.6	47.5		[61]	
Ir(tdppy)(terpy) ⁺	504	44.8	754	0.033	0.19	1.7	+1.08	[96]	
Ir(tdppy)(Brterpy)	520	19.1	690	0.032	1.7	1.9	+1.08	[95]	

^a AN solvent unless otherwise noted^b Lowest-energy absorption maximum with $\epsilon > 1500 \text{ M}^{-1} \text{ cm}^{-1}$ ^c Oxygen-free solvent^d Radiative rate constant, $k_r = \phi/\tau$ ^e Potentials vs. SCE

leagues [92]. The schematic structures of the $\text{Ir}(\text{pqpy}^-)(\text{pqpy})^{2+}$ and $\text{Ir}(\text{pqpy}^-)_2^+$ complexes, that include phenyl-quinoyl fragments which can bind both at N and C⁻ positions, are displayed in Fig. 18; some spectroscopic and electrochemical data are gathered in Table 12 [92–96].

Remarkably, owing to the extended ligand frame, these complexes show low-energy MLCT features, both in absorption and emission [92].

Low-lying MLCT states are also met in the series $\text{Ir}(\text{terpy})(\text{pbpy})_2^{2+}$, $\text{Ir}(\text{terpy})(\text{tpbpy})^+$, and $\text{Ir}(\text{terpy})(\text{tpebpy})^+$, Fig. 18 and Table 12 [93]. For these species, it is interesting that the N[^]N[^]C coordination for the pbpy, tpbpy, and tpebpy never takes place; for the latter two cases it is argued that the aryl substituent may be responsible for activation to cyclometalation of the C3' position at the central pyridyl ring.

The six positions of a bis-terdentate ligation system can be arranged in different ways, Fig. 18 [61, 94–96]. Williams and coworkers have reported on the properties of complexes exhibiting the asymmetric dipyriddylylene (N[^]C[^]N, dpyx) and 2,6-diphenyl-pyridine (C[^]N[^]C, dppy) coordination, Fig. 18 and Table 12 [61]. For $\text{Ir}(\text{dpyx})(\text{dppy})$, the emitting level is described as ³MLCT in nature, as supported by DFT calculations, with the LUMO mainly centered at the (N[^]C[^]N) fragment. For $\text{Ir}(\text{dpyx})(\text{dppy})$ and $\text{Ir}(\text{dpyx})(\text{F4-dppy})$, the luminescence quantum yield is $\phi = 0.21$ and 0.41 , respectively. This demonstrates that also Ir(III) bis-terdentate complexes can be quite good emitters, like the related Ir(III) tris-bidentate ones. In addition, for a complex where dppy coordinates as (ppy-C,N), $\text{Ir}(\text{dpyx})(\text{ppy})\text{Cl}$ (Fig. 18), the luminescence quantum yield is exceptionally high, $\phi = 0.76$, which is likely due to inhibition of photodissociation processes, see below [61].

Scandola and coworkers have explored in detail the consequences of the asymmetry of the coordination environment. On the basis of results from time-dependent DFT calculations, it is concluded that for a series of complexes including $\text{Ir}(\text{tdppy})(\text{tterpy})^+$ and $\text{Ir}(\text{tdppy})(\text{Brptterpy})$ —wherein the Ir(III) center is coordinated by 2,6-diphenylpyridine (dppy) and terpy fragments—the lowest-lying states can display a unique directional character, of dppy → terpy nature (LLCT). Table 12 collects spectroscopic and electrochemical properties for these complexes that feature intense CT absorption in the visible and emission in the red region, $\lambda_{\text{em}} = 690$ nm for $\text{Ir}(\text{tdppy})(\text{Brptterpy})$ [95, 96].

5

Interplay of Excited States and the Role of MC Levels

For the Ir(III) complexes reviewed here, the lowest-lying (and emissive) excited state can be of ³LC, ³MLCT, ³ILCT, ³MLLCT, and ³LLCT nature. Some attention should also be paid to the ³MC levels, Fig. 3. As is well known and has been widely investigated for Re(I)-, Ru(II)-, and Os(II)-polyimine

complexes [97–107], the ^3MC non-emissive levels are effective doorways to radiationless paths, which can include photodegradation of the complex (in some cases, involving ligand release [44, 106, 108–110]). If the energy gap between the emissive and higher-lying ^3MC levels, ΔE (Fig. 3c), is not too high, the latter become thermally accessible at r.t., thus affecting the emission intensity. For instance, for $\text{Ru}(\text{bpy})_3^{2+}$, the $^3\text{MLCT}$ level (actually a cluster of closely spaced MLCT levels [111]) is at ~ 2.1 eV, and thermal population of the ^3MC levels takes place with $\Delta E \sim 0.5$ eV [97], so that the ^3MC level can apparently be placed at 2.6 eV. As discussed in previous sections, Os(II) and Ir(III) are $5d^6$ metal centers, and the ^3MC levels derived from the split of the $5d$ orbitals in an octahedral ligand field are expected to be significantly higher in energy than for a $4d$ case like Ru(II), Fig. 3. As mentioned above, the $^3\text{MLCT}$ emissive level for Os(II) complexes is typically 1.6 eV [4, 88], which should inhibit thermal population of the (too high) ^3MC level. With regard to Ir(III) complexes, either from cyclometalated or non-cyclometalated ligands, this could not be the case. As seen above, their emissive level ranges from 2.0 eV (red region) to 3.0 eV (blue region) or higher, and for the most extreme blue emitters it is easy to predict a severe detrimental role of the ^3MC levels.

An assessment of the energy gap, ΔE , between emissive and ^3MC levels can be obtained by studying the temperature dependence of the luminescence properties, as illustrated by several systematic studies for Ru(II)-polypyridine complexes [3, 97–107]. This can be done by using an Arrhenius-like expression, Eq. 7 [98].

$$k_{\text{nr}} = A \exp\left(\frac{-\Delta E}{RT}\right) + k_0 \quad (7)$$

Here, A is a frequency factor, k_0 is a low temperature limiting value, and $k_{\text{nr}} = 1/\tau - k_{\text{r}}$ (for Ru(II)-polylimine emitters, $k_{\text{nr}} \cong 1/\tau$ [3]). The meaning of A and ΔE is best discussed with reference to two limiting cases, (a) and (b) [3, 98], Fig. 19.

For case (a), the ^3MC deactivation is very fast (showing that photodegradation can also be a contributing process [106, 108–110]). Consistent with this, ΔE is the energy gap between the bottom level of the emission curve (either $^3\text{MLCT}$ or ^3LC) and the level for the crossing with the ^3MC curve; in this case, A should be found in the range 10^{12} – 10^{14} s^{-1} [98].

For case (b), deactivation of the ^3MC level is so slow as to allow equilibration between the emitting level and the ^3MC level. Thus, ΔE is to a good approximation the energy gap between the bottom levels of the curves for the involved states, and it turns out that A should be orders of magnitude slower than 10^{12} s^{-1} [3, 112, 113].

For some of the Ir(III) complexes dealt with here, it could be very important to know about the role of ^3MC levels in view of applications. For instance, the use of Ir(III)-based phosphors as active materials within EL devices, could suffer from the thermal accessibility of the ^3MC levels. At the moment, in-

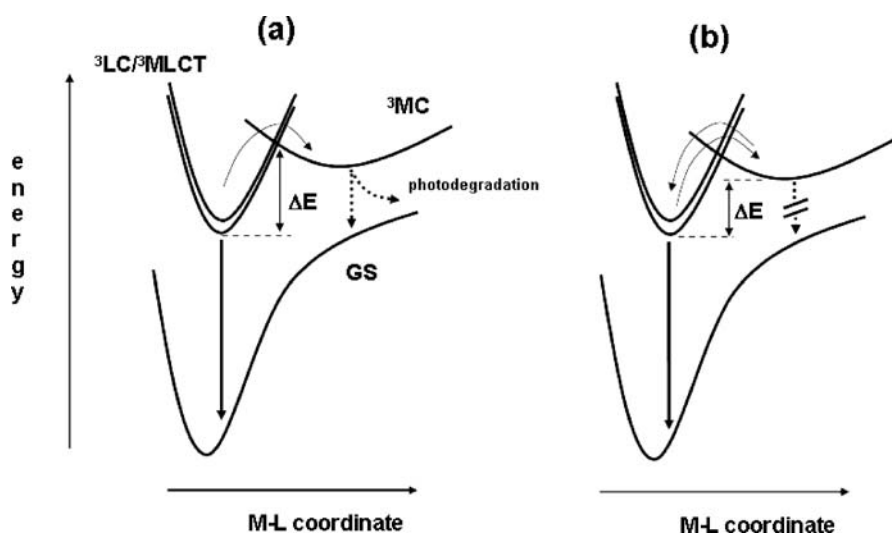


Fig. 19 Expected limiting kinetic cases for deactivation of the luminescent ${}^3\text{LC}/{}^3\text{MLCT}$ levels in Ir(III)-complexes, see text. Adapted from refs [3, 98]

investigation of the temperature dependence of the luminescence seems to be a quite uncommon occurrence for Ir(III)-polyimine complexes. Available results from a few cases studied are summarized in Table 13 [25, 54, 56].

From the low values of the frequency factor A , it seems that for $\text{Ir}(\text{terpy})_2^{3+}$ and $\text{Ir}(\text{tterpy})_2^{3+}$, Table 13, the ${}^3\text{MC}$ level is scarcely active and the appropriate kinetic reference scheme could be that of Fig. 19b. In contrast, for $\text{Ir}(\text{dmF} - \text{ppz})_2(\text{F}_7 - \text{tap})$ (Fig. 9 and Tables 5, 6 and 7), $A \sim 10^{12} \text{ s}^{-1}$ and the kinetic case of Fig. 19a seems to hold, which is consistent with the low emission intensity, $\phi = 0.008$ ($\lambda_{\text{em}} = 469 \text{ nm}$) [54]. Use of these kinetic results would

Table 13 Kinetic parameters for excited-state decay^a

	$A^b \text{ s}^{-1}$	$\Delta E^b \text{ eV}$	$k_o^b \text{ s}^{-1}$	$E^{00,c}$	Refs.
$\text{Ir}(\text{terpy})_2^{3+}$	7.6×10^9	0.22	2.1E5	2.71	[25]
$\text{Ir}(\text{tterpy})_2^{3+}$	2.2×10^7	0.13	6.0E4	2.45	[25]
$\text{Ir}(\text{F}_2 - \text{ptz})_3$	–	0.67	–	2.90	[56]
$\text{Ir}(\text{dmF} - \text{ppz})_2$ ($\text{F}_7 - \text{tap}$)	1.25×10^{12}	0.19		2.65	[54]

^a Solvent and temperature range explored are indicated in the original works

^b See Eq. 7 and concerned text

^c Emission energy level as estimated from the luminescence peak

Table 14 Luminescence properties of chloride-bridged dinuclear complexes^a

	298 K λ_{em} nm	τ μs	ϕ	77 K λ_{em} nm	τ μs	Refs.
$[(\text{ppy})_2\text{Ir}(\mu-\text{Cl})]_2$	518	0.14	0.005	483	4.0	[26, 27, 118]
$[(\text{bzq})_2\text{Ir}(\mu-\text{Cl})]_2$	-	1.40	-	-	30.0	[27]
$[(\text{ptpy})_2\text{Ir}(\mu-\text{Cl})]_2$	510	0.15	-	490	5.2	[26]
$[(\text{mppy})_2\text{Ir}(\mu-\text{Cl})]_2$	520	0.06	-	497	5.0	[26]
$[(\text{nppy})_2\text{Ir}(\mu-\text{Cl})]_2$	574	1.34	0.057	569	2.2	[118]
$[(\text{pnpy})_2\text{Ir}(\mu-\text{Cl})]_2$	651	0.42	0.047	636	3.2	[118]
$[(\text{fppy})_2\text{Ir}(\mu-\text{Cl})]_2$	545	0.40	0.004	-	-	[119]
$[(\text{fppy})_2\text{Ir}(\mu-\text{NCO})]_2$	550	4.60	0.020	-	-	[119]

^a Solvents indicated in the original papers

therefore indicate that as luminophores at r.t., $\text{Ir}(\text{terpy})_2^{3+}$ and $\text{Ir}(\text{tterpy})_2^{3+}$ are expected to be scarcely affected by the ^3MC reactivity. On the contrary, for $\text{Ir}(\text{dmF} - \text{ppz})_2(\text{F}_7 - \text{tap})$ photodamage can be a likely occurrence.

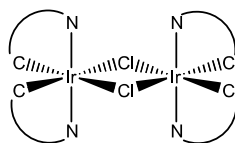
Of course, in addition to a low $^3\text{MLCT}/^3\text{LC} - ^3\text{MC}$ energy gap, limitations in the use of Ir(III)-polyimine complexes as *blue emitters* may arise in connection with some other factors. Actually, even if the phosphorescent level of the complex is lower than the lowest-lying level of a hosting material, a low energy gap between these levels can result in phosphorescence quenching of the guest and lack of exciton confinement [114, 115]. Nevertheless, quite sophisticated strategies may afford white light from devices wherein the incorporated Ir(III)-polyimine components are not designed to act as blue emitters [116].

6 Ir(III) Complexes in Multicomponent Systems

In this section the use of Ir(III) complexes in the construction of supramolecular systems for the collection and conversion of light energy will be reviewed. After a short description of a few homometallic binuclear cases containing Ir(III), the collection of light energy will be treated first, in the section addressing the energy transfer processes. The conversion of light energy into chemical energy will be addressed in the last two sections, with the former dealing with some early work on electron transfer and the latter reviewing the use of Ir(III) complexes in devices for charge separation.

6.1 Binuclear Homometallic Complexes

The direct synthesis of Ir(III) tris-chelate complexes is difficult due to steric and electronic effects of the ligands. It has been shown that a facile route to a variety of phosphorescent compounds exists through chloride-bridged dimers [46, 47]. As mentioned above, IrCl_3 reacts with an excess of the desired ($\text{C}^{\wedge}\text{N}$) ligand to give a cyclometalated complex [117]. The product of this reaction is a chloride-bridged dimer, $[(\text{C}^{\wedge}\text{N})_2\text{Ir}(\mu - \text{Cl})_2\text{Ir}(\text{C}^{\wedge}\text{N})_2]$, with the heterocyclic rings of the ($\text{C}^{\wedge}\text{N}$) ligands in a trans disposition, Scheme 2.



This cyclometalation reaction proceeds under fairly mild conditions, giving good yields (typically > 75%) of the corresponding $[(C^{\wedge}N)_2Ir(\mu-Cl)_2Ir(C^{\wedge}N)_2]$ dimer for a number of ligands having a heterocyclic nitrogen and an sp^2 -hybridized carbon positioned such that the cyclometalation reaction leads to a five-membered ring. The tendency of ppy-type ligands to form bridged species may be viewed as a result of the enhanced electron density at the metal center imposed by a larger σ donation through the Ir – C bond than would be the case in Ir – N bonded complexes of bpy-type ligands [27].

The absorption spectra of these chloro-bridged dimeric complexes are similar to the spectra that would be observed for the corresponding monomer species, providing a good evidence for the small degree of metal-metal interaction which occurs in the dimers [27]. $[(C^{\wedge}N)_2Ir(\mu-Cl)_2Ir(C^{\wedge}N)_2]$ complexes are only weakly emissive at room temperature, $\phi < 0.05$; however, they strongly phosphoresce in frozen glasses at low temperature. In Table 14 are listed luminescence properties of such chloride-bridged Ir(III) dimers; Fig. 20 shows ligands not yet illustrated in previous figures. The weak phosphorescence at room temperature has been explained by the occurrence of a rapid non-radiative decay, involving cleavage in the excited state, followed by a re-formation of the dimer in the ground state [118].

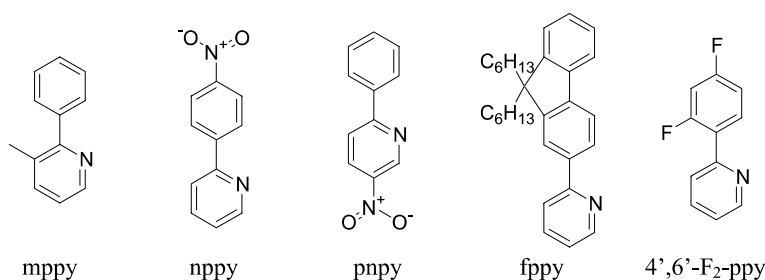


Fig. 20 Terminal ligands employed in binuclear homometallic complexes

Insertion of σ -donating alkyl groups on the phenyl- and pyridine moiety of ppy results in a higher electron density at the metal center. Nevertheless, electronic transitions in the substituted complexes occur at energies similar to those of the unsubstituted ppy derivatives, as a balance of σ -donor and π -acceptor effects from the alkyl groups during charge transfer processes [26]. On the contrary, upon substitution on the ppy ligands with strongly electron-withdrawing groups, like NO_2 , an extreme variability in the photophysical properties is manifested, and a large bathochromic shift of the emission band maximum is observed. This is a consequence of a significant decrease in the σ -donor ability of the phenyl moiety, or increase in π -accepting ability of the pyridyl moiety when an electron-withdrawing group is attached on the corresponding aromatic ring [118]. The use of isocyanate (NCO) bridging ligands has been demonstrated to increase the photoluminescence quantum

yield without shifting the emission wavelength significantly [119]. The use of pseudo-halogen ligands can either (i) affect the gap between the LUMO level of the cyclometalating ligand and the metal t_{2g} orbitals, resulting in a red or blue shift in the emission maxima, or (ii) increase the gap between the cyclometalating ligand LUMO and the metal e_g levels, thus reducing the likelihood of non-radiative decay processes through the 3MC levels and increasing the luminescence quantum yield [57]. The use of these isocyano-bridged dinuclear Ir(III) complexes as triplet emitters in OLED devices has recently been suggested [119].

Examples of binuclear Ir(III) complexes comprising organic bridges are scarce, with the linking ligands mainly making use of *p*-phenylene spacing units [120–123], Fig. 21. The luminescence properties of some of these systems are collected in Table 15. When two Ir(ppy)₂ moieties are coordinated by bpy units connected through polyphenylene spacers, the luminescence behavior is ascribable to 3MLCT transitions involving the bridging ligand [121–123]. The length of the spacer and the presence of substituents

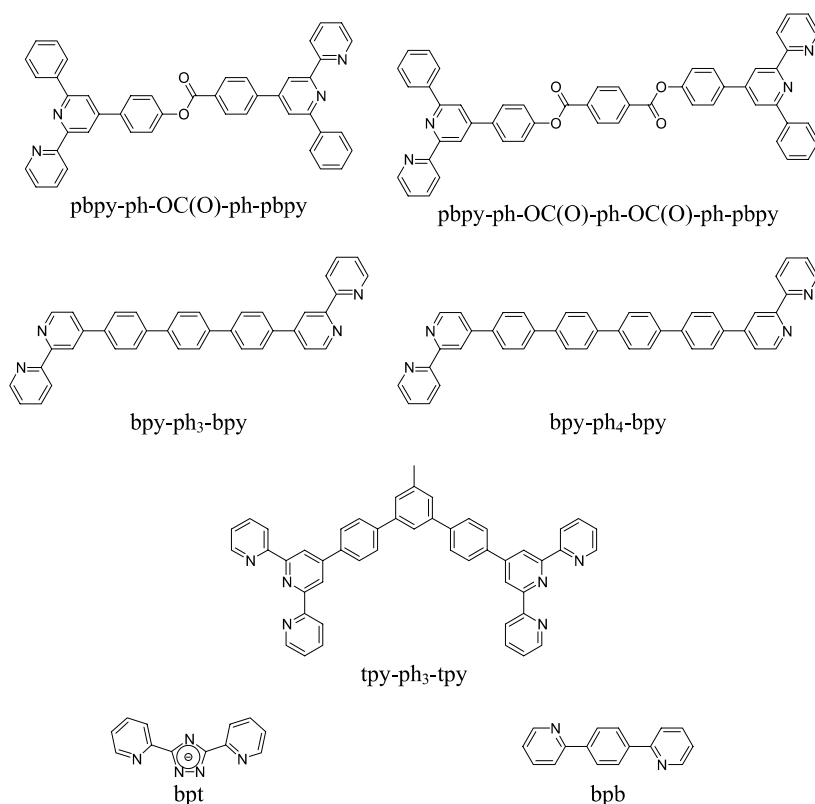


Fig. 21 Bridging ligands employed in binuclear homometallic complexes

Table 15 Luminescence properties of dinuclear complexes^a

	298 K λ_{em} nm	τ μs	ϕ	77 K λ_{em} nm	τ μs	Refs.
$[(\text{ppy})_2\text{Ir}(\mu\text{-pbpy}\text{-ph}\text{-OC(O)}\text{-ph}\text{-pbpy})\text{Ir}(\text{ppy})_2]^{2+}$	646	0.065	0.006	552	3.5	[123]
$[(\text{ppy})_2\text{Ir}(\mu\text{-pbpy}\text{-ph}\text{-OC(O)}\text{-ph}\text{-O(CO)}\text{-ph}\text{-pbpy})\text{Ir}(\text{ppy})_2]^{2+}$	631	0.069	0.007	548	3.6	[123]
$[(\text{ppy})_2\text{Ir}(\mu\text{-bpy}\text{-ph}_3\text{-bpy})\text{Ir}(\text{ppy})_2]^{2+}$	608	0.390	0.094	535	6.0	[122]
$[(\text{ppy})_2\text{Ir}(\mu\text{-bpy}\text{-ph}_4\text{-bpy})\text{Ir}(\text{ppy})_2]^{2+}$	606	0.411	0.175	537	6.2	[122]
$[(44,64\text{-ppy})_2\text{Ir}(\mu\text{-bpy}\text{-ph}_4\text{-bpy})\text{Ir}(44,64\text{-ppy})_2]^{2+}$	546	15, 2	0.117	530	2.6, 990, 49	[121]
$[(\text{tpy})\text{Ir}(\mu\text{-tpy}\text{-ph}_3\text{-tpy})\text{Ir}(\text{ppy})_2]^{2+}$	578	2.774	0.007	524	205	[120]
$[(\text{ppy})_2\text{Ir}(\mu\text{-bpt})\text{Ir}(\text{ppy})_2]^+$	484	0.070	–	473	4.8	[124]
$[(\text{ppy})_2\text{Ir}(\mu\text{-bpb})\text{Ir}(\text{ppy})_2]$	665	2.000	0.040	–	–	[125]

^a Solvents indicated in the original papers

on the cyclometalating ligands affect the photophysics of the complexes. Notably, the luminescence quantum yields are 2–3 times higher with respect to the related chloride-bridged dimers (see Table 14). When the dimers are built up with terdentate chelating ligands and a terpy fragment is connected to the bridging modules, the excited state responsible for the luminescence may be long lived, $\tau > 200 \mu\text{s}$ at 77 K [120], a likely consequence of its localization at the bridging fragments.

When the organic bridging ligand allows for a significant electronic communication between the metal centers, then a strong influence is exerted on the energy of the emitting states, see cases of $[(\text{ppy})_2\text{Ir}(\mu - \text{bpt})\text{Ir}(\text{ppy})_2]^+$ and $[(\text{ppy})_2\text{Ir}(\mu - \text{bpb})\text{Ir}(\text{ppy})_2]$, Fig. 21 and Table 15 [124, 125]. In particular, a marked red shift of the emission (4400 cm^{-1}) is observed for $[(\text{ppy})_2\text{Ir}(\mu - \text{bpb})\text{Ir}(\text{ppy})_2]$, as compared to the parent mononuclear $\text{Ir}(\text{ppy})_3$ complex. By contrast, in the $[(\text{ppy})_2\text{Ir}(\mu - \text{bpt})\text{Ir}(\text{ppy})_2]^+$ complex the efficient mixing of the filled d metal orbitals and π orbitals of the bridge, causes a strong coupling between the metal centers, resulting in a blue-shifted emission. For both complexes, the observed luminescence has been assigned to $^3\text{MLCT}$ transitions involving the charged bridging ligand [124, 125].

6.2

Energy Transfer Processes

The study of photoinduced processes in Ir(III)-based arrays has been exploited since facile synthetic methods for the preparation of Ir(III)-polyimine complexes became available. Polynuclear complexes containing, in addition to Ir(III) centers, either Os(II)-, Ru(II)-, Re(II) or Cu(I)-polyimine units linked by different bridging ligands, displayed a rich variety of photoinduced energy transfer processes. In Fig. 22 are reported some representative cases of early studies.

A dinuclear complex $[(\text{bpy})_2\text{Ru}(\text{HAT})\text{Ir}(\text{ppy})_2]^{3+}$ incorporating Ru(II) and Ir(III) centers linked via the bridging ligand HAT was reported by Kirsch-De Mesmaecker et al. [126]. In this dinuclear complex, Fig. 22a, the emission is identified as Ir-centered, and denoted SBLCT in nature ($\lambda_{\text{em}} = 760 \text{ nm}$, $\tau < 10 \text{ ns}$), consistent with $\text{Ru} \rightarrow \text{Ir}$ energy transfer.

The dinuclear complex $[(\text{bpy})_2\text{Ru}(\text{bpt})\text{Ir}(\text{ppy})_2]^{2+}$ was reported by Haasnoot et al., Fig. 22b [124]. In this complex the two metal centers are linked via a bpt bridging ligand containing a monoanionic triazole unit. Because of this electronic feature, the MLCT states localized on the two moieties involve the peripheral ligands and not the bridging ligand. In $[(\text{bpy})_2\text{Ru}(\text{bpt})\text{Ir}(\text{ppy})_2]^{2+}$, emission is only observed from the Ru-based unit and the direction of inter-component energy transfer is $\text{Ir} \rightarrow \text{Ru}$, i.e., in the opposite direction from that observed for $[(\text{bpy})_2\text{Ru}(\text{HAT})\text{Ir}(\text{ppy})_2]^{3+}$.

A further example of a mixed dinuclear complex is reported by Brewer et al. and is represented in Fig. 22c. $[(\text{terpy})\text{Ru}(\text{tpp})\text{IrCl}_3]^{2+}$ was studied to-

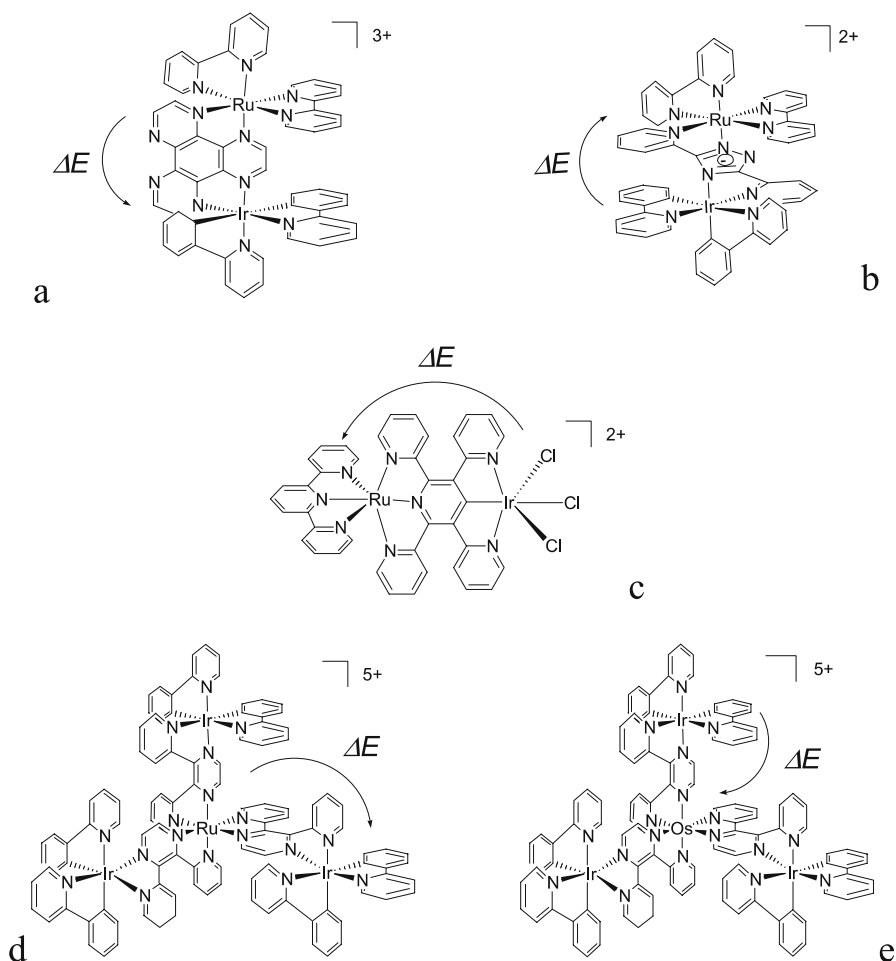


Fig. 22 Schematic structures of polynuclear complexes, see text; arrows denote energy transfer

gether with the pertinent component models [127]. Irrespective of the excited moiety, the luminescence in the array ($\lambda_{\text{em}} = 810 \text{ nm}$, $\tau = 22 \text{ ns}$), is a Ru-based emission with a $^3\text{MLCT}$ involving the tpp bridging ligand. In Fig. 22d and e are shown tetranuclear heterometallic complexes reported by Campagna et al. [128]. In the tetranuclear compounds $\{\text{M}[(\text{dpp})\text{Ir}(\text{ppy})_2]_3\}^{5+}$ with $\text{M} = \text{Ru}(\text{II})$ or $\text{Os}(\text{II})$ the direction of the energy flow is reversed depending on the nature of the central unit. In $\{\text{Ru}[(\text{dpp})\text{Ir}(\text{ppy})_2]_3\}^{5+}$ the central position is occupied by a $\text{Ru}(\text{dpp})_3^{2+}$ unit and the absorption of a photon by this chromophore results in the excitation being conveyed with unit efficiency to any one of the peripheral $(\text{dpp})\text{Ir}(\text{ppy})_2^+$ fragments, which emits. Conversely, for $\{\text{Os}[(2,3\text{-dpp})\text{Ir}(\text{ppy})_2]_3\}^{5+}$, absorption by one of

the Ir(III) chromophores is followed by a periphery-to-center excitation energy, and the emission is $\text{Os}(2,3\text{-dpp})_3^{2+}$ -based. These results agree with the known ordering of the emissive triplet state energy levels: $\text{Ru}(\text{dpp})_3^{2+} > (\text{dpp})\text{Ir}(\text{ppy})_2^+ > \text{Os}(\text{dpp})_3^{2+}$.

More recent work include examples from several groups. Neve, Campagna et al. and Quici, Campagna et al. have investigated the systems displayed in Fig. 23 [120,123]. A heterometallic cyclometalated complex $[(\text{ppy})_2\text{Ir}(\mu\text{-L-OC(O)-L})\text{Re}(\text{CO})_3\text{Br}]^+$ with $\text{L-OC(O)-L} = 4\text{-}\{(6'\text{-phenyl-2,2'}\text{-bipyridine-4'}\text{-yl})\text{benzoyloxy}\}\text{phenyl}\text{-6'}\text{-phenyl-2,2'}\text{-bipyridine}$, Fig. 23a, was electrochemically and photophysically characterized together with a series of model monomers and related homobimetallic species [120, 123]. The luminescence of the heterometallic complex was essentially dominated by the Ir-based emission, however a scarcely efficient energy transfer from the Ir center to the Re center was inferred from the wavelength dependence of the Ir-based luminescence. The very modest driving force for the energy transfer reaction ($< 0.1\text{ eV}$) together with the high reorganization energy

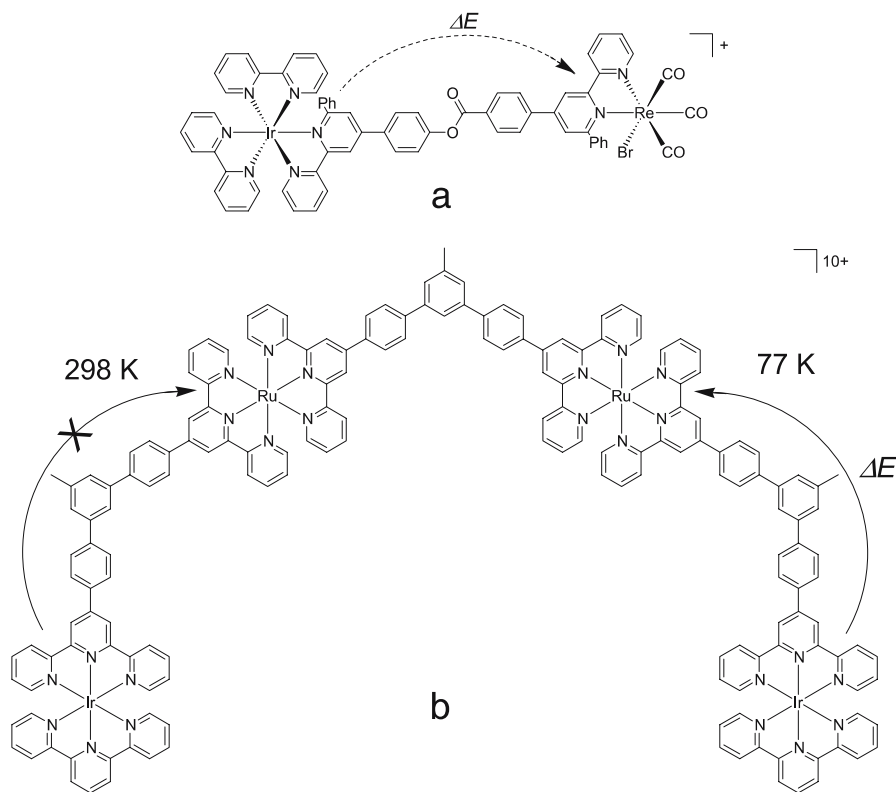


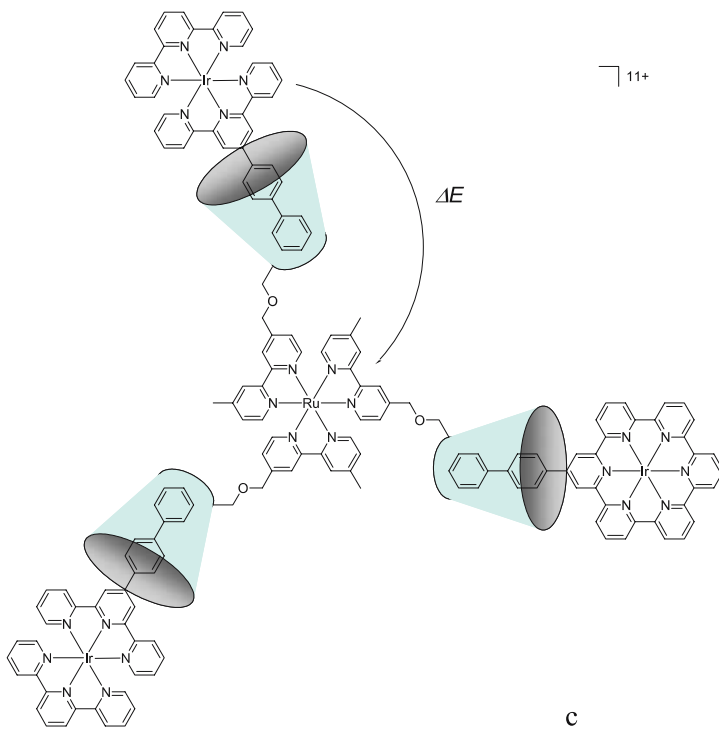
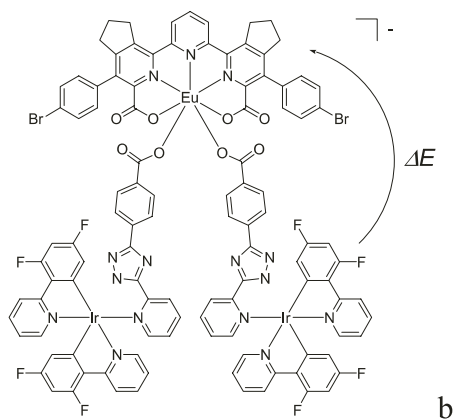
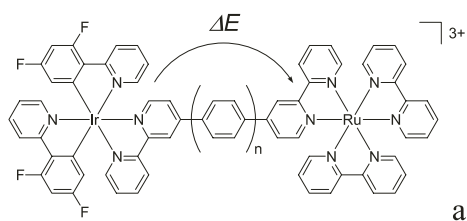
Fig. 23 Schematic structures of polynuclear complexes, see text; arrows denote energy transfer

accompanying energy transfer, were identified as the main reasons for such inefficiency. The tetranuclear system $[(\text{terpy})\text{Ir}(\text{L})\text{Ru}(\text{L})\text{Ru}(\text{L})\text{Ir}(\text{terpy})]^{10+}$, Fig. 23b, with L containing two coordinating terpyridine sub-units linked to each other by a relatively rigid polyphenyl spacer with a *meta* arrangement was recently reported [120]. At room temperature, the Ir and Ru centers emit independently and the luminescence is biphasic, with typical features of the two components units, i.e., $\lambda_{\text{em}} = 572 \text{ nm}$ and $\tau = 2.9 \mu\text{s}$ for the Ir(III) unit and $\lambda_{\text{em}} = 681 \text{ nm}$ and $\tau = 82 \text{ ns}$ for the Ru(II) unit, respectively. On the contrary at 77 K, where the lifetime of the Ir-based potential energy donor is increased to 205 μs , the only detected luminescence is Ru-based, indicating an Ir \rightarrow Ru efficient energy transfer. An energy transfer rate of the order of 10^4 s^{-1} , unable to compete with the intrinsic deactivation of the Ir donor at room temperature can be estimated.

Other contributions come from the group of De Cola [129]. A series of *para*-phenylene bridged heterodinuclear Ir/Ru complexes with increasing bridge length $[\text{Ir}-\text{ph}_n-\text{Ru}]^{3+}$, with Ir = Ir(ppyFF)₂bpy⁺ and Ru = Ru(bpy)₃²⁺, were examined, Fig. 24a [121, 129]. In these complexes selective excitation of a single metal complex unit is not possible due to the absorbance overlap of both metal complexes and connecting bridge. Both at 298 K and at 77 K, excitation at 330 nm leads to emission from the lower energy excited Ru(II)-unit only, which suggests a very fast (τ ca. 2 ps at 298 K) and nearly length independent Ir \rightarrow Ru energy transfer. This behavior was explained by a hopping mechanism (as opposed to superexchange) dominating the energy transfer process, favored by the very close energy of the ³MLCT level of the Ir(III)-based donor and the triplet state of the bridge.

An interesting application of energy transfer processes in Ir(III)-based polyimine complexes is represented by the system illustrated in Fig. 24b [130]. De Cola et al. reported the formation of this trinuclear adduct via the carboxylated groups of two Ir(III)-based centers with an Eu(III) terpyridine-based complex. The emission of the Ir center is blue-green ($\lambda_{\text{em}} = 460 \text{ nm}$ and 491 nm) and that of the Eu center is red ($\lambda_{\text{em}} = 615 \text{ nm}$). The design of the system allowed only a partial transfer (ca. 40%) of the energy of the Ir center (selectively excited at 400 nm), to the Eu(III)-based unit. This leads to a luminescence containing contributions from both centers ($\lambda_{\text{em}} = 460 \text{ nm}$, 491 nm and 615 nm), whose combination results in white luminescence, of potential interest in electroluminescent displays and for lighting applications.

A further contribution from this group, in collaboration with Pikramenou, deals with energy transfer processes in self-assembled structures of multinuclear complexes. Each ligand of a Ru(bpy)₃²⁺ unit is connected to the rim of a β -cyclodextrin receptor to form Ru(β -CD-mbpy), which can complex in a polar medium the biphenyl (or adamathyl) tail of an Ir(III)-terpyridine complex, Fig. 24c [131]. In order to provide complexation of the Ir guest and because of the low association constant, a consistent excess of the Ru(β -CD-mbpy) host is required, (80–90% of host relative to guest). Under these



◀ **Fig. 24** Schematic structures of arrays, see text; *arrows* denote energy transfer

conditions, the luminescence of the Ir unit excited at 330 nm (where also the Ru unit is excited) displays a short decay component with $\tau = 3$ ns and 35 ns, for Ir(biptpy)(terpy)³⁺ and Ir(tpyada)(terpy)³⁺, respectively. The nature of the connecting tail can affect differently the electronic coupling of the partners; this is higher for the aromatic rather than for the aliphatic guest, and can alter accordingly the rates of the energy transfer process. Rate constants of 3.3×10^8 s⁻¹ and of 2.9×10^7 s⁻¹ were derived for the biphenyl and the adamantyl guests, respectively.

An example of an Ir(III)-based binuclear complex involving Cu(I), reported by Sauvage, Collin, Flamigni et al. is displayed in Fig. 25a [132]. This binuclear complex contains an Ir(terpy)₂-type complex and an asymmetric Cu(phen)₂-type complex. It can be regarded as a pseudorotaxane where the Cu(I) center locks the axle, containing the Ir(terpy)₂-type complex, with the macrocycle containing a 2,9-diphenyl-1,10-phenanthroline. Following selective excitation of the Ir center at 390 nm, the luminescence of the Ir(III) unit is almost completely quenched. Both energy transfer (Ir→Cu) and electron transfer (Cu→Ir) are possible explanations, but a quantization of the relative weight is made difficult by the essentially non-emissive nature of unsubstituted or asymmetrically substituted Cu(I) bis-phenanthroline derivatives at the 2,9 positions.

Further examples of energy transfer processes in assemblies involving Ir(III) polyimine derivatives, from Williams et al., are shown in Fig. 25b and c [133]. These are bimetallic assemblies containing Ir and Ru centers, either an Ir(terpy)₂³⁺ connected to a Ru(bpy)₃²⁺ via a polyphenyl bridge, Fig. 25b, or a Ru(terpy)₂²⁺ connected to an Ir(ppy)₂bpy⁺ moiety, Fig. 25c. Energy transfer occurs in both arrays in the direction Ir→Ru, but whereas for (b), Fig. 25, the sensitized luminescence of the Ru center upon excitation of the Ir center can be detected also at ambient temperature, in array (c) the sensitized luminescence of the Ru(II)-terpyridine complex can only be revealed at low temperatures (165 K), due to the well-known non-emissive nature of Ru(terpy)₂²⁺ at room temperature.

In addition to polynuclear systems, energy transfer in Ir(III)-based arrays has also been exploited in simple dyads (i.e., arrays made of two units) where an aromatic group is appended to one of the ligands of the complex. An example consists of an Ir complex with an appended naphthyl unit, the complex Ir(ppy)₂(nala) where excitation of the naphthyl chromophore is followed by an efficient energy transfer to the Ir center [134]. A further example, Fig. 25d, is an assembly made of a Ir(terpy)₂³⁺ unit connected through an amidophenyl spacer to a naphthalene bisimide. In this case, upon excitation of the Ir(III) moiety, energy transfer from its ³MLCT level to the triplet localized on the naphthalene bisimide takes place with a rate constant of 4.2×10^6 s⁻¹ [135]. On the contrary, excitation of the naphthyl bisimide

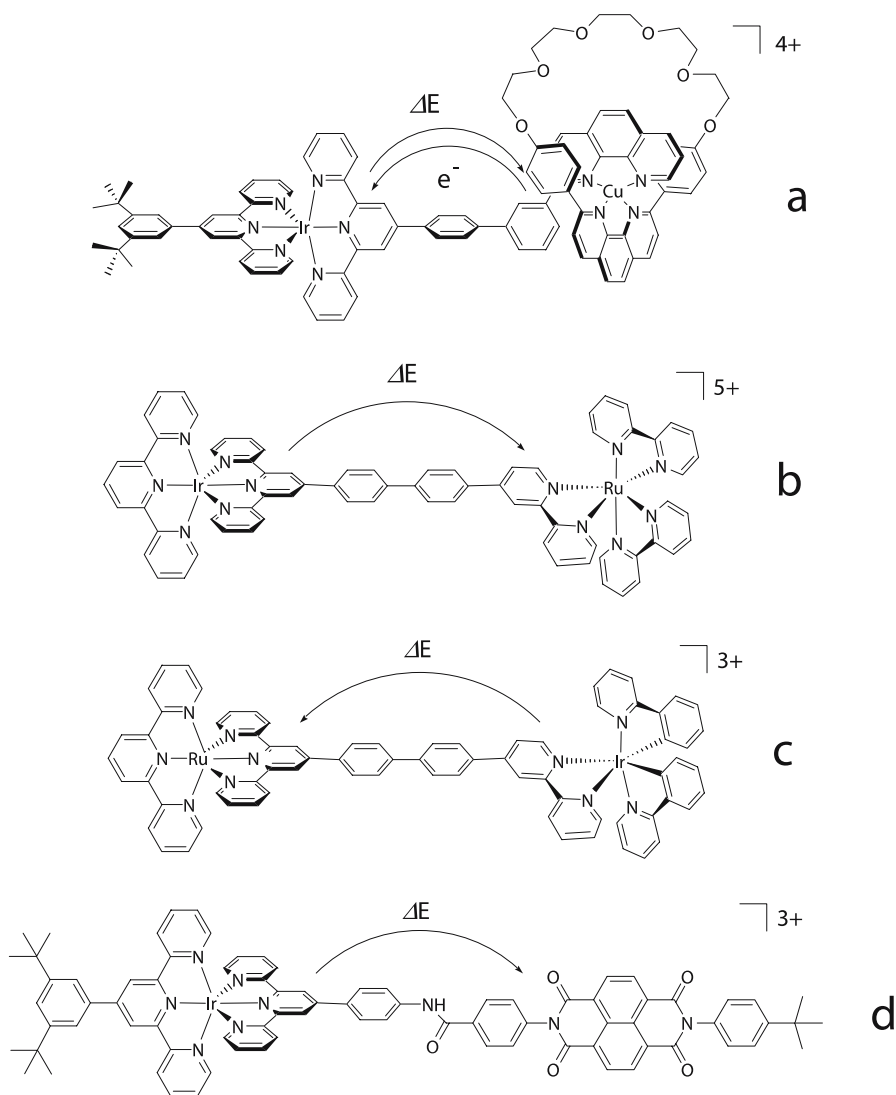


Fig. 25 Schematic structures of arrays, see text; *arrows* denote energy transfer

chromophore yields the singlet excited state of this unit which, in spite of the high energy content (3.2 eV), is unable to transfer energy to the Ir center. This is probably due to the short lifetime (ca. 50 ps) of the excited state which cannot, during its lifetime, transfer energy over the relatively long distance separating the partners (ca. 2 nm center-to-center). It should be recalled here that, due to the strong spin-orbit coupling brought about by the heavy Ir ion, also formally spin-forbidden energy transfer processes can take place.

More examples include the use of Ir(III) complexes in dendrimers [136] and as pendants in oligo- or polymeric fluorene (or carbazole), in part already discussed in Sect. 3.4 [76, 137, 138]. Both cases illustrate viable methods to solve the problem of phase separation in electroluminescent polymers doped with Ir(III) complexes and are not treated here in detail.

6.3

Electron Transfer Processes

A pioneering work in this field was authored by Brewer et al. [139]. The trinuclear complex of Fig. 26a, $\{[(bpy)_2Ru(dpb)]_2IrCl_2\}^{5+}$, containing two Ru centers and one Ir center, was extensively investigated and shown to act as a photochemical device for multiple electron collection. The electrochemical data are crucial to understanding the photoinduced processes. The two Ru(II) centers are oxidized simultaneously at 1.56 V vs. Ag/AgCl. A series of one-electron reductions (+ 0.03 V, - 0.12 V, - 0.71 V and - 0.98 V vs. Ag/AgCl) leads first to the reduction of the bridging dpb ligands which can take up to four electrons before reduction of the peripheral bpy ligands and the two-electron Ir^{III/I} step take place [139]. The first two reduction processes in the trinuclear complex are easier than the analogous processes in the mononu-

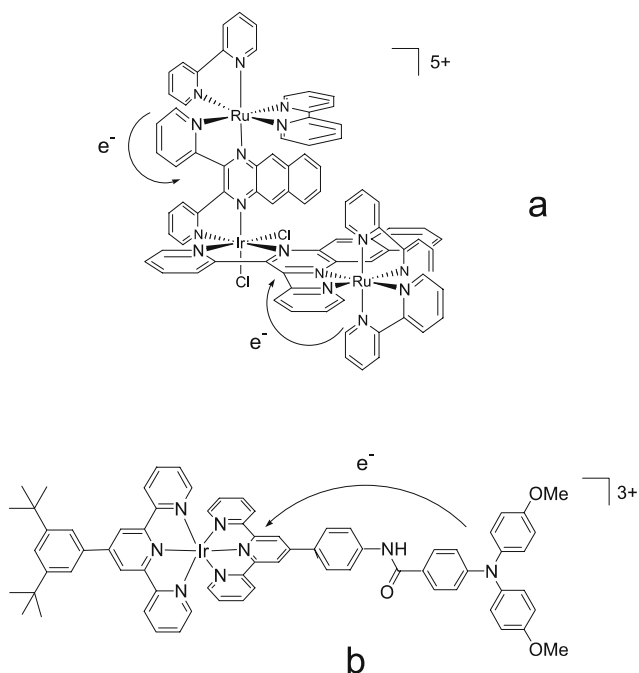


Fig. 26 Schematic structures of arrays, see text; arrows denote electron transfer

clear precursor $\text{Ir}(\text{dpb})_2\text{Cl}_2^+$. This can be ascribed to the stabilizing effect of the Ru(II) centers toward reduced species involving Ir-containing fragments. After this electrochemical behavior, an extension to systems driven by light was devised [140]. Irradiation of the peripheral Ru centers ($\lambda_{\text{exc}} = 650 \text{ nm}$) leads to the $^3\text{MLCT}$ excited state localized on the dpb fragment which undergoes excited state electron transfer with the sacrificial electron donor dimethylaniline (or triphenylamine). This leaves a reduced trinuclear complex and an oxidized sacrificial electron donor. Uptake of a second photon by the Ru unit and further reaction with the sacrificial donor leads to a doubly reduced complex with the electrons localized on the dpb fragments, $\{[(\text{bpy})_2\text{Ru}(\text{dpb}^-)]_2\text{IrCl}_2\}^{3+}$

A further example of a photoinduced electron transfer process involving Ir(III) moieties is reported in Fig. 26, structure (b), and was described by Sauvage, Collin, Flamigni et al. [141]. The dyad is made of a triarylamine electron donor (D) linked to the iridium bis-terpyridine complex (Ir) by an amidophenyl group. D has an excited state energy at ca. 3 eV, higher than the energy of the Ir(III)-complex excited state, ca. 2.5 eV, preventing any quenching of the latter by energy transfer. On the other hand, D can be oxidized at + 0.8 V (vs. SCE) and the Ir complex can be reduced at - 0.76 V (vs. SCE), so an electron transfer from the excited state of both components is possible. Selective excitation of the metal complex unit results in a complete quenching of its luminescence with the formation within 20 ps of $\text{Ir}^- - \text{D}^+$, a charge separated (CS) state with a hole on the triphenylamine unit and an electron on the terpy ligand of the iridium complex. This CS state, identified from the absorption band peaking at 765 nm, decays with a lifetime of 70 ps. Excitation of the D component around 330 nm also results in a complete quenching of the triphenylamine luminescence to yield the same CS state. In fact, when the Ir complex is excited, an electron moves from the HOMO localized at the donor to the HOMO localized at the Ir complex, and when D is excited, an electron moves from the LUMO localized at the donor to the LUMO of the Ir complex acceptor, localized at the bridging terpyridine. The electron transfer reaction occurs with a unity yield upon excitation of both components, but the lifetime of the CS state is too short to be used in any light to chemical energy conversion scheme. The addition to the Ir complex center of an ancillary electron acceptor group able to undergo a further electron transfer step (see below) is the correct strategy to increase the lifetime of the CS state.

6.4

Assemblies for Charge Separation

The topic of this section is strictly related to those of the previous sections. In fact whereas multi-step electron transfer is the basic reaction leading to charge separation, very often energy transfer reaction can occur, and not necessarily detrimentally, in arrays designed to achieve charge separation.

These are triad systems, i.e., made of three component units weakly interacting, where a separation of charges occurs over nanometric distances. All systems described here are based on a central Ir(terpy) $_2^{3+}$ unit, with functional units appended at the 4' position of the terpy ligands. As discussed above, this allows the construction of linear arrays without complications due to the formation of isomers as is the case for bidentate ligands.

The first systems of this type, reported by Collin, Sauvage, Flamigni et al., drawn in Fig. 27, have as appended units free base or zinc tetra-aryl-porphyrin on one side and gold tetra-aryl-porphyrin at the other extremity [87, 142–144]. The Ir(terpy) $_2^{3+}$ unit was introduced to replace Ru(terpy) $_2^{2+}$ used as the assembling unit in previous studies [145, 146], in order to prevent undesired competitive energy transfer processes where the metal complex played the role of energy acceptor, depleting the excited state of the porphyrin photosensitizer. The higher energy of the Ir center, ca. 2.5 eV, with respect to the Ru center, ca. 2 eV, and the lower reduction po-

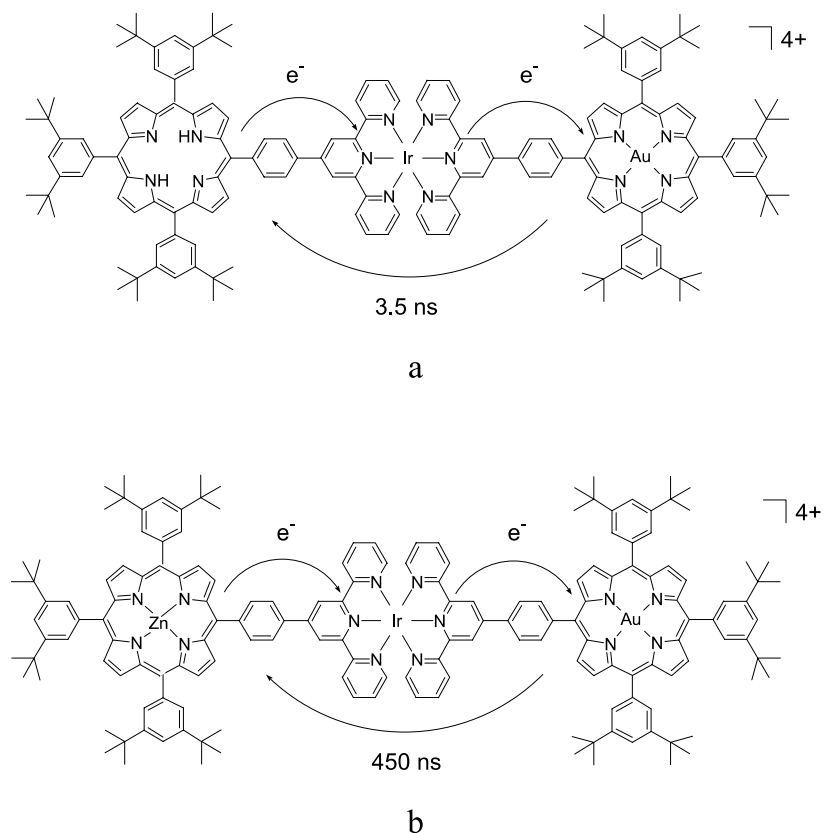


Fig. 27 Schematic structures of arrays, see text; *arrows* denote electron transfer

tential of the former, -0.75 V vs. SCE compared to -1.2 V vs. SCE for the latter, prevented the undesired energy transfer and favored electron transfer in arrays based on $\text{Ir}(\text{terpy})_2^{3+}$ [89, 147]. Excitation of the free base or zinc porphyrin unit in the compounds reported in Fig. 27, results in quenching of the porphyrin fluorescence, $\tau = 30$ ps for triad (a) and $\tau < 20$ ps for triad (b), Fig. 27, compared to a lifetime of nanoseconds for the models. This is ascribed to an electron transfer from the porphyrin excited state to the central Ir(III) complex which is then followed by a further electron transfer to the gold porphyrin unit reducible at a lower potential (-0.65 V vs. SCE) than the Ir center. The latter process occurs with a rate constant of $1.2 \times 10^{10} \text{ s}^{-1}$ in array (a), is faster than $5 \times 10^{10} \text{ s}^{-1}$ in triad (b), Fig. 27, and leads to the separation of charges over the two extreme porphyrins, separated by a center-to-center distance of ca. 3 nm. The yield of charge separation is 0.5 for triad (a) in acetonitrile and 1 for triad (b), Fig. 27, in apolar toluene. The lifetime of the CS state was disappointingly low (3.5 ns) for the triad (a) where charge recombination leads to the triplet state localized on the porphyrin moiety, close in energy to the CS state. By contrast, the lifetime of the CS state for the Zn porphyrin containing triad (b) was remarkably higher, 450 ns. In this case in fact, because of the higher level of the porphyrin triplet excited state, charge recombination leads directly to the ground state. This step, being characterized by a high driving force (ΔG^0 ca. -1.3 eV), takes place in the so-called Marcus inverted region [148] and therefore its rate is slowed down. It should be noted that excitation of the gold porphyrin unit does not yield any useful photoreactivity, in fact the triplet state decays unperturbed with a lifetime identical to the model porphyrin.

An extension of this study revealed that following selective excitation of the Ir(III)-based unit at 355 nm, rather than that of the porphyrin units at 532 nm, i.e., when the Ir center acts as a photosensitizer, the type of ensuing photoinduced process can be switched in the case of array (a), Fig. 27, from the electron transfer discussed above, to energy transfer [87].

More recently the same groups synthesized and determined the photoreactivity of a triad based on the same $\text{Ir}(\text{terpy})_2^{3+}$ unit connected via amidophenyl spacers to a triphenylamino electron donor ($E_{1/2}D^+/D$ ca. -0.8 V vs. SCE) on one side, and a naphthalene bisimide electron acceptor on the other extremity ($E_{1/2}A/A^-$ ca. -0.5 V vs. SCE), with an overall length of the triad D – Ir – A of the order of 5 nm, Fig. 28 [135]. This triad was studied in parallel with the component units and the dyads (d) of Fig. 25, and (b) of Fig. 26 mentioned above. Excitation of the Ir or the D moieties in the triad leads to a CS state $D^+ - \text{Ir} - A^-$ with a yield of ca. 10%. This is formed upon electron transfer ($D^+ - \text{Ir}^- - A \rightarrow D^+ - \text{Ir} - A^-$) from $D^+ - \text{Ir}^- - A$, in turn formed after excitation of either D or Ir units, as discussed above for the model dyad (b) of Fig. 26. Unit A can in fact be reduced more easily than the Ir unit, -0.5 V vs. -0.75 V. The low yield in the formation of $D^+ - \text{Ir} - A^-$ is due to the competition with the fast recombination to the ground state of

the primary CS state $D^+ - Ir^- - A$ ($\tau = 70$ ps, as determined in the dyad (b) of Fig. 26). What is, however, remarkable about this system is the long lifetime of the CS state, $120 \mu\text{s}$, and its scarce sensitivity to the presence of oxygen; in air equilibrated solutions the CS state lifetime is in fact $100 \mu\text{s}$. A schematic diagram of states and of intramolecular photoinduced processes is reported in Fig. 28. Excitation of the A unit does not lead to any intramolecular reactivity, but the resulting triad with an excited state localized on the acceptor unit, $D - Ir - {}^3A$ gives rise to a rich bimolecular reactivity [135].

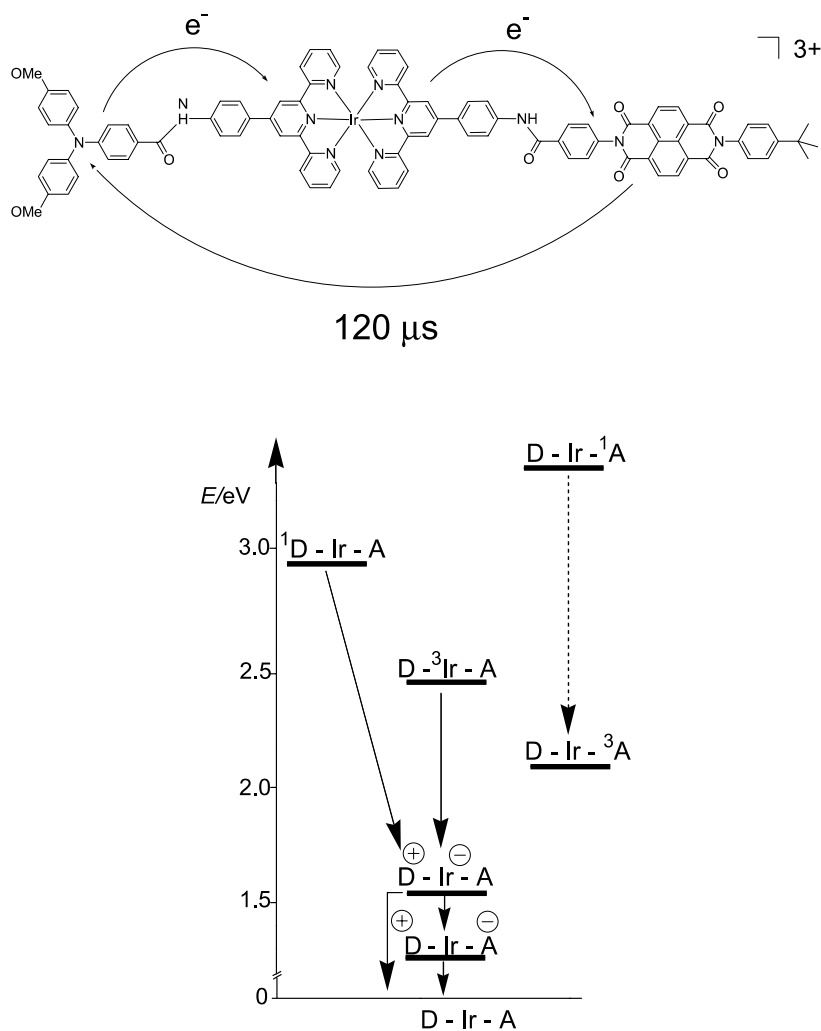


Fig. 28 Upper panel: schematic structure of a D-Ir-A triad (see text), arrows denote electron transfer steps. Lower panel: energy level diagram and elementary reactions (see text)

This system has been quite successful in providing long-lived CS states, among the longest ever obtained with assemblies based on inorganic complex units, however, an improved yield of charge separation is sought for. Addition of a further spacer between the Ir and D unit is expected to slow down the recombination of the $D^+ - Ir^- - A$ favoring the formation of $D^+ - Ir - A^-$, and this seems to be a promising strategy to increase the CS yield over the two extreme units in this type of array, and hopefully increasing at the same time the lifetime of the CS state.

7

Conclusions

The large number of investigated mononuclear luminescent complexes of the $5d^6$ Ir(III) metal ion has allowed a deep understanding of the spectroscopic and electrochemical properties for this family of complexes. Tris-bidentate and bis-terdentate arrangements have been extensively studied, both from non-cyclometalating and cyclometalating ligands. The neutral tris-cyclometalated complexes derived from the archetypical $Ir(ppy)_3$ species, exhibit outstanding luminescence properties, and their investigation as tunable dopant phosphors has been systematically operated, as we have documented in some detail. The nature of the various types of excited states influences the emissive properties, and the understanding of their interplay provides the background for approaches toward the design and use of new members (new phosphors) of this family.

Ir(III)-polyimine complexes have been shown to be quite useful units for the construction of photoactive supramolecular arrays, frequently available in fixed geometry. In several known photoactive multicomponent systems, based on hetero-metallic arrays, a rich variety of energy and electron transfer processes has been explored. In triadic systems incorporating Ir(terpy)-type components, the Ir(III)-terpyridine moiety has proved to be successful both as an assembling unit and as a valuable and versatile component that can act as an electron relay and as a photosensitizer; remarkably, in these systems very long-lived CS states ($\tau_{CS} \sim 100 \mu s$) have been observed upon light absorption. The approaches developed to fabrication of such arrays have undergone continuous improvement, which promises to result in even better performing Ir-based systems for the conversion of light into chemical energy.

Acknowledgements Acknowledgements are due to Project MACOL PM.P04.010 of CNR, Italy.

References

1. Maestri M, Balzani V, Deuschel-Cornioley C, von Zelewsky A (1992) *Adv Photochem* 17:1–68
2. Roundhill DM (1994) *Photochemistry and Photophysics of Metal Complexes*. Plenum Press, New York
3. Juris A, Balzani V, Barigelletti F, Campagna S, Belser P, Von Zelewsky A (1988) *Coord Chem Rev* 84:85
4. Kober EM, Caspar JV, Lumpkin RS, Meyer TJ (1986) *J Phys Chem* 90:3722–3734
5. Schanze KS, Macqueen DB, Perkins TA, Cabana LA (1993) *Coord Chem Rev* 122:63–89
6. Watts RJ (1991) *Comments on Inorganic Chemistry*. Gordon and Breach, London 11:303–337
7. Dixon IM, Collin JP, Sauvage JP, Flamigni L, Encinas S, Barigelletti F (2000) *Chem Soc Rev* 29:385–391
8. King KA, Spellane PJ, Watts RJ (1985) *J Am Chem Soc* 107:1431–1432
9. Tang CW, Van Slyke SA (1987) *Appl Phys Lett* 51:913–915
10. Baldo MA, Thompson ME, Forrest SR (2000) *Nature* 403:750–753
11. Adachi C, Baldo MA, Forrest SR, Thompson ME (2000) *Appl Phys Lett* 77:904–906
12. Adachi C, Baldo MA, Thompson ME, Forrest SR (2001) *J Appl Phys* 90:5048–5051
13. Evans RC, Douglas P, Winscom CJ (2006) *Coord Chem Rev* 250:2093–2126
14. Braterman PS, Song JI, Peacock RD (1992) *Inorg Chem* 31:555–559
15. Yersin H (2004) *Transition Metal and Rare Earth Compounds Iii (Topics in Current Chemistry)* 241:1–26
16. Montalti M, Credi A, Prodi L, Gandolfi MT (2006) *Handbook of Photochemistry*. Taylor and Francis, Boca Raton, FL
17. Hamann C, Von Zelewsky A, Neels A, Stoeckli-Evans H (2004) *Dalton Trans* 402–406
18. Englman R, Jortner J (1970) *Mol Phys* 18:145
19. Goze C, Chambron JC, Heitz V, Pomeranc D, Salom-Roig XJ, Sauvage JP, Morales AF, Barigelletti F (2003) *Eur J Inorg Chem* 3752–3758
20. Demas JN, Harris EW, Flynn CM, Diemente D (1975) *J Am Chem Soc* 97:3838–3839
21. Kahl JL, Hanck KW, Dearmond K (1978) *J Phys Chem* 82:540–545
22. Ohsawa Y, Sprouse S, King KA, Dearmond MK, Hanck KW, Watts RJ (1987) *J Phys Chem* 91:1047–1054
23. Ayala NP, Flynn CM, Sacksteder L, Demas JN, Degraff BA (1990) *J Am Chem Soc* 112:3837–3844
24. Dedeian K, Djurovich PI, Garces FO, Carlson G, Watts RJ (1991) *Inorg Chem* 30:1685–1687
25. Collin JP, Dixon IM, Sauvage JP, Williams JAG, Barigelletti F, Flamigni L (1999) *J Am Chem Soc* 121:5009–5016
26. Garces FO, King KA, Watts RJ (1988) *Inorg Chem* 27:3464–3471
27. Sprouse S, King KA, Spellane PJ, Watts RJ (1984) *J Am Chem Soc* 106:6647–6653
28. Tamayo AB, Alleyne BD, Djurovich PI, Lamansky S, Tsyba I, Ho NN, Bau R, Thompson ME (2003) *J Am Chem Soc* 125:7377–7387
29. Huo SQ, Deaton JC, Rajeswaran M, Lenhart WC (2006) *Inorg Chem* 45:3155–3157
30. Yang XH, Neher D, Hertel D, Daubler TK (2004) *Adv Mater* 16:161
31. Jones RAY (1984) *Physical and Mechanistic Organic Chemistry*. Cambridge University Press, Cambridge
32. Hay PJ (2002) *J Phys Chem A* 106:1634–1641

33. Jung SO, Kang Y, Kim HS, Kim YH, Yang KY, Kwon SK (2003) *Bull Korean Chem Soc* 24:1521–1524
34. Day P, Sanders N (1967) *J Chem Soc A* 1536
35. Tsuboyama A, Iwawaki H, Furugori M, Mukaide T, Kamatani J, Igawa S, Moriyama T, Miura S, Takiguchi T, Okada S, Hoshino M, Ueno K (2003) *J Am Chem Soc* 125:12971–12979
36. Li J, Djurovich PI, Alleyne BD, Yousufuddin M, Ho NN, Thomas JC, Peters JC, Bau R, Thompson ME (2005) *Inorg Chem* 44:1713–1727
37. Vlcek AA, Dodsworth ES, Pietro WJ, Lever ABP (1995) *Inorg Chem* 34:1906–1913
38. Slinker J, Bernards D, Houston PL, Abruna HD, Bernhard S, Malliaras GG (2003) *Chem Commun* 2392–2399
39. Muegge BD, Richter MM (2004) *Anal Chem* 76:73–77
40. Kim JI, Shin IS, Kim H, Lee JK (2005) *J Am Chem Soc* 127:1614–1615
41. Mayo EI, Kilsa K, Tirrell T, Djurovich PI, Tamayo A, Thompson ME, Lewis NS, Gray HB (2006) *Photochem Photobiol Sci* 5:871–873
42. Goldsmith JI, Hudson WR, Lowry MS, Anderson TH, Bernhard S (2005) *J Am Chem Soc* 127:7502–7510
43. Lowry MS, Bernard S (2006) *Chem Eur J* 12:7970
44. Adachi C, Baldo MA, Forrest SR, Lamansky S, Thompson ME, Kwong RC (2001) *Appl Phys Lett* 78:1622–1624
45. Sajoto T, Djurovich PI, Tamayo A, Yousufuddin M, Bau R, Thompson ME, Holmes RJ, Forrest SR (2005) *Inorg Chem* 44:7992–8003
46. Lamansky S, Djurovich P, Murphy D, Abdel-Razzaq F, Kwong R, Tsyba I, Bortz M, Mui B, Bau R, Thompson ME (2001) *Inorg Chem* 40:1704–1711
47. Lamansky S, Djurovich P, Murphy D, Abdel-Razzaq F, Lee HE, Adachi C, Burrows PE, Forrest SR, Thompson ME (2001) *J Am Chem Soc* 123:4304–4312
48. Colombo MG, Brunold TC, Riedener T, Gudel HU, Fortsch M, Burgi HB (1994) *Inorg Chem* 33:545–550
49. Grushin VV, Herron N, LeCloux DD, Marshall WJ, Petrov VA, Wang Y (2001) *Chem Commun* 1494–1495
50. Ragni R, Plummer EA, Brunner K, Hofstraat JW, Babudri F, Farinola GM, Naso F, De Cola L (2006) *J Mater Chem* 16:1161–1170
51. Dedeian K, Shi JM, Shepherd N, Forsythe E, Morton DC (2005) *Inorg Chem* 44:4445–4447
52. Coppo P, Plummer EA, De Cola L (2004) *Chem Commun* 1774–1775
53. Nam EJ, Kim JH, Kim BO, Kim SM, Park NG, Kim YS, Kim YK, Ha Y (2004) *Bull Chem Soc Jpn* 77:751–755
54. Yang CH, Li SW, Chi Y, Cheng YM, Yeh YS, Chou PT, Lee GH, Wang CH, Shu CF (2005) *Inorg Chem* 44:7770–7780
55. Mak CSK, Hayer A, Pascu SI, Watkins SE, Holmes AB, Kohler A, Friend RH (2005) *Chem Commun* 4708–4710
56. Lo S-C (2006) *Chem Mater* 18:5159
57. Nazeeruddin MK, Humphry-Baker R, Berner D, Rivier S, Zuppiroli L, Graetzel M (2003) *J Am Chem Soc* 125:8790–8797
58. Tamayo AB, Garon S, Sajoto T, Djurovich PI, Tsyba IM, Bau R, Thompson ME (2005) *Inorg Chem* 44:8723–8732
59. Schaffner-Hamann C, Von Zelewsky A, Barbieri A, Barigelletti F, Muller G, Riehl JP, Neels A (2004) *J Am Chem Soc* 126:9339–9348
60. Obara S, Itabashi M, Tamaki S, Tanabe Y, Ishili Y, Nozaki K, Haga M-A (2006) *Inorg Chem* 45:8907–8921

61. Wilkinson AJ, Puschmann H, Howard JAK, Foster CE, Williams JAG (2006) *Inorg Chem* 45:8685–8699
62. DiMarco G, Lanza M, Pieruccini M, Campagna S (1996) *Adv Mater* 8:576
63. Di Marco G, Lanza M, Mamo A, Stefio I, Di Pietro C, Romeo G, Campagna S (1998) *Anal Chem* 70:5019–5023
64. Lakowicz JR (1999) *Principles of Fluorescence Spectroscopy*. Kluwer Academic/Plenum Publishers, New York
65. Flamigni L, Ventura B, Barigelletti F, Baranoff E, Collin JP, Sauvage JP (2005) *Eur J Inorg Chem* 1312–1318
66. Demas JN, Harris EW, McBride RP (1977) *J Am Chem Soc* 99:3547–3551
67. Gao RM, Ho DG, Hernandez B, Selke M, Murphy D, Djurovich PI, Thompson ME (2002) *J Am Chem Soc* 124:14828–14829
68. Abdel-Shafi AA, Beer PD, Mortimer RJ, Wilkinson F (2001) *Helv Chim Acta* 84:2784–2795
69. Abdel-Shafi AA, Beer PD, Mortimer RJ, Wilkinson F (2000) *PCCP Phys Chem Chem Phys* 2:3137–3144
70. Abdel-Shafi AA, Wilkinson F (2002) *PCCP Phys Chem Chem Phys* 4:248–254
71. Glusac KD, Jiang SJ, Schanze KS (2002) *Chem Commun* 2504–2505
72. Negres RA, Gong X, Ostrowski JC, Bazan GC, Moses D, Heeger AJ (2003) *Phys Rev B* 68:1–8
73. Gong X, Ostrowski JC, Moses D, Bazan GC, Heeger AJ (2003) *Adv Funct Mater* 13:439–444
74. Zhu WG, Liu CZ, Su LJ, Yang W, Yuan M, Cao Y (2003) *J Mater Chem* 13:50–55
75. Holder E, Marin V, Kozodaev D, Meier MAR, Lohmeijer BGG, Schubert US (2005) *Macromol Chem Phys* 206:989–997
76. Chen XW, Liao JL, Liang YM, Ahmed MO, Tseng HE, Chen SA (2003) *J Am Chem Soc* 125:636–637
77. Kessler C (1999) *Nonradioactive Labeling and Detection of Biomolecules*. Springer, Berlin Heidelberg New York
78. Sammes PG, Yahioğlu G (1996) *Nat Prod Rep* 13:1–28
79. Lo KKW, Chung CK, Lee TKM, Lui LH, Tsang KHK, Zhu NY (2003) *Inorg Chem* 42:6886–6897
80. Lo KKW, Chan JSW, Lui LH, Chung CK (2004) *Organometallics* 23:3108–3116
81. Lo KKW, Chung CK, Ng DCM, Zhu NY (2002) *New J Chem* 26:81–88
82. Lo KKW, Hui WK, Chung CK, Tsang KHK, Ng DCM, Zhu NY, Cheung KK (2005) *Coordin Chem Rev* 249:1434–1450
83. Lo KKW, Li CK, Lau JSY (2005) *Organometallics* 24:4594–4601
84. Lo KKW, Lee TKM (2004) *Inorg Chem* 43:5275–5282
85. Lo KKW, Hui WK (2005) *Inorg Chem* 44:1992–2002
86. Flamigni L, Barigelletti F, Armaroli N, Collin JP, Dixon IM, Sauvage JP, Williams JAG (1999) *Coordin Chem Rev* 192:671–682
87. Flamigni L, Marconi G, Dixon IM, Collin JP, Sauvage JP (2002) *J Phys Chem B* 106:6663–6671
88. Sauvage JP, Collin JP, Chambron JC, Guillerez S, Coudret C, Balzani V, Barigelletti F, De Cola L, Flamigni L (1994) *Chem Rev* 94:993–1019
89. Baranoff E, Collin JP, Flamigni L, Sauvage JP (2004) *Chem Soc Rev* 33:147–155
90. Leslie W, Batsanov AS, Howard JAK, Williams JAG (2004) *Dalton Trans* 623–631
91. Leslie W, Poole RA, Murray PR, Yellowlees LJ, Beeby A, Williams JAG (2004) *Polyhedron* 23:2769–2777

92. Mamo A, Stefio I, Parisi MF, Credi A, Venturi M, DiPietro C, Campagna S (1997) *Inorg Chem* 36:5947–5950
93. Bexon AJS, Williams JAG (2005) *C R Chim* 8:1326–1335
94. Wilkinson AJ, Goeta AE, Foster CE, Williams JAG (2004) *Inorg Chem* 43:6513–6515
95. Polson M, Fracasso S, Bertolasi V, Ravaglia M, Scandola F (2004) *Inorg Chem* 43:1950–1956
96. Polson M, Ravaglia M, Fracasso S, Garavelli M, Scandola F (2005) *Inorg Chem* 44:1282–1289
97. Barigelletti F, Belser P, Von Zelewsky A, Juris A, Balzani V (1985) *J Phys Chem* 89:3680–3684
98. Juris A, Barigelletti F, Balzani V, Belser P, Von Zelewsky A (1985) *Inorg Chem* 24:202–206
99. Barigelletti F, Juris A, Balzani V, Belser P, Von Zelewsky A (1986) *J Phys Chem* 90:5190–5193
100. Meyer TJ (1986) *Pure Appl Chem* 58:1193–1206
101. Barigelletti F, Juris A, Balzani V, Belser P, Von Zelewsky A (1987) *J Phys Chem* 91:1095–1098
102. Kawanishi Y, Kitamura N, Tazuke S (1989) *Inorg Chem* 28:2968–2975
103. Meyer TJ (1989) *Account Chem Res* 22:163–170
104. Ryu CK, Schmehl RH (1989) *J Phys Chem* 93:7961–7966
105. Balzani V, Barigelletti F, De Cola L (1990) *Top Curr Chem* 158:31–71
106. Lumpkin RS, Kober EM, Worl LA, Murtaza Z, Meyer TJ (1990) *J Phys Chem* 94:239–243
107. Wang R, Vos JG, Schmehl RH, Hage R (1992) *J Am Chem Soc* 114:1964–1970
108. Caspar JV, Meyer TJ (1983) *Inorg Chem* 22:2444–2453
109. Caspar JV, Meyer TJ (1983) *J Am Chem Soc* 105:5583–5590
110. Durham B, Caspar JV, Nagle JK, Meyer TJ (1982) *J Am Chem Soc* 104:4803–4810
111. Hager GD, Crosby GA (1975) *J Am Chem Soc* 97:7031–7037
112. Barigelletti F, Sandrini D, Maestri M, Balzani V, Von Zelewsky A, Chassot L, Joliet P, Maeder U (1988) *Inorg Chem* 27:3644–3647
113. Barigelletti F, De Cola L, Balzani V, Belser P, Von Zelewsky A, Vvgtle F, Ebmeyer F, Grammenudi S (1989) *J Am Chem Soc* 111:4662–4668
114. Sudhakar M, Djurovich PI, Hogen-Esch TE, Thompson ME (2003) *J Am Chem Soc* 125:7796–7797
115. Chen FC, He GF, Yang Y (2003) *Appl Phys Lett* 82:1006–1008
116. Sun YR, Giebink NC, Kanno H, Ma BW, Thompson ME, Forrest SR (2006) *Nature* 440:908–912
117. Nonoyama M (1974) *Bull Chem Soc Jpn* 47:767–768
118. Carlson GA, Djurovich PI, Watts RJ (1993) *Inorg Chem* 32:4483–4484
119. Bettington S, Tavasli M, Bryce MR, Batsanov AS, Thompson AL, Al Attar HA, Dias FB, Monkman AP (2006) *J Mater Chem* 16:1046–1052
120. Cavazzini M, Pastorelli P, Quici S, Loiseau R, Campagna S (2005) *Chem Commun* 5266–5268
121. Lafolet F, Welter S, Popovic Z, De Cola L (2005) *J Mater Chem* 15:2820–2828
122. Plummer EA, Hofstraat JW, De Cola L (2003) *Dalton Trans* 2080–2084
123. Neve F, Crispini A, Serroni S, Loiseau F, Campagna S (2001) *Inorg Chem* 40:1093–1101
124. Vandiemmen JH, Hage R, Haasnoot JG, Lempers HEB, Reedijk J, Vos JG, De Cola L, Barigelletti F, Balzani V (1992) *Inorg Chem* 31:3518–3522
125. Tsuboyama A, Takiguchi T, Okada S, Osawa M, Hoshino M, Ueno K (2004) *Dalton Trans* 1115–1116

126. Ortmans I, Didier P, Kirsch-Demesmaeker A (1995) *Inorg Chem* 34:3695–3704
127. Vogler LM, Scott B, Brewer KJ (1993) *Inorg Chem* 32:898–903
128. Serroni S, Juris A, Campagna S, Venturi M, Denti G, Balzani V (1994) *J Am Chem Soc* 116:9086–9091
129. Welter S, Lafalet F, Cecchetto E, Vergeer F, De Cola L (2005) *Chem Phys Chem* 6:2417–2427
130. Coppo P, Duati M, Kozhevnikov VN, Hofstraat JW, De Cola L (2005) *Angew Chem Int Ed* 44:1806–1810
131. Haider JM, Williams RM, De Cola L, Pikramenou Z (2003) *Angew Chem Int Ed* 42:1830–1833
132. Baranoff E, Griffiths K, Collin JP, Sauvage JP, Ventura B, Flamigni L (2004) *New J Chem* 28:1091–1095
133. Arm KJ, Williams JAG (2006) *Dalton Trans* 2172–2174
134. Pawlowski V, Kunkely H, Vogler A (2004) *J Photochem Photobiol A-Chem* 161:95–97
135. Flamigni L, Baranoff E, Collin JP, Sauvage JP (2006) *Chem-Eur J* 12:6592–6606
136. Namdas EB, Ruseckas A, Samuel IDW, Lo SC, Burn PL (2004) *J Phys Chem B* 108:1570–1577
137. Tavasli M, Bettington S, Bryce MR, Al Attar HA, Dias FB, King S, Monkman AP (2005) *J Mater Chem* 15:4963–4970
138. Evans NR, Devi LS, Mak CSK, Watkins SE, Pascu SI, Kohler A, Friend RH, Williams CK, Holmes AB (2006) *J Am Chem Soc* 128:6647–6656
139. Bridgewater JS, Vogler LM, Molnar SM, Brewer KJ (1993) *Inorg Chim Acta* 208:179–188
140. Molnar SM, Nallas G, Bridgewater JS, Brewer KJ (1994) *J Am Chem Soc* 116:5206–5210
141. Baranoff E, Dixon IM, Collin JP, Sauvage JP, Ventura B, Flamigni L (2004) *Inorg Chem* 43:3057–3066
142. Dixon IM, Collin JP, Sauvage JP, Barigelletti F, Flamigni L (2000) *Angew Chem Int Ed* 39:1292
143. Flamigni L, Dixon IM, Collin JP, Sauvage JP (2000) *Chem Commun* 2479–2480
144. Dixon IM, Collin JP, Sauvage JP, Flamigni L (2001) *Inorg Chem* 40:5507–5517
145. Flamigni L, Barigelletti F, Armaroli N, Collin JP, Sauvage JP, Williams JAG (1998) *Chem-Eur J* 4:1744–1754
146. Flamigni L, Barigelletti F, Armaroli N, Ventura B, Collin JP, Sauvage JP, Williams JAG (1999) *Inorg Chem* 38:661–667
147. Baranoff E, Barigelletti F, Bonnet S, Collin JP, Flamigni L, Mobian P, Sauvage JP (2006) *Struct Bond* DOI: 10.1007/1430
148. Marcus RA, Sutin N (1985) *Biochim Biophys Acta* 811:265–322

Photochemistry and Photophysics of Coordination Compounds: Platinum

J. A. Gareth Williams

Department of Chemistry, University of Durham, Durham DH1 3LE, UK
j.a.g.williams@durham.ac.uk

1	Introduction	207
1.1	Content and Organization of the Chapter	211
2	Pt Complexes with Bidentate N[^]N Ligands	212
2.1	Pt(N [^] N)X ₂ (X = Halide)	212
2.2	Pt(N [^] N)(C≡N) ₂	217
2.3	Pt(N [^] N)(C≡CR) ₂	218
2.3.1	Applications of Acetylide Complexes	225
2.4	Pt(N [^] N)(S [^] S) and Pt(N [^] N)(S-R) ₂	227
2.4.1	Photo-oxidation Chemistry of Thiolate Complexes	232
2.4.2	Dimeric and Trimeric Complexes with Bridging Sulfurs	233
2.5	Pt(N [^] N)X ₂ (X = N-, C- and O-coordinating Ligands)	235
3	Pt complexes with N[^]N[^]N Terdentate Ligands	237
3.1	Introduction	237
3.2	[Pt(tpy)Cl] ⁺	238
3.3	[Pt(tpy)X] ⁺	239
3.4	[Pt(4'-R-tpy)Cl] ⁺	241
3.4.1	R = -C≡N or Heteroatom	241
3.4.2	R = Aryl	242
3.5	[Pt(tpy)(-C≡CR)] ⁺	244
3.6	[Pt(N [^] N [^] N)X] ⁺ with other N [^] N [^] N Ligands	247
4	Cyclometallated Complexes	250
4.1	Introduction	250
4.2	Pt(N [^] C) Complexes with Bidentate Ligands	251
4.3	Pt(N [^] N [^] C) Complexes	255
4.4	Pt(N [^] C [^] N) Complexes	258
4.5	Pt(C [^] N [^] C) and Pt(C [^] C) Complexes	262
5	Concluding Remarks	263
	References	264

Abstract This chapter provides an overview of the luminescence properties of platinum(II) complexes, exploring how the excited states involved in emission are influenced by the ligands around the metal ion. The square planar nature of d⁸ Pt(II) complexes has many implications, leading to properties and applications that are not open to d⁶ complexes. For example, axial intermolecular interactions can lead to new excited states not present in the isolated molecules. This review focuses on complexes containing one or

more chelating ligands, of which at least one contains a heterocyclic ring such as pyridine. Thus, we explore the properties of a range of bipyridyl (bpy) and terpyridyl (tpy) complexes, and how they are influenced by the identity of the other ligands that complete the coordination sphere of the Pt(II) ion, such as halide, cyanide, thiolates and acetylides. We consider the sometimes dramatic influence of substituents in the bpy/tpy ligands in producing other excited states that may be much more intensely emissive than those of the parent complexes. The influence of cyclometallation on excited states is discussed, and how it can lead to highly emissive complexes: a range of cyclometallated systems are reviewed, with bidentate and terdentate ligands incorporating one or more metal-carbon bonds. Contemporary applications in areas such as sensors, photoinduced electron transfer, and organic light-emitting devices are highlighted.

Keywords Platinum · Excited states · Luminescence · Emission · OLEDs · Sensors

Abbreviations

acac	Acetylacetonate
2ap	2-aminopyridine
4ap	4-aminopyridine
bbtb	2,6-bis(benzothiazole)benzene
bdt	1,2-benzenedithiolate
BIP	2,6-bis(2'-indolyl)pyridine
bph	biphenyl dianion
bpy	2,2'-bipyridine
bt	2-phenyl-benzothiazolato- <i>N</i> , <i>C</i> ^{2'}
bt _p	2-2'-(4',5'-benzo)thienylpyridinato- <i>N</i> , <i>C</i> ^{3'}
bzimpy	2,6-bis(benzimidazol-2-yl)pyridine
bzq	Benzoquinoline
cmc	Critical micelle concentration
CS	Charge-separated
dap	2,6-diaminopyridine
dbbpy	4,4'-di- <i>tert</i> -butyl-2,2'-bipyridine
DCM	Dichloromethane
46dfp-4dmapy	2-(4',6'-difluorophenyl)-4-(dimethylamino)-pyridinato- <i>N</i> , <i>C</i> ^{2'}
46dfppy	2-(4',6'-difluorophenyl)pyridinato- <i>N</i> , <i>C</i> ^{2'}
DFT	Density functional theory
DMF	<i>N,N</i> -dimethylformamide
dmdpybH	4-(<i>p</i> -(dimethylamino)phenyl)-2,6-dipyridyl-benzene
dmpz	3,5-dimethylpyrazole
dpdt	Meso-1,2-diphenyl-1,2-ethanedithiolate
dpm	Dipivaloylmethane
dppm	bis(diphenylphosphino)methane
dpphen	4,7-diphenyl-1,10-phenanthroline
dppyH ₂	2,6-diphenylpyridine
dpybH	2,6-di(2-pyridyl)benzene
dpypz	2,3-di(2-pyridyl)-pyrazine
edt	1,2-ethanedithiolate
en	1,2-ethylenediamine
ENDOR	Electron nuclear double resonance
EPR	Electron paramagnetic resonance (or electron spin resonance, ESR)

ILCT	Intraligand charge transfer
ISC	Intersystem crossing
LB	Langmuir–Blodgett
LC	Ligand centered
LLCT	Ligand-to-ligand charge transfer (= interligand charge transfer)
MC	Metal-centered
MeTHF	2-methyl-tetrahydrofuran
MLCT	Metal-to-ligand charge transfer
MMLCT	Metal–metal bond-to-ligand charge transfer
PET	Photoinduced electron transfer
phbpy	6-phenyl-2,2'-bipyridine
phen	1,10-phenanthroline
php	2-pyridyl-1,10-phenanthroline
ppy	2-phenylpyridinato
pq	2-phenylquinolyl- <i>N,C'</i>
PTZ	Phenothiazine
PVK	Poly(vinylcarbazole)
py	Pyridine
pyr	Pyren-1-yl
pz	pyrazole
RT	Room temperature
salen	<i>N,N'</i> -bis(salicylidene)-1,2-ethylenediamine
tbtpy	4,4',4''-tris- <i>tert</i> -butyl-2,2':6',2''-terpyridine
tbcda	1-(<i>tert</i> -butylcarboxy)-1-cyanoethylene-2,2-dithiolate
tda	Tolan-2,2'-diacetylde
TD-DFT	Time-dependent density functional theory
tdt	Toluene-3,4-dithiolate
thpy	2-(2'-thienyl)pyridine
tmen	<i>N,N,N',N'</i> -tetramethylethylenediamine
tmphen	3,4,7,8-tetramethyl-1,10-phenanthroline
tmpz	3,4,5-trimethylpyrazole
tpy	2,2':6',2''-terpyridine
tpty	4'- <i>p</i> -tolyl-2,2':6',2''-terpyridine
TRIR	Time-resolved infra-red

1

Introduction

The third row transition element platinum, along with nickel and palladium, constitute Group 10 of the periodic table. The most important oxidation state in this group is the +2, with electronic configuration d^8 . Consideration of a simple ligand-field splitting diagram reveals why d^8 metal ions have a thermodynamic preference to form square planar complexes in the presence of strong-field ligands: this geometry pushes a single unoccupied orbital to high energies, whilst allowing substantial stabilization of three of the occupied orbitals (Fig. 1). For nickel(II), it requires strong field ligands like CN^- to induce the switch-over from octahedral geometry, but for Pt(II), the ligand field is

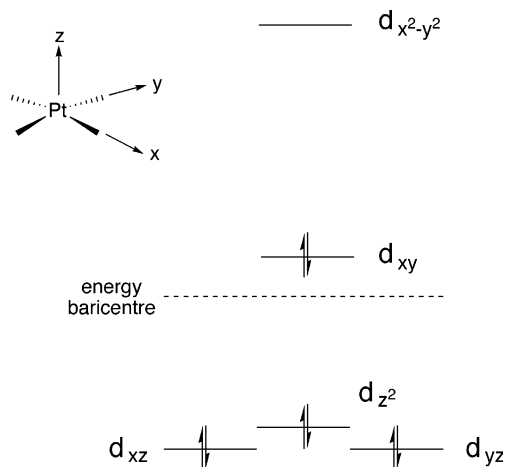


Fig. 1 Simple ligand field-splitting diagram for metal d orbitals in a square planar complex. By convention, the z axis is perpendicular to the plane of the complex and the M – L bonds lie along the x and y axes. Note that the exact ordering of the lower energy levels depends on the ligand set (e.g., relative importance of σ - and π -effects) but the $d_{x^2-y^2}$ is always unequivocally the highest

almost always sufficiently large to ensure that Pt(II) complexes are square-planar.

It is the 4-coordinate square-planar geometry that makes Pt(II) complexes very different from those of most of the other metal ions familiar to the inorganic photochemist, including Cr(III), Ru(II), Os(II), Rh(III), Ir(III) (almost always 6-coordinate octahedral), copper(I) (4-coordinate tetrahedral), and lanthanides (8 or 9 coordinate). The square planar conformation is responsible for many of the key features that characterize the absorption, luminescence and other excited state properties of platinum(II) complexes.

Ligand Field (d-d) Excited States are Subject to Efficient Non-radiative Decay

The $d_{x^2-y^2}$ orbital is strongly antibonding. If this orbital is populated through absorption of light, then the molecule will undergo a significant distortion upon formation of the excited state and Pt – L bond lengths increase. We can represent this in a simplified visual way, in terms of the d-d excited state potential energy surface having an energy minimum that is markedly displaced compared to the ground state (Fig. 2a). This is an unfavorable scenario for luminescence from an excited state, owing to the thermal accessibility of the isoenergetic crossing point where non-radiative internal conversion or inter-system crossing to the ground state can occur. One of the consequences is that platinum complexes with simple inorganic ligands (e.g., $\text{Pt}(\text{NH}_3)_4^{2+}$, PtCl_4^{2-}) are unlikely to be luminescent in fluid solution or are, at best, only weakly

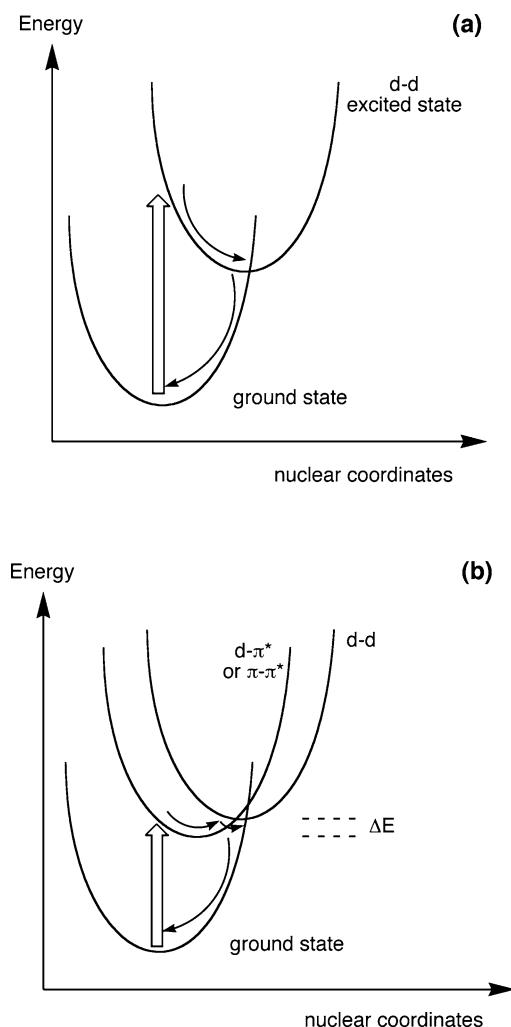


Fig. 2 **a** Illustrating the displacement of the potential energy surface for the d-d excited state in a square planar d^8 complex, formed by population of the $d_{x^2-y^2}$ orbital, compared to the ground state. **b** Even though other excited states (e.g., $d-\pi^*$ or $\pi-\pi^*$) may lie at lower energies, the d-d excited state can provide a thermally activated non-radiative decay pathway. *Thick arrows* represent absorption of light; *thin ones* indicate vibrational relaxation and non-radiative decay

so. The rate constant of non-radiative decay $\sum k_{nr}$ is large, and the problem is further exacerbated by the radiative decay rate constant k_r being typically small for Laporte-forbidden d-d transitions. In the solid state or at low temperatures, distortion of molecules is inhibited to some extent, and emission can then be observed in some instances. Pertinent examples accompanied by citations will be provided in the sections that follow [1].

Ligand Field (d-d) Excited States can Provide a Thermally Activated Deactivation Pathway for Other, Lower-lying Excited States

The introduction of conjugated aromatic ligands around a metal ion introduces ligand-centered (LC) (π - π^* or n - π^*) and charge-transfer (e.g., metal-to-ligand charge-transfer, MLCT, d - π^*) excited states into the picture. In many Pt(II) complexes, either the MLCT or the LC states, or indeed both, may lie at lower energies than the d-d states, and have intrinsically faster k_r values than the d-d (Fig. 2b). However, the d-d excited state, lurking in the background, can still exert a deleterious effect on luminescence, particularly at room temperature, since it may be thermally accessible from the lowest-energy excited state (when ΔE in Fig. 2b is comparable to kT) and hence serve as a pathway of non-radiative deactivation—effectively a drain pipe for the excited state energy. As we shall see in the subsequent sections, the most emissive Pt complexes are generally those where ΔE is large, either as a result of the emissive state being low in energy, or because the d-d state has been raised to relatively inaccessible energies.

The Planar Nature of the Complexes Allows Axial Interactions

In this respect, Pt(II) complexes are very different from those of 6-coordinate d^6 complexes, which present an effectively spherical profile to their environment. Square planar platinum complexes with sterically undemanding ligands are essentially flat, and this allows close, intimate interactions, either with other identical molecules (e.g., intermolecular stacking or dimerization in the ground state; excimer formation in the excited state) or with other molecules (e.g., exciplex formation with Lewis bases). Ground-state stacking of platinum(II) complexes may involve very specific metal-metal interactions: the d_{z^2} orbital is perpendicular to the plane of the molecule, and an intermolecular separation of the order 3–3.5 Å is appropriate for the d_{z^2} orbitals of adjacent molecules to interact in an end-on manner to form weakly bonding and antibonding $d\sigma$ and $d\sigma^*$ molecular orbitals (Fig. 3). Such interactions have long been known, and they underpinned intensive investigations of platinum complexes as one-dimensional, electrically conducting, molecular materials in the 1970s [2, 3]. In the context of optical spectroscopy and excited states, one of the implications of such interactions is that the highest occupied metal-based molecular orbital is raised in energy compared to that of the isolated molecules, so that lowest-energy optical transitions are shifted to lower energies. This can lead to a switch over in the nature of the lowest-energy excited state; for example, in Fig. 3, from π - π^* in the isolated monomers to $d\sigma^*$ - π^* in the presence of such interactions.

For complexes with planar, conjugated aromatic ligands, π - π interactions between the ligands of adjacent molecules are also possible. They are some-

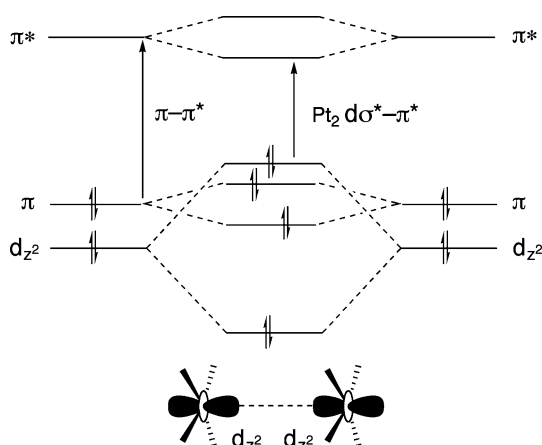


Fig. 3 Simplified frontier molecular orbital diagram showing the effect of face-to-face interactions and intermolecular d_{z^2} orbital overlap. In this example, such interaction leads to a change in the nature of the lowest-energy excited state from $\pi-\pi^*$ (ligand-centred or LC) to $d\sigma^*-\pi^*$ (metal-metal bond-to-ligand charge transfer or MMLCT)

what less sensitive to the intermolecular separations and precise dispositions of one molecule relative to the other, but can give rise to broadly similar effects.

A further key feature is the importance of the triplet states, a feature shared with other third row and many second row transition metal ions. The high spin-orbit coupling constant ξ of platinum promotes rapid intersystem crossing (ISC) from singlet to triplet excited states. For excited states with significant contribution from metal-based orbitals, ISC is normally thought to occur at a rate constant of the order of 10^{12} s^{-1} [4], which greatly exceeds typical radiative rate constants from singlet excited states ($\sim 10^8 \text{ s}^{-1}$). Thus, the observed luminescence from Pt complexes is typically anticipated to emanate from states of triplet character (unless the excited state is localized on a remote part of the ligand well removed from the metal center). The triplet-singlet transition, which gives rise to phosphorescence, is formally forbidden in purely organic systems, with a rate constant (typically $< 10^3 \text{ s}^{-1}$) that is too slow to allow phosphorescence to compete with non-radiative decay at room temperature. But in the presence of the Pt(II) ion with its high ξ parameter, $k_r(\text{T} \rightarrow \text{S})$ is accelerated typically to values of the order of 10^5 – 10^7 s^{-1} , and triplet emission on the microsecond timescale can then be observed ... provided, of course, that non-radiative decay channels do not drain the excited state faster by other pathways!

1.1

Content and Organization of the Chapter

In the sections which follow, the principles discussed above will be used in exploring the properties of a range of platinum(II) complexes. The emphasis of the chapter will be on emission—*luminescence*—from Pt(II) complexes, on the features and properties of molecules that tend to favor emission over other non-radiative processes. In other words, photophysics, as opposed to photochemistry, is our main subject here, but we also consider other excited state processes in selected systems, such as electron transfer and photooxidation.

Space constraints require selectivity in coverage, and we have chosen to focus this contribution on those complexes that contain at least one chelating ligand incorporating an *N*-heterocyclic ring (normally pyridine). This embraces all those complexes with ligands such as bipyridine, phenanthroline and terpyridine, as well as their cyclometallating cousins in which one or more of the pyridines is replaced by a phenyl ring. The selection is largely justified on the basis that it is such compounds that have constituted the vast majority of research into the development of luminescent platinum(II) complexes over the past decade. However, there are notable omissions, including many studies on platinum porphyrins and on Pt(II) ions incorporated into π -conjugated polymers. On the other hand, porphyrinic studies tend to be aimed at applied work (e.g., use in oxygen sensors and in luminescence microscopy and bioimaging [5, 6]) rather than on intrinsically new photophysics, whilst the polymer work deals with environments and issues that are rather different from those normally relevant to discrete Pt complexes [7, 8].

We begin with complexes containing one bidentate ligand coordinating through two nitrogen atoms – the designation $N^{\wedge}N$ is used to represent such a chelation mode – followed by terdentate $N^{\wedge}N^{\wedge}N$ -coordinating systems and then bi- and terdentate cyclometallated systems. Individual sections are subdivided according to the nature of the other ligands that complete the platinum ion's coordination sphere.

2

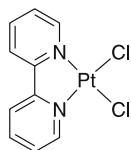
Pt Complexes with Bidentate $N^{\wedge}N$ Ligands

2.1

$Pt(N^{\wedge}N)X_2$ ($X = \text{Halide}$)

We start our discussion with what at first sight seems like one of the simplest of possible complexes, namely $Pt(bpy)Cl_2$, **1**. That the system is not simple after all is immediately apparent from the fact that it may exist in either yellow or red polymorphs. A detailed investigation of the emission

properties of the two forms, and of a number of derivatives, was carried out by Miskowski et al. [9, 10], and the results provide a useful foundation for understanding many Pt(II) complexes prepared more recently. The yellow form displays a broad, Gaussian-shaped structureless emission band in the solid state at 300 K, centred at around 640 nm. The bands become narrower upon cooling, but do not shift significantly, nor is any vibronic structure resolved even at 10 K. Pt(phen)Cl₂ behaves similarly. Such properties are characteristic of metal-centred (MC) d-d states: according to a classical description, the reduced amplitude of M–L vibrations at low temperatures simply results in a smaller spread in the ligand-field strengths. The d-d assignment is reinforced by the similarity of the spectra to that displayed by [Pt(tmen)Cl₂], where the absence of π -conjugated ligands rules out the possibility of any low-energy MLCT or LC states (tmen = N,N,N',N'-tetramethylethylenediamine).



1

The red form of Pt(bpy)Cl₂ displays a very similar emission maximum to the yellow form, but the spectral profile is more asymmetric, and narrows sharply and red-shifts upon cooling (Fig. 4, inset). At 10 K, a shoulder is resolved, 1500 cm⁻¹ to lower energy of the maximum, indicative of the involvement of the bpy ligand in the excited state through its characteristic vibrational mode, and thus suggestive of an MLCT state. The switch in the nature of the emissive excited state between the two forms is attributed to Pt–Pt interactions in the red form, which has a linear-chain structure with a Pt–Pt distance of 3.45 Å. As briefly introduced in Sect. 1, overlap of two Pt d_{z2} orbitals generates an antibonding (d σ^*) orbital that lies higher in energy than the isolated d_{z2} orbital, and the d $\sigma^* \rightarrow \pi^*$ (metal–metal-to-ligand charge transfer, or MMLCT) excited state energy is thus expected to decrease as the metal–metal distance decreases and the interaction strengthens. This accounts for the observed red-shift upon cooling: as the temperature decreases, the lattice contracts and the Pt–Pt distance shortens. The phenomenon has been quantified by means of variable-temperature X-ray crystallography [11]. The unit cell contracts anisotropically: the *c* axis (normal to the plane of the molecule) decreases to 97.6% of the room temperature value at 20 K, with a concomitant shortening of the Pt–Pt distance *R* by 0.08 Å. The emission energy decreases approximately linearly with *R*⁻³ (Fig. 4), in a manner resembling that previously found for stacked Pt(CN)₄²⁻ complexes [12].

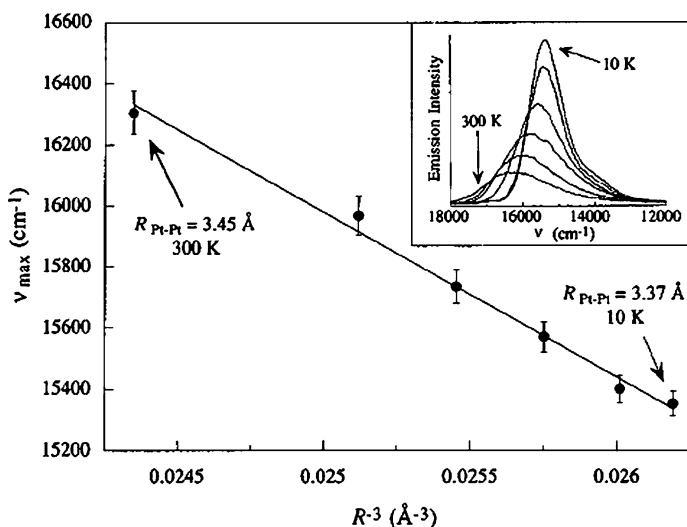


Fig. 4 Emission peak energy (ν_{max}) of the red form of $\text{Pt}(\text{bpy})\text{Cl}_2$ **1** as a function of the inverse cube of the Pt–Pt separation R [10]. The data were obtained from variable temperature X-ray crystallography. The *solid line* is the linear fit to the equation: $\nu_{\text{max}} = 29.5(55) \times 10^3 - 5.4(3) \times 10^5 R^{-3}$. The *inset*, adapted from reference [1], shows six emission spectra at different temperatures: 300, 200, 150, 100, 50 and 10 K. Reprinted with permission from [11]. © (1996) American Chemical Society

A linear decrease in the emission energy is also observed as a function of increasing pressure in the range 1 bar–17.5 kbar, over which range R is predicted to decrease by a further 0.2 \AA [13]. At a pressure of 17.5 kbar, there is an abrupt crystallographic phase transition accompanied by an increase in emission energy of 2500 cm^{-1} , a substantial broadening in the emission spectrum, and a large decrease in the emission intensity. These changes are interpreted in terms of a crystallographic phase transition to a form resembling the yellow form, a $^3\text{d-d}$ emitter.

Whilst the Pt–Pt interaction nicely explains why the HOMO in red $\text{Pt}(\text{bpy})\text{Cl}_2$ is metal-based, rather than ligand-based as it is in $[\text{Pt}(\text{bpy})(\text{en})]^{2+}$ for example, the differing behavior between the yellow and red forms of $\text{Pt}(\text{bpy})\text{Cl}_2$, namely d-d and MMLCT emitters respectively, clearly requires that the localization of the LUMO be different. Evidently, the stabilization of the π^* orbital arising from face-to-face orbital overlap (Fig. 3) is sufficient to lower it to an energy less than that of the metal-based antibonding orbital (in effect, the $d_{x^2-y^2}$ orbital). A switch to MLCT emission was observed in the complex $\text{Pt}(3,3'-(\text{MeCO}_2)_2\text{-bpy})\text{Cl}_2$ in the solid state [10], where the π^* energy is lowered as a result of the introduction of electron-withdrawing ester groups, as opposed to through stacking effects. These effects are summarized in Fig. 5.

In solution, electrochemical studies in conjunction with EPR and ^1H EN-DOR spectroscopy indicate that, for many $\text{Pt}(4,4'\text{-R}_2\text{-bpy})\text{Cl}_2$ derivatives (e.g.,

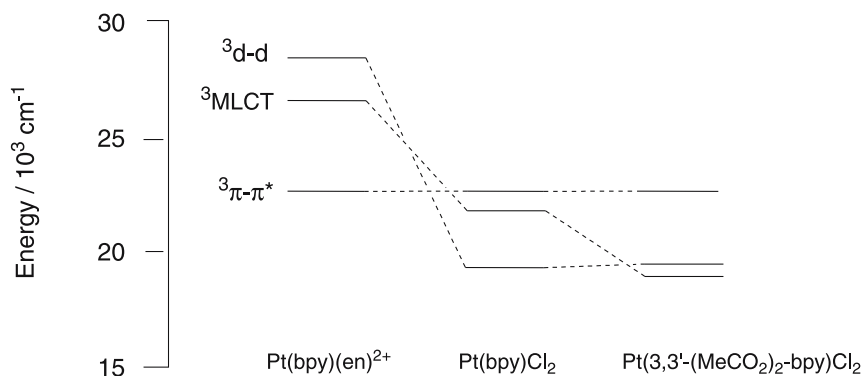


Fig. 5 Estimates of the energies of the low-lying triplet ligand-centred ($\pi-\pi^*$), charge-transfer (MLCT) and metal-centred (d-d) excited states of three platinum(II) bipyridyl complexes. Reproduced from data in [10] with permission. © (1993) American Chemical Society

R = NH₂, OEt, Me, H, Ph, Cl, CO₂Me), the singly occupied molecular orbital formed upon reduction is based predominantly on the bpy ligand [14]. The lowest energy excited states for such complexes in solution might thus be expected to be MLCT. However, these simple dihalo complexes are essentially non-emissive in fluid solution, owing to very rapid non-radiative deactivation, probably via the low-lying d-d state as discussed in Sect. 1. Unambiguous assignment of the lowest-energy excited states is therefore a difficult task. Faced with this quandary, Weinstein, George et al. have carried out a picosecond time-resolved infra-red (TRIR) study of the ester-functionalized complex Pt(4,4'-(EtCO₂)₂-bpy)Cl₂ [15]. TRIR is essentially a form of flash photolysis in which UV/visible laser excitation promotes a significant proportion of molecules to the excited state, which are then probed using fast IR absorption spectroscopy [16]. A strongly IR-active chromophore is required in an unambiguous portion of the IR spectrum, and bonds such as ester C=O, cyanide $-C\equiv N$ and acetylide $-C\equiv CR$ are often ideal. Picosecond TRIR spectra of Pt(4,4'-(EtCO₂)₂-bpy)Cl₂ were recorded at several time intervals in the range 0.5–200 ps after excitation at 400 nm (150 fs pulses). The representative spectra shown in Fig. 6 show the initial bleaching of the carbonyl ground-state absorption and formation of new $\nu(CO)$ bands 16 cm^{-1} to lower energy, followed by their rapid recovery to the baseline over a period of < 100 ps [15]. The negative shift of the $\nu(CO)$ band indicates an increase of electron density on the ester groups upon excitation, which is consistent with an MLCT assignment of the excited state. The recovery of the ground-state bands follows mono-exponential kinetics, with a lifetime of $8.7 \pm 0.8 \text{ ps}$.

Results of studies such as these reveal that the excited states of Pt(N^N)Cl₂ complexes are normally short-lived in solution, too short for emission to compete with the rapid non-radiative decay, accounting for the lack of lu-

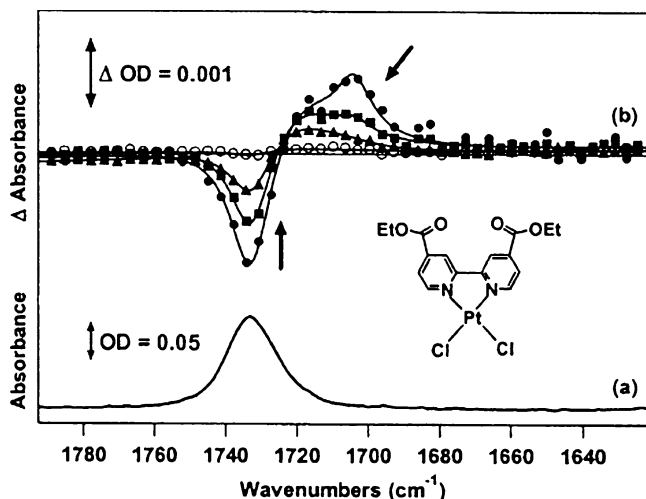
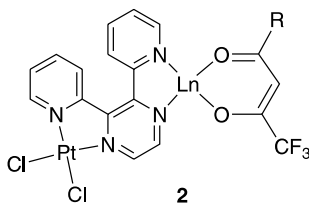


Fig. 6 **a** Ground-state IR spectrum of Pt(4,4'-(EtCO₂)₂-bpy)Cl₂ in CH₂Cl₂. **b** TRIR spectra obtained at 1.5 ps (solid circles), 4 ps (squares), 11 ps (triangles) and 50 ps (open circles) after excitation at 400 nm (150 fs pulse). Solid lines represent curve-fitted spectra and arrows indicate movement of the bands with increasing time delay following excitation. Reprinted from [15] by permission of the Royal Society of Chemistry

minescence in solution. On the other hand, it appears that the lifetime can be sufficiently long for energy transfer to suitable receptors to occur. For example, Ward and co-workers have demonstrated that the Pt(dpypz)Cl₂ moiety in **2** {dpypz = 2,3-di(2-pyridyl)-pyrazine} can be used to sensitize luminescence from near-IR emitting lanthanide ions (e.g., Ln = Nd³⁺, Er³⁺, Yb³⁺ in **2**), whose emissive excited states are sufficiently low in energy to be populated by a large variety of chromophores that absorb in the visible region [17]. Clearly, some energy transfer from the platinum center to the lanthanide ion must be occurring before complete deactivation has occurred. Time-resolved kinetic studies suggest that the rate constant for energy transfer exceeds $2 \times 10^8 \text{ s}^{-1}$ although a quantitative assessment of the efficiency of energy transfer would require quantum yields of the near-IR emission.

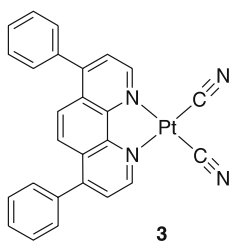


2.2

Pt(N[^]N)(C≡N)₂

These complexes provide a good introduction into the phenomena of self-quenching and excimer formation in solution. The substitution of weak-field halide ligands by strong-field cyanides lowers the energy of the highest-occupied metal-centred orbitals to below the highest π orbital of the bpy ligand. Thus, the lowest-energy excited states of Pt(N[^]N)(CN)₂ complexes are typically π - π^* in character. Moreover, the strong ligand field also raises the vacant $d_{x^2-y^2}$ orbital, so that deactivation via cross-over to the strongly distorted metal-centred states is reduced, and emission from fluid solutions at room temperature is observable. Typically, the emission spectra show clearly resolved structure, with vibrational spacings of around 1400 cm⁻¹ corresponding to the C = N and C = C stretches of the aromatic diimine, and lifetimes are on the microsecond timescale [18].

The planar nature of the complexes, coupled with the long-lifetimes of the excited states, favor intermolecular interactions and self-quenching, sometimes accompanied by excimer formation [19]. For example, Pt(5,5'-Me₂-bpy)(CN)₂ has a quantum yield of 10⁻³ in acetonitrile at room temperature, but the emission intensity and lifetime decrease with increasing concentration [18]. A linear Stern-Volmer relationship between 1/ τ and [Pt(II)] was found, from which a lifetime at infinite dilution (τ_0) of 6.3 μ s could be extrapolated [18]. Subsequent work on more soluble derivatives allowed behavior at higher concentrations to be assessed, under which conditions excimer formation has been observed [20,21]. For example, Pt(dpphen)(CN)₂ **3** (dpphen = 4,7-diphenyl-1,10-phenanthroline) displays green emission centred at 520 nm in dilute CH₂Cl₂ (10⁻⁵ M), but an increase in concentration is accompanied by the appearance of a red emission band, centred at 615 nm, which grows in at the expense of the green band, with an identical excitation spectrum [20]. The red emission is attributed to an excimer, analogous to well-known examples amongst planar organic compounds such as pyrene, and formed from the bimolecular interaction of an excited monomer with a ground-state monomer. Much higher concentrations are possible in polyethylene glycol solution, which allow a point to be reached where the green monomer emission is completely



replaced by the red excimer emission. Similar behavior was observed by Che et al. for Pt(dbbpy)(CN)₂, where excimer formation ($\lambda_{\text{max}} = 565 \text{ nm}$) in 1,2-dichloroethane is facilitated by the long monomer lifetime ($3 \mu\text{s}$, $\lambda_{00} = 456 \text{ nm}$) [21]. Time-resolved studies showed that the excimer emission does not reach a maximum until about 100 ns after excitation, reflecting the bimolecular nature of the process of excimer formation. Data for these complexes, and for representative examples of all complexes discussed in this Chapter which are emissive in solution at room temperature, are summarized in Table 1.

Nagle et al. have reviewed the kinetic scheme that underlies excimer formation, as it applies to Pt complexes [19]. A plot of $I_{\text{D}}/I_{\text{M}}$ (integrated emission intensities of excimer and monomer bands, respectively) versus concentration of the complex should be linear. The slope is determined by all the rate constants of formation and decay of both excimer and monomer, but is approximately related to the equilibrium constant for excimer formation. Typically for Pt complexes that do show excimer emission, the rate constants for formation and subsequent decay of the excimer are substantially larger than monomer decay. The decay of both monomer and excimer are thus governed by the rate of excimer formation, leading to nearly identical decay kinetics for the two species.

Despite the unambiguous $\pi\text{-}\pi^*$ assignment of the lowest excited state of Pt(N[^]N)(CN)₂ complexes in solution, Pt–Pt interactions in the solid state can raise the energy of filled metal d_{z²} orbitals beyond the ligand π , just as they do for the red form of Pt(bpy)Cl₂. Thus, Pt(bpy)(CN)₂ forms a red crystalline solid, with a Pt–Pt distance (R) of 3.35 Å at room temperature [22], the intense red emission of which is assigned to a ³MMLCT [$d\sigma^*(\text{Pt}_2) \rightarrow \pi^*(\text{bpy})$] excited state [23, 24].

2.3

Pt(N[^]N)(C \equiv CR)₂

Investigations into platinum(II) diimine complexes containing acetylide ligands have comprised a major area of interest in platinum chemistry over the past decade. As for X = –C \equiv N, the introduction of strong-field acetylide ligands into the coordination sphere of Pt(II) ensures that the energy of otherwise deactivating metal-centred d-d states is raised, and the complexes are normally quite strongly emissive in fluid solution at room temperature.

The first example of such a complex was reported by Che in 1994, who attributed the broad, structureless, room temperature emission band of Pt(phen)(–C \equiv C–Ph)₂ to a Pt(d)- $\pi^*(\text{phen})$ ³MLCT excited state ($\lambda_{\text{em}} = 578 \text{ nm}$, $\tau = 2.1 \mu\text{s}$ in CH₂Cl₂) [25]. Eisenberg et al. later examined this complex and the 4-tolyl-acetylide and 4-fluorophenyl-acetylide analogues as part of a study of the concentration-dependent self-quenching of square planar Pt(II) complexes [26]. They noted that, in CH₂Cl₂, the self-quenching of

Table 1 Photophysical data for key representative platinum complexes that are emissive in solution at room temperature^a

Complex ^b	$\lambda_{\text{abs}}/\text{nm}^c$ (ϵ) ^d	$\lambda_{\text{em}}/\text{nm}^e$	ϕ_{em}^f	$\tau_{\text{em}}/\text{ns}^g$	Solvent ^h	Assignment ⁱ	Refs.
Pt(dpphen)(CN) ₂ 3	374 (5900)	530 630	- -	100 1000	PEG	³ π - π^* Excimer	[20]
Pt(5,5'-Me ₂ bpy)(CN) ₂	340 (6700)	470, 502, 535	$\sim 10^{-3}$	6300	MeCN	³ π - π^*	[18]
Pt(dbbpy)(CN) ₂	315 (19200) ^j	456, 485, 515 565	- -	3000 -	DCM	³ π - π^* Excimer	[21]
Pt(phen)(-C \equiv C-Ph) ₂	399 (-)	578	-	2100	DCM	³ d- π^* \wedge \wedge \wedge \wedge	[25]
Pt(tmbpy)(-C \equiv C-C ₆ H ₄ - <i>p</i> -Me) ₂ 4	379 (9000)	553	0.27	1300	DCM	³ d- π^* \wedge \wedge \wedge \wedge	[29]
Pt(dbbpy)(-C \equiv C-C ₆ H ₄ - <i>p</i> -Me) ₂ 5	386 (8500)	570	0.11	800	DCM	³ d- π^* \wedge \wedge \wedge \wedge	[29]
Pt(4,4'-bpy-(CONEt ₂) ₂)(-C \equiv C-C ₆ H ₄ - <i>p</i> -Me) ₂ 6	424 (4500)	642	0.007	103	DCM	³ d- π^* \wedge \wedge \wedge \wedge	[29]
Pt(4,4'-bpy-(CO ₂ Et) ₂)(-C \equiv C-C ₆ H ₄ - <i>p</i> -Me) ₂ 7	445 (5500)	670	0.005	20	DCM	³ d- π^* \wedge \wedge \wedge \wedge	[29]
Pt(dbbpy)(-C \equiv C-C ₆ H ₄ - <i>p</i> -CF ₃) ₂ 8	389 (12400)	538	0.21	607	DCM	mixed ³ d- π^* \wedge \wedge / \wedge \wedge	[29]
Pt(dbbpy)(-C \equiv C-C ₆ H ₄ - <i>p</i> -NO ₂) ₂ 9	371 (42000)	561	0.09	3600	DCM	³ π - π^* $\text{C}\equiv\text{C-AR}$ \wedge \wedge	[29]
Pt(dbbpy)(-C \equiv C-C ₆ H ₄ - <i>p</i> -NMe ₂) ₂ 10	454 (6100)	586	0.008	250	DCM	mixed ³ d- π^* \wedge \wedge / \wedge \wedge	[29]
Pt(dbbpy)(-C \equiv C-C ₆ H ₄ - <i>p</i> -OMe) ₂ 11	401 (7500)	623	0.02	60	DCM	³ π Me ₂ - π^* \wedge \wedge \wedge \wedge	[29]
Pt(dbbpy)(tda) 12	427 (12 000)	562	0.52	2560	DCM	³ d- π^* \wedge \wedge \wedge \wedge	[30]
Pt(dbbpy)(-C \equiv C-1-pyrene) ₂ 13	450 (10 300)	662, 722	0.011	48 500	DCM	³ π - π^* $\text{C}\equiv\text{C-pyrene}$	[32]
Pt(dbbpy)tbca 16	437 (12 900)	590 (493) ^k	1.2×10^{-3}	2	DCM	³ d _{pt} /ps - π \wedge \wedge	[43]
Pt(dbbpy)(S ^{\wedge} S-bdt) 21	563 (7200)	720 (643) ^k	1.1×10^{-3}	504	DCM	³ d _{pt} /ps - π \wedge \wedge	[43]

Table 1 (continued)

Complex ^b	$\lambda_{\text{abs}}/\text{nm}^c$ (ϵ) ^d	$\lambda_{\text{em}}/\text{nm}^e$	ϕ_{em}^f	$\tau_{\text{em}}/\text{ns}^g$	Solvent ^h	Assignment ⁱ	Refs.
Pt(tmpphen)(S [^] S-tdt) 22	532 (7160)	675 (639) ^k	5.7×10^{-3}	1020	DCM	$^3\text{d}_{\text{Pt}}\text{p}s - \pi_{\text{N}}^*\text{N}^{\wedge}\text{N}$	[43]
Pt(4,4'-bpy-(CO ₂ Et) ₂)(S [^] S-tdt) 28	679 (10400)	795 (784) ^k	4×10^{-6}	68	DCM	$^3\text{d}_{\text{Pt}}\text{p}s - \pi_{\text{N}}^*\text{N}^{\wedge}\text{N}$	[43]
Pt(N [^] N [^] O [^] O-salen) 34	420 (5000)	550	0.19	3500	MeCN	$^3\text{d}_{\text{Pt}}/\text{p}o - \pi_{\text{imine}}^*$	[57, 58]
Pt(N [^] N [^] O [^] O-2,9-(o-O-C ₆ H ₄) ₂ -dpphen) 35	504 (7200)	586	0.6	5300	DCM	$^3\text{d}_{\text{Pt}}/\text{p}o - \pi_{\text{phen}}^*$	[59]
[Pt(N [^] N [^] N [^] -4'-Me ₂ N-tpy)Cl] ⁺	419 (9290)	535	0.08	1920	DCM	mixed $^3\text{d}_{\text{Pt}}-\pi_{\text{N}}^*\text{N}^{\wedge}\text{N}^{\wedge}\text{N}^{\wedge}/$	[85]
[Pt(N [^] N [^] N [^] -4'-Me ₂ N-tpy)(C \equiv N)] ⁺	415 (9260)	520, 545, 600sh	0.26	22000	DCM	$^3\text{P}_{\text{NMe}_2}-\pi_{\text{N}}^*\text{N}^{\wedge}\text{N}^{\wedge}\text{N}^{\wedge}$	[75]
[Pt(N [^] N [^] N [^] -4'-(pyren-1-yl)-tpy)Cl] ⁺ 37	476 (8990)	640, 685	0.034	6400	DCM	$\text{P}_{\text{NMe}_2}-\pi_{\text{N}}^*\text{N}^{\wedge}\text{N}^{\wedge}\text{N}^{\wedge}$ mixed $^3\pi_{\text{pyr}}-\pi_{\text{tpy}}^*/$	[70, 86]
[Pt(N [^] N [^] N [^] -tpy)(-C \equiv C-benzo-18-C-5)] ⁺ 38	480 (3805)	640 ^l	-	1 ^l	MeCN	$^1\pi_{\text{pyr}}-\pi_{\text{tpy}}^*$ ^k	[93]
Mg ²⁺ adduct	445 (4350)	625	-	-		$^3\text{d}-\pi_{\text{N}}^*\text{N}^{\wedge}\text{N}$	
[Pt(N [^] N [^] N [^] -pnp)Cl] ⁺ 39	421 (2600)	547, 591, 650	3.1×10^{-3}	230	DCM	mixed $^3\pi-\pi^*/^3\text{d}-\pi^*$	[98]
[Pt(N [^] N [^] N [^] -2-(8'-quinoliny)phen)Cl] ⁺ 40	395(-)	555, 590, 660(sh)	2×10^{-3}	310	DCM	$^3\pi-\pi^*/(^3\text{d}-\pi^*)$	[99]
[Pt(N [^] N [^] N [^] -(C ₁₈ H ₃₇) ₂ -bzimpy)Cl] ⁺ 41	382 (19200)	564, 605, 660	-	220, 45 ⁿ	CHCl ₃	$^3\pi-\pi^*$	[100]
[Pt(N [^] N [^] N [^] -BIP)(py)] ⁺ 44	418 (21800)	585	-	11-22	PVKP	$\text{d}\sigma^*(\text{Pt}_2) \rightarrow \pi^*$	[102]
[Pt(N [^] C-ppy)(en)] ⁺ 45 ^(N[^]N=en)	395 (1300)	487	0.058	1700	DMF	$^3\text{d}_{\text{Pt}}-\pi_{\text{N}}^*\text{N}^{\wedge}\text{C}$	[108]
[Pt(N [^] C-ppy)(bpy)] ⁺ 45 ^(N[^]N=bpy)	410sh (1900)	495	0.017	4000	DMF	$^3\text{d}_{\text{Pt}}-\pi_{\text{N}}^*\text{N}^{\wedge}\text{N}$	[108]
Pt(N [^] C-ppy)(acac) 46 ^(R=Me)	410sh (3700) ^q	486	0.15	2600	MeTHF	$^3\text{d}_{\text{Pt}}-\pi_{\text{N}}^*\text{N}^{\wedge}\text{C}/\pi-\pi_{\text{N}}^*\text{N}^{\wedge}\text{C}$	[109]
Pt(N [^] C-46dfppy)(dpm) Fig. 19	394 (3100) ^r	466	0.02	< 1000	MeTHF	$^3\text{d}_{\text{Pt}}-\pi_{\text{N}}^*\text{N}^{\wedge}\text{C}/\pi-\pi_{\text{N}}^*\text{N}^{\wedge}\text{C}$	[109]
Pt(N [^] C-46dfp-4dmapy)(dpm) Fig. 19	365 (6000) ^r	447	v.weak	< 1000	MeTHF	$^3\text{d}_{\text{Pt}}-\pi_{\text{N}}^*\text{N}^{\wedge}\text{C}/\pi-\pi_{\text{N}}^*\text{N}^{\wedge}\text{C}$	[109]

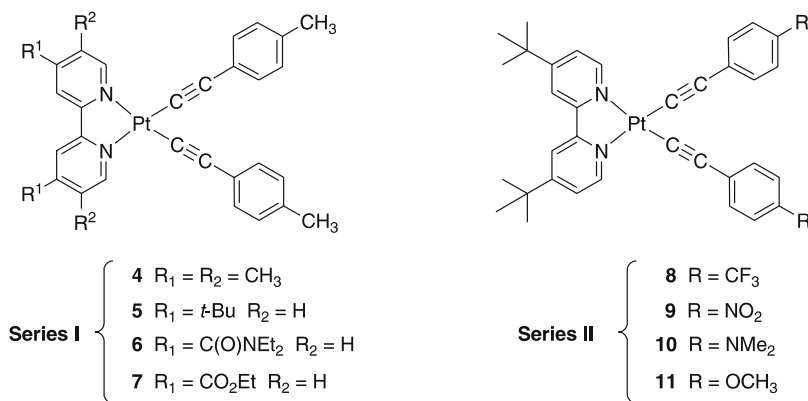
Table 1 (continued)

Complex ^b	$\lambda_{\text{abs}}/\text{nm}^c$ (ε) ^d	$\lambda_{\text{em}}/\text{nm}^e$	ϕ_{em}^f	$\tau_{\text{em}}/\text{ns}^g$	Solvent ^h	Assignment ⁱ	Refs.
Pt(N ^{^A} C-btp)(acac) Fig. 20	444 (6800) ^q	612	0.08	3400	MeTHF	$^3d_{\text{Pt}}-\pi^*/\pi-\pi^*$ $\text{N}^{\wedge}\text{C}^{\wedge}\text{N}^{\wedge}\text{C}$	[109]
Pt(N ^{^A} N ^{^A} C-phbpy)Cl 47 (R=H)	430 (1550)	565	0.025	510	DCM	$^3d_{\text{Pt}}-\pi^*$ $\text{N}^{\wedge}\text{N}^{\wedge}\text{C}$	[120]
Pt(N ^{^A} N ^{^A} C-4'-Ph-phbpy)Cl 47 (R=Ph)	435 (3500)	564	0.052	600	DCM	$^3d_{\text{Pt}}-\pi^*$ $\text{N}^{\wedge}\text{N}^{\wedge}\text{C}$	[120]
[Pt(N ^{^A} N ^{^A} C-phbpy) ₂ (μ -dppm)] ²⁺ 48 (R=H)	504sh (1900)	652	0.015	140	MeCN	$d\sigma^*(\text{Pt}_2) \rightarrow \pi^*$	[120]
Pt(N ^{^A} C ^{^A} N-dpyb)Cl 49 (R=H)	401 (7010)	491, 524, 562	0.60	7200	DCM	$^3\pi-\pi^*$	[130]
		700	-	100		Excimer	
Pt(N ^{^A} C ^{^A} N-dmdpyb)Cl 49 (R=Me ₂ N-C ₆ H ₄ -)	431 (8880)	588	0.54	12 400	DCM	$^3\text{p}_{\text{NMe}_2} - \pi^*$ $\text{N}^{\wedge}\text{C}^{\wedge}\text{N}$	[133]
N-protonated complex							
	410 (7310)	482, 514, 547	0.40	5800		$^3\pi-\pi^*$	
Pt(N ^{^A} C ^{^A} N-bbtb)Cl 50	449 (12 800) ^s	550, 597, 649, 718	0.33 at 77 K	4100	DCM/ THF (3/2)	$^3\pi-\pi^*$	[140]
Pt(C ^{^A} N ^{^A} C-dppy)(py-4-C(O)-N-15aza-C-5) 56	350 (16 070)	505	-	2700	DCM	$^3\pi-\pi^*$	[148]
		625	-	1100		Aggregate	
Pt(C ^{^A} C-bph)(py) ₂ 57 (L=py)	332 (4000)	492	0.15	3200	DCM	$^3\pi-\pi^*$	[149]

^a Data in original literature is specified as having been recorded at "room temperature" or at 298 K, except where stated otherwise; ^b The coordination mode of the ligands is shown in italics, but is omitted for the first 18 entries, all of which refer to bidentate N^{^A}N-coordinating ligands; ^c Position of the longest wavelength absorption band with $\varepsilon > 1000$; ^d ε is the molar absorptivity in units of mol⁻¹ dm³ cm⁻¹; ^e Wavelengths of the maxima in the emission spectra; ^f Luminescence quantum yield; ^g Luminescence lifetime from monoexponential fitting of the decay, except where stated otherwise; ^h The solvent is that in which the emission data was obtained; absorption data refers to the same solvent except where stated otherwise; ⁱ Refers to the likely assignment of the emissive excited state, as put forward in the publications cited; ^j In MeCN; ^k In butyronitrile at 77 K; ^l In air-equilibrated solution; ^m Non-emissive; ⁿ Biexponential decay; relative proportions 85/15; ^o Aggregate emission at elevated concentration, with corresponding band in excitation at 550 nm; ^p Rigid polymer matrix; ^q In dichloromethane solution; ^r In solution in hexanes; ^s In THF

the parent complex was accompanied by formation of an excimer emitting around 750 nm.

Seeking to establish the nature of the emissive excited state in such complexes, and to determine the influence of ligand substituents on the excited state energy and deactivation pathways, the Eisenberg and Schanze groups independently undertook systematic studies of series of $\text{Pt}(\text{N}^{\wedge}\text{N})(\text{C}\equiv\text{C}-\text{Ar})_2$ complexes, in which the acetylide ligand was varied through the introduction of electron-withdrawing or -donating substituents, whilst keeping the $\text{N}^{\wedge}\text{N}$ ligand constant, and *vice versa* [27–29]. For example, Schanze et al. prepared the two series of complexes 4–7 and 8–11 [29].

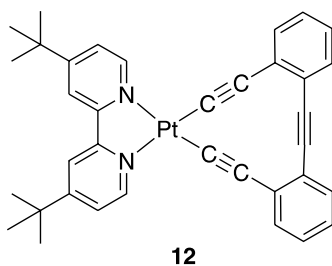


All the complexes feature a low-energy absorption band in the 350–500 nm region, attributed to a $\text{Pt} \rightarrow \text{diimine } ^1\text{MLCT}$ transition. This assignment is supported by the influence of the substituents on λ_{max} . Thus, for Series I, the energy of the band decreases by a total of nearly 3000 cm^{-1} over the sequence $4 < 5 < 6 < 7$, as the substituents become increasingly electron-withdrawing (or less strongly donating), and the diimine π^* (LUMO) energy decreases. Similarly, the emission maxima decrease in energy by 3900 cm^{-1} over the same sequence. The 77 K spectra are strongly blue-shifted compared to the 298 K spectra, consistent with a large outer-sphere reorganization energy upon formation of the excited state, and hence with a $^3\text{MLCT}$ assignment.

These conclusions were supported by transient absorption spectroscopy, which revealed signals corresponding to the formation of the diimine radical anion, with lifetimes in close agreement with the luminescence lifetimes. Time-resolved infrared spectroscopy of the acetylide $\text{C}\equiv\text{C}$ bonds provides further conclusive evidence for the MLCT assignment. Thus, in the ground state IR spectrum of 4, there are two $\nu(\text{C}\equiv\text{C})$ bands at 2115 and 2124 cm^{-1} , whilst the step-scan FTIR difference spectrum obtained 50 ns after irradiation at 355 nm reveals bleaching of the parent bands, and the formation

of a new excited-state band at 2142 cm^{-1} . The shift of the $\nu(\text{C}\equiv\text{C})$ bands to higher frequency is consistent with an excited state of $d(\text{Pt})\rightarrow\pi^*(\text{diimine})$ character: the formation of the excited state will be accompanied by a reduction in the electron density at the metal, and thus back-bonding from the metal into the $\pi^*(\text{C}\equiv\text{C})$ orbital will be reduced and the triple bond strengthened.

The photoluminescence lifetimes and quantum yields of this series of complexes decrease dramatically with decrease in the emission energy. A quantitative analysis reveals that $\ln(\sum k_{\text{nr}})$ increases linearly with decreasing excited state energy, confirming that the energy gap law is obeyed for this series (Fig. 7). In passing, we note that Castellano, in a recent study, has been able to reduce the extent of non-radiative deactivation in such complexes by incorporating the two coordinated acetylides into a rigid cyclic structure. The bidentate ligand tolan-2,2'-diacetylide (tdaH₂) was used to obtain Pt(tbbpy)(tda) **12**, which displays a particularly high quantum yield of luminescence and long lifetime ($\phi = 0.52$, $\tau = 2.56\ \mu\text{s}$ in CH_2Cl_2 at room temperature) [30].



For Series II (8–11), the lowest-energy absorption band decreases in energy in the order $\text{NO}_2 > \text{CF}_3 > \text{OMe} > \text{NMe}_2$, as the substituent on the arylacetylide becomes more electron-donating, increasing the electron density at the metal and hence lowering the $^1\text{MLCT}$ energy. However, trends in the emission energy, lifetimes and quantum yields are not clear-cut for this series (e.g., the lack of correlation of k_{nr} with excited state energy is clear from Fig. 7). In particular, there is strong evidence for a $^3\pi-\pi^*$ assignment of the emissive state in the nitro-substituted complex **9**, localized on the acetylide ligands. For example, the emission maximum for this complex is virtually the same at 80 K as at 298 K, the TRIR spectrum reveals only a very small $\Delta\nu(\text{C}\equiv\text{C})$, and the transient absorption (TA) spectrum shows a very different, broad absorption band that probably arises from the formation of the nitrophenylacetylide radical anion [29].

A striking example of the interplay between $^3\pi-\pi^*$ and $^3\text{MLCT}$ states comes from Castellano's group, who investigated complexes incorporating acetylides bound to more highly conjugated aromatic units such as 1-pyrene,

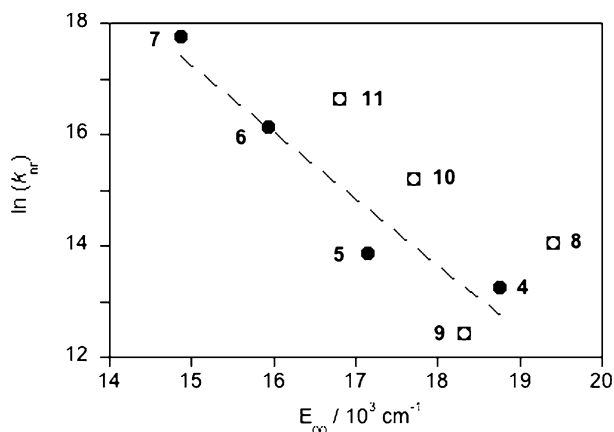
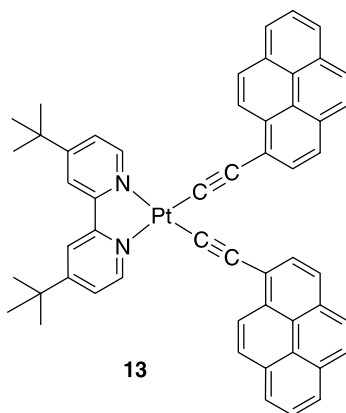


Fig. 7 Energy gap law analysis for Schanze's Pt(N^N)(-C≡C-Ar)₂ complexes in CH₂Cl₂ solution at 298 K: plot of $\ln \sum k_{nr}$ versus the 0-0 energy. Reproduced from data in [29] with permission. © (2001) American Chemical Society

1-anthracene and 1-perylene [31]. For example, the absorption spectrum of Pt(tbbpy)(-C≡C-1-pyrene)₂ **13** displays structured bands due to pyrene-acetylide π - π^* transitions, at higher energy than the Pt→diimine ¹MLCT bands around 450 nm. On the other hand, excitation into the ¹MLCT bands in fluid solution at room temperature produces long-lived ($\tau = 48.5 \mu\text{s}$) structured phosphorescence originating from the *triplet* π - π^* state of the pyrene-C≡C units, which lies around 2800 cm⁻¹ lower in energy than the ³MLCT emission observed in Pt(dbpy)(-C≡C-Ph)₂ (Fig. 8) [32]. Thus the MLCT absorption bands are able to sensitize triplet intraligand emission.



The same group has also investigated alkyl and silyl acetylides, as opposed to the aryl acetylides of most of the other studies. The σ -donor strength of the

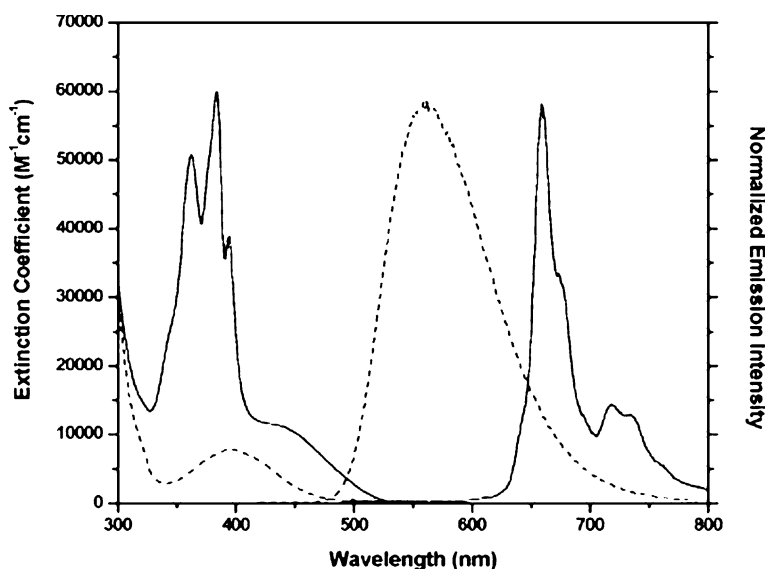


Fig. 8 Absorption (*left*) and emission (*right*) spectra of the bis-(pyrenylacetylide) platinum complex **13** (*solid lines*) and of Pt(dbppy)(-C≡C-Ph)₂ for comparison (*dotted lines*) in deoxygenated CH₂Cl₂ at room temperature; $\lambda_{\text{ex}} = 480$ nm. Reprinted with permission from [32]. © (2003) American Chemical Society

acetylide is again found to be critical in determining the ease of metal-based oxidation and hence the energy of the ³MLCT-based emission. For example, the emission maximum is blue-shifted from 557 nm for Pt(tbbpy)(-C≡C-*t*-Bu)₂ to 526 nm for Pt(tbbpy)(-C≡C-SiMe₃)₂ (CH₂Cl₂ at RT) [33].

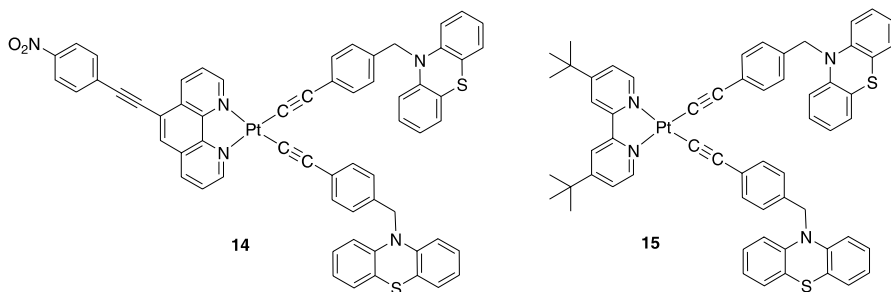
2.3.1

Applications of Acetylide Complexes

Metal complexes with MLCT excited states have long been of interest as possible chromophores for promoting long-range, photoinduced charge separation (CS) in molecular triads of the form donor–chromophore–acceptor (D–C–A). The initial short-range charge separation that occurs upon formation of the MLCT state may be followed by electron transfer from the complex to the acceptor and then from donor to complex, leading to a D⁺–C–A⁻ state that may be long-lived if the thermodynamics of charge recombination place it within the Marcus inverted region. The use of Pt(II) complexes for this purpose, in the context of other metals such as Ru(II), has been reviewed recently by Schmehl and Eisenberg [34].

The Eisenberg group has been investigating the utility of the Pt(N[^]N)(-C≡C-Ar)₂ unit as the central chromophore in such systems. Thus the complex **14** was prepared, incorporating phenothiazine (PTZ) donor groups

linked to the acetylide ligands and a nitrophenyl group on the diimine serving as the terminal electron acceptor [35]. Electrochemical measurements, in comparison with those on suitable model compounds, confirmed that the sites of most facile reduction and oxidation are associated with the nitrophenyl and PTZ groups, respectively, rather than the Pt chromophore itself, and hence that the triad can, in principle, function in the desired way. That it does so upon irradiation into the $^1\text{MLCT}$ band of the Pt chromophore ($\lambda_{\text{ex}} = 405 \text{ nm}$) was confirmed: (i) by the absence of luminescence, indicative of the introduction of a rapid, competitive deactivation pathway compared to parent $\text{Pt}(\text{N}^{\wedge}\text{N})(-\text{C}\equiv\text{C}-\text{Ar})_2$ complexes; and (ii) from the TA spectra, which show bands attributable to the $\text{PTZ}^{\cdot+}$ radical cation and the nitrobenzene radical anion, as anticipated for a $\text{D}^+ - \text{C} - \text{A}^-$ state. Based on the TA decay kinetics, the lifetime of the charge-separated state was estimated to be $70 \pm 5 \text{ ns}$ in DMF.



A series of model dyads were also studied [36]. Interestingly, although dyad **15** displays emission quenching in *acetonitrile* and formation of a CS state $\text{D}^+ - \text{C}^-$ (where the negative charge is localized on the bpy), no such behavior is observed in toluene, wherein the complex is brightly emissive with a luminescence quantum yield similar to the parent complex with no DPZ pendant. This solvent dependence of charge separation has been interpreted in terms of the differing extents to which the energies of the MLCT and CS states are influenced by solvent polarity, the latter becoming the lowest energy excited state only in the more polar solvents [36].

Che and Wong and co-workers have investigated the utility of platinum diimine bisacetylides as vapoluminescent materials [37]. In particular, the bis(4-pyridylacetylide) complex, $\text{Pt}(\text{tbbpy})(-\text{C}\equiv\text{C}-4\text{-py})_2$, displays a dramatic enhancement of green $^3\text{MLCT}$ luminescence in the solid state upon sorption of chlorocarbon vapors, particularly CH_2Cl_2 . The solid state-emission of this material is dependent upon its crystallinity and the medium from which it has been recrystallized. Thus, when crystallized from $\text{CH}_2\text{Cl}_2/\text{Et}_2\text{O}$, the emission is almost identical to that in CH_2Cl_2 solution, with a structured profile peaking at 517 nm, whereas a powdered sample obtained by grinding the crystals displays only very weak, broad and red-shifted, structureless emission

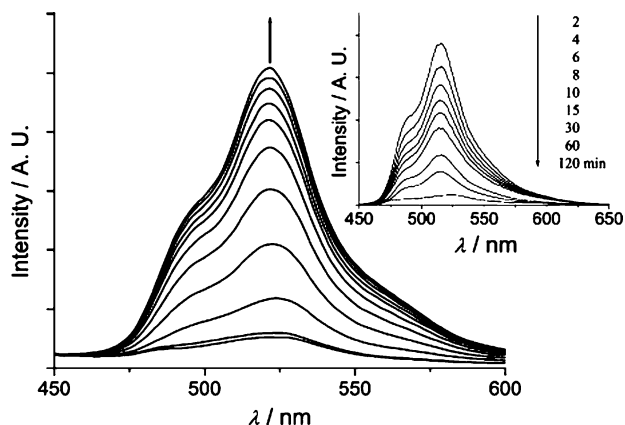


Fig. 9 Growth of the emission from a thin film of $\text{Pt}(\text{dbppy})(-\text{C}\equiv\text{C}-4\text{-py})_2$ upon exposure to N_2 saturated with CH_2Cl_2 vapor ($\lambda_{\text{ex}} = 350 \text{ nm}$, N_2 flow rate = 12 mL min^{-1} , interval between spectra = 2 min). The inset shows the emission spectral traces for this film upon removal of the CH_2Cl_2 vapor (N_2 flow rate = 90 mL min^{-1}). Reprinted with permission from [37]. © (2003) Wiley-VCH

($\lambda_{\text{max}} = 640 \text{ nm}$). When the powder is exposed to CH_2Cl_2 vapor, the intense green emission is restored; when subjected to heat or reduced pressure, it disappears. Rapid “switching-on” of the emission of a $40 \mu\text{m}$ thin film on a glass slide was observed upon exposure to N_2 gas saturated with CH_2Cl_2 vapor (Fig. 9), and the response was found to be reversible several times, offering a detection limit of 25 ppm. The crystal structure of the material, crystallized in the presence of dichloromethane, reveals one molecule of CH_2Cl_2 per complex, the disposition of which suggests that weak $\text{C}-\text{H} \cdots \pi(\text{C}\equiv\text{C})$ interactions exist between the two acidic protons of the CH_2Cl_2 molecule and the bis(acetylide) moiety, and the presence of weak $\text{Cl} \cdots \text{Cl}$ contacts between adjacent solvent molecules. It is suggested that the sensing mechanism arises from the quenching of the excited state in the “off” or powder state, through intermolecular $\text{C}-\text{H} \cdots \text{N}(\text{py})$ and/or $\text{Pt} \cdots \text{N}(\text{py})$ interactions. Diffusion of CH_2Cl_2 (or CHCl_3) into the material results in expansion of the lattice and segregation of the molecules, triggering the intense $^3\text{MLCT}$ emission.

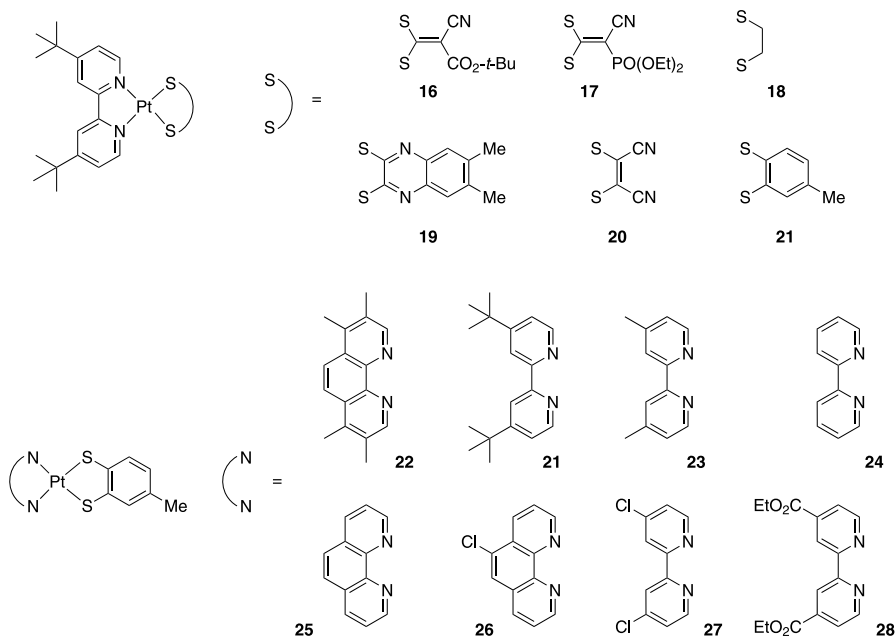
2.4

$\text{Pt}(\text{N}^{\wedge}\text{N})(\text{S}^{\wedge}\text{S})$ and $\text{Pt}(\text{N}^{\wedge}\text{N})(\text{S}-\text{R})_2$

Since an initial report by Eisenberg in 1989 [38], a large number of platinum(II) diimine dithiolate complexes are now known which are luminescent in fluid solution. Although their emission is typically weak under ambient conditions, and some earlier examples had been noted to be emissive only at 77 K [39], this class of complex is of considerable interest owing to the wide range over which the excited state energies and redox poten-

tials can be tuned. Early studies supported by electrochemical measurements and extended Hückel MO calculations indicated that, whilst the LUMO is localized unequivocally on the N[^]N ligand, the HOMO probably has substantial contributions from both the metal d(Pt) and the thiolate ligand p(S) orbitals [40, 41]. A mixed MLCT/LLCT designation might thus be appropriate, and the all-encompassing term “charge-transfer-to-diimine” has been proposed [42].

In a landmark study, Cummings and Eisenberg explored two series of Pt(diimine)(dithiolate) complexes in which the chelating ligands were systematically varied [43]. The first series consists of Pt(dbbpy)(dithiolate) complexes, with six different 1,1- or 1,2-dithiolates (S[^]S) of varying electron demand 16–21. In the second series, electron-donating or -withdrawing substituents were introduced into the N[^]N ligands, whilst the dithiolate was held constant as toluene-3,4-dithiolate (tdt) 21–28. The strategy is effectively similar to that used in the study of the bis-acetylide complexes discussed above. These two series of complexes offer dramatic support for the charge-transfer-to-diimine formulation of the lowest-energy excited state. Thus, the lowest energy absorption band red-shifts in absorption by > 4000 cm⁻¹ in Series II, on going from Pt(tmphen)(tdt) through to Pt(4,4'-(EtCO₂)₂-bpy)(tdt), as the electron-accepting nature of the diimine increases. A good correlation with Hammett constants is observed for the substituted bipyridine ligands. There is a similar range of energies for Series I. Overall for the two series, the



absorption energy can be tuned by an enormous 8160 cm^{-1} (in CH_2Cl_2 solution). Similar trends are clear in the 77 K emission spectra, where the energies of the emission maxima vary over a range of 7400 cm^{-1} (Fig. 10).

A further key feature is the very strong negative solvatochromism exhibited by these CT bands, as exemplified by $\text{Pt}(\text{dbbpy})(\text{tdt})$ in Fig. 11. The shift to higher energy in solvents of increasing polarity is typically indicative of an excited state that is less polar than the ground state. This can be understood

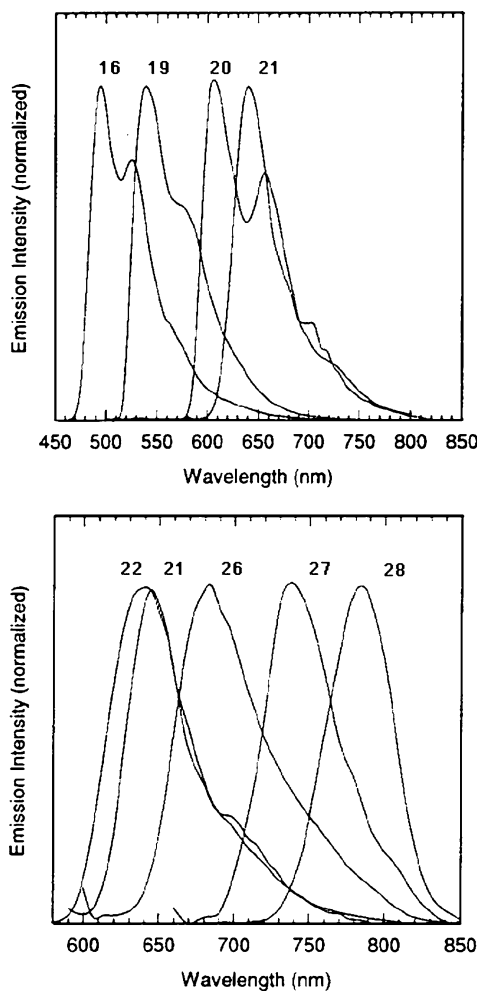


Fig. 10 Charge-transfer-to-diimine emission bands of the dbbpy series of complexes 16–21 with varying dithiolate (*top*), and the toluenedithiolate series 21–28 with varying diimine (*bottom*). The spectra were recorded in frozen butyronitrile at 77 K; their intensities have been normalized. Reprinted with permission from [43]. © (1996) American Chemical Society

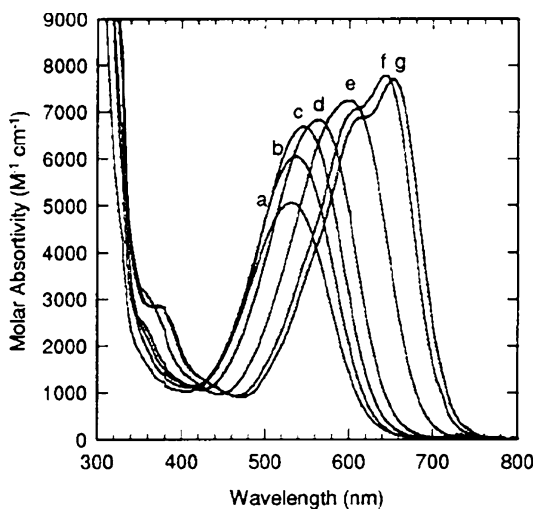


Fig. 11 Charge-transfer-to-diimine absorption band for 21 in (a) CH₃CN, (b) DMSO, (c) DMF, (d) THF, (e) CH₂Cl₂, (f) C₆H₆, and (g) C₆H₅CH₃. Reprinted with permission from [43]. © (1996) American Chemical Society

here in terms of the dipolar charge distribution in the ground state, which is greatly reduced in the excited state: the charge-transfer axis lies colinear with the dipole axis. The authors devised an empirical solvent scale based on the results for Pt(tbbpy)(tdt) to assess the relative degree of solvatochromism for the other complexes: the slopes of the plots of energy versus solvent parameter were of a similar magnitude for all the complexes, suggesting the same type of excited state in each case, and a similar degree of charge redistribution. Since the formation of a charge-transfer-to-diimine excited state formally involves the oxidation of a HOMO having dithiolate and metal orbital character and reduction of a diimine-based LUMO, a linear correlation should exist between the excited state energy and the difference between the ground state oxidation and reduction potentials [44, 45]. For the present series of complexes, a good correlation is indeed observed (Fig. 12).

The quantum yields of the complexes are of the order 10^{-3} – 10^{-4} , and lifetimes are in the range 1–1000 ns in CH₂Cl₂ at 298 K. Radiative decay constants decrease with decreasing energy, although not with the strict cubic dependence predicted by the Einstein coefficient if the electronic transition moment were to remain constant. Non-radiative decay of the Series II complexes follows the energy gap law, with $\ln(\sum k_{nr})$ increasing approximately linearly with decreasing excited state energy. No such correlation was observed for Series I, where there is more structural variation between complexes.

Investigations into bis-thiolate (as opposed to chelating dithiolate) complexes, Pt(N[^]N)(SAr)₂, have also revealed heavily mixed p(S)-p(Ar)/d(Pt)

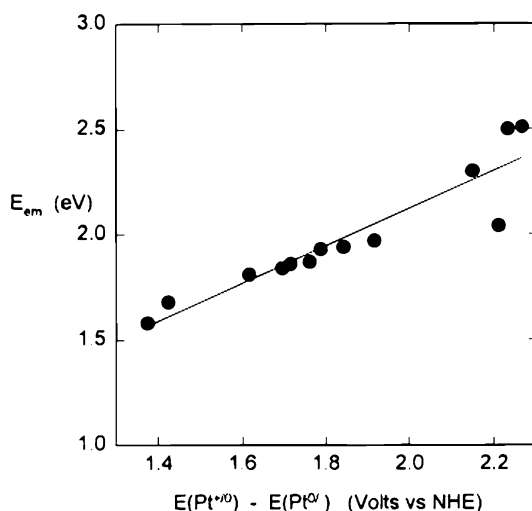
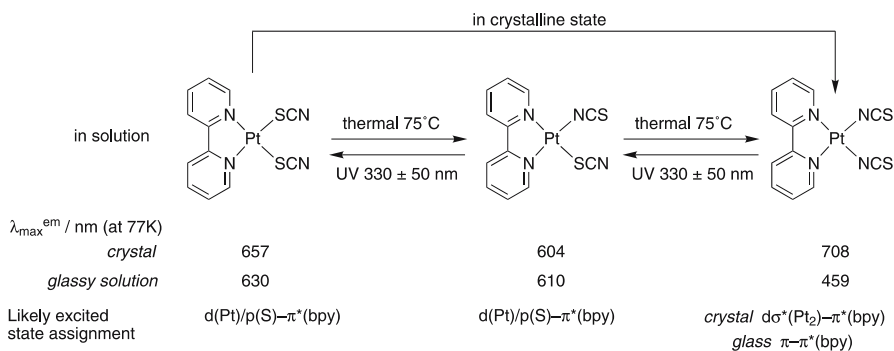


Fig. 12 Plot of emission energy (from 77 K butyronitrile spectra) against the difference between the ground state oxidation and reduction potentials for 16–29, and the linear least-squares fit. Reprinted with permission from [43]. © (1996) American Chemical Society

HOMOs and N^π-based LUMOs, using techniques such as spectroelectrochemistry and resonance Raman spectroscopy [46, 47]. These complexes, however, usually have shorter-lived excited states, and solution-state emission is unusual. The technique of time-resolved IR spectroscopy described in Sect. 2.1 has again proved useful here in probing these short-lived excited states. For example, the decay of the charge-transfer-to-diimine excited state in Pt(bpy)(*p*-S-C₆F₄-CN)₂, monitored through observation of the excited state C≡N stretching vibrations, displays initial vibrational cooling on a 2 ps timescale, and back electron transfer with a lifetime of 35 ps [47].

Finally, we note recent work on thiocyanate complexes. Thiocyanate is a well-known ambidentate ligand in transition metal chemistry, which can coordinate to metal ions either through nitrogen (M–NCS) or through sulfur (M–SCN). The controlled switching between such isomers – which may have quite different properties – is of interest in many fields. Kato and Kishi have succeeded in isolating and obtaining the crystal structures of the three linkage isomers Pt(bpy)(SCN)₂, Pt(bpy)(SCN)(NCS) and Pt(bpy)(NCS)₂, and have investigated their interconversion (Scheme 1) [48]. The first is the kinetically favored product, which is converted thermally to the third in a stepwise manner in solution via the second. Stepwise reverse isomerization occurs upon irradiation in the near-UV. In the solid state, Pt(bpy)(SCN)₂ converts directly to Pt(bpy)(NCS)₂, suggesting a concerted flipping of the two thio-



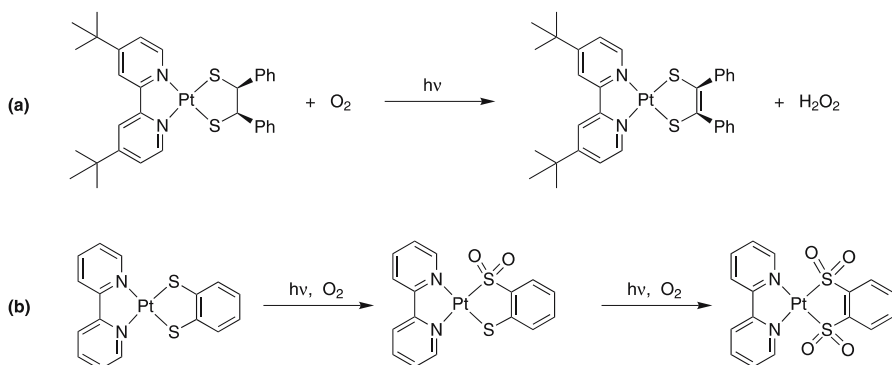
Scheme 1 Linkage isomers of bis(thiocyanate)(2,2'-bipyridine)platinum(II), their interconversion, and their emission maxima and excited states at 77 K. Based on data from [48]

cyanate ligands. The different isomers have different emission properties, as summarized in Scheme 1.

2.4.1

Photo-oxidation Chemistry of Thiolate Complexes

Extensive work by Srivastava in the 1980s revealed that many Pt(II) diimine complexes are able to sensitize the formation of singlet oxygen ($^1\text{O}_2$) in aerated solutions [49]. During this work, it was found that thiolate ligands could undergo photoinduced decomposition in oxygenated solutions [50]. Schanze et al. noted contrasting behavior in the oxidative photochemistry of Pt(dbbpy)(dpdt) and Pt(dbbpy)(edt) in the presence of O_2 (dpdt = meso-1,2-diphenyl-1,2-ethanedithiolate; edt = 1,2-ethanedithiolate) [51]. Irradiation into the charge-transfer-to-diimine band of Pt(dbbpy)(dpdt) in air-saturated MeCN led to bleaching of this band (λ_{\max} 466 nm) accompanied by the growth of a new band at lower energy (λ_{\max} 582 nm). On the basis of ^1H NMR and HRMS, this was interpreted in terms of the conversion of the dithiolate into the more strongly electron-donating dithiolene by hydrogen abstraction (Scheme 2a). In contrast, although irradiation of Pt(dbbpy)(edt) under similar conditions also led to the bleaching of the CT band, no new low-energy band was formed. In this case, photooxidation of one or both of the thiolate ligands to sulfinates ($-\text{SO}_2\text{R}$) was proposed on the basis of HRMS, although the products were insufficiently soluble for conclusive evidence to be obtained. Subsequently, Connick and Gray investigated a closely related complex, Pt(bpy)(bdt) (bdt = 1,2-benzenedithiolate) [52]. They were able to obtain crystal structures of the sulfinate Pt(bpy)(bdtO₂) and disulfinate Pt(bpy)(bdtO₄) complexes as photoproducts (Scheme 2b). Both studies concluded that the first step in the photooxidation is energy transfer from



Scheme 2 Photo-oxidation of (a) Pt(dbbpy)(dpdt) leading to the corresponding dithiole complex [48]; (b) Pt(bpy)(bdt) leading sequentially to the sulfinate and disulfinate complexes [22]

the CT excited state of the complex to $^3\text{O}_2$ to generate $^1\text{O}_2$, followed by its reaction with the ground-state of the complex, possibly involving conversion of $^1\text{O}_2$ to $\text{O}_2^{\cdot-}$ (superoxide). Interestingly, $\text{O}_2^{\cdot-}$ is not formed in the initial excited state quenching reaction, despite the large driving force for the process, suggesting that it is kinetically disfavored by being highly inverted [52].

2.4.2

Dimeric and Trimeric Complexes with Bridging Sulfurs

Sulfur's ability to bridge transition metal ions is well known, and there are numerous examples in platinum chemistry. Amongst those containing Pt(diimine) fragments, Che's group has described some intriguing *triangularo* trimetallic structures comprising three Pt(N[^]N) moieties supported by two triply bridging sulfide ligands [53]. The broad, unstructured emission observed in the solid state for these $[\text{Pt}_3(\text{N}^{\wedge}\text{N})_3(\mu_3\text{-S})_2](\text{ClO}_4)_2$ salts, both at 77 K and 298 K, was tentatively assigned to metal-centred excited states. A charge-transfer-to-diimine state is unlikely here, given the similarity in emission energy for an analogue containing a diphosphine in place of the diimine, where the phosphine π^* orbital would be much higher in energy.

Kato and co-workers have found that a pair of pyridine-2-thiolate (2-pyS) ligands can bridge between two Pt(bpy) units, either to give the *anti* isomer, in which there is a head-to-tail arrangement of the two bridging ligands and an N_3S coordination environment around each Pt center (Fig. 13a), or the *syn* isomer, with head-to-head pyridinethiolates and where one Pt center is bonded to four nitrogen atoms whilst the other has N_2S_2 coordination

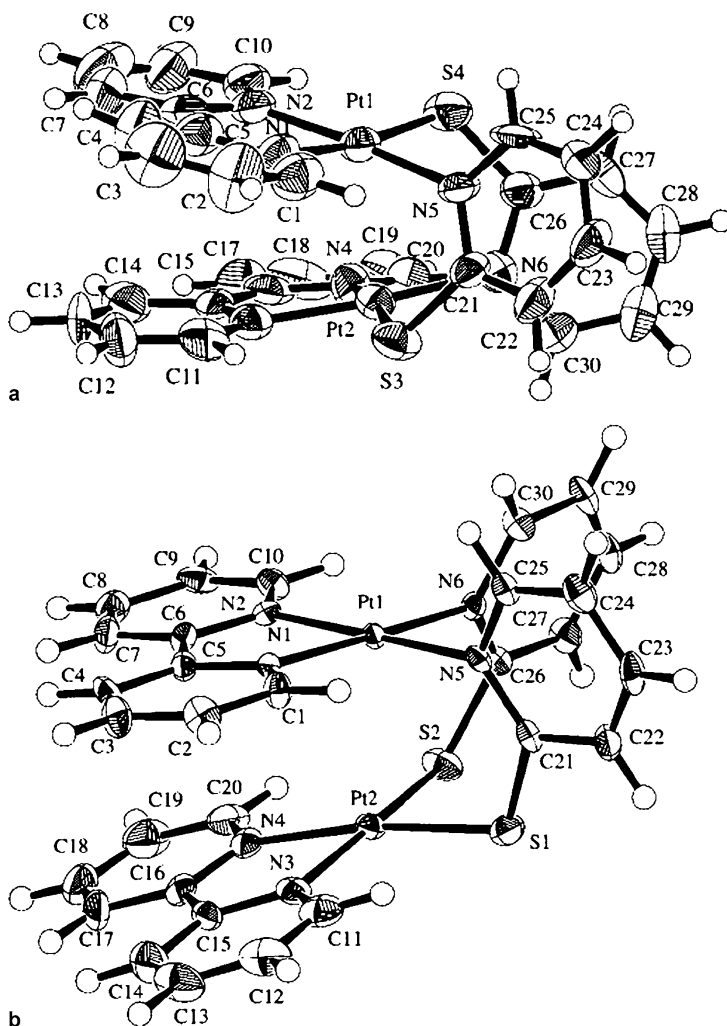


Fig. 13 Single crystal X-ray structures of the **a** *anti*, and **b** *syn* isomers of $[\text{Pt}(\text{bpy})(2\text{-pyS})]_2$. Reprinted with permission from [54]. © (2002) Wiley-VCH

(Fig. 13b) [54]. Crystals of the *anti* isomer display intense orange emission at room temperature ($\lambda_{\text{max}} = 603 \text{ nm}$; $\tau = 240 \text{ ns}$) (Fig. 14a). Given the close separations of the Pt centers in the dimer ($2.997(1) \text{ \AA}$), there will be substantial interaction of their d_{z^2} orbitals to generate an antibonding ($d\sigma^*$) orbital, such that the luminescence is probably due to an MMLCT state (Sect. 2.1). The desolvated *syn* form emits at slightly longer wavelength ($\lambda_{\text{max}} = 644 \text{ nm}$), possibly due to the shorter Pt...Pt separation in this isomer ($2.923(1) \text{ \AA}$) (Fig. 14b). This form is particularly interesting since the color of the crystals darkens and the emission red-shifts substantially upon exposure to ace-

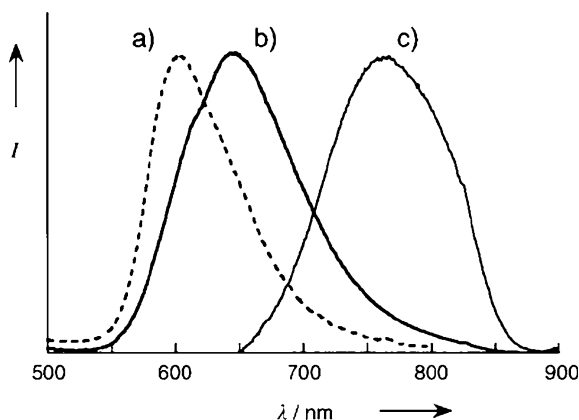


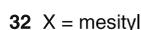
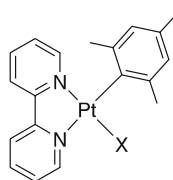
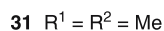
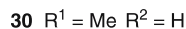
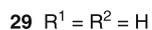
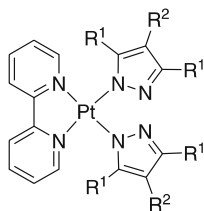
Fig. 14 Luminescence spectra of $[\text{Pt}(\text{bpy})(2\text{-pyS})]_2$ at room temperature: (a) the *anti* isomer, (b) the light-red form of the *syn* isomer, and (c) the dark-red (solvated) form of the *syn* isomer. See Fig. 13 for corresponding structures. Reprinted with permission from [54]. © (2002) Wiley-VCH

tonitrile vapor (Fig. 14c). Other solvent molecules, provided they are quite small (e.g., CH_2Cl_2 but not CHCl_3 ; EtOH but not *t*-BuOH), induce a similar effect. This vapochromic behavior, somewhat similar to that described in Sect. 2.3, seems to be related to the presence of channels in the crystal structure, into which the solvent molecules probably enter, perhaps favoring *intermolecular* contacts between the Pt centers of neighboring dimeric molecules: the Pt···Pt separation between the dimeric molecules in the solvated form is 3.384(1) Å.

2.5

$\text{Pt}(\text{N}^{\wedge}\text{N})\text{X}_2$ (X = N-, C- and O-coordinating Ligands)

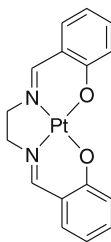
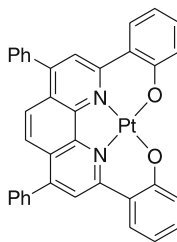
Gray and co-workers discovered that, for complexes containing pyrazolate ancillary ligands X, the introduction of methyl substituents into the pyrazole



ring leads to a remarkably clear-cut cross-over in the parentage of the emissive excited state [55]. For example, Pt(bpy)(pz)₂ **29** displays highly structured green luminescence at 77K from the bpy ³π-π* state. On the other hand, the emission is orange to red for Pt(bpy)(dmpz)₂ **30** and Pt(bpy)(tmpz)₂ **31**, and the spectral profiles are broad and unstructured (dmpz = 3,5-dimethylpyrazolate; tmpz = 3,4,5-trimethylpyrazolate). This is interpreted in terms of the known strong influence of methyl substitution in destabilizing the N lone pair and ring π orbitals of pyrazole, which will have the effect of increasing σ and π donation to the metal. The concomitant destabilization of the metal d levels lowers the energy of the ³MLCT d(Pt)→ π*(bpy), to which the emission is assigned.

Organometallic complexes containing metal-carbon(aryl) bonds have also been reported that are emissive from states of MLCT character, for example, the bis-mesityl complex **32** and analogues with other diimines [56]. Such carbon ligands are also very strongly electron-donating, and could be thought of as somewhat analogous to the methylated pyrazoles. Interestingly, we note in passing that complex **32** is unusual in that it can be reversibly oxidized to a remarkably persistent d⁷ Pt(III) species, an effect attributed to the effective protection of the axial positions by the two mesityl groups. This contrasts to the irreversible oxidation chemistry normally observed for Pt(II) complexes of the type discussed in this Chapter, and as found, for example, for **33**, which has only one such mesityl unit.

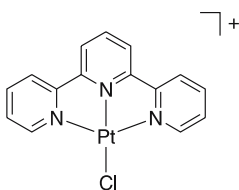
Oxygen ligands on their own are generally not suitable for forming stable complexes with the soft Pt(II) ion, but in combination with other ligands such as diimines, complexes with high thermodynamic stability can be obtained. For example, the ligand salen, *N,N'*-bis(salicylidene)-1,2-ethylenediamine, well known for its many catalytically active 1st row transition metal complexes, forms a highly luminescent platinum(II) complex **34** [57, 58]. Closely related ligands based on dpphen or tbbpy appended with ortho-phenoxy groups also give Pt(II) complexes that are strongly luminescent in solution [59]. For example, complex **35** displays a broad structureless emission centred at 586 nm, τ = 5.3 μs, φ = 0.6. The emission is attributed to a state of mixed Pt(d)/O(p)→ π*(N^N) charge-transfer character, where O(p) represents a lone pair of electrons on the phenoxide oxygen atoms.

**34****35**

3 Pt complexes with N[^]N[^]N Terdentate Ligands

3.1 Introduction

The platinum terpyridyl complex $[\text{Pt}(\text{tpy})\text{Cl}]^+$ **36** has been known since 1934 [60], and derivatives with other ligands in place of Cl were investigated in the 1970s as DNA intercalators [61]. However, it is since the early 1990s that the excited state and luminescence properties of Pt(II) terpyridyls have been investigated in detail, yielding a wealth of interesting systems with a rich variety of emissive excited states, subtly tuned according to the structures of the ligands. Much of the pioneering work on both the influence of the fourth ligand and the effect of substituents in the tpy has been led by McMillin and co-workers. Several groups have been exploring the chemistry and excited state properties of acetylides derivatives $[\text{Pt}(\text{tpy})(-\text{C}\equiv\text{C}-\text{R})]^+$, analogous to the bpy systems of Sect. 2.3.



36

One of the features of *terdentate* complexation is the additional rigidity imparted on the resulting complex, compared to bidentate systems. The d-d excited states of Pt(N[^]N) complexes are unstable with respect to a D_{2d} distortion, namely a twisting of the plane of the N[^]N ligand relative to that of the other two ligands, away from the D_{4h} square planar configuration and towards a tetrahedral conformation [62, 63]. Such distortion facilitates non-radiative decay by promoting coupling with the ground-state (Fig. 2) [64]. Terpyridines have a strong preference for a planar geometry: there is therefore very little scope for D_{2d} distortion in the complex, and non-radiative decay in this way should be greatly reduced. However, the bite angle of terpyridine is not ideal for second and third row transition metal ions: crystal structures typically reveal that whilst the central M–N bond length is similar to that in a corresponding bpy complex, the lateral M–N bond lengths are usually lengthened beyond the ideal values, due to the constraints imposed by the rigidity of the ligand. Thus, the ligand field is reduced, and the d-d excited states that promote thermally activated non-radiative decay are lowered in energy [65]. The situation is reminiscent of

that found in ruthenium(II) chemistry, where $[\text{Ru}(\text{tpy})_2]^{2+}$ is almost non-emissive under ambient conditions, in contrast to $[\text{Ru}(\text{bpy})_3]^{2+}$ [44, 45, 66]. However, in the case of Pt(tpy) complexes, by using a strong-field ancillary ligand in the fourth position, this effect can be counteracted [65]. A further key difference between $[\text{Pt}(\text{tpy})\text{X}]^+$ and $\text{Pt}(\text{bpy})\text{X}_2$ analogues is that the tpy complexes are cationic (for X = monoanionic ligand). The identity of the counter-anion can be crucial in influencing the properties, particularly in the solid state.

3.2

$[\text{Pt}(\text{tpy})\text{Cl}]^+$

The simple chloro complex highlights both of the above features very well. Thus, the color of the compound is highly dependent upon the identity of the counteranion; e.g., the ClO_4^- salt is deep red, the Cl^- and CF_3SO_3^- salts orange, and the PF_6^- salt yellow [67]. On the other hand, irrespective of the counterion, the $[\text{Pt}(\text{tpy})\text{Cl}]^+$ cation is essentially non-emissive in fluid solution at RT, attributed to the weak ligand field and hence low energy of the d-d excited states through which radiationless decay to the ground state occurs [67, 68].

The absorption spectra of $[\text{Pt}(\text{tpy})\text{Cl}]^+$ salts in solution show two sets of bands. Intense, structured bands occur at wavelengths less than about 350 nm, attributed to intraligand $\pi-\pi^*$ bands similar to those shown by $\text{Zn}(\text{tpy})\text{Cl}_2$ [68]. The somewhat weaker bands in the 350–450 nm range are assigned to $^1\text{MLCT}$ transitions: they have no counterpart in the zinc complex, which acts as a model in which the metal center cannot be oxidized and where low-energy d- π^* excited states are thus not possible.

In *dilute* glassy solution at 77 K ($< 10 \mu\text{M}$), $[\text{Pt}(\text{tpy})\text{Cl}]^+$ salts are emissive, displaying a sharply structured luminescence spectrum ($\lambda_{\text{max}}^{0-0} = 465 \text{ nm}$) with a vibronic progression of about 1400 cm^{-1} typical of tpy vibrational modes [67]. Based on the observation that the spectrum is almost identical to that of $[\text{Pt}(\text{tpy})\text{NH}_3]^{2+}$ [69] and similar to that of $\text{Zn}(\text{tpy})\text{Cl}_2$ ($\lambda_{\text{max}}^{0-0} = 435 \text{ nm}$ [70]), the emission can be assigned unambiguously to a $^3\pi-\pi^*$ state localized on the terpyridine. Moreover, a weak feature is observed at 463 nm in the excitation spectrum, corresponding to formally spin-forbidden, ground-state absorption to the $^3\pi-\pi^*$ state. That the lowest triplet excited state is $\pi-\pi^*$ in nature, whereas the lowest singlet excited state from the absorption spectrum is $^1\text{MLCT}$, reflects the fact that singlet-triplet splitting is typically much smaller for d- π^* excitations [71].

At higher concentrations in frozen glasses, additional features are observed: a broad, weakly structured band centred around 600 nm, and an unstructured band at 720 nm. These have been assigned to aggregated forms involving $\pi-\pi$ and metal-metal $d\sigma^*-\pi^*$ interactions, respectively [67]. In the solid state (as opposed to glasses), aggregate emission is typically observed,

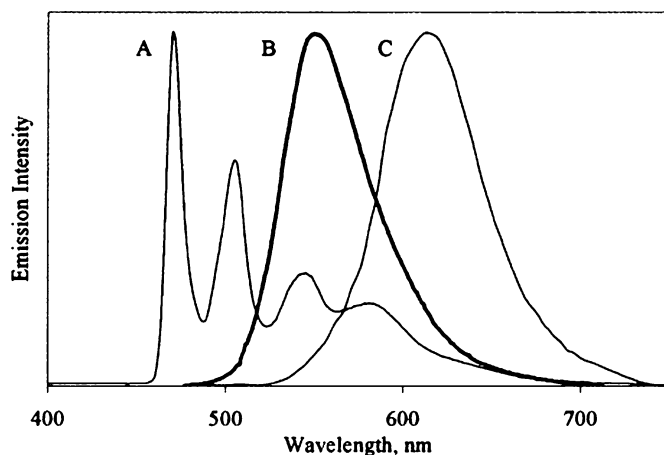


Fig. 15 Low-temperature emission from salts of $[\text{Pt}(\text{tpy})\text{Cl}]^+$. (A) ${}^3\pi-\pi^*$ emission from the SbF_6^- salt in a butyronitrile glass at 77 K; (B) ${}^3\text{MLCT}$ emission from solid $[\text{Pt}(\text{tpy})\text{Cl}]\text{SbF}_6$ at 100 K; (C) ${}^3\text{MMLCT}$ emission from solid $[\text{Pt}(\text{tpy})\text{Cl}]\text{SO}_3\text{CF}_3$ at 100 K. Reprinted from [65] with permission from Elsevier

but the behavior is strongly influenced by the identity of the counteranion, as exemplified by the dramatic difference between the SbF_6^- and CF_3SO_3^- salts (Fig. 15) [65].

3.3

$[\text{Pt}(\text{tpy})\text{X}]^+$

Replacement of the chloride ligand in $[\text{Pt}(\text{tpy})\text{Cl}]^+$ by other, stronger-field ligands, can lead to emission being observed in fluid solution at RT, as the normally deactivating d-d states are pushed to inaccessible energies. For example, for the complexes with $\text{X} = \text{NCS}$, OMe and OH , the corrected emission maxima and lifetimes are 588 nm (3.5 ns), 654 nm (180 ns) and 621 nm (170 ns), respectively, in degassed MeCN [68]. The broad, unstructured emission profiles and high radiative rate constants are suggestive of a ${}^3\text{MLCT}$ assignment. Substantially longer emission lifetimes are observed in CH_2Cl_2 , and this may reflect the ability of MeCN to act as a quencher of the $\text{d}-\pi^*$ excited state through interaction at the open (axial) coordination sites [72].

Interestingly, the emission of $[\text{Pt}(\text{tpy})(\text{OH})]^+$ is quenched in water, but is restored upon intercalation with double-stranded nucleic acids $[\text{poly}(\text{dA}\cdot\text{dT})]_2$ and $[\text{poly}(\text{dI}\cdot\text{dC})]_2$ [73]. Although intercalation can also occur at G-C-rich sequences – and indeed it does so more strongly than for A-T – emission is then quenched by electron-transfer from guanine, the most readily oxidized of the nucleobases. The initial intercalative interactions are probably followed by covalent platination of the DNA, most likely by purine-N7 displacing the OH ligand, reminiscent of cisplatin. The absorption

spectrum shifts to higher energy, in line with a neutral fourth ligand, and the emission is lost [73]. A similar “light switch” effect of $[\text{Pt}(\text{tpy})(\text{OH})]^+$ has also been observed upon formation of micelles in aqueous solution [74]. Emission is enhanced by a factor of $> 10^3$, and a luminescence lifetime of 100 ns is measured, when the concentration of sodium dodecyl sulfate in water reaches the critical micelle concentration (CMC).

More recently, McMillin, Field and co-workers have investigated the incorporation of $\text{C}\equiv\text{N}$ as the fourth ligand, achieved by treatment of the parent chloride complex with AgCN [75]. Given that CN^- is one of the very strongest of ligands in the spectrochemical series, its introduction into the coordination sphere of the Pt ion might be anticipated to raise the energy of the normally deactivating d-d excited states even more, thereby favoring the emission intensity and lifetime (cf. Sect. 2.2). However, the $d-\pi^*$ $^3\text{MLCT}$ state is also raised in energy by this substitution: the outcome is that the lowest-energy triplet excited state is now the $^3\pi-\pi^*$, and not the $^3\text{MLCT}$. Thus, a highly structured emission spectrum, with $\lambda_{\text{max}}^{0-0}$ of 465 nm is observed (as for $[\text{Pt}(\text{tpy})\text{Cl}]^+$ at 77 K). The emission is, in fact, very weak at room temperature ($\phi = 4 \times 10^{-4}$), owing to the low radiative rate constant associated with a $^3\pi-\pi^*$ transition having little metal contribution, and to the fact that the emission originates from a relatively high energy state, so that deactivation via the d-d may still be possible.

Monsù Scolaro and co-workers have prepared organometallic $\text{Pt}(\text{tpy})$ derivatives containing methyl or phenyl ligands in the fourth coordination site, $[\text{Pt}(\text{tpy})\text{Me}]^+$ and $[\text{Pt}(\text{tpy})\text{Ph}]^+$, as well as their analogues with 4'-phenyl-terpyridine [76–78]. There are close parallels between the behavior of the methylated complexes and the chloro complexes, although the former have an even stronger propensity to aggregate and stack in solution. The low-energy $^1\text{MLCT}$ bands in absorption are red-shifted compared to the chloro complexes, in line with the stronger σ -donating ability of Me and Ph compared to Cl. The emission spectra of the methyl compounds in MeOH/EtOH glasses at 77 K are highly concentration dependent, displaying $^3\pi-\pi^*$ structured emission in the 460–600 nm range at high dilution, which is accompanied, at high concentrations, by an unstructured low-energy band around 680–800 nm, assigned to a $d\sigma^*(\text{Pt}_2) \rightarrow \pi^*(\text{tpy})$ (MMLCT) state formed by aggregation. An ill-defined band at intermediate energies is attributed to an excimeric excited state involving $\pi-\pi$ stacking, but is weaker than the corresponding feature observed in $[\text{Pt}(\text{tpy})\text{Cl}]^+$ (Sect. 3.2), possibly due to the greater electron-donating ability of Me favoring the metal–metal interaction over the $\pi-\pi$. The phenyl derivatives display only the high energy $\pi-\pi^*$ structured emission irrespective of concentration, which can be rationalized in terms of the steric influence of the phenyl group in inhibiting close intermolecular contacts.

Thiolate adducts of the $\text{Pt}(\text{tpy})$ unit have been investigated, particularly in the context of the design of DNA intercalating agents [61, 79, 80]. Those

studies which have focused on the nature of the excited states have generally concluded that the intense, low-energy bands typically observed in such complexes in the 500–600 nm region are due to $p\pi(RS^-) \rightarrow \pi^*(tpy)$ charge-transfer transitions, possibly mixed with some $Pt(d) \rightarrow \pi^*(tpy)$ character, in line with the conclusions for $Pt(N^{\wedge}N)(SR)_2$ complexes discussed in Sect. 2.4 [81–84]. However, very few of the terpyridyl complexes have been reported to be emissive, Che's study of the pyrimidine-/quinoline-2-thiolate and dithiouracil adducts – which are emissive both in the solid state and in solution at 298 K – being a notable exception [53].

3.4

$[Pt(4'-R-tpy)Cl]^+$

3.4.1

R = $-C\equiv N$ or Heteroatom

The introduction of substituents into the 4'-position of the terpyridine proves to have profound effects on the photophysical properties of the platinum terpyridyl moiety, and has led to the most strongly emissive and longest-lived such complexes to date. The introduction of electron-withdrawing $-C\equiv N$ or $-SO_2Me$ substituents stabilizes the ligand π^* , as indicated by a shift of the ligand-localized reduction potential to less negative values [85]. Charge-transfer excited states involving the tpy as the acceptor are therefore expected to be stabilized, and indeed the 1MLCT absorption bands for these two complexes are displaced to longer wavelength compared to the parent unsubstituted compound. The compounds are emissive in room temperature degassed solution, with emission maxima (quantum yields) of 550 nm (0.005) and 542 nm (0.002), respectively. The luminescence – which probably originates from a state of predominant 3MLCT character – is clearly favored by a stabilization of the CT state relative to the d-d, so that thermally activated decay via the latter is inhibited (Fig. 16) [65].

Electron-donating substituents, such as $-NMe_2$ and $-SMe$ would be expected to *destabilize* the MLCT states, as reflected in the more negative reduction potentials of the respective complexes [85]. Yet it transpires that, not only do these complexes display room temperature luminescence with emission maxima very similar to that of the cyano complex, they are actually more intensely emissive with longer lifetimes. Indeed, $[Pt(4'-Me_2N-tpy)Cl]^+$ has a very impressive quantum yield of 0.08 and a long lifetime of 1.9 μs in degassed CH_2Cl_2 at room temperature [85]. This remarkable result has been interpreted by McMillin in terms of the influence of the lone pairs on the substituents, which can give rise to transitions with significant intraligand, substituent-to-terpyridine charge transfer (ILCT) character. Although such transitions occur in the UV region in the case of the free ligands, they shift to lower energy upon complexation of the tpy to

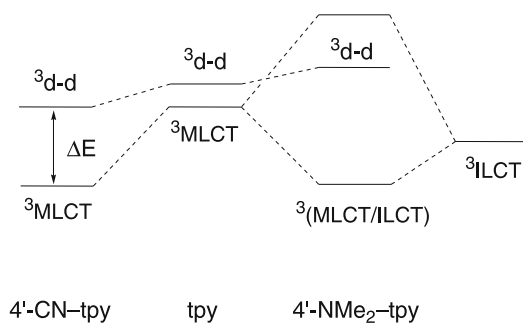


Fig. 16 Schematic of the trends in excited-state energies in $[\text{Pt}(4'\text{-R-tpy})\text{Cl}]^+$ complexes, showing the mixing of the ILCT state for the amino-substituted complex. ΔE represents the barrier to deactivation via a ³d-d state. Reproduced from data in [65] with permission from Elsevier

the positively charged metal ion. A configuration interaction between the ³ILCT and ³MLCT states leads to a lowest energy transition of mixed orbital parentage that occurs at lower energy than either of the two constituent excited states (Fig. 16). Part of the reason for the particularly long lifetime may be due to the fact that formation of the ILCT excited state is accompanied by relatively little change in equilibrium geometry, since the electron density is effectively displaced sideways to the peripheral rings rather than along the dipole axis. As noted in the introduction, the smaller the distortion, the weaker the coupling to the ground-state, favoring radiative over non-radiative decay. Replacement of the chloride ligand by cyanide now does further enhance luminescence, as the barrier to deactivation via the d-d state is raised. Thus, $[\text{Pt}(4'\text{-Me}_2\text{N-tpy})\text{CN}]^+$ has a remarkably high quantum yield of 0.26 and long lifetime of 22 μs in degassed CH_2Cl_2 at RT [75].

A key observation that supports the notion of ILCT character is the decreased susceptibility of these complexes to exciplex quenching. This normally occurs by attack of Lewis bases at the vacant coordination sites of the metal, and is promoted for MLCT excited states by the increased electrophilicity of the metal in the transient, formally oxidized + 3 state, in effect by the “hole” generated on the metal [85]. Contribution of ILCT character serves to delocalize the hole away from the metal and onto the ligand.

3.4.2

R = Aryl

Che et al. reported that the introduction of aryl rings (i.e., $\text{R} = p\text{-R}'\text{-C}_6\text{H}_4$ – where $\text{R}' = \text{MeO}, \text{Me}, \text{Br}, \text{ or } -\text{CN}$) into the 4'-position of the tpy leads to complexes which are emissive in fluid solution, with λ_{max} in the range 530–580 nm, $\tau \sim 1 \mu\text{s}$ and $\phi \sim 10^{-3}$ (10^{-2} for $\text{R}' = p\text{-MeO}$) in degassed

MeCN [69]. These results were interpreted in terms of the increased energy gap between the emissive $^3\text{MLCT}$ and deactivating d-d states.

More recently, McMillin has explored the influence of larger, fused-ring aromatic substituents which are relatively easily ionized (e.g., R = 1-naphthyl, 9-phenanthryl, 1-pyrenyl) [70, 86]. Perhaps the most remarkable system here is the 1-pyrenyl system **37**, which has an astonishingly long luminescence lifetime of 64 μs in deoxygenated CH_2Cl_2 at room temperature, $\lambda_{\text{max}} = 685 \text{ nm}$. In *aerated* solution, the complex displays a higher energy, much shorter-lived emission band, $\lambda_{\text{max}} = 640 \text{ nm}$ and $\tau = 1.0 \text{ ns}$, with an excitation spectrum identical to that of the 685 nm band. This 640 nm band is seen as a shoulder in the degassed spectrum (Fig. 17). The results have again been interpreted in terms of the involvement of ILCT states, in this case, dual emission from both the singlet and triplet states. Thus, the fast emission at 640 nm is at-

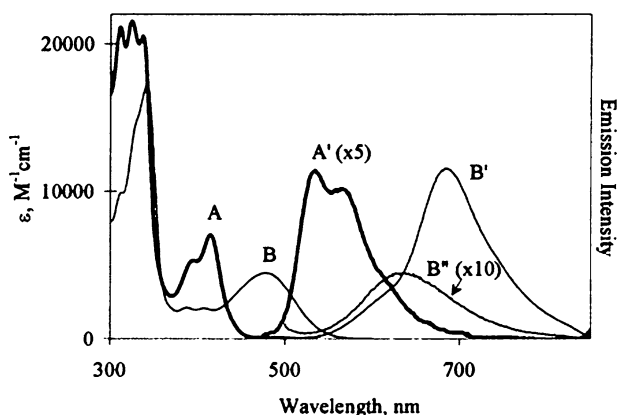
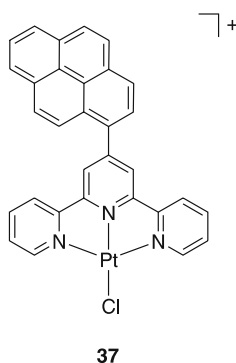


Fig. 17 Spectra of $[\text{Pt}(4'\text{-Ar-tpy})\text{Cl}]^+$ complexes in CH_2Cl_2 at room temperature. Absorption spectra: (**A**) Ar = Ph; (**B**) Ar = pyren-1-yl. Uncorrected emission spectra: (**A'**) Ar = Ph (deoxygenated solution); (**B'**) Ar = pyren-1-yl (deoxygenated); (**B''**) Ar = pyren-1-yl (air-equilibrated solution). Reprinted from [65] with permission from Elsevier

tributed to fluorescence from a $^1\text{ILCT}$ state, involving pyrene as the donor. This interpretation is supported by the similar broad, structureless emission band displayed by $\text{Zn}(4'\text{-pyren-1-yl-tpy})\text{Cl}_2$, also assigned to $^1\text{ILCT}$ emission, the higher energy of which ($\lambda_{\text{max}} = 488 \text{ nm}$) can be satisfactorily accounted for by the more negative first reduction potential of the Zn^{2+} compared to the Pt^{2+} complex. The long-lived emission of the Pt complex in deoxygenated solution must emanate from a state that comprises not just $^3\text{ILCT}$ character, but also substantial $^3\text{MLCT}$ and $^3\pi\text{-}\pi^*$ character that serve to increase the radiative rate constant compared to the low value expected in the absence of Pt. The relatively long triplet lifetime is sufficient to allow thermally activated repopulation of the singlet state, leading to the 640 nm shoulder in the deoxygenated spectrum (Fig. 17).

3.5

$[\text{Pt}(\text{tpy})(\text{-C}\equiv\text{CR})]^+$

As in the bpy systems of Sect. 2.3, the introduction of strong-field acetylide ligands into the fourth coordination site might be anticipated to lead to lower-energy, charge-transfer-to-terpyridine transitions whilst raising the energy of deactivating d-d states, promoting luminescence over non-radiative decay. A number of studies have confirmed that many $[\text{Pt}(\text{tpy})(\text{-C}\equiv\text{CR})]^+$ complexes are indeed luminescent in fluid solution, and some impressive quantum yields have now been obtained. A subtle difference compared to the platinum bipyridyl acetylides relates to the contribution of ligand-to-ligand charge transfer character to the lowest energy excited state. Castellano et al. have highlighted this point in the comparison of the $\text{-C}\equiv\text{C-}t\text{-Bu}$ and $\text{-C}\equiv\text{C-Ph}$ derivatives of the Pt(dbbpy) and Pt(tbtpy) systems [31]. These two acetylides have essentially identical σ -donor strengths, so little difference would be expected between their respective $\text{Pt}\rightarrow\text{N}^{\wedge}\text{N}$ (or $\text{Pt}\rightarrow\text{N}^{\wedge}\text{N}^{\wedge}\text{N}$) energies for a transition which has predominant MLCT character. Whilst this holds true for the pair of bpy complexes, the absorption spectra of $[\text{Pt}(\text{tbtpy})(\text{-C}\equiv\text{C-}t\text{-Bu})]^+$ and $[\text{Pt}(\text{tbtpy})(\text{-C}\equiv\text{C-Ph})]^+$ are rather different from one another in the low energy region, the phenylacetylide system showing a much broader band extending further into the red, and apparently comprising additional transitions. This probably reflects a greater contribution of acetylide $\pi(\text{C}\equiv\text{C})$ character to the HOMO for the phenyl acetylide system, leading to low-energy LLCT transitions. The lowest energy (emissive) state may then be better described as heavily mixed MLCT/LLCT, much like the $\text{Pt}(\text{N}^{\wedge}\text{N})(\text{dithiolate})$ complexes in Sect. 2.4.

These conclusions have been reinforced by at least two recent, detailed theoretical studies using TD-DFT calculations [87, 88], which reveal that the proportion of Pt(5d) metal character in the HOMO falls from around 25% for alkyl acetylides ($\text{R} = n\text{-propyl}$) to around 10% for phenylacetylide, the $\pi(\text{C}\equiv\text{C-R})$ character increasing correspondingly. For an aryl acetylide with

a strongly donating amino substituent, $-\text{C}\equiv\text{C}-\text{C}_6\text{H}_4-\text{NH}_2$, the metal character in the HOMO falls to a meagre 4%, which is lower even than its contribution to the LUMO, so that the HOMO in this instance could be characterized unambiguously as acetylide-based [87].

In their first study of complexes of this type, Yam and co-workers prepared $[\text{Pt}(\text{tpy})(-\text{C}\equiv\text{C}-\text{Ar})]^+$ salts with a range of *p*-substituted aryl groups [89]. The emission energies follow the trend that would be expected for luminescence from an $^3\text{MLCT}$ state; e.g., the energies in MeCN solution at RT decrease in the order $\text{Ar} = -\text{C}_6\text{H}_4\text{NO}_2 > -\text{C}_6\text{H}_4\text{Cl} > -\text{C}_6\text{H}_5 > -\text{C}_6\text{H}_4\text{Me}$, as the electron-donating power of the acetylide substituent increases. However, the quantum yields are quite low in solution, 10^{-3} – 10^{-2} . Superior quantum yields have been obtained in a related set of complexes prepared by Tung et al., containing 4'-tolyl-terpyridine (ttpy) in place of tpy, and including alkyl as well as aryl acetylides. For example, for $[\text{Pt}(\text{ttpy})(-\text{C}\equiv\text{C}-\text{CH}_2\text{OH})]^+$, $\phi = 0.30$ in CH_2Cl_2 at 298 K [90]. Again, the emission energies were found to decrease as the electron-richness of the acetylide increases.

Both research groups have noted the adverse effect on the emission properties exerted by strongly electron-donating aryl groups on the acetylide, especially anilines and phenols. Yam et al. found that 4-methoxyphenyl, 3,4-dimethoxyphenyl, and benzo-15-crown-5- substituted complexes are not emissive in fluid solution [82]. Dialkylamino substituents, including *N*-15-monoazacrown-5, have a similarly adverse effect on emission [91, 92]. These complexes display an intense, low-energy absorption band in solution, around 550 nm, which is attributed to a low-lying excited state of intraligand charge transfer character, a conclusion strongly reinforced by the recent DFT studies mentioned above. Presumably, this state serves to deactivate the $^3\text{MLCT}$ state. On the other hand, it can be put to advantage in the construction of sensory systems, since the binding of the lone pairs of the amine or phenolic heteroatoms to metal ions or protons will raise the energy of the ILCT state, and emission is then "switched on". The induction of emission from the complex $[\text{Pt}(\text{tpy})(-\text{C}\equiv\text{C}-p\text{-benzo-15-crown-5})]^+$ **38** upon binding of Mg^{2+} ions offers an example of this effect (Fig. 18) [93].

Intriguing aggregation effects have been observed for some $\text{Pt}(\text{tpy})$ acetylide complexes, involving Pt–Pt interactions that give rise to low energy $d\sigma^*(\text{Pt}_2) \rightarrow \pi^*(\text{tpy})$ (MMLCT) states, resembling those discussed earlier in this Chapter. For example, $[\text{Pt}(\text{tpy})(\text{C}\equiv\text{C}-\text{C}\equiv\text{CH})]\text{OTf}$ crystallizes in two distinct forms, a red form with a dimeric structure with alternating Pt...Pt distances of 3.394 and 3.648 Å, and a green form with equally spaced platinum atoms (3.388 Å apart) [94]. Upon dissolution in acetonitrile, both forms give a yellow solution with the same UV-vis spectra, and aggregation is ruled out for concentrations up to 2×10^{-3} M on the basis of the good agreement with the Beer-Lambert law. However, the addition of diethyl ether results in a color change from yellow through green to blue, accompanied by the appearance of a low energy emission band centred at 785 nm. This dramatic

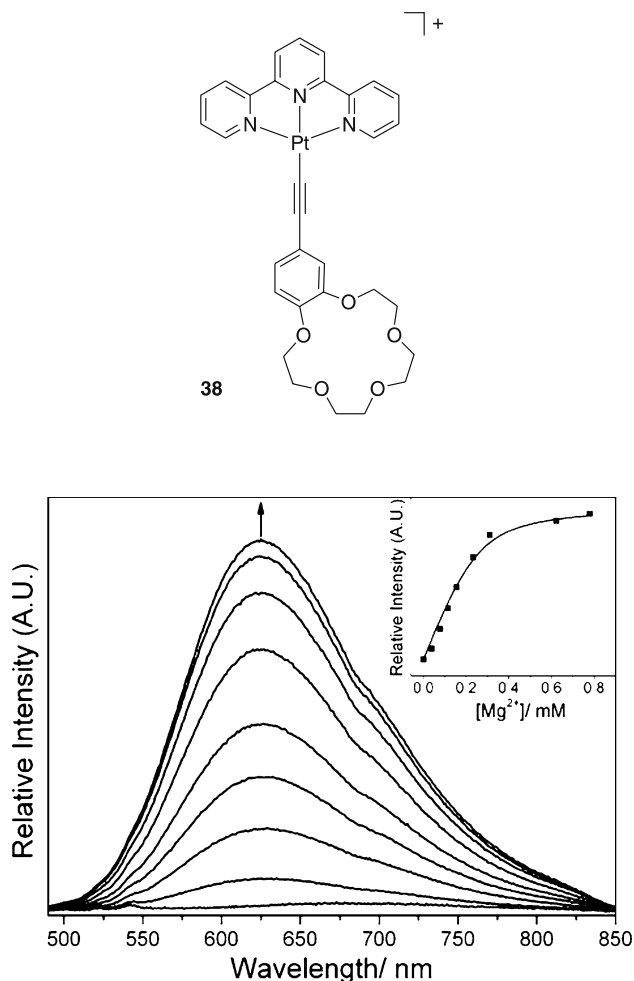


Fig. 18 Growth of emission of **38** in MeCN (2.5×10^{-4} M) upon addition of increasing amounts of $Mg(ClO_4)_2$. *Inset* shows relative intensity at 625 nm vs. $[Mg^{2+}]$ (squares) and the 1 : 1 fit (line). Reprinted from [93] by permission of the Royal Society of Chemistry

effect is attributed to an aggregation process, probably involving trimeric or oligomeric species rather than simply dimers, and triggering the formation of an MMLCT state in solution. A somewhat similar effect has been observed upon addition of poly(acrylic acid) to the same complex in solution in the presence of strong base. Under these conditions, the polymer is ionized, and the interaction of the carboxylate groups of the polyanion with the cationic Pt complexes results in the assembly of the latter, at intermolecular distances appropriate to favor Pt...Pt interactions, signalled by the appearance of new, low-energy absorption bands [95].

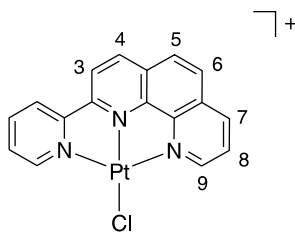
Pt(tpy) acetylides have begun to be explored for photoinduced electron transfer processes, as described for their bpy cousins in Sect. 2.3 [34, 96, 97]. The terpyridyl systems, through functionalization at the 4' position, offer the potential structural advantage of allowing linear connection of units in a donor–chromophore–acceptor array [92]. Odobel et al. have explored the rate of electron transfer between Zn- or Mg-porphyrin electron donors and Pt(tpy) units as acceptors, linked via a *p*-phenylene-bisacetylene linear bridge. Excitation of the porphyrin leads to fast electron transfer (2–20 ps) to the Pt moiety, the rate displaying a Marcus-type variation with the driving force, followed by very fast charge recombination [97].

3.6

[Pt(N[^]N[^]N)X]⁺ with other N[^]N[^]N Ligands

Two limitations of terpyridine as a ligand for platinum(II) are the fact that it is not rigidly planar when bound – there is still scope for distortion in the excited state, promoting non-radiative decay – and the poor bite angle which leads to *trans* N–Pt–N angles of around 160°, compared to an ideal angle of 180° for maximizing the ligand-field strength.

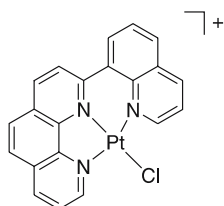
Seeking to tackle the first of these issues, McMillin and co-workers have investigated a series of partially rigidified terpyridine analogues, namely 2-pyridylphenanthroline (php) and derivatives carrying methyl groups in the phen moiety. Unlike [Pt(tpy)Cl]⁺, the new complex [Pt(php)Cl]⁺ **39** proves to be emissive in solution at room temperature: $\phi = 3.1 \times 10^{-3}$ and $\tau = 0.23 \mu\text{s}$ in degassed CH₂Cl₂ [98]. Whilst variable temperature studies do indeed reveal the sought-after sizeable energy gap between the emissive state and a deactivating pathway (presumed to be the excited d-d levels), it is likely that a major reason for the difference compared to tpy is that the excited state has substantial π - π^* character, as evident from the pronounced vibrational structure of the emission spectrum. The introduction of methyl groups into the phen unit leads to a remarkable enhancement of the emission, particularly for the 3,5,6,8-tetramethyl derivative for which $\phi = 0.055$ and $\tau = 9.3 \mu\text{s}$ in CH₂Cl₂. This is probably due to the methyl groups inducing a drop in the



39

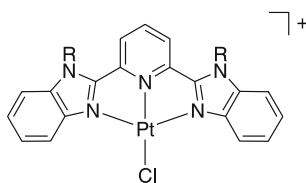
energy of the ${}^3\pi-\pi^*$ excitation, thus enhancing its contribution to the excited state character.

The second issue of how to relieve the strain in the terdentate ligand upon binding, to obtain a more appropriate bite angle and stronger ligand field, has been considered by Thummel and colleagues, who prepared the new ligand 2-(8'-quinolinyl)-1,10-phenanthroline **40** [99]. Note that this ligand resembles php, but coordination to Pt(II) will lead to one 5- and one 6-membered chelate, rather than the two 5-membered chelates in $[\text{Pt}(\text{php})\text{Cl}]^+$, so that ring strain should be relieved. The studies showed that, although the activation barrier to thermally induced quenching is indeed increased with an accompanying enhancement of the lifetime from 0.23 to 0.31 μs , the augmentation is only rather modest. By inspection of the X-ray crystal structure, it is likely that the relieved ring strain is counteracted by more severe steric interactions between ligands, leading to non-planarity and a weakening of the ligand field.



40

2,6-Bis(benzimidazol-2-yl)pyridine (bzimpy) is a terdentate $\text{N}^-\text{N}^-\text{N}^-$ -coordinating analogue of terpyridine, of which, complexes with a number of transition metal ions are known. Haga et al. explored the Pt(II) complex of such a ligand incorporating long-chain C18 alkyl groups on the pyrrolic nitrogen atoms, **41**, with a view to obtaining ordered Langmuir-Blodgett (LB) films [100]. The complex is luminescent in dilute solution ($\lambda_{\text{max}} = 560 \text{ nm}$ in CHCl_3), with a structured emission profile: the smaller HOMO-LUMO gap in bzimpy compared to tpy probably results in greater $\pi-\pi^*$ character to the lowest-energy triplet state. More concentrated solutions show an additional emission band at 650 nm, with a corresponding new shoulder at 550 nm in the excitation spectrum attributed to the formation of a ${}^3\text{MMLCT}$ state through Pt–Pt interactions, much as in Gray's study of $[\text{Pt}(\text{tpy})\text{Cl}]^+$ described earlier [67]. In contrast, such Pt–Pt interactions appear to be suppressed in the LB films prepared. At low surface pressures ($< 15 \text{ mN m}^{-1}$), the $\pi-\pi^*$ emission is observed, but increases in surface pressure result in emission centred around 580–600 nm, rather than the lower-energy Pt–Pt aggregate emission. It is proposed that this emission of intermediate energy is derived from a ligand–ligand π -stacked species, involving partial $\pi-\pi$ stacking of benzene rings and pyridyl rings in two adjacent complexes.

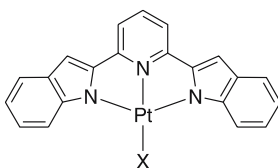


41 R = C₁₈H₃₇

42 R = CH₃

Connick and co-workers have found that the *N,N*-dimethylated bzipmy Pt(II) complex, **42**, displays interesting vapochromic effects [101]. When the counterion is Cl⁻, thin films respond to vapors of MeOH, CHCl₃, EtOH and MeCN by changing color within a few seconds from yellow to red. The PF₆⁻ salt, on the other hand, responds only to MeCN, changing from yellow to violet. Emission spectra are also affected by the vapors, albeit more weakly. On the basis of the spectroscopic evidence, it appears that the vapochromic response is associated with a decrease in the Pt – Pt separation upon uptake of the vapor, favoring the MMLCT [$d\sigma^* \rightarrow \pi^*$] transitions.

Finally in this section, we note that platinum(II) complexes of 2,6-bis(2'-indolyl)pyridine, BIP, have also been explored [102]. Although superficially similar to the bzipmy ligands, complexation of BIP involves deprotonation of the indole nitrogens, so that the bound ligand is actually a dianion, more akin to a cyclometallating ligand (vide infra) than to tpy and its relatives above. The BIP complexes **43** and **44** are luminescent in CH₂Cl₂ at 77 K ($\lambda_{\max} = 572$ and 589 nm, respectively) and in polycarbonate and PVK matrices at room temperature. The emission is assigned to a predominantly $^3\pi-\pi^*$ ligand-centred excited state, with some Pt(d) contribution in the HOMO.



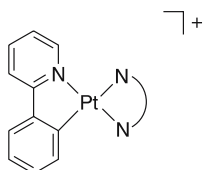
43 X = SMe₂

44 X = pyridine

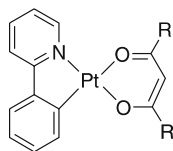
4 Cyclometallated Complexes

4.1 Introduction

Cyclometallation refers to the binding of a polydentate ligand to a metal via a covalent metal–carbon bond, the remaining bonds normally being coordinate bonds from heteroatoms such as nitrogen in the ligand. Cyclometallated complexes are thus strictly organometallic compounds. For example, 2-phenylpyridine (ppy) can bind to a variety of second and third row transition metal ions as an N[^]C ligand, forming a 5 membered chelate through the carbon atom of the phenyl ring which is *ortho* to the link to the pyridine (see the generic structures 45 and 46 below). Since the process involves a net deprotonation of the aromatic C–H, cyclometallating ligands like ppy are anionic, rather than neutral like bpy. The C⁻ ligating atom is a very strong σ donor, whilst the pyridyl group remains a good π -acceptor, so that these ligands offer the metal ion a very strong ligand-field. The important consequence for the photophysics and excited state properties is that the energy of deactivating d-d states is raised compared to analogous N[^]N complexes, much like the effect of acetylide ligands discussed earlier. Thus, many cyclometallated platinum complexes prove to be luminescent in solution under ambient conditions, some of them intensely so. It is this feature that has led to the intense recent interest in such compounds as triplet emitters in organic light-emitting devices [103].



e.g. N[^]N = en, bpy or phen



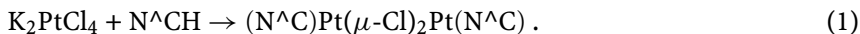
e.g. R = Me or *t*-Bu

4.2

Pt(N[^]C) Complexes with Bidentate Ligands

Von Zelewsky and Balzani showed in the mid-1980s that complexes such as *cis*-Pt(thpy)₂ {thpyH = 2-(2'-thienyl)pyridine} are luminescent in solution ($\lambda_{\text{max}} = 578 \text{ nm}$, $\tau = 2.2 \mu\text{s}$ in PrCN/EtCN mix), whilst a number of other cyclometallating heterocycles form structurally related Pt complexes that are emissive at 77 K, attributed to a ³MLCT state [104, 105]. Variable temperature emission studies subsequently confirmed that the energy gap between the emissive state and the higher energy (deactivating) state is of the order of 3700 cm^{-1} in Pt(thpy)₂, sufficiently large to close off this pathway of deactivation at room temperature [106]. A detailed review of the excited state properties of Pt(thpy)₂, including very low temperature measurements at 1.3 K in a Shpol'skii matrix, has been presented by Yersin & Donges in this journal [107].

Such bis-cyclometallated complexes have been rather eclipsed over the past decade by studies into compounds of the type [Pt(N[^]C)(L[^]L)]⁺ and Pt(N[^]C)(L[^]X), partly owing to their ease of synthesis. The formation of the original Pt(N[^]C)₂ compounds requires the use of the lithiates of the cyclometallating ligands, which are intolerant of many functional groups [104]. In contrast, the introduction of just one N[^]C ligand into the coordination sphere of Pt(II) can normally be accomplished readily upon reaction with simple salts such as K₂PtCl₄, leading to chloro-bridged dimers (Eq. 1).



The dimers can then be cleaved under mild conditions by L[^]L-coordinating diamines or diimines, such as en and bpy to give [Pt(N[^]C)(N[^]N)]⁺ complexes **45** [108], or by bidentate anionic ligands L[^]X, such as β -diketonates to give [Pt(N[^]C)(O[^]O)] complexes **46** [109]. The introduction of monodentate ligands can be achieved similarly, leading to complexes such as [Pt(N[^]C)Cl₂]⁻ [108], [Pt(N[^]C)(CO)Cl] [110], and [Pt(N[^]C)(CO)SR] [111].

Kvam and co-workers investigated the absorption and emission properties of [Pt(ppy)Cl₂]⁻, [Pt(ppy)(en)]⁺, [Pt(ppy)(bpy)]⁺ and [Pt(bpy)(phen)]⁺, using electrochemical data to assist in the assignment of the excited states [108]. The complex [Pt(ppy)Cl₂]⁻, containing weak-field chloride ligands, is luminescent at 77 K, but not at RT. The strong temperature dependence was attributed to a relatively small energy gap of 1700 cm^{-1} between the lowest emitting ³MLCT state and the upper lying d-d states, the thermally activated population of which can occur at RT, quenching the emission. The en, bpy and phen derivatives incorporate stronger-field ligands: these complexes are luminescent in DMF solution at 293 K, $\lambda_{\text{max}} \sim 486 \text{ nm}$ with microsecond lifetimes. Direct population of the emissive triplet state is observed as a weak feature at 482 nm for the en complex, for which a $d_{\text{Pt}} \rightarrow \pi^*_{(\text{N}^{\wedge}\text{C})}$

³MLCT assignment is clear-cut. On the other hand, for the bpy and phen complexes, the electrochemical data indicate that the first reduction process is localized on the diimine rather than the N^ΛC ligand, and a $d_{Pt} \rightarrow \pi^*_{(N^{\Lambda}N)}$ assignment is proposed in these cases [108].

A major systematic study of cyclometallated complexes of the form [Pt(N^ΛC)(O^ΛO)] has been reported recently by Thompson et al. [109], one of the pioneering groups investigating the application of transition metal complexes as phosphorescent emitters in organic light-emitting devices. Twenty-three different N^ΛC ligands were investigated, including several containing substituents in either the phenyl or the pyridyl rings of ppy, as well as some more extended aromatic structures. Acetylacetonate (acac) and dipivaloyl-methane (dpm) were used as the ancillary O^ΛO-chelating ligands, the latter augmenting the solubility of the complexes without significantly affecting the optical properties. DFT calculations suggest that the HOMO levels in these complexes comprise contributions from both Pt and ligand orbitals, while the LUMO is largely localized on the N^ΛC ligand. Electrochemical measurements confirm these predictions, indicating that the reversible reduction waves observed are N^ΛC ligand-based, localized primarily on the pyridine ring, whilst the irreversible oxidations are predominantly metal-based.

All of the complexes are intensely luminescent in glasses at 77 K, and several – though not all – are also quite strongly emissive in fluid solution at RT. The emission energies can be readily rationalized in terms of excited states of predominant ³MLCT character. Thus, electron-*withdrawing* F or CF₃ substituents on the 4' and 6' positions of the *phenyl* ring of ppy induce a blue shift in the emission, as the HOMO is stabilized (Fig. 19). On the other hand, the incorporation of electron-*donating* –OMe or –NMe₂ substituents into the *pyridyl* ring raises the LUMO, also resulting in a blue shift. The effects in the two rings are qualitatively additive, allowing quite substantial shifts towards the blue to be obtained (Fig. 19). Despite the high energy emission, however, Pt(46dfp-4dmapy)(dpm), shown at the top of Fig. 19, is scarcely emissive at 298 K: $\phi < 10^{-3}$ {46dfp-4dmapy = 2-(4',6'-difluorophenyl)-4-(dimethylamino)pyridinato-*N,C*^{2'}'}. Indeed, contrary to the energy gap law, as the energy of emission increases in this series, there is a corresponding decrease in the room temperature ϕ and τ values. Presumably, thermal activation to an MC state or a competing MLCT state on the ancillary β -diketonate becomes significant for the higher energy complexes. The complexes are susceptible to self-quenching and excimer formation, and a detailed study has been carried out for Pt(46dfppy)(acac) (46dfppy = 2-(4',6'-difluorophenyl)pyridinato-*N,C*^{2'}) [112].

Meanwhile, complexes with more extended π systems, or with more polarisable atoms such as sulfur incorporated into the ring, have lower oxidation potentials, and their MLCT excited states are correspondingly lower. Figure 20 illustrates the increasing red-shifts observed upon going from

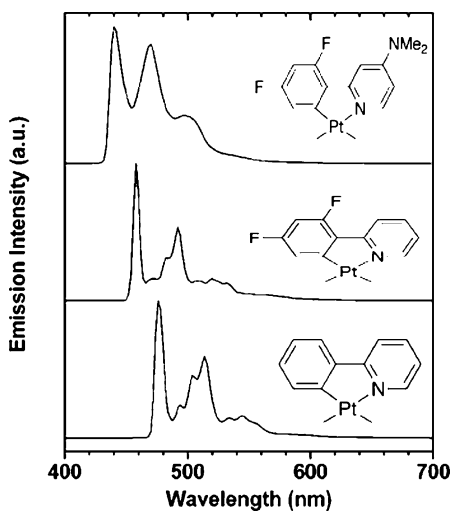


Fig. 19 From bottom to top: Emission spectra of Pt(ppy)(dpm), Pt(46dfppy)(dpm), and Pt(46dfp-4dmapy)(dpm), in MeTHF at 77 K. In the partial structures shown, the O[^]O-chelated dpm ligand has been omitted. Reprinted with permission from [109]. © (2002) American Chemical Society

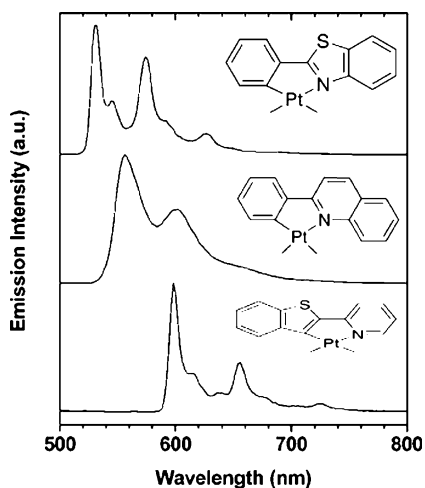


Fig. 20 From top to bottom: Emission spectra of Pt(bt)(dpm), Pt(pq)(dpm), and Pt(btp)(acac), in MeTHF at 77 K. The O[^]O-chelated β -diketone ligand is omitted from the structures shown. Reprinted with permission from [109]. © (2002) American Chemical Society

the complex with 2-phenylbenzothiazole, through 2-phenylquinolyl, to 2-(2'-benzothiazole)-pyridyl.

Large red shifts in the emission of $\text{Pt}(\text{N}^{\wedge}\text{C})(\text{O}^{\wedge}\text{O})$ complexes have also been achieved by the incorporation of stilbene pendants into the 4-position of the pyridyl ring, as reported by Guerchais et al. [113]. Indeed, it proves possible to extend the emission even further into the red through the introduction of either electron-withdrawing or electron-donating substituents into the distal aryl ring of the stilbene unit (Fig. 21). An interesting observation here is that photoinduced *cis-trans* isomerization of the $\text{C}=\text{C}$ bond can proceed readily and, at 77 K, the two isomers have very different emission energies, the *cis* form being about 4400 cm^{-1} higher, with a similar vibrational profile to the *trans* but insensitive to the substituent in the stilbene.

Thompson et al. have reported a set of pyrazolate-bridged $\text{Pt}(\text{N}^{\wedge}\text{C})$ dimers, of the general formula $(46\text{dfppy})\text{Pt}(\mu\text{-pz}')_2\text{Pt}(46\text{dfppy})$, where $\text{pz}' = \text{pyrazolate}$, 3,5-dimethylpyrazolate, 3-methyl-5-*tert*-butylpyrazolate or 3,5-bis(*tert*-butyl)pyrazolate, as well as a monomeric analogue with an Et_2B unit coordinated in place of the second platinum [114]. Single crystal X-ray crystallography reveals that the dimers adopt a boat-like conformation, which brings the platinum centers relatively close together (Fig. 22). Moreover, the introduction of the bulky substituents onto the pyrazolate bridges forces the two $\text{Pt}(\text{N}^{\wedge}\text{C})$ moieties closer together: the Pt – Pt distances range from $3.3763(7)\text{ \AA}$ for $\text{pz}' = \text{pyrazolate}$ to $2.8343(6)\text{ \AA}$ for 3,5-bis(*tert*-butyl)pyrazolate, and Pt \cdots Pt interactions would be anticipated to be en-

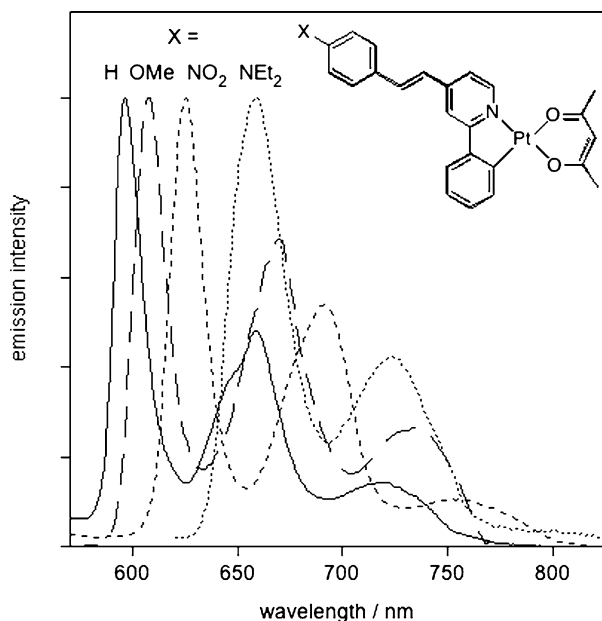


Fig. 21 Emission spectra of stilbene-appended $\text{Pt}(\text{ppy})(\text{acac})$ complexes in EPA at 77 K, showing the influence of the *para* substituent X; $\lambda_{\text{ex}} = 400\text{ nm}$

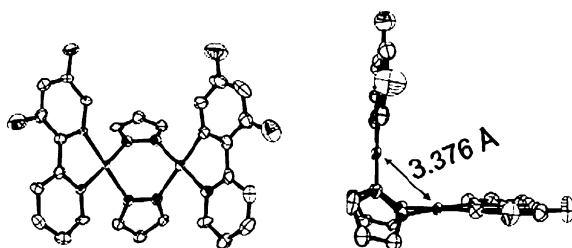


Fig. 22 ORTEP views of $(46dfppy)Pt(\mu\text{-pz})_2Pt(46dfppy)$, showing the boat-like conformation that leads to short metal-metal separations. Reprinted with permission from [114]. © (2005) American Chemical Society

hanced accordingly. That this is the case is clear from the absorption and emission properties. Thus, the complexes with one and two *tert*-butyl substituents are orange and red, respectively, with low-energy absorption bands between 400 and 500 nm that have no counterpart in the other two dimers or in the monomer, which are yellow. These additional bands are assigned to MMLCT transitions. Similarly, in the 77 K emission spectra, these two complexes display a broad, structureless, low-energy emission band, typical of such a transition, whereas the other two complexes have vibrationally structured bands at higher energy, typical of the mixed ${}^3MLCT/{}^3LC$ emission of the $Pt(N^{\wedge}C)$ monomeric complexes. In fluid solution, all four complexes are able to collapse to the MMLCT excited state giving the red emission [114].

Anionic $N^{\wedge}C$ -coordinated complexes incorporating two acetylide ligands, $[Pt(bzq)(-C\equiv C-R)_2]^-$, have been prepared, with a number of alkyl and aryl R groups [115]. They are luminescent in CH_2Cl_2 solution at room temperature, with emission around 530 nm only modestly affected by the identity of R, quantum yields of the order of 5%, and lifetimes of just under a microsecond. On the basis of TD-DFT calculations, the emission is proposed to arise from a mixed $[\pi_{(C\equiv CR)}/d_{Pt}/\pi_{(bzq)} \rightarrow \pi_{(bzq)}^*]$ transition. However, the more structured spectrum observed when $R = -C_6H_4-C\equiv C-Ph$ is likely to originate from an intraligand $\pi-\pi^*$ excited state localized on the extended acetylene $-C\equiv C-C_6H_4-C\equiv C-Ph$.

4.3

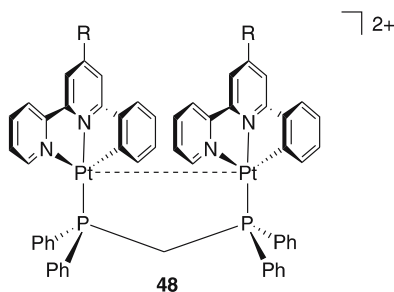
$Pt(N^{\wedge}N^{\wedge}C)$ Complexes

As noted in Sect. 3.1, one of the potential advantages of a terdentate ligand over a bidentate ligand relates to the inhibition of the D_{2d} distortion that bis-bidentate complexes can undergo, through twisting of the two planes relative to one another. The same reasoning applied to cyclometallated systems naturally suggests that if the cyclometallating ring could be incorporated into a terdentate system rather than a bidentate ligand (e.g., $N^{\wedge}N^{\wedge}C$ rather than $N^{\wedge}C$), then further increases in the efficiency of luminescence might be an-

plexes and the parent [Pt(phbpv)Cl] emit at substantially longer wavelengths (665–687 nm) than the other complexes (emission around 600 nm). Moreover, the emission for the former group is shifted to longer wavelengths (700–722 nm) upon cooling the solid to 77 K, whereas the others are blue-shifted. This contrasting behavior is interpreted in terms of an emissive $^3[d\sigma^* \rightarrow \pi^*]$ MMLCT state for the former group, stabilized upon cooling as the Pt–Pt distance decreases, and $^3d \rightarrow \pi^*$ MLCT states for the latter group of complexes [120].

The chloride ligand in [Pt(N[^]N[^]C)Cl] complexes is quite labile, and can be displaced by other ligands. Yip et al. examined a series of four pyridyl adducts, [Pt(phbpv)(py'')](ClO₄) where py'' = pyridine (py), 4-aminopyridine (4-ap), 2-aminopyridine (2-ap), and 2,6-diaminopyridine (dap) [122]. On the basis of absorption spectroscopy, the order of energy of the MLCT excited states was established as py ~ 4-ap > 2-ap > dap. In emission, the py and 4-ap complexes display structured, high-energy emission spectra ($\lambda_{\text{max}} \sim 494$ nm in MeCN at room temperature), assignable to $^3\pi-\pi^*$ states. In contrast, the 2-ap complex emits at substantially lower energy ($\lambda_{\text{max}} 534$ nm), even though the σ -donating ability of 2-ap is similar to 4-ap. The results are interpreted in terms of the role of the ortho-NH₂ groups in destabilizing the Pt $d\pi$ orbitals, through intramolecular interactions of their lone pairs with the metal center. This is supported by the X-ray crystal structures of the 2-ap and dap complexes, which reveal that the Pt–N(H₂) distances are significantly shorter than the sum of the van der Waals radii of Pt and N. Perhaps another way of thinking about this is that such interactions are able to stabilize the hole that is formally generated on the metal upon formation of an MLCT state.

Phosphines can also be introduced into the fourth site. Che's group have explored the use of bidentate or terdentate phosphines, of varying length, to bridge between two or even three Pt complexes **48** [120, 123, 124]. When dppm is used as the bridge (one carbon spacer), low-energy, structureless emission is observed in solution. The bridge holds the two Pt units sufficiently close and in the appropriate face-to-face conformation for Pt...Pt interactions in solution: emission is assigned to the MMLCT excited state. When longer bridges are used (3 or 5 carbon spacers), emission characteris-



tic of the $^3\text{MLCT}$ state is restored [120]. A complex carrying a pendent amine at the other end of the phosphine, $[\text{Pt}(\text{phbpy}) - \text{P}(\text{Ph})_2\text{CH}_2\text{NHPh}](\text{ClO}_4)$, displays pH-dependent emission. The complex is practically non-emissive in aqueous solution ($\phi < 10^{-4}$), due partly to the solvent-induced quenching that normally occurs in water, but also to photoinduced electron transfer (PET) from the amine to the excited Pt complex, an efficient deactivation pathway. Upon protonation of the amine ($\text{p}K_{\text{a}} 3.2$), the emission intensity increases by a factor of 130, as the PET process is suppressed [125].

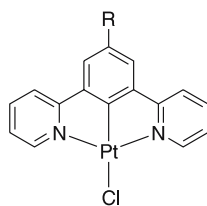
Other sensory systems have exploited the balance between $^3\text{MLCT}$ and $^3\text{MMLCT}$ emission. They include a complementary set of results based on the incorporation of the $\text{Pt}(\text{N}^{\wedge}\text{N}^{\wedge}\text{C})$ unit into a Nafion film and into MCM-41 silicates [126]. In the former, $^3\text{MLCT}$ emission is observed around 540 nm at low loadings of the complex, but this steadily loses out to the $^3\text{MMLCT}$ centred at 665 nm as the concentration of complex within the film increases. For low-loaded, unsaturated films, $^3\text{MMLCT}$ emission is promoted by the uptake of EtOH into the film. For the complex hosted in MCM-41 (2.8 wt %), the effects are essentially the opposite. Thus, the MMLCT emission dominates the spectrum, but uptake of non-polar solvent vapors such as pentane lead to the growth of the monomeric $^3\text{MLCT}$ emission band. Interactions of these types of complexes with proteins and with nucleic acids have also been explored [127, 128].

Che and workers have carried out a comprehensive study of $[\text{Pt}(\text{N}^{\wedge}\text{N}^{\wedge}\text{C})(-\text{C}\equiv\text{C}-\text{R})]$ complexes, in which over 30 derivatives were prepared containing acetylides in the fourth coordination site [129]. Based on the combination of the strong-field cyclometallating carbon, the strong-field acetylide, and the rigidity of the terdentate ligand, high efficiency luminescence would be anticipated and, indeed, all the complexes studied are luminescent in fluid solution, with quantum yields typically in the range 0.05–0.10. Some of the compounds were also doped into organic light-emitting devices: electrophosphorescent efficiencies up to 4.2 cd A^{-1} were measured.

4.4

Pt(N[∧]C[∧]N) Complexes

The superficially trivial switch in the position of the cyclometallating phenyl ring, from lateral to central, leads to substantial differences in the excited state properties. For example, $[\text{Pt}(\text{dpyb})\text{Cl}]$ (**49**, R = H) is intensely emissive in dilute CH_2Cl_2 solution at RT, with a lifetime (7.2 μs) and luminescence quantum yield (0.60) an order of magnitude greater than the corresponding values for $[\text{Pt}(\text{phbpy})\text{Cl}]$ **47** [130]. One reason for the increase in ϕ may relate to the shorter Pt–C bond length in **49** compared to **47**, as shown in the solid state by X-ray crystallography where the difference in bond lengths is about 0.14 Å. This may push the deactivating d-d excited states to yet higher energy, effectively closing off this pathway of non-radiative de-



49

cay. However, a further difference is that the excited state in the N[^]C[^]N systems is predominantly π - π^* in character, an assignment based on the highly structured profile of the emission spectrum, and on the very small Stokes shift between the highest energy emission band and the weak but distinct $S_0 \rightarrow T_1$ absorption band. A detailed theoretical study using DFT has revealed, however, that there is also significant d- π^* character, accounting for the relatively high triplet radiative rate constants [131]. The complexes undergo self-quenching accompanied by excimer formation at elevated concentrations in solution, with bimolecular self-quenching rate constants of the order of $5 \times 10^9 \text{ M}^{-1} \text{ s}^{-1}$. The excimers, $\lambda_{\text{max}} \sim 700 \text{ nm}$, are unusually intensely emissive, with quantum yields of excimer luminescence estimated to be around 0.35 [132].

The introduction of substituents into the 4-position (R) of the central phenyl ring of the N[^]C[^]N ligand allows considerable control over the emission energy. For example, an electron-withdrawing $-\text{CO}_2\text{Me}$ ester group leads to a blue-shift in the luminescence, whilst aryl groups shift the emission increasingly to the red according to their electron-donating ability (Fig. 23) [133]. The trend in decreasing energy shows an approximately linear correlation with the decreasing oxidation potential of the complexes (with the exception of $\text{R} = -\text{C}_6\text{H}_4\text{-NMe}_2$, vide infra). This can be understood in terms of the influence of the substituent on the energy of the HOMO, to which the central ring makes a substantial contribution, compared to its lack of influence on the LUMO, which is localized primarily on the pyridyl rings—the phenyl-4 position is actually a node in the LUMO.

The introduction of the strongly electron-donating pendant $\text{R} = -\text{C}_6\text{H}_4\text{NMe}_2$ leads to a switch in the nature of the lowest-energy excited state from π - π^* to one of primarily intraligand charge transfer character: this complex displays a structureless and much broader emission band than the other compounds and a high degree of positive solvatochromism. The ILCT character is reminiscent of McMillins's study of the influence of electron-donating pendants at the 4'-position of the $[\text{Pt}(\text{tpy})\text{Cl}]^+$ unit (Sect. 3.4). In the present instance, reversible switching between the ILCT and π - π^* states can be induced by simple protonation (Fig. 24). Unusually for transition-metal-based systems, both the ILCT and π - π^* excited states are highly luminescent with quantum yields of the order of 0.5.

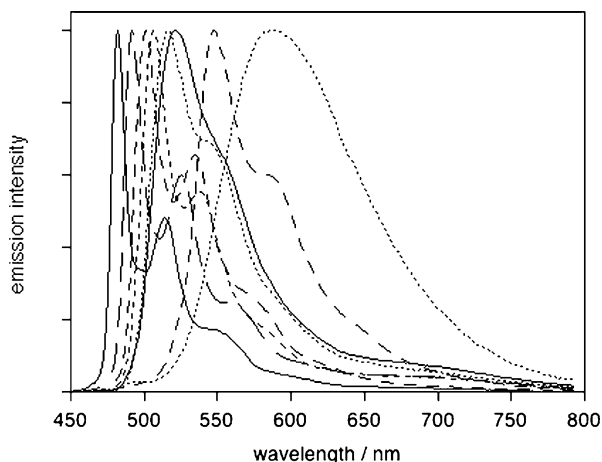


Fig. 23 Emission spectra of N^C^N complexes **49** in CH_2Cl_2 (10^{-5} M), RT, $\lambda_{\text{ex}} = 400$ nm. From left to right: R = $-\text{CO}_2\text{Me}$, H, mesityl, 2-pyridyl, 4-tolyl, 4-biphenyl, 2-thienyl, 4-(dimethyl-amino)phenyl

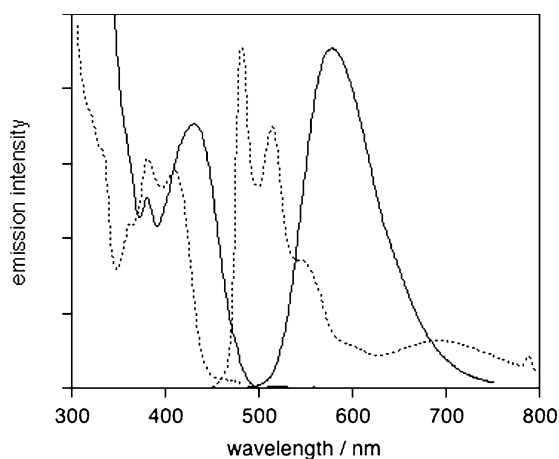
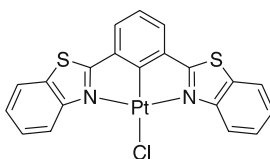
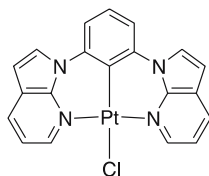


Fig. 24 Emission and excitation spectra of **49**, where R = $-\text{C}_6\text{H}_4\text{-NMe}_2$ (solid lines), in CH_2Cl_2 at RT (6×10^{-5} M), and of the same solution after addition of trifluoroacetic acid (dotted lines)

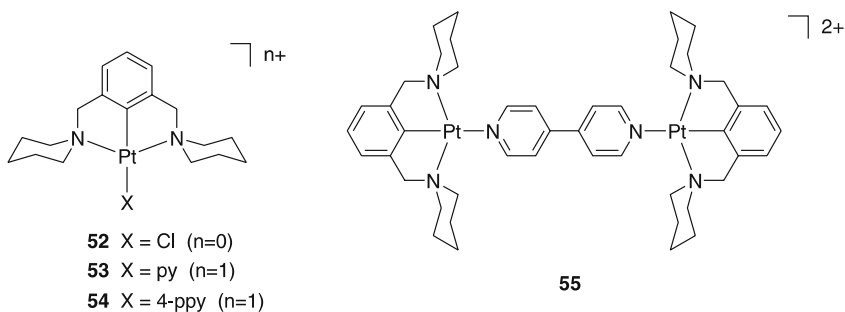
The high emissivity of these compounds renders them particularly attractive as phosphorescent dopants in OLEDs, and high efficiency devices have been obtained using them [134–137]. In particular, the high efficiency of excimer luminescence means that broad coverage of emission across the visible region can be attained (at dopant concentrations where both excimer and monomer emit) rendering the complexes of particular interest for the generation of white-light emitting devices [132]. High efficiency near-IR emitting

devices have also been fabricated [138]. Other applications of such complexes include their use in sensors for molecular oxygen [139]. The luminescence is partially quenched by O₂, but not as strongly as other commonly used phosphors such as Pt porphyrin, permitting useful responses over higher [O₂] ranges.

Related N[^]C[^]N-coordinated complexes containing benzothiazoles **50** or azaindoles **51** in place of the pyridyl rings have also been investigated [140, 141]. Complex **50** is luminescent in solution at room temperature, with π - π^* spectral properties resembling monomeric [Pt(dpyb)Cl], whilst the azaindole complexes are emissive only in the solid state or in glasses at 77 K.

**50****51**

The replacement of the π -acceptor pyridyl rings in the N[^]C[^]N unit by saturated, tertiary amine groups would be expected to lead to a reduction in the ligand field strength, and to a huge increase in the energy of both π - π^* and charge-transfer-to-N[^]C[^]N transitions in the absence of a decent π -acceptor. Lowest-energy excited states of metal-centred character might thus be anticipated (e.g., as for yellow Pt(bpy)Cl₂, Sect. 2.1). Connick and co-workers have explored complexes such as **52**–**54** [142, 143]. The halo complexes (e.g., **52** and



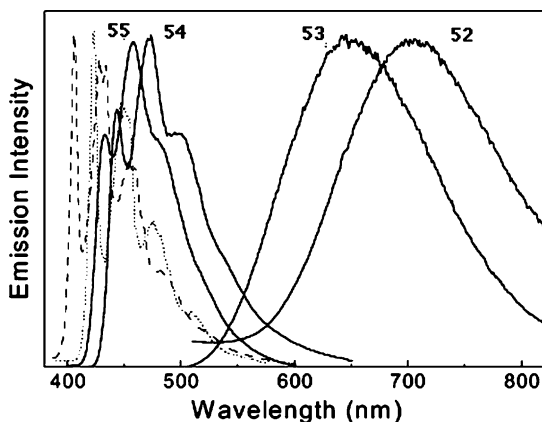


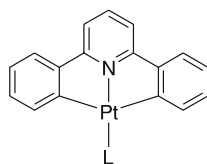
Fig. 25 Emission spectra of the N^C^N coordinated complexes 52–55 at 77 K in ethanol-methanol (4 : 1) glassy solution; the spectra of 4-phenylpyridine (*dotted line*) and 4,4'-bipyridine (*dashed line*) under the same conditions are also shown. Reprinted with permission from [142]. © (2004) American Chemical Society

its Br and I analogues) and the py complex **53** do indeed display structureless metal-centred emission bands in frozen glasses at 77 K: the emission energy decreases in the order $py > Cl > Br > I$, in line with the decreasing order of ligand field strengths. On the other hand, the introduction of 4'-ppy into the fourth coordination site **54**, or 4,4'-bpy as in the dimer **55**, introduces lowest-energy $\pi-\pi^*$ emission bands that are associated with these ligands in the fourth site (Fig. 25).

4.5

Pt(C^N^C) and Pt(C^C) Complexes

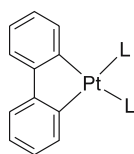
During their work on C^N -coordinated Pt(II) complexes (Sect. 4.2), von Zelewsky et al. prepared charge-neutral, doubly cyclometallated compounds of the type $[Pt(C^N^C)L]$ ($L = py, Et_2S, pz$), by means of a double lithiation of 2,6-diphenylpyridine (dppy) [144]. Following the report by Rourke and co-workers of a more straightforward route to such complexes [145], Che and Yam and colleagues have investigated the photophysics of complexes incorporating such units. For L ligands such as 4-*t*-butylpyridine and 2,6-diphenylisocyanide, $Pt(dppy)L$ **56** display high-energy ($\lambda_{max} \sim 500$ nm), vibronically structured emission spectra in glasses at 77 K, attributed to $\pi-\pi^*$ states [146]. At higher concentrations, this is accompanied by lower-energy emission from excimers, the appearance of which correlates with the presence of solid-state $\pi-\pi$ interactions in the crystal structures. On the other hand, when L is a good π -acceptor ligand such as 1-methyl-4,4'-bipyridinium or pyrazine, strongly red-shifted emission in the 650–700 nm region is at-



56

tributed to a $^3\text{MLCT } d(\text{Pt}) \rightarrow \pi^*(\text{L})$ transition. More recently, the same group has explored related complexes of 2,6-bis(2'-naphthyl)pyridine, including systems that are bridged by dppm, and which show fast and reversible vapochromic responses to halogenated solvents [147]. Yam and co-workers have found that $\text{Pt}(\text{dppy})\text{L}$ complexes containing a variety of pyridyl L ligands, including two crown-ether-linked pyridines, are emissive in solution at RT, in contrast to those with phosphines in the fourth site which are emissive only in the solid state or at low temperature [148].

Finally, we note the unique work of Rillema and co-workers, who reported on a class of remarkably emissive Pt complexes as early as 1992, before much of the work towards RT-emitting systems in preceding sections had been carried out [149]. They studied biphenyl (bph) as a $\text{C}^{\wedge}\text{C}$ -cyclometallating ligand. $\text{Pt}(\text{bph})\text{L}_2$ complexes ($\text{L} = \text{MeCN}$, py and en) were found to be bright emitters in solution ($\phi = 0.15\text{--}0.2$ in DCM). Their highly structured spectra display emission maxima ($\lambda_{\text{max}} \sim 492 \text{ nm}$) that are almost identical for each of the three complexes and for a sulfur-bridged dimer $[\text{Pt}(\text{bph})(\text{EtS})_2]_2$. An unambiguous $\pi\text{-}\pi^*$ assignment is clear-cut here. On the other hand, the ancillary ligands do influence the energy of higher-lying deactivating states. By consideration of the temperature dependence of the lifetimes over the range 140–300 K, the activation energy to this state (ΔE in Fig. 2b) was estimated to vary from 1220 cm^{-1} for $\text{L} = \text{MeCN}$ to 2490 cm^{-1} for $\text{L} = \text{en}$.



57

5 Concluding Remarks

In conclusion, this survey has sought to highlight the advances that have been made over the past decade into the design and development of luminescent platinum(II) complexes. Insight into the factors that influence not only the excited state energies, but also the relative importance of luminescence versus

non-radiative decay and ways to optimize the emission, is constantly developing from fundamental studies. Ligand design is crucial to control of excited state properties. In this respect, new synthetic strategies, particularly cross-coupling methodology that allows aryl and pyridyl rings to be linked together reliably, will play an increasingly valuable role. As the range of complexes with bespoke properties expands, applications should expand in parallel, ranging from new technological materials (e.g., sensors, light-emitting devices, solar-energy conversion—where Pt complexes have scarcely yet been considered) to biology and medicine (e.g., protein and nucleic acid probes, bioimaging).

Acknowledgements It gives the author much pleasure to thank his co-workers and friends David Rochester, Lisa Murphy, and Dr. Stéphanie Develay, for their enthusiastic work on platinum in our laboratory. We are grateful to Dr. Valeria Fattori and her team at the CNR Bologna, Dr Véronique Guerchais and colleagues at l'Université de Rennes, Dr. Julia Weinstein of the University of Sheffield, and Dr Peter Douglas at the University of Swansea, for fruitful and enjoyable collaborations.

References

1. Houlding VH, Miskowski VM (1991) *Coord Chem Rev* 111:145
2. Keller HJ (ed) (1977) *Chemistry and physics of one-dimensional metals*. Plenum Press, New York
3. Miller JS (ed) (1982) *Extended linear chain compounds*. Plenum Press, New York
4. Yeh AT, Shank CV, McCusker JK (2000) *Science* 289:935
5. Douglas P, Eaton K (2002) *Sens Actuat B* 82:1
6. de Haas RR, van Gijlswijk RPM, van der Tol EB, Veuskens J, van Gijssel HE, Tijdens RB, Bonnet J, Verwoerd NP, Tanke HJ (1999) *J Histochem Cytochem* 47:183
7. Wilson JS, Dhoot AS, Seeley AJAB, Khan MS, Köhler A, Friend RH (2001) *Nature* 413:828
8. Wilson JS, Chawdhury N, Al-Mandhary MRA, Younus M, Khan MS, Raithby PR, Köhler A, Friend RH (2001) *J Am Chem Soc* 123:9412
9. Miskowski VM, Houlding VH (1989) *Inorg Chem* 28:1529
10. Miskowski VM, Houlding VH, Che C-M, Wang Y (1993) *Inorg Chem* 32:2518
11. Connick WB, Henling LM, Marsh RE, Gray HB (1996) *Inorg Chem* 35:6261
12. Gliemann G, Yersin H (1985) *Struct Bond* 62:87
13. Wenger OS, García-Revilla S, Güdel HU, Gray HB, Valiente R (2004) *Chem Phys Lett* 384:190
14. McInnes EJJ, Farley RD, Rowlands CC, Welch AJ, Rovatti L, Yellowlees LJ (1999) *J Chem Soc Dalton Trans* 4203
15. Weinstein JA, Grills DC, Towrie M, Matousek P, Parker AW, George MW (2002) *Chem Commun*, p 382
16. George MW, Turner JJ (1998) *Coord Chem Rev* 177:201
17. Shavaleev NM, Moorcraft LP, Pope SJA, Bell ZR, Faulkner S, Ward MD (2003) *Chem Eur J* 9:5283
18. Che CM, Wan K-T, He L-Y, Poon C-K, Yam VW-W (1989) *J Chem Soc Chem Commun*, p 943

19. Pettijohn CN, Jochowitz EB, Chuong B, Nagle JK, Vogler A (1998) *Coord Chem Rev* 171:85
20. Kunkely H, Vogler A (1990) *J Am Chem Soc* 112:5625
21. Wan K-T, Che C-M, Cho K-C (1991) *J Chem Soc Dalton Trans* 1077
22. Connick WB, Henling LM, Marsh RE (1996) *Acta Crystallogr B* 52:817
23. Che C-M, He LY, Poon CK, Mak TCW (1989) *Inorg Chem* 28:3081
24. Kato M, Kosuge C, Morii K, Ahn JS, Kitagawa H, Mitani T, Matsushita M, Kato T, Yano S, Kimura M (1999) *Inorg Chem* 38:1638
25. Chan C-W, Cheng L-K, Che C-M (1994) *Coord Chem Rev* 132:87
26. Connick WB, Geiger D, Eisenberg R (1999) *Inorg Chem* 38:3264
27. Hissler M, Connick WB, Geiger DK, McGarrah JE, Lipa D, Lachicotte RJ, Eisenberg R (2000) *Inorg Chem* 39:447
28. Wadas TJ, Lachicotte RJ, Eisenberg R (2003) *Inorg Chem* 42:3772
29. Whittle CE, Weinstein JA, George MW, Schanze KS (2001) *Inorg Chem* 40:4053
30. Hua F, Kinayyigit S, Cable JR, Castellano FN (2006) *Inorg Chem* 45:4304
31. Castellano FN, Pomestchenko IE, Shikhova E, Hua F, Muro ML, Rajapakse N (2006) *Coord Chem Rev* 250:1819
32. Pomestchenko IE, Luman CR, Hissler M, Ziessel R, Castellano FN (2003) *Inorg Chem* 42:1394
33. Hua F, Kinayyigit S, Cable JR, Castellano FN (2005) *Inorg Chem* 44:471
34. Chakraborty S, Wadas TJ, Hester H, Schmehl R, Eisenberg R (2005) *Inorg Chem* 44:6865
35. McGarrah JE, Kim Y-J, Hissler M, Eisenberg R (2001) *Inorg Chem* 40:4510
36. McGarrah JE, Eisenberg R (2003) *Inorg Chem* 42:4355
37. Lu W, Chan MCW, Zhu N, Che C-M, He Z, Wong KY (2003) *Chem Eur J* 9:6155
38. Zuleta JA, Chesta CA, Eisenberg R (1989) *Inorg Chem* 111:8916
39. Vogler A, Kunkely H (1981) *J Am Chem Soc* 103:1559
40. Zuleta JA, Bevilacqua JM, Proserpio DM, Harvey PD, Eisenberg R (1992) *Inorg Chem* 31:2396
41. Miller TR, Dance IG (1973) *J Am Chem Soc* 95:6970
42. Cummings SD, Eisenberg R (1995) *Inorg Chem* 34:2007
43. Cummings SD, Eisenberg R (1996) *J Am Chem Soc* 118:1949
44. Juris A, Balzani V, Barigelletti F, Campagna S, Belser P, Von Zelewsky A (1988) *Coord Chem Rev* 84:85
45. Caspar JV, Meyer TJ (1983) *Inorg Chem* 22:2444
46. Weinstein JA, Zheligovskaya NN, Mel'nikov MYa, Hartl F (1998) *J Chem Soc Dalton Trans* 2459
47. Weinstein JA, Blake AJ, Davies ES, Davis AL, George MW, Grills DC, Lileev IV, Maksimov AM, Matousek P, Mel'nikov MYa, Parker AW, Platonov VE, Towrie M, Wilson C, Zheligovskaya NN (2003) *Inorg Chem* 42:7077
48. Kishi S, Kato M (2003) *Inorg Chem* 42:8728
49. Anbalagan V, Srivastava TS (1995) *J Photochem Photobiol A Chem* 89:113
50. Puthraya KH, Srivastava TS (1985) *Polyhedron* 4:1579
51. Zhang Y, Ley KD, Schanze KS (1996) *Inorg Chem* 35:7102
52. Connick WB, Gray HB (1997) *J Am Chem Soc* 119:11620
53. Tzeng B-C, Chan S-C, Chan MCW, Che C-M, Cheung K-K, Peng S-M (2001) *Inorg Chem* 40:6699
54. Kato M, Omura A, Toshikawa A, Kishi S, Sugimoto Y (2002) *Angew Chem Int Ed* 41:3183
55. Connick WB, Miskowski VM, Houlding VH, Gray HB (2000) *Inorg Chem* 29:2585

56. Klein A, Kaim W (1995) *Organometallics* 14:1176
57. Ardasheva LP, Shagisultanova GA (1998) *Russ J Inorg Chem* 43:85
58. Che C-M, Chan S-C, Xiang H-F, Chan MCW, Liu Y, Wang Y (2004) *Chem Commun*, p 1484
59. Lin Y-Y, Chan S-C, Chan MCW, Hou Y-J, Zhu N, Che C-M, Liu Y, Wang Y (2003) *Chem Eur J* 9:1264
60. Morgan GT, Burstall FH (1934) *J Chem Soc*, p 1498
61. Lippard SJ (1978) *Acc Chem Res* 11:211
62. Ballhausen CJ, Bjerrum N, Dingle R, Eriks K, Hare CR (1965) *Inorg Chem* 4:514
63. Balzani V, Carassiti V (1968) *J Phys Chem* 72:383
64. Andrews LJ (1979) *J Phys Chem* 83:3203
65. McMillin DR, Moore JJ (2002) *Coord Chem Rev* 229:113
66. Sauvage J-P, Collin J-P, Chambron J-C, Guillerez S, Coudret C, Balzani V, Barigelletti F, De Cola L, Flamigni L (1994) *Chem Rev* 94:993
67. Bailey JA, Hill MG, Marsh RE, Miskowski VM, Schaefer WP, Gray HB (1995) *Inorg Chem* 34:4591
68. Aldridge TK, Stacy EM, McMillin DR (1994) *Inorg Chem* 33:722
69. Yip H-K, Cheng L-K, Cheung K-K, Che C-M (1993) *J Chem Soc Dalton Trans* 2933
70. Michalec JF, Bejune SA, Cuttall DG, Summerton GC, Gertenbach JA, Field JS, Haines JS, McMillin DR (2001) *Inorg Chem* 40:2193
71. DePriest J, Zheng GY, Goswami N, Eichhorn DM, Woods C, Rillema DP (2000) *Inorg Chem* 39:1955
72. Crites Tears DK, McMillin DR (2001) *Coord Chem Rev* 211:195
73. Peyratout CS, Aldridge TK, Crites DK, McMillin DR (1995) *Inorg Chem* 34:4484
74. Wong K-Y, Lee WW-S (1997) *J Photochem Photobiol A* (102):231
75. Wilson MH, Ledwaba LP, Field JS, McMillin DR (2005) *Dalton Trans* 2754
76. Arena G, Monsù Scolaro L, Pasternack RF, Romeo R (1995) *Inorg Chem* 34:2994
77. Arena G, Calogero G, Campagna S, Monsù Scolaro L, Ricevuto V, Romeo R (1998) *Inorg Chem* 37:2763
78. Romeo R, Monsù Scolaro L, Plutino MR, Albinati A (2000) *J Organomet Chem* 593–594:403
79. Becker K, Herold-Mende C, Park JJ, Lowe G, Schirmer RH (2001) *J Med Chem* 44:2784
80. Woodhouse SL, Ziolkowski EJ, Rendina LM (2005) *Dalton Trans* 2827
81. Tzeng B-C, Fu W-F, Che C-M, Chao H-Y, Cheung K-K, Peng S-M (1999) *Dalton Trans* 1017
82. Yam VW-W, Tang RP-L, Wong KM-C, Ko C-C, Cheung K-K (2001) *Inorg Chem* 40:571
83. Rakhimov RD, Weinstein YuA, Lileeva EV, Zheligovskaya NN, Mel'nikov MYa, Butin KP (2006) *Russ Chem Bull* 52:1150
84. Chen W-H, Reinheimer EW, Dunbar KR, Omary MA (2006) *Inorg Chem* 45:2770
85. Crites DK, Cunningham CT, McMillin DR (1998) *Inorg Chim Acta* 273:346
86. Michalec JF, Bejune SA, McMillin DR (2000) *Inorg Chem* 39:2708
87. Liu X-J, Feng J-K, Meng J, Pan Q-J, Ren A-M, Zhou X, Zhang H-X (2005) *Eur J Inorg Chem* 1856
88. Zhou X, Zhang H-Z, Pan Q-J, Xia B-H, Tang A (2005) *J Phys Chem A* 109:8809
89. Yam VW-W, Tang RP-L, Wong KM-C, Cheung K-K (2001) *Organometallics* 20:4476
90. Yang Q-Z, Wu L-Z, Wu Z-X, Zhang L-P, Tung C-H (2002) *Inorg Chem* 41:5653
91. Yang Q-Z, Tong Q-X, Wu L-Z, Wu Z-X, Zhang L-P, Tung C-H (2004) *Eur J Inorg Chem* 1948

92. Wong KM-C, Tang W-S, Lu X-X, Zhu N, Yam VW-W (2005) *Inorg Chem* 44:1492
93. Tang W-S, Lu X-X, Wong KM-C, Yam VW-W (2005) *J Mater Chem* 15:2714
94. Yam VW-W, Wong KM-C, Zhu N (2002) *J Am Chem Soc* 124:6506
95. Yu C, Wong KM-C, Chan KH-Y, Yam VW-W (2005) *Angew Chem Int Ed* 44:791
96. Chakraborty S, Wadas TJ, Hester H, Flaschenreim C, Schmehl R, Eisenberg R (2005) *Inorg Chem* 44:6284
97. Monnereau C, Gomez J, Blart E, Odobel F, Wallin S, Fallberg A, Hammarström L (2005) *Inorg Chem* 44:4806
98. Moore JJ, Nash JJ, Fanwick PE, McMillin DR (2002) *Inorg Chem* 41:6387
99. Hu Y-Z, Wilson MH, Zong R, Bonnefous C, McMillin DR, Thummel RP (2005) *Dalton Trans* 354
100. Wang K, Haga M, Monjushiro H, Akiba M, Sasaki Y (2000) *Inorg Chem* 39:4022
101. Grove LJ, Rennkamp JM, Jude H, Connick WB (2004) *J Am Chem Soc* 126:1594
102. Liu Q, Thorne L, Kozin I, Song D, Seward C, D'Iorio M, Tao Y, Wang S (2002) *J Chem Soc Dalton Trans* 3234
103. Evans RC, Douglas P, Winscom CJ (2006) *Coord Chem Rev* 250:2093
104. Chassot L, Müller E, von Zelewsky A (1984) *Inorg Chem* 23:4249
105. Maestri M, Sandrini D, Balzani V, Chassot L, Jolliet P, von Zelewsky A (1985) *Chem Phys Lett* 122:375
106. Barigelletti F, Sandrini D, Maestri M, Balzani V, von Zelewsky A, Chassot L, Jolliet P, Maeder U (1988) *Inorg Chem* 27:3644
107. Yersin H, Donges D (2001) *Top Curr Chem* 214:81
108. Kvam P-I, Puzyk MV, Balashev KP, Songstad J (1995) *Acta Chem Scand* 49:335
109. Brooks J, Babayan Y, Lamansky S, Djurovich PI, Tsyba I, Bau R, Thompson ME (2002) *Inorg Chem* 41:3055
110. Mdleleni MM, Bridgewater JS, Watts RJ, Ford PC (1995) *Inorg Chem* 34:2334
111. Kovelonov YA, Blake AJ, George MW, Matousek P, Mel'nikov MYa, Parker AW, Sun X-Z, Towrie M, Weinstein JA (2005) *Dalton Trans* 2092
112. Ma B, Djurovich P, Thompson ME (2005) *Coord Chem Rev* 249:1501
113. Yin B, Niemeyer F, Williams JAG, Jiang J, Boucekkine A, Toupet L, Le Bozec H, Guerchais V (2006) *Inorg Chem* 45:8584
114. Ma B, Li J, Djurovich PI, Yousufuddin M, Bau R, Thompson ME (2005) *J Am Chem Soc* 127:28
115. Fernández S, Forniés J, Gil B, Gómez, Lalinde E (2003) *Dalton Trans* 822
116. Chan C-W, Lai T-F, Che C-M, Peng S-M (1993) *J Am Chem Soc* 115:11245
117. Constable EC, Henney RPG, Leese TA, Tocher DA (1990) *J Chem Soc Dalton Trans* 443
118. Constable EC, Henney RPG, Leese TA, Tocher DA (1990) *J Chem Soc Chem Commun*, p 513
119. Cheung T-C, Cheung K-K, Peng S-M, Che C-M (1996) *J Chem Soc Dalton Trans* 1645
120. Lai S-W, Chan MC-W, Cheung T-C, Peng S-M, Che C-M (1999) *Inorg Chem* 38:4046
121. Neve F, Crispini A, Campagna S (1997) *Inorg Chem* 36:6150
122. Yip JHK, Suwarno, Vittal JJ (2000) *Inorg Chem* 39:3537
123. Lu W, Zhu N, Che C-M (2002) *Chem Commun*, p 900
124. Lu W, Chan MCW, Zhu N, Che C-M, Li C, Hui Z (2004) *J Am Chem Soc* 126:7639
125. Wong K-H, Chan MC-W, Che C-M (1999) *Chem Eur J* 5:2845
126. Che C-M, Fu W-F, Lai S-W, Hou Y-J, Liu Y-L (2003) *Chem Commun*, p 118
127. Che C-M, Zhang J-L, Lin L-R (2002) *Chem Commun*, p 2556
128. Ma D-L, Che C-M (2003) *Chem Eur J* 9:6133

129. Lu W, Mi B-X, Chan MC-W, Hui Z, Che C-M, Zhu N, Lee S-T (2004) *J Am Chem Soc* 126:4958
130. Williams JAG, Beeby A, Davies ES, Weinstein JA, Wilson C (2003) *Inorg Chem* 42:8609
131. Sotoyama W, Satoh T, Sato H, Matsuura A, Sawatari N (2005) *J Phys Chem A* 109:9760
132. Cocchi M, Kalinowski J, Virgili D, Fattori V, Develay S, Williams JAG (2007) *Appl Phys Lett* 90:163508
133. Farley SJ, Rochester DL, Thompson AL, Howard JAK, Williams JAG (2005) *Inorg Chem* 44:9690
134. Sotoyama W, Satoh T, Sawatari N, Inoue H (2005) *Appl Phys Lett* 86:153505
135. Cocchi M, Virgili D, Fattori V, Rochester DL, Williams JAG (2007) *Adv Funct Mater* 17:285
136. Kalinowski J, Cocchi M, Virgili D, Fattori V, Williams JAG (2006) *Chem Phys Lett* 432:110
137. Virgili D, Cocchi M, Fattori V, Sabatini C, Kalinowski J, Williams JAG (2006) *Chem Phys Lett* 433:145
138. Cocchi M, Virgili D, Fattori V, Williams JAG, Kalinowski J (2007) *Appl Phys Lett* 90:023506
139. Evans RC, Douglas P, Williams JAG, Rochester DL (2006) *J Fluorescence* 16:201
140. Okamoto K, Kanbara T, Yamamoto T, Wada A (2006) *Organometallics* 25:4026
141. Song D, Wu Q, Hook A, Kozin I, Wang S (2001) *Organometallics* 20:4683
142. Jude H, Krause Bauer JA, Connick WB (2002) *Inorg Chem* 41:2275
143. Jude H, Krause Bauer JA, Connick WB (2004) *Inorg Chem* 43:725
144. Deuschel-Cornioley C, Ward T, von Zelewsky A (1988) *Helv Chim Acta* 71:130
145. Cave GWV, Fanizzi FP, Deeth RJ, Errington W, Rourke JP (2000) *Organometallics* 19:1355
146. Lu W, Chan MCW, Cheung K-K, Che C-M (2001) *Organometallics* 20:2477
147. Kui SCF, Chui SS-Y, Che C-M, Zhu N (2006) *J Am Chem Soc* 128:8297
148. Yam VW-W, Tang RP-L, Wong KM-C, Lu X-X, Cheung K-K, Zhu N (2002) *Chem Eur J* 8:4066
149. Blanton CB, Murtaza Z, Shaver RJ, Rillema DP (1992) *Inorg Chem* 31:3230

Photochemistry and Photophysics of Coordination Compounds: Gold

Vivian Wing-Wah Yam (✉) · Eddie Chung-Chin Cheng

Department of Chemistry, The University of Hong Kong,
Pokfulam Road, Hong Kong, China
wwyam@hku.hk

1	Introduction	270
2	Photophysical and Photochemical Properties of Gold(I) Complexes	272
2.1	Homoleptic Gold(I) Complexes with Phosphine Ligands	272
2.2	Gold(I) Chalcogenido and Thiolato Complexes	275
2.3	Gold(I) Alkynyl Complexes	284
2.4	Trinuclear Complexes with Exobidentate N [∧] C/N Bridging Ligands	292
2.5	Miscellaneous Gold(I) Complexes	296
3	Photophysical and Photochemical Properties of Gold(II) Complexes	296
4	Photophysical and Photochemical Properties of Gold(III) Complexes	298
4.1	Gold(III) Alkyl and Aryl Complexes with Ancillary Diimine Ligands	298
4.2	Cyclometallated Gold(III) Complexes	298
4.3	Porphyrinato Gold(III) Complexes	301
5	Conclusion	305
	References	305

Abstract Gold, in addition to its attractive historical monetary value, has attracted growing attention from the chemical perspective. A significant proportion of recent contributions has been associated with the luminescent behavior of gold compounds, some of which are associated with the presence of the weak closed-shell aurophilic interactions. In this review the photophysical properties of several classes of gold complexes in the oxidation states of + 1, + 2 and + 3 are discussed. Some of them also exhibit interesting photochemical properties. Such growth of attention has proven the potential application of gold complexes to serve as promising light-emitting molecular materials.

Keywords Gold · Excited state properties · Luminescence · Photochemistry · Photophysics

Abbreviations

bpy	bipyridyl
B15C5	benzo-15-crown-5
dcpe	1,2-bis(dicyclohexylphosphino)ethane
dcpm	bis(dicyclohexylphosphino)ethane
dmb	1,8-diisocyano- <i>p</i> -menthane

dmpm	bis(dimethylphosphino)methane
dmmp	bis(dimethylphosphinomethyl)methylphosphine, $\text{Me}_2\text{PCH}_2\text{P}(\text{Me})\text{CH}_2\text{PMe}_2$
dpmp	bis(diphenylphosphinomethyl)phenylphosphine, $\text{Ph}_2\text{PCH}_2\text{P}(\text{Ph})\text{CH}_2\text{PPh}_2$
dppb	1,4-bis(diphenylphosphino)benzene
dppe	1,2-bis(diphenylphosphino)ethane
dppf	1,1'-bis(diphenylphosphino)ferrocene
dpphen	4,7-diphenyl-1,10-phenanthroline
dppm	bis(diphenylphosphino)methane
dppn	1,8-bis(diphenylphosphino)naphthalene
dpppe	1,5-bis(diphenylphosphino)pentane
dppy	2-diphenylphosphinopyridine
DB18C6	dibenzo-18-crown-6
IL	intra ligand
<i>i</i> -mnt	1,1-dicyanoethylene-2,2-dithiolate
LLCT	ligand-to-ligand charge transfer
LMCT	ligand-to-metal charge transfer
LMMCT	ligand-to-metal-metal charge transfer
mes	mesityl
MLCT	metal-to-ligand charge transfer
MMLCT	metal-metal-to-ligand charge transfer
MV^{2+}	methyl viologen
NHC	<i>N</i> -heterocyclic carbene
Np	1-naphthyl
phen	1,10-phenanthroline
PPE	poly(<i>p</i> -phenylene-ethynylene)
PPN	bis(triphenylphosphine)iminium
SSCE	saturated sodium chloride calomel electrode
thf	tetrahydrofuran
TCNQ	7,7,8,8-tetracyanoquinodimethane
tmb	2,5-diisocyano-2,5-dimethylhexane
TPA	1,3,5-triaza-7-phosphaadamantane
tppb	1,2,4,5-tetrakis(diphenylphosphino)benzene
TPPH ₂	5,10,15,20-tetraphenylporphyrin
VOC	volatile organic compounds

1

Introduction

While gold has been regarded as precious and widely utilized as money, a store of value and in jewelery since the ancient times, the exploration and development of the coordination and organometallic chemistry of gold are also fascinating and challenging, and have attracted increasing attention from chemists. The uniqueness of the weak intermolecular attractive interaction present in between gold centers [1, 2] has attracted the increasing attention of the scientific community since the 1990s, and this has been one of the reasons that has accelerated the scientific development of gold in

both physical and chemical aspects. This intermolecular attractive Au···Au interaction, which is the most remarkable among all elements, is especially prominent in gold(I) systems. Gold(I) has a closed-shell d^{10} electronic configuration and the tendency for weak metal···metal interaction involving affinity between same charges has been attributed to the sub-bonding interaction introduced through the stabilization of the filled $5d$ -orbital-based molecular orbitals by configuration mixing with empty molecular orbitals of appropriate symmetry derived from the higher-energy $6s$ and $6p$ orbitals. The strong relativistic effects possessed by gold also cause the contraction of the $6s$ orbital and, to a smaller extent, the $6p$ orbitals, and at the same time the expansion of $5d$ orbitals [2–4]. Besides, the spin-orbit coupling would also be enhanced. All these effects would bring the $5d$ and $6s/6p$ orbitals closer in energy, having a more effective overlap and stronger interaction. Consequently, the phenomenon of mononuclear gold(I) complexes showing a tendency to undergo intermolecular aggregation via short sub-van der Waals gold-gold contacts of less than 3.4 \AA is expected and observed. Gold-gold contacts of $\sim 3.0 \text{ \AA}$ were estimated to have a bond energy of the order of $5\text{--}10 \text{ kcal mol}^{-1}$ [1]. This energy is comparable to that of standard hydrogen bonds and thus provides extra stability to polynuclear gold(I) complexes. Similarly, short intramolecular Au···Au contacts are also commonly observed based on this effect and as a result would give rise to the unique and intriguing structural properties in gold(I) complexes. The term “aurophilicity” describing this phenomenon [1, 2] was introduced by Schmidbaur and is widely accepted today. Pyykkö and co-workers suggested the dispersion (van der Waals) nature of aurophilicity by performing theoretical calculations on a gold(I) dimer, $[\text{Au}(\text{PH}_3)\text{Cl}]_2$, at the Hartree–Fock and Møller–Plesset levels, and suggested that the aurophilic attraction was caused by correlation effects and strengthened by relativistic effects rather than hybridization [5–7]. In addition, the rich photophysical properties that gold complexes exhibit have no doubt made this class of complexes an important family of luminescent metal complexes. The presence of the heavy gold center in these complexes will enhance the spin-orbit coupling of the system, which in turn will facilitate the access to triplet excited states via intersystem crossing. Relaxation of the triplet excited state by radiative decay would usually result in phosphorescence with large Stokes shifts. Subsequently, the photophysical properties and the associated photochemical studies of some of these complexes have also been initiated. The photoreactivity of gold(I) and gold(III) systems have recently been reviewed by Vogler and co-workers [8].

In this review, the photophysical and photochemical properties of selected gold systems will be described and discussed, so as to provide readers with a broad overview of the great diversity of these systems in these aspects.

2

Photophysical and Photochemical Properties of Gold(I) Complexes

2.1

Homoleptic Gold(I) Complexes with Phosphine Ligands

The first report on gold(I) luminescence dates back to 1970, when Dori and co-workers studied the photoluminescence properties of $[\text{Au}(\text{PPh}_3)\text{Cl}]$ [9]. In 1989, the fascinating photophysical properties and excited-state redox behavior of $[\text{Au}_2(\text{dppm})_2]^{2+}$ were reported independently by Fackler [10] and Che [11, 12]. It was found that the annular complex, $[\text{Au}_2(\text{dppm})_2](\text{BF}_4)_2$, exhibits strong and long-lived yellow phosphorescence, and a Au–Au bonded emissive excited state was suggested. The triplet excited state, $[\text{Au}_2(\text{dppm})_2]^{2+*}$, was also demonstrated to be strongly reducing in nature, with the excited-state redox potential $E^0[\text{Au}_2(\text{dppm})_2^{3+/2+*}]$ of $-1.6(1)$ V vs. SSCE determined via oxidative quenching experiments using a series of pyridinium acceptors [11, 12]. In the same year, the electronic absorption and magnetic circular dichroism studies of the related systems with $\text{Me}_2\text{P}-(\text{CH}_2)_n-\text{PMe}_2$ ($n = 1, 2$) as the bridging ligands were reported by Mason and co-workers [13]. Since then, growing attention has been given to the exploration of luminescent gold(I) systems. The effect of the extent of Au...Au interactions on the photophysical properties of the annular complex $[\text{Au}_2(\text{dmpm})_2](\text{ClO}_4)_2$ was investigated by Yam and co-workers, through a direct comparison with the trinuclear analogue, $[\text{Au}_3(\text{dmmp})_2](\text{ClO}_4)_3$ [14, 15]. It was found that both complexes display dual phosphorescence ($[\text{Au}_2(\text{dmpm})_2](\text{ClO}_4)_2$: $\lambda_{\text{max}} = 455$ nm, $\tau_0 = 1.2$ μs ; $\lambda_{\text{max}} = 555$ nm, $\tau_0 = 2.8$ μs . $[\text{Au}_3(\text{dmmp})_2](\text{ClO}_4)_3$: $\lambda_{\text{max}} = 467$ nm, $\tau_0 = 1.6$ μs ; $\lambda_{\text{max}} = 580$ nm, $\tau_0 = 7.0$ μs) in degassed acetonitrile solutions upon photo-excitation. The high-energy emission band was assigned to originate from an excited state of intraligand character while the low-energy band was assigned to originate from the $^3[(d\delta^*)^1(p\sigma)^1]$ excited state. The observed red shift of both the $^1[d\sigma^* \rightarrow p\sigma]$ absorption and $^3[(d\delta^*)^1(p\sigma)^1]$ phosphorescence on going from $[\text{Au}_2(\text{dmpm})_2](\text{ClO}_4)_2$ to $[\text{Au}_3(\text{dmmp})_2](\text{ClO}_4)_3$ (269 nm \rightarrow 315 nm and 555 nm \rightarrow 570 nm, respectively), is in line with the reduced $d\sigma^*-p\sigma$ and $d\delta^*-p\sigma$ energy gaps as illustrated in Fig. 1 [14]. A similar red shift was also reported for the absorption bands of the phenyl-containing phosphine counterparts, $[\text{Au}(\text{PPh}_3)_2]\text{OTf}$, $[\text{Au}_2(\text{dppm})_2](\text{OTf})_2$ and $[\text{Au}_3(\text{dpmp})_2](\text{SCN})_3$, as depicted in Fig. 2 [16]. The excited-state redox potentials, $E^0[\text{Au}_2(\text{dmpm})_2^{3+/2+*}]$ and $E^0[\text{Au}_3(\text{dmmp})_2^{4+/3+*}]$, were determined to be $-1.7(1)$ and $-1.6(1)$ V vs. SSCE, respectively [14]. The stronger reducing power of $[\text{Au}_2(\text{dmpm})_2]^{2+*}$ than $[\text{Au}_3(\text{dmmp})_2]^{3+*}$ was attributed to the fact that the latter with a charge of 3+ is more difficult to be oxidized.

Very recently, Che re-investigated [17] and reviewed [18] the $[\text{Au}_2(\text{P}^{\wedge}\text{P})_2]^{2+}$ system using the optically transparent dcpm ligand (for $\lambda \geq 250$ nm), and

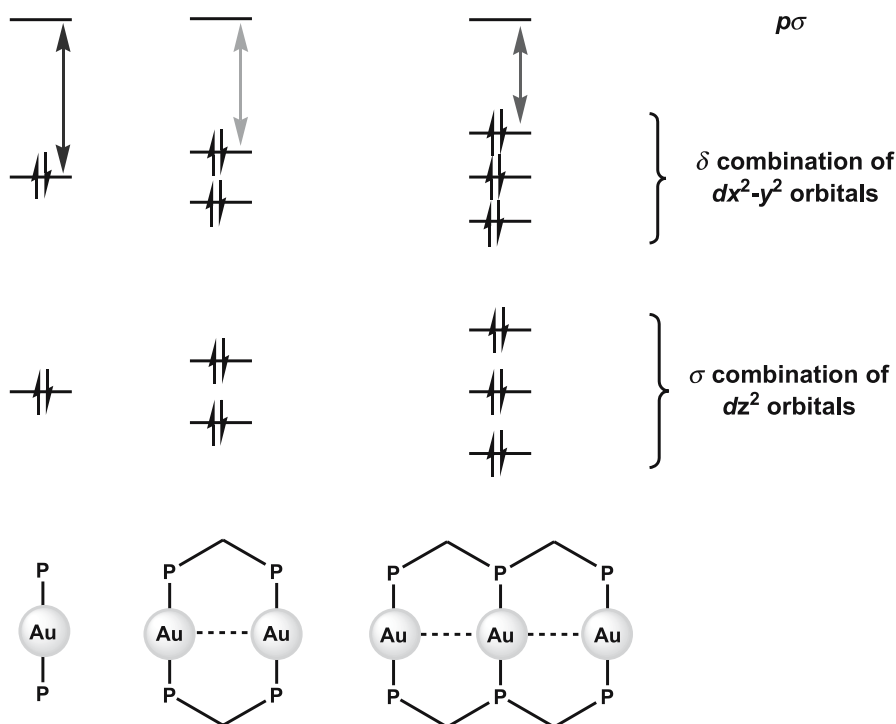


Fig. 1 Schematic molecular orbital diagram showing the effect of aurophilic contacts on the HOMO-LUMO energy gap of gold(I) phosphine complexes

the photophysical properties of $[\text{Au}_2(\text{dcpm})_2]^{2+}$ bearing a series of counter-anions (ClO_4^- , PF_6^- , CF_3SO_3^- , $[\text{Au}(\text{CN})_2]^-$, Cl^- , I^-) were studied. It was suggested that the emission energy could be readily perturbed by the presence of coordinating solvents and anions. The intrinsic $^3[(d\sigma^*)^1(p\sigma)^1]$ phosphorescence of $[\text{Au}_2(\text{R}_2\text{PCH}_2\text{PR}_2)_2]^{2+}$ should occur in the near UV region (~ 368 nm for $\text{R} = \text{Cy}$) whereas the observed blue-green emission in MeCN was attributed to the phosphorescence associated with the exciplexes formed in the presence of coordinating solvents/anions. This has been supported by theoretical calculations at the ab initio level by the single excitation configuration interaction (CIS) method using the model complex, $[\text{Au}_2(\text{H}_2\text{PCH}_2\text{PH}_2)_2]^{2+}$, in which a comparably high-energy emission at 331 nm was calculated from the 3A_u excited state in the absence of solvent- or anion-exciplex formation [19]. The weak aurophilic interaction observed in the ground state of $[\text{Au}_2(\text{H}_2\text{PCH}_2\text{PH}_2)_2]^{2+}$ is strengthened significantly in the $^1[(d\sigma^*)^1(p\sigma)^1]$ excited state, and is in line with the findings from the resonance Raman spectroscopic studies on $[\text{Au}_2(\text{dcpm})_2](\text{ClO}_4)_2$, in which

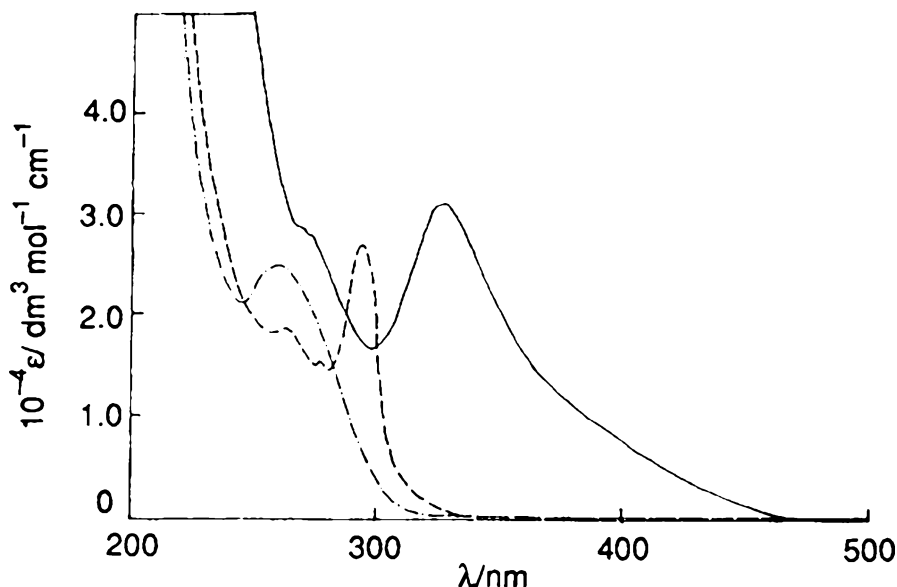


Fig. 2 Electronic absorption spectra of $[\text{Au}(\text{PPh}_3)_2]\text{OTf}$ (- · - · - ·), $[\text{Au}_2(\text{dppm})_2](\text{OTf})_2$ (- - -) and $[\text{Au}_3(\text{dmmp})_2](\text{SCN})_3$ (—) in MeCN at room temperature [16]

the ground and $^1[(d\sigma^*)^1(p\sigma)^1]$ excited state vibrational frequencies of 88 and 175 cm^{-1} were determined, respectively [20, 21]. As a result, the high-energy emission band of $[\text{Au}_3(\text{dmmp})_2](\text{ClO}_4)_3$ ($\lambda_{\text{max}} = 467\text{ nm}$) in degassed acetonitrile that was previously assigned to originate from the intraligand character could also be re-assigned to originate from the $^3[(d\sigma^*)^1(p\sigma)^1]$ excited states; whereas the low-energy emission ($\lambda_{\text{max}} = 580\text{ nm}$) was attributed to the exciplex phosphorescence due to the coordination of MeCN to $[\text{Au}_3(\text{dmmp})_2]^{3+}$ core in the excited states.

Yip and co-workers recently isolated a trinuclear gold(I) complex with 9,10-bis(diphenylphosphino)anthracene ligand, $[\text{Au}_3(\mu\text{-Ph}_2\text{PANPPH}_2)_3](\text{ClO}_4)_3$, with a cyclophane structure and interesting cyclohexane-like fluxional behavior [22]. The complex also exhibits intense emission with a structureless band maximized at 475 nm in MeCN at 298 K. The absence of any structural features in the emission band and the large Stokes shift of $\sim 4000\text{ cm}^{-1}$ suggested the excimeric nature of the emission.

Examples of luminescent gold(I) phosphine complexes with coordination number greater than two were also reported in the literature. Gray and co-workers reported a binuclear gold(I) complex, $[(\mu\text{-dcpe})\{\text{Au}(\text{dcpe})\}_2](\text{PF}_6)_2$, with each gold(I) center being 3-coordinated by one chelating dcpe and one bridging dcpe ligand (Fig. 3), and separated by 7.0501 \AA (as a $[\text{Au}(\text{CN})_2]^-$ salt) [23]. The complex was found to be strongly emissive in the green

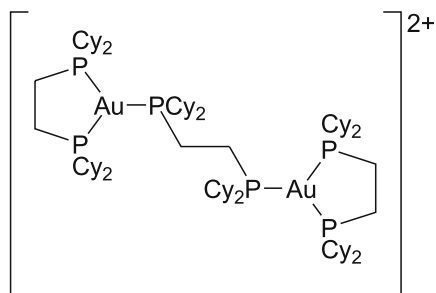


Fig. 3 Structure of the complex cation of $[(\mu\text{-dcpe})\{\text{Au}(\text{dcpe})\}_2](\text{PF}_6)_2$

region, and such emission was suggested to be associated with the sterically protected monomeric AuP_3 moiety. Fackler also explored a series of mononuclear gold(I) phosphine complexes having the AuP_3 moiety, such as $[\text{Au}(\text{PPh}_3)_3]^+$, $[\text{Au}(\text{TPA})_3]^+$ and $[\text{Au}\{\text{P}(3\text{-C}_6\text{H}_4\text{SO}_3)_3\}_3]^{8-}$ [24–26]. In general, the 3-coordinate gold(I) complexes are more strongly emissive than their 2-coordinate counterparts and the emission was attributed to originate from a metal-centered $^3[(d\sigma^*)^1(p\sigma)^1]$ excited state. A complex with a tripodal phosphine, $[\text{Au}\{\text{N}(\text{PPh}_2)_3\}]^+$, was also reported to be luminescent [27].

Yam and co-workers reported the first luminescent study of 4-coordinate gold(I) phosphine complexes, $[\text{Au}(\text{P}^\wedge\text{P})_2]\text{X}$ ($\text{P}^\wedge\text{P} = 1,8\text{-bis}(\text{diphenylphosphino})\text{naphthalene}$, 4-methyl-1,8-bis(diphenylphosphino)naphthalene; $\text{X} = \text{Cl}$, PF_6) in 2000 [28]. The complexes were shown to exhibit orange-red photoluminescence both in the solid state and in dichloromethane, and the emission origin was attributed to the triplet state derived from a $[\sigma \rightarrow \pi^*(\text{naphthyl})]$ IL transition. The PF_6^- salt of the complexes were also employed as an emissive layer in the fabrication of OLEDs.

2.2

Gold(I) Chalcogenido and Thiolato Complexes

There has been an immense research interest devoted to the d^{10} metal-chalcogenide nanoparticles due to their rich intrinsic photoluminescence properties. However, photophysical studies related to the gold(I) chalcogenides are relatively rare, possibly due to the relative instability of gold(I) chalcogenides compared to that of gold metal. Since 1999, Yam and co-workers reported the isolation of a series of luminescent hexanuclear, decanuclear and dodecanuclear gold(I) sulfido complexes, 1–3 (Fig. 4), with the ancillary diphosphine ligands acting as a “protective coating” against the formation of binary materials [29–32]. These complexes are soluble in common organic solvents and are molecular in nature, which may serve as model systems for the study of gold(I) sulfide clusters and nanoparticles. Short intramolecular auriphilic interactions, with the $\text{Au} \cdots \text{Au}$ distances

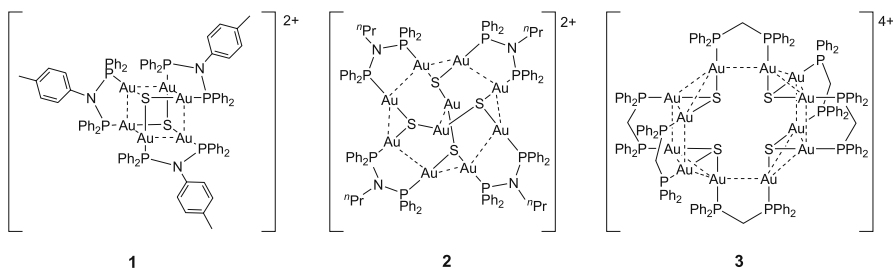


Fig. 4 Luminescent high-nuclearity gold(I) sulfido complexes 1–3

in the range of 2.939–3.3775 Å, were observed in the X-ray crystal structures of these complexes. In addition, all the complexes exhibit intriguing photophysical properties. They display an orange to red emission that has been attributed as derived from states of a $^3\text{LMMCT} [\text{S} \rightarrow \text{Au} \cdots \text{Au}]$ origin. Interestingly, complex **2** exhibits dual luminescence behavior with an additional emission band in the green region that was tentatively assigned as the metal-perturbed $^3\text{IL}(\text{diphosphine})$ phosphorescence, while an abnormally large Stokes shift of $15\,052\text{ cm}^{-1}$ (1.87 eV) was observed for **1** that is suggestive of a highly distorted excited state structure. Figure 5 displays the electronic absorption, emission and excitation spectra of **1** in dichloromethane at 298 K. Fenske reported a series of luminescent gold(I)-selenido aggregates, namely $[\text{Au}_{18}\text{Se}_8(\text{dppe})_6]\text{Br}_2$ and $[\text{Au}_{10}\text{Se}_4(\text{dpppe})_4]\text{Br}_2$ [33]. The former possesses long-lived red phosphorescence in the solid state and is capable of photosensitizing singlet oxygen in solution, while the latter shows a broad near-infrared phosphorescence at 880 nm in dichloromethane that red-shifted to 1020 nm in the solid state.

El-Sayed and Whetten reported the visible to infrared luminescence behavior of a $\text{Au}_{28}(\text{SG})_{16}$ (GSH = glutathione) monolayer protected clus-

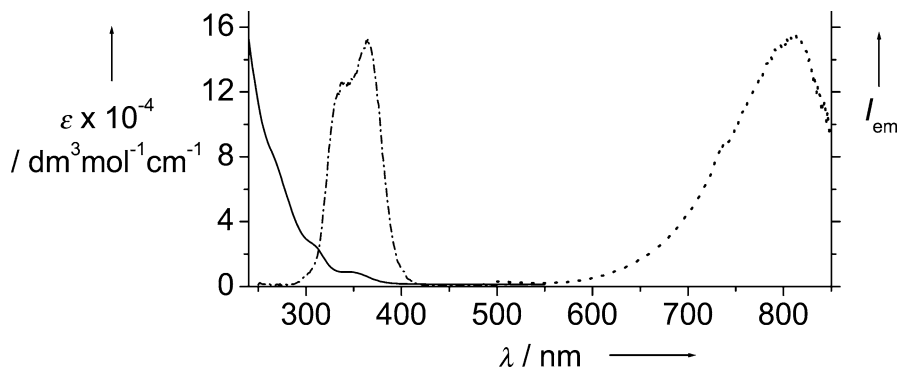


Fig. 5 Electronic absorption (—), emission (···) (excitation at 365 nm) and excitation (– · – · –) (monitored at 810 nm) spectra of **1** in dichloromethane solution at 298 K [29]

ter (MPC) [34]. Emission maxima at ~ 1.15 eV (1080 nm) and ~ 1.5 eV (~ 827 nm) were observed in D_2O . An assignment of these low-energy emission to emissive states associated with a $[S \rightarrow Au \cdots Au]$ LMMCT origin, similar to that assigned for complexes 1–3, is possible using a molecular model. Alternatively, the 1.15 eV emission band could also be attributed using the solid-state model to the intraband transition within the sp -band across the HOMO-LUMO gap, whereas the 1.5 eV emission is attributed to the interband recombination between the sp and d bands. In another study, Murray and co-workers studied the photophysical properties of a series of Au-MPCs with different core sizes and monolayers, and it was found that the NIR emission was an electronic surface-state phenomenon [35–37].

Laguna and Eisenberg collaboratively reported the rich luminescence behavior of a series of luminescent gold-silver complexes, $[E\{Au_3(dppy)\}_3Ag](BF_4)_2$ ($E = O, S, Se$) [38]. The solid-state emission energy at ambient temperature was found to change substantially on going from $E = O$ (466 nm, blue) to S (554 nm, yellow) and Se (670 nm, orange). Addition of a methyl group on the dppy ligand for the sulfido complex would blue-shift the solid-state emission to afford a green emission (534 nm) (Fig. 6). The red shift on going from $E = S$ to Se and the microsecond-ranged lifetime were in agreement with a 3LMMCT assignment of the excited state, while for the oxo complex, either a 3LMMCT or metal-centered cluster-based emission was suggested.

Balch examined an interesting reversible orthorhombic-monoclinic phase change in the crystals of $[S(AuCNC_7H_{13})_3](SbF_6)$ upon cooling [39]. At 190 K, two complex cations were found to self-associate to form a pseudo-octahedral array of six gold atoms connected by both intra- and inter-ionic

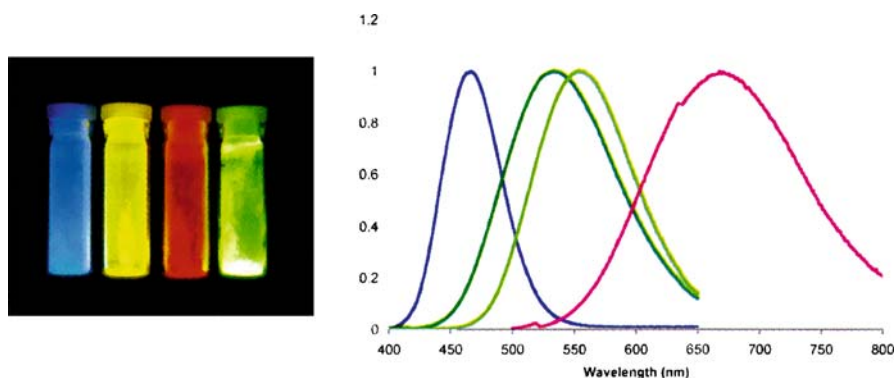


Fig. 6 Photo of the solid-state emission from $[E\{Au_3(dppy)\}_3Ag](BF_4)_2$ ($E = O, S, Se$) and $[S\{Au_3(Me-dppy)\}_3Ag](BF_4)_2$ from left to right ($\lambda_{ex} = 365$ nm) (left), and the normalized emission spectra of $[E\{Au_3(dppy)\}_3Ag](BF_4)_2$ ($E = O$ (blue), S (green), Se (red)) and $[S\{Au_3(Me-dppy)\}_3Ag](BF_4)_2$ (dark green) in the solid state at room temperature (right) [38]

aurophilic interactions. Subsequent cooling caused the clusters to become less symmetric, leading to an increase in the inter-ionic Au···Au separations in one cluster and a decrease in the other. In addition, crystalline samples of $[\text{S}(\text{AuCNC}_7\text{H}_{13})_3](\text{SbF}_6)$ showed corresponding changes in their emission properties, with a single emission at 667 nm at 298 K switched to a dual phosphorescence at 490 and 680 nm at 77 K. In contrast, no change in the crystallographic phase or luminescence properties upon cooling was observed for $[\text{S}(\text{AuCNC}_6\text{H}_{11})_3](\text{PF}_6)$, which possesses a structure similar to that of $[\text{S}(\text{AuCNC}_7\text{H}_{13})_3](\text{SbF}_6)$ at 190 K.

All these examples illustrate the wide range of structural variety and their fascinating relationship with the delicate excited state properties in these polynuclear gold(I) chalcogenido complexes.

On the other hand, the luminescence studies of the related gold(I) thiolate complexes with ancillary phosphine ligands were initiated at an earlier time. In fact, the *d-sp* configurational mixing idea was first applied by Vogler and co-workers in the interpretation of the electronic absorption and emission properties of gold(I) complexes bearing weak Au···Au interaction [40]. The tetranuclear gold(I) dithioacetate, $[\text{Au}(\text{MeCS}_2)]_4$, which was first isolated and structurally characterized to possess a rhombic Au₄ array with short Au···Au contacts of ~ 3.016 Å by Zanazzi and co-workers [41, 42], was found to display low-energy absorptions at 407 and ~ 430 nm in CS₂ at room temperature and a low-energy emission maximum at 743 nm in ethanol glass at 77 K [40]. A related $[\text{Au}(\text{piperidine})\text{Cl}]_4$, which was reported by Guy et al. to possess also a Au₄ array in the solid state [43], displayed an absorption band at 305 nm at room temperature and an emission band at 700 nm at 77 K in EtOH [40]. The significant difference in the absorption energy among these two tetranuclear complexes and yet their similarity in emission energy suggested that the emission should not be derived from states with MLCT character but rather a metal-centered *5d-6s* transition that was modified by the metal-metal interaction. The strength of the Au···Au interaction in the related binuclear anionic $[\text{Au}_2(\text{CS}_3)_2]^{2-}$, which possesses a short Au–Au contact of 2.80 Å (as a PPN⁺ salt) [44], was studied (in its ⁿBu₄N⁺ salt) using electronic absorption and resonance Raman spectroscopies by Cheng et al. [45], and a stretching frequency of 125 cm⁻¹ was identified to be the $\nu(\text{Au} - \text{Au})$ mode.

Bruce and Bruce reported the phosphorescence nature of a series of binuclear gold(I) thiolate complexes bearing bridging diphosphine ligands, $[\text{Au}_2\{\text{Ph}_2\text{P}(\text{CH}_2)_n\text{PPh}_2\}(4\text{-SC}_6\text{H}_4\text{Me})]$ ($n = 2-5$) and $[\text{Au}_2\{\text{Ph}_2\text{P}(\text{CH}_2)_n\text{PPh}_2\}(\text{SCH}_2\text{CH}_2\text{CH}_2\text{S})]$ ($n = 2-5$), and the emission with energies spanned in the range of 485–515 nm was attributed to originate from the $[\text{S} \rightarrow \text{Au}]$ LMCT excited state [46]. Although correlation studies between the extent of Au···Au interactions calculated from EXAFS and the luminescence properties were attempted, no simple, clear-cut correlation could be made. In another study, Fackler reported the luminescence study of a series of mononuclear gold(I)

thiolate complexes, with the TPA ligand that possesses a small cone angle of 102° and shows no low-energy IL transitions for $\lambda_{\text{abs}} > 210$ nm (in water) [47].

It was found that solely the emission maxima could not be used to predict the presence or absence of weak Au \cdots Au interactions. According to a LMCT assignment, a blue shift in the emission energy would be expected when the thiolate ligand is changed from -SPh to -(4-SC₆H₄Cl), and yet the presence of weak Au \cdots Au interactions in [Au(TPA)(4-SC₆H₄Cl)] (Au \cdots Au = 3.078 Å) could shift the emission maxima to the red, by as much as 2500 cm⁻¹ compared to that of [Au(TPA)(SPh)] (Au \cdots Au = 5.243 Å). The emission energy of this class of complexes was suggested to be controlled by: (1) the presence of electron-withdrawing groups on the thiolate ligand, and (2) whether there was any Au \cdots Au interaction present, either intramolecularly or intermolecularly. Electron-withdrawing groups on the thiolate ligand would stabilize the sulfur orbital, making the ligand more difficult to be oxidized and hence causing a blue shift in the emission. The presence of short Au \cdots Au contacts would destabilize the 5*dz*² orbitals (taking the Au \cdots Au interaction axis as the *z*-axis) while the empty 6*p_z* orbitals would be stabilized. This would bring a net effect of lowering the transition energy and results in a red shift in the emission energy. Such interpretation formed the basis for the LMMCT assignments that are widely used today. Replacement of the TPA ligand with PPh₃ further complicated the results and assignments. It was suggested that the π and π^* orbitals associated with PPh₃ were very close in energy to the S- and Au-based orbitals, such that a change in the substituents with different electron-withdrawing effects on the thiolate ligands could affect the relative ordering of these orbitals [47]. Yam reported the photophysical studies of a series of binuclear gold(I) thiolate complexes with bridging bis(diphenylphosphino)alkyl- and -aryl-amines, [Au₂{Ph₂PN(R)PPh₂}(4-SC₆H₄R')₂] (R = Ph, Cy, ⁿPr, ⁱPr; R' = F, Cl, Me) [48]. Interestingly, only very weak or no intramolecular Au \cdots Au interaction was identified in the crystal structure of [Au₂{Ph₂PN(C₆H₁₁)PPh₂}(4-SC₆H₄F)₂], with the corresponding non-bonded Au \cdots Au distance of 3.4779(4) Å. At room temperature, these complexes exhibit intense blue-green phosphorescence that was typical of metal-perturbed ligand-centered emission. Lowering of the temperature to 77 K in CHCl₃ glass matrices gave dual emission, in which excitation of the sample at ~ 300 nm produced a green emission centered at ~ 500 nm whereas excitation at ~ 440 nm resulted in a new orange emission band centered at ~ 600 nm. Such a new band was suggested to be derived mainly from the ³[S \rightarrow Au] LMCT excited states, although the possibility of a LLCT origin cannot be excluded. It was believed that the presence of aurophilic interactions could lower the emission energy in such systems, and were employed in the design of luminescence chemosensors for alkali metal ions. Indeed, a series of diphosphine-bridged binuclear gold(I) complexes with benzocrown-ether functionalized thiolate ligands were demonstrated to

be capable of sensing alkali metal ions, with specificity depending on the size of the crown ether pendants. Upon encapsulation of alkali metal ions of appropriate size, i.e. when the alkali metal ion was intramolecularly sandwiched between two crown ether pendants, the intramolecular Au···Au interaction became “switched on” and the emission energy would be lowered according to the change of emission nature from a $^3[S \rightarrow \text{Au}]$ LMCT to a $^3[S \rightarrow \text{Au} \cdots \text{Au}]$ LMMCT origin (Fig. 7) [49–51].

Recently, mono- and binuclear gold(I) complexes **4a–g** (Fig. 8), bearing the carboimidothiolate ligand ($\text{O}_2\text{N}-\text{C}_6\text{H}_4-\text{N}=\text{C}(\text{OMe})\text{S}^-$) were reported to be photoluminescent [52]. However, their luminescence behavior was suggested to be dominated by the intraligand donor–acceptor charge transfer, with only slight mixings of the $^3[S \rightarrow \text{Au}]$ LMCT character that has been modified by the weak Au···Au interactions.

Systems bearing dithiolate ligands were also studied by a number of research groups. Zink explored the emission nature of $[\text{Au}(\text{PET}_3)_2]^+[\text{Au}(\text{AuPET}_3)_2(i\text{-mnt})_2]^-$ in which the emission at $\sim 19600\text{ cm}^{-1}$ ($\sim 510\text{ nm}$) showed weak vibronic structures with average progressional spacings of $\sim 470\text{ cm}^{-1}$ that

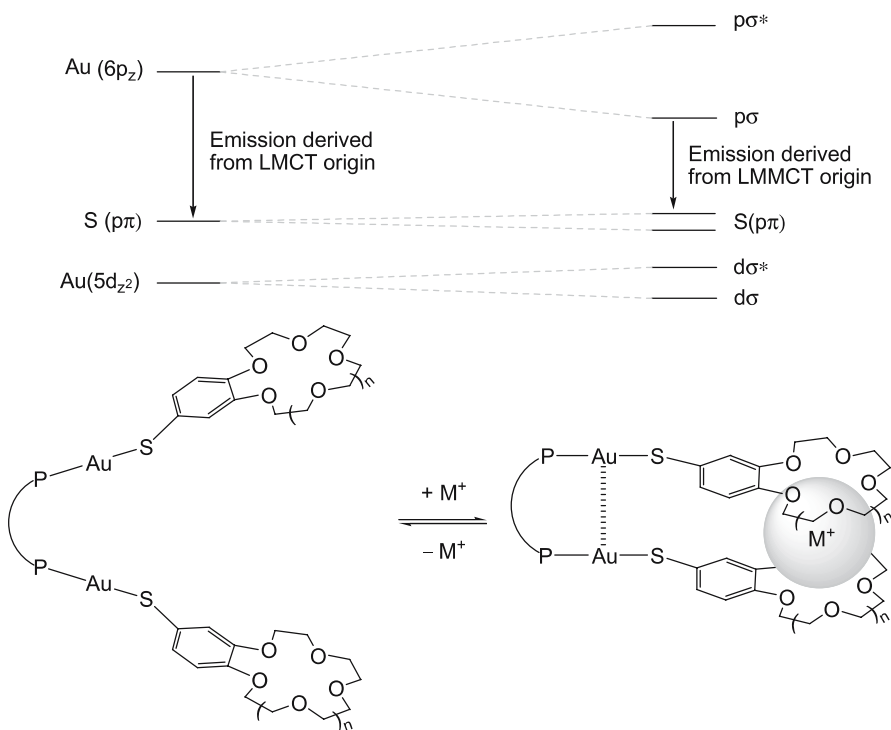


Fig. 7 Red shift in emission energy of binuclear gold(I) thiolate complexes via metal-ion encapsulation

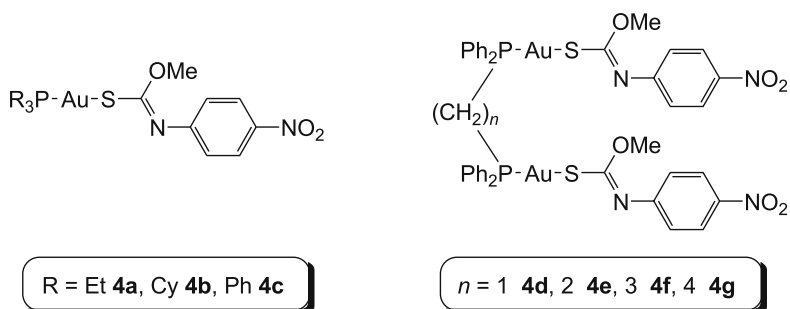


Fig. 8 Gold(I) complexes **4a–g** with thiolate ligand bearing donor-acceptor functionalities

were associated with the Au – S stretch [53]. Assignment of the emission origin was assisted by the results from the pre-resonance Raman spectrum, and the origin was attributed to a [S → Au] LMCT excited state associated with the trinuclear complex anion. A series of annular binuclear gold(I) complexes of the type $[\text{Au}_2(\mu\text{-P}^{\wedge}\text{P})(\mu\text{-S}^{\wedge}\text{S})]^{n+}$ ($n = 0, 1$) were investigated by Lin and co-workers [54], in which the observed concentration dependence of the electronic absorption, emission and variable temperature ^{31}P NMR spectra of $[\text{Au}_2(\text{dppm})(\text{S}_2\text{C}=\text{NEt}_2)](\text{PF}_6)$ provided indication for the presence of intermolecular dimerization process via the weak $\text{Au}\cdots\text{Au}$ interactions in a concentrated solution. A monomer-dimer ratio of 1.4 was observed, with an equilibrium constant of $\sim 38 \text{ M}^{-1}$, ΔH of $\sim 14 \text{ kcal mol}^{-1}$ and ΔS of $\sim -35 \text{ cal K}^{-1} \text{ mol}^{-1}$ determined. Trinuclear gold(I) dithiocarbamate complexes with bridging $\text{Ph}_2\text{PCH}_2\text{P}(\text{Ph})\text{CH}_2\text{PPh}_2$ were reported by Laguna [55]. The complexes were found to be fluxional in solution, and a red shift in the solid-state emission energy was observed upon increasing the number of dithiocarbamate ligands from 1 to 3. By using the piperazine-1,4-dicarbodithiolate and dppm as bridging ligands, Yu, Li and Yam reported the synthesis of a tetranuclear gold(I) complex **5** that crystallized as a tetramer [i.e. an Au_{16} complex [54]] (Fig. 9) by self-assembly, in which supramolecular chirality of the complex cation was induced upon the intermolecular aggregation process driven solely by weak $\text{Au}\cdots\text{Au}$ interactions [56]. Complex **5** displayed a low-energy absorption at $\sim 370 \text{ nm}$ in MeCN which is concentration-dependent, and a 5-5₂ monomer-dimer equilibrium was identified with ε_{max} (5_2), equilibrium constant and ΔG determined to be $2600 \text{ M}^{-1} \text{ cm}^{-1}$, 6800 M^{-1} and 22 kJ mol^{-1} , respectively. Complex **5**₄ exhibited intense green solid-state photoluminescence, which was slightly blue-shifted from 531 to 524 nm on lowering the temperature from 293 to 77 K. Complex **5** displayed intense orange emission at $\sim 605\text{--}608 \text{ nm}$ in MeCN and Me₂CO solutions at 293 K with an excitation band centered at 324–331 nm, whereas in ⁿPrCN glass at 77 K, the emission maximum was significantly blue-shifted to 501 nm. The emission has been attributed to originate from [S → Au] LMCT excited states, probably modified by the presence of weak $\text{Au}\cdots\text{Au}$ interac-

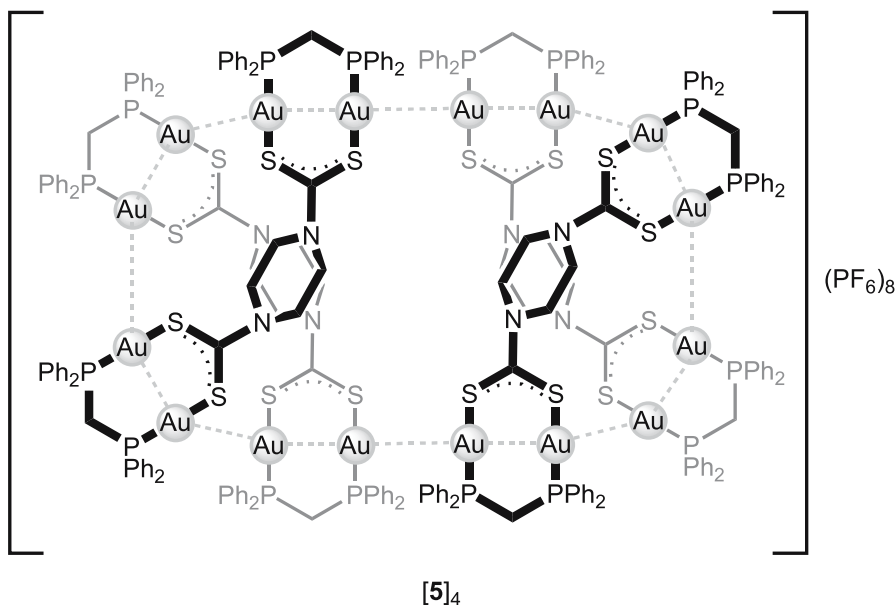


Fig. 9 Chiral Au₁₆ aggregate [5]₄ via self-assembly process

tions. The blue shift observed upon decreasing temperature was attributed to the increased rigidity of the molecular structure at low temperature, which rendered a smaller geometrical distortion in the excited states and hence a smaller Stokes shift. In contrast to the electronic absorption studies, concentration dependence was not significant on the phosphorescence energy of **5** which might be suggestive of an emission origin having a ligand-to-metal-metal charge transfer (LMMCT) character localized on the intramolecular Au··Au interaction in the Au₂ unit or one that has a predominant ligand-centered or ligand-to-ligand charge transfer character.

Eisenberg reported the interesting vapochromism and VOC-induced luminescence behavior of a phosphine-free binuclear gold(I) dithiocarbamate complex, [Au₂{S₂CN(C₅H₁₁)₂}] [57]. The crystal structures in the emissive solvated orange form and the non-emissive naked colorless form were determined, in which weak intermolecular Au··Au interactions could only be observed in the former (Au··Au_{intermol} (orange-form): 2.9617(7) Å, Au··Au_{intermol} (colorless-form): 8.135 Å). When the colorless form was brought in contact with polar aprotic solvent vapors, luminescence could be restored. The formation of linear Au··Au chains induced by solvent triggered its orange color and luminescence nature, even though there was no unusual complex-solvent interaction in the solid state. The stoichiometries of the complex to solvent molecules in the two forms were determined from NMR integration and thermogravimetric analysis, in which one acetone molecule

per 2.5 dimers and one acetone molecule per three dimers were determined, respectively, when using acetone as the triggering solvent.

Fackler and co-workers were able to correlate the relationship between the intermolecular Au...Au interactions and the presence of photo-luminescence in a series of binuclear annular gold(I) dithiophosphonate complexes with different extents of intermolecular Au...Au interactions [58, 59]. This not only enables one to predict the presence of any weak intermolecular Au...Au interactions based on the observed luminescence properties of this class of complexes, but also allows one to estimate the relative extent of such interactions.

The luminescent binuclear gold(I) dithiophosphate complexes $[\text{Au}_2\{\text{S}_2\text{P}(\text{OR})_2\}_2]$ ($\text{R} = \text{Me}, \text{Et}$) were found to possess comparable intra- and intermolecular aurophilic contacts and afforded one-dimensional Au – Au chain structures [60]. At 77 K, solid samples of $[\text{Au}_2\{\text{S}_2\text{P}(\text{OMe})_2\}_2]$ displayed multiple emission bands, with the two concentration-dependent higher energy bands at 415 nm ($\tau = 20$ ns) and 456 nm ($\tau = 2.16$ μs) assigned to ^1MC and ^3MC emission, respectively, while the lower energy band at 560 nm was attributed to a LMCT excited state. $[\text{Au}_2\{\text{S}_2\text{P}(\text{OR})_2\}_2]$ was further shown to exhibit intense luminescence of different colors and striking thermochromism of the emission in frozen glasses of different solvents.

Another interesting phenomenon, luminescence tribochromism, was demonstrated in a series of binuclear gold(I) thiouracilate diphosphine complexes, **6–7** (Fig. 10) [61]. It refers to a sustained change in the photoluminescence spectrum upon the initial application of a pressure. Complexes **6a–b**, which possess the singly deprotonated thiouracilate ligand, were found to be weakly emissive, whereas **7a–b** bearing the doubly deprotonated ligand exhibited intense blue to cyan photoluminescence. Interconversion of **6** and **7**, as indicated by the turning on-and-off of the emission, could be achieved by pressure application and recrystallization, as well as through pH control. It

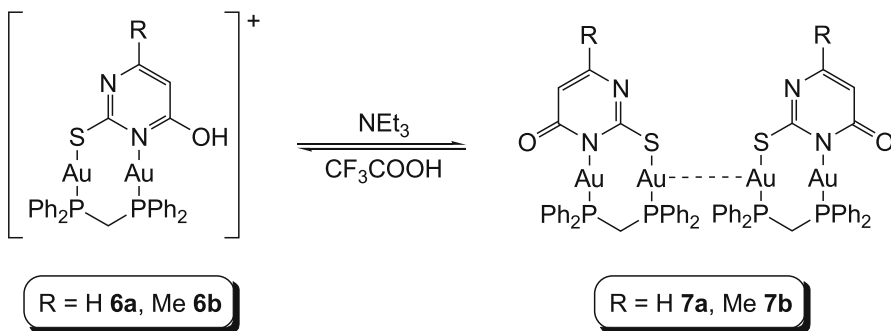


Fig. 10 Acid-base controlled interconversion of **6** and **7**

was suggested that the observation of the intense emission is a consequence of the presence of strong intermolecular Au··Au interactions.

2.3

Gold(I) Alkynyl Complexes

The gold(I) alkynyl systems represent another important class of organo-metallic gold(I) complexes. The rigid nature of the alkynyl ligand with the sp hybridized carbons gives rise to a linear $\text{C}\equiv\text{C}$ unit with an angle of 180° . These, together with the preferential linear two-coordinate geometry of gold(I), have made this class of complexes attractive as building blocks for molecular design and supramolecular architecture [62–69] that may find potential applications in molecular electronics and materials science [70–76].

Gold(I) alkynyls are also well-known to usually exhibit interesting luminescence properties. The first report dealt with the spectroscopic and photophysical properties of $[\text{Au}_2(\text{dppe})(\text{C}\equiv\text{CPh})_2]$ that possesses an intramolecular Au··Au contact of $3.153(2)$ Å [77]. The complex exhibited an IL emission at 420 nm in dichloromethane at 298 K and a solid-state emission at 550 nm at 298 K that was attributed to the $[(d\delta^*)^1(p\sigma)^1]$ phosphorescence. The related complex, $[\text{Au}_3(\text{dppm})_2(\text{C}\equiv\text{CPh})_2][\text{Au}(\text{C}\equiv\text{CPh})_2]$, which possesses a trinuclear $[\text{Au}_3(\text{dppm})_2(\text{C}\equiv\text{CPh})_2]^+$ cation and intramolecular Au··Au distances of $3.083(2)$ and $3.167(2)$ Å, showed a dual phosphorescence with the high-energy IL emission at 425 nm and the low-energy $[(d\delta^*)^1(p\sigma)^1]$ emission at 600 nm in MeCN at 298 K [78].

The photophysical properties of a series of alkynyl-bridged binuclear gold(I) complexes, $[(\text{Ph})_n(\text{Np})_{3-n}\text{PAuC}\equiv\text{CAuP}(\text{Ph})_n(\text{Np})_{3-n}]$ ($n = 0-3$) and $[\text{Fc}_2\text{PhPAuC}\equiv\text{CAuPPhFc}_2]$ have been studied by Mingos and Yam in 1994 [62]. Observation of the vibronically structured absorption bands at 296 nm was suggestive of their $^1[\sigma(\text{Au-P}) \rightarrow \pi^*(\text{Np})]$ transition origin. The red shift of solid-state emission energies of the former complexes at 77 K upon increasing the number of Np groups on the phosphines is in line with the increasing electron-richness around the Au–P bonds and the presence of a $^3[\sigma(\text{Au-P}) \rightarrow \pi^*(\text{Np})]$ excited state. However, the presence of the ferrocenyl moiety in the latter complex resulted in effective intramolecular reductive electron transfer quenching, which gave rise to its weakly emissive nature. $[(4\text{-C}_6\text{H}_4\text{OMe})_3\text{PAuC}\equiv\text{CAuP}(4\text{-C}_6\text{H}_4\text{OMe})_3]$ was reported to have a well-resolved vibronic-structured emission that ranged from 400 to 600 nm with progressional spacings of $\sim 2100\text{ cm}^{-1}$, and the emission origin was ascribed to originate from the $^3[\pi \rightarrow \pi^*(\text{C}\equiv\text{C})]$ IL excited state [79]. A series of gold(I) complexes bearing bridging phosphine or alkynyl ligands, $[(4\text{-C}_6\text{H}_4\text{Me})_3\text{PAu}(\text{BL})\text{AuP}(4\text{-C}_6\text{H}_4\text{Me})_3]$ ($\text{H}_2\text{BL} = 1,4$ -diethynylbenzene, 9,10-diethynylanthracene), $[\text{Au}_2(\text{dppn})(\text{C}\equiv\text{CR})_2]$ ($\text{R} = 4\text{-C}_6\text{H}_4\text{Ph}$, $4\text{-C}_6\text{H}_4\text{OMe}$, ${}^n\text{C}_6\text{H}_{13}$), $[\text{Au}_2(\text{dmpm})(\text{C}\equiv\text{CR})_2]$ ($\text{R} = \text{Ph}$, $4\text{-C}_6\text{H}_4\text{OMe}$) and $[\text{Au}_3(\text{dmmp})(\text{C}\equiv\text{CR})_3]$ ($\text{R} = \text{Ph}$, $4\text{-C}_6\text{H}_4\text{OMe}$) were found to be pho-

toluiminescent [80]. The complexes with bridging 1,4-diethynylbenzene and 9,10-diethynylanthracene ligands showed absorption bands at ~ 294 – 328 and 410 – 464 nm with vibrational progression spacings of 1980 and 1400 cm^{-1} respectively, and the origin was suggested to arise from the $[\pi-\pi^*(\text{alkynyl})]$ IL or $^1[\sigma(\text{Au}-\text{P}) \rightarrow \pi^*(\text{alkynyl})]$ transitions. For those alkynyl complexes having dppn as the bridging ligand, absorption bands observed at ~ 290 – 310 nm with a weaker absorption at ca. 400 nm and tailing to ~ 500 nm were suggested to arise from the $^1[\sigma(\text{Au}-\text{P}) \rightarrow \pi^*(\text{dppn})]$ transition. The binuclear dmpm and trinuclear dmmp complexes showed strong absorption bands at ~ 252 – 290 nm, which were suggested to arise from the $[\pi-\pi^*(\text{alkynyl})]$ or $[\sigma(\text{Au}-\text{P}) \rightarrow \pi^*(\text{alkynyl})]$ transitions. They also possessed absorption shoulders at ca. 320 – 332 nm that were absent in the mononuclear analogues and were assigned to originate from a $^1[d\sigma^* \rightarrow p\sigma]$ transition. However, a red shift observed in the absorption energy from the mononuclear to the trinuclear species might be suggestive of a $^1[d\sigma^*(\text{Au}-\text{Au}) \rightarrow \pi^*(\text{C}\equiv\text{CR})]$ MMLCT transition. $[(4\text{-C}_6\text{H}_4\text{Me})_3\text{PAu}(\text{C}\equiv\text{C}-4\text{-C}_6\text{H}_4\text{C}\equiv\text{C})\text{AuP}(4\text{-C}_6\text{H}_4\text{Me})_3]$ showed a vibronically structured emission band at ~ 533 nm in the solid state, which was assigned to arise from a $[\pi \rightarrow \pi^*(\text{alkynyl})]$ IL or $[\sigma(\text{Au}-\text{P}) \rightarrow \pi^*(\text{alkynyl})]$ triplet state. Similarly, the complex $[(4\text{-C}_6\text{H}_4\text{Me})_3\text{PAu}(\text{BL})\text{AuP}(4\text{-C}_6\text{H}_4\text{Me})_3]$ ($\text{H}_2\text{BL} = 9,10\text{-diethynylanthracene}$) showed solid-state emission at 580 nm that originated from $[\pi \rightarrow \pi^*(\text{anthryl})]$ IL or $[\sigma(\text{Au}-\text{P}) \rightarrow \pi^*(\text{anthryl})]$ transition. Complexes with dppn ligands displayed $[\sigma(\text{Au}-\text{P}) \rightarrow \pi^*(\text{Np})]$ phosphorescence at ~ 571 – 655 nm. The complex with the dcpn bridge exhibited a much lower energy emission maximum at 707 nm, and such a red shift could be explained by the presence of the more electron-donating cyclohexyl groups that rendered the phosphorus atoms and hence the $\sigma(\text{Au}-\text{P})$ electron-pair higher in energy. The binuclear $[\text{Au}_2(\text{dmpm})(\text{C}\equiv\text{CPh})_2]$ and $[\text{Au}_2(\text{dmpm})(\text{C}\equiv\text{C}-4\text{-C}_6\text{H}_4\text{OMe})_2]$ showed solid-state emission bands at 490 and 521 nm, respectively, while the corresponding trinuclear $[\text{Au}_3(\text{dmmp})(\text{C}\equiv\text{CPh})_3]$ and $[\text{Au}_3(\text{dmmp})(\text{C}\equiv\text{C}-4\text{-C}_6\text{H}_4\text{OMe})_3]$ have bands at 538 and 539 nm, respectively. The emission was suggested to be originated from a metal-centered $^3[(d\delta^*)^1(p\sigma)^1]$ state. The phosphorescent state of $[\text{Au}_3(\text{dmmp})(\text{C}\equiv\text{CPh})_3]$ could be quenched by electron acceptors such as 4-methoxycarbonyl-*N*-methylpyridinium ion, with a bimolecular quenching rate constant of 4.98×10^9 $\text{dm}^3 \text{mol}^{-1} \text{s}^{-1}$ in this case. The mechanisms for this photoinduced electron transfer quenching reaction, together with a related reaction between $[\text{Au}_2(\text{dppn})(\text{C}\equiv\text{C}-4\text{-C}_6\text{H}_4\text{OMe})_2]$ and MV^{2+} , were investigated using nanosecond transient absorption spectroscopy.

The binuclear $[\text{Au}_2(\text{dppb})(\text{C}\equiv\text{CR})_2]$ ($\text{R} = \text{Hex, Ph, } 4\text{-C}_6\text{H}_4\text{OMe}$) and tetranuclear $[\text{Au}_4(\text{tppb})(\text{C}\equiv\text{CR})_4]$ ($\text{R} = \text{Hex, Ph, } 4\text{-C}_6\text{H}_4\text{OMe}$) gold(I) alkynyl complexes were isolated and their spectroscopic properties studied [81]. The electronic absorption bands of these complexes at ~ 250 – 300 nm were assigned to be $^1[\sigma(\text{Au}-\text{P}) \rightarrow \pi^*(\text{Ph}_{\text{bridging}})]$ transitions. Absorption bands observed in the complexes with the dppb ligand are usually higher

in energy than those with tppb due to the more electron-deficient nature of the bridging phenyl ring in the latter. Besides, the methoxyphenylethynyl containing complexes in general are found to have a lower energy emission than those with phenylethynyls. The more electron-rich methoxy substituents would reduce the extent of metal-to-ligand back- π -donation to the alkynyl ligands [$d\pi(\text{Au}) \rightarrow \pi^*(\text{alkynyl})$], which would lead to an increased $d\pi(\text{Au})$ - $3d(\text{P})$ overlap and hence a higher $\sigma(\text{Au-P})$ orbital energy. The photoreaction between $[\text{Au}_4(\text{tppb})(\text{C}\equiv\text{C-4-C}_6\text{H}_4\text{OMe})_4]$ and MV^{2+} was traced by nanosecond transient absorption spectroscopy. The transient absorption difference spectrum showed a sharp absorption band at ~ 400 nm and another broad one at ~ 600 nm, both of which are typical for the MV^+ radical absorptions, and are indicative of the strongly reducing properties of the $[\text{Au}_4(\text{tppb})(\text{C}\equiv\text{C-4-C}_6\text{H}_4\text{OMe})_4]^*$ state. A back electron-transfer rate constant k_b of $1.94 \times 10^{10} \text{ dm}^3 \text{ mol}^{-1} \text{ s}^{-1}$ was also estimated from a plot of $\{1/\Delta A\}$ versus time for the decay trace.

The photophysical and photochemical properties of the binuclear $[\text{Au}_2(\text{dppf})(\text{C}\equiv\text{CR})_2]$ ($\text{R} = \text{Ph}$ and ^tBu) were studied [82]. The complexes were non-emissive in the solid state even at 77 K, but emission bands at ~ 410 nm in dichloromethane could be observed. The photoreaction between $[\text{Au}_2(\text{dppf})(\text{C}\equiv\text{CPh})_2]$ and the dichloromethane solvent was probed, which led to the formation of the organic C-C coupled product, $\text{PhC}\equiv\text{CC}\equiv\text{CPh}$, and the inorganic $[\text{Au}_2(\text{dppf})\text{Cl}_2]$ complex.

In addition to the widely explored phosphine systems, gold(I) alkynyls with the isocyanide ligands, which are also neutral and good σ -donor ligands, were also reported to be luminescent. $[\text{Au}\{\text{CN-2,6-C}_6\text{H}_3(\text{CH}_3)_2\}(\text{C}\equiv\text{CPh})]$ and $[\text{Au}_2(\text{L})(\text{C}\equiv\text{CPh})_2]$ [$\text{L} = \text{tmb}, \text{dmb}$] were structurally characterized, with the intermolecular $\text{Au}\cdots\text{Au}$ contacts determined to be 3.329(4) Å, 3.565(2) Å and 3.485(3) Å, respectively [83]. All the three complexes showed an intense high-energy $^1[dz^2 \rightarrow \pi^*(\text{isocyanide})]$ MLCT absorption band at ~ 240 nm, and a lower energy $[\pi \rightarrow \pi^*(\text{alkynyl})]$ IL absorption at ca. 273 and 278 nm. The complexes showed a $[\pi \rightarrow \pi^*(\text{alkynyl})]$ IL emission at ~ 420 nm in dichloromethane, whereas in the solid state a broad emission band attributed to the $^3[(d\delta^*)^1(p\sigma)^1]$ metal-centered phosphorescence was observed at ~ 550 nm.

Puddephatt and co-workers reported a series of polymeric gold(I) conjugated arylalkynyl complexes [84]. $[\text{Me}_3\text{PAuC}\equiv\text{C-2,5-C}_6\text{H}_2\text{R}_2\text{-C}\equiv\text{CAuPMe}_3]$ ($\text{R} = \text{H}, \text{CH}_3$) showed photoemission at ca. 415 nm in dichloromethane, which was suggested to arise from an excited state of $[\pi \rightarrow \pi^*(\text{alkynyl})]/[\sigma(\text{Au-P}) \rightarrow \pi^*(\text{alkynyl})]$ origin. In the solid state, the emission was red-shifted to ~ 540 nm and was suggested to originate from states of $^3[(d\delta^*)^1(p\sigma)^1]$ metal-centered parentage, based on the observed short intermolecular $\text{Au}\cdots\text{Au}$ separation of 3.1361(9) Å in the crystal structure of $[\text{Me}_3\text{PAuC}\equiv\text{C-2,5-C}_6\text{H}_2\text{Me}_2\text{-C}\equiv\text{CAuPMe}_3]$.

Wong and co-workers reported a series of dinuclear gold(I) phosphine complexes of the type $[\text{Ph}_3\text{PAuC}\equiv\text{C-X-C}\equiv\text{CAuPPh}_3]$, with various functionalized bridging bis(alkynyl)s where X could be 9-alkyl- and aryl-carbazoles [85, 86], 3,6-bis(ethynyl)-9-butylcarbazole [85], dihexylfluorene [87], diphenylfluorene [88], biphenyl [89], $-\text{C}_6\text{H}_4\text{OC}_6\text{H}_4-$, $-\text{C}_6\text{H}_4\text{SC}_6\text{H}_4-$, $-\text{C}_6\text{H}_4\text{S(=O)C}_6\text{H}_4-$ and $-\text{C}_6\text{H}_4\text{S(=O)}_2\text{C}_6\text{H}_4-$ [90]. These dinuclear complexes usually exhibit rich photoluminescence properties associated with the alkynyl localized triplet states, perturbed by the heavy gold(I) centers.

$[(2,6-\text{C}_6\text{H}_3\text{Me}_2)\text{N}\equiv\text{CAuC}\equiv\text{C}(4-\text{C}_6\text{H}_4\text{NO}_2)]$ showed a low-energy emission at 633 nm in the solid state compared to 503 nm in dichloromethane [84], and such a low-energy emission was ascribed to the electron-withdrawing effect of the NO_2 group that stabilized the π^* orbital of the alkynyl. It was believed that the stacking interactions between the phenyl rings among the alkynyl and isocyanide of the two closest molecules in the crystal structure also gave rise to the exceptionally low solid-state emission energy.

The optically transparent PCy_3 ligand ($\lambda \geq 250$ nm) was also used in making the rigid-rod complexes, $[(\text{Cy}_3\text{P})\text{Au}(\text{C}\equiv\text{C})_n\text{Au}(\text{PCy}_3)]$ ($n = 1-4$) [63, 91]. The complexes with $n = 1$ and 2 showed a well-defined absorption band extending beyond 260 nm, which was assigned as the $[5d(\text{Au}) \rightarrow 6p(\text{Au})/\pi^*(\text{phosphine})]$ transition, whereas with $n = 4$ a highly vibronic electronic absorption at $\sim 274-290$ nm with vibrational progression spacings of ~ 2010 cm^{-1} , assigned as the dipole-allowed $[\pi \rightarrow \pi^*\{(\text{C}\equiv\text{C})_4\}]$ transition, was observed. The ethynyl complex was non-emissive in dichloromethane at 298 K, while the butadiynyl counterpart showed a long-lived $^3[\pi \rightarrow \pi^*(\text{alkynyl})]$ emission at 417 nm at 298 K. The ethynyl complex showed two dominant broad emissions centered at λ_{em} 415 and 530 nm in both the solid state at 298 K and as alcoholic glass. The spin-forbidden nature of the lowest-energy $^3[\pi \rightarrow \pi^*(\text{alkynyl})]$ excited states was relaxed to a certain extent via spin-orbit coupling of the heavy gold centers for their prominence both in the electronic absorption and emission spectra. The hexatriynyl and octatetraynyl complexes exhibited sharp vibronically structured emission with the λ_{0-0} lines at 498 and 575 nm in dichloromethane, respectively, with the vibronic progressions of ~ 2120 cm^{-1} , which could readily be assigned as the $^3[\pi \rightarrow \pi^*\{(\text{C}\equiv\text{C})_n\}]$ emission. Subsequent studies on a series of mono- and binuclear gold(I) complexes with arylalkynyl moieties coordinated to $[\text{Au}(\text{PCy}_3)]^+$ have been reported [92]. Complexes with short arylalkynyl chains, including $[\text{Cy}_3\text{PAu}(\text{C}\equiv\text{CR})]$ ($\text{R} = \text{Ph}, 4-\text{C}_6\text{H}_4\text{X}$ ($\text{X} = \text{F}, \text{Cl}, \text{Me}$), $\text{C}\equiv\text{CPh}$, $\text{C}_5\text{H}_4\text{N}$) and $[\text{Cy}_3\text{PAu}(\text{BL})\text{AuPCy}_3]$ ($\text{BL} = \text{C}\equiv\text{CC}_6\text{H}_4\text{C}\equiv\text{C}$), showed emission bands at 408–488 nm in dichloromethane, whereas in the solid state a well-resolved vibronic-structured emission band at 420–493 nm with three types of progression spacings ($\sim 1100, 1600$ and 2100 cm^{-1}) were assigned to the $^3[\pi \rightarrow \pi^*(\text{arylalkynyl})]$ emission. Complexes with long arylalkynyl chains, $[\text{Cy}_3\text{PAu}(\text{C}\equiv\text{CR})]$ ($\text{R} = 4-\text{C}_6\text{H}_4\text{Ph}, \text{C}_6\text{H}_4(\text{C}\equiv\text{CC}_6\text{H}_4)_n\text{C}\equiv\text{CPh}$

($n = 1, 2$) and $[\text{Cy}_3\text{PAu}(\text{BL})\text{AuPCy}_3]$ ($\text{BL} = (\text{C}\equiv\text{CC}_6\text{H}_4)_n\text{C}\equiv\text{C}$ ($n = 2-4$), $\text{C}\equiv\text{C}(\text{C}_6\text{H}_4)_2\text{C}\equiv\text{C}$), displayed dual emissions with high-energy bands at 330–407 nm and low-energy bands at 495–558 nm. The high-energy emission was suggested to be the delayed fluorescence that occurred via a triplet-triplet annihilation mechanism. The relationship between the phosphorescence energy and the number (n) of $\{\text{C}\equiv\text{C}-\text{C}_6\text{H}_4\}$ units was illustrated from the linear plot of $\Delta E(\text{S}_0-\text{T}_1)$ (energy gap between S_0 and T_1 states) against $1/n$ in mononuclear $[(\text{Cy}_3\text{P})\text{Au}\{(\text{C}\equiv\text{C}-\text{C}_6\text{H}_4)_{n-1}\text{C}\equiv\text{CPh}\}]$ and the binuclear $[(\text{Cy}_3\text{P})\text{Au}\{(\text{C}\equiv\text{C}-\text{C}_6\text{H}_4)_n\text{C}\equiv\text{C}\}\text{Au}(\text{PCy}_3)]$ ($n = 1-4$) complexes (Fig. 11). Extrapolation of the lines reveal an estimated $\Delta E(\text{S}_0-\text{T}_1)$ value for infinite repeating units (i.e. $[(\text{Cy}_3\text{P})\text{Au}]$ -capped PPE) of ~ 626 nm (1.98 eV) and ~ 607 nm (2.04 eV) for the mono- and dinuclear species, respectively.

In addition, $[\text{TEE}][\text{Au}(\text{PCy}_3)]_4$ (TEE- H_4 = tetraethynylethene) was found to interestingly show $^1[\pi \rightarrow \pi^*(\text{TEE})]$ fluorescence emission at 428 nm, while $[\text{TEB}][\text{Au}(\text{PCy}_3)]_3$ (TEB- H_3 = 1,3,5-triethynylbenzene) displayed $^3[\pi \rightarrow \pi^*(\text{TEB})]$ phosphorescence emission at 479 nm in dichloromethane at 298 K [93]. The polymorphic nature of $[(\text{Cy}_3\text{P})\text{Au}(4-\text{C}\equiv\text{CC}_6\text{H}_4\text{NO}_2)]$ was studied by Che [94]. Two forms, namely E- and N-forms, were structurally characterized, and were polymorphs with molecular dipoles in different

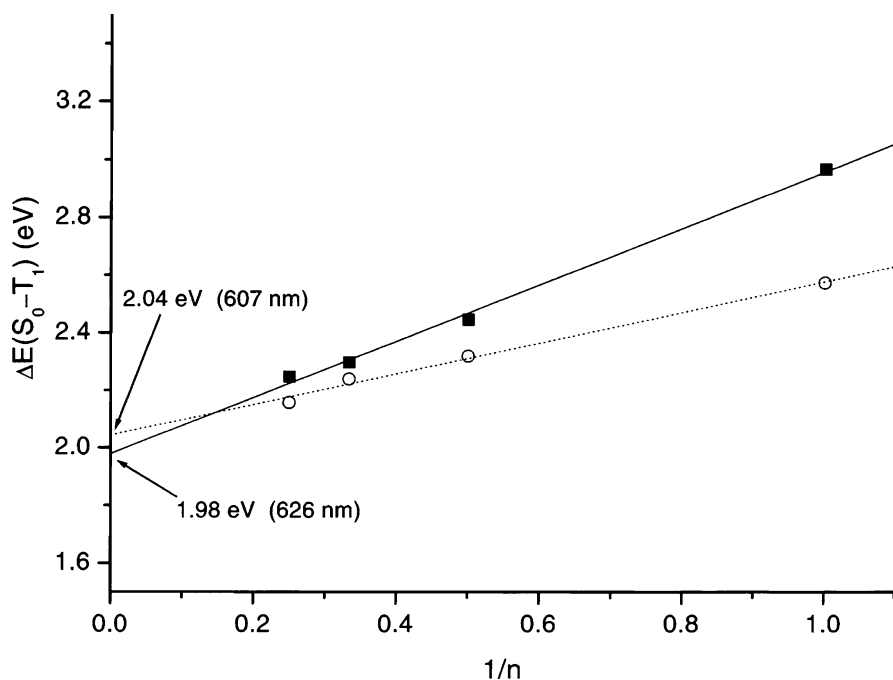


Fig. 11 Plot of $\Delta E(\text{S}_0-\text{T}_1)$ against $1/n$ in mononuclear $[(\text{Cy}_3\text{P})\text{Au}\{(\text{C}\equiv\text{C}-\text{C}_6\text{H}_4)_{n-1}\text{C}\equiv\text{CPh}\}]$ (■) and binuclear $[(\text{Cy}_3\text{P})\text{Au}\{(\text{C}\equiv\text{C}-\text{C}_6\text{H}_4)_n\text{C}\equiv\text{C}\}\text{Au}(\text{PCy}_3)]$ (○) complexes [92]

orientations and with different dihedral angles between the neighboring nitrophenyl moieties. The E-form of $[(\text{Cy}_3\text{P})\text{Au}(\text{C}\equiv\text{C}-4\text{-C}_6\text{H}_4\text{NO}_2)]$ showed ^3IL phosphorescence maxima at 504 and 538 nm at 298 K, while the N-form was non-emissive at 298 K, but it showed an emission band at 486 nm at 77 K.

The photophysical properties of a series of luminescent gold(I) phosphine mono- and diynyl complexes with nuclearity ranging from one to three, $[(\text{R}_3\text{P})\text{Au}\{(\text{C}\equiv\text{C})_2\text{R}'\}]$ ($\text{R} = \text{Ph}$, $\text{R}' = {}^n\text{Pr}$, ${}^n\text{Hex}$, Ph ; $\text{R} = 4\text{-C}_6\text{H}_4\text{Me}$, $\text{R}' = \text{Ph}$), $[\text{Au}_2(\text{P}^\wedge\text{P})(\text{C}\equiv\text{CR})_2]$ ($\text{P}^\wedge\text{P} = \text{dppe}$, $\text{R} = \text{C}\equiv\text{C}-{}^n\text{Hex}$, $\text{C}(\text{=CH}_2)\text{Me}$; $\text{P}^\wedge\text{P} = \text{dppf}$, $\text{R} = \text{C}_4\text{H}_3\text{S}$, $\text{C}_4\text{H}_2\text{SC}_4\text{H}_3\text{S}$) and $[\text{Au}_3(\text{P}^\wedge\text{P})_2(\text{C}\equiv\text{CR})_2][\text{Au}(\text{C}\equiv\text{CR})_2]$ ($\text{P}^\wedge\text{P} = \text{dcpm}$, $\text{R} = \text{C}\equiv\text{C}-{}^n\text{Hex}$, $\text{C}(\text{=CH}_2)\text{Me}$, $\text{C}_4\text{H}_3\text{S}$, $\text{C}_4\text{H}_2\text{SC}_4\text{H}_3\text{S}$; $\text{P}^\wedge\text{P} = \text{dppm}$, $\text{R} = \text{C}\equiv\text{C}-{}^n\text{Hex}$, $\text{C}(\text{=CH}_2)\text{Me}$, $\text{C}_4\text{H}_3\text{S}$, $\text{C}_4\text{H}_2\text{SC}_4\text{H}_3\text{S}$; $\text{P}^\wedge\text{P} = \{(4\text{-C}_6\text{H}_4\text{Me})_2\text{PCH}_2\text{P}(4\text{-C}_6\text{H}_4\text{Me})_2\}$, $\text{R} = \text{C}(\text{=CH}_2)\text{Me}$, $\text{C}_4\text{H}_3\text{S}$; $\text{P}^\wedge\text{P} = \text{dmpm}$, $\text{R} = \text{C}(\text{=CH}_2)\text{Me}$, $\text{C}_4\text{H}_3\text{S}$) have been reported by Yam and co-workers [95]. In general, the high-energy absorption bands were suggested to arise from intraligand phosphine-centered and $[\pi \rightarrow \pi^*(\text{C}\equiv\text{C})]$ IL transitions, whereas the low-energy absorption bands were assigned as $[\sigma(\text{Au}-\text{P}) \rightarrow \pi^*(\text{C}\equiv\text{C})]$ or metal-perturbed $[\pi \rightarrow \pi^*(\text{C}\equiv\text{C})]$ IL mixed with $[5d(\text{Au}) \rightarrow \pi^*(\text{C}\equiv\text{C})]$ MLCT transitions. Both the electronic absorption and emission energies were found to be dependent on the nature of the alkynyl ligands as well as the nuclearity of the metal complexes. The trinuclear complexes were found to possess the lowest emission energy, and such could be attributed to the presence of weak $\text{Au}\cdots\text{Au}$ interactions that would raise the metal-centered $d\sigma^*$ orbital energy, causing a shift of the emission energy of the $^3[\sigma(\text{Au}-\text{P}) \rightarrow \pi^*(\text{C}\equiv\text{C})]$ or the metal-perturbed $[\pi \rightarrow \pi^*(\text{C}\equiv\text{C})]$ $^3\text{IL}/[5d(\text{Au}) \rightarrow \pi^*(\text{C}\equiv\text{C})]$ $^3\text{MLCT}$ origin that was modified by $\text{Au}\cdots\text{Au}$ interactions (or alternatively the $^3\text{MMLCT}$) to the red.

Binuclear gold(I) alkynyls of the type $[\text{Au}_2\{\text{Ph}_2\text{PN}(\text{R})\text{PPh}_2\}(\text{C}\equiv\text{CR}')_2]$ were studied [96]. Similar to the previously reported dppe counterpart, these binuclear gold(I) complexes exhibited short aurophilic contacts shorter than 3.2 Å. Photoluminescence behavior was observed in both 77 K glass and in the solid state. However, the presence of the nitrogen heteroatom in the diphosphine bridge changed significantly their emission origin. Through the systematic variation of the substituents on the alkynyl and the diphosphine ligands and with the aid of theoretical calculations, the emission origin was attributed to be derived from the $^3[\pi(\text{ArC}\equiv\text{C}) \rightarrow \pi^*(\text{PNP})]$ LLCT states that mixed with $^3[\pi(\text{ArC}\equiv\text{C}) \rightarrow 6s/6p(\text{Au})]$ LMCT and metal-centered $^3[5d(\text{Au}) \rightarrow 6s/6p(\text{Au})]$ characters, of which the latter two were perturbed by the presence of weak $\text{Au}\cdots\text{Au}$ interaction in the solid state. Such findings are different from that assigned for the dppe analogue having metal-based $[(d\delta^*)^1(p\sigma)^1]$ and alkynyl-based IL excited states in the solid state and in fluid solution, respectively [97].

The luminescence behavior of a binuclear gold(I) alkynyl complex with a bridging dppf ligand, $[(\text{dppf})\text{Au}_2\{\text{C}\equiv\text{CC}(\text{Me})=\text{CH}_2\}_2]$, was also reported

and was shown to be switched on upon copper(I) or silver(I) encapsulation via π -bond coordination from the alkynyl moieties [98]. Lagunas and co-workers further exemplified the idea using $[(P^{\wedge}P)Au_2(C\equiv CPh)_2]$ ($P^{\wedge}P$ = 4,6-bis(diphenylphosphino)dibenzofuran as the bridging ligand. A hexanuclear gold(I)-copper(I) mixed metal adduct, $\{[(P^{\wedge}P)Au_2(C\equiv CPh)_2]_2Cu_2\}$, could be isolated, after the addition of copper(I) [99].

Ethynylcrown ether containing bi- and tetranuclear gold(I) crown ether complexes, $\{[(Ph_3P)AuC\equiv C]_2\text{-}4,5\text{-}B15C5\}$ and $\{[(Ph_3P)AuC\equiv C]_4\text{-}4,4',5,5'\text{-}DB18C6\}$ were reported, which exhibited intense absorptions at $\sim 268\text{--}335$ nm, with tails extending to ~ 400 nm for the binuclear complex and ~ 500 nm for the tetranuclear complex [100]. The high-energy absorptions were assigned as IL transitions characteristic of triphenylphosphine, whereas the low-energy absorptions were assigned as $[\pi \rightarrow \pi^*]$ IL transitions of the alkynyl ligands. Both complexes show emission bands at $530\text{--}560$ nm in dichloromethane and in the solid state at both room temperature and 77 K, which were suggested to arise from $[\sigma(Au\text{-}P) \rightarrow \pi^*(C\equiv C)]$ or metal-perturbed $[\pi \rightarrow \pi^*(C\equiv C)]$ IL excited states. Electronic absorption changes upon addition of alkali metal ion were also observed. The binuclear gold(I) complex with the benzo-15-crown-5 moiety had a binding affinity towards sodium ion, while the tetranuclear gold(I) complex bearing the benzo-18-crown-6 showed a preferential binding towards potassium ion.

Very recently, linear binuclear and macrocyclic tetranuclear gold(I) phosphine complexes with azo-containing alkynyl ligands, $[(Ph_3P)Au(C\equiv CC_6H_4N=NC_6H_4C\equiv C)Au(PPh_3)]$ and $[(dppm)Au_2(C\equiv CC_6H_4N=NC_6H_4C\equiv C)_2Au_2(dppm)]$ respectively, were reported [101]. The azo complexes were found to have a low-energy absorption band at $\sim 380\text{--}390$ nm and an absorption tail at ~ 500 nm, attributed to the $[\pi \rightarrow \pi^*(azo)]$ and $[n \rightarrow \pi^*(azo)]$ IL transitions, respectively. The photoisomerization of the azo moieties in these complexes were studied, and the coordination and decoordination of silver(I) at the alkynyl groups in the tetranuclear macrocycle were also achieved and employed for modulating the photoswitching processes, as shown in Fig. 12. It is noteworthy to mention that a related structurally characterized tetranuclear complex, $[(dpppe)Au_2\{(NC_5H_4)_2C_4H_4(C_5H_4N)_2\}Au_2(dpppe)]$, which has a central cyclobutane ring formed by a $[2 + 2]$ cycloaddition reaction of two bis(pyridyl)ethylene ligands, was communicated to be isolated upon the recrystallization of the polymeric $[(dpppe)Au(NC_5H_4CH=CHC_5H_4N)Au]_{\infty}$ in the open laboratory conditions [102, 103].

With the more sophisticated dialkynylcalixarenes as ligands, tetranuclear gold(I) alkynyl complexes **8a** and **8b** (Fig. 13), in which both σ - and π -coordinated gold(I) centers are present and exhibit short intramolecular $Au \cdots Au$ contacts of $3.1344(8)$ and $3.2048(8)$ Å, were obtained [104]. The complexes were found to be strongly luminescent at $\sim 591\text{--}616$ nm in the solid state, whereas in chloroform solution or 77 K $CHCl_3$ -MeOH-EtOH glass

the emission band has a maximum at ~ 587 nm upon photoexcitation at ~ 350 – 370 nm. The luminescence quantum yield determined in CHCl_3 solution at 298 K was ~ 0.2 . The large Stokes shift, luminescence lifetime in the microsecond regime, and the slight perturbation of the emission energy upon changing the substituents on the dialkynylcalixarene ligand suggest the emission origin to be derived from states of metal-cluster-centered character that have been modified by $\text{Au}\cdots\text{Au}$ interactions and mixed with metal-perturbed $[\pi \rightarrow \pi^*(\text{C}\equiv\text{C})]$ intraligand states.

Besides, a series of phosphine containing gold(I) alkynylcalix[4]crown-5 complexes, $[(\text{R}_n\text{R}'_{3-n}\text{P})\text{Au}]_2\text{L}$ ($n = 0$ – 3) ($\text{R} = \text{Ph}$, $\text{R}' = 2\text{-C}_6\text{H}_4\text{Me}$, $4\text{-C}_6\text{H}_4\text{Me}$; $\text{H}_2\text{L} = 5,17\text{-diethynyl-25,27-dimethoxycalix[4]crown-5}$) were synthesized [105, 106]. In general, these complexes showed high-energy [phosphine/ethynylcalixcrown] IL absorptions at 270–300 nm and low-energy absorptions at ~ 342 nm that were characteristic of the gold(I) alkynyl system. All the complexes showed an emission band at 578–585 nm in dichloromethane that was suggested to be derived from a triplet state of metal-perturbed IL or $[\sigma(\text{Au-P}) \rightarrow \pi^*(\text{phosphine})]$ character. The binding properties of the complexes towards alkali metal ions (Na^+ and K^+) could be fine-tuned by a change in the different steric requirements of the auxiliary phosphine ligands.

2.4

Trinuclear Complexes with Exobidentate N[^] C/N Bridging Ligands

Homoleptic trinuclear gold(I) complexes bearing exobidentate N- and/or C-donor ligands represent an important class of luminescent molecular gold(I) materials. This stems from the fact that the trinuclear Au_3 units, which possess intramolecular aurophilic contacts, can also form extensive intermolecular stacking through aurophilic interactions. Their structural aspects have been reviewed recently [107]. Such intermolecular aggregations are easily perturbed upon changing the size and types of substituents present on the ligands, solvents, pH and temperature, and the rich photophysical behavior associated with these supramolecular structures are usually very different from that for the monomeric trinuclear units. In 1997, Balch reported the remarkable solvent-stimulated luminescence (or solvoluminescence) of solid samples of $[\text{Au}_3(\text{MeN}=\text{COMe})_3]$ **9** (Fig. 14) [108, 109]. Complex **9** displayed an emission band with a maximum at 422 nm in chloroform, whereas in the solid state it exhibited a dual luminescence behavior with maxima at 446 and 552 nm. The crystal structure revealed indefinite columnar stacks of the triangular trinuclear units, both in the eclipsed and staggered conformations in a 2 : 1 ratio, with the intra- and intermolecular $\text{Au}\cdots\text{Au}$ contacts of 3.308(2) and 3.346(1) Å, respectively. When a polycrystalline sample of **9** that had been previously photo-irradiated at the near-UV wavelength was exposed to a drop of solvents such as acetone, chloroform, dichloromethane,

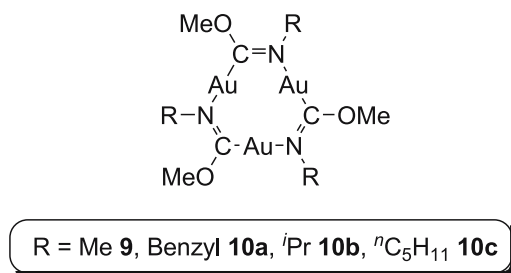


Fig. 14 Solvoluminescent and polymorphic trinuclear gold(I) complex **9** and its related counterparts **10a–c**

toluene, hexane, methanol and water in the dark, a spontaneous yellow emission that could be readily correlated with the long-lived low-energy emission in the dual luminescence of **9** in the solid state could be observed. This gives an indication that the solvoluminescence behavior is related to the intermolecular aggregation present in the solid rather than the discrete trinuclear monomers.

Replacement of the *N*-methyl groups with the bulkier *N*-benzyl or *N*-isopropyl groups did not reproduce any columnar stack in the crystal structure that was found in **9**, and no solvoluminescent behavior was observed [110, 111]. The closest intermolecular Au–Au contact of 3.662 and 6.417 Å in the crystal packing in **10a** and **10b** (Fig. 14), respectively, indicated the absence of any intermolecular aurophilic interaction.

Alteration of the intermolecular aurophilic Au₃ stacking was also achieved by intercalation using planar π -conjugated acids. For instance, intercalation using electron-accepting nitro-9-fluorenones and TCNQ has been reported by Balch and Fackler, respectively, of which the crystalline adducts formed did not exhibit any luminescence nor solvoluminescence behavior but rather low-energy charge-transfer absorptions beyond 460 nm for the former and 600 nm for the latter were observed [112–114]. The polymorphic nature of **9** and **10c** (Fig. 14) has also been reported, and the results further indicated the crucial role of intermolecular {Au₃} stacking in governing the photoluminescence and solvoluminescence behaviors in this class of complexes [111]. Intercalation with perfluoronaphthalene resulted in the enhancement of the singlet-triplet intersystem crossing and phosphorescence of the perfluoronaphthalene, whereas intercalation of perfluorobenzene caused a quenching of the blue Au₃ luminescence [113–115]. Similar intercalation with the trinuclear organometallic mercury(II) complex, [Hg₃(μ -C,C-C₆F₄)₃], afforded a sandwiched complex that exhibited weak intermolecular Au···Hg interactions and a red shift in the emission energy [116]. Intercalation of **11** and **12** (Fig. 15) using metal ions such as Ag⁺ and Tl⁺ ions was demonstrated by Burini and Fackler [117]. In general, short intermolecular metallophilic contacts of ~ 3 Å were observed upon the sandwiching of the metal ions

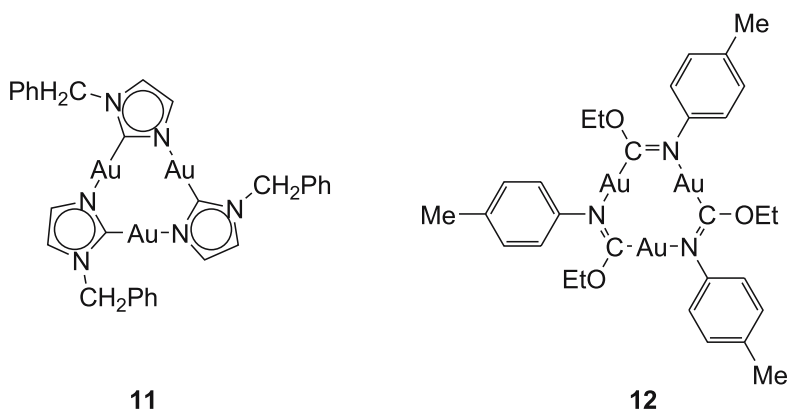


Fig. 15 Structure of the trinuclear gold(I) complexes **11** and **12**

by the Au₃ moieties, and at the same time the sandwiched complexes exhibited luminescence thermochromism with a red shift in emission energy upon lowering the temperature from ambient to 77 K. Coppens and Omary reported the synthesis of Au₃ complex, **13** (Fig. 16), using a triazolate ligand and the complex was shown to exhibit multiple phosphorescence bands both in the solid state and in solution due to the different inter-convertible effective symmetries in the crystal structures that are governed by the crystal temperature and solution concentration [118]. The quenching properties of **13** towards protonation by Brønsted acids and π -intercalation were also reported.

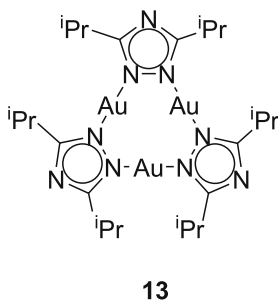


Fig. 16 Structure of the trinuclear gold(I) triazolate complex **13**

With the previously demonstrated ability of trinuclear gold(I) pyrazolate complexes that possess long-alkyl chains to form columnar mesophases [119–121], Aida and co-workers synthesized a series of luminescent Au₃ complexes bearing dendritic poly(benzyl ether) functionalized pyrazole ligands [122]. By controlling the dendron generation, superhelical fibres with extensive intermolecular Au₃ stacking could be obtained, which resulted in an

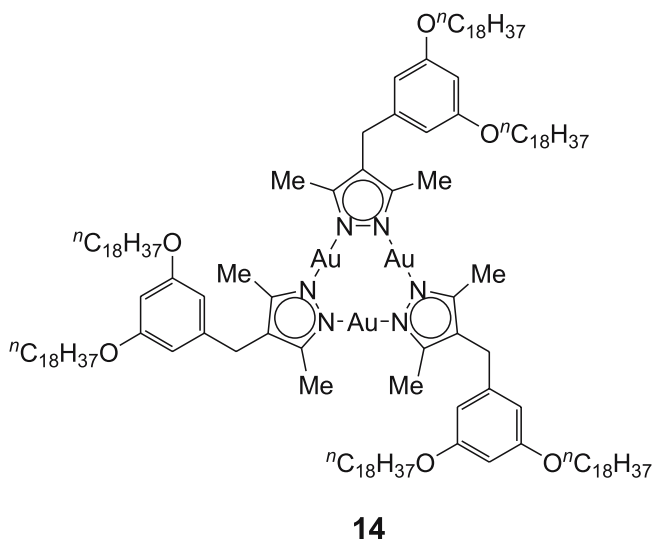


Fig. 17 Phosphorescent trinuclear gold(I) organogel

effective energy transfer from the dendritic wedge to the columnar $\{\text{Au}_3\}_n$ core (the antenna effect). Subsequent works by the same group showed the gelation properties of **14** (Fig. 17) and reversible RGB-color switching could be achieved through the intervention of the Au_3 stacking by Ag^+ ions (Fig. 18) [123].

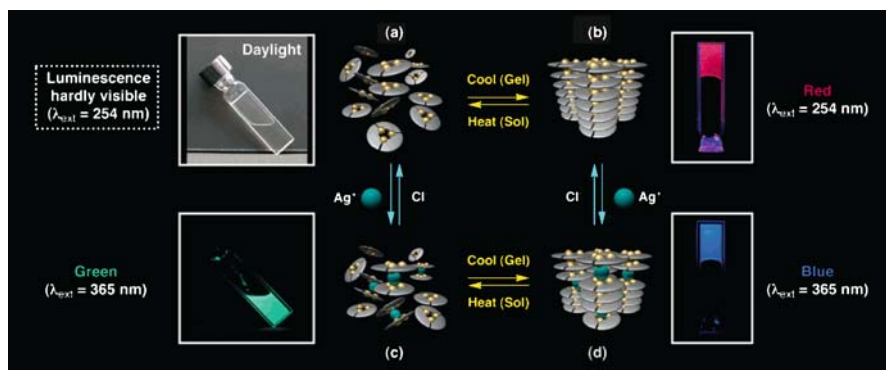


Fig. 18 Luminescence profiles of **14** in hexane. Pictures and schematic self-assembling structures of (a) sol, (b) gel, (c) sol containing AgOTf (0.01 equiv.), and (d) gel containing AgOTf (0.01 equiv.) [123]

2.5

Miscellaneous Gold(I) Complexes

A fluorescent cationic tetranuclear gold(I) rectangle, $[(\mu\text{-Ph}_2\text{PAnPPh}_2)\text{Au}_2(\mu\text{-4,4' -bpy})_2\text{Au}_2(\mu\text{-Ph}_2\text{PAnPPh}_2)]\text{X}_4$ ($\text{X} = \text{PF}_6, \text{NO}_3$), was assembled using 9,10-bis(diphenylphosphino)anthracene and 4,4'-bipyridyl [124]. The molecular rectangle has a cavity of $7.921(3) \times 16.76(3)$ Å as reflected from its crystal structure, and its complexation behavior towards various aromatic molecules at the cavity was demonstrated.

Leznoff and co-workers reported the structural characterization and the polymorphic nature of a gold(I)-copper(II) coordination polymer, $[\text{Cu}\{\text{Au}(\text{CN})_2\}_2(\text{dmsO})_2]_\infty$ [125]. In a green polymorphic form it possessed a 1-D chain structure with five-coordinate copper(II) centers, while a 2-D corrugated sheet structure with six-coordinate copper(II) centers was characterized in the blue polymorph, both of which are linked together to form a 3-D structure via aurophilic interactions. These two polymorphs exhibited virtually identical vapochromic behavior towards water, MeCN, dioxane, dmf, pyridine and ammonia, with the formation of $[\text{Cu}\{\text{Au}(\text{CN})_2\}_2(\text{solvent})_x]_\infty$.

Recently, there has been a blooming growth of study on the use of NHC ligands as alternatives and extensions for organic phosphines, due to the good σ -donating ability of the carbene ligands and hence they are capable of stabilizing metal centers in both high and low oxidation states. More importantly, the steric and electronic properties of the NHC ligands can be fine-tuned easily by the variation of the organic groups attached to the nitrogen atoms.

In this regard, Lin and co-workers have reported a series of mononuclear gold(I) complexes with one or two NHC ligands coordinated to the metal centers [126, 127]. Complexes of the type $[\text{Au}(\text{NHC})_2]^+$, $[\text{Au}(\text{NHC})\text{X}]$ ($\text{X} = \text{halide}$), $[\text{Au}(\text{NHC})(\text{C}\equiv\text{CPh})]$, $[\text{Au}(\text{NHC})(\text{SPh})]$ and $[\text{Au}(\text{NHC})(\text{NR})]$ ($\text{NR} = \text{carbazolate}$) were isolated, and most of them were shown to be luminescent.

Catalano and co-workers also reported a series of mononuclear, trinuclear and polymeric homo- and heterometallic gold(I) complexes, with the NHC ligands having additional nitrogen-donor groups (such as 2-pyridyl and 2-pyridinylmethyl) attached to the carbene nitrogens [128, 129]. All the NHC-containing gold(I) complexes studied were also reported to be emissive in nature.

3

Photophysical and Photochemical Properties of Gold(II) Complexes

Compared to the extensively studied luminescent gold(I) complexes, reports on the gold(II) systems are much less explored. Within the scanty list of examples, very few of them have had their electronic spectroscopy investigated. Fackler and co-workers investigated the spectroscopic properties of a se-

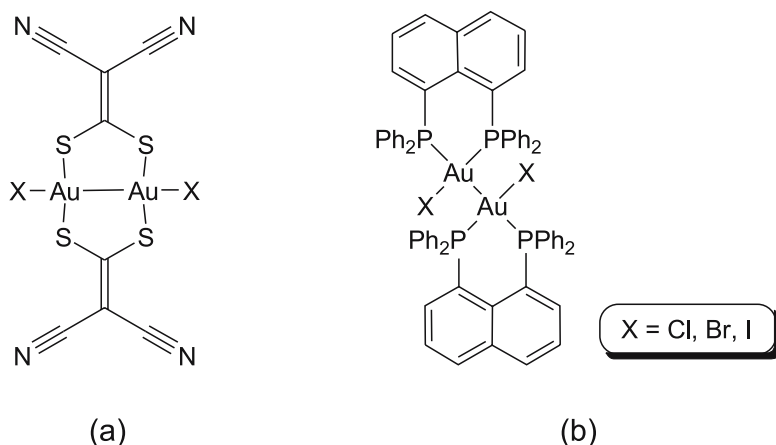


Fig. 19 Luminescent binuclear gold(II) complexes

ries of binuclear annular gold(II) complexes with bridging dithiolato ligands, $(^n\text{Bu}_4\text{N})_2[\text{Au}_2(i\text{-mnt})_2\text{X}_2]$ ($\text{X} = \text{Cl}, \text{Br}, \text{I}$) (Fig. 19a) [130]. A low-energy absorption band was observed for these complexes, with an energy trend of $\text{X} = \text{Cl}$ (550 nm) > Br (586 nm) > I (640 nm) which follows the order of decreasing electronegativity of the halo ligands and increasing Au-Au bond distance ($\text{X} = \text{Cl}$ (2.550 Å) < Br (2.570 Å)). These absorptions were assigned as $[\sigma \rightarrow \sigma^*]$ transitions.

Yam and co-workers reported a novel series of binuclear cationic gold(II) complexes, $[\{\text{Au}(\text{dppn})\text{X}\}_2](\text{PF}_6)_2$ ($\text{X} = \text{Cl}, \text{Br}, \text{I}$) (Fig. 19b) [131, 132], with an unsupported formal $\text{Au}^{\text{II}}-\text{Au}^{\text{II}}$ bond. Although a similar low-energy absorption band with an energy trend of $\text{X} = \text{Cl}$ (520 nm) > Br (544 nm) > I (602 nm) (Fig. 20) that follows the order of decreasing electronegativity of the halo ligands was also observed, such a trend was not in agreement with the increasing $\text{Au}^{\text{II}}-\text{Au}^{\text{II}}$ bond distances ($\text{X} = \text{Br}$ (2.6035 Å) < Cl (2.6112 Å) < I (2.6405 Å)) and a direct assignment of a $[\sigma \rightarrow \sigma^*]$ transition was not possible. Instead, this low-energy absorption was suggested to involve a transition of substantial $[d\sigma(\text{Au}_2)/p\pi(\text{X}) \rightarrow d\sigma^*(\text{Au}_2)]$ metal-centered/LMCT character that mixed with a $[p\sigma(\text{P}) \rightarrow d\sigma^*(\text{Au}_2)]$ LMCT character. The three halo complexes were also found to be luminescent in nature. An emission energy trend of $\text{X} = \text{Cl}$ (555 nm) > Br (580 nm) > I (685 nm) in 77 K glass was observed (Fig. 20), with excitation bands that were similar to those of the low-energy absorptions. An emission with origin similar to that assigned for the low-energy absorptions was suggested.

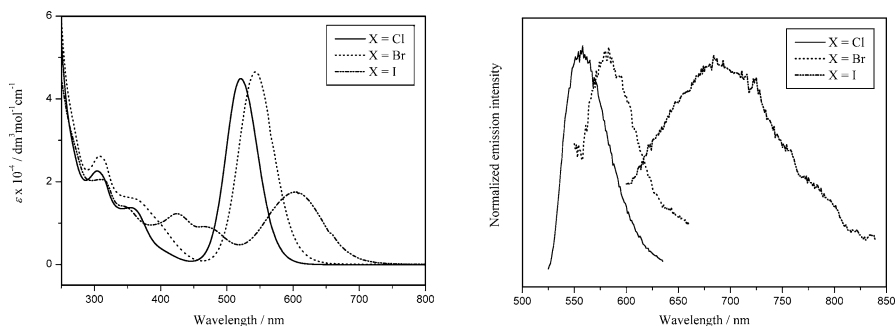


Fig. 20 Electronic absorption spectra in dichloromethane at 298 K (*left*) and normalized emission spectra in solvent glass at 77 K (*right*) for $[\{\text{Au}(\text{dppn})\text{X}\}_2](\text{PF}_6)_2$ (X = Cl, Br, I) [132]

4

Photophysical and Photochemical Properties of Gold(III) Complexes

4.1

Gold(III) Alkyl and Aryl Complexes with Ancillary Diimine Ligands

Although there have been numerous reports on luminescent platinum(II) complexes, related studies on the isoelectronic gold(III) systems are much less explored. A probable reason may be the presence of low-energy $d-d$ ligand field (LF) states and the high electrophilicity of the gold(III) center. The presence of a non-emissive low-lying $d-d$ state would quench the luminescent excited states by thermal equilibrium or energy transfer. It was suggested that the introduction of good σ -donor ligands would render the metal center more electron rich, with the additional advantage of raising the energy of the $d-d$ states, which would then improve the chance of obtaining luminescent gold(III) complexes. This concept was demonstrated by the report of a series of luminescent organogold(III) diimine complexes, $[\text{AuR}_2(\text{L}^{\wedge}\text{L})]\text{ClO}_4$ (R = mes, CH_2SiMe_3 ; $\text{L}^{\wedge}\text{L}$ = 2,2'-bpy, phen, dpphen) [133]. Detailed systematic comparison studies with the $[\text{AuCl}_2(\text{L}^{\wedge}\text{L})]\text{ClO}_4$ and the platinum(II) analogues suggest that several possible assignments for the emission could be made including metal-perturbed $[\pi \rightarrow \pi^*]$ IL, $[\text{Au} \rightarrow \pi^*(\text{N}^{\wedge}\text{N})]$ MLCT, $[\text{R} \rightarrow \pi^*(\text{N}^{\wedge}\text{N})]$ LLCT, or mixtures of them in origin.

4.2

Cyclometallated Gold(III) Complexes

In addition to the organogold(III) diimine system described in the previous section, ancillary aryls could also be incorporated as part of the diimine ligand moiety in obtaining luminescent gold(III) complexes. A series of cyclometallated chlorogold(III) complexes, $[\text{Au}(\text{N}^{\wedge}\text{N}^{\wedge}\text{C})\text{Cl}]^+$ **15a,b**

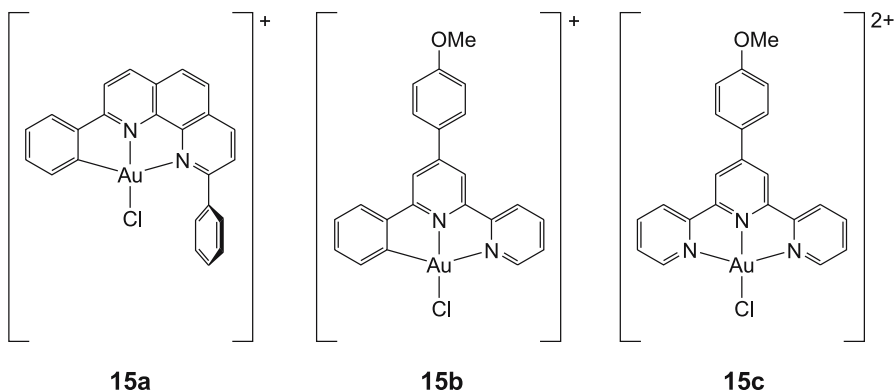


Fig. 21 Structure of the cyclometallated chlorogold(III) complexes **15a–b**, and the related terpyridyl counterpart **15c**

(Fig. 21) were reported to be luminescent in the solid-state, in fluid solution and in 77 K glass matrices [134, 135]. The richly vibronic-structured emission of **15a** with progressional spacings of $\sim 1400\text{ cm}^{-1}$ in various media, together with the luminescence lifetimes in microsecond range and the insensitivity of emission energies to solvents supported an emission origin of triplet intraligand parentage. Perturbation of emission by the gold(III) metal center was observed when the results were compared to those for the free N^N^C ligand and the related platinum(II) complex, $[\text{Pt}(N^N^C)(\text{MeCN})]^+$. The excited state of **15a** was found to be a powerful photo-oxidant toward 1,4-dimethoxybenzene and thf, resulting in the generation of the 1,4-dimethoxybenzene cation radical and the oxidative ring cleaved product of thf, respectively. The emission of **15b** was quenched and blue-shifted upon intercalation to calf-thymus DNA, with the quenching rate constant in between that for $\text{poly}(dG-dC)_2$ and $\text{poly}(dA-dT)_2$, revealing the lack of specificity at the GC and AT sites. The terpyridyl analogue **15c** (Fig. 21) was also studied for comparison.

More recently, the dianionic bis-cyclometallated diarylpyridine ligands were employed in the synthesis of luminescent bis-cyclometallated gold(III) complexes, **16a–f** (Fig. 22) [136] and **17a–e** (Fig. 23) [137, 138]. The electronic absorption spectra of **16a–d** exhibited characteristic vibronically structured bands at 383–404 nm that were attributed to the metal-perturbed $[\pi \rightarrow \pi^*]$ IL transitions. They are also emissive in MeCN at 77 K with the emission maximum at $\sim 483\text{--}485\text{ nm}$ that originates from the metal-perturbed $[\pi \rightarrow \pi^*]$ IL phosphorescence, in view of the relative insensitivity of the emission energy to the nature of the ancillary ligand, such as chloro, phosphine, thiolate or imidazole. The binuclear complexes, **16e,f**, exhibit similar absorption and emission patterns as the mononuclear analogue **16b**, but the energies are red-shifted due to the plausible intramolecular $\pi\text{--}\pi$ stacking of the $\{\text{Au}(C^N^C)\}$

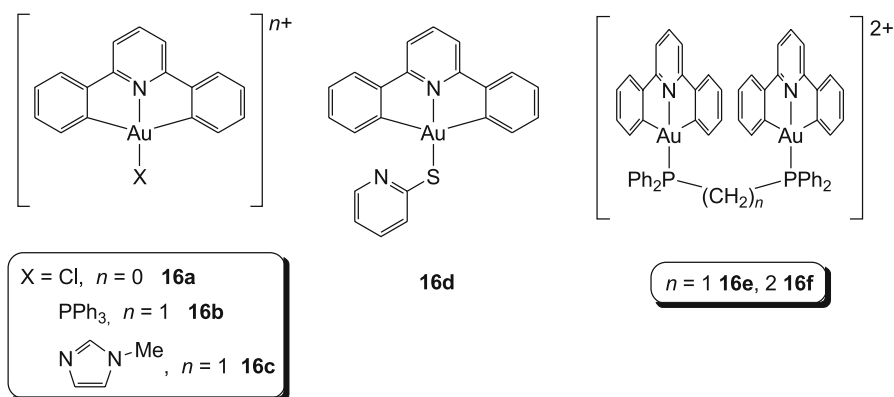


Fig. 22 Structure of the bis-cyclometallated gold(III) complexes **16a-f**

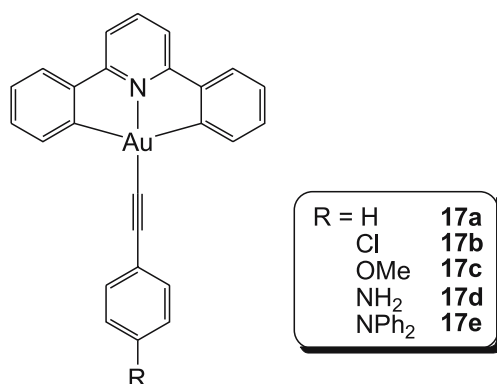


Fig. 23 Structure of the bis-cyclometallated gold(III) alkynyl complexes **17a-e**

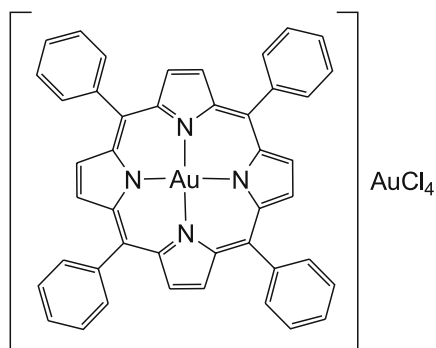
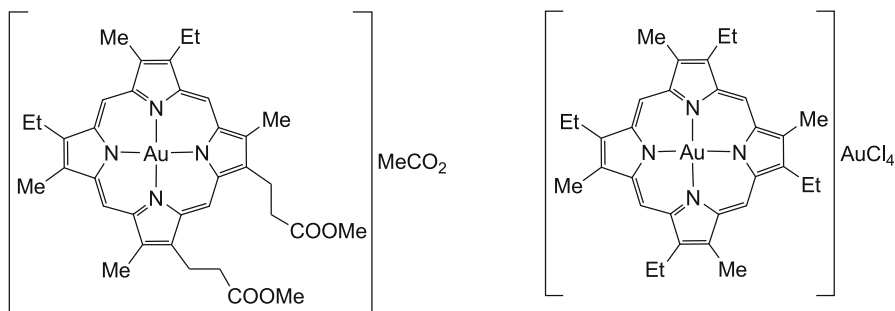
moieties in the binuclear complexes that gives rise to the presence of excimeric characters in the excited states. It is noteworthy to mention that the chloro complexes usually do not emit in fluid solution at room temperature, and one way to make this class of complexes emissive is to increase the IL character by introducing extra phenyl rings on the ligand, similar to that for **15a,b**. Yam and co-workers used an alternative strategy in enhancing the emissive character of the gold(III) complexes by introducing the strongly σ -donating alkynyl ligands to the gold(III) center so as to raise the energy of the $d-d$ states and to reduce its electrophilicity. Complexes **17a-e** were found to exhibit luminescence in various media at both low and ambient temperature. Complexes **17a-c** exhibited characteristic vibronically structured absorption bands at 362–402 nm and emission maxima at 474–476 nm in dichloromethane at 298 K, which were attributed to the metal-perturbed [$\pi \rightarrow \pi^*(\text{C}^{\wedge}\text{N}^{\wedge}\text{C})$] IL transitions and phosphorescence, respectively, involv-

ing charge transfer from the phenyl to the pyridyl rings. In addition to the typical C^N^C ligand absorption, **17d** and **17e** also displayed a low-energy absorption tail at ~ 415 and 460 nm, respectively, which were ascribed to an admixture of [$\pi \rightarrow \pi^*(\text{C}^{\text{N}}^{\text{C}})$] IL and [$\pi(\text{C}\equiv\text{CC}_6\text{H}_4\text{NR}_2) \rightarrow \pi^*(\text{C}^{\text{N}}^{\text{C}})$] LLCT transitions due to the presence of the good electron-donating amino group on the phenyl alkynyl ligands. The emission energies of **17d** and **17e** in dilute solutions are significantly red-shifted to 611 and 620 nm, respectively, and the structureless feature of the emission band supports an assignment of a $^3[\pi(\text{C}\equiv\text{CC}_6\text{H}_4\text{NR}_2) \rightarrow \pi^*(\text{C}^{\text{N}}^{\text{C}})]$ LLCT origin. Interestingly, **17a–e** displayed a low-energy structureless emission band at 550–588 nm in the solid state, and such a red shift was attributed to dimeric or excimeric emission arising from the π - π stacking of the planar $\{\text{Au}(\text{C}^{\text{N}}^{\text{C}})\}$ units, in agreement with the short inter-planar distance of 3.384 Å as observed in the crystal structure of **17a**. Complexes **17a** and **17e** were also demonstrated to possess interesting electroluminescence properties and were employed as both electrophosphorescent emitters and dopants in the fabrication of multilayer organic-light-emitting devices (OLEDs) [138]. Dopant concentration- and voltage-dependent tunable OLEDs were fabricated and a maximum external quantum efficiency of 5.5%, corresponding to a current efficiency of 17.6 cd A⁻¹ and luminance power efficiency of 14.5 lm W⁻¹ could be achieved in one of the multilayer OLEDs.

4.3

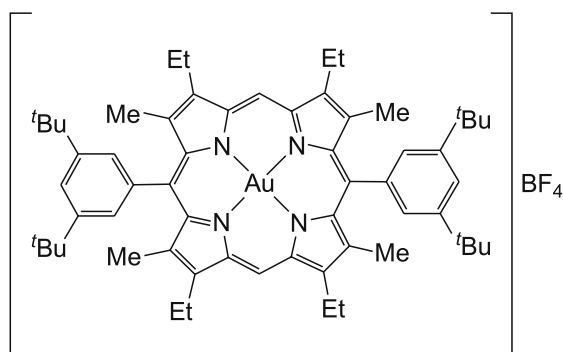
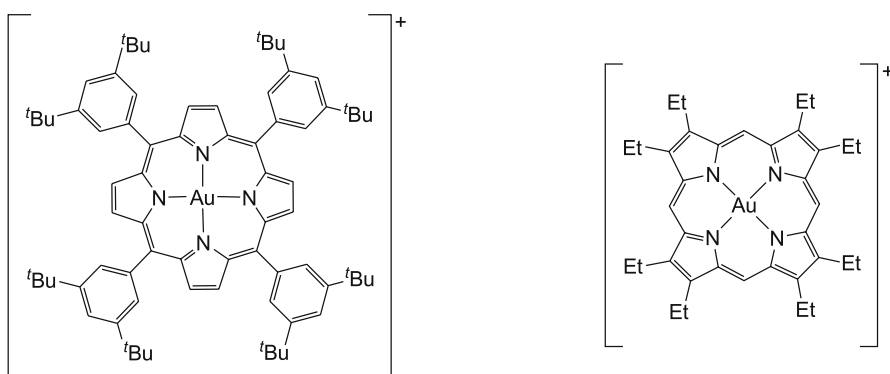
Porphyrinato Gold(III) Complexes

Exploration of the photophysical properties of gold(III) porphyrin complexes was initiated by Fleischer and Laszlo in the late 1970s, where the electronic absorption properties of $[\text{Au}(\text{TPP})](\text{AuCl}_4)$ **18** (Fig. 24) in pyridine and chloroform were found to possess two absorption bands (λ/nm ($\epsilon / \text{M}^{-1}\text{cm}^{-1}$): ~ 410 (~ 10⁵); ~ 520 (~ 10⁴)), both of which were blue-shifted with respect to the closed *d*-shell metalloporphyrin and were classified as *hypso* [139]. Later, related studies of **18** in various solvents in the presence of tetraalkylammonium perchlorate were carried out by Jamin and Iwamoto in 1978, where an additional weak low-energy band was observed at ~ 600 nm with molar extinction coefficients of the order of 10³ M⁻¹cm⁻¹ [140]. These three bands at ~ 410, 520 and 600 nm were assigned as the Soret, the Q(1,0) (or β) and the Q(0,0) (or α) bands, respectively. Parallel studies with the analogous complexes **19a,b** (Fig. 25) were also demonstrated [140]. Gouterman and co-workers demonstrated for the first time the phosphorescence nature of the gold(III) porphyrin-type complex [141]. Complex **18** was found to exhibit no fluorescence, but rather a vibronically structured phosphorescence at ~ 700 nm in 77 K ethanol: glycerol (11 : 1 v/v) glass with a phosphorescence quantum yield of 6×10^{-3} was observed. Its luminescence decay was found to be non-single exponential with lifetimes of 64 and 183 μs . In a related

**18****Fig. 24** Structure of the gold(III) porphyrin complex **18****19a****19b****Fig. 25** Structure of **19a** and **19b**

study, it was determined that the depopulation of the first or lowest energy singlet excited state of **20** (Fig. 26) in EtOH at room temperature occurred with a time constant of 240 fs to the charge-transfer state [142]. Albinsson and co-workers subsequently investigated the photophysical properties of the triplet states of **20**, **21a** and **21b** (Fig. 27) in various media at different temperatures [143]. It was found that, in addition to the previously reported biexponential phosphorescence decay in the microsecond range corresponding to the two degenerate triplet excited states, there existed a “dark” state with a lifetime in the range of 20–50 ns attributed to the optically forbidden $^1\text{LMCT}$ state. This LMCT state was suggested to act as a gate for the triplet state formation versus the deactivation process to the ground state.

Pioneering works by Harriman and Sauvage reported the zinc(II)-gold(III) bis(porphyrin)-type complexes with diimine linkers, where the photoinduced electron transfer process from the zinc(II) porphyrin excited state to the

**20****Fig. 26** Structure of 20**21a****21b****Fig. 27** Structure of 21a and 21b

cationic gold(III) porphyrin moiety could be tuned by complexation of copper(II) centers at the central diimine bridge [144–147]. In addition, systems involving ruthenium(II), osmium(II) and iridium(III) centers were also investigated and will be discussed elsewhere in this volume. The gold(III) porphyrin moieties, capable of being easily reduced, have been utilized as electron acceptors in the photoactive multi-component “donor-bridge-acceptor” (D-B-A) assemblies involving photoinduced electron transfer processes [148–155]. The understanding of the underlying redox properties and origins of the gold(III) porphyrin systems becomes crucial in the design of efficient D-B-A systems. Kadish, Fukuzumi and Crossley’s groups investigated the redox nature of the gold(III) porphyrin systems using spectroelectrochemistry and ESR studies, in which the substituent on the porphyrin ring was found to

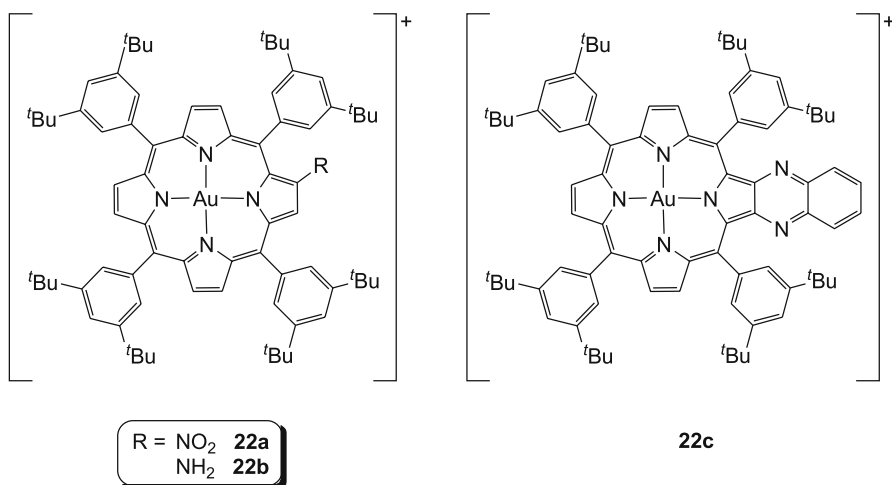


Fig. 28 Structure of **22a–c**

play an important role in governing the nature of the reduction process [156]. In general, gold(III) porphyrins are capable of undergoing three successive reductions. For **21a** and **22b, c** (Fig. 28), the first reduction indeed involves the metal-centered [Au(III) → Au(II)] reduction, followed by the two successive reductions at the porphyrin ring to afford the porphyrin π -anion radicals [156, 157]. When electron-withdrawing groups such as NO₂ were attached to the porphyrin ring, i.e. **22a** (Fig. 28), the π^* orbitals of the whole porphyrin ring were essentially lowered in energy, and the site of the first reduction would switch from the gold(III) center to the porphyrin ring. The

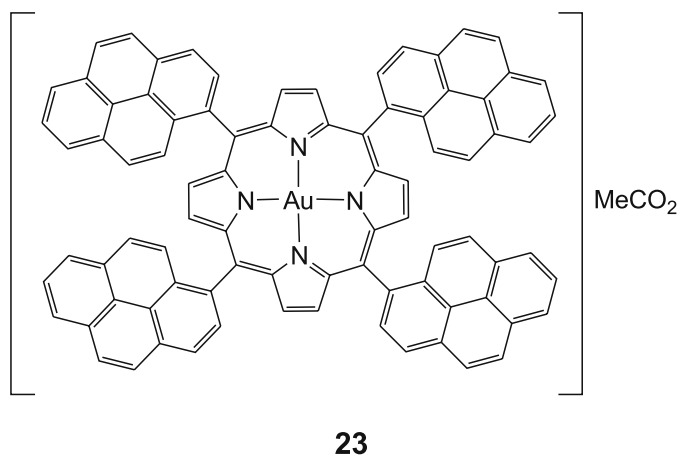


Fig. 29 Structure of the pyrene-functionalized gold(III) porphyrin complex **23**

photocatalytic oxidative degradation of guanine by a pyrene-functionalized gold(III) porphyrin complex, **23** (Fig. 29) was studied by Knör, in which a quantum yield of 0.03 ± 0.01 and an initial turnover frequency of 66 h^{-1} were demonstrated at 298 K [158].

5 Conclusion

Coordination and organometallic complexes of gold(I) often display interesting luminescence properties. The presence of the heavy gold(I) centers, with the enhancement of intersystem crossing, provides an effective means for the access of the spin-forbidden triplet states by heavy-atom effect upon photoexcitation to the singlet excited states. Auophilic contacts are usually observed in the solid state structure of gold(I) complexes and do play a role in perturbing the luminescence nature of this type of complexes, when there is an involvement of orbitals from the gold metal center. Luminescent gold(III) complexes are much less explored compared to that of gold(I), and yet could be obtained in general by raising the energy level of the low-lying $d-d$ states via coordination of good σ -donor ligands. Examples of luminescent gold(II) complexes are rare, and photoexcitation of gold(II) complexes usually results in the weakening of the metal-metal bond due to the promotion of electron density to the anti-bonding σ^* (Au-Au) orbitals, which accounts for their general instability.

Acknowledgements The authors acknowledge financial support from the University Development Fund (UDF) of The University of Hong Kong, the URC Seed Funding for Strategic Research Theme on Organic Optoelectronics, the University of Hong Kong Foundation for Educational Development and Research Limited, a CERG Grant from the Research Grants Council of the Hong Kong Special Administrative Region, China (Project No. HKU 7049/05P) and the National Natural Science Foundation of China and the Research Grants Council of Hong Kong Joint Research (NSFC-RGC) Scheme (Project No. N_HKU 737/06).

References

1. Schmidbaur H (1995) *Chem Soc Rev* 391
2. Schmidbaur H (1990) *Gold Bull* 23:11
3. Kaltsoyannis N (1997) *J Chem Soc Dalton Trans* 1
4. Thayer JS (2005) *J Chem Ed* 82:1721
5. Pyykkö P, Zhao Y (1991) *Angew Chem Int Ed Engl* 30:604
6. Pyykkö P (2004) *Angew Chem Int Ed* 43:4412
7. Rehr JJ, Zaremba E, Kohn W (1975) *Phys Rev B* 12:2062
8. Vogler A, Kunkely H (2001) *Coord Chem Rev* 219-221:489
9. Ziolo RF, Lipton S, Dori Z (1970) *J Chem Soc Chem Commun* p 1124

10. King C, Wang JC, Khan MNI, Fackler JP Jr (1989) *Inorg Chem* 28:2145
11. Che CM, Kwong HL, Yam VWW, Cho KC (1989) *J Chem Soc Chem Commun* p 885
12. Che CM, Kwong HL, Poon CK, Yam VWW (1990) *J Chem Soc Dalton Trans* 3215
13. Jaw HRC, Savas MM, Rogers RD, Mason WR (1989) *Inorg Chem* 28:1028
14. Yam VWW, Lai TF, Che CM (1990) *J Chem Soc Dalton Trans* 3747
15. Yam VWW, Lee WK (1993) *J Chem Soc Dalton Trans* 2097
16. Li D, Che CM, Peng SM, Liu ST, Zhou ZY, Mak TCW (1993) *J Chem Soc Dalton Trans* 189
17. Fu WF, Chan KC, Miskowski VM, Che CM (1999) *Angew Chem Int Ed* 38:2783
18. Che CM, Lai SW (2005) *Coord Chem Rev* 249:1296
19. Zhang HX, Che CM (2001) *Chem Eur J* 7:4887
20. Leung KH, Phillips DL, Tse MC, Che CM, Miskowski VM (1999) *J Am Chem Soc* 121:4799
21. Phillips DL, Che CM, Leung KH, Mao Z, Tse MC (2005) *Coord Chem Rev* 249:1476
22. Yip JHK, Prabhavathy J (2001) *Angew Chem Int Ed* 40:2159
23. McCleskey TM, Gray HB (1992) *Inorg Chem* 31:1733
24. King C, Khan MNI, Staples RJ, Fackler JP Jr (1992) *Inorg Chem* 31:3236
25. Forward JM, Assefa Z, Fackler JP Jr (1995) *J Am Chem Soc* 117:9103
26. Assefa Z, Forward JM, Grant TA, Staples RJ, Hanson BE, Mohamed AA, Fackler JP Jr (2003) *Inorg Chim Acta* 352:31
27. Khan MNI, Staples RJ, King C, Fackler JP Jr, Winpenny REP (1993) *Inorg Chem* 32:5800
28. Yam VWW, Chan CL, Choi SWK, Wong KMC, Cheng ECC, Yu SC, Ng PK, Chan WK, Cheung KK (2000) *Chem Commun* p 53
29. Yam VWW, Cheng ECC, Zhu N (2001) *Angew Chem Int Ed* 40:1763
30. Yam VWW, Cheng ECC, Zhou ZY (2000) *Angew Chem Int Ed* 39:1683
31. Yam VWW, Cheng ECC, Cheung KK (1999) *Angew Chem Int Ed* 38:197
32. Yam VWW, Cheng ECC (2000) *Gold Bull* 34:20
33. Lebedkin S, Langetepe T, Sevillano P, Fenske D, Kappes MM (2002) *J Phys Chem B* 106:9019
34. Link S, Beeby A, FitzGerald S, El-Sayed MA, Schaaff TG, Whetten RL (2002) *J Phys Chem B* 106:3410
35. Huang T, Murray RW (2001) *J Phys Chem B* 105:12498
36. Lee D, Donkers RL, Wang G, Harper AS, Murray RW (2004) *J Am Chem Soc* 126:6193
37. Wang G, Huang T, Murray RW, Menard L, Nuzzo RG (2005) *J Am Chem Soc* 127:812
38. Wang QM, Lee YA, Crespo O, Deaton J, Tang C, Gysling HJ, Gimeno MC, Larraz C, Villacampa MD, Laguna A, Eisenberg R (2004) *J Am Chem Soc* 126:9488
39. Gussenhoven EM, Fettinger JC, Pham DM, Malwitz MM, Balch AL (2005) *J Am Chem Soc* 127:10838
40. Vogler A, Kunkely H (1988) *Chem Phys Lett* 150:135
41. Piovesana O, Zanazzi PF (1980) *Angew Chem Int Ed Engl* 19:561
42. Chiari B, Piovesana O, Tarantelli T, Zanazzi PF (1985) *Inorg Chem* 24:366
43. Guy JJ, Jones PG, Mays MJ, Sheldrick GM (1977) *J Chem Soc Dalton Trans* 8
44. Vicente J, Chicote MT, González-Herrero P, Jones PG (1995) *J Chem Soc Chem Commun* p 745
45. Cheng ECC, Leung KH, Miskowski VM, Yam VWW, Phillips DL (2000) *Inorg Chem* 39:3690
46. Jones WB, Yuan J, Narayanaswamy R, Young MA, Elder RC, Bruce AE, Bruce MRM (1995) *Inorg Chem* 34:1996
47. Forward JM, Bohmann D, Fackler JP Jr, Staples RJ (1995) *Inorg Chem* 34:6330

48. Yam VWW, Chan CL, Cheung KK (1996) *J Chem Soc Dalton Trans* 4019
49. Yam VWW, Li CK, Chan CL (1998) *Angew Chem Int Ed Engl* 37:2857
50. Yam VWW, Chan CL, Li CK, Wong KMC (2001) *Coord Chem Rev* 216-217:171
51. Li CK, Lu XX, Wong KMC, Chan CL, Zhu N, Yam VWW (2004) *Inorg Chem* 43:7421
52. Ho SY, Cheng ECC, Tiekink ERT, Yam VWW (2006) *Inorg Chem* 45:8165
53. Hanna SD, Khan SI, Zink JI (1996) *Inorg Chem* 35:5813
54. Tang SS, Chang CP, Lin IJB, Liou LS, Wang JC (1997) *Inorg Chem* 36:2294
55. Bardaji M, Laguna A, Jones PG, Fischer AK (2000) *Inorg Chem* 39:3560
56. Yu SY, Zhang ZX, Cheng ECC, Li YZ, Yam VWW, Huang HP, Zhang R (2005) *J Am Chem Soc* 127:17994
57. Mansour MA, Connick WB, Lachicotte RJ, Gysling HJ, Eisenberg R (1998) *J Am Chem Soc* 120:1329
58. van Zyl WE, López-de-Luzuriaga JM, Fackler JP Jr (2000) *J Mol Struct* 516:99
59. van Zyl WE, López-de-Luzuriaga JM, Mohamed AA, Staples RJ, Fackler JP Jr (2002) *Inorg Chem* 41:4579
60. Lee YA, McGarrah JE, Lachicotte RJ, Eisenberg R (2002) *J Am Chem Soc* 124:10662
61. Lee YA, Eisenberg R (2003) *J Am Chem Soc* 125:7778
62. Müller T, Choi SWK, Mingos DMP, Murphy D, Williams DJ, Yam VWW (1994) *J Organomet Chem* 484:209
63. Che CM, Chao HY, Miskowski VM, Li Y, Cheung KK (2001) *J Am Chem Soc* 123:4985
64. Lu W, Xiang HF, Zhu N, Che CM (2002) *Organometallics* 21:2343
65. Mingos DMP, Yau J, Menzer S, Williams DJ (1995) *Angew Chem Int Ed Engl* 34:1894
66. Mohr F, Jennings MC, Puddephatt RJ (2003) *Eur J Inorg Chem* 217
67. Puddephatt RJ (2001) *Coord Chem Rev* 216-217:313
68. McArdle CP, Van S, Jennings MC, Puddephatt RJ (2002) *J Am Chem Soc* 124:3959
69. Mohr F, Eisler DJ, McArdle CP, Atieh K, Jennings MC, Puddephatt RJ (2003) *J Organomet Chem* 670:27
70. Yam VWW (2004) *J Organomet Chem* 689:1393
71. Long NJ, Williams CK (2003) *Angew Chem Int Ed* 42:2586
72. Paul F, Lapinte C (1998) *Coord Chem Rev* 431:178
73. Bruneau C, Dixneuf PH (1999) *Acc Chem Res* 32:311
74. Bruce MI, Ke M, Low PJ, Skelton BW, White AH (1998) *Organometallics* 17:3539
75. Cadierno V, Gamasa MP, Gimeno J (1998) *Organometallics* 17:697
76. Roidl G, Enkelmann V, Adams RD, Bunz UHF (1999) *J Organomet Chem* 578:144
77. Li D, Hong X, Che CM, Lo WC, Peng SM (1993) *J Chem Soc Dalton Trans* 2929
78. Che CM, Yip HK, Lo WC, Peng SM (1994) *Polyhedron* 13:887
79. Hong X, Cheung KK, Guo CX, Che CM (1994) *J Chem Soc Dalton Trans* 1867
80. Yam VWW, Choi SWK (1996) *J Chem Soc Dalton Trans* 4227
81. Yam VWW, Choi SWK, Cheung KK (1996) *Organometallics* 15:1734
82. Yam VWW, Choi SWK, Cheung KK (1996) *J Chem Soc Dalton Trans* 3411
83. Xiao H, Cheung KK, Che CM (1996) *J Chem Soc Dalton Trans* 3699
84. Irwin MJ, Vittal JJ, Puddephatt RJ (1997) *Organometallics* 16:3541
85. Liu L, Wong WY, Poon SY, Cheah KW (2005) *J Inorg Organomet Polym Mat* 15:555
86. Liu L, Wong WY, Shi JX, Cheah KW, Lee TH, Leung LM (2006) *J Organomet Chem* 691:4028
87. Liu L, Wong WY, Poon SY, Shi JX, Cheah KW, Lin Z (2006) *Chem Mater* 18:1369
88. Wong WY, Liu L, Poon SY, Choi KH, Cheah KW, Shi JX (2004) *Macromolecules* 37:4496
89. Liu L, Poon SY, Wong WY (2005) *J Organomet Chem* 690:5036

90. Poon SY, Wong WY, Cheah KW, Shi JX (2006) *Chem Eur J* 12:2550
91. Lu W, Xiang HF, Zhu N, Che CM (2002) *Organometallics* 21:2343
92. Chao HY, Lu W, Li Y, Chan MCW, Che CM, Cheung KK, Zhu N (2002) *J Am Chem Soc* 124:14696
93. Lu W, Zhu N, Che CM (2003) *J Organomet Chem* 607:11
94. Lu W, Zhu N, Che CM (2003) *J Am Chem Soc* 125:16081
95. Yam VWW, Cheung KL, Yip SK, Cheung KK (2003) *J Organomet Chem* 681:196
96. Yip SK, Lam WH, Zhu N, Yam VWW (2006) *Inorg Chim Acta* 359:3639
97. Li D, Hong X, Che CM, Lo WC, Peng SM (1993) *J Chem Soc Dalton Trans* 2929
98. Yam VWW, Cheung KL, Cheng ECC, Zhu N, Cheung KK (2003) *Dalton Trans* 1830
99. de la Riva H, Nieuwhuyzen M, Fierro CM, Raithby PR, Male L, Lagunas MC (2006) *Inorg Chem* 45:1418
100. Lu XX, Li CK, Cheng ECC, Zhu N, Yam VWW (2004) *Inorg Chem* 43:2225
101. Tang HS, Zhu N, Yam VWW (2006) *Organometallics* 26:22
102. Puddephatt RJ (1998) *Chem Commun* p 1055
103. Puddephatt RJ (2001) *Coord Chem Rev* 216-217:313
104. Yip SK, Cheng ECC, Yuan LH, Zhu N, Yam VWW (2004) *Angew Chem Int Ed* 43:4954
105. Yam VWW, Cheung KL, Yuan LH, Wong KMC, Cheung KK (2000) *Chem Commun* p 1513
106. Yam VWW, Yip SK, Yuan LH, Cheung KL, Zhu N, Cheung KK (2003) *Organometallics* 22:2630
107. Burini A, Mohamed AA, Fackler JP Jr (2003) *Comments Inorg Chem* 24:253
108. Vickery JC, Olmstead MM, Fung EY, Balch AL (1997) *Angew Chem Int Ed Engl* 36:1179
109. Fung EY, Olmstead MM, Vickery JC, Balch AL (1998) *Coord Chem Rev* 171:151
110. Balch AL, Olmstead MM, Vickery JC (1999) *Inorg Chem* 38:3494
111. White-Morris RL, Olmstead MM, Attar S, Balch AL (2004) *Inorg Chem* 44:5021
112. Olmstead MM, Jiang F, Attar S, Balch AL (2001) *J Am Chem Soc* 123:3260
113. Rawashdeh-Omary MA, Omary MA, Fackler JP Jr (2001) *J Am Chem Soc* 123:9689
114. Omary MA, Mohamed AA, Rawashdeh-Omary MA, Fackler JP Jr (2005) *Coord Chem Rev* 249:1372
115. Mohamed AA, Rawashdeh-Omary MA, Omary MA, Fackler JP Jr (2005) *Dalton Trans* 2597
116. Burini A, Fackler JP Jr, Galassi R, Grant TA, Omary MA, Rawashdeh-Omary MA, Pietroni BR, Staples RJ (2000) *J Am Chem Soc* 122:11264
117. Burini A, Bravi R, Fackler JP Jr, Galassi R, Grant TA, Omary MA, Pietroni BR, Staples RJ (2000) 39:3158
118. Yang C, Messerschmidt M, Coppens P, Omary MA (2006) *Inorg Chem* 45:6592
119. Barberá J, Elduque A, Giménez R, Oro LA, Serrano JL (1996) *Angew Chem Int Ed Engl* 35:2832
120. Barberá J, Elduque A, Giménez R, Lahoz FJ, López JA, Oro LA, Serrano JL (1998) *Inorg Chem* 37:2960
121. Kim SJ, Kang SH, Park KM, Kim H, Zin WC, Choi MG, Kim K (1998) *Chem Mater* 10:1889
122. Enomoto M, Kishimura A, Aida T (2001) *J Am Chem Soc* 123:5608
123. Kishimura A, Yamashita T, Aida T (2005) *J Am Chem Soc* 127:179
124. Lin R, Yip JHK, Zhang K, Koh LL, Wong KY, Ho KP (2004) *J Am Chem Soc* 126:15852
125. Lefebvre J, Batchelor RJ, Leznoff DB (2004) *J Am Chem Soc* 126:16117
126. Wang HMJ, Chen CYL, Lin IJB (1999) *Organometallics* 18:1216

127. Wang HMJ, Vasam CS, Tsai TYR, Chen SH, Cheng AHH, Lin IJB (2005) *Organometallics* 24:486
128. Catalano VJ, Malqitz MA, Etogo AO (2004) *Inorg Chem* 43:5714
129. Catalano VJ, Etogo AO (2005) *J Organomet Chem* 690:6041
130. Khan MNI, Wang S, Fackler JP Jr (1989) *Inorg Chem* 28:3579
131. Yam VWW, Choi SWK, Cheung KK (1996) *Chem Commun* p 1173
132. Yam VWW, Li CK, Chan CL, Cheung KK (2001) *Inorg Chem* 40:7054
133. Yam VWW, Choi SWK, Lai TF, Lee WK (1993) *J Chem Soc Dalton Trans* 1001
134. Chan CW, Wong WT, Che CM (1994) *Inorg Chem* 33:1266
135. Liu HQ, Cheung TC, Peng SM, Che CM (1995) *J Chem Soc Chem Commun* p 1787
136. Wong KH, Cheung KK, Chan MCW, Che CM (1998) *Organometallics* 17:3505
137. Yam VWW, Wong KMC, Hung LL, Zhu N (2005) *Angew Chem Int Ed* 44:3107
138. Wong KMC, Zhu X, Hung LL, Zhu N, Yam VWW, Kwok HS (2005) *Chem Commun* p 2906
139. Fleischer EB, Laszlo A (1969) *Inorg Nucl Chem Letts* 5:373
140. Jamin ME, Iwamoto RT (1978) *Inorg Chim Acta* 27:135
141. Antipas A, Dolphin D, Gouterman M, Johnson EC (1978) *J Am Chem Soc* 100:7705
142. Andréasson J, Kodis G, Lin S, Moore AL, Moore TA, Gust D, Mårtensson J, Albinsson B (2002) *Photochem Photobiol* 76:47
143. Eng MP, Ljungdahl T, Andréasson J, Mårtensson J, Albinsson B (2005) *J Phys Chem A* 109:1776
144. Brun AM, Harriman A, Heitz V, Sauvage JP (1991) *J Am Chem Soc* 113:8657
145. Chambron JC, Chardon-Noblat S, Harriman A, Heitz V, Sauvage JP (1993) *Pure Appl Chem* 65:2343
146. Harriman A, Sauvage JP (1996) *Chem Soc Rev* 25:41
147. Blanco MJ, Jiménez MC, Chambron JC, Heitz V, Linke M, Sauvage JP (1999) *Chem Soc Rev* 28:293
148. Dixon IM, Collin JP, Sauvage JP, Flamigni L (2001) *Inorg Chem* 40:5507
149. Kilså K, Kajanus J, Macpherson AN, Mårtensson J, Albinsson B (2001) *J Am Chem Soc* 123:3069
150. Andersson M, Linke M, Chambron JC, Davidsson J, Heitz V, Hammarström L, Sauvage JP (2002) *J Am Chem Soc* 124:4347
151. Andréasson J, Kodis G, Ljungdahl T, Moore AL, Moore TA, Gust D, Mårtensson J, Albinsson B (2003) *J Phys Chem A* 107:8825
152. Flamigni L, Talarico AM, Chambron JC, Heitz V, Linke M, Fujita N, Sauvage JP (2004) *Chem Eur J* 10:2689
153. Winters MU, Pettersson K, Mårtensson J, Albinsson B (2005) *Chem Eur J* 11:562
154. Pettersson K, Wiberg J, Ljungdahl T, Mårtensson J, Albinsson B (2005) *J Phys Chem A* 110:319
155. Ohkubo K, Santic PJ, Tkachenko NV, Lemmetyinen H, Wenbo E, Ou Z, Shao J, Kadish KM, Crossley MJ, Fukuzumi S (2006) *Chem Phys* 326:3
156. Ou Z, Kadish KM, Wenbo E, Shao J, Santic PJ, Ohkubo K, Fukuzumi S, Crossley MJ (2004) *Inorg Chem* 43:2078
157. Kadish KM, Wenbo E, Ou Z, Shao J, Santic PJ, Ohkubo K, Fukuzumi S, Crossley MJ (2002) *Chem Commun* p 356
158. Knör G (2001) *Inorg Chem Commun* 4:160

Author Index Volumes 251–281

Author Index Vols. 26–50 see Vol. 50
Author Index Vols. 51–100 see Vol. 100
Author Index Vols. 101–150 see Vol. 150
Author Index Vols. 151–200 see Vol. 200
Author Index Vols. 201–250 see Vol. 250

The volume numbers are printed in italics

- Accorsi G, see Armaroli N (2007) 280: 69–115
Ajayaghosh A, George SJ, Schenning APHJ (2005) Hydrogen-Bonded Assemblies of Dyes and Extended π -Conjugated Systems. 258: 83–118
Akai S, Kita Y (2007) Recent Advances in Pummerer Reactions. 274: 35–76
Albert M, Fensterbank L, Lacôte E, Malacria M (2006) Tandem Radical Reactions. 264: 1–62
Alberto R (2005) New Organometallic Technetium Complexes for Radiopharmaceutical Imaging. 252: 1–44
Alegret S, see Pividori MI (2005) 260: 1–36
Alfaro JA, see Schuman B (2007) 272: 217–258
Amabilino DB, Veciana J (2006) Supramolecular Chiral Functional Materials. 265: 253–302
Anderson CJ, see Li WP (2005) 252: 179–192
Anslyn EV, see Collins BE (2007) 277: 181–218
Anslyn EV, see Houk RJT (2005) 255: 199–229
Appukkuttan P, Van der Eycken E (2006) Microwave-Assisted Natural Product Chemistry. 266: 1–47
Araki K, Yoshikawa I (2005) Nucleobase-Containing Gelators. 256: 133–165
Armaroli N, Accorsi G, Cardinali Fç, Listorti A (2007) Photochemistry and Photophysics of Coordination Compounds: Copper. 280: 69–115
Armitage BA (2005) Cyanine Dye–DNA Interactions: Intercalation, Groove Binding and Aggregation. 253: 55–76
Arya DP (2005) Aminoglycoside–Nucleic Acid Interactions: The Case for Neomycin. 253: 149–178

Bailly C, see Dias N (2005) 253: 89–108
Balaban TS, Tamiaki H, Holzwarth AR (2005) Chlorins Programmed for Self-Assembly. 258: 1–38
Baltzer L (2007) Polypeptide Conjugate Binders for Protein Recognition. 277: 89–106
Balzani V, Bergamini G, Campagna S, Puntoriero F (2007) Photochemistry and Photophysics of Coordination Compounds: Overview and General Concepts. 280: 1–36
Balzani V, Credi A, Ferrer B, Silvi S, Venturi M (2005) Artificial Molecular Motors and Machines: Design Principles and Prototype Systems. 262: 1–27
Balzani V, see Campagna S (2007) 280: 117–214
Barbieri CM, see Pilch DS (2005) 253: 179–204
Barbieri A, see Flamigni L (2007) 281: 143–204
Barchuk A, see Daasbjerg K (2006) 263: 39–70
Bargon J, see Kuhn LT (2007) 276: 25–68
Bargon J, see Kuhn LT (2007) 276: 125–154

- Barigelletti F, see Flamigni L (2007) 281: 143–204
- Bayly SR, see Beer PD (2005) 255: 125–162
- Beck-Sickingler AG, see Haack M (2007) 278: 243–288
- Beer PD, Bayly SR (2005) Anion Sensing by Metal-Based Receptors. 255: 125–162
- Bergamini G, see Balzani V (2007) 280: 1–36
- Bergamini G, see Campagna S (2007) 280: 117–214
- Bertini L, Bruschi M, de Gioia L, Fantucci P, Greco C, Zampella G (2007) Quantum Chemical Investigations of Reaction Paths of Metalloenzymes and Biomimetic Models – The Hydrogenase Example. 268: 1–46
- Bier FF, see Heise C (2005) 261: 1–25
- Blum LJ, see Marquette CA (2005) 261: 113–129
- Boiteau L, see Pascal R (2005) 259: 69–122
- Bolhuis PG, see Dellago C (2007) 268: 291–317
- Borovkov VV, Inoue Y (2006) Supramolecular Chirogenesis in Host–Guest Systems Containing Porphyrinoids. 265: 89–146
- Boschi A, Duatti A, Uccelli L (2005) Development of Technetium-99m and Rhenium-188 Radiopharmaceuticals Containing a Terminal Metal–Nitrido Multiple Bond for Diagnosis and Therapy. 252: 85–115
- Braga D, D’Addario D, Giaffreda SL, Maini L, Polito M, Grepioni F (2005) Intra-Solid and Inter-Solid Reactions of Molecular Crystals: a Green Route to Crystal Engineering. 254: 71–94
- Bräse S, see Jung N (2007) 278: 1–88
- Braverman S, Cherkinsky M (2007) [2,3]Sigmatropic Rearrangements of Propargylic and Allenic Systems. 275: 67–101
- Brebion F, see Crich D (2006) 263: 1–38
- Breinbauer R, see Mentel M (2007) 278: 209–241
- Breit B (2007) Recent Advances in Alkene Hydroformylation. 279: 139–172
- Brizard A, Oda R, Huc I (2005) Chirality Effects in Self-assembled Fibrillar Networks. 256: 167–218
- Broene RD (2007) Reductive Coupling of Unactivated Alkenes and Alkynes. 279: 209–248
- Bromfield K, see Ljungdahl N (2007) 278: 89–134
- Bruce IJ, see del Campo A (2005) 260: 77–111
- Bruschi M, see Bertini L (2007) 268: 1–46
- Bur SK (2007) 1,3-Sulfur Shifts: Mechanism and Synthetic Utility. 274: 125–171
- Campagna S, Puntoriero F, Nastasi F, Bergamini G, Balzani V (2007) Photochemistry and Photophysics of Coordination Compounds: Ruthenium. 280: 117–214
- Campagna S, see Balzani V (2007) 280: 1–36
- del Campo A, Bruce IJ (2005) Substrate Patterning and Activation Strategies for DNA Chip Fabrication. 260: 77–111
- Cardinali F, see Armaroli N (2007) 280: 69–115
- Carney CK, Harry SR, Sewell SL, Wright DW (2007) Detoxification Biominerals. 270: 155–185
- Castagner B, Seeberger PH (2007) Automated Solid Phase Oligosaccharide Synthesis. 278: 289–309
- Chaires JB (2005) Structural Selectivity of Drug–Nucleic Acid Interactions Probed by Competition Dialysis. 253: 33–53
- Cheng EC-C, see Yam VW-W (2007) 281: 269–310
- Cherkinsky M, see Braverman S (2007) 275: 67–101
- Chiorboli C, Indelli MT, Scandola F (2005) Photoinduced Electron/Energy Transfer Across Molecular Bridges in Binuclear Metal Complexes. 257: 63–102

- Chiorboli C, see Indelli MT (2007) 280: 215–255
- Coleman AW, Perret F, Moussa A, Dupin M, Guo Y, Perron H (2007) Calix[n]arenes as Protein Sensors. 277: 31–88
- Cölfen H (2007) Bio-inspired Mineralization Using Hydrophilic Polymers. 271: 1–77
- Collin J-P, Heitz V, Sauvage J-P (2005) Transition-Metal-Complexed Catenanes and Rotaxanes in Motion: Towards Molecular Machines. 262: 29–62
- Collins BE, Wright AT, Anslyn EV (2007) Combining Molecular Recognition, Optical Detection, and Chemometric Analysis. 277: 181–218
- Collyer SD, see Davis F (2005) 255: 97–124
- Commeyras A, see Pascal R (2005) 259: 69–122
- Coquerel G (2007) Preferential Crystallization. 269: 1–51
- Correia JDG, see Santos I (2005) 252: 45–84
- Costanzo G, see Saladino R (2005) 259: 29–68
- Cotarca L, see Zonta C (2007) 275: 131–161
- Credi A, see Balzani V (2005) 262: 1–27
- Crestini C, see Saladino R (2005) 259: 29–68
- Crich D, Brebion F, Suk D-H (2006) Generation of Alkene Radical Cations by Heterolysis of β -Substituted Radicals: Mechanism, Stereochemistry, and Applications in Synthesis. 263: 1–38
- Cuerva JM, Justicia J, Oller-López JL, Oltra JE (2006) Cp_2TiCl in Natural Product Synthesis. 264: 63–92
- Daasbjerg K, Svith H, Grimme S, Gerenkamp M, Mück-Lichtenfeld C, Gansäuer A, Barchuk A (2006) The Mechanism of Epoxide Opening through Electron Transfer: Experiment and Theory in Concert. 263: 39–70
- D'Addario D, see Braga D (2005) 254: 71–94
- Danishesky SJ, see Warren JD (2007) 267: 109–141
- Darmency V, Renaud P (2006) Tin-Free Radical Reactions Mediated by Organoboron Compounds. 263: 71–106
- Davis F, Collyer SD, Higson SPJ (2005) The Construction and Operation of Anion Sensors: Current Status and Future Perspectives. 255: 97–124
- Deamer DW, Dworkin JP (2005) Chemistry and Physics of Primitive Membranes. 259: 1–27
- Debaene F, see Winssinger N (2007) 278: 311–342
- Dellago C, Bolhuis PG (2007) Transition Path Sampling Simulations of Biological Systems. 268: 291–317
- Deng J-Y, see Zhang X-E (2005) 261: 169–190
- Dervan PB, Poulin-Kerstien AT, Fechter EJ, Edelson BS (2005) Regulation of Gene Expression by Synthetic DNA-Binding Ligands. 253: 1–31
- Dias N, Vezin H, Lansiaux A, Bailly C (2005) Topoisomerase Inhibitors of Marine Origin and Their Potential Use as Anticancer Agents. 253: 89–108
- DiMauro E, see Saladino R (2005) 259: 29–68
- Dittrich M, Yu J, Schulten K (2007) PcrA Helicase, a Molecular Motor Studied from the Electronic to the Functional Level. 268: 319–347
- Dobrawa R, see You C-C (2005) 258: 39–82
- Du Q, Larsson O, Swerdlow H, Liang Z (2005) DNA Immobilization: Silanized Nucleic Acids and Nanoprinting. 261: 45–61
- Duatti A, see Boschi A (2005) 252: 85–115
- Dupin M, see Coleman AW (2007) 277: 31–88
- Dworkin JP, see Deamer DW (2005) 259: 1–27

- Edelson BS, see Dervan PB (2005) 253: 1–31
- Edwards DS, see Liu S (2005) 252: 193–216
- Ernst K-H (2006) *Supramolecular Surface Chirality*. 265: 209–252
- Ersmark K, see Wannberg J (2006) 266: 167–197
- Escudé C, Sun J-S (2005) DNA Major Groove Binders: Triple Helix-Forming Oligonucleotides, Triple Helix-Specific DNA Ligands and Cleaving Agents. 253: 109–148
- Evans SV, see Schuman B (2007) 272: 217–258
- Van der Eycken E, see Appukkuttan P (2006) 266: 1–47
- Fages F, Vögtle F, Žinić M (2005) Systematic Design of Amide- and Urea-Type Gelators with Tailored Properties. 256: 77–131
- Fages F, see Žinić M (2005) 256: 39–76
- Faigl F, Schindler J, Fogassy E (2007) Advantages of Structural Similarities of the Reactants in Optical Resolution Processes. 269: 133–157
- Fan C-A, see Gansäuer A (2007) 279: 25–52
- Fantucci P, see Bertini L (2007) 268: 1–46
- Fechter EJ, see Dervan PB (2005) 253: 1–31
- Fensterbank L, see Albert M (2006) 264: 1–62
- Fernández JM, see Moonen NNP (2005) 262: 99–132
- Fernando C, see Szathmáry E (2005) 259: 167–211
- Ferrer B, see Balzani V (2005) 262: 1–27
- De Feyter S, De Schryver F (2005) Two-Dimensional Dye Assemblies on Surfaces Studied by Scanning Tunneling Microscopy. 258: 205–255
- Fischer D, Geyer A (2007) NMR Analysis of Bioprotective Sugars: Sucrose and Oligomeric (1→2)- α -D-glucopyranosyl-(1→2)- β -D-fructofuranosides. 272: 169–186
- Flamigni L, Barbieri A, Sabatini C, Ventura B, Barigelletti F (2007) Photochemistry and Photophysics of Coordination Compounds: Iridium. 281: 143–204
- Flood AH, see Moonen NNP (2005) 262: 99–132
- Fogassy E, see Faigl F (2007) 269: 133–157
- Fricke M, Volkmer D (2007) Crystallization of Calcium Carbonate Beneath Insoluble Monolayers: Suitable Models of Mineral–Matrix Interactions in Biomineralization? 270: 1–41
- Fujimoto D, see Tamura R (2007) 269: 53–82
- Fujiwara S-i, Kambe N (2005) Thio-, Seleno-, and Telluro-Carboxylic Acid Esters. 251: 87–140
- Gansäuer A, see Daasbjerg K (2006) 263: 39–70
- Garcia-Garibay MA, see Karlen SD (2005) 262: 179–227
- Gelinck GH, see Grozema FC (2005) 257: 135–164
- Geng X, see Warren JD (2007) 267: 109–141
- Gansäuer A, Justicia J, Fan C-A, Worgull D, Piester F (2007) Reductive C–C Bond Formation after Epoxide Opening via Electron Transfer. 279: 25–52
- George SJ, see Ajayaghosh A (2005) 258: 83–118
- Gerenkamp M, see Daasbjerg K (2006) 263: 39–70
- Gevorgyan V, see Sromek AW (2007) 274: 77–124
- Geyer A, see Fischer D (2007) 272: 169–186
- Giaffreda SL, see Braga D (2005) 254: 71–94
- Giernoth R (2007) Homogeneous Catalysis in Ionic Liquids. 276: 1–23
- de Gioia L, see Bertini L (2007) 268: 1–46
- Di Giusto DA, King GC (2005) Special-Purpose Modifications and Immobilized Functional Nucleic Acids for Biomolecular Interactions. 261: 131–168

- Greco C, see Bertini L (2007) 268: 1–46
- Greiner L, Laue S, Wöltinger J, Liese A (2007) Continuous Asymmetric Hydrogenation. 276: 111–124
- Grepioni F, see Braga D (2005) 254: 71–94
- Grimme S, see Daasbjerg K (2006) 263: 39–70
- Grozema FC, Siebbeles LDA, Gelinck GH, Warman JM (2005) The Opto-Electronic Properties of Isolated Phenylenevinylene Molecular Wires. 257: 135–164
- Guiseppe-Elie A, Lingerfelt L (2005) Impedimetric Detection of DNA Hybridization: Towards Near-Patient DNA Diagnostics. 260: 161–186
- Gunnlaugsson T, see Leonard JP (2007) 281: 1–44
- Guo Y, see Coleman AW (2007) 277: 31–88
- Haack M, Beck-Sickinger AG (2007) Multiple Peptide Synthesis to Identify Bioactive Hormone Structures. 278: 243–288
- Haase C, Seitz O (2007) Chemical Synthesis of Glycopeptides. 267: 1–36
- Hahn F, Schepers U (2007) Solid Phase Chemistry for the Directed Synthesis of Biologically Active Polyamine Analogs, Derivatives, and Conjugates. 278: 135–208
- Hansen SG, Skrydstrup T (2006) Modification of Amino Acids, Peptides, and Carbohydrates through Radical Chemistry. 264: 135–162
- Harmer NJ (2007) The Fibroblast Growth Factor (FGF) – FGF Receptor Complex: Progress Towards the Physiological State. 272: 83–116
- Harry SR, see Carney CK (2007) 270: 155–185
- Heise C, Bier FF (2005) Immobilization of DNA on Microarrays. 261: 1–25
- Heitz V, see Collin J-P (2005) 262: 29–62
- Herrmann C, Reiher M (2007) First-Principles Approach to Vibrational Spectroscopy of Biomolecules. 268: 85–132
- Higson SPJ, see Davis F (2005) 255: 97–124
- Hirao T (2007) Catalytic Reductive Coupling of Carbonyl Compounds – The Pinacol Coupling Reaction and Beyond. 279: 53–75
- Hirayama N, see Sakai K (2007) 269: 233–271
- Hirst AR, Smith DK (2005) Dendritic Gelators. 256: 237–273
- Holzwarth AR, see Balaban TS (2005) 258: 1–38
- Homans SW (2007) Dynamics and Thermodynamics of Ligand–Protein Interactions. 272: 51–82
- Houk RJT, Tobey SL, Anslyn EV (2005) Abiotic Guanidinium Receptors for Anion Molecular Recognition and Sensing. 255: 199–229
- Huc I, see Brizard A (2005) 256: 167–218
- Ihmels H, Otto D (2005) Intercalation of Organic Dye Molecules into Double-Stranded DNA – General Principles and Recent Developments. 258: 161–204
- Iida H, Krische MJ (2007) Catalytic Reductive Coupling of Alkenes and Alkynes to Carbonyl Compounds and Imines Mediated by Hydrogen. 279: 77–104
- Imai H (2007) Self-Organized Formation of Hierarchical Structures. 270: 43–72
- Indelli MT, Chiorboli C, Scandola F (2007) Photochemistry and Photophysics of Coordination Compounds: Rhodium. 280: 215–255
- Indelli MT, see Chiorboli C (2005) 257: 63–102
- Inoue Y, see Borovkov VV (2006) 265: 89–146
- Ishii A, Nakayama J (2005) Carbodithioic Acid Esters. 251: 181–225
- Ishii A, Nakayama J (2005) Carboselenothioic and Carbodiselenoic Acid Derivatives and Related Compounds. 251: 227–246

- Ishi-i T, Shinkai S (2005) Dye-Based Organogels: Stimuli-Responsive Soft Materials Based on One-Dimensional Self-Assembling Aromatic Dyes. *258*: 119–160
- James DK, Tour JM (2005) *Molecular Wires*. *257*: 33–62
- James TD (2007) Saccharide-Selective Boronic Acid Based Photoinduced Electron Transfer (PET) Fluorescent Sensors. *277*: 107–152
- Jelinek R, Kolusheva S (2007) Biomolecular Sensing with Colorimetric Vesicles. *277*: 155–180
- Jones W, see Trask AV (2005) *254*: 41–70
- Jung N, Wiehn M, Bräse S (2007) Multifunctional Linkers for Combinatorial Solid Phase Synthesis. *278*: 1–88
- Justicia J, see Cuerva JM (2006) *264*: 63–92
- Justicia J, see Gansäuer A (2007) *279*: 25–52
- Kambe N, see Fujiwara S-i (2005) *251*: 87–140
- Kane-Maguire NAP (2007) Photochemistry and Photophysics of Coordination Compounds: Chromium. *280*: 37–67
- Kann N, see Ljungdahl N (2007) *278*: 89–134
- Kano N, Kawashima T (2005) Dithiocarboxylic Acid Salts of Group 1–17 Elements (Except for Carbon). *251*: 141–180
- Kappe CO, see Kreamsner JM (2006) *266*: 233–278
- Kaptein B, see Kellogg RM (2007) *269*: 159–197
- Karlen SD, Garcia-Garibay MA (2005) Amphidynamic Crystals: Structural Blueprints for Molecular Machines. *262*: 179–227
- Kato S, Niyomura O (2005) Group 1–17 Element (Except Carbon) Derivatives of Thio-, Seleno- and Telluro-Carboxylic Acids. *251*: 19–85
- Kato S, see Niyomura O (2005) *251*: 1–12
- Kato T, Mizoshita N, Moriyama M, Kitamura T (2005) Gelation of Liquid Crystals with Self-Assembled Fibers. *256*: 219–236
- Kaul M, see Pilch DS (2005) *253*: 179–204
- Kaupp G (2005) Organic Solid-State Reactions with 100% Yield. *254*: 95–183
- Kawasaki T, see Okahata Y (2005) *260*: 57–75
- Kawashima T, see Kano N (2005) *251*: 141–180
- Kay ER, Leigh DA (2005) Hydrogen Bond-Assembled Synthetic Molecular Motors and Machines. *262*: 133–177
- Kellogg RM, Kaptein B, Vries TR (2007) Dutch Resolution of Racemates and the Roles of Solid Solution Formation and Nucleation Inhibition. *269*: 159–197
- Kessler H, see Weide T (2007) *272*: 1–50
- Kimura M, Tamaru Y (2007) Nickel-Catalyzed Reductive Coupling of Dienes and Carbonyl Compounds. *279*: 173–207
- King GC, see Di Giusto DA (2005) *261*: 131–168
- Kirchner B, see Thar J (2007) *268*: 133–171
- Kirgan RA, Sullivan BP, Rillema DP (2007) Photochemistry and Photophysics of Coordination Compounds: Rhenium. *281*: 45–102
- Kita Y, see Akai S (2007) *274*: 35–76
- Kitamura T, see Kato T (2005) *256*: 219–236
- Kniep R, Simon P (2007) Fluorapatite-Gelatine-Nanocomposites: Self-Organized Morphogenesis, Real Structure and Relations to Natural Hard Materials. *270*: 73–125
- Koenig BW (2007) Residual Dipolar Couplings Report on the Active Conformation of Rhodopsin-Bound Protein Fragments. *272*: 187–216
- Kolusheva S, see Jelinek R (2007) *277*: 155–180

- Komatsu K (2005) The Mechanochemical Solid-State Reaction of Fullerenes. *254*: 185–206
- Kremsner JM, Stadler A, Kappe CO (2006) The Scale-Up of Microwave-Assisted Organic Synthesis. *266*: 233–278
- Kriegisch V, Lambert C (2005) Self-Assembled Monolayers of Chromophores on Gold Surfaces. *258*: 257–313
- Krische MJ, see Iida H (2007) *279*: 77–104
- Kuhn LT, Bargon J (2007) Transfer of Parahydrogen-Induced Hyperpolarization to Heteronuclei. *276*: 25–68
- Kuhn LT, Bargon J (2007) Exploiting Nuclear Spin Polarization to Investigate Free Radical Reactions via in situ NMR. *276*: 125–154
- Kumaresan D, Shankar K, Vaidya S, Schmehl RH (2007) Photochemistry and Photophysics of Coordination Compounds: Osmium. *281*: 101–142
- Lacôte E, see Albert M (2006) *264*: 1–62
- Lahav M, see Weissbuch I (2005) *259*: 123–165
- Lambert C, see Kriegisch V (2005) *258*: 257–313
- Lansiaux A, see Dias N (2005) *253*: 89–108
- LaPlante SR (2007) Exploiting Ligand and Receptor Adaptability in Rational Drug Design Using Dynamics and Structure-Based Strategies. *272*: 259–296
- Larhed M, see Nilsson P (2006) *266*: 103–144
- Larhed M, see Wannberg J (2006) *266*: 167–197
- Larsson O, see Du Q (2005) *261*: 45–61
- Laue S, see Greiner L (2007) *276*: 111–124
- Leigh DA, Pérez EM (2006) Dynamic Chirality: Molecular Shuttles and Motors. *265*: 185–208
- Leigh DA, see Kay ER (2005) *262*: 133–177
- Leiserowitz L, see Weissbuch I (2005) *259*: 123–165
- Leonard JP, Nolan CB, Stomeo F, Gunnlaugsson T (2007) Photochemistry and Photophysics of Coordination Compounds: Lanthanides. *281*: 1–44
- Lhoták P (2005) Anion Receptors Based on Calixarenes. *255*: 65–95
- Li WP, Meyer LA, Anderson CJ (2005) Radiopharmaceuticals for Positron Emission Tomography Imaging of Somatostatin Receptor Positive Tumors. *252*: 179–192
- Liang Z, see Du Q (2005) *261*: 45–61
- Liese A, see Greiner L (2007) *276*: 111–124
- Lingerfelt L, see Guiseppi-Elie A (2005) *260*: 161–186
- Listorti A, see Armaroli N (2007) *280*: 69–115
- Litvinchuk S, see Matile S (2007) *277*: 219–250
- Liu S (2005) 6-Hydrazinonicotinamide Derivatives as Bifunctional Coupling Agents for ^{99m}Tc-Labeling of Small Biomolecules. *252*: 117–153
- Liu S, Robinson SP, Edwards DS (2005) Radiolabeled Integrin $\alpha_v\beta_3$ Antagonists as Radiopharmaceuticals for Tumor Radiotherapy. *252*: 193–216
- Liu XY (2005) Gelation with Small Molecules: from Formation Mechanism to Nanostructure Architecture. *256*: 1–37
- Ljungdahl N, Bromfield K, Kann N (2007) Solid Phase Organometallic Chemistry. *278*: 89–134
- De Lucchi O, see Zonta C (2007) *275*: 131–161
- Luderer F, Walschus U (2005) Immobilization of Oligonucleotides for Biochemical Sensing by Self-Assembled Monolayers: Thiol-Organic Bonding on Gold and Silanization on Silica Surfaces. *260*: 37–56

- Maeda K, Yashima E (2006) Dynamic Helical Structures: Detection and Amplification of Chirality. *265*: 47–88
- Magnera TF, Michl J (2005) Altitudinal Surface-Mounted Molecular Rotors. *262*: 63–97
- Maini L, see Braga D (2005) *254*: 71–94
- Malacria M, see Albert M (2006) *264*: 1–62
- Marquette CA, Blum LJ (2005) Beads Arraying and Beads Used in DNA Chips. *261*: 113–129
- Mascini M, see Palchetti I (2005) *261*: 27–43
- Matile S, Tanaka H, Litvinchuk S (2007) Analyte Sensing Across Membranes with Artificial Pores. *277*: 219–250
- Matsumoto A (2005) Reactions of 1,3-Diene Compounds in the Crystalline State. *254*: 263–305
- McGhee AM, Procter DJ (2006) Radical Chemistry on Solid Support. *264*: 93–134
- Mentel M, Breinbauer R (2007) Combinatorial Solid-Phase Natural Product Chemistry. *278*: 209–241
- Meyer B, Möller H (2007) Conformation of Glycopeptides and Glycoproteins. *267*: 187–251
- Meyer LA, see Li WP (2005) *252*: 179–192
- Michl J, see Magnera TF (2005) *262*: 63–97
- Milea JS, see Smith CL (2005) *261*: 63–90
- Mizoshita N, see Kato T (2005) *256*: 219–236
- Modlinger A, see Weide T (2007) *272*: 1–50
- Möller H, see Meyer B (2007) *267*: 187–251
- Montgomery J, Sormunen GJ (2007) Nickel-Catalyzed Reductive Couplings of Aldehydes and Alkynes. *279*: 1–23
- Moonen NNP, Flood AH, Fernández JM, Stoddart JF (2005) Towards a Rational Design of Molecular Switches and Sensors from their Basic Building Blocks. *262*: 99–132
- Moriyama M, see Kato T (2005) *256*: 219–236
- Moussa A, see Coleman AW (2007) *277*: 31–88
- Murai T (2005) Thio-, Seleno-, Telluro-Amides. *251*: 247–272
- Murakami H (2007) From Racemates to Single Enantiomers – Chiral Synthetic Drugs over the last 20 Years. *269*: 273–299
- Mutule I, see Suna E (2006) *266*: 49–101
- Naka K (2007) Delayed Action of Synthetic Polymers for Controlled Mineralization of Calcium Carbonate. *271*: 119–154
- Nakayama J, see Ishii A (2005) *251*: 181–225
- Nakayama J, see Ishii A (2005) *251*: 227–246
- Narayanan S, see Reif B (2007) *272*: 117–168
- Nastasi F, see Campagna S (2007) *280*: 117–214
- Neese F, see Sinnecker S (2007) *268*: 47–83
- Nguyen GH, see Smith CL (2005) *261*: 63–90
- Nicolau DV, Sawant PD (2005) Scanning Probe Microscopy Studies of Surface-Immobilised DNA/Oligonucleotide Molecules. *260*: 113–160
- Niessen HG, Woelk K (2007) Investigations in Supercritical Fluids. *276*: 69–110
- Nilsson P, Olofsson K, Larhed M (2006) Microwave-Assisted and Metal-Catalyzed Coupling Reactions. *266*: 103–144
- Nishiyama H, Shiomi T (2007) Reductive Aldol, Michael, and Mannich Reactions. *279*: 105–137
- Niyomura O, Kato S (2005) Chalcogenocarboxylic Acids. *251*: 1–12
- Niyomura O, see Kato S (2005) *251*: 19–85

- Nohira H, see Sakai K (2007) 269: 199–231
Nolan CB, see Leonard JP (2007) 281: 1–44
- Oda R, see Brizard A (2005) 256: 167–218
Okahata Y, Kawasaki T (2005) Preparation and Electron Conductivity of DNA-Aligned Cast and LB Films from DNA-Lipid Complexes. 260: 57–75
Okamura T, see Ueyama N (2007) 271: 155–193
Oller-López JL, see Cuerva JM (2006) 264: 63–92
Olofsson K, see Nilsson P (2006) 266: 103–144
Oltra JE, see Cuerva JM (2006) 264: 63–92
Onoda A, see Ueyama N (2007) 271: 155–193
Otto D, see Ihmels H (2005) 258: 161–204
Otto S, Severin K (2007) Dynamic Combinatorial Libraries for the Development of Synthetic Receptors and Sensors. 277: 267–288
- Palchetti I, Mascini M (2005) Electrochemical Adsorption Technique for Immobilization of Single-Stranded Oligonucleotides onto Carbon Screen-Printed Electrodes. 261: 27–43
Pascal R, Boiteau L, Commeyras A (2005) From the Prebiotic Synthesis of α -Amino Acids Towards a Primitive Translation Apparatus for the Synthesis of Peptides. 259: 69–122
Paulo A, see Santos I (2005) 252: 45–84
Pérez EM, see Leigh DA (2006) 265: 185–208
Perret F, see Coleman AW (2007) 277: 31–88
Perron H, see Coleman AW (2007) 277: 31–88
Pianowski Z, see Winssinger N (2007) 278: 311–342
Piestert F, see Gansäuer A (2007) 279: 25–52
Pilch DS, Kaul M, Barbieri CM (2005) Ribosomal RNA Recognition by Aminoglycoside Antibiotics. 253: 179–204
Pividori MI, Alegret S (2005) DNA Adsorption on Carbonaceous Materials. 260: 1–36
Piwnica-Worms D, see Sharma V (2005) 252: 155–178
Plesniak K, Zarecki A, Wicha J (2007) The Smiles Rearrangement and the Julia–Kocienski Olefination Reaction. 275: 163–250
Polito M, see Braga D (2005) 254: 71–94
Poulin-Kerstien AT, see Dervan PB (2005) 253: 1–31
de la Pradilla RF, Tortosa M, Viso A (2007) Sulfur Participation in [3,3]-Sigmatropic Rearrangements. 275: 103–129
Procter DJ, see McGhee AM (2006) 264: 93–134
Puntoriero F, see Balzani V (2007) 280: 1–36
Puntoriero F, see Campagna S (2007) 280: 117–214
- Quiclet-Sire B, Zard SZ (2006) The Degenerative Radical Transfer of Xanthates and Related Derivatives: An Unusually Powerful Tool for the Creation of Carbon–Carbon Bonds. 264: 201–236
- Ratner MA, see Weiss EA (2005) 257: 103–133
Raymond KN, see Seeber G (2006) 265: 147–184
Rebek Jr J, see Scarso A (2006) 265: 1–46
Reckien W, see Thar J (2007) 268: 133–171
Reggelin M (2007) [2,3]-Sigmatropic Rearrangements of Allylic Sulfur Compounds. 275: 1–65

- Reif B, Narayanan S (2007) Characterization of Interactions Between Misfolding Proteins and Molecular Chaperones by NMR Spectroscopy. *272*: 117–168
- Reiher M, see Herrmann C (2007) *268*: 85–132
- Renaud P, see Darmency V (2006) *263*: 71–106
- Revell JD, Wennemers H (2007) Identification of Catalysts in Combinatorial Libraries. *277*: 251–266
- Rillema DP, see Kirgan RA (2007) *281*: 45–102
- Robinson SP, see Liu S (2005) *252*: 193–216
- Sabatini C, see Flamigni L (2007) *281*: 143–204
- Saha-Möller CR, see You C-C (2005) *258*: 39–82
- Sakai K, Sakurai R, Hirayama N (2007) Molecular Mechanisms of Dielectrically Controlled Resolution (DCR). *269*: 233–271
- Sakai K, Sakurai R, Nohira H (2007) New Resolution Technologies Controlled by Chiral Discrimination Mechanisms. *269*: 199–231
- Sakamoto M (2005) Photochemical Aspects of Thiocarbonyl Compounds in the Solid-State. *254*: 207–232
- Sakurai R, see Sakai K (2007) *269*: 199–231
- Sakurai R, see Sakai K (2007) *269*: 233–271
- Saladino R, Crestini C, Costanzo G, DiMauro E (2005) On the Prebiotic Synthesis of Nucleobases, Nucleotides, Oligonucleotides, Pre-RNA and Pre-DNA Molecules. *259*: 29–68
- Santos I, Paulo A, Correia JDG (2005) Rhenium and Technetium Complexes Anchored by Phosphines and Scorpionates for Radiopharmaceutical Applications. *252*: 45–84
- Santos M, see Szathmáry E (2005) *259*: 167–211
- Sato K (2007) Inorganic–Organic Interfacial Interactions in Hydroxyapatite Mineralization Processes. *270*: 127–153
- Sauvage J-P, see Collin J-P (2005) *262*: 29–62
- Sawant PD, see Nicolau DV (2005) *260*: 113–160
- Scandola F, see Chiorboli C (2005) *257*: 63–102
- Scarso A, Rebek Jr J (2006) Chiral Spaces in Supramolecular Assemblies. *265*: 1–46
- Schaumann E (2007) Sulfur is More Than the Fat Brother of Oxygen. An Overview of Organosulfur Chemistry. *274*: 1–34
- Scheffer JR, Xia W (2005) Asymmetric Induction in Organic Photochemistry via the Solid-State Ionic Chiral Auxiliary Approach. *254*: 233–262
- Schenning APHJ, see Ajayaghosh A (2005) *258*: 83–118
- Schepers U, see Hahn F (2007) *278*: 135–208
- Schindler J, see Faigl F (2007) *269*: 133–157
- Schmehl RH, see Kumaresan D (2007) *281*: 101–142
- Schmidtchen FP (2005) Artificial Host Molecules for the Sensing of Anions. *255*: 1–29 Author Index Volumes 251–255
- Scandola F, see Indelli MT (2007) *280*: 215–255
- Schmuck C, Wich P (2007) The Development of Artificial Receptors for Small Peptides Using Combinatorial Approaches. *277*: 3–30
- Schoof S, see Wolter F (2007) *267*: 143–185
- De Schryver F, see De Feyter S (2005) *258*: 205–255
- Schulten K, see Dittrich M (2007) *268*: 319–347
- Schuman B, Alfaro JA, Evans SV (2007) Glycosyltransferase Structure and Function. *272*: 217–258
- Seeber G, Tiedemann BEF, Raymond KN (2006) Supramolecular Chirality in Coordination Chemistry. *265*: 147–184

- Seeberger PH, see Castagner B (2007) 278: 289–309
- Seitz O, see Haase C (2007) 267: 1–36
- Senn HM, Thiel W (2007) QM/MM Methods for Biological Systems. 268: 173–289
- Severin K, see Otto S (2007) 277: 267–288
- Sewell SL, see Carney CK (2007) 270: 155–185
- Shankar K, see Kumaresan D (2007) 281: 101–142
- Sharma V, Piwnica-Worms D (2005) Monitoring Multidrug Resistance P-Glycoprotein Drug Transport Activity with Single-Photon-Emission Computed Tomography and Positron Emission Tomography Radiopharmaceuticals. 252: 155–178
- Shinkai S, see Ishi-i T (2005) 258: 119–160
- Shiomi T, see Nishiyama H (2007) 279: 105–137
- Sibi MP, see Zimmerman J (2006) 263: 107–162
- Siebbeles LDA, see Grozema FC (2005) 257: 135–164
- Silvi S, see Balzani V (2005) 262: 1–27
- Simon P, see Kniep R (2007) 270: 73–125
- Sinnecker S, Neese F (2007) Theoretical Bioinorganic Spectroscopy. 268: 47–83
- Skrydstrup T, see Hansen SG (2006) 264: 135–162
- Smith CL, Milea JS, Nguyen GH (2005) Immobilization of Nucleic Acids Using Biotin-Strept(avidin) Systems. 261: 63–90
- Smith DK, see Hirst AR (2005) 256: 237–273
- Sormunen GJ, see Montgomery J (2007) 279: 1–23
- Specker D, Wittmann V (2007) Synthesis and Application of Glycopeptide and Glycoprotein Mimetics. 267: 65–107
- Sromek AW, Gevorgyan V (2007) 1,2-Sulfur Migrations. 274: 77–124
- Stadler A, see Kremsner JM (2006) 266: 233–278
- Stibor I, Zlatušková P (2005) Chiral Recognition of Anions. 255: 31–63
- Stoddart JF, see Moonen NNP (2005) 262: 99–132
- Stomeo F, see Leonard JP (2007) 281: 1–44
- Strauss CR, Varma RS (2006) Microwaves in Green and Sustainable Chemistry. 266: 199–231
- Suk D-H, see Crich D (2006) 263: 1–38
- Suksai C, Tuntulani T (2005) Chromogenetic Anion Sensors. 255: 163–198
- Sullivan BP, see Kirgan RA (2007) 281: 45–102
- Sun J-S, see Escudé C (2005) 253: 109–148
- Suna E, Mutule I (2006) Microwave-assisted Heterocyclic Chemistry. 266: 49–101
- Süssmuth RD, see Wolter F (2007) 267: 143–185
- Svith H, see Daasbjerg K (2006) 263: 39–70
- Swerdlow H, see Du Q (2005) 261: 45–61
- Szathmáry E, Santos M, Fernando C (2005) Evolutionary Potential and Requirements for Minimal protocells. 259: 167–211
- Taira S, see Yokoyama K (2005) 261: 91–112
- Takahashi H, see Tamura R (2007) 269: 53–82
- Takahashi K, see Ueyama N (2007) 271: 155–193
- Tamiaki H, see Balaban TS (2005) 258: 1–38
- Tamaru Y, see Kimura M (2007) 279: 173–207
- Tamura R, Takahashi H, Fujimoto D, Ushio T (2007) Mechanism and Scope of Preferential Enrichment, a Symmetry-Breaking Enantiomeric Resolution Phenomenon. 269: 53–82
- Tanaka H, see Matile S (2007) 277: 219–250
- Thar J, Reckien W, Kirchner B (2007) Car-Parrinello Molecular Dynamics Simulations and Biological Systems. 268: 133–171

- Thayer DA, Wong C-H (2007) Enzymatic Synthesis of Glycopeptides and Glycoproteins. 267: 37–63
- Thiel W, see Senn HM (2007) 268: 173–289
- Tiedemann BEF, see Seeber G (2006) 265: 147–184
- Tobey SL, see Houk RJT (2005) 255: 199–229
- Toda F (2005) Thermal and Photochemical Reactions in the Solid-State. 254: 1–40
- Tortosa M, see de la Pradilla RF (2007) 275: 103–129
- Tour JM, see James DK (2005) 257: 33–62
- Trask AV, Jones W (2005) Crystal Engineering of Organic Cocrystals by the Solid-State Grinding Approach. 254: 41–70
- Tuntulani T, see Suksai C (2005) 255: 163–198
- Uccelli L, see Boschi A (2005) 252: 85–115
- Ueyama N, Takahashi K, Onoda A, Okamura T, Yamamoto H (2007) Inorganic–Organic Calcium Carbonate Composite of Synthetic Polymer Ligands with an Intramolecular NH \cdot · · O Hydrogen Bond. 271: 155–193
- Ushio T, see Tamura R (2007) 269: 53–82
- Vaidya S, see Kumaresan D (2007) 281: 101–142
- Varma RS, see Strauss CR (2006) 266: 199–231
- Veciana J, see Amabilino DB (2006) 265: 253–302
- Ventura B, see Flamigni L (2007) 281: 143–204
- Venturi M, see Balzani V (2005) 262: 1–27
- Veziñ H, see Dias N (2005) 253: 89–108
- Viso A, see de la Pradilla RF (2007) 275: 103–129
- Vögtle F, see Fages F (2005) 256: 77–131
- Vögtle M, see Žinić M (2005) 256: 39–76
- Volkmer D, see Fricke M (2007) 270: 1–41
- Volpicelli R, see Zonta C (2007) 275: 131–161
- Vries TR, see Kellogg RM (2007) 269: 159–197
- Walschus U, see Luderer F (2005) 260: 37–56
- Walton JC (2006) Unusual Radical Cyclisations. 264: 163–200
- Wannberg J, Ersmark K, Larhed M (2006) Microwave-Accelerated Synthesis of Protease Inhibitors. 266: 167–197
- Warman JM, see Grozema FC (2005) 257: 135–164
- Warren JD, Geng X, Danishefsky SJ (2007) Synthetic Glycopeptide-Based Vaccines. 267: 109–141
- Wasielewski MR, see Weiss EA (2005) 257: 103–133
- Weide T, Modlinger A, Kessler H (2007) Spatial Screening for the Identification of the Bioactive Conformation of Integrin Ligands. 272: 1–50
- Weiss EA, Wasielewski MR, Ratner MA (2005) Molecules as Wires: Molecule-Assisted Movement of Charge and Energy. 257: 103–133
- Weissbuch I, Leiserowitz L, Lahav M (2005) Stochastic “Mirror Symmetry Breaking” via Self-Assembly, Reactivity and Amplification of Chirality: Relevance to Abiotic Conditions. 259: 123–165
- Wennemers H, see Revell JD (2007) 277: 251–266
- Wich P, see Schmuck C (2007) 277: 3–30
- Wicha J, see Plesniak K (2007) 275: 163–250
- Wiehn M, see Jung N (2007) 278: 1–88

- Williams JAG (2007) Photochemistry and Photophysics of Coordination Compounds: Platinum. *281*: 205–268
- Williams LD (2005) Between Objectivity and Whim: Nucleic Acid Structural Biology. *253*: 77–88
- Wingssinger N, Pianowski Z, Debaene F (2007) Probing Biology with Small Molecule Microarrays (SMM). *278*: 311–342
- Wittmann V, see Specker D (2007) *267*: 65–107
- Wright DW, see Carney CK (2007) *270*: 155–185
- Woelk K, see Niessen HG (2007) *276*: 69–110
- Wolter F, Schoof S, Süßmuth RD (2007) Synopsis of Structural, Biosynthetic, and Chemical Aspects of Glycopeptide Antibiotics. *267*: 143–185
- Wöltinger J, see Greiner L (2007) *276*: 111–124
- Wong C-H, see Thayer DA (2007) *267*: 37–63
- Wong KM-C, see Yam VW-W (2005) *257*: 1–32
- Worgull D, see Gansäuer A (2007) *279*: 25–52
- Wright AT, see Collins BE (2007) *277*: 181–218
- Würthner F, see You C-C (2005) *258*: 39–82
- Xia W, see Scheffer JR (2005) *254*: 233–262
- Yam VW-W, Cheng EC-C (2007) Photochemistry and Photophysics of Coordination Compounds: Gold. *281*: 269–310
- Yam VW-W, Wong KM-C (2005) Luminescent Molecular Rods – Transition-Metal Alkynyl Complexes. *257*: 1–32
- Yamamoto H, see Ueyama N (2007) *271*: 155–193
- Yashima E, see Maeda K (2006) *265*: 47–88
- Yokoyama K, Taira S (2005) Self-Assembly DNA-Conjugated Polymer for DNA Immobilization on Chip. *261*: 91–112
- Yoshikawa I, see Araki K (2005) *256*: 133–165
- Yoshioka R (2007) Racemization, Optical Resolution and Crystallization-Induced Asymmetric Transformation of Amino Acids and Pharmaceutical Intermediates. *269*: 83–132
- You C-C, Dobrawa R, Saha-Möller CR, Würthner F (2005) Metallosupramolecular Dye Assemblies. *258*: 39–82
- Yu J, see Dittrich M (2007) *268*: 319–347
- Yu S-H (2007) Bio-inspired Crystal Growth by Synthetic Templates. *271*: 79–118
- Zampella G, see Bertini L (2007) *268*: 1–46
- Zard SZ, see Quiclet-Sire B (2006) *264*: 201–236
- Zarecki A, see Plesniak K (2007) *275*: 163–250
- Zhang W (2006) Microwave-Enhanced High-Speed Fluorous Synthesis. *266*: 145–166
- Zhang X-E, Deng J-Y (2005) Detection of Mutations in Rifampin-Resistant *Mycobacterium Tuberculosis* by Short Oligonucleotide Ligation Assay on DNA Chips (SOLAC). *261*: 169–190
- Zimmerman J, Sibi MP (2006) Enantioselective Radical Reactions. *263*: 107–162
- Žinić M, see Fages F (2005) *256*: 77–131
- Žinić M, Vögtle F, Fages F (2005) Cholesterol-Based Gelators. *256*: 39–76
- Zipse H (2006) Radical Stability—A Theoretical Perspective. *263*: 163–190
- Zlatušková P, see Stibor I (2005) *255*: 31–63
- Zonta C, De Lucchi O, Volpicelli R, Cotarca L (2007) Thione–Thiol Rearrangement: Miyazaki–Newman–Kwart Rearrangement and Others. *275*: 131–161

Subject Index

- Acetylide complexes 225
Anion sensor molecules 94
Antenna 8
Autofluorescence 2
Avidin 172
- Bidentate ligands, mononuclear complexes 150
Bioconjugates 172
Bioinorganic applications 88
Bis(thiocyanate)(2,2'-bipyridine)platinum(II) 232
Black chromophores 104
Blue emission 159, 182
- Calixarenes 13
Carbon dioxide reduction 87
Charge separation 194
Chromophore excitation 5
CO loss 133
Cp*Re(CO)₃ 97
Cryptates 12
Cyclometalating ligands 143
-, terdentate 176
Cyclometallated complexes 250
- Dipyridyphenazine ligand 80
DOTA 3
Dy(III) 3
- Eilatin 104
Electrochemistry 143
Electroluminescent (EL) polymers 171
Electroluminescent devices 139
Electron transfer 112, 193
-, intramolecular 112
Emissive excited states 152
- Energy transfer 112, 186
-, aromatic hydrocarbon donors/acceptors 125
-, triplet-mediated 6
Er(III) 3
Eu(III) complexes 1
Excited states, MC levels 178
- Fe(II)-polyimines 147
Fluorotyrosines 89
- Gd(III) 3
Gold(I) complexes 272
-, phosphine ligands, homoleptic 272
Gold(I) alkynyl complexes 284
Gold(I) chalcogenido/thiolato complexes 275
Gold(II) complexes 296
Gold(III) complexes 298
-, cyclometallated 298
-, porphyrinato 301
Gold(III) alkyl/aryl complexes, ancillary diimine ligands 298
- Heteroleptic complexes 154
Ho(III) 3
Homoleptic complexes 157
Homometallic complexes, binuclear 182
Host-guest molecules 86
Human serum albumin (HSA) 172
4-Hydroxytamoxifen 90
- Imidazole tetrafluorobenzene ligands 89
Iodoacetamide 172
Ir(III) complexes, multicomponent systems 143, 182
-, oxygen sensing 167
Ir(III) metal center, octahedral coordination 146

- Ir(III)-cyclometalated complexes, cationic 163
-, phosphorescence tuning 154
Ir(ppy)₂(LL) complexes, covalently linked to substrates 169
Iridium complexes 143
Isoelatin bis-phenanthroline 104
- Lanthanides, luminescent sensors/switches 2, 18, 96
Light emitting devices 90
- Metal-element multiple bonds 46
Metallo dendrimers 90
N-Methyl salicylimine 156
Molecular polygons 82
Multicomponent arrays 143
- N[^]C/N bridging ligands, exobidentate 292
N[^]N[^]N ligands, terdentate 172
Nd(III) 3
Nitric oxidase synthase 89
Nitridorhenium complexes 52
- OLEDs 93, 107, 154
Organometallic photoreactions 133
Os carbonyl clusters, M-M cleavage 130
Os complexes 135
-, imine ligands 102
-, organometallic 129
-, quenchers 116
-, transition metal complexes 102
Os(II)-diimines 103
Os(II)-polyimines 147
Osmium imine complexes 102
Oxorhenium complexes, high-valent 47
Oxygen sensing, Ir(III) complexes 167
- Phenothiazine (PTZ) donor 225
2-Phenylpyridines 151
Phosphorescence 143
Photochemistry 76
Photoinduced processes 143
Photoswitch 79
Photovoltaic cells 137
Picolinic acid 156
Platinum(II) diimine dithiolate 227
Podands 11
Poly(amidoamine) dendrimers 90
- Poly(*p*-phenylenevinylene) backbone 81
Polyfluorene 171
Polymer systems 80
Pr(III) 3
Proton sensor ligands 94
Pt complexes, N[^]N bidentate ligands 212
-, N[^]N[^]N terdentate ligands 237
Pt(C[^]C) complexes 262
Pt(C[^]N[^]C) complexes 262
Pt(diimine)(dithiolate) 228
Pt(dpphen)(CN)₂ 217
Pt(N[^]C) complexes, bidentate ligands 251
Pt(N[^]C[^]N) complexes 258
Pt(N[^]N)(C≡CR)₂ 218
Pt(N[^]N)(C≡N)₂ 217
Pt(N[^]N)(S-R)₂ 227
Pt(N[^]N)(S[^]S) 227
Pt(N[^]N)X₂ 212, 235
Pt(N[^]N[^]C) complexes 255
[Pt(N[^]N[^]N)X]⁺ 247
[Pt(4'-R-tpy)Cl]⁺ 241
Pt(tbbpy)(tda) 223
[Pt(tpy)(-C≡CR)]⁺ 244
[Pt(tpy)Cl]⁺ 238
[Pt(tpy)X]⁺ 239
- Radiopharmaceuticals, Re complexes 90
Re(I), carbonyl complexes 97
-, pyridine/diimine ligands 55
Re(II), complexes 53
Re/Pd square 83
Rectangles 84
ReO⁺² core 48
Rhenium complexes, cancer studies 92
Rhenium hydride complexes 54
Rhenium tricarbonyl complexes 56
Rhenium-rhenium bonds 55
Ru(II)-polyimines 147
- Self-quenching 77
Sensitisation process 5
Sensors 94, 135
Sm(III) 3
Solvent effects 9
Squares 84
- Tamoxifen 90
Tb(III) complexes 1

-
- Terdentate ligands, mononuclear
complexes 172
- Tetrakis(carboxymethyl)-
tetraazacyclododecane (DOTA)
3
- Thiolate complexes 232
- Tm(III) 3
- Toluene-3,4-dithiolate 228
- Transient detection 75
- Triangles 84
- Yb(III) 3
- Zinc porphyrin 82
- Zn salen 82
- Zn(II) tetraphenylporphyrin 114